

Energy, Environment, and Sustainability

Santanu De
Avinash Kumar Agarwal
V. S. Moholkar
Bhaskar Thallada *Editors*

Coal and Biomass Gasification

Recent Advances and Future Challenges



 Springer

Energy, Environment, and Sustainability

Series editors

Avinash Kumar Agarwal, Department of Mechanical Engineering, Indian Institute of Technology, Kanpur, Uttar Pradesh, India

Ashok Pandey, Distinguished Scientist, CSIR-Indian Institute of Toxicology Research, Lucknow, India

This books series publishes cutting edge monographs and professional books focused on all aspects of energy and environmental sustainability, especially as it relates to energy concerns. The Series is published in partnership with the International Society for Energy, Environment, and Sustainability. The books in these series are editor or authored by top researchers and professional across the globe. The series aims at publishing state-of-the-art research and development in areas including, but not limited to:

- Renewable Energy
- Alternative Fuels
- Engines and Locomotives
- Combustion and Propulsion
- Fossil Fuels
- Carbon Capture
- Control and Automation for Energy
- Environmental Pollution
- Waste Management
- Transportation Sustainability

More information about this series at <http://www.springer.com/series/15901>

Santanu De · Avinash Kumar Agarwal
V. S. Moholkar · Bhaskar Thallada
Editors

Coal and Biomass Gasification

Recent Advances and Future Challenges

 Springer

Editors

Santanu De
Department of Mechanical Engineering
Indian Institute of Technology Kanpur
Kanpur, Uttar Pradesh
India

V. S. Moholkar
Department of Chemical Engineering
Indian Institute of Technology Guwahati
Guwahati, Assam
India

Avinash Kumar Agarwal
Department of Mechanical Engineering
Indian Institute of Technology Kanpur
Kanpur, Uttar Pradesh
India

Bhaskar Thallada
Bio-Fuels Division
CSIR-Indian Institute of Petroleum (IIP)
Dehradun, Uttarakhand
India

ISSN 2522-8366

ISSN 2522-8374 (electronic)

Energy, Environment, and Sustainability

ISBN 978-981-10-7334-2

ISBN 978-981-10-7335-9 (eBook)

<https://doi.org/10.1007/978-981-10-7335-9>

Library of Congress Control Number: 2017958629

© Springer Nature Singapore Pte Ltd. 2018

This work is subject to copyright. All rights are reserved by the Publisher, whether the whole or part of the material is concerned, specifically the rights of translation, reprinting, reuse of illustrations, recitation, broadcasting, reproduction on microfilms or in any other physical way, and transmission or information storage and retrieval, electronic adaptation, computer software, or by similar or dissimilar methodology now known or hereafter developed.

The use of general descriptive names, registered names, trademarks, service marks, etc. in this publication does not imply, even in the absence of a specific statement, that such names are exempt from the relevant protective laws and regulations and therefore free for general use.

The publisher, the authors and the editors are safe to assume that the advice and information in this book are believed to be true and accurate at the date of publication. Neither the publisher nor the authors or the editors give a warranty, express or implied, with respect to the material contained herein or for any errors or omissions that may have been made. The publisher remains neutral with regard to jurisdictional claims in published maps and institutional affiliations.

Printed on acid-free paper

This Springer imprint is published by Springer Nature

The registered company is Springer Nature Singapore Pte Ltd.

The registered company address is: 152 Beach Road, #21-01/04 Gateway East, Singapore 189721, Singapore

Preface

Energy demand has been rising remarkably due to increasing population and urbanization. Global economy and society are significantly dependent on the energy availability because it touches every facet of human life and its activities. Transportation and power generation are major examples of energy. Without the transportation by millions of personalized and mass transport vehicles and availability of 24×7 power, human civilization would not have reached contemporary living standards.

First International Conference on ‘Sustainable Energy and Environmental Challenges’ (SEEC-2017) was organized under the auspices of ‘International Society for Energy and Environmental Sustainability’ (ISEES) by the ‘Center of Innovative and Applied Bioprocessing’ (CIAB), Mohali, from February 26–28, 2017. ISEES was founded at IIT Kanpur in January 2014 with the aim of spreading knowledge in the fields of energy, environment, sustainability, and combustion. The society’s goal is to contribute to the development of clean, affordable, and secure energy resources and a sustainable environment for the society and to spread knowledge in the above-mentioned areas and spread awareness about the environmental challenges, which the world is facing today. ISEES is involved in various activities such as conducting workshops, seminars, conferences in the domains of its interests. The society also recognizes the outstanding works done by the young scientists and engineers for their contributions in these fields by conferring them awards under various categories.

This conference provided a platform for discussions between eminent scientists and engineers from various countries including India, USA, South Korea, Norway, Malaysia, and Australia. In this conference, eminent speakers from all over the world presented their views related to different aspects of energy, combustion, emissions, and alternative energy resource for sustainable development and a cleaner environment. The conference started with four mini-symposiums on very topical themes, which included (i) New Fuels and Advanced Engine Combustion, (ii) Sustainable Energy, (iii) Experimental and Numerical Combustion, and (iv) Environmental Remediation and Rail Road Transport. The conference had 14 technical sessions of topics related to energy and environmental sustainability and a

panel discussions on 'Challenges, Opportunities and Directions of Technical Education and Research in the Area of Energy, Environment and Sustainability' to wrap up the 3 day technical extravaganza. The conference included 2 plenary talks, 12 keynote talks, 42 invited talks from prominent scientists, 49 contributed talks, and 120 posters. A total of 234 participants and speakers attended this three-day conference, which hosted Dr. V. K. Saraswat, Member NITI Ayog, India, as a chief guest for the award ceremony of ISEES. This conference laid out the road map for technology development, opportunities, and challenges in this technology domain. The technical sessions in the conference included Advances in IC Engines and Fuels; Conversion of Biomass to Biofuels; Combustion Processes; Renewable Energy: Prospects and Technologies; Waste to Wealth—Chemicals and Fuels; Energy Conversion Systems; Numerical Simulation of Combustion Processes; Alternate Fuels for IC Engines; Sprays and Heterogeneous Combustion of Coal/Biomass; Biomass Conversion to Fuels and Chemicals—Thermochemical Processes; Utilization of Biofuels; and Environmental Protection and Health. All these topics are very relevant for the country and the world in the present context. The society is grateful to Prof. Ashok Pandey for organizing and hosting this conference, which led to germination of this series of monographs, which included 16 books related to different aspects of energy, environment, and sustainability. This is the first time that such voluminous and high-quality outcome has been achieved by any society in India from one conference.

The editors would like to express their sincere gratitude to the authors for submitting their work in a timely manner and revising it appropriately at short notice. We would like to express our special thanks to Dr. Sminu Bhaskaran, Prof. Sudip Ghosh, Prof. Pankaj Kalita, Prof. Malay Karmakar, Prof. Mayank Kumar, Dr. Chanchal Loha, Prof. H. S. Mukunda, Prof. V. Prabu, Prof. M. R. Ravi, and Prof. R. Vinu, who reviewed various chapters of this monograph and provided their valuable suggestions improving the manuscripts. We acknowledge the support received from various funding agencies and organizations for the successful conduct of the first ISEES conference SEEC-2017, where these monographs germinated. These include Department of Science and Technology, Government of India (special thanks to Dr. Sanjay Bajpai); TSI, India (special thanks to Dr. Deepak Sharma); Tesscorn, India (special thanks to Sh. Satyanarayana); AVL India; Horiba, India; Springer (special thanks to Swati Mehershi); CIAB (Special thanks to Dr. Sangwan).

Gasification provides a clean alternative approach over direct combustion for production of electricity, fuels, fertilizers, and other useful chemicals from any carbonaceous feedstock, such as coal, oil, gas, biomass, and municipal solid wastes. The product of gasification consists of a mixture of H_2/CO , commonly referred as syngas, which may be directly used in gas engines, spark ignition engines, and solid oxide fuel cells, produce electricity by burning it in gas turbine of an integrated gasification combined cycle power plant, produce combined heat and power, used to produce methanol and hydrogen, or converted into synthetic fuel via the Fischer–Tropsch process. Besides the quality of feedstock, several other parameters influence the efficiency of gasification, such as operating temperature, pressure, and the

type of reactor. Several types of gasifiers are currently available for commercial use: moving bed, fluidized bed, entrained flow, and plasma gasifier. Research is being directed to study gasification in different gasifiers and optimize their design, reduce tar, increase conversion efficiency, cleaning of hot gases, to name a few.

In this book, science and technology of gasification process are described. It also covers state-of-the-art experimental techniques, modeling and numerical simulations of gasification, and environment-friendly approaches, such as integration with solar energy, utilization of municipal solid wastes. The recent advances and future directions of research in the field of gasification are also discussed. The book is envisaged to benefit a relatively broad audience, including beginners, graduate students in chemical and thermal engineering, seasoned researchers, and engineers working in designing and operating gasifiers.

The monograph is intended for engineers/practitioners who are working in the area of gasification. We hope that the book would be of great interest to the professionals and postgraduate students involved in gasification technology, experimentation, and numerical simulation of gasification. The main objective of this monograph is to promote a better and more accurate understanding of gasification and related technologies, besides recent advances and future challenges. The topics are organized into four different sections: (i) fundamentals of gasification, (ii) experiments, modeling and numerical simulations of gasification, (iii) integration of renewable energy and utilization of wastes, and (iv) advanced topics of gasification.

Kanpur, India
Kanpur, India
Guwahati, India
Dehradun, India

Santanu De
Avinash Kumar Agarwal
V. S. Moholkar
Bhaskar Thallada

Contents

Part I Fundamentals of Gasification

Feedstock Characterization for Pyrolysis and Gasification	3
B. Rajasekhar Reddy and R. Vinu	
Thermodynamics and Kinetics of Gasification	37
M. R. Ravi and Sangeeta Kohli	
Gasifiers: Types, Operational Principles, and Commercial Forms	63
Chanchal Loha, Malay K. Karmakar, Santanu De and Pradip K. Chatterjee	
Hydrodynamics of Circulating Fluidized Bed Systems	93
Malay K. Karmakar, Chanchal Loha, Santanu De and Pradip K. Chatterjee	
Investigation of Biomass Gasifier Product Gas Composition and its Characterization	115
Pankaj Kalita and Debarshi Baruah	
Gas Cleaning and Tar Conversion in Biomass Gasification	151
Sudip Ghosh	

Part II Experiments, Modeling and Numerical Simulations of Gasification

Measurement Techniques: Cold Flow Studies	175
Premkumar Kamalanathan and Rajesh Kumar Upadhyay	
Cavity Models for Underground Coal Gasification	207
Preeti Aghalayam	
Gasification of Mixed Biomass: Analysis Using Equilibrium, Semi-equilibrium, and Kinetic Models	223
Debarshi Mallick, Buljit Buragohain, Pinakeswar Mahanta and Vijayanand S. Moholkar	

Numerical Modelling of Fluidized Bed Gasification: An Overview	243
Saurabh Gupta, Sminu Bhaskaran and Santanu De	
Entrained Flow Gasification: Current Status and Numerical Simulations	281
Mayank Kumar	
Advanced Numerical Methods for the Assessment of Integrated Gasification and CHP Generation Technologies	307
Ahmed M. Salem, Umesh Kumar, Ainul Nadirah Izaharuddin, Harnek Dhani, Tata Sutardi and Manosh C. Paul	
Transient Cold Flow Simulation of a Fast Fluidized Bed Fuel Reactor for Chemical Looping Combustion	331
Ramesh K. Agarwal, Mengqiao Yang and Subhdeep Banerjee	
Part III Integration of Renewable Energy and Utilization of Wastes	
Sustainability Assessment of the Biomass Gasification Process for Production of Ammonia	351
Pratham Arora, Andrew Hoadley and Sanjay Mahajani	
Recent Advances in Power Generation Through Biomass and Municipal Solid Waste Gasification	369
Natarianto Indrawan, Ajay Kumar and Sunil Kumar	
Solar-Assisted Gasification Based Cook Stoves	403
Ankur Kaundal, Satvasheel Powar and Atul Dhar	
Part IV Advanced Technologies of Gasification	
Dual Fluidized Bed Gasification of Solid Fuels	425
Sminu Bhaskaran, Saurabh Gupta and Santanu De	
New Pathways in Clean Combustion of Biomass and Coal via Partial Gasification	455
H. S. Mukunda and Suresh Attanoor	
Synergistic Effects in Gasification of Coal/Biomass Blends: Analysis and Review	473
Debarshi Mallick, Pinakeswar Mahanta and Vijayanand S. Moholkar	
Chemical Looping and Plasma Technologies for Gasification of Coal and Biomass	499
Barnali Bhui and Prabu Vairakannu	
Author Index	521

Editors and Contributors

About the Editors



Dr. Santanu De is an Assistant Professor in the Mechanical Engineering, IIT Kanpur, since December 2014. He received a Bachelor of Engineering from the North Bengal University in 2002 and an M.Tech. from IIT Kanpur in 2004, both in Mechanical Engineering. He received his Ph.D. in Aerospace Engineering from the Indian Institute of Science, Bangalore, in 2012. Prior to his joining at IIT Kanpur, he served 2 years at the Michigan Technological University as a Postdoctoral Research Associate and 1 year at the Institute of Combustion Technology (ITV), University of Stuttgart. He also worked as a Scientist at the Liquid Propulsion Systems Center, Indian Space Research Organization, between 2004 and 2005. His primary areas of research are numerical modeling of turbulent combustion, spray atomization and combustion, coal gasification and combustion. He is an Associate Editor of the 'Journal of Energy, Environment and Sustainability.'

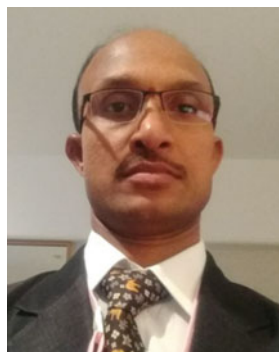


Prof. Avinash Kumar Agarwal joined IIT Kanpur in 2001 and is currently a Poonam and Prabh Goyal Endowed Chair Professor. He was at ERC, University of Wisconsin, Madison, USA, as a Postdoctoral Fellow (1999–2001). His areas of interest are IC engines, combustion, alternative fuels, hydrogen, conventional fuels, lubricating oil tribology, optical diagnostics, laser ignition, HCCI, emission and particulate control, and large bore engines. He has published more than 160 peer-reviewed international journal and conference papers. He is Associate Editor of ASME Journal of Energy Resources Technology and International Journal of Vehicle Systems Modelling and Testing. He has edited 'Handbook of Combustion' (5 volumes; 3168 pages), published by Wiley VCH, Germany. He is a Fellow of SAE (2012), Fellow of ASME (2013), and a Fellow of INAE (2015). He is the recipient of several prestigious awards such as NASI-Reliance Industries Platinum Jubilee Award-2012; INAE

Silver Jubilee Young Engineer Award-2012; Dr. C. V. Raman Young Teachers Award: 2011; SAE International's Ralph R. Teetor Educational Award-2008; INSA Young Scientist Award-2007; UICT Young Scientist Award-2007; INAE Young Engineer Award-2005. He is the recipient of Prestigious Shanti Swarup Bhatnagar Award-2016 in Engineering Sciences. He is the first combustion/IC engine researcher to get this honor.



Dr. V. S. Moholkar is a Full Professor of Chemical Engineering and Head of Center for Energy at Indian Institute of Technology (IIT) Guwahati. He received bachelors (1993) and masters (1996) in Chemical Engineering from Institute of Chemical Technology (ICT) Mumbai, followed by Ph.D. from University of Twente in 2002. He has been Head of the Chemical Engineering Department at IIT Guwahati during 2012–2015. His main research interests are sonochemistry, cavitation-assisted physical, chemical and biological processing, and thermo- and biochemical routes to biofuels. As of June 2017, he has published more than 120 papers in renowned international journals that have received more than 3800 citations (with *h*-index of 39). He has also filed two US patents (in collaboration with CTI Nanotech, CA, USA) on the application of hydrodynamic cavitation reactors for biomass pretreatment and bioalcohol synthesis. He has graduated 10 Ph.D. and 24 M.Tech. students. He has been elected Fellow of Royal Society of Chemistry (FRSC) in July 2016. He was admitted as Senior Member of American Institute of Chemical Engineers (MAIChE (Sr.)) in August 2016. He is a Chartered Member of Institution of Chemical Engineers, UK, and Chartered Engineer (CEng) registered with Engineering Council of UK.



Dr. Bhaskar Thallada, FBRS, FRSC, Principal Scientist, is currently heading the Thermo-catalytic Processes Area, Bio-Fuels Division (BFD), at CSIR-Indian Institute of Petroleum, Dehradun, India. He received his Ph.D. from CSIR-Indian Institute of Chemical Technology (IICT), Hyderabad, and thereafter spent 7 years as a Postdoc and as a Faculty at Okayama University, Japan. He has more than 120 publications in SCI journals of international repute with *h*-index of 32 and around 3500 citations and contributed 18 chapters to renowned publishers and 13 patents. In addition, he is the project leader/coordinator for several projects for biomass and waste valorization. His vast research experience covers various fields of science revolving around his expertise in heterogeneous catalysis, thermochemical conversion of biomass, waste plastics, and e-waste (WEEE) plastics into value-added hydrocarbons. He is on the editorial board of five international peer-reviewed journals and served as an editor for two books. He received the Distinguished Researcher Award from AIST (2013), Japan, and Most Progressive Researcher Award from FSRJ, Japan (2008). He is also the Fellow of Royal Society of Chemistry (FRSC), UK; Fellow of Biotech Research Society (FBRS), India; Fellow,

National Environmental Science Academy (NESA), India; Member, Management Council (BRSI). He received the Raman Research Fellowship for the year 2013–2014. He has been selected for the visiting fellowship under Chinese Academy of Sciences (CAS), China Presidential International Fellowship Initiative, for 2016. He was also a JSPS Visiting Scientist to Tokyo Institute of Technology, Japan, during 2009. He is a member of the scientific and organizing committee of several international symposia in India and abroad and visited several countries to deliver invited/plenary lectures.

Contributors

Ramesh K. Agarwal Washington University in St. Louis, St. Louis, MO, USA

Preeti Aghalayam Department of Chemical Engineering, Indian Institute of Technology Madras, Chennai, India

Pratham Arora The Energy and Resources Institute (TERI), Delhi, India

Suresh Attanoor Fire & Combustion Research centre, Jain University, Bengaluru, India

Subhdeep Banerjee Washington University in St. Louis, St. Louis, MO, USA

Debarshi Baruah Centre for Energy, Indian Institute of Technology Guwahati, Guwahati, Assam, India

Sminu Bhaskaran Department of Mechanical Engineering, Indian Institute of Technology Kanpur, Kanpur, India

Barnali Bhui Department of Chemical Engineering, Indian Institute of Technology Guwahati, Guwahati, Assam, India

Buljit Buragohain Center for Energy, Indian Institute of Technology Guwahati, Guwahati, Assam, India; Department of Mechanical Engineering, Girijananda Chowdhury Institute of Management and Technology, Azara, Guwahati 781017, Assam, India

Pradip K. Chatterjee CSIR-Central Mechanical Engineering Research Institute, Durgapur, West Bengal, India

Santanu De Department of Mechanical Engineering, Indian Institute of Technology Kanpur, Kanpur, India

Harnek Dhami Systems, Power & Energy Research Division, School of Engineering, University of Glasgow, Glasgow, UK

Atul Dhar School of Engineering, IIT Mandi, Mandi, India

Sudip Ghosh Department of Mechanical Engineering, Indian Institute of Engineering Science and Technology, Shibpur, Howrah, WB, India

Saurabh Gupta Department of Mechanical Engineering, Indian Institute of Technology Kanpur, Kanpur, India

Andrew Hoadley Department of Chemical Engineering, Monash University, Melbourne, Australia

Natarianto Indrawan Environmental Science Program, Oklahoma State University (OSU), Stillwater, OK, USA; Department of Mechanical Engineering, Institut Teknologi Nasional, Bandung, Indonesia

Ainul Nadirah Izaharuddin Systems, Power & Energy Research Division, School of Engineering, University of Glasgow, Glasgow, UK

Pankaj Kalita Centre for Energy, Indian Institute of Technology Guwahati, Guwahati, Assam, India

Premkumar Kamalanathan Department of Chemical Engineering, Indian Institute of Technology, Guwahati, Assam, India

Malay K. Karmakar CSIR-Central Mechanical Engineering Research Institute, Durgapur, West Bengal, India

Ankur Kaundal School of Engineering, IIT Mandi, Mandi, India

Sangeeta Kohli Indian Institute of Technology Delhi, New Delhi, India

Ajay Kumar Biosystems and Agricultural Engineering Department, OSU, Stillwater, OK, USA

Mayank Kumar Department of Mechanical Engineering, Indian Institute of Technology Delhi, Delhi, India

Sunil Kumar CSIR - National Environmental Engineering Research Institute, Nagpur, India

Umesh Kumar Systems, Power & Energy Research Division, School of Engineering, University of Glasgow, Glasgow, UK

Chanchal Loha CSIR-Central Mechanical Engineering Research Institute, Durgapur, West Bengal, India

Sanjay Mahajani Department of Chemical Engineering, Indian Institute of Technology Bombay, Mumbai, India

Pinakeswar Mahanta Department of Mechanical Engineering, Indian Institute of Technology Guwahati, Guwahati, Assam, India; Center for Energy, Indian Institute of Technology Guwahati, Guwahati, Assam, India

Debarshi Mallick Department of Mechanical Engineering, Indian Institute of Technology Guwahati, Guwahati, Assam, India

Vijayanand S. Moholkar Center for Energy, Indian Institute of Technology Guwahati, Guwahati, Assam, India; Department of Chemical Engineering, Indian Institute of Technology Guwahati, Guwahati, Assam, India

H. S. Mukunda Fire & Combustion Research centre, Jain University, Bengaluru, India

Manosh C. Paul Systems, Power & Energy Research Division, School of Engineering, University of Glasgow, Glasgow, UK

Satvasheel Powar School of Engineering, IIT Mandi, Mandi, India

B. Rajasekhar Reddy Department of Chemical Engineering and National Center for Combustion Research and Development, Indian Institute of Technology Madras, Chennai, India

M. R. Ravi Indian Institute of Technology Delhi, New Delhi, India

Ahmed M. Salem Systems, Power & Energy Research Division, School of Engineering, University of Glasgow, Glasgow, UK

Tata Sutardi Systems, Power & Energy Research Division, School of Engineering, University of Glasgow, Glasgow, UK

Rajesh Kumar Upadhyay Department of Chemical Engineering, Indian Institute of Technology, Guwahati, Assam, India

Prabu Vairakannu Department of Chemical Engineering, Indian Institute of Technology Guwahati, Guwahati, Assam, India

R. Vinu Department of Chemical Engineering and National Center for Combustion Research and Development, Indian Institute of Technology Madras, Chennai, India

Mengqiao Yang Washington University in St. Louis, St. Louis, MO, USA

Part I
Fundamentals of Gasification

Feedstock Characterization for Pyrolysis and Gasification

B. Rajasekhar Reddy and R. Vinu

Abstract Gasification and pyrolysis are promising thermochemical processing technologies for the conversion of complex feedstocks like coal, lignocellulosic biomass and refuse-derived fuels (RDF) into energy and fuels. The quality of the products such as syngas and liquid oil and the process efficiencies depend greatly on the operating parameters of the process, which in turn depend on feedstock characteristics. Hence, it is imperative to map the salient properties of the feedstock to the process characteristics. This review highlights the techniques adopted for characterizing different varieties of coal, biomass and RDF. The various physico-chemical and thermal properties discussed in this chapter include density, porosity, specific surface area, thermal conductivity, specific heat, calorific value, thermal stability, pyrolysate composition, proximate and elemental composition, and ash composition. A compendium of proximate analysis (moisture, volatile matter, fixed carbon, ash), ultimate analysis (elemental C, H, N, S, O) and higher heating value data for a large number of solid fuels is provided. The implications of these on the process and product characteristics are addressed. As ash is known to act as a catalyst in the pyrolysis process and cause issues like corrosion and deposition in gasifier systems, the effect of its composition on relevant process parameters is discussed. Finally, the existing challenges and requirements in fuel characterization are discussed.

B. Rajasekhar Reddy · R. Vinu (✉)

Department of Chemical Engineering and National Center for Combustion Research and Development, Indian Institute of Technology Madras, Chennai 600036, India
e-mail: vinu@iitm.ac.in

B. Rajasekhar Reddy
e-mail: rajasekharreddy104@gmail.com

1 Introduction

There is an increasing global interest in thermochemical conversion technologies for the conversion of renewable, non-renewable and waste feedstocks to liquid, solid and gaseous fuels to meet the increasing energy and fuel demands. The Technology Roadmap for Bioenergy for Heat and Power by International Energy Agency [1] envisages a threefold increase in world's bioenergy supply from 50 EJ in 2012 to 160 EJ in 2050, with 100 EJ used up for heat and power generation. Moreover, biofuels are projected to contribute to 27% of the transportation fuels by 2050 by replacing petroleum-based gasoline, diesel, kerosene and jet fuels (Technology Roadmap-Biofuels for Transport, International Energy Agency [2]). In order to meet these preset targets, it is vital to improve the conversion efficiency, cost and overall sustainability of the existing technologies. The promising thermochemical technologies for the production of energy (heat and power), fuels and fine chemicals include combustion, gasification, pyrolysis, hydrothermal liquefaction and hydrothermal liquefaction. Of the above, the first three technologies have reached commercial stage, while the last two are still in pilot and demonstration stages. Gasification is a versatile thermochemical process as it can handle a wide variety of feedstocks to produce energy, fuels and chemicals, while combustion and pyrolysis primarily cater to delivering energy and liquid products, respectively. The primary product of gasification, called as synthesis gas or syngas or producer gas, is a mixture of CO and H₂. Syngas can be combusted using air for thermal power, converted to high-energy hydrogen fuel through water-gas shift reaction or converted to hydrocarbon fuels via catalytic Fischer–Tropsch synthesis process.

Gasification refers to thermochemical conversion of any carbonaceous feedstock to a gaseous product with a reasonable heating value, which is then used as a fuel gas or feedstock for chemicals. Gasification includes pyrolysis, partial oxidation and hydrogenation processes. In the initial stages up to 600 °C, pyrolysis occurs, and at high temperatures, 700–1600 °C, partial oxidation and hydrogenation occur. Gasification eventually results in the production of syngas by partial oxidation. In partial oxidation, oxidant can be oxygen, air and/or steam. Partial oxidation can be applied to solid, liquid and gaseous feedstocks, such as coals, residual oils and natural gas. The ratio of carbon monoxide to hydrogen depends on the type of feedstock, its properties and the operating conditions. The overall gasification process includes three major operations, viz. (a) pretreatment of the feedstock (characterization of feedstock, drying, crushing, grinding, pelletization), (b) gasification itself, and (c) gas clean-up. In many cases, pretreatment of feedstock is performed to increase the output gas and gas quality. Figure 1 depicts the typical gasification process which involves primary treatment, reaction and flue emissions which include ammonia and carbonyl sulphide (COS).

During gasification, the gases are generated via several reactions of the original fuel with the gasifying agent at high temperatures. The gas can be used for combined production of heat and power or for the production of alternative fuels. In the case of autothermal gasification, the gasifying agent is oxygen. The reactions of

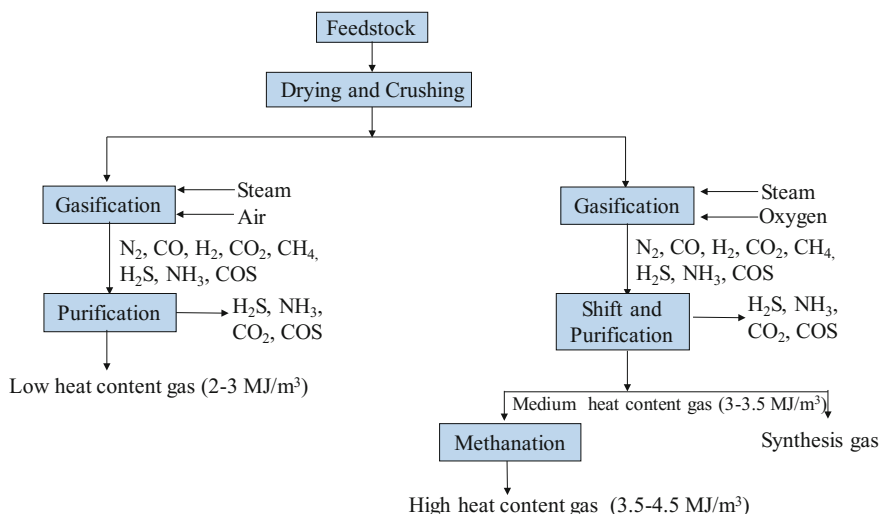


Fig. 1 Schematic of the major steps involved in gasification in air and oxygen ambience

oxygen are exothermic, while that of a moderator is endothermic. In the case of allothermal gasification, the gasification agent is composed only of a moderator (steam, carbon dioxide), and the heat needed for the endothermic process has to be supplied from an external source. Moderator controls the process by consuming the heat generated by exothermic reactions of oxygen. At the same time, it introduces additional oxygen, which is needed for the higher conversion of carbon in the fuel to gases. At present, in most cases, steam is used as the moderator for gasification, but carbon dioxide can play a very similar role and is sometimes considered for the following two reasons: (a) the CO₂ available from a carbon capture technology can be used and (b) to avoid the formation of NO_x at high temperatures by replacing N₂ with CO₂. However, the substitution of H₂O with CO₂ affects the gas composition and the overall process behaviour, because CO₂ acts as a moderator for biomass gasification. Various factors such as coal rank, pore structure and ash behaviour have important influence on coal and biomass char gasification reactivity. Figure 2 depicts the sequence of steps and the major transformations involved in gasification.

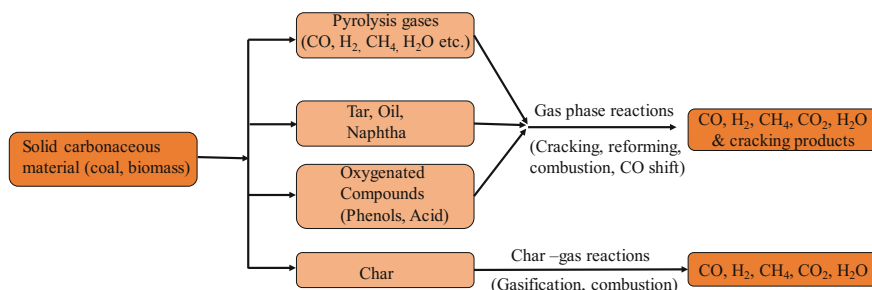
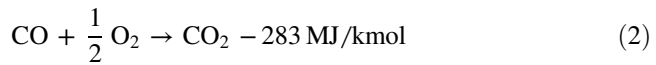
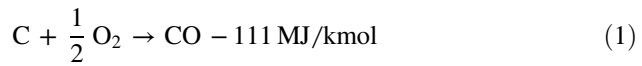
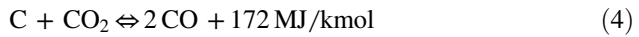


Fig. 2 Sequence of major reactions in gasification. Redrawn from Higman and Tang [3]

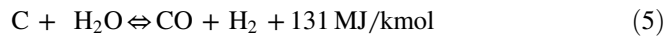
Importantly, pyrolysis is a subset of gasification, and it involves a complex set of cracking reactions that leads to the formation of tarry volatile compounds, hydrocarbons, oxygenates and non-condensable gases. The composition of the pyrolysates is complicated as it hugely depends on the type of feedstock and its biochemical or maceral composition. The condensable volatiles are further decomposed in the gas phase via secondary reactions such as cracking, reforming, combustion and CO shift to form the non-condensable gases as depicted in Fig. 2. During the gasification of solid carbon, whether in the form of coal, coke, biomass or char, the principal chemical reactions involving carbon, carbon monoxide, hydrogen, water (or steam) and methane are given below [4]. The enthalpies of the reactions are also provided. The negative and positive values signify exothermic and endothermic reactions, respectively. Owing to the high gasification temperature, thermodynamically as well as in practice, no hydrocarbons are present in appreciable quantities in syngas except methane.



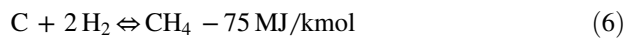
Boudouard reaction,



Water gas reaction,



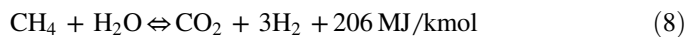
Methanation reaction,



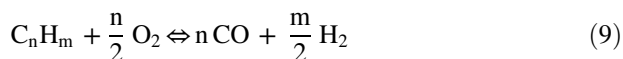
CO shift reaction,



Steam methane reforming reaction,



For real fuels including coal, which also contains hydrogen, the overall reaction can be written as



where for a gas, such as pure methane, $m = 4$ and $n = 1$; hence, $m/n = 4$, and for oil, $m/n \approx 2$; hence, $m = 2$ and $n = 1$, and for coal, $m/n \approx 1$; hence, $m = 1$ and $n = 1$.

Feedstock characterization plays an important role in achieving the required syngas composition. The composition of feedstocks such as coal, biomass and wastes is very complex and varies spatiotemporally. The detailed petrographic composition of the organic components of the coal, often characterized by maceral analysis, has little influence on most gasification processes [5]. The essential parameters for gasification are fixed carbon content, which is identified by the maturity of coals, water and ash content, and ash characteristics. However, for biomass-based feedstocks, the amount of volatile matter and the organic composition of the volatiles are important because they determine the secondary gas phase cracking to form non-condensable gases. As coal is the main feedstock for gasification even today on a commercial scale, a majority of the analyses techniques that are established are based on coal.

Figure 3 depicts the Van Krevelen diagram, in which the various feedstocks and liquid fuels are laid on a scale of atomic H/C and O/C ratios. An understanding of the elemental composition of the feedstock would provide the parametric information required for the optimization of pyrolysis or gasification process. From the

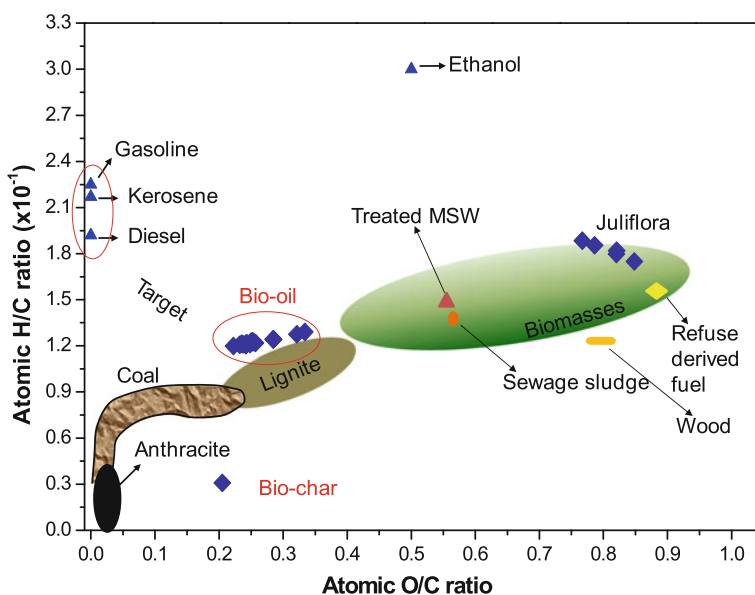


Fig. 3 Van Krevelen diagram for coals, biomasses and petroleum/biomass-derived products. The bio-oil and biochar data correspond to *Prosopis juliflora* biomass pyrolysis. Redrawn and modified from [6]

figure, it is evident that renewable feedstocks such as biomasses are rich in oxygen, whereas coal is rich in carbon. The presence of oxygen in biomass leads to a lot of issues when it comes to both pyrolysis and gasification. The oxygen present in biomass is not free oxygen, but bound by covalent bonds in the polymeric cellulose, hemicellulose and lignin. Pyrolysis of these components results in the release of oxygenates comprising a number of functional groups like alcohol, acids, aldehydes, ketones and esters [7]. Owing to such a complex mixture, the chemistry of gas phase combustion of these vapours will certainly affect the gasifier performance. In terms of pyrolysis oil, which is a condensed form of these volatiles, these components lead to storage issues and poor heating value among other variations in physicochemical properties. The composition of bio-oil is also depicted in the figure, which shows that catalytic treatments are required to improve the quality of pyrolysis oil derived from biomass (also known as bio-oil), especially in terms of further reducing the oxygen and increasing the hydrogen content, to make it equivalent to petroleum-derived fuels. Similarly, the oxygen content in biochar should be reduced so that it is similar to high-rank coal.

This chapter is intended to uncover the fundamentals of characterization of various solid fuels such as coal, lignocellulosic biomass and refuse-derived fuel, especially in terms of their composition, physicochemical and thermodynamic properties. After classifying the feedstocks based on their availability, their composition and molecular structure are discussed. The salient properties such as density, porosity, specific surface area, thermal conductivity and heat capacity are discussed in reference to gasification process. The chemical characterization of solid fuels using thermogravimetric analysis, proximate analysis, ultimate analysis, heating value determination, ash composition analysis and ash fusion temperature is examined. Besides presenting the different properties for salient feedstocks from the literature and their implications on pyrolysis and gasification process, this chapter also provides a list of standard methods for the determination of the aforesaid properties.

2 Classification of Feedstocks

Solid fuels used as feedstocks for pyrolysis and gasification can be broadly classified into two major groups, viz. non-renewable and renewable feedstocks. Figure 4 depicts the salient categories. Coal is the major non-renewable feedstock. Based on the carbon content and heating value, coal is further classified into anthracite (highest rank), bituminous/sub-bituminous (medium rank), peat/lignite (low rank). Pyrolysis coal chars represent a form of densified coals and are also included in this category. The renewable feedstocks include lignocellulosic biomass, municipal solid wastes (MSW) and refuse-derived fuel (RDF). Lignocellulosic biomass can be further divided into woody and non-woody or agro-residue

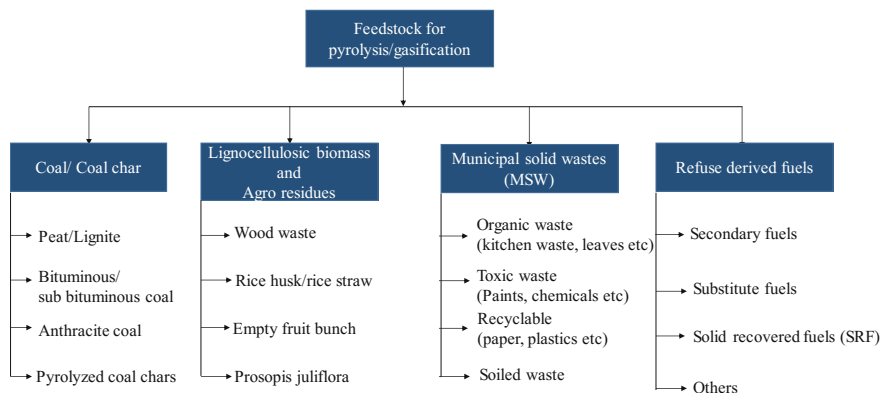


Fig. 4 Schematic of feedstock classification

biomass. Examples of woody biomass include sawdust, wood bark, wood chips and construction debris composed primarily of wooden materials. There are a number of agro-residues known today, and the important ones in the Indian context include rice straw (or paddy straw), wheat straw, sugarcane residues like bagasse, tops and leaves, *Prosopis juliflora*, rice husk, maize, cotton, empty palm fruit bunch and oilseeds. In fact, India ranks third in the world in the agro-residue generation after China and Brazil with annual generation 620 million metric tons [8]. MSW represents a complex mixture of a number of waste components including biomass wastes, plastics, garden wastes, paper, metals, inerts, cloths, jute, organic and food wastes. MSW also contains significant moisture. RDF is a valorized form of MSW, which can include dried and pelletized MSW or moderately segregated plastic wastes. Usually, the heating value of RDF is more than that of MSW. To gain a reasonable understanding of pyrolysis and gasification processes, and deduce the reactor behaviour, a thorough characterization of feedstocks is imperative.

3 Constituents of Different Feedstocks

3.1 Coal

Coal is formed from ancient plant material accumulated in subsurface environments, which prevents the complete decay of the organic matter. The formation occurs by the reduction of plant debris to simple forms such as pure carbon and simple compounds of carbon and hydrogen (hydrocarbons). In the initial stages of decay of dead plants, a soft, woody material known as peat is formed. Peat is not considered as a good fuel, because it burns poorly and releases a lot of smoke. If peat is allowed to remain in the ground for longer periods of time, it eventually becomes compacted as layers of sediments due to overburden or lithostatic

pressure. The additional pressure and heat of the overburden gradually converts peat into another form of coal known as lignite or brown coal. Continued compaction by overburden then converts lignite into bituminous (or soft) coal and finally into anthracite (or hard) coal.

Coal is classified according to its heating value and relative content of elemental carbon. Anthracite contains highest amount of pure carbon (about 86–98%) and has the highest higher heating value (31.4–36.3 MJ/kg) among all forms of coal. Bituminous coals contain lower amount of carbon (from 46 to 86%) and relatively lower higher heating values (19.3–36.3 MJ/kg) [9]. Bituminous coals are often subdivided on the basis of their heating value as low-, medium-, and high-volatile bituminous and sub-bituminous coals. Lignite is the poorest of the true coals in terms of higher heating value (12.9–19.3 MJ/kg), and contains about 46–60% carbon [9]. As shown in Fig. 5, in matured coals such as anthracite and bituminous types, aromatic rings occupy 80–85% of the coal molecular structure, and the remaining is constituted by hydroxyl groups, and nitrogen and sulphur compounds. Pyrolysis of medium- to low-rank coals results in pyrolysates that contain significant amount of phenols and naphthalene derivatives owing to the cracking of these functional units.

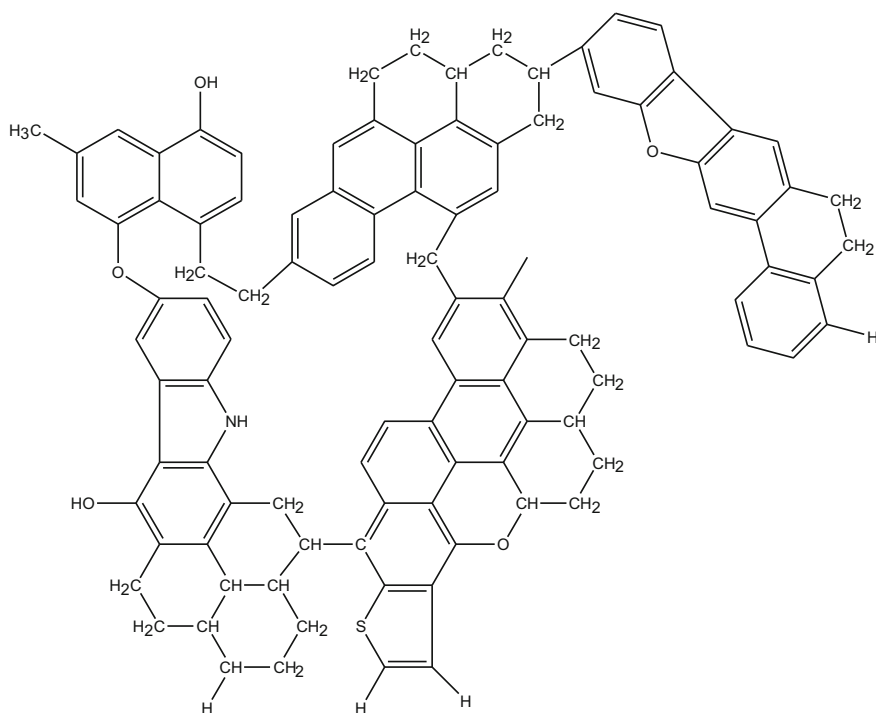


Fig. 5 Model structure of bituminous coal [10]

3.2 Lignocellulosic Biomass

Lignocellulosic biomass is composed of three different types of natural polymers, viz. cellulose, hemicellulose and lignin. Biomass is typically composed of 65–85 wt % of sugar polymers (principally cellulose and hemicellulose) with another 10–25 wt% of lignin [11]. The molecular structures of cellulose, hemicellulose and lignin are provided in Figs. 6 and 7. Cellulose is a linear polymer made of repeating glucose units which are linked together by β -1, 4-glycosidic bonds. It is a major constituent as it accounts for 40–50 wt% of dry wood. It contains intramolecular, intermolecular, interchain and intersheet hydrogen bonds, which imparts crystallinity and strength to the plant fibres. The typical number of glucose units in cellulose ranges from 5000 to 10000 [11]. Hemicellulose is an amorphous, branched polymer made up of hexose (e.g. glucose, galactose, mannose) and pentose sugars (usually xylose and arabinose) all of which are highly substituted with acetic acid. Unlike cellulose, the number of monomeric repeat units in hemicelluloses is only c.a. 150. Lignin, which constitutes the third main component of biomass, is an amorphous, three-dimensional polyphenolic material with no exact structure [11]. Lignin fills the space in the cell wall between the cellulose fibres and hemicelluloses

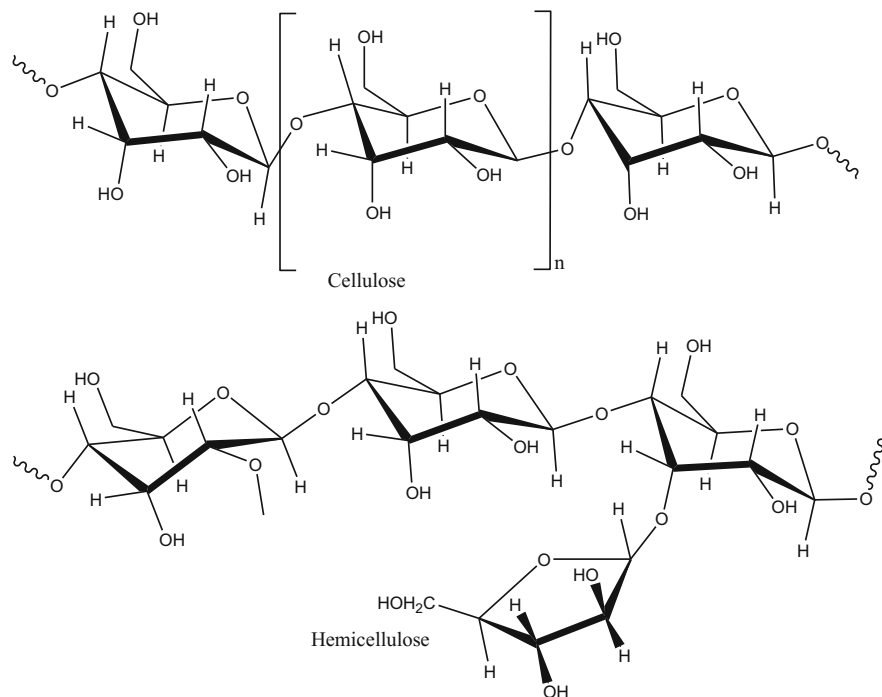


Fig. 6 Structure of cellulose and hemicellulose [12]

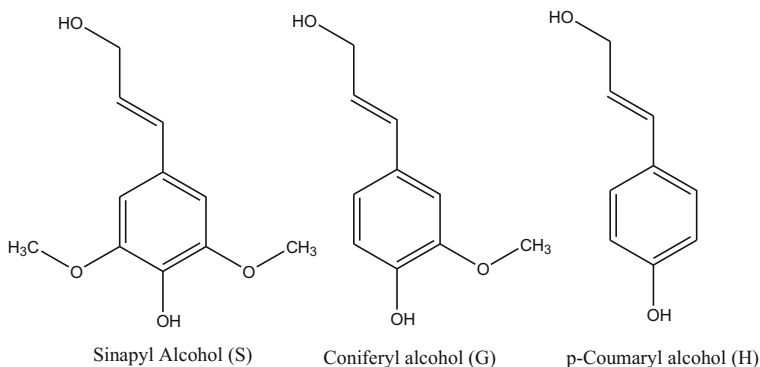


Fig. 7 Structure of monolignols, the primary building blocks of lignin [13]

bundles. It is covalently linked to hemicellulose and cellulose via lignin-carbohydrate complexes, and it acts a binder of fibrous carbohydrate structures.

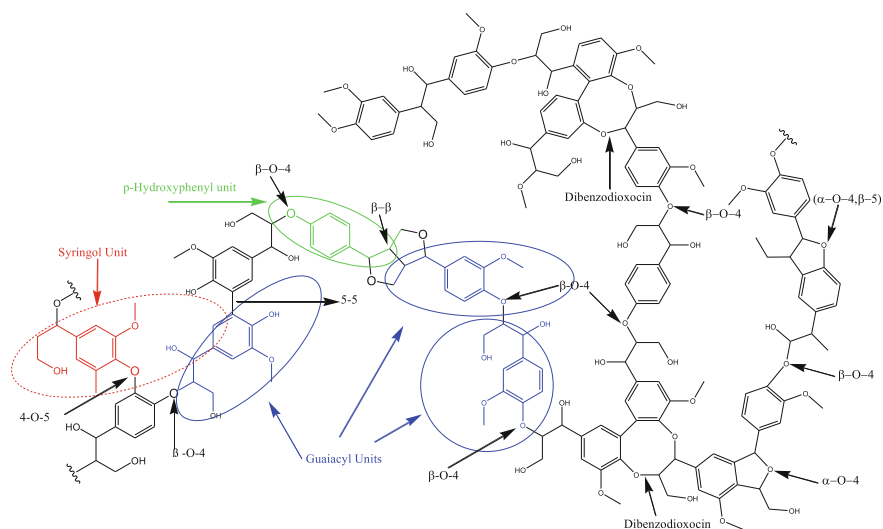
The structure of lignin is complex and is yet to be fully understood. In raw lignocellulosic biomass, lignin is primarily a complex, cross-linked and branched macromolecule that adds strength and rigidity to cell walls. It is widely accepted that lignin composition and its content in biomass vary with the type of plant species. For example, lignin accounts for 30% by weight in softwood, while this share falls to 20–25% in hardwood. Herbaceous biomasses such as grasses contain only 10–15% of lignin. As shown in Fig. 7, lignin is made of three major phenolic sub-units, viz. sinapyl (3, 5-dimethoxy, 4-hydroxycinnamyl), coniferyl (3-methoxy 4-hydroxycinnamyl) and p-coumaryl (4-hydroxycinnamyl) alcohols, joined by ether and C-C linkages [13]. The three monolignol compounds are also known as syringyl (S), guaiacyl (G) and p-hydroxyphenyl (H) sub-units. Table 1 depicts the distribution of primary lignin units in different types of biomasses.

Generally, softwood lignin contains more guaiacyl units, hardwood lignin contains more guaiacyl and syringyl units, and grass lignin presents a mixture of all three aromatic units. Figure 8 depicts a model structure of lignin with specific linkages such as α -O-4, β -O-4, β - β , 4-O-5, β -5, 5-5 and dibenzodioxocin [7]. During thermal treatment, these bonds are essentially cleaved to produce smaller molecules. More literature on the experiments and kinetics of lignin pyrolysis can be found in Ranzi et al. [14] and Zhou et al. [13].

In addition to cellulose, hemicellulose and lignin, biomass contains minor amount of extractives and ash. Extractives are those components like fats, waxes, alkaloids, proteins, pectins, gum, resins, starches and oils that can be extracted from biomass using polar and non-polar solvents [11]. Ash represents inorganic metals and salts. The biochemical composition of a number of Indian biomass varieties is shown in Table 2.

Table 1 Abundance of the primary lignin units in different types of plants [7]

Monolignol	Grass (%)	Coniferous wood (%)	Broadleaf wood
Sinapyl alcohol (S)	25–50	0–1	50–75%
Coniferyl alcohol (G)	25–50	90–95	25–50%
p-coumaryl alcohol (H)	10–25	0.5–3.4	Trace

**Fig. 8** Representative model structure of lignin. Redrawn from [7, 13]**Table 2** Biochemical composition (%) of different biomasses [15]

Components	Bagasse	Casuarina leaves	Coir pith	Groundnut shell	Rice husk	Sawdust	Wheat husk
Cellulose	40.8	40.2	26.8	33.7	34.8	34.5	37.8
Hemicellulose	21.8	16.8	17.2	17.3	26.7	19.7	30.8
Lignin	19.2	22.2	30.5	29.7	20.3	29.7	22.5
Extractives	13.4	17.34	22.0	15.0	4.2	7.8	7.5
Ash	4.8	2.86	3.7	3	17	9	1.6

4 Physical Properties

Theoretically, almost all feedstocks with moisture content in the 5–30% range can be gasified. However, it is known that feedstock properties, such as (a) specific surface area, (b) size, (c) shape, (d) moisture content, (e) volatile matter and (f) carbon content, affect gasification process and gasifier performance. Therefore, understanding the physical properties would give an idea about the right

pretreatment technique to be adopted for a particular feedstock [16]. The properties such as size, shape, specific surface area and the moisture content of the feedstock govern the type and scope of pregasification operations like storage, conveyance, crushing, drying and feeding systems. The content of volatile matter, carbon and the calorific value are crucial for the selection of gasification process and its conditions. As discussed earlier, gasification involves pyrolysis and char oxidation as the major sub-processes. Besides the feedstock characteristics, the nature and behaviour of char are crucial for the overall efficiency of gasification. This is partly signified by the amount of fixed carbon in the feedstock. Effect of feedstock particle size on the gasification is clearly described and reported in the literature. Generally, with increase in particle diameter, the syngas evolution also increases, as the larger particles contain high-volatile matter for the same mass as compared to the smaller particles. However, heating rate is significantly low for bigger particles compared to smaller ones [17]. Moreover, drying to lower the moisture content may be problematic and has not been optimized for biomass conversion processes. The emissions during drying involve the release of low molecular weight C1–C3 oxygenates and particulate emissions besides water. It is reported that at low drying temperatures (under 100 °C), the emissions consist mainly of monoterpenes and sesquiterpenes [18]. As far as pyrolysis is concerned, high moisture content in the feedstock affects the oil quality, especially the heating value, density, viscosity and storage stability of the oil. Predrying the feedstock is a common practice when the final product of interest is pyrolysis oil, which is either used directly for secondary heating applications or further catalytically upgraded to chemicals and fuels.

4.1 Density and Specific Gravity

Feedstock density plays an important role in commercial processes. Increasing the bulk density of the feedstock by pelletization is a common practice to facilitate the transportation of large quantities of the material. This is very much applicable to low-dense materials like biomass and MSW feedstocks. Simple mechanical pressing is a common technique to remove moisture from mixed feedstocks like MSW. The process of slow pyrolysis at low temperatures (200–300 °C), also called as torrefaction, is employed to remove the physicochemically bound moisture and small molecule oxygenates to densify the feedstock [19]. Such processes improve both the physical density and energy density. Coals are usually denser compared to biomass and mixed wastes.

There are different types of density measurements for porous solids such as coal. They are (a) true density, (b) apparent density, (c) particle density, (d) bulk density and (e) in-place density [16]. The true density of coal is defined as the mass divided by the volume occupied by actual, pore-free solid in coal. While determining the mass of coal is straightforward, determining the volume presents some challenges. The precise determination of true density requires complete filling of the structure with a fluid that has no interaction with the solid. No fluid meets these requirements

completely. Helium has traditionally been considered as the fluid of choice as it is not significantly adsorbed by coal at room temperature. The use of helium gives a more accurate determination of coal density, but there is evidence that part of the pore system may be inaccessible to helium as well [20]. Therefore, when helium is used as the agent for determining coal density, the density, sometimes called as helium density, may differ from the true density and may actually be lower than the latter.

The density of coal varies widely depending on the coal type. The relative density of anthracite coal is of the order of 1.3–1.55, whereas that of bituminous coal and lignite is 1.45 and 1.25, respectively [21, 22]. Table 3 depicts the typical bulk densities of different coals and biomasses. The standard method for the determination of true density (i.e. true specific gravity) of coal/coke is ASTM D-167. Empirical correlation from elemental analysis is also available to determine the true density and is given by Speight [16],

$$\rho_{\text{He}} = 1.534 - 0.05196[\%H] + 0.0007375[\%O] - 0.02472[\%N] + 0.0003853[\%S] \quad (10)$$

where ρ_{He} is the helium density (g/cm^3) and H, O, N and S are the respective weight per cent of the various elements on dry ash-free basis.

Coal density is a useful parameter for deducing the spatial structure of coal molecules. The relationship between density and porosity suggests that emphasis must be given to density and its determination. Porosity measurement, in turn, provides useful information on the technical behaviour of coal towards its end use. Particle density is required for calculating the porosity of individual coal particles.

Table 3 Bulk density and thermal conductivity data for biomass materials [23, 24]

Sample	Bulk density (kg/m^3)	Thermal conductivity (W/(m-K))	Heat capacity (J/(g-K))
Brown (High volatile) coal	910	0.088	1.347
Bituminous (Hard coal)	1160	0.157	1.270
Anthracite	1530	0.228	0.907
Pine	406	0.086	–
White wood	506	0.102	–
Cherry	534	0.108	–
White oak	615	0.113	–
Sewage sludge	760	0.130	–
Softwood	360	0.009	–
Pinewood	450	0.110	–
Maple	710	0.158	–
Fir	540	0.140	–

The apparent density of coal is determined by immersing a weighed sample of coal in a liquid followed by accurate measurement of the liquid that is displaced using a pycnometer [21]. For this procedure, the liquid should (a) wet the surface of the coal, (b) not absorb strongly onto the coal surface, (c) not cause swelling of coal and (d) penetrate the pores of the coal. The particle density is the weight of a unit volume of solid, including the pores and cracks. The bulk density is the mass of an assembly of coal particles in a container divided by the volume of the container [25]. The in-place density (or bank density) of coal is the means by which coal in the seam can be expressed as tons per acre per foot of the seam thickness and/or tons per square mile per foot of the seam thickness. The in-place density must be determined on water-saturated samples to accommodate the equilibrium moisture that exists under the in-place (seam) conditions.

4.2 Porosity and Specific Surface Area

The pore structures of coals and chars have been shown to have important effects on the combustion and oxidation of carbon particles [21, 26, 27]. Oxidation rates are higher for high surface area chars. However, the small pores in coal may restrict the transport of reactants and products to and from the internal surfaces. Porosity is the fraction (or percentage) of the volume of coal that is occupied by pores and can be calculated from the equilibrium moisture content [20]. Since coal is a porous material, porosity can have a large influence on coal behaviour during mining, preparation and utilization operations. Porosity dictates the rate at which methane can diffuse out of the coal in the seam. The preparation and pretreatment operations can also influence the porosity of coal via removal of mineral matter during washing and removal of light volatiles during the drying step. The calculation of porosity is derived from the determination of the true specific gravity (ASTM D-167), and the relationship is as follows:

$$\text{Porosity} = 100 - 100 \left(\frac{\text{apparent specific gravity}}{\text{true specific gravity}} \right) \quad (11)$$

Another method of determining porosity involves measuring the density of coal by helium and mercury displacement. Thus, the porosity of coal is calculated from the relationship.

$$P = 100 \times \rho_{\text{Hg}} \left(\frac{1}{\rho_{\text{Hg}}} - \frac{1}{\rho_{\text{He}}} \right) \quad (12)$$

where P is the porosity, ρ_{Hg} is the mercury density, and ρ_{He} is the helium density.

By determining the apparent density of coal in fluids of different but known dimensions, it is possible to calculate the pore size (or pore volume). The open pore

volume (V), i.e. the pore volume accessible to a particular fluid, can be calculated from the relationship.

$$V = \frac{1}{\rho_{\text{Hg}}} - \frac{1}{\rho_a} \quad (13)$$

where ρ_a is the apparent density in the fluid under consideration. Pore volume can be calculated from the relationship

$$V_p = \frac{1}{\rho_{\text{Hg}}} - \frac{1}{\rho_{\text{He}}} \quad (14)$$

While the above methods are well established, nitrogen adsorption–desorption porosimetry is adopted nowadays to evaluate all the pore-related parameters including specific surface area and pore size or pore volume distribution. The BET (Brunauer–Emmett–Teller) theory applies to systems of multilayer adsorption and usually utilizes inert gases that do not react with material surfaces as adsorbates to quantify the specific surface area. Specific surface area is a scale-dependent property, with no single true value of specific surface area definable, and thus, quantities of specific surface area determined through BET theory may depend on the adsorbate molecule utilized and its adsorption cross section. Further details are available elsewhere [28]. There is no direct relationship between specific surface area and the rank of coal. However, high-rank coals exhibit comparatively low specific surface area when compared to low-rank coals. Coal and biomass chars exhibit high specific surface areas owing to the devolatilization during the pyrolysis process. The specific surface area data for representative coal, biomass and their chars are available in Table 4.

Table 4 Specific surface area of different coals and biomass materials [29, 30, 31]

Feedstock	BET surface area (m^2/g)
High-volatile bituminous coal	2
Low-volatile bituminous coal	4
Anthracite coal	2
Switchgrass	1.3
Sorghum	1.0
Red cedar	2.1
Rice husk char	90.5
Corn straw char	89.6
Sawdust char	52.3
Bituminous coal char	7.1

5 Thermodynamic Properties

5.1 Heat Capacity

The heat capacity of a material is the heat required to raise the temperature of unit weight of a substance by 1 degree. The ratio of the heat capacity of one substance to the heat capacity of water at 15 °C is the specific heat. The heat capacity of coal can be measured by standard calorimetric methods that have been developed for other materials (ASTM C-351). The specific heat of coal usually increases with its moisture content, decreases with carbon content and increases with volatile matter, whereas mineral matter has little influence on the specific heat. Estimates of the specific heat of coal have also been made according to the Kopp's law which assumes that the molecular heat of a solid material is equal to the sum of the atomic heats of the constituents. The atomic heat so derived is divided by the atomic weight to give the (approximate) specific heat. From the data for various coals, an empirical relationship between the specific heat (C_p) and the elemental composition has been developed [16].

$$C_p \text{ (J/g/K)} = 0.189[\%C] + 0.874[\%H] + 0.491[\%N] + 0.360[\%O] + 0.215[\%S] \quad (15)$$

5.2 Thermal Conductivity

Thermal conductivity plays a very important role in gasification. As gasification is carried out at high temperatures, feedstock should possess minimum thermal conductivity, so that thermal lag in the gasifier can be eliminated. Thermal conductivity (k) is the rate of transfer of heat by conduction (Q) through a unit area (A) across a unit thickness (d) of the sample causing a unit difference in temperature ($T_2 - T_1$) and is given by Carslaw and Jaeger [32]:

$$Q = k \frac{A (T_2 - T_1)}{d} \quad (16)$$

From the literature, it is evident that monolithic coal is considered to be a medium conductor of heat. The thermal conductivities of anthracite and bituminous coals fall in the range of 0.209–0.376 W/(m K) and 0.127–0.292 W/(m-K), respectively [16]. Pulverized coals possess lower thermal conductivity than the monolithic counterparts. The thermal conductivity of coals generally increases with increase in the apparent density of the coal as well as with volatile matter content, ash content and temperature. There is little information about the influence of water on the thermal conductivity of coal. However, as the thermal conductivity of water is about three times higher than that of coal, the thermal conductivity of coal is

expected to increase in the presence of water. Table 3 depicts the thermal conductivities of representative coals and biomasses. There are other properties such as plastic and agglutinative properties, agglomeration index and free swelling index which are not directly relevant to pyrolysis and gasification. Therefore, they are not discussed here.

6 Characterization Techniques

6.1 Thermogravimetric Analysis

Thermogravimetric (TG) analysis is a standard method to determine the typical temperature regimes of decomposition of fossil fuels, biomass and solid wastes. It is a valuable technique to study the kinetics of pyrolysis and gasification using a small amount of sample (few tens of milligrams). The TG analysis provides a rapid, sensitive and reproducible measurement of residual mass of the sample when (a) the temperature is increased at a particular rate (dynamic) or (b) the sample is held at a particular temperature for desired time period (isothermal). To study pyrolysis of solid fuels, inert gas such as nitrogen or helium can be used, while for gasification studies, air or CO₂ can be used as the medium. The primary output of TG analysis includes a three-column matrix of time, temperature and sample mass retained. The first derivative of the mass remaining is called as derivative mass loss or differential thermogram (DTG).

Figure 9 depicts the typical mass loss and differential mass loss data for high ash coal and rice husk under pyrolysis conditions. Three distinct regimes of mass loss can generally be observed in the TG and DTG profiles. The initial mass loss in 100–120 °C range corresponds to the removal of physically bound water from the material. The wide region after the moisture removal corresponds to active pyrolysis. The specific temperature range of mass loss in active pyrolysis depends on the material pyrolyzed. For coals, the evolution of volatiles starts at 350 °C, whereas for biomasses devolatilization starts at 220 °C. From the DTG of rice husk in Fig. 9, it can be observed that specific components of biomass decompose in different temperature regimes. The hump at 300 °C corresponds to hemicellulose degradation, while cellulose decomposes in a well-defined temperature regime of 300–400 °C. Lignin decomposition starts at around 200 °C and end at 700–800 °C. Figure 10 depicts the DTG curves of a variety of biomasses and coals in CO₂ atmosphere. It is evident that pyrolysis takes place initially, and at high temperatures (900–1100 °C), gasification takes place via the Boudouard reaction [33].

Mathematical modelling to predict the product gas composition during pyrolysis and gasification requires the knowledge of reaction kinetics of devolatilization of the feedstock. Thermogravimetric analysis is very useful in determining the apparent kinetics of pyrolysis and gasification using empirical models available in the literature. The interested reader is referred to the articles by Oyedun et al. [34], Muller et al. [35] and Varhegyi et al. [36].

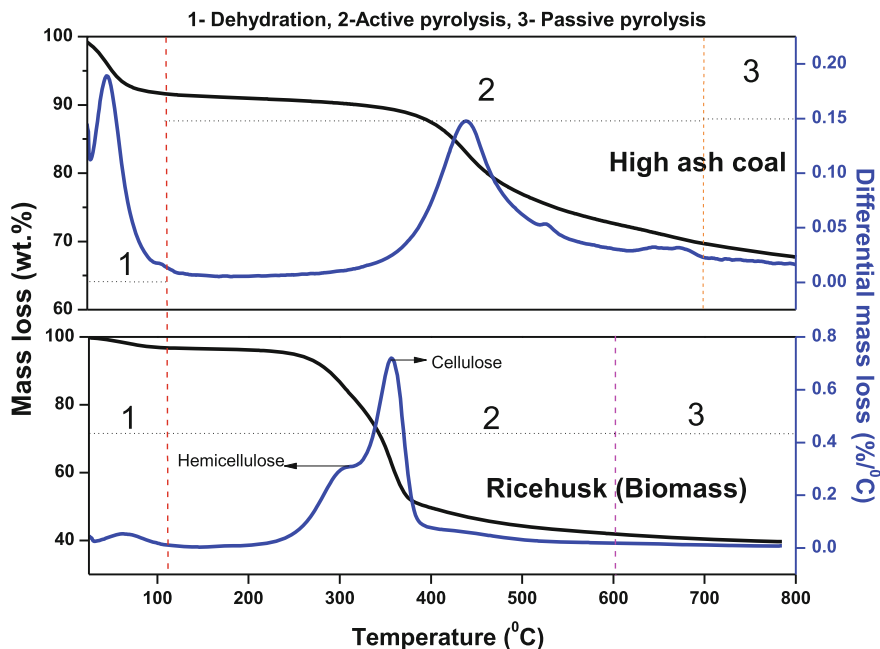


Fig. 9 Thermogravimetric mass loss and differential mass loss data for high ash coal and rice husk. Experiments were done in N_2 ambience (100 mL/min) at $10\text{ }^\circ\text{C min}^{-1}$

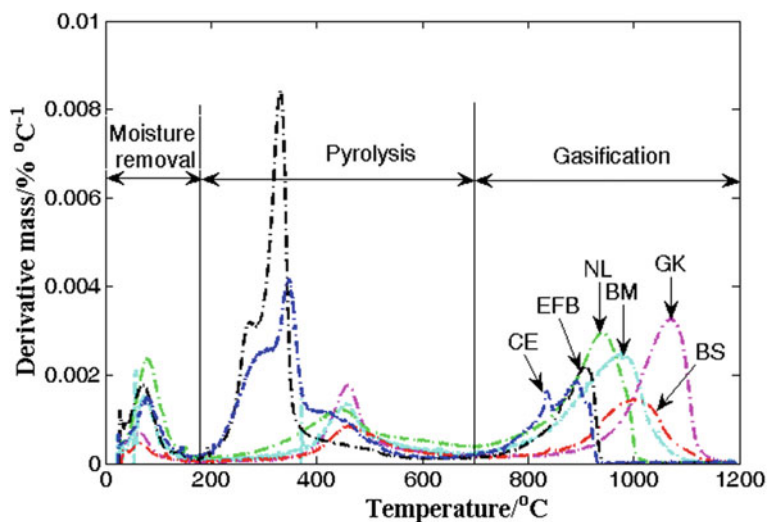


Fig. 10 Differential mass loss curves for different coals and biomasses in CO_2 atmosphere (20% in N_2) at $20\text{ }^\circ\text{C min}^{-1}$. GK-Godavarikhani, BM-Bellampalli, BS-Bilaspur, NL-Neyveli lignite, EFB-Empty fruit bunch, CE-*Causurina equisetifolia* Adapted from Naidu et al. [33] with permission from Springer

It is important to note that TG analysis provides only the overall mass loss data of the solid fuel, while it does not provide information about the volatiles released at various time periods. For this purpose, it is valuable to integrate a gas chromatograph/mass spectrometer (GC/MS) or Fourier transform infrared spectrometer (FTIR) with the TG analyser, so that the identity of the vapours/gases or functional groups can be understood. These hyphenated techniques are valuable to propose mechanisms of transformation of coal, biomass and mixed solid wastes. Figure 11 depicts the TG-FTIR profiles of different solid fuels including waste tyre rubber, biomass waste, MSW plastic and RDF [37]. It is evident that the species evolution pattern is different from these feedstocks. Increase in absorbance corresponding to a particular wave number is indicative of the increase in concentration of a functional group. This study showed that CO and OH groups evolve in significant concentrations from a majority of the feedstocks. The MSW plastic pyrolysis is characterized by the evolution of hydrocarbon C-H functional groups, which is expected. It is worthwhile to note that hyphenated techniques generate a huge data set that needs to be processed with care to decipher valuable product evolution and mechanistic information. Besides TG-FTIR, TG-MS can yield valuable information on the concentration profiles of calibrated organic species with temperature and time.

In recent times, analytical fast pyrolysis integrated with GC/MS has gained increasing interest in pyrolysis studies to understand the organic composition of primary pyrolysis vapours. This involves pyrolyzing a small sample mass (<1 mg) at fast heating rates (>1000 °C/s) and analysing the products using a GC/MS. Owing to kinetically limited conditions, the pyrolysis vapours are representative of primary products of cracking. Under gasification conditions, these pyrolysates are

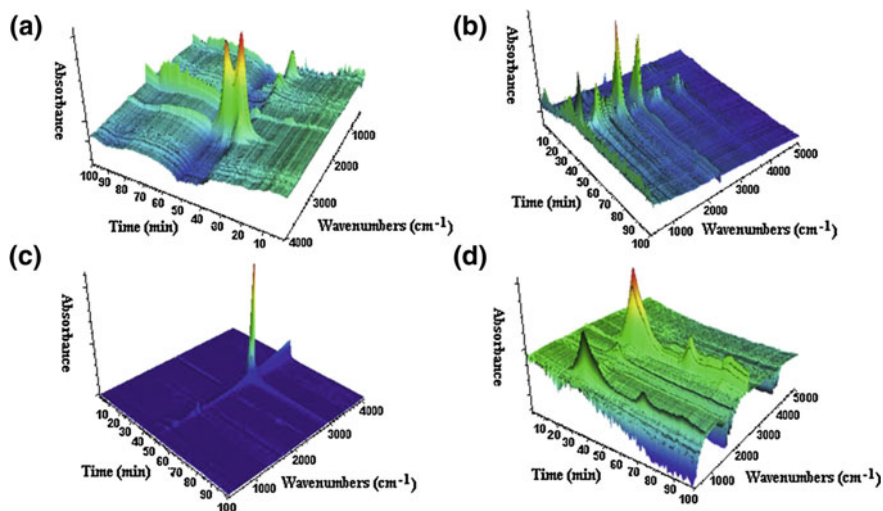


Fig. 11 TG-FTIR profiles of pyrolysis of **a** waste tyre rubber, **b** pinewood waste, **c** MSW plastic and **d** RDF. The temperatures corresponding to 30 min, 50 min, 70 min and 90 min are 325 °C, 525 °C, 725 °C and 900 °C, respectively. Adapted from [37], with permission from Elsevier

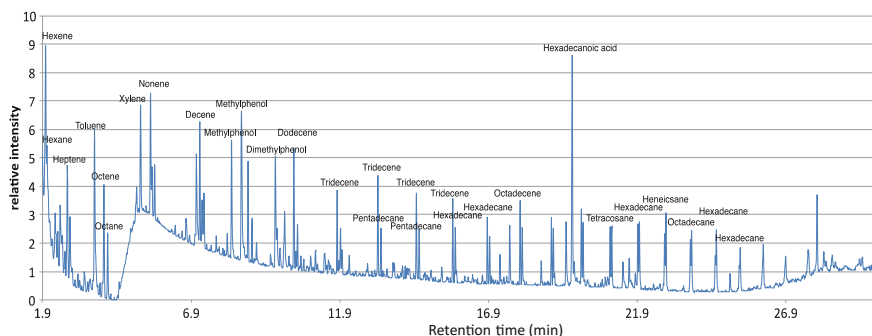


Fig. 12 GC/MS total ion chromatogram obtained from fast pyrolysis medium ash Indian coal at 700 °C using analytical pyrolyzer. The coal contains 31.2 wt% volatiles, 21.8 wt% ash, 47 wt% fixed carbon, 58 wt% C, 4.15 wt% H, 1.7 wt% N and 0.25 wt% S. For the experiments, 0.3 mg of powdered coal sample was taken in a stainless steel cup and dropped into the quartz furnace of a single-shot micropyrolyzer (Frontier Lab, Japan). The pyrolysates were analysed using a Shimadzu GC/MS (QP-2010 Plus). The flow rate of the vapours through the UA-5 alloy capillary column was 1.59 mL/min. The column oven was initially maintained at 40 °C for 1 min followed by a ramp at 10 °C/min to 300 °C, and held at 300 °C for 15 min. The electron ionization voltage was 70 eV, and the compounds were scanned in a mass range of 10–400 Da

oxidized in the gas phase. Thus, this information will be valuable in developing secondary gas phase pyrolysis and combustion mechanisms. Figure 12 depicts a typical GC chromatogram when medium ash Indian coal is fast pyrolyzed at 700 °C. It is evident that the products of Indian coal pyrolysis include a number of linear chain alkanes and alkenes in C6–C20 range along with some phenols and aromatic hydrocarbons. This data will also be useful for the design of efficient pyrolysis reactors for recovering oil from coal as well as biomass for liquid fuel applications. The interested reader is referred to the articles by Tsuge et al. [38] and Vinu et al. [39] for a better understanding of pyrolysis GC/MS.

6.2 Proximate Analysis

Proximate analysis involves the determination of moisture, volatile matter, fixed carbon and ash content in the feedstock. This is a standard characterization used to determine the rank of coals and to understand the potential of a particular feedstock for pyrolysis or gasification. Generally, high-volatile matter and low fixed carbon-containing feedstocks such as synthetic polymers and plastics are suitable for pyrolysis process, as they yield more amount of liquid products. The amount of volatile matter in the feedstock is the theoretical maximum amount of condensable organics that can be derived via pyrolysis process. However, high fixed carbon-containing materials like coals are suited for gasification and combustion. Biomass is amenable to both gasification and pyrolysis as their composition lies in

between polymers and coals. High moisture content in the feedstock is indicative of low heating value (or calorific value), while high-volatile matter/fixed carbon ratios are related to the reactivity of the fuel. Ash deeply influences the transport, handling and management costs. It is also influential in corrosion and slag formation. A number of standard methods are available to perform proximate analysis. ASTM specifies the analysis conditions for the determination of various properties. These include ASTM E-871 for moisture (UNE-EN 14774 for biomasses); ASTM E-830, D-1102 or UNE-EN 14775 for ash; ASTM E-872 and ASTM E-1755 for volatile matter [40, 41]. Fixed carbon is usually determined by difference. Generally, moisture is determined by heating the sample to 105 °C from room temperature at 10–15 °C/min and maintaining for a specified period of time. The decrease in mass of the sample is noted as moisture content. The sample temperature is then increased to 950 °C in inert atmosphere at a specific heating rate (typically 16 °C/min) and maintained at this temperature for 7–10 min. This leads to the release of organic volatiles by thermal decomposition of the feedstock. After the sample mass reaches a steady value at the final temperature, the mass difference is noted to determine the volatile matter. To determine the fixed carbon, the ambience is changed from inert to reactive air and the sample is maintained isothermally at 850 °C. The final sample left is noted as the amount of ash. Fixed carbon can be determined as the oxidized portion of the residue left after volatile generation, i.e. % fixed carbon = 100 – (%Ash + %Volatile matter).

Proximate analysis can be performed using a simple muffle furnace or in a TG analyser. TG analysers are preferred these days as the heating rate and sample temperature can be controlled well. Table 5 represents the proximate analysis results of different ranks of coals (entries 1–14), biomasses (entries 15–44) and MSW (entries 44–50). It can be seen that coals contain high amounts of ash, biomasses contain high-volatile matter and sewage sludge and MSW contain significant amount of moisture. It is important to note that composite fuels like MSW and RDF are heterogeneous, and hence, the results can vary if the sample taken for proximate analysis is not representative. Therefore, it is important to utilize more quantity of the sample while using these feedstocks. While the ASTM methods are originally developed for coals, specific European standard methods are also available for biomasses. The various standard methods are listed in Appendix A.

6.3 *Elemental Analysis*

Elemental or ultimate analysis involves the determination of C, H, N, S and O in the feedstock. The carbon in the feedstock includes carbon present as organic carbon and any carbon present as mineral carbonate. Hydrogen includes hydrogen present in the organic components as well as hydrogen in all of the water associated with the feedstock. Nitrogen is usually assumed to occur within the organic matrix of coal or biomass. Sulphur generally occurs in three forms in coal, viz. as organic

Table 5 Proximate, ultimate and higher heating value (or calorific value) analysis of different feedstocks

S. No.	Fuel	Proximate analysis (wt%, db)			Ultimate (elemental) analysis (wt%, daf)					HHV (MJ/kg)	Ref.
		VM	FC	Ash	C	H	N	S	O*		
1	Indian coal	35.2	43.1	21.7	72.3	5.1	2.2	0.2	20.2	17.9	A
2	Indonesian coal	47.7	43.5	8.82	69.1	5.1	0.2	3.1	22.5	30.0	A
3	Yilan sub-bituminous coal	36.7	40.2	23.1	66.8	5.5	1.4	0.4	25.9		B
4	Colombian coal ^a	32.3	42.3	25.4	76.6	5.4	1.6	1.9	14.5	23.6	C
5	Bituminous coal ^b	39.0	50.6	9.8	78.1	5.2	2.8	1.1	12.8	30.5	D
6	Taiwan coal	31.7	54.6	13.7	86.6	4.9	1.7	0.6	6.2	27.3	E
7	Australian coal	29.6	54.2	16.2	77.2	5.4	0.9	0.4	16.1	25.8	F
8	Indonesian coal ^a (Open blue)	50.8	46.4	2.8	70.2	5.6	3.3	0.3	20.7	15.4	F
9	Indonesian coal ^b (Wara)	49.5	46.5	4.1	72.5	5.2	1.1	0.2	21.0	17.2	F
10	South African coal	14.4	77.5	8.1	93.5	3.1	1.6	0.6	1.2	31.8	G
11	Sulcis coal	43.3	42.6	14.2	73.6	5.2	1.9	8.3	11.0	25.3	G
12	Godavarikhani coal	30.5	40.2	29.3	79.1	5.7	2.2	0.8	12.1	23.0	H
13	Bellampalli coal	33.0	42.9	24.1	74.3	6.4	1.6	0.5	17.3	19.7	H
14	Bilaspur coal	29.6	19.8	50.5	66.4	5.6	2.9	1.2	23.9	11.7	H
15	Oil palm shell	39.7	58.9	1.4	42.7	3.3	0.4	1.1	52.5		I
16	Bagasse	81.8	15.3	2.9	45.1	6.0	0.4		48.5	16.3	I
17	Coconut coir	82.1	17.0	0.9	48.0	5.8	0.2		46.0	14.7	I
18	Coconut shell	79.6	19.7	0.7	50.6	5.7	0		43.7	20.5	I
19	Groundnut shell	78.1	16.0	5.9	51.3	6.1	0.8		41.8	18.7	I
20	Millet husk	66.1	15.8	18.1	52.2	7.3	0.1		40.3	17.5	I
21	Rice husk	62.4	14.1	23.5	50.8	6.7	0.8		41.8	15.3	I
22	Rice straw	64.3	15.9	19.8	46.0	6.2	0.5		47.3	16.8	I
23	Wheat straw	74.5	14.3	11.2	53.5	6.1	0.1		40.3	18.0	I
24	Corn stakes	74.7	18.5	6.8	45.0	5.7	0		49.4	16.5	I
25	Corn cob	83.0	14.2	2.8	49.0	5.1	0		45.9	18.1	I
26	Subabul wood	84.8	14.3	0.9	48.6	5.9	0		45.5	19.8	I
27	Wood pine chips	80.0	19.4	0.6	52.1	6.1	0.3		41.5	21.0	J
28	Willow SRC	83.4	15.0	1.59	51.0	6.0	0.1		42.9	18.9	J
29	Miscanthus giganteus	82.1	16.4	1.5	49.4	6.4	0.3		43.9	19.9	J
30	Switchgrass	82.9	14.4	2.7	48.2	6.0	0.4		45.4	19.1	J
31	Straw-wheat straw	71.9	17.8	10.3	44.3	6.0	3.9		45.8	18.2	J
32	Lignin	74.6	22.0	3.4	53.1	5.9	1.1		39.8	22.2	J
33	Cellulose ^b	88.3	11.0	0.74	43.6	6.5	0.2		49.7	17.4	J
34	Red maple	83.0	14.7	0.03	47.3	6.3	2.3	0	44.1	19.3	D

(continued)

Table 5 (continued)

S. No.	Fuel	Proximate analysis (wt%, db)			Ultimate (elemental) analysis (wt%, daf)					HHV (MJ/kg)	Ref.
		VM	FC	Ash	C	H	N	S	O*		
35	Yellow poplar	81.7	15.9	0.53	48.1	6.4	2.2	0	43.3	18.6	D
36	Melon seed husk	77.3	2.0	20.7	47.5	6.1	0.8	0.1	45.5	19.1	K
37	Wood chips	79.7	19.4	0.9	58.1	6.2	0.1	0	35.5	20.0	K
38	Wood	80.8	19.2	0	51.5	5.3	0.2	0	43.0	20.3	G
39	Empty fruit bunch	76.4	16.6	7.0	76.8	8.4	1	5.4	8.4	15.5	H
40	Casuarina equisetifolia	75.4	19.1	5.6	54.9	6.7	2.2	0.6	35.7	17.8	H
41	Switchgrass	78.0	16.9	5.1	43.2	5.7	0.6	0.3	50.2	7.4	I
42	Sorghum	75.1	19.3	5.6	40.7	6.4	0.5	0.2	52.2	9.4	I
43	Red cedar	78.5	17.0	4.5	47.5	6.3	0.4	1.1	44.7	9.1	I
44	Corncob	82.5	15.9	1.6	46.8	6.0	0.3	0.2	46.7		I
45	Sewage sludge	53.9	7.6	38.5	54.8	7.5	8.4	2.9	26.4	14.1	L
46	Sewage sludge ^b	62.3	6.5	31.2	52.3	8	6.7	0.7	32.3	11.3	O
47	Refuse-derived fuel ^a	46.6	21.2	32.2	46.4	6.8	1.6	0.1	45.1	14.3	M
48	MSW-A	83.1	13.5	3.4	53.3	8.0	0.7	0.1	37.9	23.7	N
49	MSW-B	86.7	10.7	2.7	59.7	9.4	0.6	0.1	30.2	27.4	N
50	Treated MSW	71.0	6.3	22.7	58.5	8.2	1.2		32.2	17.8	I

Db—dry basis, daf—dry ash-free basis, VM—volatile matter, FC—fixed carbon, C—carbon, H—hydrogen, N—nitrogen, S—sulphur, O—oxygen

HHV—High heating value, * By difference

A—[42]; B—[43]; C—[44]; D—Singh et al. [45]; E—[46]; F—[47]; G—[48]; H—[49]; I—[50]; J—[51]; K—[52]; L—[53]; M—[54]; N—[55] (model municipal solid waste mixtures); O—[56]

^aMoisture content in this fuel is 45.2%

^bMoisture content in this fuel is 70%

sulphur compounds; as inorganic sulphides that are, for the most part, primarily iron sulphides, pyrite and marcasite (FeS_2); and as inorganic sulphates (e.g. Na_2SO_4 , CaSO_4) [16]. A number of studies report the oxygen content in the feedstock as a difference, i.e. $\%O = 100 - \%C - \%H - \%N - \%S - \%Ash$. However, oxygen can also be determined absolutely using elemental analysers. Lignocellulosic biomass usually contains negligible amount of sulphur and low amount of nitrogen (<2 wt %) in it. Importantly, the analytical values may be represented in as received basis, dry basis (db) or dry ash-free basis (daf). Trace elements that occur in coal are often included as a part of the ultimate analysis. In order to carry out proper calculations, elemental composition and the standard heat of formation of the fuels are essential. A typical elemental analysis system consists of a combustion tube in which the feedstock is heated to >1000 °C. The gases are then passed through a GC with thermal conductivity detector (TCD). The nitrogen, carbon, hydrogen and sulphur in the material are converted to N_2 , CO_2 , H_2O and SO_2 , respectively, as the material

Table 6 Elemental composition of different varieties of coals (Higman and Tam [3])

Coal rank	Carbon	Hydrogen	Oxygen
	% w/w dry ash free		
Peat	58	6	35
Lignite	71	5	23
Sub-bituminous	75	5	16
Bituminous	81	6	10
High volatile	88	4	4
Low volatile			
Anthracite	94	3	2

is combusted, and these are analysed using GC-TCD. Nitrogen is converted to NO_x , which is then reduced to N_2 using a copper-based catalyst.

The standard method for ultimate analysis of coal and coke (ASTM D-3176) and for biomass (UNE-EN 15104) includes the determination of elemental carbon, hydrogen, sulphur and nitrogen together with the ash in the material as a whole. The test methods recommended for elemental analysis include the determination of carbon and hydrogen (ASTM D-3178), nitrogen (ASTM D-3179) and sulphur (ASTM D-3177; ISO 334; ISO 351, UNE-EN 15289), with associated determination of moisture (ASTM D-3173, UNE-EN 14774) and ash (ASTM D-3174, UNE-EN 14775) to convert the data to daf basis. Table 6 depicts the carbon, hydrogen and oxygen on daf basis for different ranks of coals. It is evident that anthracite coal contains highest carbon content (94 wt%) and peat contains lowest carbon. Table 5 depicts the elemental composition of different feedstocks including coal, biomass, MSW and RDF. It can be seen from the table that biomasses contain high amount of oxygen (40–50 wt%), while coals contain high amount of carbon (70–90 wt%).

Elemental analysis is vital to close the mass balance in pyrolysis and gasification processes. Elemental analysis of solid residue (char) and condensates (pyrolysis oil or tar) together with a comprehensive non-condensable gas composition can aid in mass balance calculations. In pyrolysis studies that focus on pyrolysis oil, carbon selectivity is usually reported to evaluate the potential of the process for fine chemicals and biofuels production. Carbon content in ash and the feedstock can be used to calculate the carbon conversion (CC) in the gasifier using the following expression:

$$CC = \left(100 - \frac{m_{ash} \times \%C_{ash}}{m_{feed} \times \%C_{feed}} \right) \quad (17)$$

where m_{ash} , m_{feed} , $\%C_{ash}$ and $\%C_{feed}$ denote the mass of ash residue, mass of feedstock, carbon content in ash and carbon content in the feedstock, respectively. Moreover, in practice, the information about trace elements such as chlorine is also important, as it causes fouling and corrosion problems. Other elements that deserve importance include mercury, arsenic and selenium.

6.4 Calorific Value

Calorific value refers to the heat produced by combustion of a unit quantity of feedstock in a bomb calorimeter with oxygen under a specified set of conditions (ASTM D-121; ASTM D-2015; ASTM D-3286; ISO1928; UNE-EN 15149). For the analysis of solid carbonaceous fuel, the calorific value is determined in a bomb calorimeter either by a static (isothermal) method or by an adiabatic method, with a correction made if net calorific value is of interest. The calorific value is a direct indication of the heat content (or energy value) and represents the combined heats of combustion of the carbon, hydrogen, nitrogen and sulphur in the organic matter. The calorific value is usually expressed as gross calorific value (GCV) or the higher heating value (HHV), and net calorific value (NCV) or lower calorific value (LHV). The difference between HHV and LHV denotes the latent heat of condensation of the water vapour produced during the combustion process. The HHV assumes that all of the vapour produced during the combustion process is fully condensed, while the LHV assumes that the water is removed with the combustion products without being condensed. HHV of the feedstock is widely used in many calculations. The HHVs of coal, biomass and other feedstocks vary considerably, depending on the ash, moisture content and the amount of oxygen. Coals are also classified according to their HHVs (ASTM D-388). For quick reference, Table 5 presents the typical HHVs of different feedstocks.

A number of empirical models have been developed to evaluate the HHV from proximate and ultimate analysis of the feedstocks. The energy content of coal can be expressed as the useful heating value (UHV), which requires both ash and moisture content [16].

$$\text{UHV (kcal/kg)} = 8900 - 138 \times [\text{Ash (wt.\%)} + \text{Moisture (wt.\%)}] \quad (18)$$

To estimate HHV from elemental composition data, the Dulong's correlation is widely used, which is given by Channiwala and Parikh [57] and Vargas-Moreno et al. [58]:

$$\text{HHV (MJ/kg)} = 0.3383[\%C] + 1.443([\%H] - [\%O]/8) + 0.0942[\%S] \quad (19)$$

The Dulong's correlation is best suited for low-oxygen feedstocks. For high oxygen-containing coals, the deviations are as large as 5–7%. The Starche and Lant correlation is a modified version of Dulong's correlation with an accuracy of 2% for the whole range of coals. It is given by Channiwala and Parikh [57] and Vargas-Moreno et al. [58]:

$$\text{HHV (MJ/kg)} = 0.3406[\%C] + 1.4324[\%H] - 0.1532[\%O] + 0.1047[\%S] \quad (20)$$

While a number of correlations are available for biomasses, we present here a relation proposed by Vargas-Moreno et al. [58] that is applicable for a wide variety of plant types:

$$\text{HHV (MJ/kg)} = 0.3491[\%C] + 1.1783[\%H] - 0.1034[\%O] + 0.1005[\%S] - 0.0151[\%N] - 0.0211 [\%Ash] \quad (21)$$

The interested reader is referred to the review article by Vargas-Moreno et al. [58] for a compendium of empirical correlations for HHV of a variety of feedstocks including, coal, biomass including woods, agro-residues, plastics, MSW, RDF, petroleum crude oils, biomass-derived oils and sewage sludge.

6.5 *Equilibrium Moisture*

One of the important factors which affects pyrolysis and gasification is the moisture content of the feedstock. High moisture content may pose adverse effect on the pyrolysis oil and syngas quality. Moreover, high moisture content reduces the operating temperature, which in turn hinders the efficiency, stability and quality of output syngas. Therefore, reducing the moisture content of the feedstock to a certain level prior to gasification process is essential. However, it is challenging and requires special conditions such as lower humidity and higher temperature environment. In a large-scale plant, installing a drying unit to reduce the moisture content in the feedstock prior to gasification or pyrolysis is often a commercial decision rather than technical one. Most of the feedstocks are hygroscopic in nature and are usually affected by the humidity and temperature of the surroundings during their storage [59, 60]. While reducing the moisture content of the feedstock is important, maintaining the moisture content within stipulated levels for a specific period of time is also essential. The design and selection of proper storage system to maintain the moisture content requires the knowledge of equilibrium moisture content (EMC). Partial information can be obtained from the psychrometric chart. However, EMC depends on specific gravity, porous nature and other properties of the feedstock. While limited literature is available on this, EMC varies significantly depending on location and atmospheric conditions. Therefore, a continuous monitoring is required to determine EMC of the feedstock.

6.6 *Ash Analysis*

The mineral matter content of the feedstock greatly impacts their utilization in combustion and gasification systems. The inorganic components present in coal and biomass can lead to the formation of deposits on heat transfer surfaces, thereby reducing the thermal efficiency, and cause corrosion and erosion of structural materials. Moreover, some mineral species such as MgO, NaO, SiO₂ are known to act as catalysts in pyrolysis of, especially, biomasses and lead to variation in the composition of the volatile fraction [49]. The catalytic effect is broadly seen in biomass feedstocks than with coals. Different techniques are available to analyse

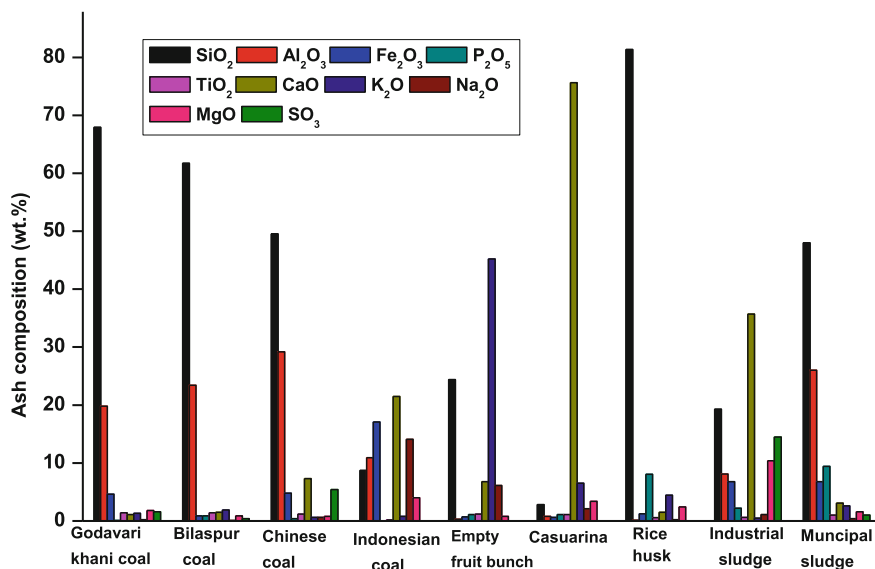


Fig. 13 Ash composition (wt% in ash) of different feedstocks [63, 49]

the mineral matter. These include (a) chemical fractionation, which is used to determine the organically bound inorganics of low-rank coals, (b) X-ray fluorescence analysis and (c) X-ray diffraction (XRD). Figure 13 depicts the ash composition of different coals, biomasses and municipal solid waste. Inorganic materials such as Si, Al, Ti, Ca, Mg, Na, K, Fe, P are determined in the form of their oxides. For biomasses, the concentration of these elements can be determined according to UNE-EN 15290 method, whereas Mn, Zn, Cu, Ni and Cr present in ppm levels can be determined according to UNE-EN 15297 method. From Fig. 13, it can be seen that SiO₂ content is high in coals followed by Al₂O₃, while CaO and K₂O are high in some biomasses like casuarina and empty fruit bunch. SiO₂ content is high in rice husk and also high in rice straw. The review articles by Vassilev et al. [61] and Baxter et al. [62] provide the typical proximate, elemental and ash composition of a variety of biomasses. A general trend is observed in the ash composition of different types of biomass feedstocks. Woody biomasses are rich in CaO, MgO and Mn, while herbaceous biomass and agro-residues are rich in K₂O, SiO₂, Cl, MgO and P₂O₅. Other types of contaminated biomass may contain Cl and S in addition to some of the aforesaid constituents.

6.7 Ash Fusion Temperature

The ash fusion temperature (AFT) characterizes the melting of solid ash and its transformation to liquid state. This temperature is an important parameter for the

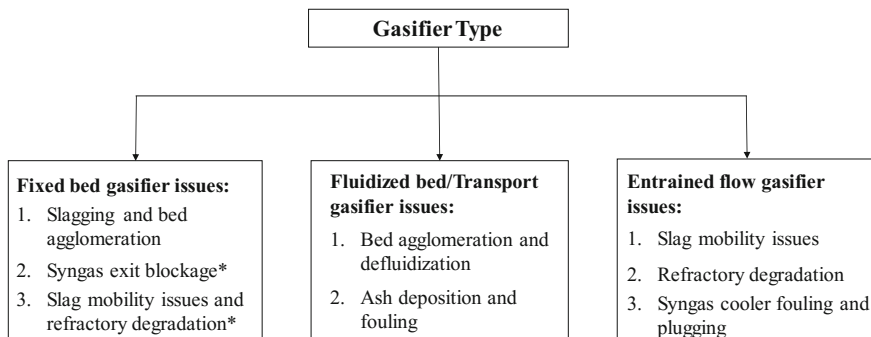


Fig. 14 Operation-related issues due to mineral matter in various types of gasifiers (*specific to slagging of fixed bed gasifiers) [64]

design and operation of gasification systems. For ash fusion temperature analysis, ash sample is moulded in the form of a cone and combusted in a furnace. The transformation of ash is monitored continuously using a high-resolution camera, and four key transition temperatures corresponding to change in configuration of the cone are noted. According to ASTM D1857, these include initial deformation temperature, softening point temperature, hemisphere temperature and floating temperature. Importantly, ash composition determines the various transition temperatures. For fluid bed processes, it determines the upper limit of the operating temperature, since above this temperature, agglomeration of the particles occurs. For entrained flow process, the gasification temperature must be above the floating temperature to allow the molten ash to be drawn off as molten slag. Importantly, entrained flow processes operate significantly above the floating temperature, owing to slag viscosity requirements.

The salient operation-related issues due to ash in typical gasifiers are listed in Fig. 14. Another important ash characteristic is the relationship between the fusion temperature and ash viscosity. This requires the determination of ash viscosity at high temperatures, which is a challenge. There has been much effort devoted to determining a method to predict the AFT from the chemical composition of the ash, but the validity of the results obtained has generally been limited to coals of similar origin that were used to test the proposed model, at least with any degree of accuracy. Coals with high SiO_2 content possess AFT around $1450\text{ }^\circ\text{C}$ [63], while for biomasses containing high CaO and K_2O , the AFT is around $1350\text{--}1400\text{ }^\circ\text{C}$. Recent works using thermodynamic models such as FactSageTM have eased the understanding of multicomponent and multiphase equilibria existing in molten ash and their fusion temperatures. Song et al. [65] systematically varied the amounts of SiO_2 , Al_2O_3 , CaO , Fe_2O_3 and MgO added to four different Chinese coal ashes under an inert (Ar) atmosphere, and studied the phase composition, phase behaviour and liquidus temperatures using FactSageTM software. They observed that the ash AFTs decreased initially with increasing CaO , Fe_2O_3 and MgO addition, while they again increased with further increase in content of these oxides. Interestingly, AFTs

increased with increase in $\text{SiO}_2/\text{Al}_2\text{O}_3$ ratio, which was also verified by thermodynamic simulations. It is imperative to note that such variations are often specific to a particular type of coal ash and cannot be extrapolated to different varieties of coal/biomass ash.

7 Conclusion and Future Prospects

In this chapter, a number of fundamental characteristics of solid fuels like coal, lignocellulosic biomass and mixed wastes like MSW and RDF are discussed for their use in pyrolysis and gasification processes. These are complicated feedstocks in terms of their molecular structure. An understanding of the physicochemical and thermal properties of the feedstock like bulk density, size, porosity, specific surface area, thermal conductivity, specific heat, heating value, pyrolysate composition and elemental composition will aid in optimizing the reactor/reaction conditions to achieve better yield of syngas via gasification and oil via pyrolysis process. The experimental techniques to determine the salient properties are also described in this monograph. A number of ASTM standard methods available today to determine the above properties are based on coal as the feedstock, although a few European standards are now available to characterize renewable feedstocks like biomass (refer Appendix A), which are very different compared to coal. The major issue in characterizing mixed solid wastes like MSW or RDF lies in the heterogeneity of the feedstock, which warrants a reasonable mass of sample being taken for characterization techniques. In this regard, studies that utilize milligrams of samples in TG analysers or analytical elemental analysers should report the standard deviation in data corresponding to multiple sample analyses. Moreover, reporting the data on a dry basis or dry ash-free basis will essentially mask the moisture and ash content in these mixed feedstocks, as these two parameters directly or indirectly influence the effectiveness of gasification and pyrolysis. Therefore, reporting the data on as received basis assumes importance.

For biomass feedstocks, an understanding of biochemical composition is also valuable to develop kinetic and reactor models for pyrolysis and gasification reactions. Ranzi and co-workers[14, 66, 67] have developed robust methods to describe the structure of complex solid fuels in terms of reference species, which is then utilized to describe the mechanism of devolatilization and gasification of these feedstocks. The semi-empirical kinetic models involving homogeneous gas phase reactions and heterogeneous reactions of solid char can be used to describe the process in terms of both particle and reactor scales. One of the major issues in process industries that utilize coals, biomasses and RDF for energy generation via gasification lies in ash handling during and after the process. As discussed in Sect. 6.7, ash composition determines the phase behaviour of ash, which in turn affects the ash fusion temperature. Ash composition and process conditions also determine the type of problem that one might encounter, i.e. clinkering, slagging and fouling. In this direction, focused research on ash behaviour from a wide variety

of coal and biomass materials is required, especially in terms of development of empirical, yet predictive models to reasonably describe the phenomena. One of the experimental difficulties lies in the determination of viscosity of molten ash or slag at high (gasification) temperatures. Development of a comprehensive database of ash composition versus their behaviour at different conditions will be a useful contribution in this direction.

Acknowledgements The authors thank National Center for Combustion Research and Development (NCCRD) at IIT Madras for funding. NCCRD is funded by Department of Science and Technology (DST), India.

Appendix A: List of Standard Methods for the Determination of Various Properties of Coal and Biomass

ASTM D-121. Standard Terminology of Coal and Coke.

ASTM D-167. Standard Test Method for Apparent and True Specific Gravity and Porosity of Lump Coke.

ASTM C-351. Standard Test Method for Mean Specific Heat of Thermal Insulation.

ASTM D-388. Standard Classification of Coals by Rank.

ASTM E-830. Standard Test Method for Ash in the Analysis Sample of Refuse-Derived Fuel.

ASTM E-871. Standard Test Method for Moisture Analysis of Particulate Wood Fuels.

ASTM E 872. Standard Test Method for Volatile Matter in the Analysis of Particulate Wood Fuels.

ASTM D-1102. Standard Test Method for Determination of Ash in Woody Biomass.

ASTM E-1755. Standard Test Method for Ash in Biomass.

ASTM D-1857. Standard Test Method for Fusibility of Coal and Coke Ash.

ASTM D-2015. Standard Test Method for Gross Calorific Value of Coal and Coke by the Adiabatic Bomb Calorimeter.

ASTM D-3173. Standard Test Method for Moisture in the Analysis Sample of Coal and Coke.

ASTM D-3174. Standard Test Method for Ash in the Analysis Sample of Coal and Coke from Coal.

ASTM D-3176. Standard Practice for Ultimate Analysis of Coal.

ASTM D-3177. Standard Test Methods for Total Sulfur in the Analysis Sample of Coal and Coke.

ASTM D-3178. Standard Test Methods for Carbon and Hydrogen in the Analysis Sample of Coal and Coke.

ASTM D-3179. Standard Test Methods for Nitrogen in the Analysis Sample of Coal and Coke.

ASTM D-3286. Standard Test Methods for Gross Calorific Value of Coal and Coke by the Isoperibol Bomb Calorimeter.

ISO 334. Determination of Total Sulfur: Eschka Method.

ISO 351. Determination of Total Sulfur: High Temperature Combustion Method.

ISO 1928. Determination of Gross Calorific Value and Calculation of Net Calorific Value.

UNE-EN 14774. Standard Test Method for Determination of Moisture content in Biomass.

UNE-EN 14775. Standard Test Method for Determination of Ash Content in the Biomass.

UNE-EN 14918. Standard Test Method for Determination of Higher Heating Value in Biomass.

UNE-EN 15290. Standard Test Method for Determination of Si, Al, Ti, Ca, Mg, K, Na, Fe and P Content of Biomass Ash.

UNE-EN 15297. Standard Test Method for Determination of Mn, Zn, Cu, Ni and Cr Content of Biomass Ash.

UNE-EN 15104. Standard Test Method for Determination of C, H, N Content in Biomass.

UNE-EN 15289. Standard Test Method for Determination of Cl, S Content in Biomass.

References

1. Technology roadmap-bioenergy for heat and power (2012). International Energy Agency. https://www.iea.org/publications/freepublications/publication/2012_Bioenergy_Roadmap_2nd_Edition_WEB.pdf. Accessed Aug. 2016
2. Technology roadmap-biofuels for transport (2011). International Energy Agency. http://www.iea.org/publications/freepublications/publication/Biofuels_Roadmap_WEB.pdf. Accessed Aug. 2016
3. Higman C, Tam S (2014) Advances in coal gasification, hydrogenation, and gas treating for the production of chemical and fuels. *Chem Rev* 114:1673–1708
4. Higman C, Burgt MV (2003) Gasification. Gulf Professional Publishing, Elsevier. ISBN 0-7506-7707-4
5. Speight JG (1983) The chemistry and technology of coal. Marcel Dekker, New York
6. Suriapparao DV, Pradeep N, Vinu R (2015) Bio-oil production from *Prosopis juliflora* via microwave pyrolysis. *Energy Fuels* 29:2571–2581
7. Li C, Zhao X, Wang A, Huber GW, Zhang T (2015) Catalytic transformation of lignin for the production of chemicals and fuels. *Chem Rev* 115:11559–11624
8. Sansaniwal SK, Rosen MA, Tyagi SK (2017) Global challenges in the sustainable development of biomass gasification: an overview. *Renew Sustain Energy Rev* 80:23–43
9. Miller BG (2005) Coal energy systems. Elsevier Academic Press, U.S.A
10. Heredy LA, Wender I (1980) Model structure for a bituminous coal. Rockwell International Corporation, Washington
11. Mohan D, Pittman CU Jr, Steele PH (2006) Pyrolysis of wood/biomass for bio-oil: a critical review. *Energy Fuels* 20:848–889

12. Lasa H, Salaiques E, Mazumder J, Lucky R (2011) Catalytic steam gasification of biomass: catalysts, thermodynamics and kinetics. *Chem Rev* 111:5404–5433
13. Zhou X, Broadbelt LJ, Vinu R (2016) Mechanistic understanding of thermochemical conversion of polymers and lignocellulosic biomass. In: Van Geem K (ed) *Advances in chemical engineering: thermochemical process engineering*, vol 49. Elsevier, U.K., pp 95–198
14. Ranzi E, Cuoci A, Faravelli T, Frassoldati A, Migliavacca G, Pierucci S, Sommariva S (2008) Chemical kinetics of biomass pyrolysis. *Energy Fuels* 22:4292–4300
15. Prakash P, Sheeba KN (2016) Prediction of pyrolysis and gasification characteristics of different biomass from their physico-chemical properties. *Energy Sources Part A: Recover Util Environ Eff* 38:1530–1536
16. Speight JG (2005) *Handbook of coal analysis*. Wiley Interscience, New Jersey
17. Feng Y, Xiao B, Goerner K, Cheng G, Wang J (2011) Influence of particle size and temperature on gasification performance in externally heated gasifier. *Smart Grid Renew Energy* 2:158–164
18. Bhavya B, Singh R, Bhaskar T (2015) Preparation of feedstocks for gasification for synthetic fuel production, Chapter 3, *Gasification for synthetic fuel production*. Elsevier
19. Van der Stelt MJC, Gerhauser H, Kiel JHA, Ptasincki KJ (2011) Biomass upgrading by torrefaction for the production of biofuels: a review. *Biomass Bioenerg* 35:3748–3762
20. Berkowitz N (1979) *An introduction to coal technology*. Academic Press, SanDiego, CA
21. Floess JK, Longwell JP, Sarofim AF (1988) Intrinsic reaction kinetics of micro porous carbons. 1: noncatalyzed chars. *Energy Fuels* 2:18–26
22. Walker PL, Verma SK, Rivera-Utrilla J, Davis A (1988) Densities, porosities and surface areas of coal macerals as measured by their interaction with gases, vapours and liquids. *Fuel* 67:1615–1623
23. Mason PE, Darvell LI, Jones JM, Williams A (2016) Comparative study of the thermal conductivity of solid biomass fuels. *Energy Fuels* 30:2158–2163
24. Golachowska MK, Gajewski W, Musial T (2014) Determination of the effective thermal conductivity of solid fuels by the lase flash method. *Arch Thermodyn* 35:3–16
25. Mahajan OP, Walker PL (1978) In: *Analytical methods for coal and coal products*. Academic Press, San Diego, CA, Chap, p 4
26. Hurt RH, Dudek DR, Longwell JP, Sarofim AF (1988) The phenomenon of gasification-induced carbon densification and its influence on pore structure evolution. *Carbon* 26:433–449
27. Kang S-W, Sarofim AF, Beér JM (1989) Particle rotation in coal combustion: Statistical, experimental and theoretical studies. *Symp (Int) Combust* 22:145–153
28. Lowell SS (2004) *Characterization of porous solids and powders: Surface area, pore size and density*. Springer, Dordrecht
29. Linge HG (1988) The surface area of coal particles. *Fuel* 68:111–113
30. Luan J, Wu X, Wu G, Shao D (2013) Analysis of char specific surface area and porosity from the fast pyrolysis of biomass and pulverized coal. *Adv Mater Res* 608:383–387
31. Qian K, Kumar A, Patil K, Bellmer D, Wang D, Yuan W, Huhuke RL (2013) Effects of Biomass feedstocks and gasification and gasification conditions on the physiochemical properties of char. *Energies* 6:3972–3986
32. Carslaw HS, Jaeger JC (1959) *Conduction of heat in solids*, 2nd edn. Oxford University Press, Oxford
33. Naidu VS, Aghalayam P, Jayanti S (2016) Evaluation of CO₂ gasification kinetics for low-rank Indian coals and biomass fuels. *J Therm Anal Calorim* 123:467–478
34. Oyedun AO, Tee CZ, Hanson S, Hui CW (2014) Thermogravimetric analysis of the pyrolysis characteristics and kinetics of plastics and biomass blends. *Fuel Process Technol* 128: 471–481
35. Muller A, Hauenstein HD, Stoesser P, Kreitzberg T, Kneer R, Kolb T (2015) Gasification kinetics of biomass and fossil based fuels: comparison study using fluidized bed and thermogravimetric analysis. *Energy Fuels* 29:6717–6723

36. Varhegyi G, Bobaly B, Jakab E, Chen H (2011) ‘Thermogravimetric study of biomass pyrolysis kinetics. A distributed activation energy model with prediction tests. *Energy Fuels* 25:24–32
37. Singh S, Wu C, Williams PT (2012) Pyrolysis of waste materials using TGA-MS and TGA-FTIR as complementary characterization techniques. *J Anal Appl Pyrol* 94:99–107
38. Tsuge S, Ohrani H, Watanabe C (2011) *Pyrolysis-GC/MS handbook of synthetic polymers*. Elsevier, Oxford, UK
39. Vinu R, Ojha DK, Nair V (2016) Polymer pyrolysis for resource recovery In: Reedijk J (ed) Elsevier reference module in chemistry, molecular sciences and chemical engineering. Elsevier, Waltham, MA. <https://doi.org/10.1016/B978-0-12-409547-2.11641-5>
40. Demirbas A (2004) Combustion characteristics of different biomass fuels. *Prog Energy Combust Sci* 30:219–230
41. Khalil RA, Meszaros E, Gronli MG, Varhegyi G, Mohai I, Marosvolgyi B, Hustad JE (2008) Thermal analysis of energy crops Part I: the applicability of a macro-thermo balance for biomass studies. *J Anal Appl Pyrol* 8:52–59
42. Reddy BR, Vinu R (2016) Microwave assisted pyrolysis of Indian and Indonesian coals and product characterization. *Fuel Process Technol* 154:96–103
43. Raveendran K, Ganesh A, Khilar KC (1995) Influence of mineral matter on biomass pyrolysis characteristics. *Fuel* 74:1812–1822
44. Barraza J, Coley-Silva E, Pineres J (2016) Effect of temperature, solvent/coal ratio and beneficiation on conversion and product distribution from direct coal liquefaction. *Fuel* 172:153–159
45. Singh K, Zondlo J (2017) Co-processing coal and torrefied biomass during direct liquefaction. *J Energy Inst* 90:497–504
46. Lu KM, Lee WH, Chen WH, Lin TC (2013) Thermogravimetric analysis and kinetics of co-pyrolysis of raw/torrefied wood and coal blends. *Energy* 105:57–65
47. Moon C, Sung Y, Ahn S, Kim T, Choi G, Kim D (2013) Thermochemical and combustion behaviours of coals of different ranks and their blends for pulverized-coal combustion. *Appl Therm Eng* 54:111–119
48. Ferrara F, Orsini A, Plaisant A, Pettinau A (2014) Pyrolysis of coal, biomass and their blends: performance assessment by thermogravimetric analysis. *Biores Technol* 171:433–441
49. Naidu VS, Aghalayam P, Jayanti S (2016) Synergetic and inhibition effects in carbon dioxide gasification of blends of coals and biomass fuels of Indian origin. *Biores Technol* 209:157–165
50. Kirubakaran V, Sivaramakrishnan V, Nalini R, Sekhar T, Premalatha M, Subramanian R (2009) A review on gasification of biomass. *Renew Sustain Energy Rev* 13:179–186
51. Phyllis 2 (2014) Database for biomass and waste. Energy Research Centre, Netherlands. <https://www.ecn.nl/phyllis2>
52. Nyakumal B, Oladokunl O, Dodo Y, Wong S, Uthman H, Halim M (2016) Fuel characterization and thermogravimetric analysis of melon (*Citrullus Colocynthis L.*) seed husk. *Chem Chem Technol* 10:493–497
53. Werle S (2014) Impact of feedstock properties and operating conditions on sewage sludge gasification in a fixed bed gasifier. *Waste Manag Res* 32:954–960
54. Lina KS, Wanga HP, Liua SH, Changa NB, Huanga YJ, Wangb HC (1999) Pyrolysis kinetics of refuse-derived fuel. *Fuel Proc Technol* 60:103–110
55. Suriapparao DV, Vinu R (2015) Bio-oil production via catalytic microwave pyrolysis of model municipal solid waste component mixtures. *RSC Advances* 5:57619–57631
56. Menendez JA, Dominguez A, Inguanzo M, Pis, JJ (2004) Microwave pyrolysis of sewage sludge: analysis of the gas fraction. *J Anal Appl Pyrolysis* 71:657–667
57. Channiwala SA, Parikh A (2002) A unified correlation for estimating HHV of solid, liquid and gaseous fuels. *Fuel* 81:1051–1063
58. Vargas-Moreno JM, Callejon-Ferre AJ, Perez Alonso J, Velazquez-Marti B (2012) A review of the mathematical models for predicting the heating value of biomass material. *Renew Sustain Energy Rev* 16:3065–3083

59. Hartley ID, Wood LJ (2008) Hygroscopic properties of densified softwood pellets. *Biomass Bioenergy* 32:90–98
60. Singh RN (2004) Equilibrium moisture content of biomass briquettes. *Biomass Bioenergy* 26:251–253
61. Vassilev SV, Baxter D, Andersen LK, Vassileva CG (2010) An overview of the chemical composition of biomass. *Fuel* 89:913–933
62. Baxter D, Andersen LK, Vassilev G, Morgan TJ (2012) An overview of the organic and inorganic phase composition of biomass. *Fuel* 94:1–33
63. Deng C, Zhang C, Tan P, Fang Q, Chen G (2015) The melting and transformation characteristics of minerals during co-combustion of coal with different sludges. *Energy Fuels* 29:6758–6767
64. Krishnamoorthy V, Pisupati SV (2015) A critical review of mineral matter related issues during gasification of coal in fixed, fluidized, and entrained flow gasifiers. *Energies* 8:10430–10463
65. Song WJ, Tang LH, Zhu XD, Wu YQ, Zhu ZB, Koyama S (2010) Effect of coal ash composition on ash fusion temperatures. *Energy Fuels* 24:182–189
66. Ranzi R, Corbetta M, Manenti F, Pierucci S (2014) Kinetic modelling of the thermal degradation and combustion of biomass. *Chem Eng Sci* 110:2–12
67. Ranzi E, Faravelli T, Manenti F (2016) Pyrolysis, gasification and combustion of solid fuels. In: Van Geem K (ed) *Advances in chemical engineering: thermochemical process engineering*, vol 49. Elsevier, UK, pp 1–94

Thermodynamics and Kinetics of Gasification

M. R. Ravi and Sangeeta Kohli

Abstract This chapter deals with the basic thermodynamics and chemical kinetics pertaining to the various physicochemical phenomena that are collectively termed as the phenomenon of gasification. Although the phenomena associated with the gasification of various feedstocks differ from each other in detail, the underlying thermodynamics is more or less common and is attempted to be captured here. The technology of gasification also has a wide variety, and this results in different phenomena having varying grades of importance in each. Thermodynamics of a phenomenon is described in terms of conservation equation for mass and the first law, often discussed under the headings of stoichiometry and energetics of a phenomenon, and in terms of the second law, which determines the equilibrium state at the end of the phenomenon, and thus defines the product compositions in gasification when the reactor is maintained at a given pressure and temperature. The variety of phenomena involved in gasification, namely drying of feedstock, its pyrolysis, homogeneous and heterogeneous reactions which form part of the gasification in the form of oxidation and reduction reactions, proceed at different rates in a given system, and also vary widely between different types of gasification systems. Hence, it is important to study the kinetics of these phenomena, in addition to the study of thermodynamic equilibrium states pertaining to these phenomena. Owing to the fact that each of these phenomena is extremely complex, in mathematical modelling of these phenomena, often apparent mechanism and their thermodynamics and kinetics are studied. This leads to a variety of models and thermodynamic and kinetic data in the literature, often in apparent conflict with each other. This chapter also attempts to identify some of these conflicts through the experience of the authors in modelling gasification phenomena.

M. R. Ravi (✉) · S. Kohli
Indian Institute of Technology Delhi, New Delhi, India
e-mail: ravimr@iitd.ac.in

S. Kohli
e-mail: skohli@iitd.ac.in

1 Introduction

Liquid and gaseous fuels from petroleum origin are being depleted at an ever-accelerating rate, and gaseous fuels from fossil origin have also been employed to greater and greater extents in the recent years. Mankind seems to have an insatiable appetite for energy, so much so that the definition of development has become almost synonymous with an increase in per capita consumption of energy. While the validity of such a model of development in itself is a matter of debate, various projections regarding energy scenario for the future have been pinning the hopes of energy security of mankind on the utilization of coal as well as renewable resources such as biomass, solar and wind energies. Thermochemical and biochemical conversion of solid fuels into gaseous and liquid fuels helps in extending the utility of solid fuels to applications where a liquid or gaseous fuels alone can be used.

1.1 Historical Background

Gasification of coal was discovered in the eighteenth century and was the prime source of energy for lighting and indoor heating in England in the latter half of the nineteenth century. Town gas was actually a by-product when coke was produced by heating coal [4, 18]. With the advent of electric bulb in early 1900s and liquid fuels for indoor heating subsequently, town gas became obsolete. During World War II, after the allied forces destroyed German refineries, synthesis of hydrocarbon liquids for aviation and water gas to run road vehicles was widespread in Germany. Again, in post-war period, the technology fell out of favour owing to resurgence of oil as fuel. Subsequently, the oil embargo in 1974 renewed the interest in gasification, and research on gasification resumed and pilot units were installed. Once oil crunch relented in the 1980s, interest in gasification again dipped lower.

Amongst coal gasification technologies, oxy-gasification in place of air gasification became feasible after commercial cryogenic separation of oxygen was demonstrated in the 1920s. Fluidized bed gasification was initiated in the 1930s, and the entrained flow gasification technology found the light of the day in the 1940s. South African oil giant Sasol had the largest commercial gasification system by the 1970s, where coal gas was converted to hydrocarbons using the Fischer–Tropsch synthesis [18].

The flexibility of the technology to different types of feedstock has also led to the use of gasification phenomenon for different solid and liquid residues of petroleum refineries, for municipal solid wastes, etc. Co-firing of multiple feedstocks based on availability has also been in practice. Integration of coal gasification in combined-cycle power plants is also in pilot demonstration stage.

In India, biomass gasification using moving bed downdraft gasification systems has been in commercial use at small scales up to about 1250 kWe [9]. Notwithstanding all developments in the technology, owing to the lack of clarity at policy level,

commercial success of these technologies does not appear feasible in near future. While coal gasification, despite its high cost, is promoted under the banner of clean coal technologies, biomass gasification, which is clearly a nonentity in comparison with the former in terms of feasible scales of feedstock availability, often is made to compete in economic terms with the fossil counterparts. The net result is that biomass gasification loses out in economic terms: this again is the result of the international pricing policy of fossil fuels, which treats these fuels as income rather than asset [34], and does not account for the cost of the lost opportunity with its depletion. A clear policy framework on the pricing and use of biomass energy would go a long way in empowering the sectors of the society which have an abundance of biomass feedstock and create business opportunities in renewable energy. In addition to economic criteria, the ethical considerations also need to be borne in mind. If policy does not regulate utilizing land resources for cultivating biomass which would eventually end up being utilized for automotive fuel in another part of the world, the population supplying feedstock may be at a disadvantage: while they produce biomass that supplements fossil fuels elsewhere, they would be paying for their own energy at prices determined by fossil fuel pricing policy decided elsewhere. It should also be recognized that cultivation of biomass for fuel may also compromise on the land available for growing foodgrains. Policy framework should promote the use of decentralized resources like biomass in a decentralized manner, so as to empower communities that have an abundance of this resource.

2 Thermochemical Conversion Processes

2.1 Basic Phenomena in Thermochemical Conversion

Conversion of a solid fuel into a liquid or gaseous fuel through heating is termed as thermochemical conversion. Basu [4] states the motivation of conversion of fuel from one form to another as:

- (i) Improvement in the heating value of the fuel by rejecting non-combustible components such as water and nitrogen
- (ii) Removal of elements such as sulphur or nitrogen in fuel which when oxidized can constitute harmful emissions
- (iii) Reduction in the carbon-to-hydrogen mass ratio of a fuel

When a solid fuel is heated, it first loses moisture and becomes dry. This process is referred to as *drying*. On further heating, *volatile matter* present in the solid fuel gets liberated, leaving behind *char*, which is mostly carbonaceous, and *ash*, which contains non-combustible inorganic mineral matter. This process is referred to as *pyrolysis* or *devolatilization*.

In the presence of oxygen, further heating of the solid fuel results in *oxidation* of the volatiles and the char and the extent of oxidation would depend on the amount of

oxygen available for the process. In case of biomass combustion in excess oxygen, near-complete oxidation takes place releasing heat of combustion of char and volatile matter, and producing carbon dioxide and water vapour as major products, besides oxidation products of other constituents of the solid fuel such as sulphur. However in the case of gasification, oxygen supply is substantially lower than stoichiometric requirements for complete combustion. In such a case, oxygen is typically consumed by the most reactive constituents of the volatile matter and partly by the char, and in the reducing environment that ensues, products of complete oxidation such as carbon dioxide and water vapour undergo a *reduction* process, resulting in final products that contain substantial quantities of carbon monoxide and hydrogen and small quantities of methane. This fuel is often referred to as *producer gas* or *syngas*.

It is often desirable to enhance the hydrogen content of the producer gas since a higher hydrogen content makes the producer gas a fuel with higher calorific value and more desirable values of combustion properties such as flame speed. This is even more important in the case of feedstocks that have low hydrogen content such as some coals. In order to achieve this, a metered quantity of steam is introduced into the reactor. The processes listed above may produce solid, liquid or gaseous fuels depending on the process parameters, as discussed below.

2.2 *Types of Thermochemical Conversion of Fuels*

Thermochemical conversion processes could be classified based on the desired end product and the process followed. When the desired end product is a solid fuel of higher quality, the processes are *charcoal making* or *charring* and *torrefaction*. While charring is carried out at atmospheric pressure, torrefaction is carried out at low pressures. When the desired product is a liquid fuel, the processes are *fast pyrolysis*, *flash pyrolysis* and *ultra-rapid pyrolysis*. Both above sets of processes use pyrolysis as the main thermochemical conversion process. When the pyrolysis is carried out at low rates of heating the feedstock (<10 °C/min), volatile yield is low and char yield is high, and this is desirable when solid fuel is the desired product. On the other hand, when liquid fuel is the desired product, the heating rate should be substantially higher (>1000 °C/min). At such high heating rates, the char yield is practically eliminated, and nearly all the feedstock is converted to volatile matter, which is subsequently condensed to make bio-oil.

Gasification methods are adopted when the desired product is a gaseous fuel. Gasification is classified based on the process adopted: when the feedstock particles are large, and are allowed to flow by gravity, the gasification process happens in a *moving bed*. If the flow of air/gas is upwards, i.e. in countercurrent with the feedstock flow, the gasifier is termed as *updraft* or *countercurrent* gasifier. If the flow of air/gas is downwards, i.e. co-current in the direction of flow of feedstock, the gasifier is a *downdraft* or *co-current* gasifier. Similarly, there are *cross-draft* gasifiers where the flow directions of feedstock and air are perpendicular to each other. Ironically,

moving bed gasifiers are also referred to as *fixed bed* gasifiers, to contrast them with fluidized bed gasifiers.

When the particles are smaller, and are fluidized by the air or oxygen (and steam where applicable) used to gasify them, the gasifier is a *fluidized bed* gasifier, and depending on the extent of fluidization, there are bubbling fluidized bed and circulating fluidized bed gasifiers. When the feedstock particles are fed into the stream of air/oxygen (and steam) so that the particles are entrained in a highly turbulent flow of the gaseous medium, the gasifier is called an *entrained flow* gasifier. These gasification systems could be operated at atmospheric pressure or at elevated pressures depending on process requirements.

When oxygen is used in place of air in gasification, the gas has a much higher fraction of combustibles and hence much higher calorific value as compared to when air is used; since in the latter case, nearly half of the producer gas is nitrogen. Also, since the inert constituent is practically absent, the temperatures of the reactor can be much higher in the former case.

Hydrogasification and *catalytic hydrogenation* processes are used to add hydrogen to char in a hydrogen environment leading to the production of methane. These, and the *Fischer–Tropsch synthesis* processes lead to the production of hydrocarbons such as substitute natural gas (SNG) from gasification products.

3 Modelling of Gasification Phenomena

Any system needs to be modelled so that its input–output relations can be obtained even before a real system is built, so that the design could be optimized for desired operation even before it is built. Once a system is designed, a model can also help in predicting the performance of the system at design as well as off-design conditions. Modelling a gasification system from first principles needs an understanding the thermodynamics and reaction kinetics underlying the gasification process. This section throws light on what these models can do and what their limitations are.

3.1 Thermodynamic Modelling

Thermodynamics has the special characteristic of being able to describe a process and predict its outcome with almost no regard to the details of the system in which the process happens. This feature of thermodynamics is of great value to modelling of phenomena and predicting their outcomes even before the conceptual design of a system is undertaken. After the system is erected and commissioned, thermodynamic laws help in identifying the optimal points of operation of the system at which its performance is the most desirable. Thus, thermodynamic analysis of a system is a powerful tool at the design as well as operation stage. The primary laws governing

the process used by thermodynamics are the conservation law of mass, first law of thermodynamics and the second law.

In understanding gasification, it is necessary to know the composition of the feedstock either in the form of an empirical/molecular formula or in terms of its ultimate analysis (elemental contents of C, H, O, etc., of the feedstock on mass or molar basis). Since pyrolysis is an important process in gasification, it is also necessary to know the proximate analysis of the feedstock, i.e. the moisture, volatile matter, ash and residual char content of the fuel under normal conditions of combustion. The most important necessity of any thermodynamic process is the conservation of the elemental atoms/mass, and the total mass of the feedstock, air/oxygen, steam, etc., during gasification. These provide a few basic equations that need to be always satisfied, and this is the first ingredient of a thermodynamic model of the phenomena.

The second most fundamental equation in thermodynamic analysis of any system is the first law of thermodynamics, which is a statement of conservation of energy in the appropriate form needed for the phenomenon. This law needs to be satisfied at all the levels of the system or process: the entire gasification system needs to satisfy first law; at the same time, each component of the system should also satisfy conservation of energy. The entire gasification process should satisfy energy conservation laws, and so should each basic phenomenon that constitutes gasification, viz. drying, pyrolysis, oxidation, reduction, etc., should each satisfy the first law of thermodynamics.

Since most basic phenomena of gasification are chemical reactions, the first law for these phenomena would involve the basic enthalpies of formation of all species considered in the reactions. The detailed chemical reaction mechanisms of pyrolysis, oxidation and reduction are extremely complex. Often, these phenomena are modelled by a minimal reduced set of representative reactions, details of which would be presented in Sect. 4. The energetics of these reactions constitute the application of first law to the phenomena that they represent, viz. pyrolysis, oxidation or reduction.

The favoured direction of a reaction is decided by its spontaneity, which is the domain of the second law of thermodynamics. Given the temperature, pressure and the participating species, second law of thermodynamics is used to determine the end state of a reaction at which the system would go to thermodynamic equilibrium, given adequate time for the equilibrium to establish. The species composition at equilibrium would give the end product of gasification in a thermodynamic model of gasification.

In summary, thermodynamic model of a gasification system would need as input the following [18]:

- (i) elemental composition/proximate and ultimate analysis and standard heats of formation of the feedstock fuels and their higher/lower heating values
- (ii) standard enthalpy and entropy data along with temperature dependence for all the species of substances involved in the various phenomena

It would use the equations of :

- (a) elemental balance of the species involved (C, H, O, N, S) and conservation of mass equations including that for ash. Ash is treated as one substance, and its elemental composition is not considered,
- (b) first law of thermodynamics corresponding to the various processes that takes into account the enthalpies of formation of the constituent streams and the sensible and latent heat addition/ subtraction in the various processes and
- (c) the equilibrium conditions either in the form of equilibrium constants of constituent reactions as a function of temperature or in the form of Gibbs functions of constituent streams that can eventually be minimized for the process to obtain equilibrium conditions.

The model would be capable of predicting:

1. gas composition
2. required proportions of feedstock, oxidizer and steam
3. effects of various operating thermodynamic conditions such as pressure, temperature, feedstock to air/oxygen/steam ratios, etc., on the gas composition
4. overall efficiency of the conversion process at different operating conditions
5. optimal conditions of operation, based on the above predictions.

However, since the time of residence of the reacting species in the system is not infinitely long, the predictions obtained from a thermodynamic model are usually the maximum achievable yields of the desired product from a reacting system [4, 22]. Since a thermodynamic model does not account for the details of the gasification system and the time of residence of reactants in the system, thermodynamic model predictions are restricted in practical applicability.

3.2 Kinetic Modelling

In order to account for the finite time available for the reactions, a kinetic model is necessary, which considers the progress of a reaction as it happens in the reactor, accounting for the geometry and fluid flow and hence the residence time.

In a moving bed gasifier, the particle sizes are larger ($> 15\text{--}20$ mm), and hence the time needed for the diffusion phenomena of heat and mass are significantly higher. Residence time requirement in such gasifiers is determined by the time scale of diffusion, which is the slowest phenomenon, especially in the regions where devolatilization occurs. The rates of oxidation are significantly higher, and in the presence of the high temperatures resulting out of rapid oxidation, the particle sizes also decrease in this region. As the particles move into the reduction zone, particle sizes decrease further owing to consumption of char by surface reactions. In the reduction reactions involving solid char, consumption rates are determined by the reaction rates at the surface. Thus in a moving bed gasification system, the lengths of drying, devolatilization, oxidation and reduction zones reflect the rates at which these reactions proceed:

oxidation zone is the shortest, followed by reduction and pyrolysis zones. Drying zone being the farthest from the exothermic oxidation zone is usually the longest.

In the fluidized bed and entrained flow reactors, particle sizes are smaller (< 10 mm). As the particle sizes decrease, the residence time requirement also falls exponentially [18]. The extent of devolatilization in such reactors depends on the final temperatures attained by the particles. It is desirable to provide adequate residence times so that the particles attain the required temperature to complete the devolatilization, without which the volatiles may contaminate the product gases in the form of tar, much as it happens in moving bed gasifiers. The kinetics of oxidation of the products of devolatilization is the least understood, but fortunately, since oxidation is a rapid phenomenon, its kinetics are not as important [18]. In the char gasification (reduction) process where the products of oxidation react with the char to produce the final products, the overall reaction rate is determined by the surface reactivity of the char, which is a function of the porosity and crystal structure of char/fixed carbon and the catalytic effects of the ash components. If we consider the resistance offered by the reaction rate constant at the surface, internal diffusion rates of gaseous reactants through the pores of individual particles and the surface diffusion rates of gaseous reactants that hinder the progress of a reaction, surface reactivity can be expressed as the reciprocal of the sum of these resistances. Higman and Burgt [18] delineate the different temperature regimes of char gasification:

- Low-Temperature Zone: chemical reaction is slow and is the rate controlling step.
- Medium-Temperature Zone: chemical reactions are faster, but the rate-limiting step is the internal diffusion of gaseous reactants into the pores of solid particles.
- High-Temperature Zone: the bulk surface diffusion of the gaseous reactants is the rate-limiting step.

In addition to the classification of a model as thermodynamic or kinetic, gasification models are also classified on the basis of the way they handle spatial variation of the phenomena in a reactor, as discussed below.

3.3 Classification of Gasification Models

Based on how a gasifier model treats spatial distribution of the phenomena in a reactor, gasification models could be classified as zero-, one- or multi-dimensional models. In fact, since in many gasification systems the predominant phenomena in different parts of the gasifier may be one of drying, pyrolysis, oxidation or reduction, it is also possible to use thermodynamic or kinetic model for each phenomenon differently in different parts of the reactor: for example, one may choose an equilibrium model for oxidation in the combustion zone of a gasifier, while using kinetic models in the pyrolysis and reduction regions. In the following paragraphs, some of these features of modelling are discussed briefly.

3.3.1 Zero-Dimensional Models

These are the most rudimentary models of gasification. They consider the entire gasifier as a single control volume, and apply the conservation of mass/elements, energy and thermodynamic equilibrium equations for determining the product composition and temperature at the end of gasification. Often, drying and pyrolysis phenomena are not modelled and the oxidation - reduction equations are solved for equilibrium. Such models are good as a quick estimate of product composition of a gasifier and are suitable where the reactions are reasonably fast so that the residence time is adequate to assume equilibrium. These models are also referred to as *well-stirred reaction models* of gasification.

3.3.2 One-Dimensional Models

In many types of gasification systems, different geometric regions can be identified where different phenomena predominate. For example, the region immediately downstream of oxidizer inlet is the oxidation zone, where oxidation reactions predominate, so much so that the other phenomena occurring there could be ignored or treated with less importance. In a downdraft moving bed gasification system, the topmost zone is the drying zone; the zone immediately upstream of the oxidation zone is the pyrolysis zone and that which is immediately downstream of the oxidation zone is the gasification or reduction zone. In such cases, the reactor could be divided into control volumes in the flow direction and each control volume could model the various phenomena using different approaches depending on the temperature and composition of the gases and solids in the control volume. The flow from one control volume to another is also appropriately modelled, accounting for the pressure losses in the gasifier. Then the gasifier model consists of a one-dimensional sequence of control volumes, each of which is treated as well-stirred in itself, and the variation from one control volume to another is computed. Such models are also referred to as *plug flow models*.

3.3.3 Multi-dimensional Models

The models which resolve the spatial variation of the various quantities such as temperature, pressure and composition and also account for the flow phenomena of solids and gases using the respective momentum equations in addition to the other constitutive thermodynamic and kinetic equations governing gasifications can be classified as multi-dimensional models. General purpose CFD simulation software could be used for this purpose. Such models are also referred to as *CFD models*.

3.3.4 Discussion

Although there is an increased amount of information generated by the models as we progress from zero-dimensional to multi-dimensional models, the cost of computation grows nonlinearly as well. And, contrary to popular perception that more detailed models should always be better than the less detailed ones, it is observed that the additional information available from more detailed models comes at such a large additional time, effort and cost that one often looks for the most judicious choice amongst these models. One-dimensional models with appropriate phenomenological representation of all basic phenomena occurring in a gasifier are most often found to be adequate and appropriate. For example, a CFD model is justified only when one would like to know what effect a particular shape of the air/oxygen nozzle has on the gasification process, and if the question is about the number and size of the nozzles rather than their shape or position, it is unnecessary to resort to CFD. Comparing the time required for simulations, a three-dimensional CFD model often takes a thousand times or more computational time taken by a one-dimensional simulation. Thus, a judicious choice of the phenomenological representation of the process often pays better dividends than a large spatially resolved computation, and the decision in favour of one or the other must be based on what improvements in predictions one is looking for.

4 Mechanisms of Gasification Phenomena

In this section, a brief discussion on the mechanisms of the basic phenomena of gasification introduced in Sect. 2.1 is presented, enabling the reader to visualize the phenomena and understand the ways to simplify and model these phenomena.

4.1 Drying

Moisture content in a given feedstock can have seasonal variations. It can also vary from feedstock to feedstock. Since moisture in the feedstock absorbs energy to evaporate, a lower moisture content permits higher reactor temperatures in a gasifier and hence is better for the gasification process. Complete absence of moisture is also not desirable in gasification, as the presence of moisture improves the H-C ratio and hence yields gas of higher calorific value. In biomass gasification, 10–15% moisture is usually deemed desirable. Fresh wood has moisture content usually in the range from 30 to 60%. But it can also be as high as 80% for feedstocks like paddy straw [19]. In such cases, pre-drying of biomass before use in a gasifier is recommended. Moisture content of coal feedstock also varies with the rank and grade of the coal, which vary from source to source.

Heat liberated in the reactor by the exothermic reactions such as oxidation of volatiles and char is transferred to the fresh feedstock through a combination of heat transfer mechanisms. These include conduction through the feedstock particles and between particles of feedstock, radiation from the hot zones of the reactor to the feedstock and convection from the hot gases in contact with the feedstock particles. Depending on the particle size, the time required for heat transfer from the surface of a particle to its interior would vary. The moisture from the interior of the particle has to diffuse out due to gradient in moisture concentrations and departure of the particle from its equilibrium moisture content at the prevailing surrounding temperature around the particle. Thus, the drying process is determined by the rate of heat and mass transfer in the feedstock bed and in the particles.

Since thermal diffusivities are often a few orders of magnitude higher than mass diffusivities, it is assumed that the feedstock particle is in thermal equilibrium with the surrounding medium, implying that heat transfer is faster than mass transfer. Hence under this assumption, mass transfer determines the rate of drying. This assumption usually holds true in moving bed gasifiers. Hence, there the mechanism of drying can be assumed to be through diffusion. As the feedstock moves progressively to higher temperature zones, there is greater departure from thermal equilibrium between the particle and the surrounding medium. In these stages of moving bed gasification, the loosely bound moisture is irreversibly removed. Heat conduction from the high-temperature region further assists in this process. Drying continues until a temperature of about 200°C is attained.

McCabe et al. [26] determined the analytical solution for one-dimensional mass diffusion in a spherical particle of wood, and this expression is commonly used to model drying of particles in a moving bed gasifier.

$$\frac{X_{m,out} - X_{m,eqb}}{X_{m,in} - X_{m,eqb}} = \frac{8}{\pi^2} \left(e^{-\alpha_1\beta} + \frac{1}{9}e^{-9\alpha_1\beta} + \dots \right) \quad (1)$$

Here X_m denotes the mass fraction of moisture in biomass, subscripts *in*, *out* and *eqb* denote inlet, outlet and equilibrium conditions. α_1 is the first eigenvalue and is equal to $(\pi/2)^2$ and β is the Fourier number given by (Dt_{res}/r_p^2) with D being the diffusion coefficient and t_{res} the residence time of a particle in a control volume. The value of diffusion coefficient is by and large of the order 10^{-10} as suggested by Simpson [39], who also performed experiments and gave the following expression for equilibrium moisture content in wood.

$$X_{m,eqb} = \frac{1800}{W} \left(\frac{Kh}{1 - Kh} + \frac{K_1Kh + 2K_1K_2K^2h^2}{1 + K_1Kh + 2K_1K_2K^2h^2} \right) \quad (2)$$

where the coefficients K , K_1 , K_2 and W are functions of temperature, obtained by Simpson [38] from an absorption model due to Hailwood and Horrobin [17]:

$$h = \frac{\omega_a}{\omega_{a,sat}} = \frac{\omega_a}{\frac{p_{v,sat}M_w}{p_aM_a}}$$

$$W = 349 + 1.29T + 0.0135T^2$$

$$K = 0.805 + 0.000736T - 0.00000273T^2$$

$$K_1 = 6.27 - 0.000938T - 0.000303T^2$$

$$K_2 = 1.91 - 0.0407T - 0.000293T^2$$

T is the temperature in °C, ω_a is the specific humidity of the incoming air in kg/kg dry air, $p_{v,sat}$ is the saturation vapour pressure of water vapour at temperature T and M_w and M_a are molecular weights of water and air, respectively.

4.1.1 Kinetics of Drying

As the particle sizes are made smaller, as in the case of fluidized bed or entrained flow gasifiers, the time required for the conduction of heat into the particle and diffusion of moisture from the particle becomes smaller and smaller, so much so that the time taken for these phenomena becomes negligibly small compared to that required for gasification [4]. In such a case, the drying phenomenon is often modelled as instantaneous, and the above expressions are not used. It is also customary to model the drying process as a first-order reaction of the form



The rate constant k_{dry} is obtained using thermogravimetric analysis of the feedstock in the range of temperatures less than 200 °C where drying happens. Thermogravimetric analysis involves heating a small sample of the feedstock under controlled temperature rise rates in controlled atmosphere of inert gases to obtain mass loss as a function of time and hence mass loss rate. Then, using the expression for the rate of the first-order reaction in Eq. 3, the rate constant k_{dry} is evaluated:

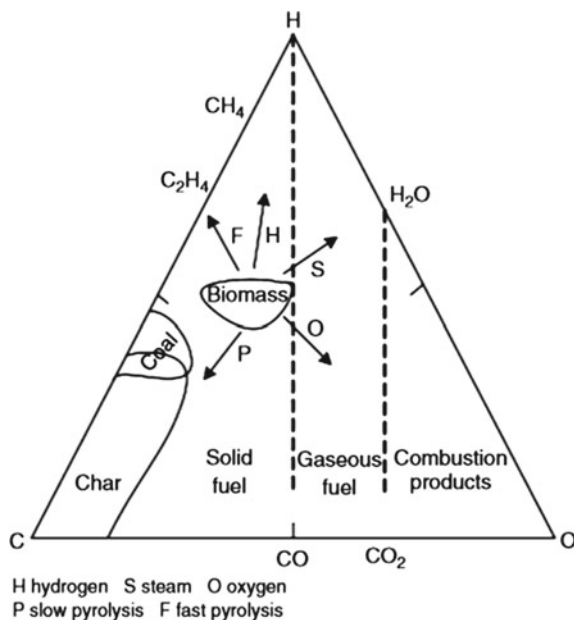
$$-\frac{dm_{\text{WF}}}{dt} = k_{\text{dry}}m_{\text{WF}} \quad (4)$$

Depending on the type of gasifier and the kind of data/equipment available, drying is modelled using either an equilibrium or a kinetic model.

4.2 Pyrolysis

Pyrolysis is thermal decomposition of feedstock by virtue of heating. No external agent like an oxidizing agent is needed in pyrolysis. The thermal decomposition

Fig. 1 C-H-O diagram of the gasification process [4]



leads to breaking of large hydrocarbon compounds of feedstock into smaller simpler gaseous molecules and char. Typical temperatures at which pyrolysis occurs in gasification systems range from 300 to 650°C. Depending on the heating rates, the products composition and yields of pyrolysis can vary [29]. If the time required to heat the fuel to the pyrolysis temperature is much longer than the characteristic pyrolysis reaction time, then the pyrolysis is considered slow, else it is fast. One important trend is that the char percentage in the pyrolysis products decreases with increasing pyrolysis temperature. Referring to Fig. 1, the solid biomass during slow pyrolysis moves towards the carbon corner of the ternary diagram, and more char is formed. On the other hand, the process moves towards the C-H axis, opposite to the oxygen corner, in the case of fast pyrolysis.

Rapid heating of biomass to a moderate temperature of around 400–600 °C yields higher volatiles and hence more liquid, whereas slower heating to similar temperatures will produce more char. Debdoubi et al. [10] reported that the liquid yield from Esparto increased from 45 to 68.5% when the heating rate increased from 5–25 °C/min to 400–500 °C/min. However, heating rates alone do not determine the pyrolysis products. Residence time also plays an important role in this regard. If heating is slow, the removal of volatiles from the reactor is slow and gradual which permits secondary reactions to occur between char particles and volatiles, leading to secondary char formation. A more detailed classification of pyrolysis is delineated in Table 1.

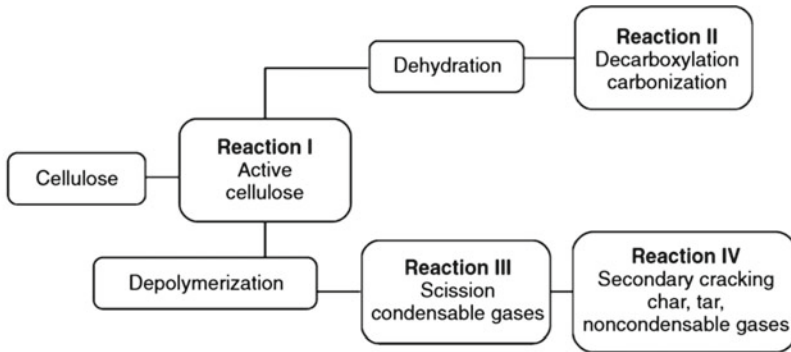
Pyrolysis is a complex phenomenon which leads to numerous products which vary greatly with the feedstock used apart from the heating rates and temperature.

Table 1 Characteristics of some pyrolysis processes [4]

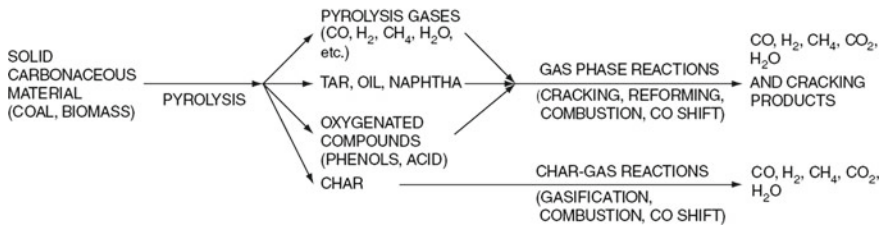
Pyrolysis process	Residence time	Heating rate	Final temperature (°C)	Products
Carbonization	Days	Very low	400	Charcoal
Conventional	5–30 min	Low	600	Char, bio-oil, gas
Fast	<2 s	Very High	500	Bio-oil
Flash	<1 s	High	<650	Bio-oil, chemicals, gas
Ultra-rapid	<0.5 s	Very High	1000	Chemicals, gas
Vacuum	2–30 s	Medium	400	Bio-oil
Hydropyrolysis	<10 s	High	<500	Bio-oil
Methanopyrolysis	<10 s	High	<700	Chemicals

Pyrolysis can be seen as two-stage process. The initial step leads to condensable gases and char. Subsequently, these condensable gases break down to non-condensable gases like CO, CO₂, H₂O, CH₄, etc. The final products can be said to be in three categories, namely solid (primarily char), liquids (tar, heavy hydrocarbons and water) and gaseous products (CO₂, H₂O, CH₄, C₂H₆, etc.). Although char is usually thought to be carbon, more generally it contains oxygen and hydrogen as well. Biomass contains very low amounts of inorganic ash. Biomass char has a lower heating value (LHV) of 32 MJ/kg as reported by Diebold and Bridgwater [11] which is higher than the biomass itself. On the other hand, the LHV of the liquid products, also known as tar, bio-oil or bio-crude, is in the range of 13 to 18 MJ/kg. While the parent biomass usually has a LHV in the range of 19.5 to 21 KJ/kg.

Shafizadeh [35] reported that the pyrolysis products of wood can be seen as the combination of thermal responses of its three major components: cellulose, hemicellulose (xylan) and lignin. It was found that hemicellulose component is the least stable and decomposes at 225–325 °C while the cellulose component decomposes at higher temperatures in narrower range of 325–375 °C and lignin decomposes gradually within the temperature range of 250–500 °C. For cellulose, the Broido–Shafizadeh model [7] is most common and has also been applied to biomass [6]. As per this model, pyrolysis involves a first reaction which gives *active cellulose*. This is an unstable species. It is followed by two parallel competing reactions: dehydration and depolymerization. Dehydration further involves decarboxylation and carbonization and is more prominent at low temperatures (less than 300 °C) [42] and slow heating rates [31]. Depolymerization further involves scission, formation of tar and condensable gases. This is prominent at high temperatures (over 300 °C) [42] and faster heating rates [31]. If the condensable vapor is allowed to escape the reactor, it can condense as bio-oil or tar, and if it is held within the reactor, it can undergo secondary reactions leading to cracking of the vapor into secondary char, tar and gases. Figure 2a summarizes this model.



(a) Modified Broido-Shafizadeh model of cellulose [7]



(b) Reaction sequence for gasification of coal or biomass [18]

Fig. 2 Some models proposed in literature for pyrolysis of cellulose and biomass

Solomon [41] presents a detailed review of work done on coal, which shows that the mechanisms of pyrolysis of coal and biomass are quite similar in nature but different in detail. Higman and Burgt [18] also indicate that the mechanisms of pyrolysis of coal and biomass follow a similar path, in two stages as shown in Fig. 2b. Mallick et al. [25] present a review of the mechanisms available in the literature for pyrolysis of coal and biomass.

The following tentative design norms are used for heating in a pyrolyzer:

- For maximizing char production, slow heating rate (<0.01–2.0 °C/min), a low final temperature and a long gas residence time are used.
- For maximizing liquid yield, high heating rate, a moderate final temperature (450–600 °C) and a short gas residence time are used.
- For maximize gas production, slow heating rate, a high final temperature (700–900 °C) and a long gas residence time are used.

4.2.1 Kinetics of Pyrolysis

Modelling pyrolysis kinetics requires the specification of rate constants of the constituent reactions. Table 2 gives the rate constants of the reactions of the Broido–

Table 2 Rate constant parameters for pyrolysis of cellulose according to the Broido–Shafizadeh Model [7]

Reaction	A_i (1/s)	E_i (kJ/mol)	Source
I. First degradation (active cellulose)	2.8×10^{19}	243	[7]
II. Dehydration (char and gas)	1.31×10^{10}	153	[7]
III. Depolymerization (tars)	3.16×10^{14}	198	[7]
IV. Secondary cracking (gas, char)	4.28×10^6	107.5	[23]

Shafizadeh model [7] for cellulose. Hemicellulose produces lesser tar and char content as compared to cellulose while lignin produces around 55% char [42]. Here, the reaction rate constant k_i of each stage I – IV can be expressed in terms of the pre-exponential factor A_i and activation energy E_i as

$$k_i = A_i \exp \frac{E_i}{RT}$$

The Broido–Shafizadeh model, although a more accurate model for pyrolysis of biomass, is not so frequently used in gasification modelling owing to the complex nature of the model. Rather simpler one stage global pyrolysis models and two-stage semi-global models are more commonly used. The generalized reaction for one stage global model is:



The rate of pyrolysis can then be given as

$$-\frac{dM_b}{dt} = k_{\text{pyr}}(M_b - M_c) \quad (6)$$

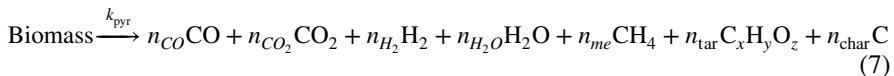
where M_b is the mass of biomass remaining in the volume of interest and M_c is the mass of char remaining after complete pyrolysis of the volume of interest, and k_{pyr} is the apparent rate constant of the single-step reaction in Eq. 5. Reliable data on the pre-exponential factor A and the activation energy E are not easily available for fast pyrolysis [31]. For slow pyrolysis, there are some values available in literature. Table 3 gives these rate constants.

The composition of volatiles can vary depending on the type of gasifier and feedstock used. Usually, the low molecular weight (CO , CO_2 , H_2 , H_2O) gases are taken explicitly while the rest of the gases are lumped into representative gas compositions with a general composition of $\text{C}_x\text{H}_y\text{O}_z$, labelled as *tar* or *heavy hydrocarbons*,

Table 3 Kinetic rate constants for the one-step single-reaction global model for biomass feedstock

Constituent	Fuel temperature (K)	E (kJ/mol)	A (1/s)	Source
Cellulose	520–1270	166.4	3.9×10^{11}	[27]
Hemicellulose	520–1270	123.7	1.45×10^9	[27]
Lignin	520–1270	141.3	1.2×10^8	[27]
Wood	321–720	125.4	1.0×10^8	[30]
Wood	–	150.96	7×10^7	[33]
Almond shell	730–880	95–121	1.8×10^6	[14]
Beech sawdust	450–700	84 (T > 600 K)	2.33×10^4	[1]

and *methane equivalent* (me) or *light hydrocarbons*, often simplified to CH₄. The pyrolysis reaction is then represented in a simplified form as



Three of the unknowns in the above equation are determined using atomic balances of elements C, H and O, respectively, and the remainder is obtained using experimental results available in the literature.

Similar literature for coal pyrolysis in moving bed gasifiers is available. The more recent designs of coal gasification systems are less pyrolysis-dominated and more partial oxidation-dominated, and the rate equations for drying and pyrolysis are often not needed in determining the product composition of gasification of coal [18].

4.3 Oxidation and Reduction

The primary route to thermochemical conversion of a solid fuel into a liquid or gaseous fuel is either pyrolysis or partial oxidation or a combination of these two. As discussed in the earlier sections, pyrolysis determines the overall rate when the particle sizes are large and the diffusion of mass is the rate-determining step. On the other hand, when the particle sizes are small, the heating rates automatically become higher at any point in the solid feedstock, and this leads to a larger fraction of volatile matter and less and less char. For production of gaseous fuels from pyrolysis alone, temperatures at the end of pyrolysis are required to be higher than those needed for the production of liquid fuels.

Partial oxidation often provides the source of heating required for the pyrolysis reactions in most gasification systems. In the case of moving bed gasifiers, pyrolysis and partial oxidation happen in distinctly different parts of the gasification reactor, so much so that distinct *drying zone*, *pyrolysis zone*, *oxidation zone* and *reduction zone* get established in such gasifiers, and heat released in the exothermic reactions in

Table 4 Homogeneous reactions in a gasifier along with their rates

Reaction	Reaction rate	Reference
$H_2 + \frac{1}{2}O_2 \rightarrow H_2O$	$r_1 = 1.0 \times 10^{11} \exp\left(-\frac{42000}{RT}\right)[H_2][O_2]$	[47]
$CH_4 + \frac{3}{2}O_2 \rightarrow CO_2 + 2H_2O$	$r_2 = 9.2 \times 10^6 \exp\left(-\frac{80000}{RT}\right)[CH_4]^{0.5}[O_2]$	[8], [47]
$C_6H_{6.2}O_{0.2} + 4.45O_2 \rightarrow 3.1H_2O + 6CO$	$r_3 = 9.2 \times 10^6 \exp\left(-\frac{80000}{RT}\right)[C_6H_{6.2}O_{0.2}]^{0.5}[O_2]$	[8]
$CO + \frac{1}{2}O_2 \rightarrow CO_2$	$r_5 = 1.0 \times 10^{11} \exp\left(-\frac{126000}{RT}\right)[CO][O_2]^{0.5}[H_2O]^{0.5}$	[8]
$CH_4 + H_2O \rightarrow 3H_2 + CO$	$r_9 = 9.1 \times 10^{10} \exp\left(-\frac{131000}{RT}\right)\left([CH_4][H_2O] - \frac{[CO][H_2]^3}{K_{eq9}}\right)$	[44]
$CO + H_2O \rightarrow CO_2 + H_2$	$r_6 = 2.78 \exp\left(-\frac{12600}{RT}\right)\left([CO][H_2O] - \frac{[CO_2][H_2]}{0.0265 \exp\left(-\frac{32900}{RT}\right)}\right)$	[24]

the oxidation zone is transferred to the other endothermic zones through appropriate heat transfer mechanisms as discussed in Sect. 4.1. Basu [4] illustrates a separate combustion zone and gasification zone in fluidized bed and entrained flow gasifiers, where the region closest to the inlet of the oxidizer acts as the combustion zone and the downstream region after all oxygen has been consumed acts as the gasification region.

In all gasifiers, solid particle is heated to undergo drying and pyrolysis first. Subsequently, the volatiles, as well as char, undergo oxidation in the presence of oxygen. Once the oxygen is exhausted by the oxidation reactions, since the supply of oxygen to such reactors is only a fraction of the stoichiometric oxygen required for complete oxidation of the solid fuel, there is a reducing environment, with char particles acting as reducing agents for the remaining gaseous compounds. Thus, the chemical reactions associated with oxidation and reduction are a combination of homogeneous (gas phase) reactions and heterogeneous (gas-solid) reactions involving char particles. Tables 4 and 5 summarize the reactions occurring in the gasifier along with their rates.

In a gasifier, there are four possible gasification reactions of char, namely with oxygen, hydrogen, steam and carbon dioxide. Usually, the rate of gasification with oxygen is the fastest, followed by gasification with steam, carbon dioxide and hydrogen in that order [4]. The combustion of char with oxygen ($C + O_2 \rightarrow CO_2$) is one of the most exothermic reactions occurring in the gasifier ($\Delta H_R^\circ = -394$ kJ/mol). This heat of reaction is useful in sustaining the pyrolysis and even the char gasification reactions which are primarily endothermic.

In Table 5, ρ_i is the partial density of species i , T is the temperature in kelvin, A_v is the surface to volume ratio of char, M_i is molecular mass of species i in kg/kmol, D_c is the diffusion coefficient, d_c is the diameter of char particles, Re is the Reynolds number, Sc is the Schmidt number, R is the universal gas constant in kJ/kmol-K, P_i

Table 5 Heterogeneous reactions in a gasifier along with their rates

Reaction	Reaction rate	Reference
$C + \frac{1}{2}O_2 \rightarrow CO$	$r_{c1} = \rho_{O_2} A_v \left(\frac{2M_c}{M_{O_2}} \right) \left(\frac{h_{D1} K_1}{h_{D1} + K_1} \right)$ $K_1 = 1.74T \exp \left(-\frac{9 \times 10^3}{T} \right)$ $h_{D1} = \frac{0.8D_c}{d_c} (2 + 1.1Re^{0.6} Sc^{1/3})$	[8]
$C + CO_2 \rightarrow 2CO$	$r_{c2} = 1.3 \times$ $10^8 \exp \left(\frac{-215000}{RT} \right) \left(\frac{P_{CO_2}}{10^5} \right)^{0.38} \times mf_{char}$	[2]
$C + H_2O \rightarrow CO + H_2$	$r_{c3} = 2.62 \times$ $10^8 \exp \left(\frac{-231000}{RT} \right) \left(\frac{P_{H_2O}}{10^5} \right)^{0.57} \times mf_{char}$	[3]
$C + 2H_2 \rightarrow CH_4$	$r_{c4} = \rho_{H_2} A_v \left(\frac{M_c}{2M_{H_2}} \right) \left(\frac{h_{D1} K_2}{h_{D1} + K_2} \right)$ $K_1 = 10^4 T \exp \left(-\frac{21700}{T} \right)$ $h_{D1} = 0.8D_c d_c (2 + 1.1Re^{0.6} Sc^{1/3})$	[47]

Here, ρ_i is the partial density of species i , T is the temperature in kelvin, A_v is the surface to volume ratio of char, M_i is molecular mass of species i in kg/kmol, D_c is the diffusion coefficient, d_c is the diameter of char particles, Re is the Reynolds number, Sc is the Schmidt number, R is the universal gas constant in kJ/kmol-K, P_i is the partial pressure of species i and r_{ci} = reaction rate of reaction i in kg of char consumed per m^3 per second. All the concentrations are in $kmol/m^3$ and reaction rates in $kmol/m^3s$

is the partial pressure of species i and r_{ci} = reaction rate of reaction i in kg of char consumed per m^3 per second. All the concentrations are in $kmol/m^3$ and reaction rates in $kmol/m^3s$. As already highlighted, char is not just pure carbon but also contains hydrogen and oxygen. However, most gasification models assume char to be pure carbon. The char from biomass is usually more porous and reactive than coal char. While the porosity of biomass char is in the range from 40 to 50%, the porosity of coal char is around 2 to 18% (Encinar et al. [12]). Also, the values of reactivity of char from various sources are different. It is generally observed that the reactivity of char from coal decreases with char conversion while that of char from biomass increases. Such a reverse trend for char from biomass is attributed to alkali metal constituents in biomass which have catalytic activity in char reactivity [32].

5 Case Study: Modelling a Downdraft Biomass Gasifier

In this section, a case study of the authors' experience in modelling of downdraft biomass gasifiers is discussed to demonstrate the modelling approaches discussed in this chapter. Firstly, the work of Kumar [20] is presented, which involved the modelling

of a 20 kWe downdraft biomass gasifier using a one-dimensional phenomenological model. This work was subsequently augmented by Kumar [21] to incorporate a radiation model between the hot oxidation zone and the remaining zones. Sutar [43] adapted the model to simulate a 4 kWth downdraft biomass gasifier. Golchha and Jatrelle [16] developed a two-dimensional CFD model for the 20 kWe downdraft biomass gasifier. The following paragraphs summarize the models and experience of the aforementioned work.

5.1 Gasifier Model of Kumar [20]

Kumar [20] developed the phenomenological model of a 20 kWe gasifier at IIT Delhi. The fluid flow through the gasifier was modelled by appropriately accounting for pressure drops in the gasifier and the gas cooling and cleaning systems. The pressure loss coefficients of various components were determined experimentally. The pressure loss in the fuel bed was modelled using the Ergun equation [13], and minor losses were accounted for using standard pressure loss coefficients. Heat transfer in the gasifier was modelled by one-dimensional steady-state heat conduction equation, using an effective thermal conductivity model due to Slavina et al. [40] that correct for the effects of radiation. Drying was modelled using Eq. 1. Kinetic rate of pyrolysis was modelled using Eq. 6, and the rate constant k_{pyr} was taken from Roberts [33] as:

$$k_{\text{pyr}} = 7 \times 10^7 \exp\left(-\frac{1560}{T}\right) \quad (8)$$

Pyrolysis product gas composition was modelled as a mixture of CO, CO₂, H₂, H₂O, methane equivalent (me) (C_{1.16}H₄), tar (C₆H_{6.2}O_{0.2}), and char was modelled as pure carbon. Char fraction was determined from the composition of wood in terms of cellulose, hemicellulose and lignin, and the data from Tillman et al. [45] on char fractions of these substances at the end of pyrolysis. Gas composition was determined from the elemental balances of C, H and O. The three additional equations needed to close the system were obtained from the ratio of CO/CO₂, H₂O/CO₂ and me/CO₂ as a function of temperature, using curve-fits to the data of Boroson [5].

Oxidation was modelled using a heuristic model for oxygen consumption in the order of decreasing affinity for oxygen, followed by water gas shift equilibrium equation at the temperature of the respective control volume. Reduction reactions were modelled using a kinetic model consisting of the fifth reaction in Table 4 (the water gas shift reaction) and the last three reactions listed in Table 5, but using the reaction rate constants recommended by Wang and Kinoshita [46] and Giltrap [15]. Char reactivity factor in each of the reduction reactions was taken to be 1000 as per recommendations of Giltrap [15].

Thermodynamic and transport property data were obtained from handbooks and curve-fitted for use in the model. Each module was individually validated against available references, and the predictions of temperatures and gas compositions were verified against measurements from the same gasifier by Kumar [20]. Figure 3 shows the comparison of measured and predicted temperature profiles and CO and H₂ con-

tent [20], which show a good agreement. These results were also published in Sharma et al. [36].

5.2 Radiation Model of Kumar [21]

Figure 3 shows a temperature profile which has an unusually sharp rise at the beginning of the oxidation zone, which is identified by the location of the tuyeres for air inflow in the model. This is owing to the shortcoming of the effective conductivity model representing the effect of radiation. In order to correct this, Kumar [21] implemented a radiation model in the above simulations. He used the Schuster–Schwarzschild approximation of one-dimensional heat transfer due to radiation [28], also known as the flux method. Here, the entire sphere around any point in a participating medium is divided into two hemispheres, in the positive and negative directions of the one-dimensional coordinate, and the radiant flux to and from both directions is accounted for in the energy balance of the one-dimensional control volume. Kumar [21] assumed that the gas is completely transparent and does not participate in radiation. Thus, he wrote separate energy equations for the gaseous and solid parts of each control volume, and obtained the temperature profiles of both phases separately, while accounting for the heat transfer between the phases. Radiant fluxes, as mentioned above, were taken into account only in the solid phase energy equation. This resulted in a substantial improvement in prediction of temperatures, as illustrated in Fig. 4. Sutar [43] made improvements to the thermodynamic and transport property data of the model and adapted it to predict the temperatures and gas compositions for a 4 kWth gasifier, a much smaller system compared to the one analysed by Kumar [20] and Kumar [21]. He also made measurements of these quantities and compared the predictions with these values. He found that the predictions of temperature were in quite good agreement with measured values, but the gas compositions showed significant variations. This may be due to the smaller size of the gasifier, for which the assumptions on the validity of the equilibrium model for oxidation and kinetic models for pyrolysis and reduction may need to be reviewed.

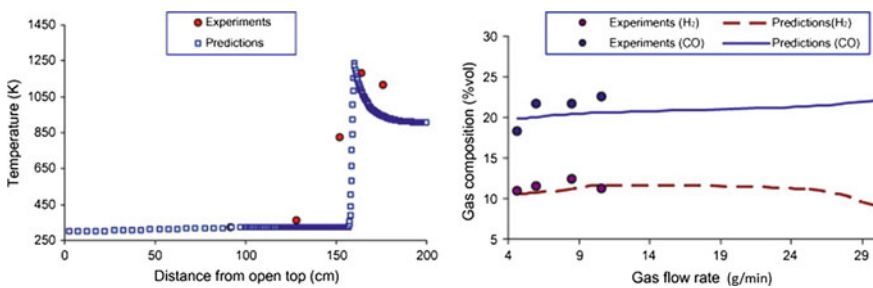
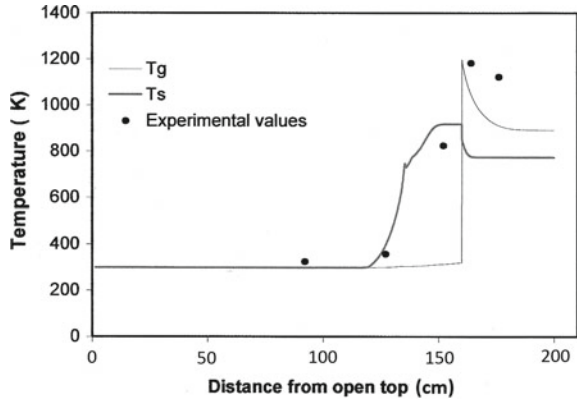


Fig. 3 Comparison of predictions and measurements of Kumar [20]

Fig. 4 Comparison of predictions on Kumar [21] with measurements of Kumar [20]



5.3 CFD Model of Golchha and Jatrelle [16]

Golchha and Jatrelle [16] developed a two-dimensional axisymmetric CFD simulation model using the commercial software ANSYS Fluent for the 20 kW_e downdraft biomass gasifier. The fuel bed was treated as a porous bed with negligible solid velocity. Models for fluid flow and heat transfer were similar to that of Kumar [20] but in the two-dimensional form. Drying, pyrolysis, oxidation and reduction were modelled using the kinetics approach presented in Sect. 4. Table 6 shows the results obtained from the work and its comparison with the range of values from experimental data in the literature. Figure 5 shows the temperature profile along the axis of the gasifier as predicted by the model in comparison with experimental data of Kumar [20]. As can be seen from these results, a good agreement was obtained with experimental data in terms of temperature profiles as well as gas composition.

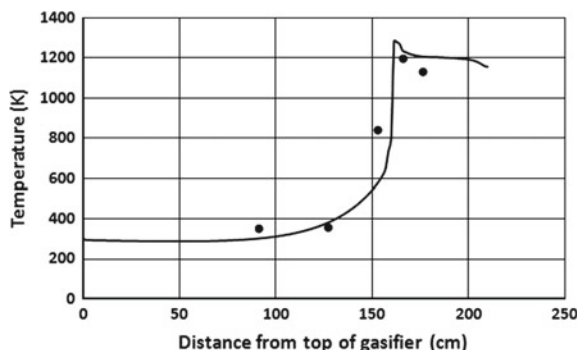
5.4 Discussion

Although a substantial body of literature seems to be available on the phenomena of gasification and their modelling, when one sets out to implement the models pub-

Table 6 Predicted gas compositions Golchha and Jatrelle [16] compared with experimental data from literature

Species	Golchha and Jatrelle [16] (mole fractions %)	Range in literature (mole fractions %)
H ₂	11.6	8–10
CO	19.5	22–25
CH ₄	4.5	3–4

Fig. 5 Temperature profile along gasifier centreline Golchha and Jatrelle [16] and comparison with experimental data Kumar [20]



lished in literature for simulating an existing gasifier, one is faced with several hurdles and inconsistencies. For example, the implementation of pyrolysis model in the work of Kumar [20] and Sharma et al. [37] seemed to be a straightforward one. However, while working on the implementation of the model published by established researchers in the subject, basic inconsistencies were encountered: the proportions of cellulose, hemicellulose and lignin and the respective C-H-O contents did not add up to that of wood used in such publications. Eventually, after an elaborate search in literature for consistent data, the experimental work of Boroson [5] was found helpful in closing the system of equations.

Similarly, when Golchha and Jatrelle [16] set out to model the chemistry of gasification, which also seemed to have been well-researched, they found that none of the sets of apparent rate constants in any one publication in the literature could be directly used. Whenever one tries to verify the rate equations in one publication with its respective cited source, one often encounters errors in units, transcription or typography. It was thus necessary to pick up all available threads in the literature and trace each of them back to their origins in order to get the most consistent set of rate constants for use in the work of Golchha and Jatrelle [16]. Thus, although there is a substantial progress in the understanding of the basic phenomena, there is a lot left to be desired in the literature in terms of correctness of published models or their presentation. Given the fact that the number of publications in every area has increased substantially, it is rather taxing on young researchers to learn not to trust any single work in the literature until it is found (a) to be consistent with its sources and (b) it really works and produces credible predictions when used. Having said this, it is sincerely believed that the rate expressions given in Tables 4 and 5 are correct.

6 Conclusions

Thermochemical conversion of solid fuels into gaseous fuels and its thermodynamics and kinetics formed the subject matter of this chapter. It started with basic intro-

ductions of the processes and technologies and went on to describe what constitutes thermodynamic and kinetic modelling of these phenomena. It also brought out the limitations and restrictions of the different types of modelling approaches in predicting the temperatures, gas compositions and in optimizing desired performance and process parameters. The chapter ended with presentation of a few case studies of modelling downdraft biomass gasifiers using thermodynamic and CFD models, and the difficulties one encounters while implementing such models.

Acknowledgements The contribution of Rishabh Golchha, undergraduate student of Mechanical Engineering, IIT Delhi, in collecting and scrutinizing literature, and in drafting the chapter is gratefully acknowledged.

References

1. Barooah JN, Long VD (1976) Rates of thermal decomposition of some carbonaceous materials in a fluidized bed. *Fuel* 55(2):116–120
2. Barrio M, Hustad J (2008) CO₂ gasification of birch char and the effect of co inhibition on the calculation of chemical kinetics. *Prog Thermochem Biomass Convers* 47
3. Barrio M, Gøbel B, Risnes H, Henriksen UB, Hustad J, Sørensen L (2000) Steam gasification of wood char and the effect of hydrogen inhibition on the chemical kinetics. In: Conference on progress in thermochemical biomass conversion
4. Basu P (2010) Biomass gasification and pyrolysis: practical design and theory. Academic press
5. Boroson ML, Howard JB, Longwell JP, Peters WA (1989) Product yields and kinetics from the vapor phase cracking of wood pyrolysis tars. *AIChE J* 35(1):120–128
6. Boutin O, Lédé J (2001) Use of a concentrated radiation for the determination of cellulose thermal decomposition mechanisms. *Prog Thermochem Biomass Convers* 1034–1045
7. Bradbury AG, Sakai Y, Shafizadeh F (1979) A kinetic model for pyrolysis of cellulose. *J Appl Polym Sci* 23(11):3271–3280
8. Bryden KM, Ragland KW (1996) Numerical modeling of a deep, fixed bed combustor. *Ener Fuels* 10(2):269–275
9. Dasappa S, Mukunda H, Paul P, Rajan NKS (2003) Biomass to energy: the science and technology of the IISc bio-energy systems. 1st ed India, ABETS
10. Deboudi A, Colacio E, Blesa M, Hajjaj L et al (2006) The effect of heating rate on yields and compositions of oil products from esparto pyrolysis. *Int J Ener Res* 30(15):1243–1250
11. Diebold J, Bridgwater A (1997) Overview of fast pyrolysis of biomass for the production of liquid fuels. In: Developments in thermochemical biomass conversion, Springer, pp 5–23
12. Encinar JM, González JF, Rodríguez JJ, Ramiro MJ (2001) Catalysed and uncatalysed steam gasification of eucalyptus char: influence of variables and kinetic study. *Fuel* 80(14):2025–2036
13. Ergun S (1952) Fluid flow through packed columns. *Chem Eng Prog* 48:89–94
14. Font R, Marcilla A, Verdu E, Devesa J (1990) Kinetics of the pyrolysis of almond shells and almond shells impregnated with cobalt dichloride in a fluidized bed reactor and in a pyroprobe 100. *Indust Eng Chem Res* 29(9):1846–1855
15. Giltrap D, McKibbin R, Barnes G (2003) A steady state model of gas-char reactions in a downdraft biomass gasifier. *Solar Ener* 74(1):85–91
16. Golchha R, Jatrele T (2017) CFD simulation of a downdraft gasifier and its experimental validation. B. Tech. Dissertation, Mechanical engineering, IIT Delhi, New Delhi
17. Hailwood A, Horrobin S (1946) Absorption of water by polymers: analysis in terms of a simple model. *Trans Faraday Soc* 42:B084–B092

18. Higman C, van der Burgt M (2003) Gasification. Gulf Professional Publishing
19. Kitani O, Hall CW, Wagener K (1989) Biomass handbook. Gordon and Breach Science Publishers
20. Kumar A (2006) Simulation of a biomass gasifier-engine system. PhD thesis, IIT Delhi, New Delhi
21. Kumar VK (2009) Modelling of a biomass gasification system. M. Tech. Dissertation, Mechanical engineering, IIT Delhi, New Delhi
22. Li X, Grace J, Watkinson A, Lim C, Ergdenler A (2001) Equilibrium modeling of gasification: a free energy minimization approach and its application to a circulating fluidized bed coal gasifier. *Fuel* 80(2):195–207
23. Liden A, Berruti F, Scott D (1988) A kinetic model for the production of liquids from the flash pyrolysis of biomass. *Chem Eng Commun* 65(1):207–221
24. Macak J, Malecha J (1978) Mathematical model for the gasification of coal under pressure. *Indust Eng Chem Process Design Dev* 17(1):92–98
25. Mallick D, Mahanta P, Moholkar VS (2017) Co-gasification of coal and biomass blends: chemistry and engineering. *Fuel* 204:106–128
26. McCabe WL, Smith JC, Harriott P (1993) Unit operations of chemical engineering, vol 5. McGraw-Hill New York
27. Min K (1977) Vapor-phase thermal analysis of pyrolysis products from cellulosic materials. *Combust Flame* 30:285–294
28. Modest MF (2003) Radiative heat transfer. Academic Press
29. Nikitin NI (1966) The chemistry of cellulose and wood. Davey Publishers
30. Nolan PF, Brown D, Rothwell E (1973) Gamma-radiographic study of wood combustion. In: Symposium (International) on combustion, Elsevier, vol 14, pp 1143–1150
31. Reed TB (2002) Encyclopedia of biomass thermal conversion: the principles and technology of pyrolysis, gasification & combustion. Biomass Energy Foundation Press
32. Risnes H, Sørensen LH, Hustad J (2001) CO₂ reactivity of chars from wheat, spruce and coal. *Prog Thermochem Biomass Convers* pp 61–72
33. Roberts A (1970) A review of kinetics data for the pyrolysis of wood and related substances. *Combust Flame* 14(2):261–272
34. Schumacher EF (1973) Small is beautiful, vol 90. Harper & Row, New York
35. Shafizadeh F, Chin PP (1977) Thermal deterioration of wood. ACS Publications
36. Sharma AK (2011) Modeling and simulation of a downdraft biomass gasifier 1. model development and validation. *Ener Convers Manag* 52(2):1386–1396
37. Sharma AK, Ravi M, Kohli S (2006) Modeling heat transfer in biomass gasifier. Paper code: HMT-2006-C184. In: Proceedings of 18th National and 7th ISHMT-ASME, Heat transfer conference, p 315
38. Simpson WT (1993) Determination and use of moisture diffusion coefficient to characterize drying of northern red oak (*quercus rubra*). *Wood Sci Technol* 27(6):409–420
39. Simpson WT (2007) Predicting equilibrium moisture content of wood by mathematical models. *Wood Fiber Sci* 5(1):41–49
40. Slavin A, Arcas V, Greenhalgh C, Irvine E, Marshall D (2002) Theoretical model for the thermal conductivity of a packed bed of solid spheroids in the presence of a static gas, with no adjustable parameters except at low pressure and temperature. *Int J Heat Mass Trans* 45(20):4151–4161
41. Solomon PR, Serio MA, Suuberg EM (1992) Coal pyrolysis: Experiments, kinetic rates and mechanisms. *Prog Ener Combust Sci* 18(2):133–220
42. Soltes E, Elder T (1981) Pyrolysis. organic chemical from biomass. IS Goldstein Florida, CRC Press
43. Sutar KB (2015) Development of downdraft gasifier cookstoves for domestic application. PhD thesis, IIT Delhi, New Delhi
44. Suyitno, Thoharudin, Suhendra B (2011) Mechanism of the char reduction reaction in a staged gasification: sensitivity of water gas shift reaction. *Int J Eng Technol* 11(2):86–93

45. Tillman D, Rossi A, Kitto W (1981) Wood combustion—principles. Processes and Economics Academic Press, New York
46. Wang Y, Kinoshita C (1993) Kinetic model of biomass gasification. Solar Ener 51(1):19–25
47. Yucel O, Hastaoglu MA (2016) Kinetic modeling and simulation of throated downdraft gasifier. Fuel Process Technol 144:145–154

Gasifiers: Types, Operational Principles, and Commercial Forms

Chanchal Loha, Malay K. Karmakar, Santanu De
and Pradip K. Chatterjee

Abstract Carbonaceous solid materials are converted into gaseous fuel through the gasification process. A limited supply of steam, air, oxygen, or a combination of these serves as gasifying agent. Depending upon the gasifying agent used, the fuel gas will contain mainly hydrogen, carbon monoxide, carbon dioxide, methane, higher hydrocarbons, and nitrogen (if air is used). In gasification, different technologies are used depending upon the requirement. Technologies used for gasification can broadly be classified into four groups; fixed bed or moving bed gasification, fluidized bed gasification, entrained bed gasification, and plasma gasification. In the present chapter, a detail discussion on the design, working principle, merits and demerits of different types of gasifiers are presented. Some of the important commercial gasifiers installed worldwide are also discussed.

Keywords Gasifier • Fixed bed • Fluidized bed • Entrained flow
Commercial gasifiers

C. Loha (✉) · M. K. Karmakar · P. K. Chatterjee
CSIR-Central Mechanical Engineering Research Institute, Durgapur 713209,
West Bengal, India
e-mail: chanchalcmeri@gmail.com

M. K. Karmakar
e-mail: malaycmeri@gmail.com

P. K. Chatterjee
e-mail: pradipcmeri@gmail.com

S. De
Department of Mechanical Engineering, Indian Institute of Technology
Kanpur, Kanpur 208016, India
e-mail: santanu80@gmail.com

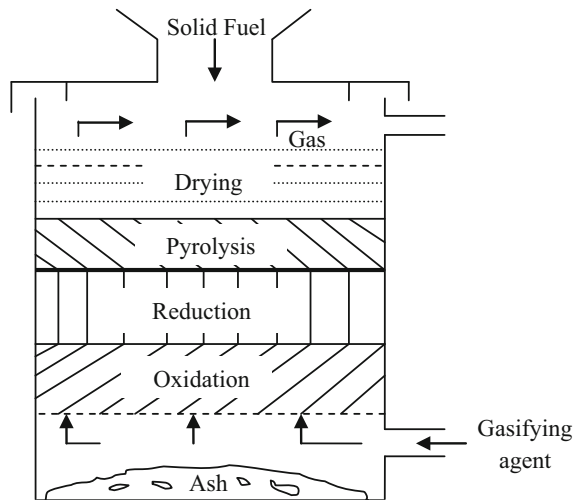
1 Introduction

Gasification is the thermochemical conversion process through which the carbonaceous solid fuels are converted into a gaseous fuel. The gaseous fuel contains hydrogen, carbon monoxide, water vapor, carbon dioxide, methane, nitrogen, and higher hydrocarbons. The gaseous fuel also contains some contaminants like char particle, ash and some higher hydrocarbons, or tar. Gasification is basically a partial oxidation process. The term partial oxidation means that less oxygen is used in gasification than it is required for complete combustion of the same amount of fuel. Gasification generally occurs in a gasifier at an elevated temperature/pressure where a gasifying agent is directly contacted with the carbonaceous material causing a series of chemical reactions to occur that convert the feed to fuel gas and ash/ slag. The heat released by partial oxidation provides the heat required for gasification reactions. A limited supply of steam, oxygen, air, or a combination of these serves as gasifying agent. Gasification with steam or oxygen produces fuel gas with medium to higher calorific value. The gasification with oxygen is not economic, yet because it requires huge investment for production of oxygen. Gasification with steam is snatching more attention in the recent years because it produces fuel gas which contains higher amount of hydrogen, it is capable of maximizing the fuel gas production involving higher heating rate, it has advantageous residence time characteristics, and it is capable of efficient tar and char reduction through steam reforming [1]. On the other hand, the gasification with air dilutes the gas due to the presence of nitrogen in the air. Gasification offers better option compared to more established combustion process to convert carbonaceous solid fuels into electricity and other useful products. With the advancement of gasification technology and its advantageous features will make it an increasingly important part of the world's energy and industrial markets, particularly in clean energy generation. The process of gasification is quite complex which comprises of a series of physical and chemical reactions within the gasifier. In a gasifier, the carbonaceous fuel undergoes different processes and/or reactions. In order to carry out the gasification process, different types of gasifiers could be used. These gasifiers have their own advantages and disadvantages. Different types of gasifiers with their principle of operation, advantages, and disadvantages are discussed below in detail.

2 Fixed Bed Gasifiers

Fixed bed gasifiers are the oldest gasifiers. They are also known as moving bed gasifiers. There are three major kinds of fixed or moving bed gasifiers which are updraft gasifier, downdraft gasifier, and cross-draft gasifier. These names are given based on the directions of the flows of the fuel and the oxidant in the gasifier. Fixed bed gasifiers are suitable for small-scale application up to 10 MW. Therefore, fixed bed gasifiers are mostly used for decentralized power generation using biomass.

Fig. 1 Updraft or countercurrent gasifier [3]



2.1 Updraft Gasifier

Figure 1 shows the schematic diagram of an updraft gasifier. It consists of a fixed bed of carbonaceous fuel through which the gasifying agent flows. Fuel in the form of large particles is loaded into the top of the gasifier. The gasifying agent is introduced at the bottom of the gasifier. The fuel moves slowly from top to the bottom and reacts with the gasifying agent which flows countercurrently upward in the gasifier. Therefore, the updraft gasifier is also called countercurrent gasifier. The basic configuration of an updraft gasifier is similar to the common configuration of a blast furnace. Typical reaction zones of an updraft gasifier are shown in Fig. 1. The fuel moves down through a drying zone where the moisture is removed from the fuel, followed by a pyrolysis zone where volatiles are evaporated from the fuel and char is produced. Water vapor goes upward and leaves the gasifier along with the product gas. Char continues to move downward and gets reduced in the gasification zone and finally it's combusted in the oxidation zone where the gasifying agent is introduced [2]. Because of high temperature (up to 1300 °C) in the oxidation zone, ash is mostly removed as liquid. Here, the risk of ash fusion or solidification of slag is less due to the presence of oxidation zone at the bottom of the reactor which prevents the blockage in the flow path of the reactor when proceeding to the zone with lower temperature. The gaseous pyrolysis products are carried upward by the upward flowing hot gas stream. The product gas from the gasifier consists mainly of the pyrolysis products and the gaseous products from char reduction and oxidation reactions. The product gas passes over a relatively cold drying region before exit. The fuel used for these types of gasifiers must have high mechanical strength and should form a porous bed. The thermal efficiency of this type of gasifier is high but the throughput is relatively low. As the pyrolysis product passes over a relatively cold drying zone but not through the

high-temperature oxidation zone, the exit gas temperature is relatively low. Due to relatively low gas temperature, the production of tar ($\sim 50 \text{ g/Nm}^3$) is significant from these types of gasifiers.

Advantages

- Effective heat transfer due to countercurrent flow
- Can process fuel with high moisture as the product gas dries the wet fuel as it moves downwards
- Less sensitive to the amount of ash in the fuel because the highest temperature is attained at the bottom of the reactor near the ash discharge point [3]
- Less complex fuel preparation is required due to the use of coarse fuel particles
- Product gas leaves the gasifier at relatively low temperature which eliminates the need of expensive high-temperature heat recovery system
- High cold gas efficiency
- High methane content in product gas
- Relatively simple and low-cost process

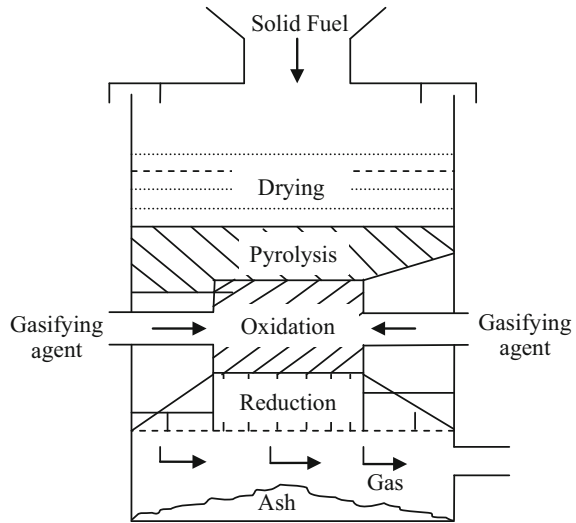
Disadvantages

- Higher amount of tar in the product gas [4]
- Not suitable for scale-up due to the possibility of channeling through the bed which can be dangerous and explosive situations may occur
- Limited ability to handle fines from fuel
- Requires carefully controlled feed size distribution because of long feedstock residence time and slag flow characteristics.

2.2 Downdraft Gasifier

Figure 2 shows the schematic diagram of a downdraft gasifier. Here, the solid fuel is introduced from the top, the gasifying agent is introduced at some intermediate level, and the product gas is taken out from the bottom. As the solid fuel and the gas move in the same direction, the downdraft gasifier is also called co-current gasifier. The product gas leaves the downdraft gasifier at high temperature. Heat from the product gas is generally recovered by preheating the gasifying agent which may result in higher efficiency almost equivalent to the updraft gasifier. Tar which is produced in downdraft gasifier passes through a hot bed of char which converts much of the tar to gaseous product. Typical reaction zones of a downdraft gasifier are shown in Fig. 2. Fuel introduced from the top gets dried in the drying zone. The water vapor produced during drying flows downward and adds to the water vapor formed in the oxidation zone. Some amount of water vapor reacts with the char in the reduction zone and rest leaves the gasifier with the product gas. Then the fuel comes to the pyrolysis zone where char and gaseous species are produced. The pyrolysis products (gas and char) flow downwards into the oxidation zone. As can

Fig. 2 Downdraft or co-current gasifier [3]



be seen from the figure that there is a throat in the oxidation zone where the gasifying agent is introduced and the oxidation reactions take place. The pyrolysis gas and char are partially combusted in the oxidation zone, and a sharp rise in the temperature occurs. The products from the oxidation zone move downward into the reduction zone. In the reduction zone, the gases and char coming from the oxidation zone get reduced and finally a combustible fuel gas is produced. The sensible heat of gases and char provide the heat required for reduction reactions. In downdraft gasifier, the reaction products are thoroughly mixed in the high-temperature turbulent oxidation zone around the throat which helps in tar conversion. Some tar conversion also takes place below the throat on a residual charcoal bed where the gasification process is completed. As a result of tar conversion, tar production in downdraft gasifiers is less than in the case of updraft gasifiers [5]. In these types of gasifiers, the maximum fuel size is limited to the size of the throat. The arrangement of the reaction zones in downdraft gasifier restricts the use of high ash fuel. In this type of gasifier, some of the ash constituents may melt at the high-temperatures oxidation zone which could form bigger lumps upon cooling in the gasification zone. These lumps formation frequently put obstruction to the overall flow of solid and also to the ash discharge at the bottom of the gasifier.

Advantages

- The major advantage of downdraft gasifier is the production of relatively clean gas which contains less amount of tar, ash, and shoot [4]
- The downdraft gasifier is easier to control than the updraft gasifier
- Low sensitivity to the fines from fuel [6]
- Requires minimal tar cleanup from the product gas

- Fuel minerals remain with the char/ash which generally reduce the need for a cyclone separator
- Relatively simple and low-cost process

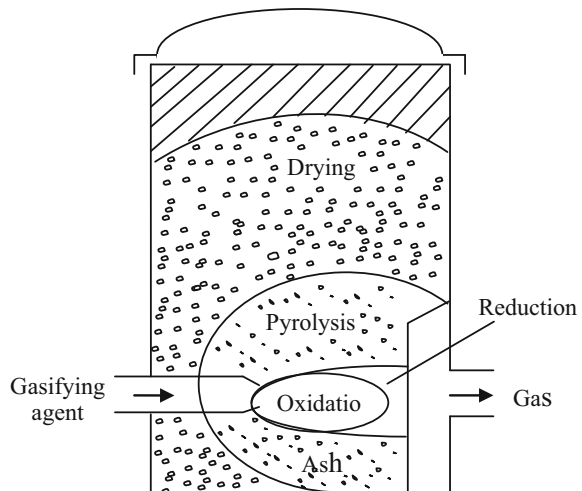
Disadvantages

- Downdraft gasifiers are fuel-specific. Fluffy and low-density materials may create flow problems and also excessive pressure drop [7]
- Fuel needs to be dried to a low moisture content [7]
- It generally suffer from many problems when high ash content fuel is used
- Lower efficiency due to lower carbon conversion and exit of product gas at high temperature (without heat exchanger)
- Impractical for scale-up because it requires to maintain high temperature over a given cross-sectional area (throat).

2.3 Cross-Draft Gasifier

Figure 3 shows the schematic diagram of a cross-draft gasifier. Here, the fuel is introduced from the top of the gasifier. The gasifying agent is introduced from one side of the gasifier, and the product gas is taken out from the other side. The exit of the product gas and the entry of the gasifying agent are kept almost at the same level. As the fuel moves down through the gasifier, it is dried, devolatilized, pyrolyzed, and finally gasified before leaving the gasifier. The oxidation zone is located near the entry of the gasifying agent, and the gasification zone is located near the exit. The pyrolysis zone is located above the oxidation/reduction zone, and the drying zone is located above the pyrolysis zone. In cross-draft gasifier ash bin, oxidation zone and reduction zone are separated which impose the restriction for using different type of fuels. The exit gas temperature in cross-draft gasifier is very

Fig. 3 Cross-draft gasifier [8]



high which has an effect on gas composition like it produces gas with higher carbon monoxide content and low hydrogen and methane content.

Advantages

- Cross-draft gasifiers are compact and can be operated at small scale
- Gas cleaning requirement is less
- Start-up time is much faster compared to downdraft and updraft gasifiers
- The load following ability is quite good due to concentrated high-temperature zone with temperature up to 2000 °C
- Do not need grate because ash falls to the bottom and does not come in the way of normal operation

Disadvantages

- Poor carbon dioxide reduction and high gas velocity
- Requires low ash fuel because of separated ash bin, oxidation, and reduction zones
- High exit gas temperature reduces its thermal efficiency [8]
- Not suitable for scale-up.

3 Fluidized Bed Gasifiers

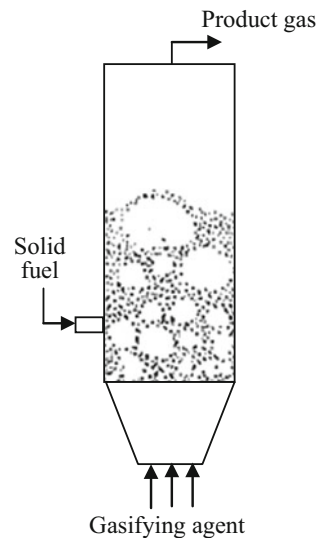
Fluidization is the operation by which a bed of solid particles is transformed into a fluid-like state by the application of gas. The fluidized bed system requires the feedstock to be finely ground into small particles, and the gasifying/fluidizing gases are introduced through a distributor plate near the bottom of the reactor. In fluidized bed gasifier drying, pyrolysis, oxidation, and reduction zones are not apparent at any specific region of the gasifier like in fixed bed gasifiers. These processes occur in the entire gasifier, and thus the fluidized bed gasifiers are more homogeneous type of reactors. In a fluidized bed gasifier, the gasifying agent also acts as the fluidizing agent to fluidize the particle bed. The distinct advantages of fluidized bed over fixed bed gasifiers are uniform and controllable temperature due to excellent gas–solid mixing, high carbon conversion rate, low tar production, flexibility in terms of use of different types of fuel, feed rate, particle size, and moisture content [9]. In fluidized bed gasifiers, reaction rates are much faster than in the fixed bed gasifiers because of intimate gas–solid contact and the increased solids surface area resulted from smaller particle size. Because of the aforementioned features, scale-up and operation of the fluidized bed gasifiers are much easier. The fluidized bed gasifiers are designed to be accompanied by a cyclone separator downstream of the gasifier to capture the particles that are entrained by gas and leave the gasifier as a result of the fluidity of the bed and the velocity of the gas rising through the bed. After separation, these particles are either recycled back into the gasifier or removed from the gasifier. Most of the problems associated with the fixed bed gasifiers could

be overcome in fluidized bed gasifiers. Therefore, fluidized bed gasifiers are more popular than fixed bed gasifiers. There are different types of fluidized bed gasifiers like bubbling fluidized bed gasifier, jetting fluidized bed gasifier, circulating fluidized bed gasifier, and dual fluidized bed gasifier. The residence time of fuel particles in fluidized bed gasifiers is generally less than that of fixed bed gasifiers. However, the residence time may be increased by re-circulating the particles again and again like in circulating fluidized bed gasifiers. Fluidized bed gasifiers are suitable for small to medium scale (500 kW to 50 MW) application. Although the fluidized bed gasifiers are used for gasification of both coal and biomass, but they are becoming more popular for biomass gasification due to lower gasification temperature of biomass compared to coal. Different types of fluidized bed gasifiers are discussed below.

3.1 Bubbling Fluidized Bed Gasifier

Figure 4 presents the schematic diagram of a bubbling fluidized bed gasifier. In a typical reactor with solid particles, when the velocity of fluidizing gas is increased, a situation is reached when the solid particles are just suspended by the upward flowing gas. At this situation, the drag force between particles and fluid counterbalance the weight of particles and the pressure drop between any two points along the height of the bed equals the weight of fluid and particles in that section. At this point, the bed is called to be at minimum fluidization condition and corresponding velocity is called the minimum fluidization velocity. With an increase in velocity beyond the minimum fluidization velocity, bubble formation starts. These small

Fig. 4 Bubbling fluidized bed gasifier [3]



bubbles grow in size while traveling through the bed. On the way up through the bed, bubbles withdraw particles from surroundings and thereby set the particles in motion. On reaching the bed surface, bubbles burst and particles splash into freeboard region [3]. However, the bed of particles does not expand much beyond its volume at minimum fluidization condition. Such a bed is called bubbling fluidized bed. In bubbling fluidized bed gasifier, generally an inert bed material is used where the gasification of fuel takes place. Solid fuel is introduced either from the top of the gasifier on the bed of particles or deep inside the bed. The deeper introduction of the fuel into the gasifier will allow sufficient residence time for fine fuel particles that would otherwise be entrained by the fluidizing gas. In bubbling fluidized bed, the volume flow rate of gasifying/fluidizing agent is such that its velocity is sufficient to suspend the solid particles but not high enough to blow them out from the gasifier. The result is a bed of solids which simulate a boiling action ensuing intimate contact between solid and gas which lead to a uniform temperature distribution inside the gasifier. Solid particles flow rapidly and repeatedly from bottom to top of the bed and back again, while the gas flows up through void space in between solid particles and in the bubbles with higher velocity. Some of the small particles are transported with the gas and leaves the gasifier at the top. A cyclone separator is used to trap these particles that exit from the fluidized bed gasifier, and these particles are either returned to the bed of the gasifier or removed from the system as fly ash. But, most of the fine ash particles fall back to the bed and can be continuously removed from the bottom of the gasifier as bottom ash. In bubbling fluidized bed gasifier, the height of the freeboard region should be enough to restrict bed materials from blown out of the system. The tar production in bubbling fluidized bed gasifier is less than the updraft gasifier but more than the downdraft gasifier. The rate of gasification and the movement of particles in bubbling fluidized bed gasifier largely depend upon the size of fuel particles. With small particles, the gasification process is rapid and it might be complete near the fuel feeding zone before reaching to the center of the bed, resulting in oxygen slip and a void center in the bed. For this reason, fuel feeding is done through multi-feeding points in bubbling fluid bed gasifier. The typical superficial gas velocity in a bubbling fluidized bed is around 1–2 m/s.

Advantages

- Nearly uniform temperature distribution inside the gasifier due to intense gas-particle mixing [10]
- Fuel flexibility and ability to accept wide range of fuel particle size distribution
- Possibility to scale-up
- Ash does not melt due to the lower operating temperature and can easily be removed from the reactor
- Sulfur- and chlorine-containing constituents of the fuel can be absorbed in the inert bed material, thus eliminating the fouling hazard and reducing the maintenance cost
- Load flexibility and high heat transfer rates

- Gives the possibility to use catalyst to increase tar conversion
- Ability to operate with various throughputs with same diameter unit by changing the appropriate bed material

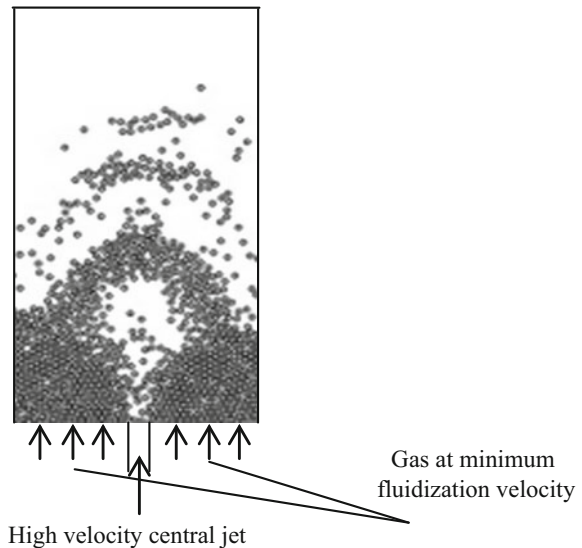
Disadvantages

- Large size bubbles may create problem result of gas bypassing through the bed
- The gasification reactions cannot reach to their chemical equilibrium because of relatively short residence times
- Tar formation is more than downdraft gasifier (without catalyst).

3.2 Jetting Fluidized Bed Gasifier

Figure 5 shows the schematic diagram of a jetting fluidized bed gasifier. It is basically a bubbling fluidized bed with a high-velocity gas jet of gas applied at the center. A part of the fluidizing agent is fed through the center jet and the remaining part is fed to the rest of the inlet with minimum fluidized bed velocity to keep entire bed in fluidized condition. Vertically upward injecting gas jet results in the formation of a bubble plume or a flame-like permanent jet, depending on the properties of bed particles. Presence of a high-velocity jet in the fluidized bed gasifier increases the solid circulation rate which in turn enhances the gas-particle contact resulting in a better carbon conversion in the gasifier [11].

Fig. 5 Jetting fluidized bed gasifier [11]



Advantages

- A high-temperature central region increase the carbon conversion
- Keeps the bed fluidize even with small agglomerates by breaking and re-circulating them [11]
- Higher throughput compared to the bubbling fluidized bed

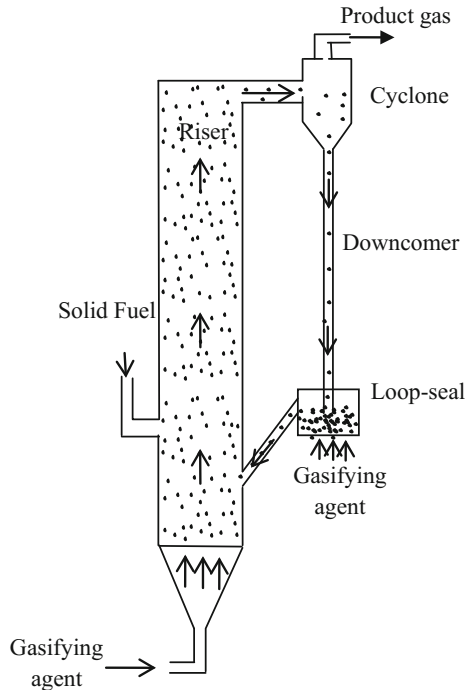
Disadvantages

- Possibility of clinker formation at high temperature
- Overheating at the freeboard zone.

3.3 Circulating Fluidized Bed Gasifier

Figure 6 shows the schematic of a circulating fluidized bed gasifier. Generally, it consists of a high-velocity riser, a cyclone separator, a downcomer, and a loop-seal/L-valve. If the velocity of gasifying agent is increased beyond the bubbling fluidized bed, solid particles are distributed across the whole riser height and most of the particles are entrained by the gas. Particles are separated from the gas with the help of cyclone separator, come down through the loop-seal through the

Fig. 6 Circulating fluidized bed gasifier [3]



downcomer, and return to the bottom of the riser, forming a solids circulation loop. Then it becomes a circulating fluidized bed or fast fluidized bed gasifier. In circulating fluidized bed, particles arrested by cyclone separator are generally fed back to the riser either by using a loop-seal or L-valve. The solid circulation flux is controlled by the gas velocity in the riser and as well as in the loop-seal. The driving force for the solid circulation is the pressure difference in different parts of the circulating fluidized bed system. Higher gas velocity in circulating fluidized bed results in more intense mixing of the gas and particles in the bed which provides excellent gas–solid contact [12]. High relative velocity between the gas and particles also enables it for very high heat and mass transfer rates within the circulating fluidized bed system. Unlike bubbling fluidized bed, there is no distinct separation between dense particle zone and dilute particle zone. The advantage of circulating fluidized bed over bubbling fluidized bed is mainly due to the longer overall residence time. The residence time of solid particles in the circulating fluid bed gasifier is determined by the solids circulation rate, collection efficiency of the solids in the cyclone separator, and the number of circulations. In a circulating fluidized bed gasifier, a fuel particle generally takes 1–10 s to complete one circulation, and thus, the total residence time could be as high as 10,000 s by re-circulating many times [13]. Due to higher gas velocity and recycling of the particles, complete mixing could be achieved regardless of fuel type. Generally, the circulating fluidized bed designs are more flexible but are still limited by the amount of fine particles that can be processed. The typical gas velocity in a circulating fluidized bed may vary from 5 to 10 m/s [14].

Advantages

- High conversion rates due to re-circulation of particles
- Low-quality fuel with high ash, low heating value, high sulfur, and moisture can be utilized
- Throughput is very high [2]
- Suitable for rapid reactions
- High possibility to scale-up of the gasifier
- High heat and mass transport rates are possible
- Low tar production

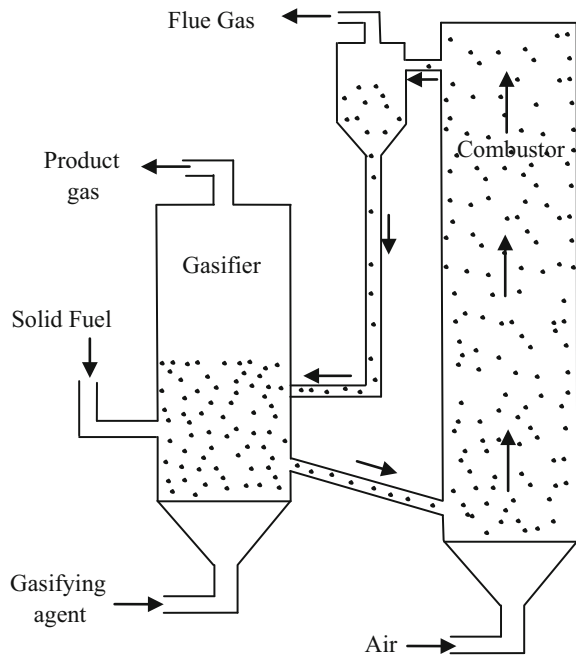
Disadvantages

- Temperature gradients occur in the direction of solid flow
- The size of fuel particles determines minimum transport velocity
- High velocity of particles may result in erosion
- Heat exchange is less efficient compared to a bubbling fluidized bed gasifier [15]
- The high gas velocities and the re-circulation of solids make it more expensive.

3.4 Dual Fluidized Bed Gasifier

Another form of fluidized bed system which is also used for gasification of high volatiles fuel is the dual fluidized bed gasifier as shown in Fig. 7. It consists of two fluidized bed chambers, one is gasification chamber and the other is combustion chamber [16]. The gasification chamber is generally in bubbling fluidized bed condition, and the combustion chamber is in fast fluidized bed condition. In the gasification chamber, the gasifying agent (mostly steam) is brought into contact with the solid fuel to be gasified. There is continuous discharge of bed material with un-reacted char particles from the gasification chamber, which is then fed to combustion chamber generally operated with air where the remaining char is burned and the bed material is heated. Then the hot bed material from the combustion chamber is circulated to the gasification chamber to supply the heat required for the endothermic steam gasification reactions. A controlled amount of excessive fuel may be used to provide sufficient heat required to achieve a particular gasification temperature in the gasification chamber. The gasification with steam produces a hydrogen-rich product gas with higher calorific value compared with that of air gasification [17]. The dual bed gasification technology is especially suitable for gasification of biomass because of higher volatiles content in biomass compared to coal. Here, only the volatile part of biomass is used for the fuel gas production. The fixed carbon is transferred to the combusted chamber where it is combusted to

Fig. 7 Dual fluidized bed gasifier [17]



supply the heat. In this process, the slow gasification reactions of fixed carbon with steam/carbon dioxide could be avoided.

Advantages

- Gasification and combustion reactions are separated
- Nitrogen-free product gas could be obtained without having any air separation unit [18]
- No external heat supply is required even if the gasification is done using steam [17]. Heat required for gasification is supplied from combustion chamber by circulation of hot particles
- Fuel containing high amount of volatiles could be gasified very efficiently
- Possibility to scale-up

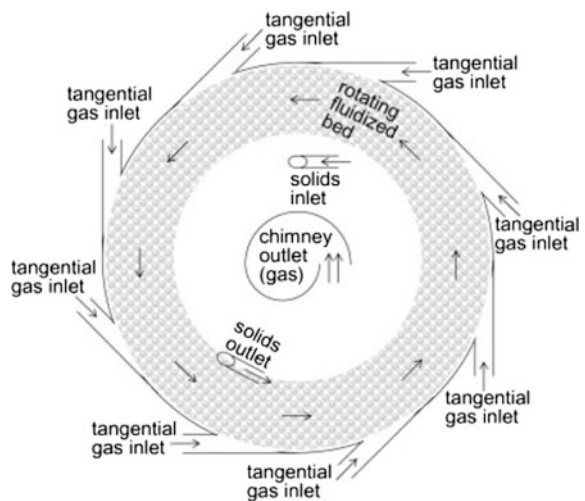
Disadvantages

- Difficult to maintain continuous circulation of particles
- Relatively complex construction makes it expensive
- Difficult to avoid slight gas mixing between two chambers.

3.5 Vortex Chamber Fluidized Bed Gasifier

Figure 8 shows the schematic of a vortex chamber fluidized bed. The shape of the vortex chamber is cylindrical. Gas is inserted tangentially into the chamber through multiple inlet slots located at the periphery of the vortex chamber. Gas leaves the vortex chamber through centrally located chimney. Gas flow inlet and outlet directions are shown in figure. Vortex is formed inside the chamber due to

Fig. 8 Vortex chamber fluidized bed [19]



tangential injection of gas. While particles are injected into the vortex chamber, particles are fluidized and a rotating bed of particles is formed inside the vortex chamber due to the contact of particles and gas. Particles experience a radially outwards centrifugal force due to their rotational motion. Particles also experience a radially inwards gas-particle drag force due to the movement of gas from periphery to the centrally located chimney. When the radially outwards centrifugal force on particles dominates the radially inwards gas-particle drag force, a stable rotating bed of particles is formed against the outer cylindrical wall of the vortex chamber. The value of the centrifugal force is determined by the rotational speed of particle, and its value could be a multiple of earth gravity which allows the vortex chamber fluidized bed to operate at much higher fluidization gas velocities and increased gas–solid slip velocities compared to the conventional fluidized beds [19].

Advantages

- Fluidization at higher slip velocity (1–10 m/s) [20]
- Higher particle loading per unit volume of the reactor
- Shorter residence time
- Enhanced heat and mass transfer
- Very fine particles can be fluidized [21]

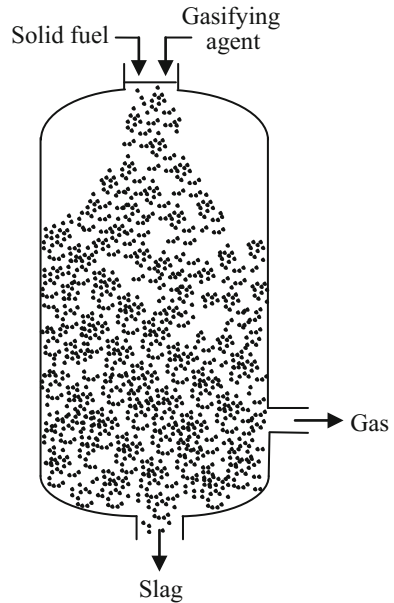
Disadvantages

- High power requirement due to high gas velocity
- High attrition due to high shear in rotating particle bed.

4 Entrained Flow Gasifier

Figure 9 shows the schematic diagram of an entrained flow gasifier. Here, solid fuel and the gasifying agent are fed from the top and they flow co-currently to the gasifier. Very fine fuel particles are required for entrained flow gasifier compared to the fluidized bed gasifiers. Oxygen or air both can be used as the gasifying agent, but most of the commercial plants use oxygen as the gasifying agent. Here, the velocity of gasifying agent is even higher than in circulating fluidized bed gasifier. The small fuel particles are entrained by the gasifying agent, and they flow through the gasifier in a dense cloud. The residence time of particles is very less which requires the entrained flow gasifier to be operated at high temperature (about 1200–1500 °C). High temperature and extremely turbulent flow inside the gasifier cause rapid fuel conversion which also allows high throughput. The gasification reactions occur at a very high rate. Product gas from entrained flow gasifier contains lesser amount of tar and condensable gases due to high-temperature operation. The major part of the ash is removed as slag because the operating temperature of the gasifier is well above the ash fusion temperature. It has the ability to gasify any type of fuels. However, fuels with low moisture and ash content are favored to reduce the oxygen consumption.

Fig. 9 Entrained flow gasifier [3]



Entrained flow gasifiers are suitable for large-scale application (>100 MW). It is a well-researched and developed technology for gasification of fossil fuel like coal, refinery waste. The entrained flow gasification technology has been commercialized in large-scale integrated gasification combined cycle (IGCC) coal power plants. In most cases, the gasifiers are operated under pressure (~20–50 bar) with pure oxygen and with capacities in the order of several hundreds of MW [13]. However, the application of entrained flow gasifiers in biomass gasification is still under development. Most of the integrated gasification combined cycle (IGCC) plants installed worldwide used the entrained flow gasification technology.

Advantages

- High throughput and suitable for high capacities [22]
- High carbon conversion efficiency
- High-quality product gas
- Low tar yield due to high-temperature operation
- Short residence time

Disadvantages

- Fuel preparation cost is high due to very fine particle size requirement
- More sophisticated reactor design due to high-temperature operation
- Some fuels can form corrosive slag which may damage the inner wall
- Low cold gas efficiency [23]
- Higher amount of gasifying agent requirement.

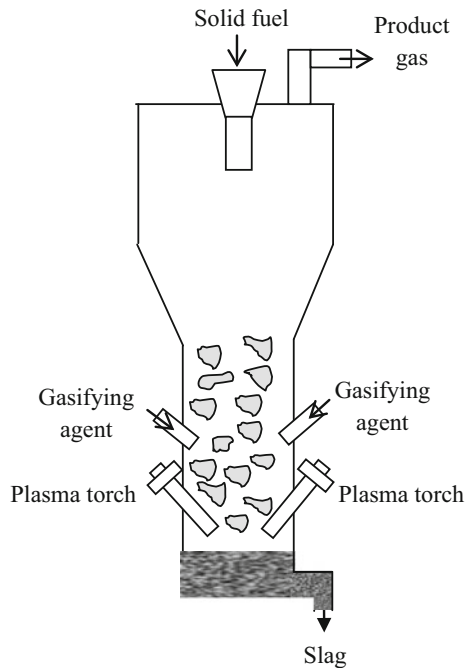
5 Plasma Gasifier

Figure 10 shows the schematic diagram of a typical plasma gasifier. Here, the gasifier is heated by a plasma system (plasma torch or plasma arc) located near the bottom of the gasifier. In the gasifier, the fuel is generally introduced from the top of the gasifier and it passes through the plasma zone. Gasifying agent is introduced near the plasma system and work as ionized gas. Gasification takes place at very high temperatures driven by the plasma system [24]. The high operating temperature breaks down the fuel into their respective elemental constituents which significantly increases the rate of the various reactions occurring in the gasification zone and also helps to converts all organic materials into a fuel gas. The gas is taken out from the top of the gasifier. Any residual material from inorganic constituents of the fuel is melted and produces a vitrified slag.

Advantages

- Hazardous and toxic materials like municipal solid waste, hospital waste can safely be gasified [25]
- Waste material can be fed without prior segregation
- Greatly reduce the waste volume
- Produce stable slag which is highly resistant to leaching

Fig. 10 Plasma gasifier



Disadvantages

- Highly energy consuming process
- High capital cost
- Net energy production is small or sometimes negative.

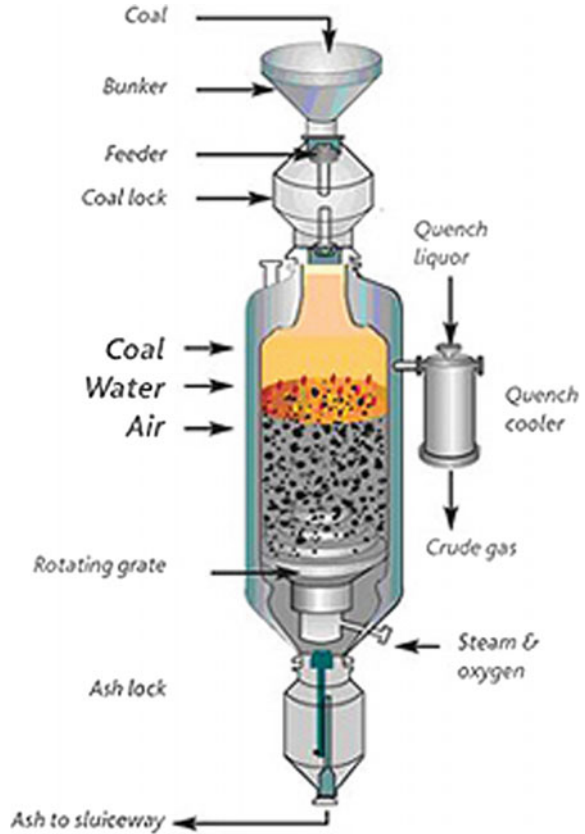
6 Commercial Gasifiers

Gasification is a century-old technology which flourished before and during World War II. After World War II, the gasification technology was largely abandoned due to the ready availability of liquid fuels at reasonable cost. Thereafter, the interest in gasification technology has undergone many ups and downs, driven by energy and chemical markets, and geopolitical forces. The first commercial-scale coal gasification technology was established in South Africa in 1955 for the production of coal-to-liquids. During the 1970s, the thrust was given in the USA for the development of coal gasification technology to generate energy from domestic coal and to reduce the reliance on imported oil. The growth of gasification technology continues from 1980s to 1990s with the installation of coal-to-natural-gas plants and integrated gasification combined cycle (IGCC) plants in USA, Europe, Japan, and China. The projects on development gasification technology for production of cleaner energy from coal were accelerated rapidly in the early 2000s because the energy prices continued to increase very rapidly. Thereafter, the projects on the development of coal gasification technology in USA slowed down significantly with the drop in natural gas prices as well as the utilization of shale gas resources. However, up to the early 2010s, the development of coal gasification technology continues in China to feed its industrialization-driven demand for chemicals. Recently, the growth in the coal gasification industry has in general slowed down throughout the world and there is renewed interest in biomass gasification technology due to increased environmental concerns of using fossil fuels along with their availability and price. In the present paragraph, some of the important commercial gasifiers installed worldwide are presented below.

LURGI Gasifier

LURGI gasifier is the first and most widely used commercial fixed bed gasifier. The Lurgi process was developed in two directions. In one direction, the pilot plant was built to carry out the gasification at pressures up to 100 bar. By increasing the pressure, the methane content of the gas was increased from 9 to 17 vol% and the thermal efficiency of the process was increased from 80 to 85%, while the amount of converted coal also roughly doubled. Another development of the Lurgi process is the slagging gasifier technology. Figure 11 shows the schematic diagram of a Lurgi slagging gasifier [26]. Here, coal is used as the fuel and steam and oxygen are used as the gasifying medium. Coal is introduced at the top of the gasifier through a lock hopper. From the lock hopper, coal is fed to the gasifier via a rotary distributor. The gasifying agent is introduced from the bottom, and the produced fuel gas leaves

Fig. 11 LURGI slagging gasifier [26]



the gasifier around 500 °C. The fuel gas leaving the gasifier is cooled and quenched to condense tar and oil. In order to cool the gasifier, a water jacket is provided inside the gasifier which also produces some amount of steam used in the gasifier. Thus, the steam consumption can greatly be reduced. The temperature at the bottom of the gasifier is approximately 2000 °C. Thus, ash is removed in the form of slag and it is removed in molten state. Therefore, another advantage is that the material obtained by cooling the molten slag immobilized heavy metals and other pollutants in its matrix, thus its disposal is less problematic [27].

High-Temperature Winkler (HTW) Gasifier

High-temperature winkler (HTW) gasifier is an improved version of the original Winkler gasifier. The HTW gasifier is a pressurized circulating fluidized bed gasifier which can gasify a wide range of fuels like coal and biomass. The schematic of a typical HTW gasifier is shown in Fig. 12. Fuel is pressurized in a lock hopper and then stored in a charge bin. Fuel is fed to the gasifier either through a gravity pipe or through a screw feeder. Air or oxygen and steam are used as the gasifying agent, which are injected into the gasifier through separate nozzles. The

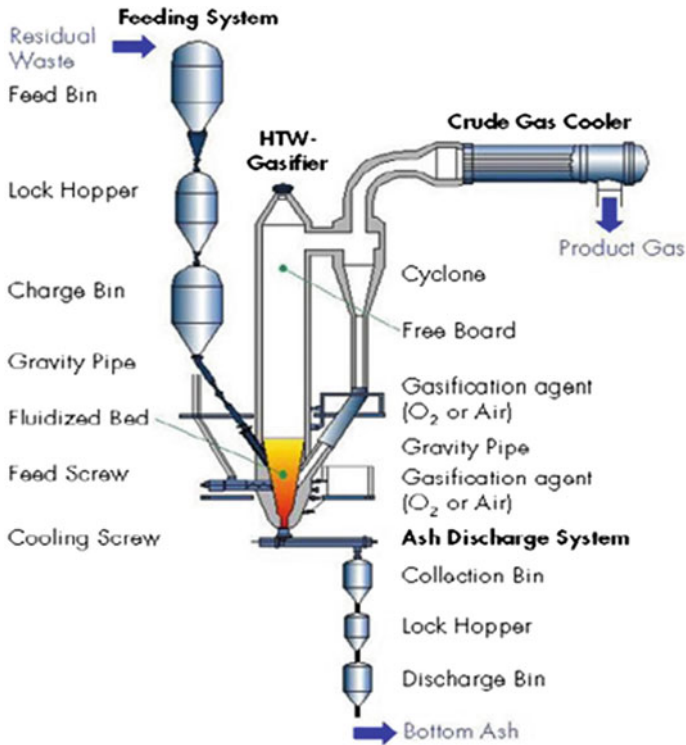


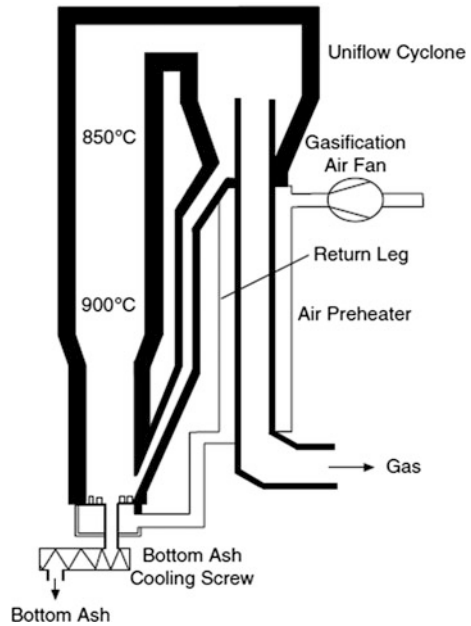
Fig. 12 Winkler gasifier [28]

nozzles are arranged in several levels which are located in both the fluidized bed region and the freeboard region. The purpose of injecting the gasifying agent at the freeboard is to improve the gas quality and the conversion rate by increasing the temperature. The gasifier is operated at about 10 bar pressure. The temperature at the bed is 800–1000 °C, and at the freeboard is 900–1200 °C [28]. There are two temperature zones which exist of about 800 °C. The temperature is maintained below the ash-softening point to avoid particle agglomeration. Fine ash and char particles entrained by the fuel gas are removed through cyclone separator. The solid particles removed from the gas in the cyclone separator are recirculated to the gasifier in order to maximize the carbon conversion. The fuel gas exits from the gasifier at high temperature and does not contain any higher hydrocarbons like tar. Ash is removed from the bottom of the gasifier by means of an ash discharge system which generally consists of an ash screw, lock hopper, and discharge bin. The key advantage of this technology is that it can also gasify low-rank coals with a higher ash-softening temperature.

FOSTER WHEELER Atmospheric CFB Gasifier

It is an atmospheric pressure circulating fluidized bed gasifier as shown in Fig. 13 [29]. The reactor is refractory-lined reactor. Air is used as the gasifying agent.

Fig. 13 FOSTER
WHEELER atmospheric CFB
gasifier [29]



Depending upon the fuel and the application, the operating temperature in the gasifier varies from 800 to 1000 °C. Fuel is fed into the gasifier above certain distance from the distributor plate. Fuel undergoes gasification and produces fuel gas and char. Big char particle flows down to the more dense bed in the riser, and small char particles flow up together with gas. These smaller particles are separated by cyclone separator and return to the bottom of the riser. Ash is collected from the bottom.

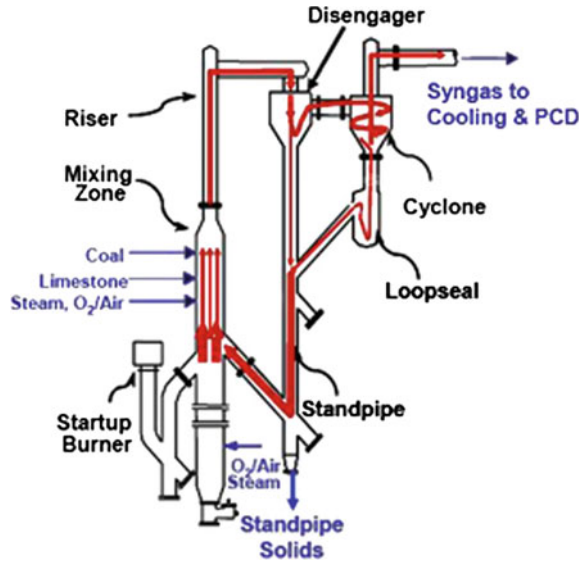
Kellogg, Brown, and Root (KBR) Transport Gasifier

KBR transport gasifier is basically a circulating fluidized bed gasifier which consists of mixing zone, riser, disengager, cyclone separator, loop-seal, standpipe, and J-leg [30]. A typical KBR CFB gasifier is shown schematically in Fig. 14. Steam and air/oxygen are used as the gasifying agent. The gasifying agent is introduced at lower mixing zone as well as at upper mixing zone. Fuel is introduced at the upper mixing zone and reacts with the gasifying agent to produce fuel gas. The gas and solids move up through the riser and enter the disengager. In disengager, larger particles are separated from gas by gravity. Most of the particles are separated at the disengager and remaining particles are separated in the cyclone separator. Particles separated at disengager directly come to the standpipe while particles separated at cyclone come to the standpipe via loop-seal. These particles are recycled back to the gasifier through the J-leg.

MILENA Gasifier

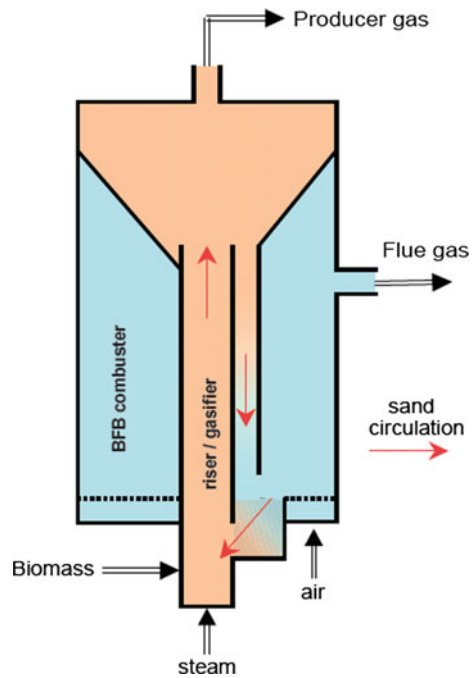
Energy Research Centre of the Netherland (ECN) developed the MILENA gasification process to convert solid biomass into gas that can be used in gas engine/gas

Fig. 14 KBR CFB gasifier [30]



turbine/fuel cell after purification [31]. The MILENA gasification process is shown schematically in Fig. 15. It consists of two integrated reactors; riser/gasifier and the bubbling fluidized bed combustor. Biomass is injected at the riser/gasifier, and it is

Fig. 15 MILENA gasifier [3]

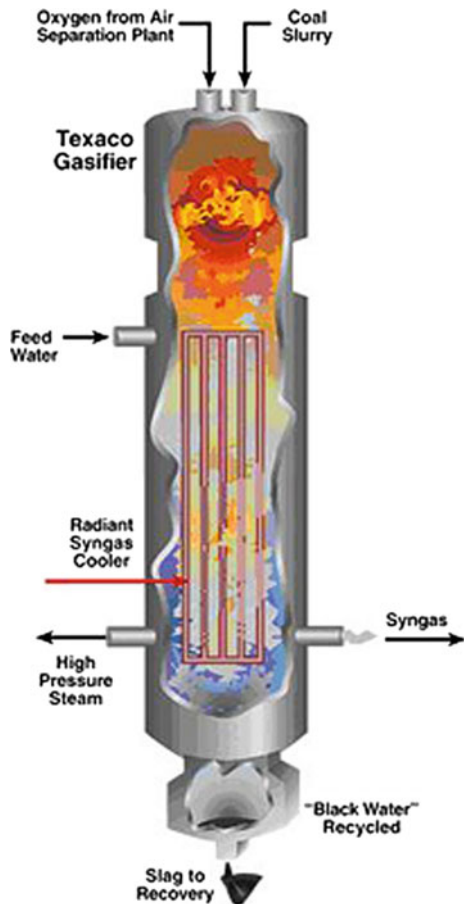


gasified by using steam. Biomass is converted into fuel gas and char. Most of the char is separated from the fuel gas and falls down in the combustor. Remaining fine char particles are entrained by the fuel gas and left with the fuel gas from the top of the riser/gasifier. Air is used in the combustor to burn the char. The flue gas produced and remaining ash leave the combustor bed from a side port. The heat required for the endothermic gasification reactions in the riser/gasifier is provided by transferring hot bed material from the combustor through the opening between riser/gasifier and combustor at the bottom. Here, the yield of hydrocarbons in the product gas is generally high like the CH₄ concentration could reach more than 12 vol.%. Higher amount of hydrocarbons in the product gas has a positive effect on the efficiency. Therefore, the higher cold gas efficiency (79–82%) could be achieved.

GE ENERGY Gasifier

GE ENERGY gasifier is a single stage, downward-feed, entrained flow gasifier developed to generate fuel gas from coal/water slurry [32] as shown in Fig. 16.

Fig. 16 GE ENERGY gasifier [32]

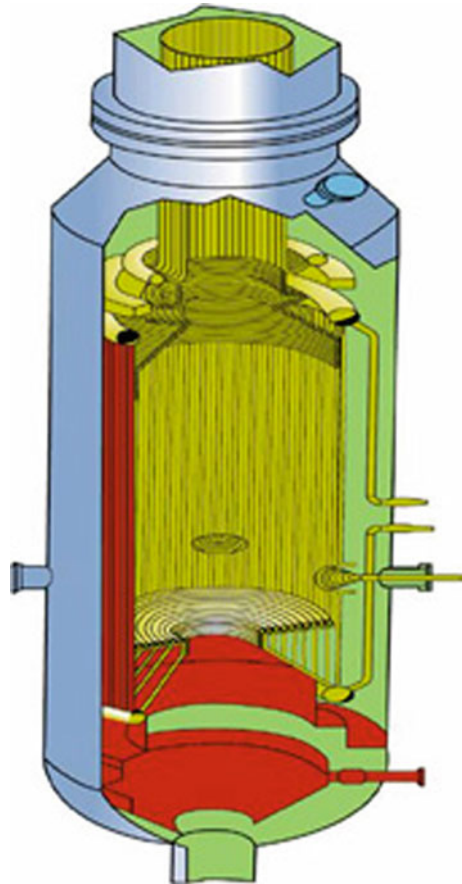


However, the gasifier is also operated with wide range of fuel like natural gas, heavy oil, coal, and petcoke. Oxygen is used as the gasifying agent. Coal slurry and oxygen are introduced from the top of the gasifier. The coal is gasified at high temperature ($\sim 1200\text{--}1500\text{ }^{\circ}\text{C}$) and pressure ($>2\text{ MPa}$) and produces fuel gas and slag. The product gas mostly contains hydrogen (H_2) and carbon monoxide (CO). No hydrocarbon liquids are produced in this high temperature. Syngas is cooled using a radiant syngas cooling system before leaving the gasifier, and high-pressure steam is generated. Slag is quenched in a water pool located at the bottom and removed from the gasifier through a lock hopper. Fine particulate matter and char are collected from the fuel gas and recycled back to the gasifier.

SHELL Gasifier

Shell coal gasification process (SCGP) uses entrained flow gasifier which can operate with wide variety of fuels like coal, petcoke, and biomass [33]. The configuration of a typical SHELL gasifier is shown in Fig. 17. Here, pulverized coal is

Fig. 17 SHELL gasifier [33]



used as the fuel and mixture of oxygen, and steam is used as the gasifying agent. Coal is introduced through pressurized lock hoppers. Coal reacts with oxygen at about 1500–1600 °C temperature and pressure around 2.4–4.0 MPa to produce syngas which consists only small amounts of carbon dioxide. Inside the gasifier, refractory line with water/steam tube membrane wall is used which can produce steam required for gasification. Ash is converted into molten slag which is vitrified due to cooling and forms a protective layer against the refractory. Produced

Table 1 Commercial gasifiers installed worldwide

Country	Type of gasifier	Capacity	Plant/project name
USA	Downdraft	1 MW	CLEW
	Downdraft	40 KW	Stwalley Engg.
	Lurgi	1900.3 MW	Great Plains Synfuels Plants
	GE ENERGY	1150 MW	Edwardsport IGCC
Canada	SHELL	1025 MW	Long Lake Intergated Upgrading Project
Germany	SHELL	984.3 MW	Leuna Methanol Plant
Italy	GE ENERGY	1300 MW	SARLUX IGCC Project
	GE ENERGY	1203 MW	ISAB Energy IGCC Project
South Africa	Lurgi	7048 MW	Sasol Synfuels II (West)
	Lurgi	7048 MW	Sasol Synfuels II (Eest)
Austria	CFB	10 MW	Zeltweg BioCoComb Project
	Dual CFB	8 MW	Gussing
	CFB	35 MW	Pols Bark Gasification Project
Finland	FOSTER WHEELER CFB	60 MW	Lathi Kymijarvi Project
	FOSTER WHEELER CFB	65 MW	ECOGAS Energy Plant Varkaus
India	Downdraft	8 MW	Balamurugan Chemical Pvt. Ltd
	Downdraft	1.5 MW	BMC Pvt. Ltd.
	Downdraft	1.8 MW	ITC Ltd
	Downdraft	1.05 MW	Acclaim Technology Services
	Downdraft	1 MW	Gomathy, Arashi
	Downdraft	600 kW	Sri Sasthaa Energy Pvt. Ltd.
Brazil	CFB	32 MW	Brazillian BIG-GT Plant
Malaysia	SHELL	1032.4	Bintulu GTL Plant
China	GE ENERGY	1750	Shenhua Baotou Coal-to-Olefins Plant
	GE ENERGY	1167	Sanwei Neimenggu Mechnol Plant
	SHELL	1124	Tianjin Chemical Plant
	SHELL	861	Shenhua Erdos
	SHELL	3373	Inner Mongolia Chemical Plant

slag flows down the reactor and collected into a water bath where it is removed through a lock hopper arrangement. The syngas which leaves the gasifier at relatively high temperature is utilized to produce superheated steam. Most of the fly ash entrained by syngas is removed by cyclone separator or commercial filters. The bottom ash is captured with a wet scrubber.

Some of the large gasification projects from different countries in the world based on the above-gasification technologies are listed in Table 1. However, there are many other commercial gasifiers which also exists.

7 Future Scope of R&D

Based on the operation of different gasifiers and future trend, some of the important areas are identified in the following section which may be of prime interest for future R&D work in this filed.

- The design of low tar gasifiers could be a major area of research interest which needs to be explored further. If the amount of tar in the product gas coming out from the gasifier is low, it will reduce the load on the gas cleaning system as well as it will reduce the maintenance requirement and shelf life of the sophisticated downstream application systems.
- A fundamental problem related to the design of the gasifier is the high degree of empiricism. Most of the design data are limited to the experience acquired during operation. There are very few attempts to find a rational and theoretical basis for selection of the various dimensions required to fabricate a gasifier. Thus, the development of engineering design methods for gasifiers should form an important topic for further R&D studies.
- The supercritical water gasification could be a future technology which can convert coal/biomass to hydrogen-rich gas efficiently and in a cleaner way. The properties of supercritical water such as low viscosity, low dielectric constant, and high diffusivity make it an ideal solvent for coal or biomass to take homogeneous reactions.
- The demand for small scale and modular gasifiers for biomass and waste is increasing because they do not require the larger gasifiers like industrial applications. Therefore, the development of modular gasifiers is another future technology which may allow the unit to be moved where the demand exists.
- Development of a gasifier design suitable for low energy density and flaky materials like a variety of loose biomass and its standardization for commercialization needs to be addressed.
- Development of low-temperature non-slagging gasifier will be another interesting work to reduce the plant capital and operating costs.
- The underground coal gasification (UCG), a technology of harnessing the energy of coal without the usual environmental impacts, may probably be the future technology. Though the process exists since the nineteenth century, but it

was not commercially viable. However, the advancement in technology and the rising price of gas are making it feasible for accessing the vast resources of coal that are too deep to mine.

8 Summary

In the above chapter, different types of gasifiers with their operational principle, advantages, and disadvantages are discussed in detail. It is observed that fixed beds gasifiers are simple in construction and easy to operate. They are generally suitable for small-scale application. In fixed bed gasifiers, different reaction zones are separated. Based on the operational principle, it is observed that the updraft gasifiers are best suited for thermal application. In order to use the updraft gasifiers for power generation, excessive gas cleaning is required. But, downdraft gasifiers are suitable for both thermal and power application due to its key advantage of production of gas with low tar content. In fluidized bed gasifiers, uniform temperature is obtained due to intense gas-particle mixing which make them suitable for up-scaling. Large-scale fluidized bed gasifiers are commercially established in many countries. In fluidized bed, bubbling bed gasifiers are comparatively simple, but the carbon conversion rate is low. The carbon conversion rate is increased by re-circulating the particles in circulating fluidized bed. The throughput in circulating fluidized bed gasifiers is high due to rapid carbon conversion resulted from high gas velocity. Dual fluidized bed gasifier is a special type of circulating fluidized bed gasifier which is more suitable for fuels containing high amount of volatiles because here separate chambers are used for gasification and combustion. Entrained flow gasifier is a leading technology for large-scale application, though the requirement of an air separation unit makes it costlier. There are many recent commercial installation of entrained flow gasifier for generating energy from coal. However, this technology is not much explored for biomass gasification. There are also some other types of gasifiers like plasma gasifier and vortex chamber gasifier which are discussed. Plasma gasifier is a relatively new technology which is becoming popular, particularly for environment-friendly disposal of hazardous solid waste.

It is observed from the above discussion that each of the gasifiers has its own merits and demerits. There is no general rule exists for the selection of gasifiers. The selection of a gasifier is primarily done based on fuel type and availability, downstream application of product gas, and scale of application required. However, there are other factors like environmental restriction, capital investment, social acceptance. which may also play major role.

References

1. Loha C, Chatterjee PK, Chattopadhyay H (2011) Performance of fluidized bed steam gasification of biomass— Modeling and experiment. *Energy Convers Manag* 52:1583–1588
2. Bridgwater AV (1995) The technical and economic feasibility of biomass gasification for power generation. *Fuel* 74:631–653
3. Loha C (2013) Studies on fluidized bed gasification of biomass. PhD thesis, Jadavpur University, Kolkata, India
4. Quevedo RAG (2015) Fundamental Kinetic Studies of CO₂ and Steam Gasification. PhD thesis, Graduate program in chemical and petroleum engineering Calgary, Alberta
5. Hein D, Karl J (2006) Conversion of biomass to heat and electricity. In *Energy technologies (Subvolume C: Renewable Energy)*, vol. 3, Chapter 5.2. Springer, Germany, pp 374–413
6. Rajvanshi AK (1986) Biomass gasification. In: *Alternative Energy in Agriculture (Chapter 4 in book)*, vol II. CRC Press, pp 83–102
7. Latif A (1999) A study of the design of fluidized bed reactors for biomass gasification. PhD thesis, Department of Chemical Engineering, University of London
8. Buragohani B, Mahanta P, Moholkar VS (2010) Biomass gasification for decentralized power generation: the Indian perspective. *Renew Sustain Energy Rev* 14:73–92
9. Kunii D, Levenspiel O (1991) *Fluidization engineering*, 2nd edn. Butterworth-Heinemann, Boston
10. Loha C, Chattopadhyay H, Chatterjee PK (2013) Energy generation from fluidized bed gasification of rice husk. *J Renew Sustain Energy* 5:043111–1–10
11. Chatterjee PK (1993) Fluidized bed gasification of coal. PhD Thesis, Mechanical Engineering Department, University of Burdwan, India
12. Pena JAP (2011) Bubbling fluidized bed (BFB), when to use this technology? In: *IASA, Industrial fluidization South Africa, Johannesburg, South Africa*
13. Basu P (2006) *Combustion and gasification in fluidized beds*. CRC Press, Boca Raton, FL, USA
14. Van der Aarsen FG (1985) Fluidized bed wood gasifier—performance and modeling. Dissertation TH Twenty University Publication
15. Babu SP (2006) Thermal gasification of biomass. In: *Workshop No. 1: perspectives on biomass gasification*. IEA Bioenergy Agreement, Task 33. International Energy Agency, Paris, France
16. Xu G, Murakami T, Suda T, Matsuzaw Y, Tani H (2009) Two-stage dual fluidized bed gasification: Its conception and application to biomass. *Fuel Process Technol* 90:137–144
17. Karmakar MK (2010) Thermochemical fluidized bed gasification of biomass. PhD thesis, Department of Chemical Engineering, NIT Durgapur, India
18. Pfeifer C, Koppatz S, Hofbauer H (2011) Steam gasification of various feedstock's at a dual fluidized bed gasifier: impacts of operation conditions and bed materials. *Biomass Conv Biorefin* 1:39–53
19. de Wilde J, de Broqueville A (2007) Rotating fluidized beds in static geometry: experimental proof of concept. *AIChE J* 53:793–810
20. Ekatpure RP, Suryawanshi VU, Heynderickx GJ, de Broqueville A, Marin GB (2011) Experimental investigation of a gas–solid rotating bed reactor with static geometry. *Chem Eng Process* 50:77–84
21. Quevedo J, Pfeffer R, Shen Y, Dave R, Nakamura H, Watano S (2006) Fluidization of nanoagglomerates in a rotating fluidized bed. *A.I.Ch.E J* 52:2401–2412
22. Ramos A, Monteiro E, Silva V, Rouboa A (2018) Co-gasification and recent developments on waste-to-energy conversion: A review. *Renew Sust Eng Rev* 81:380–398
23. Knoef H (ed) (2005) *Handbook on biomass gasification*. In: BTG, Enschede, The Netherlands
24. Messerle VE, Ustimenko AB (2007) Solid fuel plasma gasification. In: *Advanced combustion and aerothermal technologies*. NATO science for peace and security series C. Environmental security pp 141–156

25. Lemmens B, Elslander H, Vanderreydt I, Peys K, Diels L, Oosterlinck M, Joos M (2007) Assessment of plasma gasification of high caloric waste stream. *Waste Manage* 27:1562–1569
26. van de Venter E (2005) Sasol-Lurgi Coal gasification technology and low rank coal. In: Gasification Technologies Council Conference, San Francisco, 10–12 Oct 2005
27. Szechy G, Szebeny I (1995) Development of coal gasification technologies. *Periodica Polytechnica Ser Chem Eng* 39:87–99
28. Toporov D, Abraham R (2015) Gasification of low-rank coal in High temperature Winkler (HTW) process. *J South Afr Inst Min Metall* 115:589–97
29. Granatstein DL (2002) Case study on lahten lampovoima gasification project kymijarvi power station, Lathi, Finland. IEA Bioenergy agreement-Task 36, Nov 2002
30. Smith PV (2005) BR transport gasifier. Gasification Technologies, San Francisco, California 9–12 Oct 2005
31. van der Meijden C, MILENA gasification technology. Energy research Centre of the Netherlands (ECN). <http://www.milenatechnology.com>
32. GE Energy (formerly Chevron Texaco) Gasifier. National Energy Technology Laboratory (NETL). <https://www.netl.doe.gov/research/coal/energy-systems/gasification/gasifipedia/ge>
33. Coal gasification. Converting coal, petroleum coke and biomass into high value products and power. Shell Global Solutions. <https://www.shell.com>

Hydrodynamics of Circulating Fluidized Bed Systems

Malay K. Karmakar, Chanchal Loha, Santanu De and Pradip K. Chatterjee

Abstract Fluidized bed reactors are used in different industries to carry out multiphase chemical reactions. In these reactors, the fluid is passed through the reactor bed having granular solid materials. The velocity of the fluid is kept high enough to suspend these materials resulting to behave them like fluids. Such reactors are classified as bubbling bed, fast circulating bed or dual bed systems combining two beds depending upon the fluid velocities and constructions of the reactors. For combustion and gasification processes, circulating or dual fluidized bed systems are often preferred because they are more efficient having high throughput. However, the hydrodynamics of such fluidized beds, using normally low-grade feedstocks, is very complex and plays a critical role for successful operation of the plant. Lots of experimental and theoretical investigations are done in this area; however, the available information on the hydrodynamics is limited. In this chapter, the hydrodynamics of circulating fluidized bed systems has been discussed.

Keywords Hydrodynamics · Fluidized bed · Circulating · Low-grade feedstock

M. K. Karmakar (✉) · C. Loha · P. K. Chatterjee
CSIR-Central Mechanical Engineering Research Institute, Durgapur 713209,
West Bengal, India
e-mail: malaycmeri@gmail.com

C. Loha
e-mail: chanchalcmeri@gmail.com

P. K. Chatterjee
e-mail: pradipcmeri@gmail.com

S. De
Department of Mechanical Engineering, Indian Institute of Technology Kanpur,
Kanpur 208016, India
e-mail: santanu80@gmail.com

1 Introduction

In fluidized bed systems, the oxidant also acts as the fluidizing agent of the inert bed solids. The fuel is fed near the bottom of the reactor and evenly distributed in the bed. In a bubbling fluidized bed, the gas velocity is kept low. The gas moves through the voids in the bed and forms bubbles in higher bed heights. Some bed particles are entrained into the freeboard from these fast moving bubbles, and part of fly ash is also transported with the gas and leaves the reactor at the top. When the gas velocity is further increased, the solids are distributed along the entire riser height and some of them escape through the exit of riser. The particles are separated in the cyclone and are recirculated to the fluid bed near the bottom through a return leg. This becomes then a circulating fluidized bed (CFB). The advantage of circulating fluidized beds over the bubbling fluidized bed is the longer overall residence time. A fuel particle may take 1–10 s to pass once through the reaction chamber. However, as the particle is likely to recirculate a number of times in the CFB loop, the total residence time could be as high as 10,000 s as given in Basu [1]. The schematic view of bubbling fluidized bed and circulating fluidized bed gasifier is shown in Figs. 1 and 2.

The superficial gas velocity in a bubbling fluidized bed system is kept around 1–2 m/s depending on the particle characteristics. In a circulating fluidized bed system, it may go up to 5–10 m/s typically as given in Van den Aarsen [2]. The solids, in circulating bed systems, not only circulate in the outer loop through the return leg, but there is also internal circulation of the solids in the riser, which fall back from the higher region and move downwards near the riser wall.

The major advantages of fluidized bed gasifiers, as reported by Van den Aarsen [2], are their feedstock flexibility, resulting from easy control of temperature which can be kept below the range of ash melting/fusion point and their ability to deal

Fig. 1 Fluidized bed gasifier

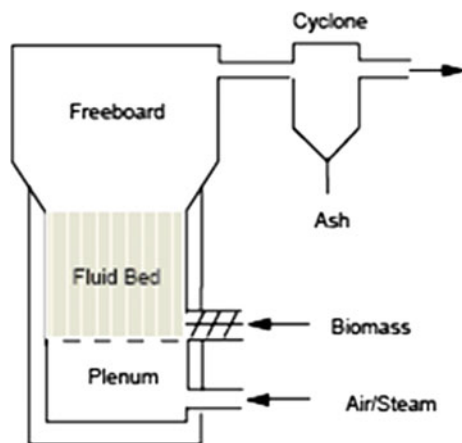
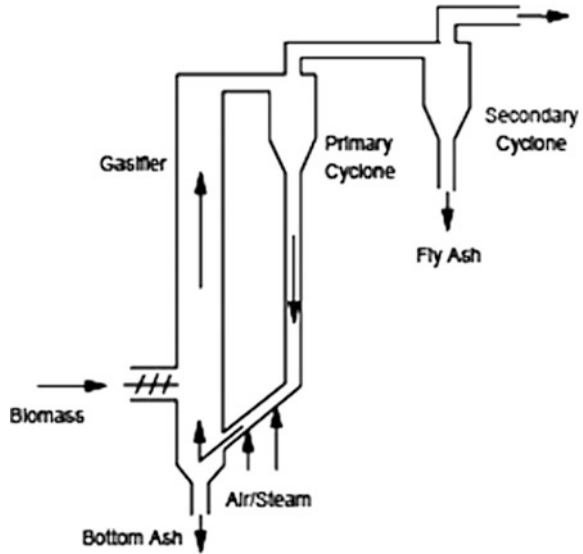


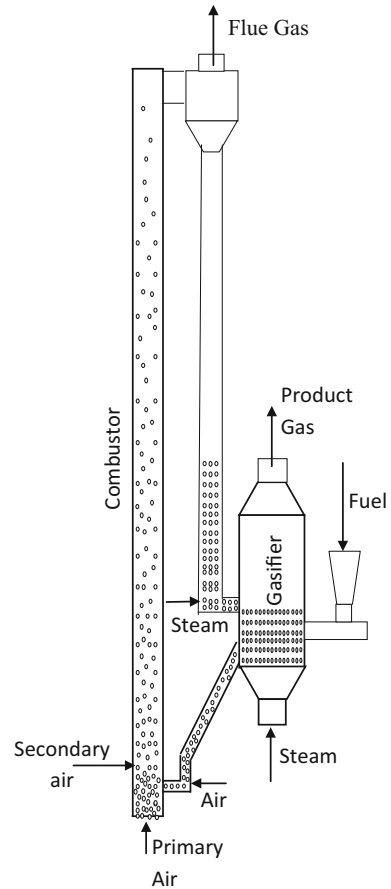
Fig. 2 Circulating fluidized bed gasifier



with fluffy and fine grained materials (in case of sawdust, etc.) without the need of pre-processing. However, problems with feeding, instability of the bed and fly ash sintering in the gas channels may occur with few fuels. Other drawbacks of the fluidized bed gasifiers lie in the tar content of product gas (up to 500 mg/m^3), the incomplete carbon burnout and poor response to load changes. The product gas from fluidized beds suffers from high dust content because of the unrestrained fine fly ash particles. The tar content from fluidized bed gasifiers is less than that from fixed-bed updraft gasifiers but higher compared to the content from fixed-bed downdraft gasifiers.

In case of dual fluidized bed gasifiers, as shown in Fig. 3, the gasifying agent (mostly steam) is the fluidizing gas that is brought into contact with the fuel in first fluid bed. Continuous transfer of bed materials with unreacted char particles from the first fluidized bed takes place to the second fluidized bed. The second bed is operated with air and acts as the combustor to burn the remaining char to get the bed particles heated. Hot bed materials from the second fluidized bed are then circulated back to the first fluidized bed to supply the heat for the endothermic gasification reactions. This technology is especially interesting for biomass gasification due to the higher volatiles content in the biomass compared to coal. Here only the volatiles are used for synthesis gas production. Use of the fixed carbon for conversion into energy gas is renounced; therefore, the slow gasification reactions of fixed carbon with steam or carbon dioxide are avoided. However, the fixed-carbon content is burnt to supply the heat. The dust load from this technology is the same as for all fluidized bed gasifiers but if steam is used in the first fluidized bed, the producer gas is not diluted by nitrogen from the air.

Fig. 3 Dual fluidized bed system



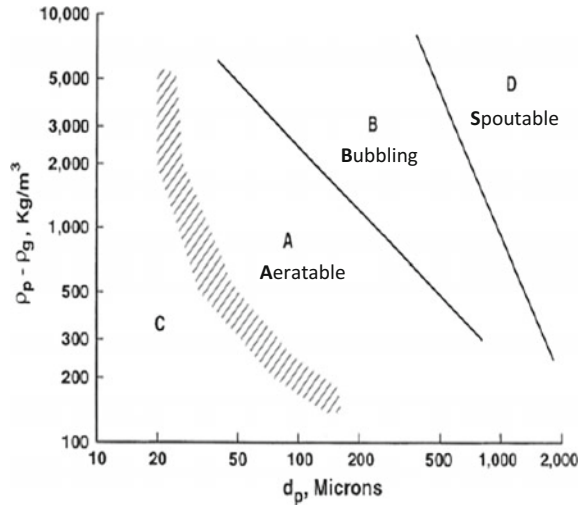
2 Some Definitions

2.1 Bed Particles

Geldart [3] observed the nature of fluidizing particles and categorized his observations by plotting particle diameter against the relative density difference between the fluid and the solid particles. Particle classification or particle types and sizes have very strong influence on the behaviour as well as hydrodynamics of fluidized beds. The observations on particle fluidization character made by Geldart [3, 4] are shown in Fig. 4 in which the characteristics of the four different particles are classified:

- (a) Group A is classified as ‘aeratable’ particles. These materials have small mean diameter ($30 \mu\text{m} < d_p < 100 \mu\text{m}$) and/or low particle density ($< 1.4 \text{ g/cm}^3$).

Fig. 4 Geldart classification of bed particles [3] against density—Geldart [2.44]



This category typically includes fluid cracking catalysts. The solids are fluidized generally at low gas velocities without the formation of bubbles.

- (b) Group B is called ‘sand-like’ particles. The group mostly covers particles having size from 100–1000 μm and density from 1.4 to 4 g/cm^3 . Bubbles in the bed of group B particles are formed when the gas velocity exceeds the minimum fluidization velocity. Typical examples of group B particles are glass beads and coarse sand.
- (c) Group C materials are ‘cohesive’ in nature. These are very fine powders usually less than 30 μm , and they are extremely difficult to fluidize because the particle-to-particle forces are larger compared to those resulting from the action of gas. Typical examples of group C materials are talc, flour and starch. In small beds, group C particles are not easily fluidized due to very high cohesiveness and channeling tends to occur in the bed.
- (d) Group D is ‘spoutable’ type of particles having either large diameters ($d_p > 1000 \mu\text{m}$) or dense. They can not be easily fluidized in deep beds. Generally, a jet is formed in the bed with increased gas velocity and the materials are blown upwards with the jet in a spouting motion. Roasting coffee beans, lead shot and some roasting metal ores are examples of group D materials.

2.2 Minimum Fluidization Velocity

The minimum fluidization velocity is the main criteria required for design and development of fluidized bed reactors. However, in industrial applications, fluidized bed reactors are mostly operated at superficial gas velocities well above the

minimum fluidization velocities, and therefore, the minimum fluidization velocity is not a parameter with a precise significance.

The minimum fluidization velocity is defined as the superficial velocity at which the pressure drop of the gas is equal to the weight of the bed of particles. The minimum fluidization velocity can be measured and it is characteristic of solid particles of a certain density and size. The pressure drop through fixed beds can be correlated by Ergun [5] using the equation:

$$\frac{\Delta P}{L} g_c = 150 \frac{(1 - \varepsilon_m)^2}{\varepsilon_m^3} \frac{\mu_g U_o}{(\phi d_p)^2} + 1.75 \frac{1 - \varepsilon_m}{\varepsilon_m^3} \frac{\rho_g U_o^2}{\phi d_p} \quad (1)$$

where

$$\varepsilon_m = 1 - \frac{M_{bed}}{\rho_s L A_{bed}} \quad (2)$$

The above pressure drop equation represents two factors, the viscous and the kinetic energy losses. At low Reynolds numbers the viscous losses predominate and Eq. (1) becomes:

$$\frac{\Delta P}{L} g_c = 150 \frac{(1 - \varepsilon_m)^2}{\varepsilon_m^3} \frac{\mu_g U_o}{(\phi d_p)^2}, \quad \text{Re}_p = \frac{d_p \rho_g U_o}{\mu_g} < 20 \quad (3)$$

At high Reynolds numbers, only kinetic energy losses need to be considered and thus Eq. (1) becomes:

$$\frac{\Delta P}{L} g_c = 1.75 \frac{1 - \varepsilon_m}{\varepsilon_m^3} \frac{\rho_g U_o^2}{\phi d_p}, \quad \text{Re}_p = \frac{d_p \rho_g U_o}{\mu_g} > 1000 \quad (4)$$

Later on, Agarwal and O' Neill [6] proposed an alternative formula for Eq. (1) which is apparently a valid extension of Ergun equation. Therefore, Eq. (1) can be put into dimensionless form as given below:

$$\frac{\Delta P}{g(\rho_s - \rho_g)(1 - \varepsilon_m)L} = 150 \frac{1 - \varepsilon_m}{\varepsilon_m^3} \frac{\text{Re}_p}{\phi^2 A_r} + \frac{1.75 \text{Re}_p^2}{\phi \varepsilon_m^3 A_r} \quad (5)$$

The onset of fluidization occurs when drag force by upward moving gas equals to weight of particles, i.e.

(ΔP in bed) (Area of bed) = (Volume of bed) (Fraction of solids) (sp. weight of solids)

$$\Delta P \cdot A_{bed} = (A_{bed} L_{mf}) (1 - \varepsilon_{mf}) (\rho_s - \rho_g) \frac{g}{g_c} \quad (6)$$

where

$$\epsilon_{mf} = 1 - \frac{M_{bed}}{\rho_s L_{mf} A_{bed}} \tag{7}$$

By rearranging, we can find for minimum fluidization conditions that

$$\frac{\Delta P}{L_{mf}} = (1 - \epsilon_{mf}) (\rho_s - \rho_g) \frac{g}{g_c} \tag{8}$$

In a bed at onset of fluidization, the voidage (ϵ_{mf}) is slightly more than in a packed bed and it basically represents the maximum expanded position of a packed bed. The superficial velocity of gas at minimum fluidization condition, U_{mf} , is found by combining Eqs. (1) and (8) which gives a quadratic equation of U_{mf} .

$$\frac{1.75}{\phi \epsilon_{mf}^3} \left(\frac{d_p U_{mf} \rho_g}{\mu_g} \right)^2 + \frac{150(1 - \epsilon_{mf})}{\phi^2 \epsilon_{mf}^3} \left(\frac{d_p U_{mf} \rho_g}{\mu_g} \right) = \frac{d_p^3 \rho_g (\rho_s - \rho_g) g}{\mu_g^2} \tag{9}$$

Figure 5 shows the pressure drop versus air velocity for uniformly sized bed materials.

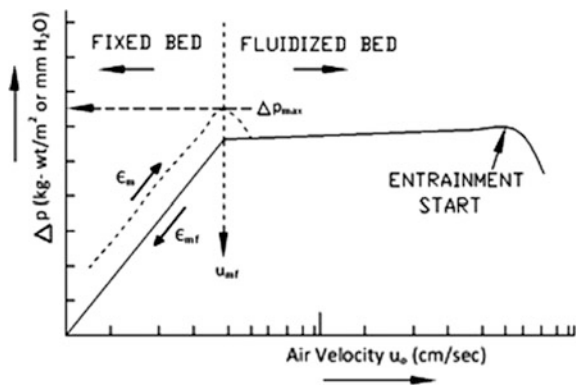
Eq. (9) can also be written as:

$$Re_{mf} = \frac{d_p U_{mf} \rho_g}{\mu_g} = \left[(33.7)^2 + 0.0408 \frac{d_p^3 \rho_g (\rho_s - \rho_g) g}{\mu_g^2} \right]^{\frac{1}{2}} - 33.7 \tag{10}$$

or

$$Re_{mf} = \sqrt{(33.7)^2 + 0.0408 A_r} - 33.7 \tag{11}$$

Fig. 5 Pressure drop versus air velocity for a fluidized bed system, Kunii and Levenspiel [7]



where Re_{mf} is the particle Reynolds number at onset of fluidization. Eq. (11) can also be represented in generic form as:

$$Re_{mf} = \sqrt{C_1^2 + C_2 A_r} - C_1 \quad (12)$$

where C_1 and C_2 are constants having values 33.7 and 0.0408, respectively, and A_r is the Archimedes number, or Galileo number (G_a) in some literature, which is defined by Eq. (13) below:

$$A_r \text{ or } G_a = \frac{d_p^3 \rho_g (\rho_s - \rho_g) g}{\mu_g^2} \quad (13)$$

A tightly packed bed can require a pressure drop greater than the bed weight minus buoyancy to unlock the particles, producing a hump in the pressure drop curve as the velocity increases as shown in Fig. 7. However, decreasing the velocity gradually from the fluidized state avoids the hump leading to hysteresis. Thus, it is better to decrease the velocity for the experimental determination of minimum fluidization.

2.3 Terminal Velocity of Particles

The gas flow rate through a fluidized bed is limited on two factors—the minimum fluidized bed velocity and the entrainment of solids by the gas. When entrainment occurs, these solid particles must be recirculated or supplemented by fresh material to maintain bed inventory for steady-state operation. The maximum gas flow rate is dependent on the terminal or free-fall velocity of the particles as explained by Kunii and Levenspiel [7] which can be estimated from fluid mechanics by:

$$U_t = \left[\frac{4gd_p(\rho_s - \rho_g)}{3\rho_g C_d} \right]^{1/2} \quad (14)$$

where C_d is the experimentally determined drag coefficient.

The terminal velocity U_t , for both spherical and non-spherical particles, can be obtained from Fig. 6 given in Brown et al. [8] on the basis of experimental correlation of the dimensionless groups between $C_d \cdot Re_p^2$ and Re_p , where

$$Re_p = \frac{d_p \cdot \rho_g \cdot U_t}{\mu} \quad (15)$$

and the velocity independent group.

$$C_d \cdot Re_p^2 = \frac{4 \cdot g \cdot d_p^3 \cdot \rho_g (\rho_s - \rho_g)}{3 \cdot \mu^2} \tag{16}$$

To determine U_t , the value of $C_d \cdot Re_p^2$ is obtained from the known values of d_p , ρ_g , ρ_s and μ and then the corresponding value of Re_p is obtained from Fig. 6 from which U_t is calculated using Eq. (15).

The other method of finding the particle terminal velocity U_t for spherical particles uses analytical expressions for the drag coefficient C_d . Unfortunately, no single simple expression can represent the experimental findings in the flow regime of interest. The value of C_d for a particular range of Reynolds number is obtained as follows:

$$C_d = \frac{24}{Re_p} \quad \text{For } Re_p < 0.4 \tag{17}$$

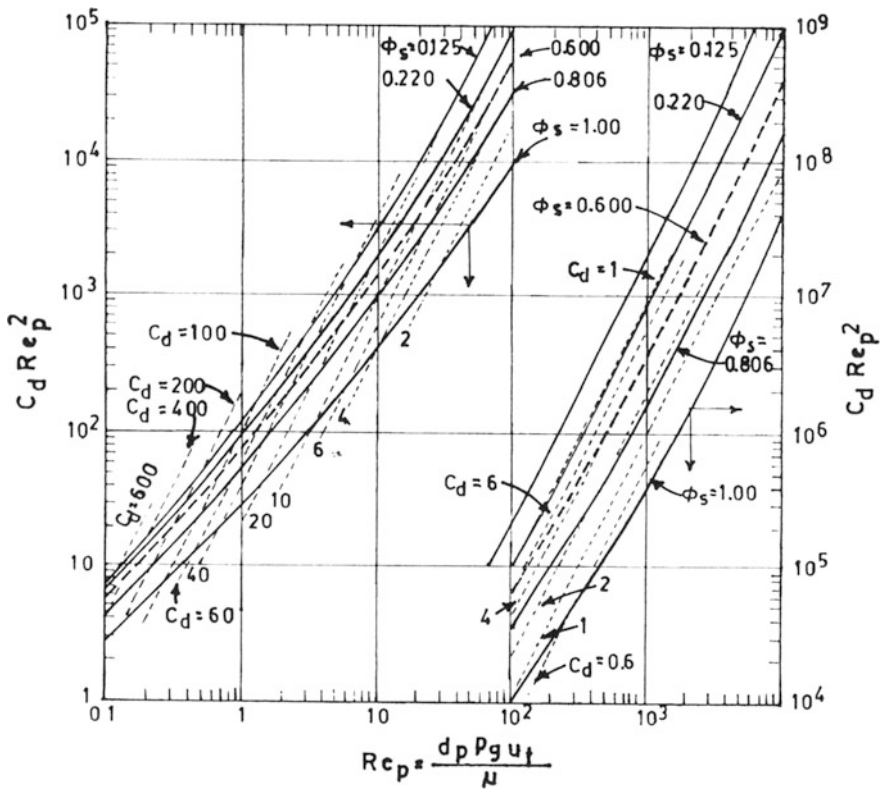


Fig. 6 Chart for determining the terminal velocity of particles falling through fluids, Brown et al. [8]

$$C_d = \frac{10}{\text{Re}_p^{1/2}} \quad \text{For } 0.4 < \text{Re}_p < 500 \quad (18)$$

$$C_d = 0.43 \quad \text{For } 500 < \text{Re}_p < 200,000 \quad (19)$$

The expressions for terminal velocity given by Ryu et al. [9] at different Reynolds number ranges are presented as below:

$$U_t = \frac{g(\rho_s - \rho_g)d_p^2}{18\mu} \quad \text{For } \text{Re}_p < 0.4 \quad (20)$$

$$U_t = \left[\frac{4}{225} \cdot \frac{g(\rho_s - \rho_g)^2 d_p^2}{\rho_g \mu} \right]^{1/3} d_p \quad \text{For } 0.4 < \text{Re}_p < 500 \quad (21)$$

$$U_t = \left[\frac{3.1g(\rho_s - \rho_g)d_p}{\rho_g} \right]^{1/2} \quad \text{For } 500 < \text{Re}_p < 200,000 \quad (22)$$

To control entrainment of solids from a bed, the gas velocity for fluidized bed operations should be maintained between U_{mf} and U_t . In determining U_{mf} , the mean diameter of particles actually present in the bed should be considered; however, in calculation of U_t , the smallest size of particles present in the bed is considered.

3 Theoretical Aspects—Hydrodynamics of Circulating Fluidized Bed System

The fast fluidization is encountered at much higher multiples of the minimum fluidization velocity, perhaps 100 times or more. The momentum flux of the gas is so high that most of the particles in the bed are entrained and drag out of the riser. In order to maintain a steady state in this regime, particles must be introduced into the bottom of the riser at the same rate at which they are being dragged out. Interestingly, such condition causes the bed of particles to disappear into a much more disperse concentration of particles.

In fast fluidized beds, non-uniform behaviour is observed in both axial and lateral directions. There are several models suggested by Bolton and Davidson [10], Rhodes and Getdart [11], Kunii and Levenspiel [12] and Yang [13]. On the basis of these models, the hydrodynamics of the fast beds is discussed and empirical correlations have been presented to analyze the overall distribution of particle suspension densities.

3.1 Riser Voidage—Axial Direction

The lower part of riser operates in turbulent fluidized mode which comprises of two phases, namely, the dense or emulsion phase and the bubble phase. The volume fraction of solids in such bed is obtained by applying modified two phase theory as proposed by Johnsson et al. [14]. The emulsion phase is made by the solid bed particles as well as the interstitial gas flow in bed particles. The gas velocity, U_{mf} , and the voidage, ϵ_{mf} , at minimum fluidizing condition is determined from Ergun [15].

$$U_{mf} = \frac{\mu_g}{d_p \rho_g} \left[\left(33.7^2 + 0.0408 \frac{d_p^3 \rho_g (\rho_s - \rho_g) g}{\mu_g^2} \right)^{\frac{1}{2}} - 33.7 \right] \quad (23)$$

and

$$\frac{\Delta p}{L_{mf}} = (1 - \epsilon_{mf}) (\rho_s - \rho_g) \frac{g}{g_c} \quad (24)$$

The bubble phase consists of gas bubbles flowing upward, assumed to be free of solids. The effective voidage in the bottom zone, ϵ_{dz} , is expressed as follows.

$$\epsilon_{dz} = \delta_b + (1 - \delta_b) \cdot \epsilon_{mf} \quad (25)$$

where δ_b , is the volume fraction of bubbles which can be calculated as:

$$\delta_b = \frac{1}{1 + \frac{1.3(0.15 + U_{pa} - U_{mf})^{0.33}}{0.26 + 0.7 \exp(-3.3d_p)} \cdot (U_{pa} - U_{mf})^{-0.8}} \quad (26)$$

In transport zone, the axial voidage profile is obtained from the exponential correlation from the entrainment model proposed by Zenz and Weil [16].

$$\frac{\epsilon_{Tz} - \epsilon_{\infty}}{\epsilon_{Dz} - \epsilon_{\infty}} = \exp[-a(h_{Tz} - h_{Dz})] \quad (27)$$

where a is the decay factor of solid volume fraction and h_{Tz} is the height of the particular point in transport zone. In the literature, different correlations are available for the decay factor a . Adanez et al. [17] conducted an experiment in a circulating fluidized bed system using sand and coal as bed materials under group B of Geldart classification and proposed the following correlation for determining the decay factor.

$$\alpha(U - U_t)^2 D^{0.6} = 0.88 - 420d_p \quad (28)$$

The extreme upstream voidage in transport section, ε_∞ , in Eq. (3.92), depends on superficial gas velocity, terminal velocity of particle, solid density and elutriation rate, and this voidage at infinity is given in [18] as:

$$(1 - \varepsilon_\infty) = \frac{K_\infty}{\rho_s(U - U_t)} \quad (29)$$

where K_∞ is the particle elutriation rate constant for uniform size particles and is obtained using following correlation as proposed by Wen and Chen [19].

$$K_\infty = \rho_s \alpha_i (U - U_t) \quad (30)$$

where

$$\alpha_i = 1 - \left(1 + \frac{f_s(U - U_t)^2}{2gD} \right)^{-\frac{1}{4.7}} \quad (31)$$

Here, f_s is the coefficient of friction, evaluated from the correlations from Wen and Chen [19].

$$\begin{aligned} \frac{f_s \rho_s}{d_p^2} \left(\frac{\mu_g}{\rho_g} \right)^{2.5} &= 5.17 \left[\frac{\rho_g(U - U_t)d_p}{\mu_g} \right]^{-1.5} D^2 \\ &\text{for } \frac{\rho_g(U - U_t)d_p}{\mu_g} \leq \frac{2.38}{D} \end{aligned} \quad (32)$$

and

$$\begin{aligned} \frac{f_s \rho_s}{d_p^2} \left(\frac{\mu_g}{\rho_g} \right)^{2.5} &= 12.3 \left[\frac{\rho_g(U - U_t)d_p}{\mu_g} \right]^{-2.5} D \\ &\text{for } \frac{\rho_g(U - U_t)d_p}{\mu_g} \geq \frac{2.38}{D} \end{aligned} \quad (33)$$

Wen and Chen [19] recommended Eqs. (30)–(33) considering bed particles diameters in the range of 37–3400 μm and density of 860–7850 kg/m^3 with gas velocity in the range of 0.1–10 m/s in riser having diameters ranges from 0.034 to 2.06 m.

Axial distribution of the average voidage in a fast bed is typically shown in Fig. 7 given in Li et al. [20].

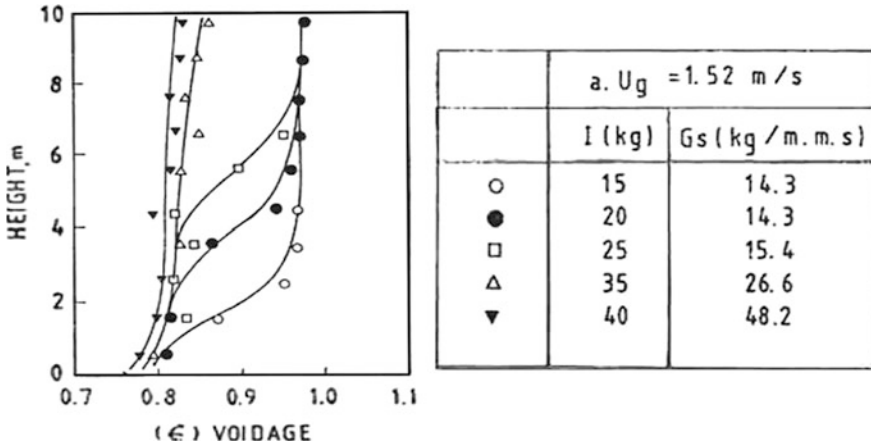


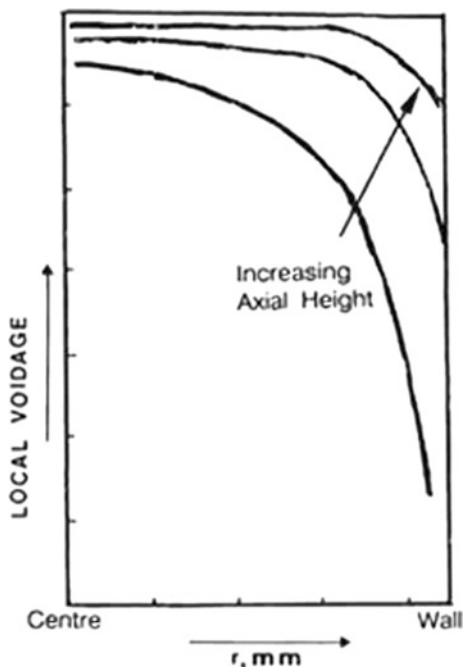
Fig. 7 Axial profile of average bed voidages for FCC particles, Li et al. [20]

3.2 Riser Voidage—Radial Direction

In fast bed riser, the fluidizing gas travels upwards in a plug flow and the velocity near the wall is much lower than that in the core of the bed. The solids move up and down about the bed in the form of clusters and the concentrations of clusters are higher near the wall than near the reactor. However, in very dilute beds of coarse particles, the clusters are less likely to form. In the core, the particles move upwards through a dilute suspension forming occasional clusters. These solids tend to move in radial direction due to hydrodynamic interactions, and upon reaching the low gas velocity wall zone, they experience lower fluid drag, and therefore, the particles start falling. The solids falling near the wall are occasionally picked up in the up flowing gas of the core, resulting their upward journey. These results in two lateral fluxes: one towards the wall and another from the wall. A generalized equation for the lateral flux of solid is yet to be developed [21].

The upward and downward movements of particles in the core and annulus result in an internal circulation in the bed. The area of annular zone decreases along the height of the riser. The voidage along with the velocities of both gas and solid phases change continuously along the axis towards the wall. The voidage is the highest on the axis of column and the lowest on the wall. The radial voidage distribution is much flatter in the upper section of the bed with lower circulation rates [21]. A typical radial void profile in a fast bed is shown in Fig. 8.

Fig. 8 Radial voidage profile across the cross section of riser, Basu and Fraser [21]



3.3 Gas–Solid Slip Velocity

During the bulk motion of gas and solids in fast beds, the slip velocity, U_{slip} , between them is written as

$$U_{slip} = \frac{U}{\varepsilon} - \frac{G_s}{\rho_s(1 - \varepsilon)} \quad (34)$$

In dispersed phase, the solids generally travel upward through the core of the bed and the slip velocity is of the order of terminal velocity of the individual particles. Near the periphery or the walls, the gas velocity is much lower and it even flows downward sometimes. When the solids descend along the wall, they do not have a very high slip velocity. However, this situation does not consider the formation of clusters which move at different velocities and may account for the high mass transfer rate observed in many processes [21].

3.4 Pressure Drop in Riser

The pressure profile in riser is a key parameter and an important characteristic of CFB; The CFB riser is generally divided into two regions: dense turbulent bed zone

and dilute transport zone. Pressure heads for solids suspension, gas–solids friction and particle acceleration are the main factors which contribute the pressure drop in riser.

The riser bottom zone generally has a constant pressure drop, ΔP_{dz} , for a particular bed height, and it is determined by static heads of bed particles. Solids acceleration and deceleration are assumed to compensate each other as well as there is negligible friction forces exist amongst solid particles and particles to wall. Therefore, it is given as follows:

$$\Delta P_{dz} = (1 - \varepsilon_{dz})\rho_s h_{dz}g \quad (35)$$

where h_{dz} is the bed height in dense zone.

In transport zone of riser, the pressure drop is determined from the solids hold up which can be represented by the following formulations.

$$\Delta P_{TZ} = \int_{h_{DZ}}^{h_{TZ}} (1 - \varepsilon(h))\rho_s g dh \quad (36)$$

where $\varepsilon(h)$ can be obtained from Eq. (27)

The pressure drop due to solids friction given in Loffler et al. [18] is as follows:

$$\Delta P_{Tz,fric} = \int_{h_{sz}}^{h_{tz}} f_s \frac{U_s^2}{2} \frac{4}{D} (1 - \varepsilon_{hTZ})\rho_s g dh \quad (37)$$

Since the dilute-phase transport section in riser is considered to behave like a fully developed vertical pneumatic zone, the correlation for estimating particle velocity beyond the acceleration region, developed by Yang [21], may be employed.

$$U_s = U - U_t \sqrt{\left(1 + \frac{f_s U_s^2}{2gD}\right) \varepsilon_{TZ}^{4.7}} \quad (38)$$

where

$$f_s \frac{\varepsilon_{tz}^3}{(1 - \varepsilon_{tz})} = 0.0126 \left[(1 - \varepsilon_{tz}) \frac{U_t}{U_s} \right]^{-0.979}, \quad \text{for } \frac{U_t}{U_s} > 1.5 \quad (39)$$

and

$$f_s \frac{\varepsilon_{tz}^3}{(1 - \varepsilon_{tz})} = 0.0410 \left[(1 - \varepsilon_{tz}) \frac{U_t}{U_s} \right]^{-1.021}, \quad \text{for } \frac{U_t}{U_s} < 1.5 \quad (40)$$

Eqs. (37)–(40) are solved iteratively to evaluate the voidage ε_{tz} , the solid friction factor, f_s , and the solid velocity, U_s .

3.5 Pressure Drop Between Riser Exit and Cyclone Inlet

The pressure drop in horizontal section between riser and cyclone may be considered from Patience et al. [22].

$$\Delta P_{RE} = G_s(2.84 + 0.0108U_h^2) \quad (41)$$

where G_s and U_h are the solid mass flux and the gas velocity in this section, respectively.

3.6 Pressure Drop in Cyclone

The cyclone pressure drop is directly proportional to the square of inlet velocity, and it is employed by the equation given by Gimbut et al. [23].

$$\Delta P_{CYC} = \alpha \frac{\rho_g U_{CYC}^2}{2} \quad (42)$$

where α is a function of cyclone dimension and it is expressed in [3.30] as.

$$\alpha = 16 \frac{a_{CYC} \cdot b_{CYC}}{D_e^2} \quad (43)$$

3.7 Pressure Drop in Downcomer and L-Valve

Determination of gas flow rate and the corresponding pressure drop through the downcomer and L-valve sections of a circulating fluidized bed system is not an easy task [24].

Variations of voidage in downcomer depend on solids flow mode. The solids movement in downcomer is considered to be transitional packed bed flow in presence of aeration flow through L-valves. When these aeration taps are turned off, the solids form a packed bed in the downcomer causing no solids flow. While the aeration flow is on, air flows through the particles and the relative movement between gas and solids produces a drag force on the particles in the direction of flow. This phenomenon was also observed by Zhang and Rudolph [25] that the transitional packed bed flow occurs when the solids flow by aeration.

When the solids in downcomer are in transitional packed bed flow condition, the slip velocity causes to increase the voidage linearly. In this state, the voidage in downcomer is more than compact bed voidage (ϵ_c), but less than voidage at minimum fluidization condition (ϵ_{mf}). Therefore, this voidage above the aeration point is taken as per the correlation given by Tong et al. [26].

$$\epsilon_{DC} = \frac{1}{2}(\epsilon_{mf} + \epsilon_c) \quad (44)$$

Pressure drop due to solids flow by aeration can be expressed by the Ergun [15] equation that is a function of slip velocity suggested by Knowlton and Hirsan [27].

$$\frac{\Delta P_{DC}}{L_{DC}} = \frac{150\mu(1 - \epsilon_{DC})^2 U_{SLDC}}{(\phi d_p)^2 \epsilon_{DC}^3} + \frac{1.75\mu(1 - \epsilon_{DC}) U_{SLDC}^2}{(\phi d_p) \epsilon_{DC}} \quad (45)$$

The slip velocity for gas flowing up the downcomer can be expressed as:

$$U_{SLDC} = \frac{G_s}{\rho_s(1 - \epsilon_{DC})} + \frac{U_{GDC}}{\epsilon_{DC}} \quad (46)$$

The slip velocity for gas flowing down the downcomer can be expressed as:

$$U_{SLDC} = \frac{G_s}{\rho_s(1 - \epsilon_{DC})} - \frac{U_{GDC}}{\epsilon_{DC}} \quad (47)$$

The pressure drop between the aeration point in L-valve and the solids discharge to the fast bed, ΔP_{LV} , can be obtained by solid mass flux (G_s), L-valve diameter (D_{LV}), mean particle size (d_p) and length of valve (L_{LV}) as proposed by Geldart and Jones [28]. The correlation is given as follows:

$$\frac{\Delta P_{LV}}{L_{LV}} = 216 G_s^{0.17} D_{LV}^{-0.63} d_p^{-0.15} \quad (48)$$

3.8 Pressure Loop in CFB System

The position of the point of inflection separating the lean and dense regions of a fast bed is a function of the solid circulation rate and the solids inventory in the system. This effect arises out of the pressure balance around the circulating fluidized bed loop which is explained in Fig. 9 presented by Basu and Fraser [29].

The dense bottom section of the fast bed results in higher pressure drops per unit height of the bed than that in the upper section, which is leaner. For a given bed inventory, the solids are distributed between the bed and the downcomer in such a way that the pressure drops through the two legs of the loop balance each other. The

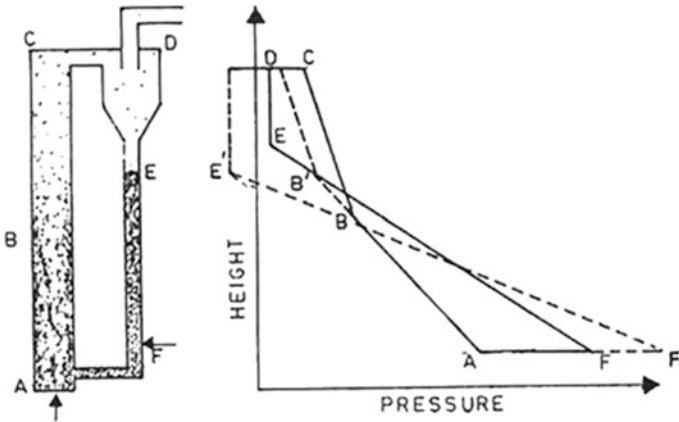


Fig. 9 Pressure balance in CFB loop, dotted line shows the pressure profile at higher circulation rate, Basu and Fraser [29]

pressure drop across the L-valve is proportional to the solid flow rate. The solids flow rate is increased by increasing the aeration flow rate which in turn increases the pressure drop per unit length of the moving packed bed in the downcomer. The pressure drop in the cyclone is proportional to the square of the gas velocity at the entry. The pressure drop across the stand pipe depends on the height of solids in it. For stable operations, the pressure balance around the loop may be written as

$$\Delta P_{F-A} + \Delta P_{A-B} + \Delta P_{B-C} + \Delta P_{C-D} = \Delta P_{D-E} + \Delta P_{E-F} \quad (49)$$

The pressure balance depends on the different operating parameters. The response of the bed to the variations of operating parameters can be estimated from the above equation.

3.9 Solid Recirculation in CFB Loop

The solids circulation rate, G_s , has been determined from the following correlation:

$$G_s = \rho_s (1 - \varepsilon_{Tz}) U_s \quad (50)$$

4 Practical Aspects—Circulating Fluidized Bed System

Conventional bubbling fluidized bed gasifiers are available for small- to-medium scale application, but these systems have low conversion efficiency in addition to other drawbacks. On the other hand, the CFB gasification technology is suitable for

large-scale application which can handle high ash fuels like peat, lignite, etc. The system is more efficient as the fuel conversion ratio is high, and it is also environment friendly. The CFB technology enhances heat and mass transfer, raise reaction rate, strengthen fast pyrolysis, reduction and shift as well as other gas–solid reactions, etc., which make the productivity of the CFBG much higher and gas quality much better than other kinds of air-blown gasifiers. Although it is proven that the CFB technology has many advantages, it is still an emerging technology. It needs more focus on research to facilitate the operational issues for steady-state operation of the plant. The hydrodynamics of such systems is still not fully understood by the researchers.

An important aspect of CFB systems is the ability to control the solid circulation rate and the most important factor that controls the solids circulation rate is the riser gas velocity.

The diameter of the solids exit at the cyclone is critical. Cyclone designs are usually optimized for fine particles, and the presence of coarse particles is often not taken into account in calculations. If a too low value is chosen it may result to the blockage of the cyclone with unconverted fuel particles, which on its turn will lead to the loss of bed material in the reactor. For CFB system to be stable for longer duration, it is important that there is continuous circulation of particles in the endless loop and there should be overall pressure balance in the system. The algebraic sum of pressure drop across each part of the circulation loop is considered to be equal to zero. Frequently, a loop seal is used to facilitate the movement of solids from high-pressure downcomer to a fast bed riser.

5 Few Prototypes/Demonstration Plants

Atmospheric bubbling fluidized bed gasifier (ABFBG) has been proved to be reliable with a variety of feedstocks at pilot scale and commercial applications in small- to-medium scale, capacity up to about 25 MWth. They are limited in their capacity size range as they have not been scaled up significantly and the gasifier diameter is significantly larger than that of atmospheric circulating fluidized bed gasifier (ACFBG) for the same feedstock capacity. Pressurized fluidized bed gasifier systems either circulating (PCFBG) or bubbling (PBFBG) are considered of medium market attractiveness due to the more complex operation of the installation and to the additional costs related to the construction of all pressurized vessels. On the other hand, pressurized fluidized bed systems have the advantage in integrated combined cycle applications as the need to compress the fuel gas prior its utilization in the combustion chamber of the gas turbine is avoided.

There are increasing number of fluidized bed biomass gasifiers which are built and commissioned world wide. Unfortunately, these biomass projects around the globe have struggled to reach commercialization. The potentially high in efficiency has made biomass integrated gasification combined cycle (BIGCC) attractive to

many developers and governments. Some of such significant gasifier plants are listed below.

- (a) ARBRE, UK Project [30]—The ARBRE IGCC project of capacity 8 MW near Eggborough in the UK is a wood-fuelled atmospheric circulating fluidized bed gasifier. The plant contains an atmospheric-pressure circulating fluidized bed gasifier coupled to a tar-cracking vessel. After cooling and cleaning in conventional equipment, the energy-rich gas is fired in a modified 5 MW Alstom Power Typhoon gas turbine.
- (b) FERCO, Vermont Biomass Gasification Project [31]—The Burlington Vermont gasifier is the first commercial scale demonstration of the FERCO indirectly heated biomass gasification process. The gasification plant is the largest operation of its type in the USA and was the first process to integrate a biomass gasifier with a gas turbine during pilot operations at Battelle's Columbus, OH facilities. The project was sized to gasify up to 200 tonne per day of wood chips. The Burlington plant is coupled to the McNeil Station of the Burlington Electric Department and is being used to evaluate and demonstrate the gasification technology both as a producer of fuel gas and in a combined cycle with a gas turbine power generation system.
- (c) RENGAS Process [32]—The GTI/IGT RENGAS process employs a 20 bar pressurized bubbling fluidized bed process. The process was extensively tested with a variety of biomass materials, including bark sludge mixtures, bagasse and pelletized alfalfa stems in a 12 TPD PDU at IGT test facilities in Chicago. Subsequently, US DOE selected the IGT process for scale-up and demonstration, using bagasse, at the HC&S sugar mill at Paia in Hawaii. As this 100 TPD demonstration plant had limited success in handling the low-density shredded bagasse, the project was terminated. A typical gas composition obtained in the IGT PDU with bagasse at 2.24 MPa and 8500 C is 19% H₂, 26% CO, 37% CO₂, 17% CH₄, and 1% C₂ +. The heating value of this fuel gas is approximately 13 MJ/Nm³. The project participants included US DOE Biomass Power Program, IGT, Westinghouse Electric Corporation, State of Hawaii, PICHTR and HC&S.
- (d) Värnamo, Sweden [33]—The only large-scale IGCC project that has run for any appreciable length of time is in Värnamo, Sweden. It was developed by Sydkraft AB and Foster Wheeler. The gasifier was a pressurized, air-blown circulating fluidized bed designed to gasify wood and wood waste. The project included warm gas clean-up and firing in a combustion turbine provided by European Gas Turbines. The demonstration project produced 6 MWe and 9 MW heat released to district heating system to the city of Värnamo from a total fuel input equivalent to 18 MW.
- (e) 2 MWe Biomass Gasification Plant, Güssing, Austria [34]—The combined heat and power (CHP) plant has a fuel capacity of 8 MW and an electrical output of about 2 MWe with an electrical efficiency of about 25%. Wood chips with a water content of 20–30% are used as fuel. This is the fast internal circulating fluidized bed (FICFB) process, conceptualized and researched by Prof.

Hofbauer and his team at Technical University Vienna, which employs indirect-heating to gasify biomass with air to produce synthesis gas. The plant consists of a dual fluidized bed steam gasifier, a two stage gas cleaning system, a gas engine with an electricity generator and a heat utilization system.

6 Conclusion

The chapter gives a brief overview on the hydrodynamics of CFB systems having L-valves. Different correlations have been presented to understand the basic hydrodynamics and the gas–solid flow structure of the system. The effects of superficial gas velocity and particle size on the voidage across various sub-components, the pressure profiles in CFB loop and the overall solid recirculation have been discussed. Emphasis has also been given on how the solid circulation rate is dependent on the aeration flow in L-valve, bed inventory and particle size. Though the CFB concept is very old, the CFB technology is not fully developed because of the complexity of the system. This chapter has been written in a simpler way for better understanding of the hydrodynamics of the system.

References

1. Basu P (1999) Combustion of coal in circulating fluidized-bed boilers: a review. *Chem Eng Sci* 54:5547–5557
2. Van den Aarsen FG (1985) fluidised bed wood gasifier—performance and modelling. Dissertation TH Twente. University Publication
3. Geldart D (1973) types of gas fluidization. *Powder Technol* 7:285–292
4. Geldart D (1978) Homogenous fluidization in fine powder using various gases and pressures. *Powder Technol* 19:133–136
5. Ergun S (1952) *Chem Eng Prog* 48:89–94
6. Agarwal PK, O' Neill BK (1988) *Chem. Eng Sci* 43:2487
7. Kunii D, Levenspiel O (1969) Fluidization engineering, Chapter 3. Wiley, p 76
8. Brown GG et al (1950) Unit operations. Wiley, New York
9. Ryu H-J et al (1999) *J Korean Inst Chem Eng* 37(3):479
10. Bolton LW, Davidson JF (1988) Recirculation of particles in fast fluidized risers. In: Basu P, Large JF (eds) *Circulating fluidized bed technology II*. Pergamon Press, Oxford, pp 139–146
11. Rhodes MJ, Getdart D (1988) the hydrodynamics of recirculating fluidized beds. In: Basu P (ed) *Circulating fluidized bed technology II*. Pergamon Press, Oxford, pp 139–146
12. Kunii D, Levenspiel O (1990) Entrainment of solids from fluidized beds II Operation of fast Fluidized bed. *Powder Technol* 61:193–206
13. Yang WC (1988) A model for dynamics of circulating fluidized bed loop. In: Basu P Large JF (eds) *Circulating fluidized bed technology II*, Pergamon Press, Oxford, pp 181–192
14. Johnsson F, Andersson S, Leckner B (1991) Expansion of a freely bubbling fluidized bed. *Powder Technol* 68:117–123
15. Ergun S (1952) Fluid flow through packed columns. *Chem Eng Prog* 48(2):89

16. Zenz FA, Weil NA (1958) A theoretical-empirical approach to mechanism of particle entrainment from fluidized beds. *AIChE J* 4:472–479
17. Adanez J, Gayan P, Gracia-Labiano F, Diego LF (1994) Axial voidage profiles in fast fluidized beds. *Powder Technol* 31:259–268
18. Löffler G, Kaiser S, Bosch K, Hofbauer H (2003) Hydrodynamics of a dual fluidized-bed gasifier—part I: simulation of a riser with gas injection and diffuser. *Chem Eng Sci* 58:4197–4213
19. Wen CY, Chen LH (1982) Fluidized bed freeboard phenomena: entrainment and elutriation. *AIChE J* 28:117–128
20. Basu P, Large JF, Li et al (eds) (1988) *Circulating fluidized bed technology II*. Pergamon Press Plc
21. Yang W (1978) A correlation for solid friction factor in vertical pneumatic conveying lines. *AIChE* 24:548–552
22. Patience GS, Chaouki J, Grandjean BPA (1990) Solids flow metering from pressure drop measurement in circulating fluidized beds. *Powder Technol* 61:95
23. Gimbut J, Chuah TG, Fakhru'l-Razi A, Choong TSY (2005) The influence of temperature and inlet velocity on cyclone pressure drop: a CFD study. *Chem. Eng Process* 44:7–12
24. Daous MA, Al-Zahrani AA (1998) Modeling solids and gas flow through an L-valve. *Powder Technol* 99:86–89
25. Zhang JY, Rudolph V (1991) Transitional packed bed flow in standpipes. *Can J Chem Eng* 69:1242
26. Tong H, Hongzhong L, Xuesong L, Qiayu Z (2003) Hydrodynamic modeling of the L-valve. *Powder Technol* 129:8–14
27. Knowlton TM, Hirsan I (1978) L-valve characterized for solids flow—design parameters examined for valve use in coal gasification. *Hydrocarbon Process* 57:149
28. Geldart D, Jones P (1991) The behaviour of L-valves with Granular Powders. *Powder Technol* 67:163–174
29. Basu P, Fraser SA (eds) (1991) *Circulating fluidized bed boilers—design and operations*, Butterworth-Heinemann
30. Morris M, Waldheim L, Update on project ARBRE, U K—A wood-fuelled combined-cycle demonstration plant. <http://www.icheme.org/literature/conferences/gasi/Gasification%20Conf%20Papers/Session%20%20presentation-Morris%20et%20al.pdf>
31. Paisley MA, Irving JM, Overend RP (2001) A promising power option—the FERCO SILVAGAS biomass gasification process—operating experience at the Burlington gasifier. In: *Proceedings of ASME turbo expo 2001, ASME turbo expo land, sea, & air, 4–7 June 2001, New Orleans, Louisiana, USA*
32. Babu SP, Biomass gasification for hydrogen production—process description and research needs. <http://www.ieahia.org/pdfs/Tech%20Report,%20Babu,%20IEA%20Bioenergy%20Thermal%20Gas%20Task.pdf>
33. Stahl K, Waldheim L, Morris M, Johnsson U, Gardmark L, Biomass IGCC at Varnamo, Sweden—past and future. http://gcep.stanford.edu/pdfs/energy_workshops_04_04/biomass_stahl.pdf
34. Hofbauer H., Rauch R., Bosch K., Koch R. and Aichernig C., Biomass CHP Plant Güssing—A Success Story, <http://members.aon.at/biomasse/strassbourg.pdf>

Investigation of Biomass Gasifier Product Gas Composition and its Characterization

Pankaj Kalita and Debarshi Baruah

Abstract Over the years, gasification technology has been established as one of the efficient thermochemical conversion processes catering to a wide variety of applications like thermal, power generation and liquid fuel production through Fischer–Tropsch route. However, there are issues with the conversion devices when the biomass feed material changes and hence understanding of product gas behaviour and its variability is important in order to utilize the biomass gasification technology effectively in the long run. The current chapter addresses these issues relating to biomass characterization, product gas estimation and utilization, and advances in this technology. Furthermore, an example of an equilibrium model formulation for prediction of product gas generated from rice husk has been presented, and a brief about reaction kinetics has been discussed. A comparison of model result and experimental data has also been briefly presented. The recent trends in biomass gasification research show a promising future for this technology. Moreover, techno-economic evaluations prove that biomass gasification is not only technically viable but also a sound economic option. It is expected that biomass gasification will contribute more to the global energy requirements and thus to the economy in the coming future.

Nomenclature

V_g	Gas production rate (m^3/s)
q_g	Net calorific value of gas (kJ/m^3)
m_b	Rate of consumption of feedstock (kg/s)
q_b	Lower heating value of the feedstock (kJ/kg)
H_{sens}	Sensible heat in the gas (kW) given as, $H_{sens} = C_p V_g (T_g - T_a)$
C_p	Specific heat of gas ($\text{kJ}/\text{m}^3\text{ }^\circ\text{C}$)

P. Kalita (✉) · D. Baruah
Centre for Energy, Indian Institute of Technology Guwahati,
Guwahati 781039, Assam, India
e-mail: pankajk@iitg.ernet.in

D. Baruah
e-mail: debarshi_b@iitg.ernet.in

T_g	Gas temperature ($^{\circ}\text{C}$)
T_a	Ambient temperature ($^{\circ}\text{C}$)
C	Mass fraction of carbon
H	Mass fraction of hydrogen
O	Mass fraction of oxygen
N	Mass fraction of nitrogen
S	Mass fraction of sulphur
M_C	Molecular weight of carbon = 12.00 gm/mol
M_H	Molecular weight of hydrogen = 1.10 gm/mol
M_O	Molecular weight of oxygen = 16.00 gm/mol
M_N	Molecular weight of nitrogen = 14.01 gm/mol
M_S	Molecular weight of sulphur = 32.07 gm/mol
m	Amount of oxygen per kmol of wood in the gasification reaction
x_1, x_2, x_3, x_4 and x_5	Coefficients of constituents of the product species of gasification reaction
M_{bm}	Molecular weight of biomass
Φ	Relative moisture content of biomass
M_{H_2O}	Molecular weight of water
w	H_2O molar fraction in biomass
H_f^0 wood	Heat of formation of wood
H_f^0 $H_2O(l)$	Heat of formation of liquid H_2O
H_{vap}	Heat of formation of vaporized H_2O
H_f^0 $H_2O(vap)$	Heat of formation of water vapour
H_f^0 CO	Heat of formation of carbon monoxide
H_f^0 CO_2	Heat of formation of carbon dioxide
H_f^0 CH_4	Heat of formation of methane
ΔT	$T_2 - T_1$
T_1	Ambient temperature at the reduction zone
T_2	Gasification temperature at the reduction zone
C_{pH_2}	Specific heat of hydrogen
C_{pCO}	Specific heat of carbon monoxide
C_{pCO_2}	Specific heat of carbon dioxide
C_{pH_2O}	Specific heat of water vapour
C_{pCH_4}	Specific heat of methane
C_{pN_2}	Specific heat of nitrogen
X	Non-dimensional mass of sample undergoing reaction
t	Time (s)
A	Pre-exponential or frequency factor (s^{-1})
E	Activation energy of the decomposition reaction (kJ mol^{-1})
R	Universal gas constant ($\text{kJ mol}^{-1} \text{K}^{-1}$)
T	Absolute temperature (K)
n	Order of reaction

m_t	Weight of sample at time 't' (gm)
m_o	Initial weight of sample (gm)
m_f	Final weight of sample remaining at the end of the reaction (gm)
h	Enthalpy (J/kg)
h_g	Enthalpy of gas (J/kg)
k	Thermal conductivity (W/mK)
\dot{m}_g	Mass flux of gas ($\text{kg m}^{-2}\text{s}^{-1}$)
Q_i	Heat of combustion (J/kg)
x	Spatial variables (m)
ρ	Density (kg/m^3)
T_o	Initial temperature ($^{\circ}\text{C}$)
ρ_0	Initial density (kg/m^3)
T_{∞}	Environmental temperature ($^{\circ}\text{C}$)
T_r	Radiation source temperature ($^{\circ}\text{C}$)
\bar{h}	Convection heat transfer coefficient ($\text{W/m}^2\text{C}$)
ε_r	Radiation source emissivity
ε_m	Emissivity of the material
α_m	Absorptive of the material
σ	Stefan–Boltzmann constant ($5.78 \times 10^{-8} \text{ W/m}^2\text{-K}^4$)

1 Biomass Gasification Around the Globe: Brief History and Scenario

Gasification was discovered in the eighteenth century in both France and England. By 1850, the gasification technology was matured enough for certain parts of England to be lighted up by lanterns utilizing so-called 'town gas' [1]. World War I ushered in the phase when small gasifiers were developed for charcoal and biomass feedstock to operate vehicles, boats, trains and small electric generators [2]. All these gasifiers were fixed bed gasifiers, mostly downdraft by construction. By the beginning of World War II, the interest on wood-gas-driven vehicles was even more and by end of the war, there were more than 700,000 wood-gas generators powered trucks, cars and buses in Europe and probably more than a million worldwide [3]. However, with the end of war and wide spread availability of low-cost oil, this technology was pushed into oblivion with very few wood-gas vehicles left behind. This forgotten technology has started to gain interest again from the 1970s after the oil embargo of 1973 and the subsequent global oil crisis [4]. After the year 2000, biomass gasification has gained further momentum due to

issues related to global warming, political instability of oil-producing countries and shift towards renewable and carbon-neutral fuels [5].

Fluidized bed technology came into being when Fritz Winkler from Germany first obtained a patent for a fluidized bed hot gas generators in 1921. Fluidized bed processes came into wide use in the petroleum industry in post-World war period. These processes are also used extensively in the chemical and metallurgical fields [6]. Today there are number of CFB plants operating all over the world, and the size of the plant installations is increasing. The world's largest CFB power plant (Lagisza) of capacity 460 MW_e began commercial operation in 2009 and marked the beginning of a new era in the evolution of this technology. A recent example of a successful commercial CFB gasification plant is the 2 × 80 MW_{th} gasifier by Metso in Lahti, Finland, started operation in 2013 using biomass and solid waste [7]. In 2014, a total of 747 gasification projects having 1741 gasifier were planned, out of which 234 projects with 618 gasifiers were commercialized. In 2013, another 61 projects with 202 gasifiers were under construction, and 98 additional projects with 550 numbers of gasifiers were in planning [8]. This indicates, in current state of affairs, biomass gasification stands as one of the leading technologies in bioenergy conversion worldwide.

2 Biomass Gasification in India: Brief History and Current Scenario

India is currently the fourth largest economy of the world and with a second largest population of more than 1.3 billion. To sustain this economic growth, one of the most important factors is energy. The total installed capacity by end of 2016 had reached to 310 GW with the power generation shares from thermal (69.4%), hydro (13.9%), renewables (14.8%) and nuclear (1.9%). The share from bioenergy is ranked 3rd among the renewables after solar energy and wind energy [9]. Biomass-powered systems, mainly via biomass gasification route, have been applied in a variety of applications including rural, industrial and grid-connected systems. Looking back at the history of biomass gasification in India, it is seen to be a well-established technology in the Indian context. Research and experimentation on gasifier systems in India date back to early 1980s [10]. In later part of that decade, Indian government had also launched a National Biomass Gasifier Programme under which approximately 1700 units of equivalent capacity of 35 MW_e were installed till the year 2000 [11]. Since 2000, the commercialization and implementation of biomass gasification systems in India have picked up pace. Reports of both grid-connected and decentralized biomass gasification plants can be seen from the Indian literature in the last few years [12–15]. The current status of biomass power in India at the end of 2016 is summarized in Table 1.

In spite of these statistics, bioenergy is yet to emerge as a leading contributor, providing roughly 2% of India's total power generation. According to 2013

Table 1 Grid-interactive and off-grid biomass-based power generation in India (2016–17) [9]

Sector	Installed capacity (MW)
<i>I. Grid-interactive power (MW)</i>	
Biopower (biomass gasification and bagasse co-generation)	7907.34
Waste to power	114.08
<i>II. Off-grid/captive power (MWe)</i>	
Waste to energy	163.35
Biomass (non-bagasse) co-generation	651.91
Biomass gasifiers	
• Rural	18.34
• Industrial	168.54

estimate, there is 500 metric tons per year availability of biomass in India, mostly surplus agricultural residues, which measures up to a generation potential of 17.5 GW [16]. In the current year, MNRE has revaluated the biomass potential available in India to 25 GW and has also upscale the target of biopower to an installed capacity of 10 GW by 2022 [9]. To meet this target, effective policy for large-scale deployment of biomass gasification plants is the need of the hour.

3 Biomass Gasification Technology

3.1 Feedstock

Feedstock of a biomass gasifier can be of a wide variety such as sawdust, rice husk, solid wastes, wood chips, briquettes. These are naturally occurring organic material and are collectively called biomass. Biomass is a natural substance available, which stores solar energy by the process of photosynthesis in the presence of sunlight [17]. Ligno-cellulosic biomass is mainly composed of cellulose and hemicellulose (60–80% dry basis), lignin (10–25%), and some extractives and minerals [18]. Different biomasses have significant variations in their physical, chemical and morphological properties which affect the characteristics of the gasification process [19].

Besides, the choice of a biomass significantly depends on its heating value. Biomass wastes with high heating value contribute to more energy recovery and better system performance in terms of efficiency and economy [20]. Due to this, the quality of gas generated from gasification of coal of average calorific value 25 MJ/kg will be much superior from that obtained by gasification of rice straw of calorific value 14.5 MJ/kg [21]. Moreover, coal gasification is different from biomass gasification as biomass has higher oxygen-to-carbon ratio compared to coal. This influences the biomass gasification process which is a partial oxidation process. Moreover, the hydrogen-to-carbon ratio is also higher in biomass as shown in Van Krevelen diagram (Fig. 1).

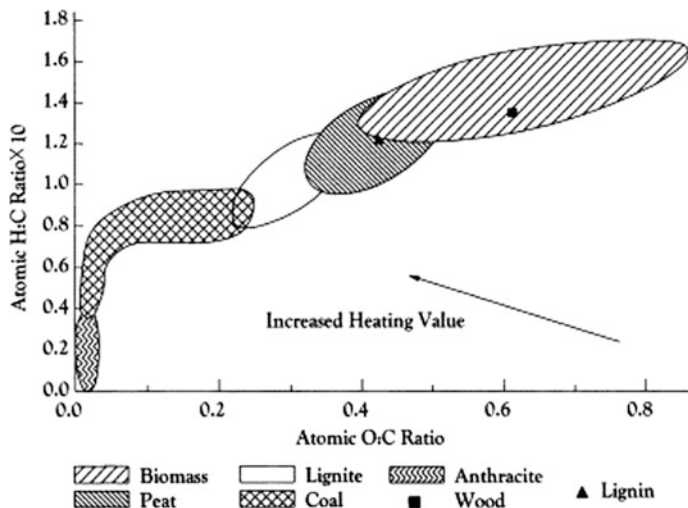


Fig. 1 Van Krevelen diagram showing H/C and O/C ratio of biomass compared to coals [32]

3.2 Types of Gasifiers

On the basis of reactor design or scheme of interaction of gasifying agent and solid fuels in the gasification reactor, generally gasifiers are subdivided into the following categories: fixed (moving) bed gasifiers, fluidized bed gasifiers and entrained-flow gasifiers.

In a fixed bed gasifier, the gasification reaction takes place over a stationary stage inside the reactor called the grate. Feeding is usually done from the top of the reactor, and the air is allowed either through the top or the bottom. After reactor, the product gas is collected from the outlet placed in position opposite to the air inlet, i.e. if the air is introduced from the top, the product gas is collected from the bottom of the reactor. The circulation of the gas in a fixed bed is slow due to which no effective motion is imparted to the particles (generally large in size), and the gas percolates through gaps between particles in the bed. The solids therefore remain relatively stationary inside a fixed bed reactor with slight movements downward as the feedstock is consumed in the reaction. The movement of feed through such gasifiers is due to gravity due to which they are also sometimes referred to as moving bed gasifiers. Fixed bed gasifiers are again categorized into three categories based on the relative direction of flow paths of air (inflow) and gas (outflow): (i) updraft gasifier, (ii) downdraft gasifier and (iii) crossdraft gasifier as shown in Fig. 2.

In updraft gasifiers, biomass is fed at the top of the reactor, moves downwards and is converted as it goes along. After conversion, the biomass reaches the bottom of the reactor in the form of ashes which are continuously removed. A continuous biomass feed allow to balance biomass conversion and keeping the biomass bed in

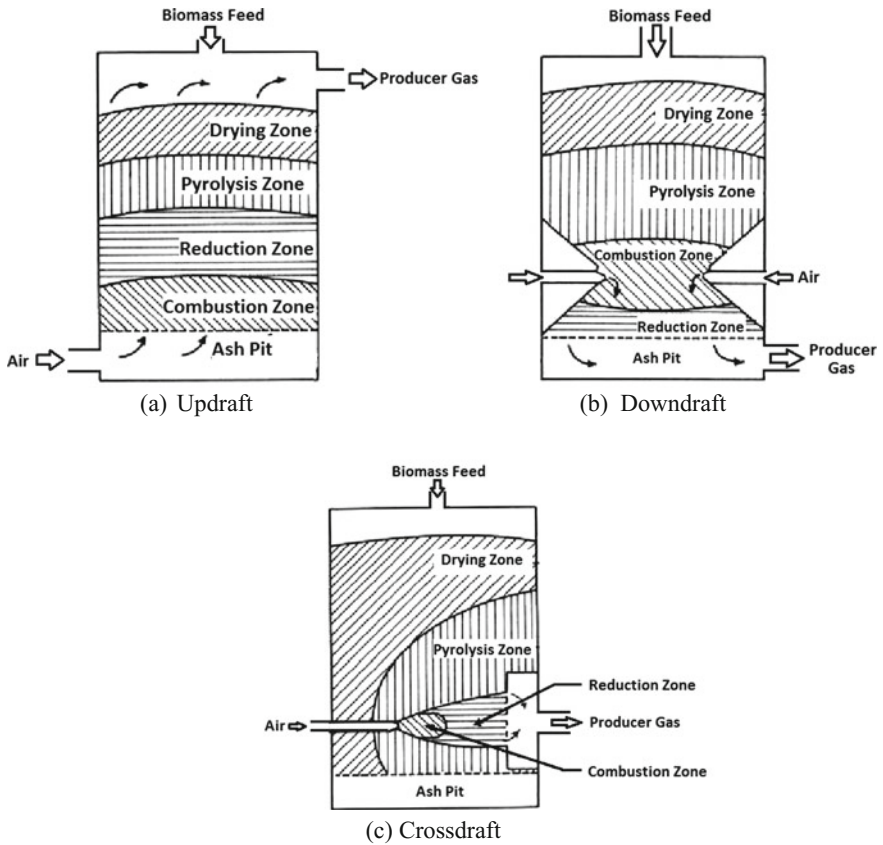


Fig. 2 Different types of fixed bed gasifiers [4]

a constant level and thus maintaining a stationary state into the gasifier. The air-intake is located at the bottom of the reactor and the produced gas leaves at the top. The biomass is then moving counter-currently to the gas flow and passes first through the drying zone, then through the pyrolysis zone, afterwards through the reduction zone and finally through the oxidation zone.

The working of a fluidized bed gasifier involves injecting the gasifying agent a high velocity through the bottom of the reactor to flow through the bed material consisting of solid fuel particles, inert particles for heat retention and transfer, and chars. After reaction, the producer gas flows out from top of the reactor. Compared to a fixed bed gasifier, the gas flow rate in fluidized bed is much higher. As gas velocity increases, the particles detach from neighbouring particles resulting in expansion of the bed and the bed of particles behaves like a fluid. This marks the beginning of fluidization. When gas velocity increases further, bubbles of excessive gas are generated that bypass the bed and such condition of the bed is called a bubbling fluidized bed. With furthermore increase of gas velocity, the particles are

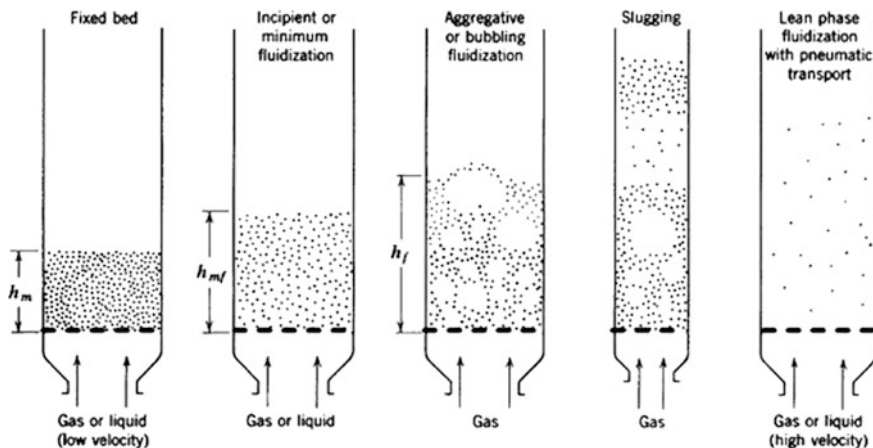


Fig. 3 Fluidization regimes in a gas–solid fluidized bed [78]

captured in the flow and are led away. This is called turbulent fluidized condition, and upper bed surface in this state is unidentifiable. These regimes of fluidization are shown in Fig. 3.

Fluidized bed gasifiers operate between bubbling to circulation fluidized regimes. In addition to biomass, inert particles like silica sand and dolomite are added to the bed for enhancing heat transfer between the gas and solid phases. Normally, 90–98% by weight of the total bed particles is constituted by these inert materials [22]. The gasification reactions occur by intensive mixing and heat transfer between the solid fuel particles and the gasifying agent. Fluidized bed gasifier operation involves heating the bed to the required temperature for gasification and subsequent feeding of solid fuel into the reactor. The gasification agents like air, pure oxygen, steam or their mixture, which also acts as a fluidization agent, are fed from the bottom of the gasifier, and its injection into the bed is made even by passing through a distributor. As mentioned before, in bubbling fluidized bed, the gas flow rate requires to be between minimum fluidization velocity and terminal velocity. On the other hand, in circulating fluidized beds, the gas flow rate required is more than terminal velocity with fine particles being entrained and carried out of the gasifier by the producer gas. For separation of the particulates, the producer gas is fed into a cyclone separator from where the gas exits from the top of the cyclone and separated particles are recirculated back to the bed from the bottom of the cyclone. Representation diagrams of bubbling fluidized bed and circulating fluidized bed are shown in Fig. 4.

In entrained-flow gasifiers, very finely pulverized feedstock is gasified in an oxygen/air and steam mixture. Entrained beds are utilized for large-scale generations of over 100 MW and often use fossil fuels in blends with biomass. Operating temperatures are high (up to 2000 °C), and high operating pressures up to 35 bar are often utilized [23]. Generally, the ash in entrained beds melts down due to high

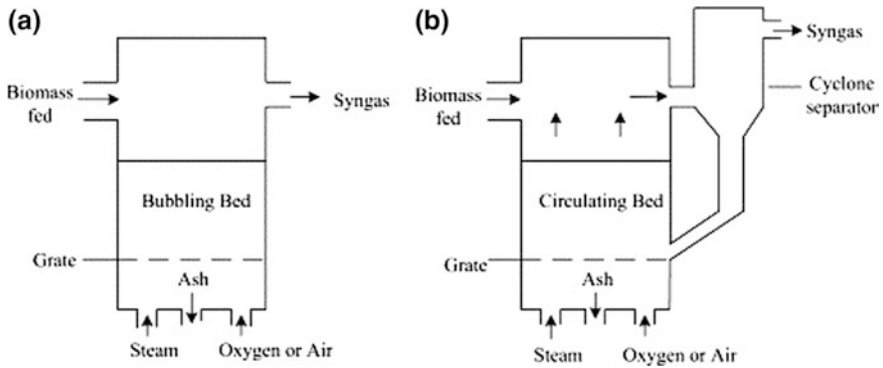


Fig. 4 a Bubbling fluidized bed gasifier, b circulating fluidized bed gasifier [79]

temperatures and is collected from the bottom as slag. Due to a short residence time of only a few seconds in entrained-flow reactors, the feedstock needs to be finely pulverized which is difficult in case of fibrous biomass. Torrefaction is one method used to unify the inhomogeneous feedstock, improve grindability and process efficiency as basis for use of biomass within a complex industrial plant [24].

3.3 Gasifier Product Gas

Biomass undergoes a series of thermochemical reactions inside the gasifier reactor to yield a fuel gas called producer gas or syngas. Biomass gasification utilizes the principle of oxidation first, then reduction of the products of oxidation, hence leading to the production of CO and H₂. These are the combustible components of producer gas along with traces of CH₄. The other non-combustible components of producer gas are CO₂, N₂ and traces of other gases [7]. Typical composition of producer gas from biomass gasification of wood in downdraft systems may be given as H₂ = 12–20%, CO₂ = 9–15%, CO = 17–22%, CH₄ = 2–3%, N₂ = 50–54%, and the range of calorific value is 5–5.9 MJ/Nm³ [25]. Significant variations may be there in the product gas composition and heating value based on feedstock used, type of reactor and various other process parameters. Based on the output gas and feedstock used, the gasifier efficiency can be calculated in two ways:

$$\text{Cold Gas Efficiency: } \eta_{CGE} = \frac{(V_g q_g)}{(m_b q_b)} \quad (1)$$

$$\text{Hot Gas Efficiency: } \eta_{HGE} = \frac{(V_g q_g + H_{sens})}{(m_b q_b)} \quad (2)$$

The hot gas efficiency is used for thermal applications where gas cooling is not required and cold gas efficiency is used when gas needs to be pre-cooled before utilization in engine [26].

3.4 Utilization of Producer Gas

The significance of biomass gasification lies in the fact that producer gas is highly suited to a variety of applications. The generated gas can be used for power generation, engine applications, thermal requirements, industrial needs, liquid fuel conversion, etc. Few literatures of such examples of applications of biomass gasification are discussed in Table 2.

From the above discussion, it is evident that biomass gasification is versatile process with flexibility of utilization for number of applications. But there are issues plaguing this process which cause problems for utilization of producer gas. One of the major problems of biomass gasification is the formation of tars [27–29]. Other

Table 2 Utilization of biomass gasification for different applications

Investigator(s)	System and utility	Discussion/Observation
Jorapur and Rajvanshi [80]	Sugar cane leaf- and bagasse-based downdraft gasification for industrial heating applications	<ul style="list-style-type: none"> • Thermal output obtained in range of 288–1080 MJ per hour with 40–100 kg per hour fuel consumption • Gas inlet to burner above 300 °C without pre-cooling resulted in no tar formation even after 700 h running
Mande et al. [81]	Process heat required for the curing of large cardamom	<ul style="list-style-type: none"> • Proposed use of low-cost wood-based gasifier in place of traditional <i>bhattis</i> • High conversion efficiency, high thermal efficiency and clean and smokeless flue gas from gasification can result in better product
Jayah et al. [82]	Potential for downdraft wood gasifier for tea drying	<ul style="list-style-type: none"> • Tested an indigenously built gasifier and found to have a conversion efficiency of 80% • Analysis showed the life cycle cost of energy produced by the gasifier is 8% less than the cost of energy from a conventional wood heater • Wood consumption is also reduced by 12%

(continued)

Table 2 (continued)

Investigator(s)	System and utility	Discussion/Observation
Tippayawong et al. [83]	Gasification of cashew nut shells by downdraft gasifier for thermal application in cashew nut-processing factory	<ul style="list-style-type: none"> • Gas produced with lower heating value about 3.51 MJ/m³ and system thermal efficiency above 20% • Saving in fuel cost of approximately \$150 a month was obtained by substitution of cashew nut shell feed in place of wood
Dutta and Baruah [84]	Gasification of uprooted tea shrub for thermal needs in black tea manufacturing	<ul style="list-style-type: none"> • Tea shrub feedstock having a HHV of 18 MJ/kg yielded producer gas of calorific value 4.2 MJ/m³ • If 28% thermal energy for tea drying comes from biomass gasification, equivalent reduction of CO₂ emission of 1299.5 tonnes
Sutar et al. [85]	Small downdraft gasifiers for domestic cooking purposes	<ul style="list-style-type: none"> • Designed, developed and tested two compact gasifiers of 4 and 2.5 kW_{th} with maximum gasification efficiency of order of 80% • In both gasifiers, a decrease in gasification efficiency is noted with increase in fuel particle size • Air flow rate is optimum when maximum temperature is achieved without significantly decreasing residence time
Sridhar et al. [86]	Engine operation with producer gas feeding from downdraft gasifier	<ul style="list-style-type: none"> • Producer gas utilized in a modified SI engine with compression ratio (CR) as high as 17:1 • Shaft power of 20 kW is obtained at maximum CR with overall efficiency of 20% and no knocking
Ramadas et al. [87]	Coir-pith- and wood-chip-based gasification for power generation by CI engine generator	<ul style="list-style-type: none"> • Engine runs on dual fuel mode with diesel and individual feeding of wood-chip producer gas and coir-pith producer gas • Maximum brake thermal efficiency was 19.9% using coir-pith and 21% using wood chips, both at 70% load • Above this load, decrease in brake thermal efficiency and increase in specific energy consumption are noted
Yin et al. [88]	Rice husk-based CFB gasification and power generation	<ul style="list-style-type: none"> • 1 MW CFB gasifier with rice husk feed for running 5 parallel 200 kW gas engines in rice mill

(continued)

Table 2 (continued)

Investigator(s)	System and utility	Discussion/Observation
		<ul style="list-style-type: none"> • Optimum performance obtained at loads above 800 kW, with rice husk consumption 1.7 kg/kWh, cold gas efficiency 65%, engine efficiency 26.5% and total system efficiency of 18%
Wu et al. [89]	Wood dust-based 1000 kW _e CFB gasification and generation plant for timber mill	<ul style="list-style-type: none"> • Cold gas efficiency is 70–80% and considering rated efficiency of the engine-generator system, the plant efficiency ranges around 17–19% • Economic analysis shows a gross profit of 2.32 million Yen/year and payback period is calculated as 3 years
Rinaldini et al. [90]	Poplar and pine wood-chip gasification in a downdraft gasifier for partial substitution in CI engine	<ul style="list-style-type: none"> • Gasifier is a downdraft single throat Imbert-type reactor of 85 kW_{th} capacity coupled to 2.8 litre turbocharged common rail diesel engine • Higher heating value of the syngas is about 5 MJ/Nm³, and diesel substitution rate of about 60% is obtained with 50 Nm torque
Boerrigter et al. [91]	Development of two demonstration plants for integrated biomass gasification (BG) and Fischer–Tropsch (FT) synthesis	<ul style="list-style-type: none"> • One system consisted of oxygen-blown CFB gasifier with tar cracker and wet gas cleaning and other oxygen-blown CFB gasifier with OLGA tar removal unit and a similar wet gas cleaning • Technical feasibility for Fischer–Tropsch synthesis from biosyngas from both systems was proven by test run of 500 h
Clausen et al. [92]	Model of plants producing dimethyl ether (DME) or methanol by catalytic conversion of a syngas generated by 2-stage gasification of woody biomass	<ul style="list-style-type: none"> • Feasibility of small-scale plants with 5 MW_{th} biomass input considered with cold gas efficiency of 93% • Plant models indicate energy efficiencies from biomass to DME/methanol and electricity of 51–58% • If utilization of waste heat for district heating is considered, total efficiencies measure up to 87–88% • However, the energy efficiencies were slightly lower than what could be achieved by large-scale plants

problems include ash slagging or clinkering [30, 31] and low heating value of gas [32]. However, to counter these problems, many mitigation methods have been put into practice and many more are under research. These have been addressed in another chapter of this compilation.

4 Parameters Affecting Biomass Gasification

4.1 *Feedstock Properties*

Biomass feedstock in gasification has a wide range of variation in their physical, chemical and morphological properties which affect the gasification process characteristics [19]. The selection of feedstock is important as the composition of biomass significantly affects the product gas composition. Biomass with higher carbon and oxygen content is found to yield higher percentage of combustibles in product gas [33].

Moisture is an important parameter as feedstock having moisture higher than 30% is difficult to ignite and result in lowering of the calorific value of the product gas due to energy consumed to remove the additional moisture. Moisture also hampers the oxidation temperature in the gasifier which in turn increases tar content [30].

Biomass with high ash content and mineral matter cause problems in gasification. Low melting point ash fuses together to form slag or clinker which hampers the flow of biomass in the reactor [12].

Biomass gasification is also sensitive to particle size. Pérez et al. [34] concluded that increase in size of feed causes reduction of the reaction surface which inhibits the transport of mass and heat to the gasification process in a downdraft gasifier. Effect of particle size is more pronounced in fluidized beds due to their influence on the suspension density profile [26].

4.2 *Operating Parameters*

Bed temperature is one of the most important operating parameters which affect both the heating value and the product gas composition. Wu et al. [35] found that calorific value of the producer gas decreases as the gasification temperature increases. This can be explained from the fact that higher temperatures are more suited to oxidation. However, a high operating temperature in the gasifier results in lower tar formation due to enhancement of cracking [36].

Gil et al. [37] studied the performance of biomass gasification with three gasifying agents—air, steam-O₂ mixtures and pure steam. The best results of the three cases on comparison showed that the superiority order in terms of LHV of the

product gas is 'steam > steam-O₂ mixture > air'. However, the tar yields in the three cases were also of the same order.

The equivalence ratio (ER) is stated to be the most important operating parameter by Narvaez et al. [38] as bed temperature, tar yield and gas quality are directly dependent on it. Their experiment on increasing ER from 0.20 to 0.45 resulted in a decrease of heating value of product gas by 2 MJ/Nm³. However, the tar yield also decreased about 50 wt%.

5 Equilibrium Modelling

Modelling involves representation of a complex process in form of mathematical equations based on fundamental physical, chemical and thermodynamic principles. To predict the composition of producer gas produced from a biomass gasifier, an equilibrium model may be used. The resulting producer gas composition can be utilized to evaluate calorific value of the produced gas. Zainal et al. [39] studied the development of equilibrium modelling to predict the gasification process in a downdraft gasifier. By using the equilibrium model, the composition of producer gas and hence, calorific value was determined. The effects of initial moisture content in wood and temperature in the gasification zone on the calorific value had also been investigated. As reported, results of the model are compared reasonably well with experimental data. Lapuerta et al. [40] predict the producer gas composition as a function of the fuel/air ratio by means of an equilibrium model. A kinetic model was used to establish the freezing temperature, which is used for equilibrium calculations in combination with the adiabatic flame temperature. Ruggiero and Manfrida [41] emphasize the potential of the equilibrium model considering the Gibbs free energy. This proceeding can be used under different operating conditions for predicting producer gas composition and the corresponding heating value. Hughes et al. [42] utilized model to stimulate effect of change of moisture percentage in feedstock of biomass gasifier. Ergüdenler et al. [43] used mathematical modelling for validation utilizing experimental data from 400 kW thermal dual-distributor-type fluidized bed gasifier. It was shown that consideration of tar formation in the model improved upon the results. Yang et al. [44] formulated a mathematical model for prediction of the main chemical and physical processes and the mathematical model is used to study the influence of temperature, oxygen concentration and flow rate of the feed gas. As reported, predicted gas species concentration profiles and their maximum values are in reasonable agreements with the measurements. Mathieu et al. [45] also studied the modelling of the biomass gasification process and more particularly the wood gasification. Various authors have developed correlation for calculation of higher heating value [46, 47]. As reported, the developed correlation can be used for HHV computation of any solid fuel and biomass material, from its proximate analysis.

5.1 Theory and Formulation of Model

Before developing a mathematical model, it is very much essential to understand the theory and chemical reactions that take place inside the biomass gasifier. Keeping this in mind, the following subsection discusses the theory, chemical reactions and equilibrium model formulation. As reported in various literatures [26], typically the following physicochemical reactions take place in a gasifier

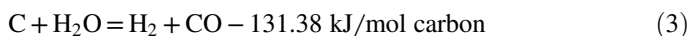
- (1) Drying (>150 °C)
- (2) Pyrolysis (devolatilization) (150–700 °C)
- (3) Combustion (700–1500 °C)
- (4) Reduction (800–1100 °C)

Drying, pyrolysis and reduction are endothermic processes which absorb heat. Moisture of the fuel is removed in drying process. Non-condensable gases, liquids and water vapour are removed in the pyrolysis process leaving behind char. Combustion is an exothermic process where the fuel is oxidized, followed by reduction which reduces the products of combustion into combustible gases in an endothermic manner.

Some authors [26] consider gasification to be a 3-stage process, viz. devolatilization, rapid-rate methane formation and low-rate char gasification. The devolatilization or pyrolysis process starts slowly at less than 350 °C and accelerates at a rapid rate to 700 °C. In this process, the products that are evolved and their chemical composition depend largely on gas composition, temperature and pressure. Pyrolysis generally produces three products, namely (a) light gases such as H_2 , CO_2 , CO , H_2O , CO , (b) tar, a black, viscous and corrosive liquid composed of heavy organic and inorganic molecules and (c) char, a solid residue mainly containing carbon.

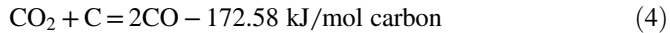
Char combustion is a very essential reaction inside the gasifier as it provides all the requisite thermal energy for the endothermic reactions to occur. When oxygen is the gasifying agent, it oxidizes the combustible particles in the bed forming CO_2 and H_2O . These again undergo reduction while reacting with the char produced from devolatilization. Ultimately, the complete process of gasification yields combustible gases such as H_2 , CO and CH_4 through the above-mentioned series of reactions. Following are the major chemical reactions takes place.

i. Water–Gas reaction: In this reaction, partial oxidation of carbon takes place in presence of steam. Steam can be from inlet air, water vapour released from feed-stock or pyrolysis reaction.

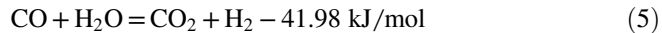


In some gasifiers, steam is supplied as the gasification medium with or without air or oxygen.

ii. Boudouard reaction: Carbon dioxide produced from combustion reacts with char to produce combustible carbon monoxide in this endothermic reaction.

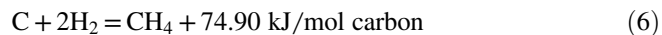


iii. Shift Conversion: Steam is reduced by carbon monoxide in this endothermic reaction, and it is desirable as H_2 has a higher heating value compared to CO



This endothermic reaction, known as water–gas, results in an increase in the ratio of hydrogen to carbon monoxide in the gas and is employed in the manufacture of synthesis gas.

iv. Methanation: Methane could also form in the gasifier through the following overall reaction:



Ni-based catalysts can be used to accelerate this reaction at 1100 °C and 6–8 bar. Formation of methane is desirable when the product gas is utilized as feedstock for other chemical processes. Moreover, the reaction enriches the product gas as methane is having a high heating value.

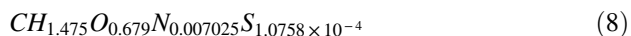
5.2 Biomass Composition and Chemical Formula

Utilizing the ultimate analysis results of biomass and the mass fractions of the elements present, the chemical formula for biomass fuel can be substituted as $\text{C}_n\text{H}_m\text{O}_p\text{N}_q\text{S}_r$ assuming $n = 1$. The remaining can be calculated from the following expressions

$$m = \frac{HM_C}{CM_H}, \quad p = \frac{OM_C}{CM_O}, \quad q = \frac{NM_C}{CM_N}, \quad r = \frac{SM_C}{CM_S} \quad (7)$$

In this section, the calculations are shown for biomass say sawdust. The proximate and ultimate analysis reported [48] is given in Table 3.

Thus from expression 7, the formula of the fuel used based on a single atom of carbon is



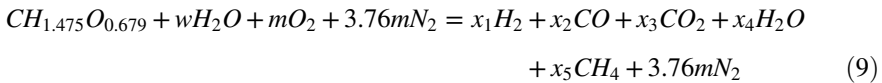
Using the substitution formula of the biomass fuel, its specific molar weight, quantity of water per mole of biomass, the stoichiometric air-to-fuel ratio and formation enthalpy of biomass may be calculated.

Table 3 Proximate and ultimate analysis of saw dust

Characteristics of material	Saw dust
Volatile matter %	77.01
HHV kJ/kg	15,019.75
<i>Elemental analysis weight %</i>	
C	48.52
H	6.39
O	44.65
N	0.13
S	0.32
Ash %	0.76

5.3 Chemical Equilibrium

Estimation of the components of product gas of a gasifier can be done based on chemical equilibrium between the different species and assuming that the tar content of the gas is negligible. Then, the general equation for biomass gasification may be written as



Therefore, H_2O molar fraction in biomass (H_2O/mol of biomass)

$$w = \frac{M_{bm} \times \Phi}{M_{H_2O} \times (1 - \Phi)} \quad (10)$$

The molecular weight of the biomass considered in the present case will be,

$$\begin{aligned} M_{bm} &= CH_{1.475}O_{0.679}N_{0.007025}S_{1.0758 \times 10^{-4}} \\ &= 24.44 \text{ gm/mol} \end{aligned}$$

When Φ is known, w becomes a constant with no change of value.

As seen in Eq. (9), there are six variables x_1 , x_2 , x_3 , x_4 , x_5 and m which represent the five unknowns in the product and oxygen required for the gasification reaction. To evaluate the six unknowns, six number of equations will be required. These are formulated based on the reaction takes place inside the gasifier. The chemical reactions that take place inside the gasifier are as follows:





Eqs. (11) and (12) on combining give the shift reaction



The equilibrium constant for methane formulation (Eq. 13) is

$$K_1 = \frac{P_{CH_4}}{(P_{H_2})^2} = \frac{x_5}{x_1^2} \quad (15)$$

The equilibrium constant for the shift reaction (Eq. 14) is

$$K_2 = \frac{P_{CO_2} \times P_{H_2}}{P_{CO} \times P_{H_2O}} = \frac{x_1 \times x_3}{x_2 \times x_4} \quad (16)$$

Carbon balance from Eq. (9):

$$1 = x_2 + x_3 + x_5 \quad (17)$$

Hydrogen balance from Eq. (9):

$$2w + 1.475 = 2x_1 + 2x_4 + 4x_5 \quad \text{Or} \quad w + 0.737 = x_1 + x_4 + 2x_5 \quad (18)$$

Oxygen balance from Eq. (9):

$$w + 0.679 + 2m = x_2 + 2x_3 + x_4 \quad (19)$$

Since gasification process is assumed to be adiabatic, hence the equation for the heat balance will be,

$$\begin{aligned} & H_f^0 \text{ wood} + w(H_f^0 \text{ H}_2\text{O}(l) + H_{(vap)}) + mH_f^0 \text{ O}_2 + 3.76mH_f^0 \text{ N}_2 \\ & = x_1H_f^0 \text{ H}_2 + x_2H_f^0 \text{ CO} + x_3H_f^0 \text{ CO}_2 + x_4H_f^0 \text{ H}_2\text{O}(vap) + x_5H_f^0 \text{ CH}_4 \\ & + \Delta T(x_1C_{pH_2} + x_2C_{pCO} + x_3C_{pCO_2} + x_4C_{pH_2O} + x_5C_{pCH_4} + 3.76mC_{pN_2}) \end{aligned} \quad (20)$$

The Eq. (20) can be simplified as,

$$dH_{\text{wood}} + wdH_{\text{H}_2\text{O}(l)} = x_1dH_{\text{H}_2} + x_2dH_{\text{CO}} + x_3dH_{\text{CO}_2} + x_4dH_{\text{H}_2\text{O}(vap)} + x_5dH_{\text{CH}_4} + 3.76mdH_{\text{N}_2} \quad (21)$$

where

$$dH_{(\text{for any gas})} = \text{Heat of formation} + \text{enthalpy change} = H_f^0 + \Delta H, \Delta H = \Delta T \times C_{p(g)}$$

$$dH_{H_2O(l)} = H_{f_{H_2O(l)}}^0 + H_{(vap)} \text{ and } dH_{wood} = H_{f_{wood}}^0 \quad (22)$$

Equations (15)–(19) and (21) represent six equations with six unknowns. Eqs. (15) and (16) are nonlinear equations while the rest (Eqs. 17–19 and 21) are linear equations. On reduction, one linear and two nonlinear equations can be formed from the above system of equations.

From Eq. (17),

$$x_5 = 1 - x_2 - x_3 \quad (23)$$

From Eq. (18),

$$x_4 = w + 0.737 - x_1 - 2x_5 \quad (24)$$

Substituting the value of x_5 in Eq. (24) gives,

$$x_4 = w + 0.737 - x_1 - 2(1 - x_2 - x_3) \text{ or} \quad (25)$$

$$x_4 = -x_1 + 2x_2 + 2x_3 + w - 1.263$$

From Eq. (19),

$$m = 1/2 (x_2 + 2x_3 + x_4 - w - 0.679) \quad (26)$$

By substituting the value of x_4 , in the above equation, we have

$$m = 1/2 (-x + 3x_2 + 4x_3 - 1.94) \quad (27)$$

Equation (15) implies,

$$x_5 = x_1^2 K_1 \quad (28)$$

By substituting the value of x_5 , in the above equation, we have

$$1 - x_2 - x_3 = x_1^2 K_1 \Rightarrow x_1^2 K_1 + x_2 + x_3 - 1 = 0 \quad (29)$$

From Eq. (16),

$$x_1 x_3 = x_2 x_4 K_2 \quad (30)$$

By substituting the value of x_4 , in the above equation, we have

$$-K_1x_1x_3 + (w - 1.263)K_2x_2 + 2K_2x_2^2 - x_1x_3 + 2K_2x_2x_3 = 0 \quad (31)$$

Now substituting the values of x_4 , x_5 and m in Eq. (21), we have

$$\begin{aligned} & (dH_{H_2} - dH_{H_2O(g)} - 1.88dH_{N_2})x_1 + (dH_{CO} + 2dH_{H_2O(g)} - dH_{CH_4} + 5.64dH_{N_2})x_2 \\ & + (dH_{CO_2} + 2dH_{H_2O(g)} - dH_{CH_4} + 7.52dH_2)x_3 + (dH_{H_2O(g)} - dH_{H_2O(l)})w \\ & + dH_{CH_4} - 1.263dH_{H_2O(g)} - 3.6472dH_{N_2} - dH_{wood} \end{aligned} \quad (32)$$

To simplify Eq. (32), the known constants are simplified as follows:

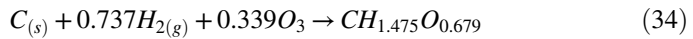
$$\begin{aligned} A &= dH_{H_2} - dH_{H_2O(g)} - 1.88dH_{N_2} \\ B &= dH_{CO} + 2dH_{H_2O(g)} - dH_{CH_4} + 5.64dH_{N_2} \\ C &= dH_{CO_2} + 2dH_{H_2O(g)} - dH_{CH_4} + 7.52dH_2 \\ D &= dH_{H_2O(g)} - dH_{H_2O(l)} \\ E &= dH_{CH_4} - 1.263dH_{H_2O(g)} - 3.6472dH_{N_2} - dH_{wood} \end{aligned}$$

Therefore, the Eq. (32) simplifies to

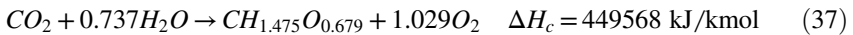
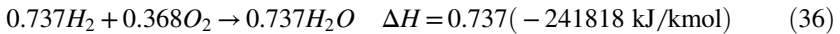
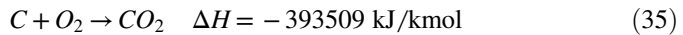
$$Ax_1 + Bx_2 + Cx_3 + Dw + E = 0 \quad (33)$$

Three remaining equations are there, two nonlinear (29) and (31) and one linear Eq. (33). The set of equation has to be solved using the multivariable Newton-Raphson method.

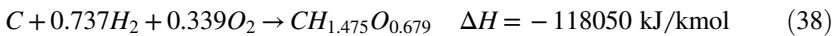
For the formation of 1 mol of solid biomass wood from ($CH_{1.475}O_{0.679}$) solid carbon, hydrogen and oxygen, the heat of formation equation is



Practically, the above reaction is not possible to occur. $CH_{1.475}O_{0.679}$ is formed based on the following reactions:



Equation (35) + (36) + (37) \Rightarrow



The following correlation has been reported in [49] for calculation of equilibrium constants K_1 (shift reaction Eq. (14)) and K_2 (methane formation reaction Eq. (15)):

$$K_1 = \exp(4000T^{-1} - 3.5) \quad (39)$$

and

$$K_2 = \exp(10000T^{-1} - 12.2) \quad (40)$$

The dependence of specific heat on temperature is given by an empirical equation, and the most simplified version for calculation of enthalpy of formation of methane is

$$C_{pmh} = R \left(A + BT_{am} + \frac{C}{3} (4T_{am}^2 - T_1T_2) + \frac{D}{T_1T_2} \right) \quad (41)$$

where

$T_{am} = (T_1 + T_2)/2$ is the arithmetic mean temperature, and A, B, C and D are the constants for the properties of the gases concerned. T_1 = ambient temperature and T_2 = gasification temperature.

Therefore, enthalpy of formation can be calculated by,

$$\Delta H = C_{pmh}(T_2 - T_1) \quad (42)$$

The heating value, i.e. ΔH_c , can be measured by experiment using calorimeter, and according to Reed [47], the heat of formation of any biomass material can be calculated with good accuracy from the following correlation

$$\Delta H_c = HHV \text{ (kJ/kmol)} = 0.236(146.58C + 56.878H - 51.53O - 6.58A + 29.45) \quad (43)$$

HHV can also be calculated with the help of the correlation developed by Channiwala [46]. The correlation is as follows,

$$HHV \text{ (MJ/kg)} = 0.3491C + 1.1783H + 0.1005S - 0.1034O - 0.0151N - 0.0211A, \quad (44)$$

With the ranges as $0\% \leq C \leq 92.25\%$, $0.43\% \leq H \leq 25.15\%$, $0\% \leq O \leq 50.00\%$, $0\% \leq N \leq 5.60\%$, $0\% \leq S \leq 94.08\%$, $0\% \leq A \leq 71.4\%$, $4.745 \leq HHV \leq 55.343 \text{ MJ/kg}$

Table 4 Composition of producer gas composition at 750 °C

Fuels	Composition of producer gas (%)					
	H_2	CO	CO_2	H_2O	CH_4	N_2
Saw dust	2.22	26.74	21.84	6.91	1.08	41.16
Rice husk	2.60	22.64	37.71	16.42	1.36	19.31
Bamboo dust	2.43	22.75	25.97	10.54	1.40	36.92

Table 5 Comparison of calorific value

Fuel	Calorific value (kJ/kg)
Saw dust	15,019.75
Rice husk	13,521.98
Bamboo dust	14,490.15

where C, H, O, S, N and A are the mass fractions of carbon, hydrogen, oxygen, sulphur, nitrogen and ash, respectively in the dry biomass.

HHV by proximate analysis is investigated by Parikh et al. [46],

$$HHV \text{ (MJ/kg)} = 0.3536FC + 0.1559VM - 0.0078ASH, \quad (45)$$

with the ranges as, FC: 1.0–91.5%, VM: 0.92–90.6%, ASH: 0.12–77.7%.

The results of the equilibrium model are presented under the results and discussion part.

The result of the equilibrium model used to predict the producer gas composition at gasification temperature of 750 °C for three different biomasses such as rice husk, saw dust and bamboo dust obtained by Kalita and Mahanta [48] is presented in Table 4. In this model, it was assumed that the initial moisture content present in the biomass to be 20%.

Table 5 shows the comparison of calorific value for the three biomasses obtained numerically by Kalita and Mahanta.

Result of the present model is compared with the model developed by Zainal et al. [39]. In the present study, gasification temperature 750 °C is found to be best in terms of quality and quantity of producer gas composition. Calorific value of saw dust and bamboo dust is close to each other, whereas the calorific value of rice husk is lower compared to the other two.

The validation of any model by comparison with experimental results is necessary to ascertain the appropriateness of the model. Figures 5 and 6 show the comparison of producer gas composition for rice husk at equivalent ratios ER = 0.3 and 0.4.

From the above figures, it has been observed that experimental and model results are almost similar for all the compositions. However, higher values of hydrogen and carbon monoxide percentage have been observed at ER = 0.3. Methane percentage is observed to be more at ER = 0.4.

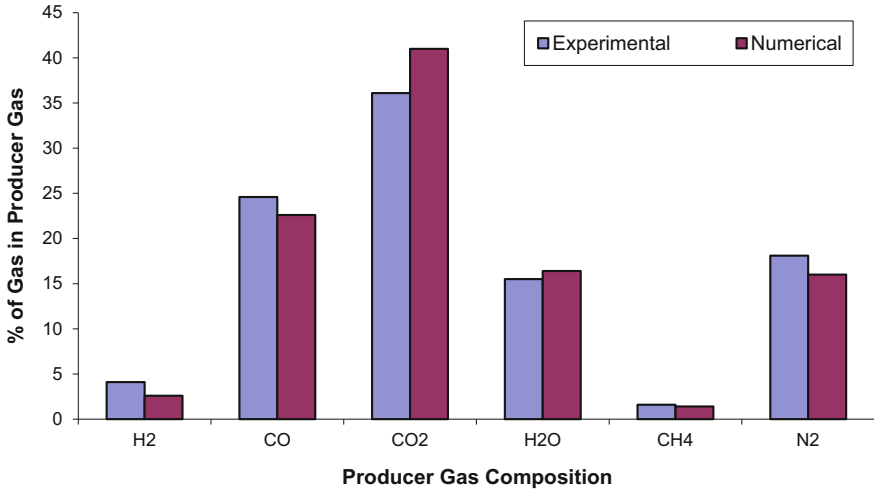


Fig. 5 Comparison of gas composition of rice husk (ER = 0.3)

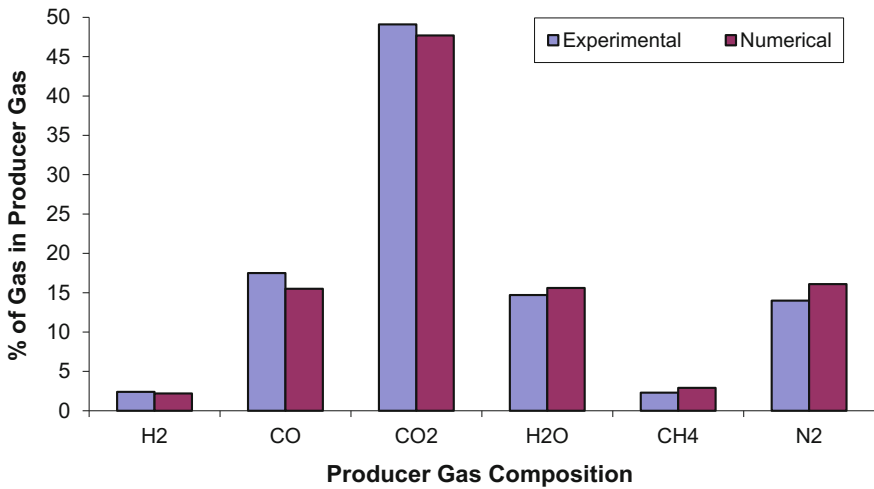


Fig. 6 Comparison of gas composition of rice husk (ER = 0.4)

Figures 7, 8 and 9 show the variation of gas composition of producer gas composition for rice husk at three different temperatures such as 650 °C, 750 °C and 850 °C, respectively. From these figures, it has been observed that % of CO

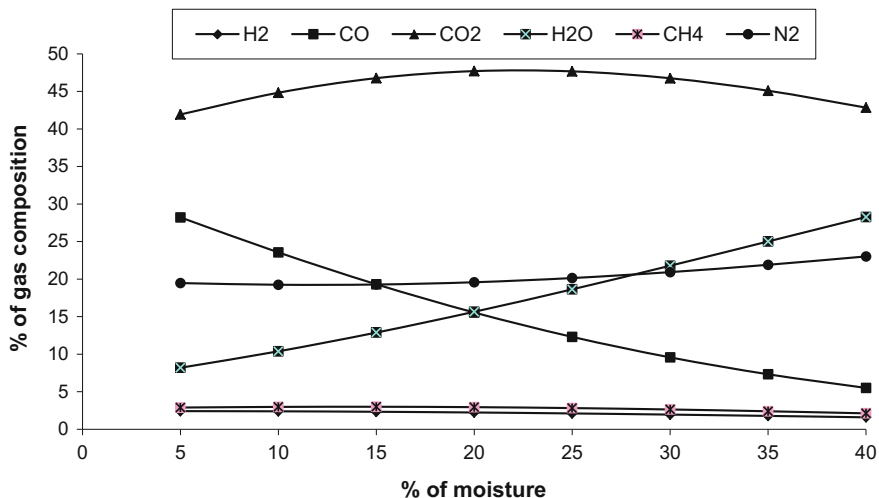


Fig. 7 Variation of moisture content on product gas composition at 650 °C

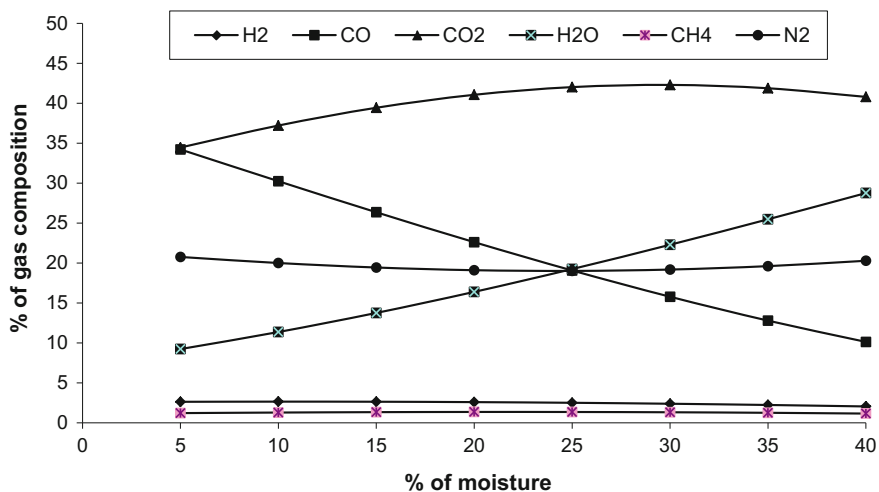


Fig. 8 Variation of moisture content on product gas composition at 750 °C

decreases with the increase in % of moisture content. Opposite pattern has been observed in case of CO₂ up to moisture content 20% before start decreasing. The decrease in % of CO₂ shows better conversion into CO in the gasification process. Percentage of H₂ and CH₄ remains constant up to 20% moisture content then

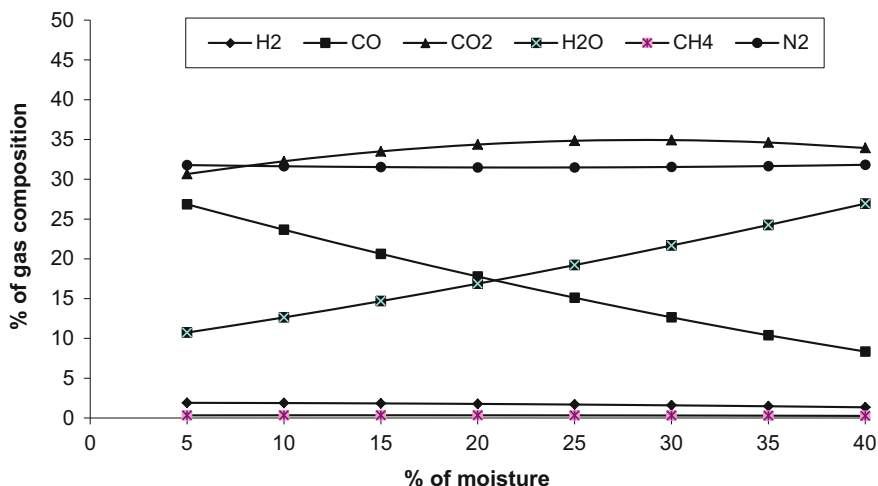


Fig. 9 Variation of moisture content on product gas composition 850 °C

decreases as moisture content increases. Percentage of N_2 and H_2O increases almost linearly with the increase in moisture content. More % of CO , H_2 and CH_4 has been observed at gasification temperature 750 °C.

6 Reaction Kinetics

The knowledge of properties and behaviour of biomass with time and temperature in a reactor are very essential for designing an efficient gasification unit. The design of biomass gasifier requires understanding of reaction chemistry such as reaction kinetics, conversion or yield, thermodynamics and process parameters (e.g. operating temperature and pressure as well as heat of reaction) which affects the reaction. The effective heat and mass transfer properties of fluidized beds provide the possibility of using various types of biomass wastes with different compositions and heating values [50]. Thermal analysis has been widely used in pyrolysis research [51–54]. Thermogravimetric analysis (TGA), differential thermal analysis (DTA), differential scanning calorimetry (DSC) or a combination of the same is used for the pyrolysis of the biomass containing cellulose, hemicelluloses and lignin [54–56]. As reported [57–59], wide variation of experimental conditions such as rate of heating, medium of heating has been applied in TGA.

The determination of kinetic parameters from TG data was based on the following Arrhenius rate expression [60].

$$\frac{dX}{dt} = -Ae^{-\left(\frac{E}{RT}\right)}X^n \quad (46)$$

Kinetic parameters were determined from typical curves of TG data over the entire temperature range in a continuous manner [61]. The values of A , E and n may be calculated by using a multiple linear regression. As proposed by the above authors, the linearized form of the Arrhenius equation is as follows

$$y = B + Cx + Dz \quad (47)$$

The parameters y , x , z , B , C and D in Eq. (47) are defined as follows:

$$\begin{aligned} y &= \ln\{[-1 / (m_o - m_f)] [dm/dt]\} \\ x &= 1 / (RT) \\ z &= \ln[(m_t - m_f) / (m_o - m_f)] \\ B &= \ln A \\ C &= -E \\ D &= n \end{aligned}$$

In this analysis, the rate expression is integrated numerically for two reaction zones separately over the given temperature ranges. The simplified form of the rate expression (Eq. 46) for fourth-order Runge–Kutta is as follows:

$$\begin{aligned} \frac{dX}{dt} &= -Ae^{-\left(\frac{E}{RT}\right)}X^n \\ \Rightarrow \frac{dX}{dT} \left(\frac{dT}{dt}\right) &= -Ae^{-\left(\frac{E}{RT}\right)}X^n \\ \Rightarrow \frac{dX}{dT} &= -\frac{1}{\beta}Ae^{-\left(\frac{E}{RT}\right)}X^n = f(X, T) \\ \text{where } \beta &= \frac{dT}{dt} = \text{Heating rate} \end{aligned} \quad (48)$$

If the temperature range is divided into ‘ p ’ parts with the interval ‘ h ’, then by integrating Eq. (48)

$$X(T_{p+1}) - X(T_p) = \int_{T_p}^{T_{p+1}} \left(\frac{dX}{dT}\right) dT = \int_{T_p}^{T_{p+1}} X'(T) dT \quad (49)$$

The values of X can be found out at regular interval of temperature at two different temperature zones. Ode 45 in MATLAB[®] may be used to calculate the value of X .

6.1 Model Formulation and Description

The following nonlinear partial differential equation (PDE) gives the energy conservation for 1D heat transfer undergoing thermal decomposition;

$$\frac{\partial}{\partial t} [\rho h] = \frac{\partial}{\partial x} \left[K \frac{\partial T}{\partial x} \right] - \frac{\partial}{\partial x} [\dot{m}_g h_g] - Q_i \frac{\partial \rho}{\partial t} \quad (50)$$

The rate of change of internal energy per unit volume is represented by the term on the left-hand side of (Eq. 50). The first term on the right-hand side of the above equation represents the conduction flux. The convection energy is given by the second term. The last term of the equation represents the rate of heat generation or consumption resulting from the decomposition.

With the following boundary and initial condition, the above differential equation can be solved

$$-K \frac{\partial T}{\partial x} = f(T) \text{ for } x=0, t > 0 \quad (51)$$

$$\frac{\partial T}{\partial x} = 0, \dot{m}_g = 0 \text{ for } x=l, t > 0 \quad (52)$$

$$T = T_o, \rho = \rho_o, \dot{m}_g = 0 \text{ for } 0 \leq x \leq l, t = 0 \quad (53)$$

The function $f(T)$ is defined as

$$f(T) = \bar{h}(T_\infty - T) + \sigma(\epsilon_r d_m T_r^4 - \epsilon_m T_k^4) \text{ for } x=0, t > 0 \quad (54)$$

Kalita et al. [62, 63] evaluated the kinetic parameters of both first and second reaction zones of rice husk and sawdust by using multivariable regression analysis. These kinetic parameters are utilized in the numerical technique in order to predict the mass degradation with temperature in both the reaction zones at three heating rates, viz. 10, 30 and 80 K/min, respectively. The predicted degradation results are well comparable with the experimental results in both the reaction zones for all the three heating rates.

In order to predict the TG curve, the kinetic parameters of both first and second reaction zones were used which were evaluated by using multiple regression analysis. Numerical technique called fourth-order Runge–Kutta in MATLAB[®] software was used to predict the TG curve. Figure 10 shows the experimental TG and DTG curves for rice husk at 80 K/min, and Fig. 11 shows the comparison of experimental and numerical curves at the same heating rate.

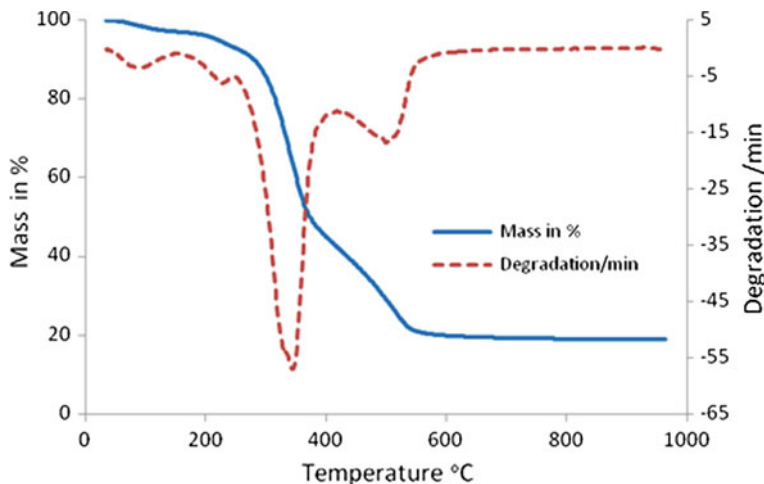


Fig. 10 TG and DTG curves of the rice husk at the heating rate of 80 K/min

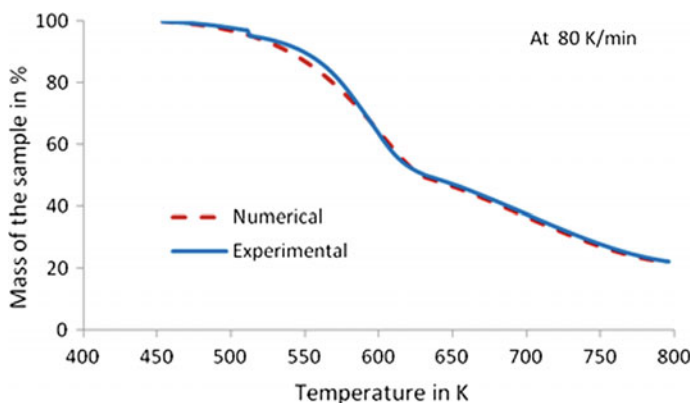


Fig. 11 Comparison of experimental and numerical curves at 80 K/min

7 Recent Advances in Biomass Gasification

In the recent years, biomass gasification has been a widely researched area and has seen technological advances in reactor design, gas cleaning and conditioning methods, and utilization avenues. It is due to continued research that success stories of commercial IGCC plants [64, 65] and FT fuel plants [66] are available. Co-gasification of biomass and coal blends is also a fairly new concept for utilization of low-grade coals along with improvement of gas heating value and energy efficiency with reduction in tar content of the product gas [67]. Recent topics of research interest are waste heat recovery devices, improved tar-cracking methods,

Table 6 Features of emerging technologies in biomass gasification [93]

Technology	Features
Combination of gasification and gas clean-up in one reactor	<ul style="list-style-type: none"> ● Robust and cost-effective design ● Extensive research required for commercialization
Multistaged gasification	<ul style="list-style-type: none"> ● Pyrolysis and gasification individually in single controlled stages ● Higher quality syngas ● High process efficiency
Distributed pyrolysis plants integrated to central gasification plant	<ul style="list-style-type: none"> ● Char–oil slurry produced in distributed plants ● Gasification for syngas and biofuel synthesis in central plant ● Utilization of low-grade biomass with cost-effective transportation in form of char–oil slurry ● Economic feasibility doubtful
Plasma gasification	<ul style="list-style-type: none"> ● Plasma used as heat source and/or tar-cracking agent ● Decomposition of any organic matter or hazardous waste ● High capital cost and power requirement, low efficiency
Supercritical water gasification	<ul style="list-style-type: none"> ● Liquid and biomass with high moisture can be gasified ● No requirement of pre-treatment ● Energy and investment high
Sorption enhanced reforming and biomass gasification with CO ₂ capture	<ul style="list-style-type: none"> ● Gasification in presence of catalyst and sorbent ● In situ carbon capture, enhanced H₂ and reduced tar content ● Research on catalyst and sorbents are required
Co-generation of heat and power (CHP)	<ul style="list-style-type: none"> ● Increased process efficiency ● Suitable for decentralized production
Polygeneration of heat, power and H ₂	<ul style="list-style-type: none"> ● Generation of H₂ along with increase of plant efficiency ● Process design is complex
Polygeneration of heat, power and SNG	<ul style="list-style-type: none"> ● Generation of renewable fuel along with increase of plant efficiency ● Not economical without SNG distribution system
Biomass gasification integrated to Fischer–Tropsch (FT) process	<ul style="list-style-type: none"> ● Syngas from biomass gasification utilized to produce renewable transportation fuel ● Process design complex

reuse of biochar as feedstock, value-added products from ash and tar, steam gasification for hydrogen yield, pre-treatment of raw feedstock, etc. [68]. Some of the emerging technologies under current research in the field of biomass gasification and their features are discussed in Table 6.

8 Techno-Economic Analysis

The gap between research and commercialization of biomass gasification systems is bridged by techno-economic analysis. It is an important tool to assess feasibility of any technology in terms of performance and economics before actual deployment to field. Many researchers have worked on techno-economic analysis of biomass gasification applied to various utilities. Lau et al. [69] studied the feasibility of hydrogen production from gasification of biomass. The potential feedstocks considered in this study were sugarcane bagasse, nut shells and switchgrass. For design calculations, process scales ranging from 500 to 4000 tonnes per day for each type of biomass were considered. Sensitivity analyses were conducted for each feedstock and plant size, comparing various capital costs, feedstock costs and internal rates of return. On simulation, hydrogen production rates were found to be 78.1 for bagasse, 84.1 for switchgrass and 88.3 for the nutshells (g of H₂/kg dry biomass). Arena et al. [70] had conducted an analysis with two configurations for biomass-to-energy gasification-based systems—both with same bubbling fluidized bed gasifier of capacity 100 kg/h—but one system with gas engine and other with externally fired gas turbine. The economic analysis was carried considering parameters such as total plant costs, operating costs, taxes and revenue collection from sale of generated energy. They concluded that compared to the gas turbine system, the gas engine has higher reliability and provides a higher internal rate of return for the investigated range of electrical energy production between 100 and 600 kW_e. Rodrigues et al. [71] conducted a techno-economic analysis of a co-fired biomass-integrated gasification system based on sugar cane residue feedstock with natural gas. Performance modelling of the system was conducted over a wide range from 20 to 300 MW_e. With mixing of low calorific value gas and natural gas, electricity cost was reduced and cost-effectiveness of up to 50% proportion of natural gas in the mixture was reported. The sensitivity of the system was also analysed in terms of efficiency, combined cycle capital costs, gas clean-up equipment and biomass fuel costs. Sara et al. [72] carried out a techno-economic analysis of hydrogen production using a 100 kW_{th} bubbling fluidized bed gasifier integrated with a Portable Purification Unit (PPS). The sensitivity of hydrogen production cost was also studied with respect to capital cost, operating cost and hydrogen production efficiency. Findings indicate that 50% reduction of PPS cost, which is a major cost, and the variation of steam-to-biomass ratio in the range of 1–1.5 will result in fluctuation of production cost between 12.75 and 9.5 €/kg. A techno-economic assessment on viability of municipal solid waste gasification in fixed bed (downdraft) reactors for electricity generation in Brazil was presented by Luz et al. [73]. They considered three scenarios with gasification plants of different generation capabilities per ton of solid municipal waste, based on the different population of inhabitants, and also different economic scenarios based on varying interest rates. The economic feasibility was evaluated using economic indicators like the net present value and the internal rate of return, whereas technical feasibility was assessed by installed capacity, capacity utilization factor, specific electrical power generation and efficiency. It was

concluded that economic feasibility is enhanced with the installation of bigger units, because higher the capacity of the installation lower the specific costs and higher the benefits. Many such literatures on techno-economic evaluation of biomass gasification applications are present which promote its viability and extensive use [74–77].

9 Conclusion

The product gas of biomass gasification is highly versatile, but sensitive to a number of parameters like feedstock, gasifying agent, equivalence ratio. For proper utilization, the characterization of this product gas is important by way of modelling or simulations. Many aspects of biomass gasification are under wide research. However, research emphasis is required at present on gasification of fuel blends, process optimization, gas cleaning, gas reforming and hydrogen separation for fuel cell application. Various analyses show that biomass gasification is feasible for deployment both technologically and economically. Use of gasification is also evident in industrial sectors such as tea industry, sugar industry, food processing industry. However, for promotion of extensive industrial use, hybrid systems with biomass gasification coupled to conventional systems like integrated gasification combined cycle (IGCC) for better conversion efficiency may be looked upon. Decentralized electrification in rural areas through gasification mode is also a very promising option in developing countries. In current state of affairs, biomass gasification is an appropriate technology available for wide-scale implementation considering the global biomass potential from agricultural residues, solid wastes and forest residues.

Acknowledgements The work reported here is a part of a research project (project no. ECR/2016/001830) funded by Science and Engineering Research Board (SERB), Government of India. The financial support provided by the SERB for the project is gratefully acknowledged.

References

1. Singer C, Holmyard EJ, Hall AR, William TI (eds) (1958) A history of technology. Volume IV. The industrial revolution. Oxford, UK, Clarendon Press, pp c1750–c1850
2. Rambush NE (1923) Modern gas producers. Benn Bros. Ltd., London
3. Egloff G, Van Arsdell PM (1941) Octane rating relationship of aliphatic, alicyclic, mononuclear, aromatic hydrocarbons, alcohols. Ethers and Ketons J I Petrol 27:121
4. Rajvanshi AK (1986) Biomass gasification. Altern Energy Agric 2(4):82–102
5. Basu P (2013) Biomass gasification, pyrolysis and torrefaction: practical design and theory. Academic press
6. Kalita P, Mahanta P, Saha UK (2015) Pressurized circulating fluidized bed technology. Energy Sci Technol Hydrogen Other Technol 11:481–526

7. Honkola T (2013) Industrial gasification demonstration plants by Metso, Finnish–Swedish Flame Days, Jivaskyle, Finland
8. Sansaniwal SK, Pal K, Rosen MA, Tyagi SK (2017) Recent advances in the development of biomass gasification technology: A comprehensive review. *Renew Sustain Energy Rev* 72:363–384
9. MNRE annual report 2016–17, Govt of India
10. Verbong G, Christiaens W, Raven R, Balkema A (2010) Strategic Niche management in an unstable regime: biomass gasification in India. *Environ Sci Policy* 13(4):272–281
11. Jain BC (2000) Commercialising biomass gasifiers: Indian experience. *Energy Sustain Dev* 4(3):72–82
12. Mukhopadhyay K (2004) An assessment of a biomass gasification based power plant in the sunderbans. *Biomass Bioenergy* 27(3):253–264
13. Dasappa S, Subbukrishna DN, Suresh KC, Paul PJ, Prabhu GS (2011) Operational experience on a grid connected 100kWe biomass gasification power plant in Karnataka, India. *Energy Sustain Dev* 15(3):231–239
14. Singh J (2015) Overview of electric power potential of surplus agricultural biomass from economic, social, environmental and technical perspective—a case study of Punjab. *Renew Sustain Energy Rev* 42:286–297
15. Palit D, Sarangi GK (2014) Renewable energy programs for rural electrification: Experience and lessons from India. In: 3rd international conference developments in renewable energy technology (ICDRET), IEEE, May 2014, pp 1–6
16. Kumar A, Kumar N, Baredar P, Shukla A (2015) A review on biomass energy resources, potential, conversion and policy in India. *Renew Sustain Energy Rev* 45:530–539
17. Aswathanarayana U, Harikrishnan T, Kadher-Mohien TS (eds) (2010) *Green energy: technology, economics and policy*. CRC Press
18. Kalita P (2010) Characterization of loose biomass for gasification. MTech dissertation, IIT Guwahati, India
19. Moilanen A, Nasrullah M, Kurkela E (2009) The effect of biomass feedstock type and process parameters on achieving the total carbon conversion in the large scale fluidized bed gasification of biomass. *Environ Prog Sustain* 28(3):355–359
20. Nemtsov DA, Zabaniotou A (2008) Mathematical modelling and simulation approaches of agricultural residues air gasification in a bubbling fluidized bed reactor. *Chem Eng J* 143(1):10–31
21. Saikia M, Bhowmik R, Baruah D, Dutta B, Baruah DC (2013) Prospect of bioenergy substitution in tea industries of North East India. *IJMERE* 3(3):1272–1278
22. Van Loo S, Koppejan J (2008) *The handbook of biomass combustion and co-firing*. Earthscan, London
23. Basu P (2010) *Biomass gasification and pyrolysis: practical design and theory*. Elsevier Inc/ Academic Press, UK
24. Weiland F, Nordwaeger M, Olofsson I, Wiinikka H, Nordin A (2014) Entrained flow gasification of torrefied wood residues. *Fuel Process Technol* 125:51–58
25. Puig-Arnabat M, Bruno JC, Coronas A (2010) Review and analysis of biomass gasification models. *Renew Sustain Energy Rev* 14(9):2841–2851
26. Basu P (2006) *Combustion and gasification in fluidized beds*. Taylor and Francis Group/CRC Press, London
27. Li C, Suzuki K (2009) Tar property, analysis, reforming mechanism and model for biomass gasification—an overview. *Renew Sustain Energy Rev* 13(3):594–604
28. Palma CF (2013) Modelling of tar formation and evolution for biomass gasification: a review. *Appl Energy* 111:129–141
29. Milne TA, Evans RJ, Abatzoglou N (1998) Biomass gasifier “Tars”: their nature, formation, and conversion. National Renewable Energy Laboratory, Golden, CO (US)
30. McKendry P (2002) Energy production from biomass (part 3): gasification technologies. *Bioresource Technol* 83(1):55–63

31. Wang L, Weller CL, Jones DD, Hanna MA (2008) Contemporary issues in thermal gasification of biomass and its application to electricity and fuel production. *Biomass Bioenergy* 32(7):573–581
32. McKendry P (2002) Energy production from biomass (part 2): conversion technologies. *Bioresource Technol* 83(1):47–54
33. Asadullah M, Miyazawa T, Ito SI, Kunimori K, Yamada M, Tomishige K (2004) Gasification of different biomasses in a dual-bed gasifier system combined with novel catalysts with high energy efficiency. *Appl Catal A-Gen* 267(1):95–102
34. Pérez JF, Melgar A, Benjumea PN (2012) Effect of operating and design parameters on the gasification/combustion process of waste biomass in fixed bed downdraft reactors: an experimental study. *Fuel* 96:487–496
35. Wu CZ, Yin XL, Ma LL, Zhou ZQ, Chen HP (2009) Operational characteristics of a 1.2-MW biomass gasification and power generation plant. *Biotechnol Adv* 27(5):588–592
36. Devi L, Ptasiński KJ, Janssen FJ (2003) A review of the primary measures for tar elimination in biomass gasification processes. *Biomass Bioenergy* 24(2):125–140
37. Gil J, Corella J, Aznar MP, Caballero MA (1999) Biomass gasification in atmospheric and bubbling fluidized bed: effect of the type of gasifying agent on the product distribution. *Biomass Bioenergy* 17(5):389–403
38. Narvaez I, Orío A, Aznar MP, Corella J (1996) Biomass gasification with air in an atmospheric bubbling fluidized bed. Effect of six operational variables on the quality of the produced raw gas. *Ind Eng Chem Res* 35(7):2110–2120
39. Zainal ZA, Ali R, Lean CH, Seetharamu KN (2001) Prediction of performance of a downdraft gasifier using equilibrium modeling for different biomass materials. *Energy Convers Manage* 42(12):1499–1515
40. Lapuerta M, Hernández JJ, Tinaut FV, Horrillo A (2001) Thermochemical behaviour of producer gas from gasification of lignocellulosic biomass in SI engines. SAE technical paper
41. Ruggiero M, Manfredi G (1999) An equilibrium model for biomass gasification processes. *Renew Energy* 16(1–4):1106–1109
42. Hughes WE, Larson ED (1998) Effect of fuel moisture content on biomass-IGCC performance. *Trans-ASME, J Eng Gas Turb Power* 120:455–459
43. Ergüdenler A, Ghaly AE, Hamdullahpur F, Al-Taweel AM (1997) Mathematical modeling of a fluidized bed straw gasifier: Part III—Model verification. *Energy Source* 19(10):1099–1121
44. Yang W, Ponzio A, Lucas C, Blasiak W (2006) Performance analysis of a fixed-bed biomass gasifier using high-temperature air. *Fuel Process Technol* 87(3):235–245
45. Mathieu P, Dubuisson R (2002) Performance analysis of a biomass gasifier. *Energy Convers Manage* 43(9):1291–1299
46. Parikh J, Channiwalwa SA, Ghosal GK (2005) A correlation for calculating HHV from proximate analysis of solid fuels. *Fuel* 84(5):487–494
47. Reed TB (1985) Principles and technology of biomass gasification. *Advances in solar energy*. Springer, US, pp 125–174
48. Kalita P, Mahanta P (2009) Equilibrium model development for prediction of producer gas composition of a cyclone gasifier. In: Proceedings on computer aided modeling and simulation in computational mechanics (CAMSCM), Itanagar, pp 167–180
49. de Souza-Santos ML (2010) Solid fuels combustion and gasification: modelling, simulation. CRC Press
50. Yassin L, Lettieri P, Simons SJ, Germanà A Techno-economic performance of energy-from-waste fluidized bed combustion and gasification processes in the UK context. *Chem Eng J* 146(3):315–327
51. Pipatmanomai S, Paterson N, Dugwell D, Kandiyoti R (2004) Kinetic modeling of coal pyrolysis in an atmospheric wire-mesh reactor. In: Joint international conference on “sustainable energy and environment” (SEE), Thailand, pp 589–594
52. Lau CW, Niksa S (1993) The impact of soot on the combustion characteristics of coal particles of various types. *Combust Flame* 95(1–2):1–21

53. Cuoci A, Faravelli T, Frassoldati A, Grana R, Pierucci S, Ranzi E, Sommariva S (2009) Mathematical modelling of gasification and combustion of solid fuels and wastes. *Chem Eng Trans* 18:989–994
54. Sommariva S, Maffei T, Migliavacca G, Faravelli T, Ranzi E (2010) A predictive multi-step kinetic model of coal devolatilization. *Fuel* 89(2):318–328
55. Alén R, Kuoppala E, Oesch P (1996) Formation of the main degradation compound groups from wood and its components during pyrolysis. *J Anal Appl Pyrol* 36(2):137–148
56. Mansaray KG, Ghaly AE (1997) Physical and thermochemical properties of rice husk. *Energy Source* 19(9):989–1004
57. Kaupp A (2013) *Gasification of rice hulls: theory and praxis*. Springer
58. Boateng AA, Walawender WP, Fan LT, Chee CS (1992) Fluidized-bed steam gasification of rice hull. *Bioresource Technol* 40(3):235–239
59. Bridgwater AV (1995) The technical and economic feasibility of biomass gasification for power generation. *Fuel* 74(5):631–653
60. Ergudenler A, Ghaly AE (1992) Determination of reaction kinetics of wheat straw using thermogravimetric analysis. *Appl Biochem Biotech* 34(1):75
61. Duvvuri MS, Muhlenkamp SP, Iqbal KZ, Welker JR (1975) The pyrolysis of natural fuels. *J Fire Flamm* 6(2):468–477
62. Kalita P, Clifford MJ, Jiamjiroch K, Kalita K, Mahanta P, Saha UK (2013) Characterization and analysis of thermal response of rice husk for gasification applications. *J Renew Sustain Energy* 5(1):013119
63. Kalita P, Mohan G, Pradeep Kumar G, Mahanta P (2009) Determination and comparison of kinetic parameters of low density biomass fuels. *J Renew Sustain Energy* 1(2):023109
64. Ståhl K, Neergaard M (1998) IGCC power plant for biomass utilisation, Värnamo, Sweden. *Biomass Bioenergy* 15(3):205–211
65. Acosta A, Aineto M, Iglesias I, Romero M, Rincon JM (2001) Physico-chemical characterization of slag waste coming from GICC thermal power plant. *Mater Lett* 50(4):246–250
66. Dautzenberg K, Hanf J (2008) Biofuel chain development in Germany: Organisation, opportunities, and challenges. *Energy Policy* 36(1):485–489
67. Mallick D, Mahanta P, Moholkar VS (2017) Co-gasification of coal and biomass blends: chemistry and engineering. *Fuel* 204:106–128
68. Sansaniwal SK, Pal K, Rosen MA, Tyagi SK (2017) Recent advances in the development of biomass gasification technology: a comprehensive review. *Renew Sustain Energy Rev* 72:363–384
69. Lau FS, Bowen DA, Dihu R, Doong S, Hughes EE, Remick R, Slimane R, Turn SQ, Zabransky R (2002) Techno-economic analysis of hydrogen production by gasification of biomass. In: *Proceedings of the 2002 US DOE hydrogen and fuel cells annual program/lab R&D review*
70. Arena U, Di Gregorio F, Santonastasi M (2010) A techno-economic comparison between two design configurations for a small scale, biomass-to-energy gasification based system. *Chem Eng J* 162(2):580–590
71. Rodrigues M, Faaij AP, Walter A (2003) Techno-economic analysis of co-fired biomass integrated gasification/combined cycle systems with inclusion of economies of scale. *Energy* 28(12):1229–1258
72. Sara HR, Enrico B, Mauro V, Vincenzo N (2016) Techno-economic analysis of hydrogen production using biomass gasification-a small scale power plant study. *Energy Proc* 101:806–813
73. Luz FC, Rocha MH, Lora EE, Venturini OJ, Andrade RV, Leme MM, del Olmo OA (2015) Techno-economic analysis of municipal solid waste gasification for electricity generation in Brazil. *Energy Convers Manage* 103:321–337
74. Buragohain B, Mahanta P, Moholkar VS (2010) Biomass gasification for decentralized power generation: the Indian perspective. *Renew Sustain Energy Rev* 14(1):73–92

75. Dell'Antonia D, Cividino SR, Malev O, Pergher G, Gubiani R (2014) A techno-economic feasibility assessment on small-scale forest biomass gasification at a regional level. *Appl Math Sci* 8(131):6565–6576
76. Andersson J, Lundgren J (2014) Techno-economic analysis of ammonia production via integrated biomass gasification. *Appl Energy* 130:484–490
77. Nouni MR, Mullick SC, Kandpal TC (2007) Biomass gasifier projects for decentralized power supply in India: a financial evaluation. *Energy Policy* 35(2):1373–1385
78. Kunii D, Levenspiel O (2013) *Fluidization engineering*. Elsevier
79. Samiran NA, Jaafar MN, Ng JH, Lam SS, Chong CT (2016) Progress in biomass gasification technique—with focus on Malaysian palm biomass for syngas production. *Renew Sustain Energy Rev* 62:1047–1062
80. Jorapur R, Rajvanshi AK (1997) Sugarcane leaf-bagasse gasifiers for industrial heating applications. *Biomass Bioenergy* 13(3):141–146
81. Mande S, Kumar A, Kishore VV (1999) A study of large-cardamom curing chambers in Sikkim. *Biomass Bioenergy* 16(6):463–473
82. Jayah TH, Fuller RJ, Aye L, Stewart DF (2007) The potential for wood gasifiers for tea drying in Sri Lanka. *Int Energy J* 2(2)
83. Tippayawong N, Chaichana C, Promwangkwa A, Rerkkriangkrai P (2011) Gasification of cashew nut shells for thermal application in local food processing factory. *Energy Sustain Dev* 15(1):69–72
84. Dutta PP, Baruah DC (2014) Gasification of tea (*Camellia sinensis* (L.) O. Kuntze) shrubs for black tea manufacturing process heat generation in Assam, India. *Biomass Bioenergy* 66:27–38
85. Sutar KB, Kohli S, Ravi MR (2017) Design, development and testing of small downdraft gasifiers for domestic cookstoves. *Energy* 124:447–460
86. Sridhar G, Paul PJ, Mukunda HS (2001) Biomass derived producer gas as a reciprocating engine fuel—an experimental analysis. *Biomass Bioenergy* 21(1):61–72
87. Ramadas AS, Jayaraj S, Muralidharan C (2006) Power generation using coir pith and wood derived producer gas in a diesel engine. *Fuel Process Technol* 87:849–853
88. Yin XL, Wu CZ, Zheng SP, Chen Y (2002) Design and operation of a CFB gasification and power generation system for rice husk. *Biomass Bioenergy* 23(3):181–187
89. Wu C, Yin X, Zheng S, Huang H, Chen Y (2008) A demonstration project for biomass gasification and power generation in China. *Progress in thermochemical biomass conversion*, p 465
90. Rinaldini CA, Allesina G, Pedrazzi S, Mattarelli E, Savioli T, Morselli N, Puglia M, Tartarini P (2017) Experimental investigation on a common rail diesel engine partially fuelled by syngas. *Energy Convers Manage* 138:526–537
91. Boerrigter H, Calis HP, Slort DJ, Bodestaff H (2004) Gas cleaning for integrated biomass gasification (BG) and Fischer-Tropsch (FT) systems; experimental demonstration of two BG-FT systems. *Acknowledgement/Preface*, p 51
92. Clausen LR, Elmegaard B, Ahrenfeldt J, Henriksen U (2011) Thermodynamic analysis of small-scale dimethyl ether (DME) and methanol plants based on the efficient two-stage gasifier. *Energy* 36(10):5805–5814
93. Sikarwar VS, Zhao M, Clough P, Yao J, Zhong X, Memon MZ, Shah N, Anthony EJ, Fennell PS (2016) An overview of advances in biomass gasification. *Energy Environ Sci* 9(10):2939–2977

Gas Cleaning and Tar Conversion in Biomass Gasification

Sudip Ghosh

Abstract Producer gas, derived from biomass gasification, contains a wide variety of compounds organic as well as inorganic, apart from the gas species and particulate matters. The hydrocarbon compounds present in the raw gas, which have comparatively lower molecular weights, act as fuel in gas turbine or gas engines. Hydrocarbons with higher molecular masses are collectively called tars. Relatively simpler tars often polymerize into more complex structures. These heavier species quickly condense, some even solidify, and choke the particulate filters and other restrictions and valves in the gas paths, causing serious obstruction to continuous operation of the application components. Some other impurities, like sulphides and halides, too cause damages to the materials of downstream equipment. It is, therefore, essential to remove the tars and impurities in the product gas to the extent possible. Tars also pollute the environment if discharged untreated. If, however, tars could be cracked and converted to permanent gas species, the producer gas calorific value could be improved substantially. Tars can be eliminated or effectively converted or their production rates can be reduced by certain measures. They include installing separation devices, modifying the conditions and parameters of gasification, modifying the gasifier design, using additives and catalysts. This chapter discusses these measures or processes that are aimed at tackling the tars.

Keywords Biomass • Gasification • Tars • Gas cleaning • Tar cracking

1 Introduction

Biomass gasification is a thermochemical conversion process in which solid biomass gets converted into combustible gas mixture that is traditionally known as producer gas. The producer gas contains CH_4 , CO , CO_2 , H_2 and N_2 as its primary

S. Ghosh (✉)

Department of Mechanical Engineering, Indian Institute of Engineering Science and Technology, Shibpur, Howrah 711103, WB, India
e-mail: ghoshsudip@mech.iiests.ac.in; sudipghosh.becollege@gmail.com

© Springer Nature Singapore Pte Ltd. 2018

S. De et al. (eds.), *Coal and Biomass Gasification*, Energy, Environment, and Sustainability, https://doi.org/10.1007/978-981-10-7335-9_6

151

constituents along with some amount of water vapour. A part of unconverted charcoal and fly ash particles get carried over by the producer gas during gasification. Some other species are also found in traces or in far less amounts compared to the permanent gas species. The presence of these species makes the product gas harmful for the downstream components, and the gas needs to be cleaned before its end use. Because of this harmful nature these species together are called contaminants or impurities. Apart from particulates, a couple of halides or sulphides and a few alkali metals, a variety of heavier carbonaceous (rather, hydro-carbonaceous) compounds, many of them being aromatics, make up these contaminants. These carbonaceous contaminants are all described by a common term called tars. Various definitions of tar exist. The IEA gasification task force recognizes “all organics boiling at temperature above that of benzene” as tars. Varying degree of gas cleaning is required to render the producer gas suitable for use in the final energy conversion devices like internal combustion engines, gas turbines and fuel cells.

During biomass gasification, the first process which takes place (after drying) is pyrolysis, occurring in the pyrolysis zone of the gasification reactor. During pyrolysis, the dried biomass breaks up to form a range of volatile gases, liquids and char. The volatiles, liquids and char then react and recombine in a series of reactions to form many high molecular mass hydrocarbon compounds while some permanent gas species like CH_4 , CO , H_2 , H_2O and CO_2 get liberated [1]. Some low-molecular-mass hydrocarbons and oxygenated compounds [2–3] are also generated in the process, but they usually do not pose high threat to the downstream components and can be used as fuel. But higher molecular mass hydrocarbons act as hindrance during application of producer gas. By tar, we therefore usually mean these higher molecular mass hydrocarbons. Tars are therefore unavoidable by-products of gasification. Tar compounds can condense or polymerize into more complex structures causing problems (chocking and attrition) for the downstream components such as pipes, filters, blowers, combustors, heat exchangers and the work producing engines or turbines. Besides, the total efficiency gets reduced and the system cost increases. In order to manage and contain tar species within acceptable levels, a detailed understanding of different tar species and their formation, characteristics and reaction affinities is essential.

The composition, properties and quantity of tar in producer gas vary remarkably depending upon the biomass feedstock, gasifier type and gasification conditions. Biomass-derived tars consist of several hundreds of hydro-carbonaceous species, which include single-ring to five-ring aromatic compounds. Municipal solid wastes (MSWs), which often has 60–70% biomass content, give rise to similar tar mix as biomass during gasification [4, 5]. Typical tar compounds derived from biomass gasification can be classified into three categories, i.e. primary, secondary and tertiary tars as shown in Fig. 1. The primary tar compounds are produced during pyrolysis process itself by direct breakdown of the constituents of biomass like cellulose, hemi-cellulose and lignin. The primary tar compounds are condensable oxygenated organic molecules. Milne and Evans [6] listed variety of compounds and mixed oxygenates in this group: acids, alcohols, sugars, aldehydes, ketones, phenols, furans, guaiacols, syringols, etc. Each of these species reacts with surrounding

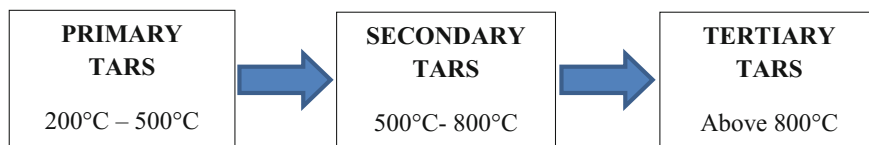


Fig. 1 Transformation of tars

Table 1 Tar classification based on molecular mass ([7, 9])

Groups	Compounds
Light aromatics (single ring)	1,2,4-Trimethylbenzene, Ethylbenzene, Toluene, Propylbenzene, Styrene, Xylenes
Heterocyclic aromatics	Benzofuran, Cresols, Dibenzofuran, Dibenzophenol, Isoquinoline, Phenol, Pyridine, Quinoline
Light PAHs (2–3 ring)	Acenaphthalene, Anthracene, Biphenyl, Fluorene, Indene, Methylnaphthalene, Naphthalene, Phenanthrene
Heavy PAHs (3–6 ring)	Chrysene, Fluoranthene, Pyrene, Perylene
GC-undetectable (7-ring or higher)	Very heavy tars that cannot be detected by GC

species and converts into secondary tar at relatively higher temperature and subsequently into tertiary tar compounds. Secondary tar compounds are molecules heavier than the primary ones. Olefins and phenols are two important constituents of this kind of tar. Tertiary tar compounds which mainly consist of polyaromatic hydrocarbons (PAHs), benzene, naphthalene, etc. are very stable [6]. Once secondary and tertiary tars are produced, no primary tar can be found in the mixture.

Another kind of classification exists, which is based on the molecular weights of the compounds and number of rings. They can be summarized as shown in Table 1 [7]. Yet another popular approach is to identify and combine several tar components into to

Table 2 Tar compounds identified under distinct subgroups [8]

Subgroups	Compounds
Aromatic compounds	Indene, Mesitylene, Phenylacetylene, Styrene
Aromatic nitrogen compounds	Carbazole, Isoquinoline, Indole, Quinoline
Furans	2-Methylbenzofuran, Benzofuran, Dibenzofuran
Guaiacols	Eugenol, Guaiacol, Isoeugenol
Naphthalenes	1-Methylnaphthalene, 2-Methylnaphthalene, Naphthalene
PAHs (except Naphthalenes)	4,5-Methylphenanthrene, Acenaphthylene, Acenaphthene, Anthracene, Biphenyl, Fluorene, Fluoranthene, Phenanthrene, Pyrene
Phenols	Phenol, 2-Methylphenol, 4-Methylphenol, 2,6 Dimethylphenol; 2,4-Dimethylphenol, 3,5-Dimethylphenol, Catechol

subgroups as shown in Table 2 [8]. The subgroups are primarily based on their related chemical structures and properties.

2 Formation of Tars

Biomass essentially consists of three types of polymers: cellulose, hemi-cellulose and lignin, in near-equal proportions, though varying with types of biomass. For example, woody biomass contains higher proportion of lignin than straw [10]. In a gasifier, the biomass fuel first undergoes heating and drying. Once heated sufficiently (over 200 °C), pyrolysis process initiates, where the complex polymers are broken down. Primary pyrolysis products are char, liquids, vapours and gases (Fig. 2). Cellulose and hemi-cellulose mainly get converted into liquids, and the other product gases and char are formed due to degradation of lignin [11]. At low temperature, formation of liquid predominates while at high temperature and high heating rate, gas generation rate tends to increase because of faster devolatilization of lignin.

Figure 3 shows the pyrolysis zone along with drying and other reaction zones for the fixed bed gasifiers. Although drying continues in the pyrolysis zone, most of the moisture gets removed in the drying zone, below 200 °C. As the temperature approaches 300 °C, the reduction of high molecular weight constituents of the biomass, mainly amorphous cellulose, starts forming carbonyl and carboxyl group radicals. Carbon monoxide and carbon dioxide are also liberated during the reduction process. As the temperature rises further, the resultant crystalline cellulose gets decomposed further, forming char, liquid tars and gaseous products. The

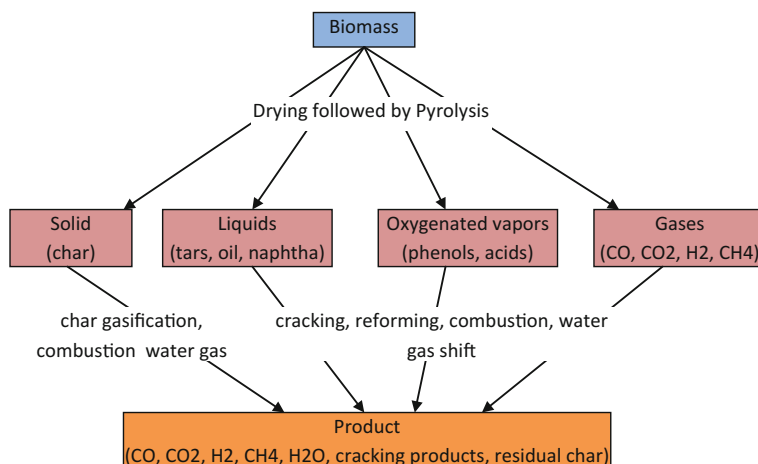


Fig. 2 Products of biomass pyrolysis (adapted from [12])

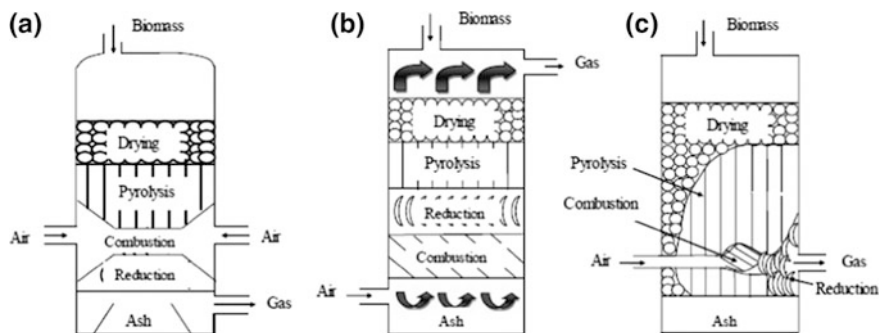


Fig. 3 Drying, pyrolysis and reaction zones of gasifiers [13]

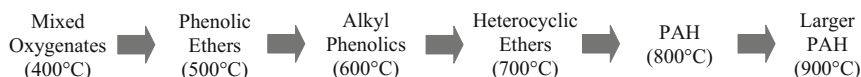


Fig. 4 Tar maturation and transition [6, 15]

hemi-cellulose also gets decomposed forming volatile gases, char and tars. The lignin gets decomposed at relatively higher temperature (up to 500 °C) and forms methanol, acetic acid and acetone [13].

The pyrolysis products pass through different phases of maturation as the temperature increases, as shown in Fig. 4. The initial biomass constituents get progressively destroyed and the secondary and tertiary processes take over, forming secondary and tertiary products such as ethers, phenols and PAHs. Evans and Milne [14] nicely described schematically the changing severity of pyrolysis through the different reaction regimes, as shown in Fig. 5.

In the temperature span 700–800 °C, secondary tars reach maximum level, beyond which they transform to tertiary tars of alkyl and PAH types, as can be seen in Fig. 6 [6]. The yield of condensable tars is influenced greatly by the reaction temperature as shown by Baker et al. [17] (Fig. 7, [18]). When flash pyrolysis occurs at relatively higher temperature (600–650 °C), tar yield is greatly reduced.

Baker et al. [17] showed that in fluid bed steam gasification, tar levels of 15%, found at 600 °C, could be reduced to 4% at 750 °C. For oxygen-blown fluid beds, tar levels were found to be 4.3% at 750 °C and 1.5% at 810 °C. In an entrained flow gasifier, operated at 1000 °C, tar level was found to be 1% only. Table 3 segregates the chemicals under different temperature regimes as was done by Elliot [15].

The dependence of tars production on the type of gasifier is a recognized fact. Lesser amounts of tars are produced in downdraft gasifiers than in fixed bed gasifiers under similar air equivalence ratio. Variations in the relative locations of drying, pyrolysis, oxidation and reduction zones play significant roles along with

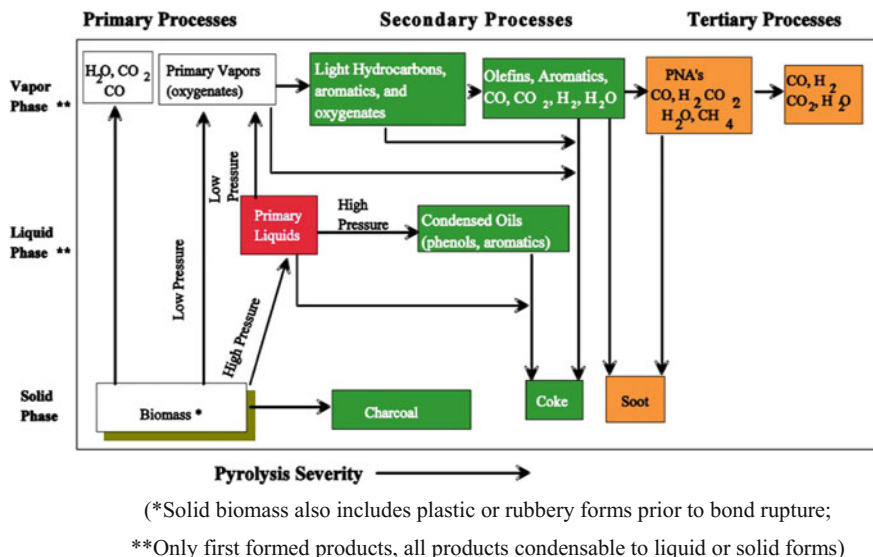


Fig. 5 Reaction zones on the pyrolysis pathway [16]

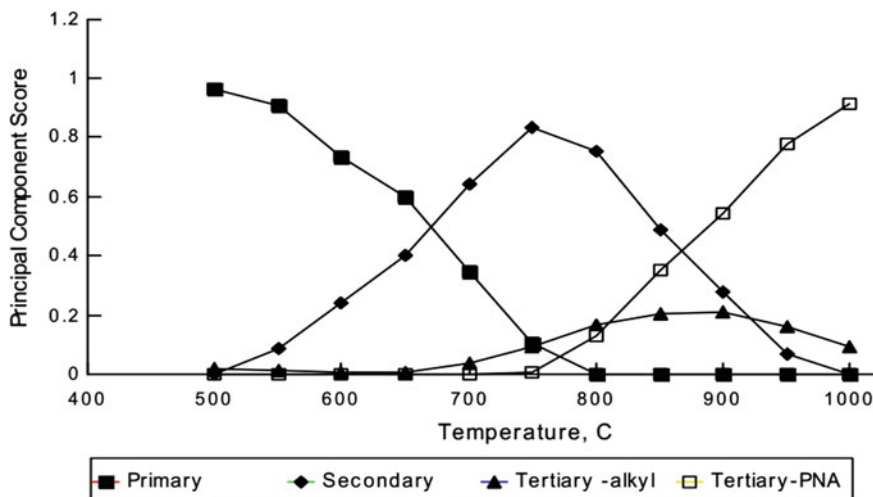


Fig. 6 Tar transition: primary-secondary-tertiary

characteristics of bed materials, operational parameters and kinetic features. A good review in this regard could be found in NREL’s 1998 report on biomass tars [6]. Wide variations exist in the estimates for raw producer gas tar loading, particularly

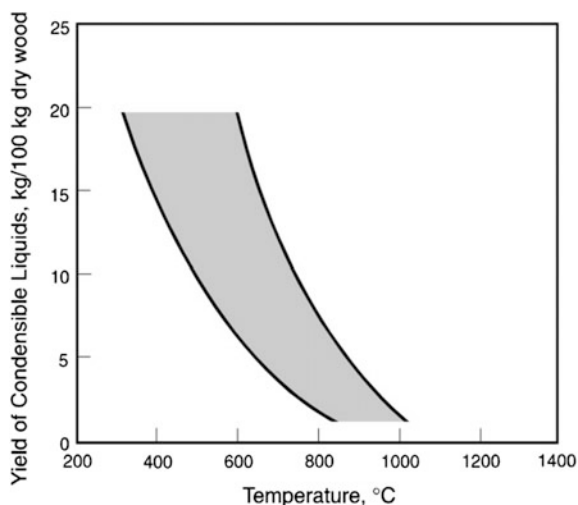


Fig. 7 Temperature versus tar yield

Table 3 Tar chemicals formed at different temperature zones [15]

Flash pyrolysis (conventional) 450–500 °C	Flash pyrolysis (high-temperature) 600–650 °C	Steam gasification (conventional) 700–800 °C	Steam gasification (high-temperature) 900–1000 °C
Acids	Benzenes	Acenaphthylenes	Acenaphthylene
Aldehydes	Benzofurans	Benzantracenes	Acephenanthrylene
Alcohols	Benzaldehydes	Fluorenes	Benzopyrenes
Ketones	Biphenyls	Phenanthrenes	Fluranthene
Furans	Catechols	Benzaldehydes	Naphthalene
Guaiacols	Naphthalenes	Naphthalenes	Phenanthrene
Phenols	Phenanthrenes	Naphthofurans	Pyrene
Syringols	Phenols	Phenols	PAHs (heavier)

for updraft systems. According to Milne and Evans [6], whose reports are primarily based on NREL studies, the average tar level in updraft gasifiers is about 50 g/Nm^3 . An ECN study [9] stated the level to be in the order of 100 g/Nm^3 . Hassler et al. [19] had put the level as $10\text{--}150 \text{ g/Nm}^3$. Better agreement is found on the tar loading of raw gas of downdraft and fluidized bed gasifiers. In downdraft gasifiers, the average loading is less than 1 g/Nm^3 . Fluidized bed systems (including the CFBs) usually have tar loading inbetween the average values for the other two, typically about 10 g/Nm^3 [6, 9]). Representative ranges for fixed and moving bed gasifiers have been reported by Stevens [20] as shown in Table 4.

Table 4 Representative tar and particulate levels of gasifiers [20]

Gasifier type	Particulate loading (g/Nm ³)			Tar loading (g/Nm ³)		
	Low	High	Representative range	Min	Max	Representative range
Fixed bed						
Updraft	0.01	10	0.1–0.2	0.04	6	0.1–1.2
Downdraft moving bed	0.1	3	0.1–1	1	150	20–100
Fluid bed (BFB)	1	100	2–20	<0.1	23	1–15
Fluid bed (CFB)	8	100	10–35	<1	30	1–15

3 Gas Cleaning

Cleaning aims to remove or convert, apart from tars, particulates (unburnt char as well as ash) and other non-tar impurities such as alkali metals (Na, K), compounds of heavier metals like Pb and Hg, halides, sulphur compounds (H₂S, COS, SO₂), nitrogenous compounds (ammonia, HCN), etc. Removing impurities and contaminants is the core objective of traditional gas cleaning, which mostly employs physical separation devices. Most often, a combination of these devices are used to achieve the desired separation. Conventionally, scrubbers (both wet and venturi), cyclone separators, filters (metallic, fabric, bed and bag types) are used in a sequence to clean raw producer gas. The heavier (high-boiling) tar species, unless removed, quickly condense, some even solidify and choke the pipe bends and valves in the gas path, particulate filters and other restrictions, causing serious obstruction to continuous operation of the application components. Some other impurities, like sulphides and halides, cause damages to the materials of downstream equipment. Hence, it is essential to remove or considerably reduce the level of tars and impurities in the product gas. Table 5 shows the types of impurities present in the producer gas, related issues of concern and the usual removal techniques adopted for them [12].

Table 5 Impurities and their removal techniques

Impurities	Issues	Treatments
Particulates (ash, unconverted char)	Erosion	Cyclones, ESP, barrier filters
Tars (vapours and liquids)	Clogging and deposition, corrosion	Wet scrubbers, ESP, barrier filters, catalytic beds
Alkali metals (Na/K-salts)	Hot gas corrosion	Cooler, scrubber, filter
N (ammonia/HCN)	Combustion NO _x	Wet scrubber
Halides (Cl, F)	Catalyst poisoning, corrosion	Scrubber, activated carbon
Sulphur (H ₂ S, COS, SO ₂)	corrosion	Scrubber, activated carbon/Fe

Table 6 Impurities and their tolerance levels for different applications

Impurities	Unit	IC engines	Gas turbines	MCFC	SOFC
Particulates (size)	mg/Nm ³ (μm)	<50 (<10)	<30 (<5)	10 ppm (w) (<3 μm) Aromatics: 0.5% (v) Cyclics: 0.5% (v)	
Tars	mg/Nm ³	<100	<10.0–		
Alkali metals	mg/Nm ³	<0.1	<0.1	<10 ppm	–
N-species	ppm(v)	–	<50	<1 vol.%	<5000 ppm
S-species	ppm(v)	<20	<20	<0.5 H ₂ S (anode) <1 SO ₂ (cathode)	<0.5 H ₂ S
Halides	ppm(v)	–	<1	<1	<1

The selection of individual separating devices and their combination depends on the requirement of the end equipment. While the combustion engines (IC engines, gas turbines) could tolerate some impurities to a certain level each, non-combustion systems (like fuel cells) and fuel synthesis systems (that often employ contaminant-sensitive catalysts) require very stringent levels of contaminants. Table 6 shows acceptable limits of contaminants for combustion engines and high-temperature fuel cells, viz. solid oxide fuel cell (SOFC) and molten carbonate fuel cell (MCFC) [11–5, 19]). It might be noted here that even when the product gas is used for fuel synthesis (such as methanation and Fischer–Tropsch (FT) synthesis), rather than for direct consumption in engines or fuel cells, the producer gas impurities need to be at levels that the processes can accept. Both methanation reactor for synthetic natural gas (SNG) generation and FT reactors for synthetic oil production employ catalysts that are damaged or degenerated by the presence of tars and other contaminants like HCN, H₂S and COS [22].

Typical cleaning trains employed for IC engine application are shown in Fig. 8. Raw gas from the gasifier is usually passed through a wet scrubber and then through two stages of fabric filters before feeding to the engine (Fig. 8a). For better separation of impurities, as may be required for 100% producer gas-fed engines, additional scrubbers, cyclone separator and bed filters are added to the train (Fig. 8b).

3.1 Wet Scrubber

Wet scrubbing has been and is a widely employed technique for gas cleaning for combustion engine application. Aimed primarily at removal of tars, a wet scrubber uses a liquid water spray tower, typically maintaining an operating temperature in the range of 35–60 °C for effective removal of condensed vapour [23]. Tar-laden hot raw gas from gasifier undergoes fast cooling and liquid droplet separation.

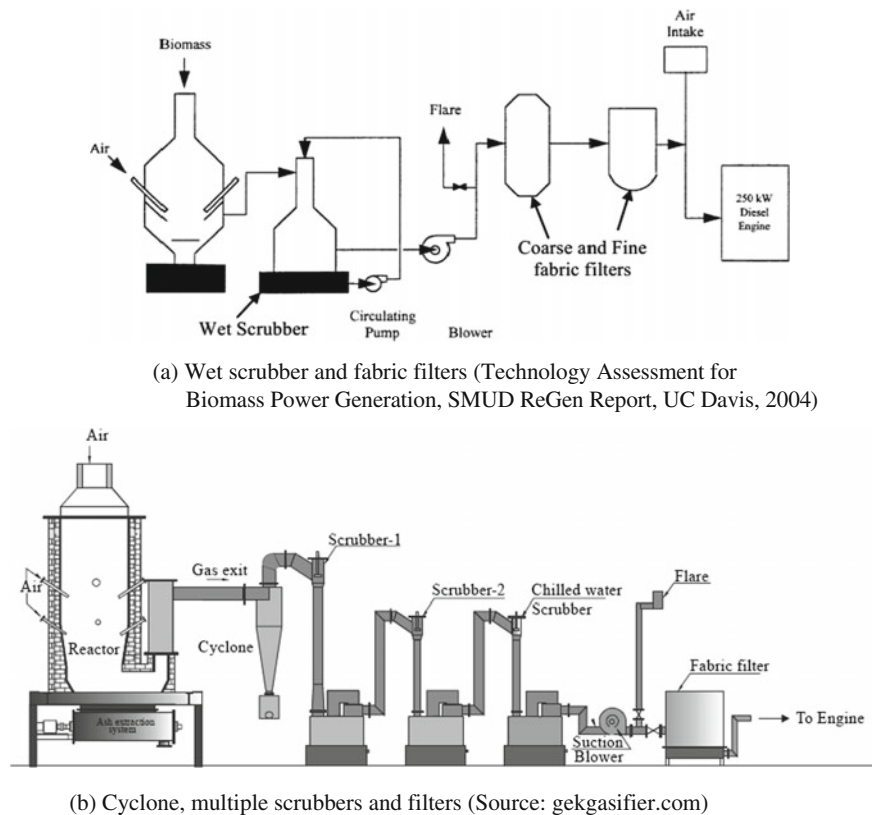


Fig. 8 Gas-cleaning trains in a gasifier-gas engine systems

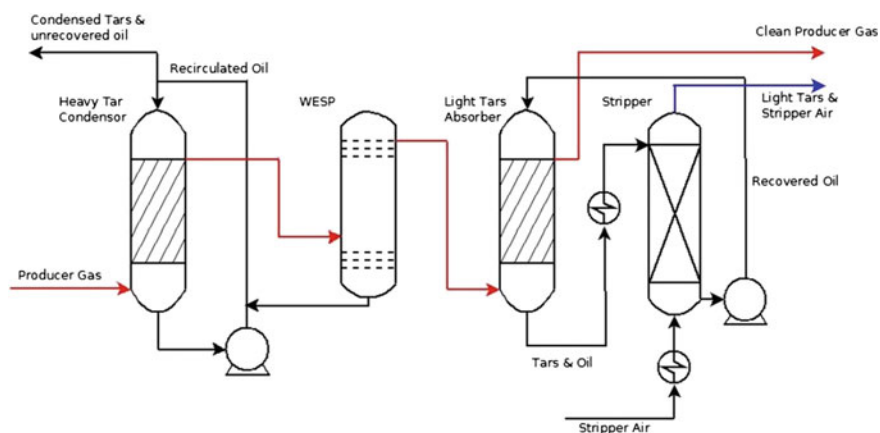
Some designs employ a separate quench cooler prior to the separation chamber [19].

A number of scrubber designs are available; spray towers, sieve plate scrubber, impingement scrubbers, baffle scrubbers, packed bed scrubber, cyclone spray scrubber and venturi scrubbers [24]. Apart from tars, scrubbing also removes particulates to a considerable extent. A venturi design creates a higher pressure drop across the venturi throat (2.5–25 kPa), allowing a better spray into the gas stream. Gas velocity in the throat area is typically in the range of 60–125 m/s. Particulate removal efficiency is proportional to the pressure drop across the venturi. Venturi scrubbers can thus remove up to 99.9% of particles of sizes over 2 μm (typically 95–99% of particles over 1 μm , Baker et al. [25], [20]). Often, a spray tower is used in combination with a venturi scrubber or a cyclonic demister to achieve higher degree of removal for both tars and particulates. Table 7 shows the removal efficiency of different scrubbers and scrubber combinations [20].

Wet scrubbers are widely used in small-scale biomass gasification systems. But the ones that are of relatively simple construction and are economical do not always

Table 7 Removal efficiency of different scrubbers and scrubber combinations

Scrubber types and combinations	Tar removal efficiency (%)	Scrubber type	Pr drop (cm water)	Particle size for 80% removal (μm)
Spray scrubber	Up to 60	Spray tower	1.5–4	10
Venturi scrubber	50–90	Impingement	5–125	1–5
Spray + venturi	83–90	Packed bed	5–125	1–10
Venturi + cyclonic	93–99	Venturi scrubber	10–250	0.2–0.8
Vortex scrubber	63–78			

**Fig. 9** OLGA scrubbing system developed by the ECN [26]

yield effective separation of all types of tars and particulates. The problem is more acute for small-scale systems when biomass feeds have higher moisture level and the system operates at unsteady conditions due to low thermal mass.

In some wet scrubbing system, oil or bio-oil (like rape methyl ester—RME) is used, instead of water, as the scrubbing medium [23]. OLGA is one such non-water scrubbing system developed by the ECN, Netherlands. The scrubber liquid, after getting saturated with tar and condensate in scrubber, is regenerated and recycled to the scrubber. Figure 9 gives the schematic of the OLGA system.

3.2 Barrier Filters

Barrier filters usually follow a scrubbing unit, which ensures that a cooled gas stream, after partial removal of tars and particulates, enters the filtering materials. Many different types of barrier filters are in use in biomass gasification systems,

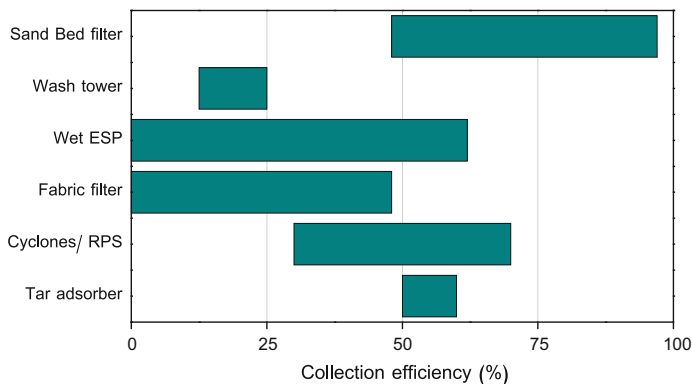


Fig. 10 Collection efficiency (%) for heavy tars of different gas-cleaning systems

particularly in small-scale applications. The presence of particulates, removal of which is also the objective of barrier filters, form caked mixtures together with the separated tar droplets, making the problem of separation compounded. Fabric bag filters and metallic sieve-type filters suffer mostly due to this solid tars accumulation plugging the pores of the surfaces. Teflon (PTFE)-based filter materials usually have a maximum operating temperature of 230 °C while fabric filters developed for IISc/Dasag gasification system operate at about 350 °C [20].

Packed bed filters made of fine sawdust, wood chips, cork and sand are used extensively in smaller-scale biomass gasification, giving effective filtration of tars and fine particulates. Packed beds can yield very high tar separation efficiency with proper design, suitable bed material and good maintenance, as can be seen from Fig. 10 [19].

3.3 Other Cleaning Devices

Many other cleaning devices have been developed for producer gas or mixed gas with different levels tar loading and other contaminants, such as, wet electrostatic precipitator (wet ESP), cyclones and rotational particle separators (RPS), absorber beds.

Wet ESPs remove tar droplets from product gas streams using the principles of high-discharge ionization and migration of ionized droplets to a collecting electrode, similar to removing dry ionized particulates from mixed gas stream removal, with ionization of the tar droplet followed by migration of the ionized droplet to a charged collecting point. A wire and tube construction is preferred for tar collection instead of plate collectors used for dry particulates. Wet ESPs operate at temperatures up to 150 °C, and the collecting surfaces are washed continuously to remove the tar deposits. They have high removal efficiency (as high as 99%) and have a

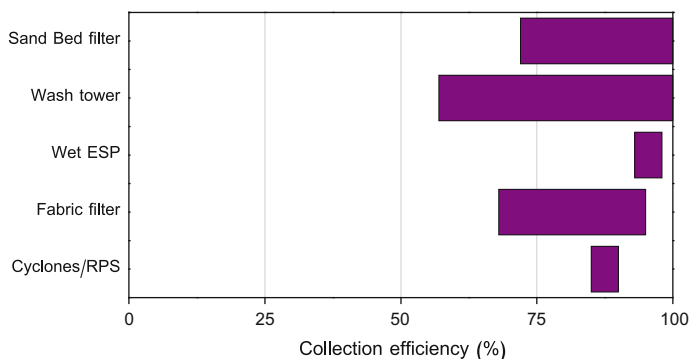


Fig. 11 Particulate collection efficiency (%) of the cleaning devices [19]

mature technology. However, high capital and operating costs stand in the way of their wider deployment [19].

Cyclones, RPS filters and vortex separators use centrifugal actions to separate particulates and tar aerosols. Like barrier filters, particulates and tars create sticky deposits on separator surfaces, creating operational problems in tar removal and maintenance. Particulates and aerosols of lower sizes, under $1\ \mu\text{m}$, cannot be removed in these devices. Finer particulates, when required to be removed sufficiently, are removed by employing packed beds, impingement or vortex scrubbers or hot gas ceramic barrier filters (candle filters). Figure 11 compares the particle collection efficiency of different devices.

3.4 Removal of Other Contaminants

When raw gas undergoes cleaning in a train of separation devices, several other contaminants, apart from tars and particulates, also get converted or separated from the gas stream, partially or near-completely.

Alkali compounds, mostly in the form of salts of Na and K (owing to their presence in the biomass feeds), stay in vaporized form in the hot raw gas if the temperature is sufficiently high ($700\ ^\circ\text{C}$ or higher). The alkali vapours, therefore, are able to evade the filtering devices unless condensed [20]. Gas cooler or spray scrubber forces these alkali vapours to condense, which then form fine solids (ash) and together with tars, get removed in cyclones and barrier filters.

Halides, also formed during gasification, remain in vapour phase in raw gas. Upon cooling (in cooler or scrubber), they transformed to corresponding aqueous acid and can thus be separated from gas stream.

Ammonia, the major nitrogenous species in gas, also gets effectively removed in wet scrubbing. Similarly, alkaline wet scrubbing can remove sulphur species considerably from the raw gas.

4 Hot Gas Clean-Up (HGCU)

The cleaning technologies discussed so far mostly fall in the low-temperature category, typically operating below normal boiling point of water. Although some of them, operate at temperature above 300 °C. Need was felt to develop a reliable and a better barrier filter that could remove particulates and aerosols at elevated temperature that could retain gas sensible heat content as much as possible. Gasifier-gas turbine for integrated gasification combined cycle (IGCC) and later gasifier-fuel cell systems was the main driving forces. The first biomass IGCC (BIGCC) demonstration at Varnamo, Sweden, employed ceramic candles and later metallic filters, where warm gas at about 350 °C was passed through them before being fed to the GT [20]. Subsequently, ceramic candle filters were tested at higher temperature, some facilities employing them at 700 °C. Recent developments open up the prospect of using candle filters at 1000 °C and beyond [27].

While low-temperature cleaning train is more separation-based, the hot gas clean-up (HGCU) is a combination of separation and conversion. A hot gas clean-up system, employing components at medium to high-temperature levels, would provide better heat integration to the system. Removing tars and other contaminants, without much compromising the sensible heat of the raw product gas, poses a great challenge. One of the major objectives of HGCU is to decompose heavy aromatic tar species and to convert them into non-condensable permanent gas species. Thus, tar conversion or tar cracking is the essence of HGCU. Tar conversion not only tackles issue of contamination; it also retains much of the heating value of the producer gas by converting the tars species into usable gas species and thus improving the gas quality.

Integration of solid oxide fuel cells (SOFC) with biomass gasification holds the promise of reliable high-efficiency distributed generation. For SOFC, the biomass-derived producer gas needs to be cleaned sufficiently so as to remove most all the contaminants to very low levels. If conventional low-temperature gas-cleaning strategy is taken, clean gas after gas clean-up needs to be preheated (therefore incurring energy penalty) to a level acceptable to the SOFC stack, which usually operates in the temperature range of 900–1000 °C. Figure 12 shows the low-temperature, medium-temperature and high-temperature clean-up routes for SOFC application.

The hot gas filters employed in medium-temperature case would not require gas cooling if gasifier exit raw gas temperature corresponds to their typical operating temperature ranges (350–450 °C). After filtration, the producer gas may be passed through a catalytic partial oxidation (CPO) reactor and a catalytic reformer. The CPO ensures sustenance of temperature level required by the reformer catalyst, which then transforms tars and sulphur containing hydrocarbons to lighter S-free hydrocarbons and permanent gas species like CO, CO₂, H₂, H₂O and H₂S. H₂S is then removed by passing the gas over an active bed sorption material like ZnO [29]. This medium-temperature clean-up train has been successfully demonstrated in biomass-integrated gasification fuel cell (B-IGFC) process system implemented at

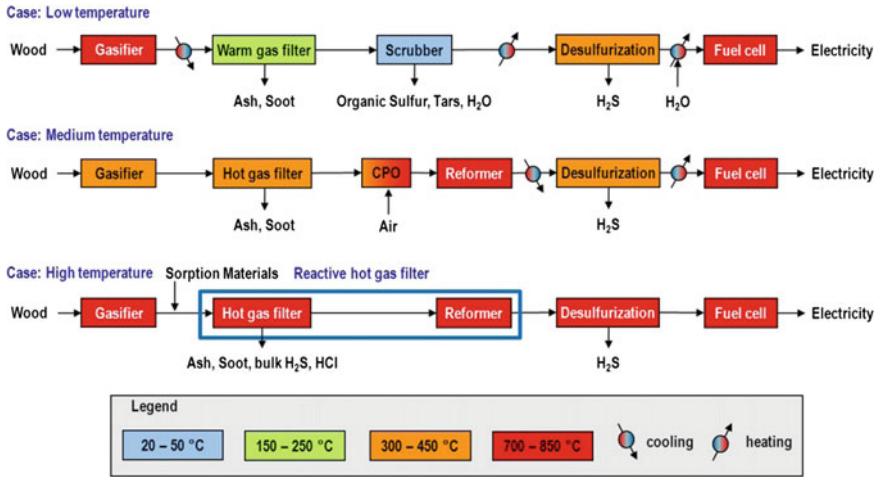


Fig. 12 Conventional and hot gas clean-up for SOFC [28]

Paul Scherrer Institute (PSI) [28, 30]. Use of HGCU components collectively at temperature level of 700–800 °C, as proposed by Rhyner [28], would offer the best heat integration, suitable for high-temperature gasifiers and requiring no cooling of hot gas. A reactive hot gas filter has been proposed in this configuration that integrates the hot gas filtration, sorption of acid gas and catalytic reforming in a single combined unit, operable at a temperature level of 850 °C.

5 Tar Cracking and Conversion

Tar cracking and conversion of heavier hydrocarbons into lower molecular weight hydrocarbons and non-condensable permanent gas species can be done in different ways. They are primarily categorized as follows:

- Thermal cracking
- Steam reforming
- Partial oxidation and
- Catalytic conversion.

5.1 Thermal Cracking

Thermal cracking is the simplest process of tar cracking, requiring no additives or catalyst. The temperature is increased to an extent such that the heavy tar

compounds crack into smaller and low-molecular-mass hydrocarbons and other lighter gases such as carbon monoxide, methane, hydrogen and water vapour. To promote thermal cracking, in above process some amount of hydrogen, air and oxygen are supplied as per requirement. Steam is also used as an input parameter to crack the tar into lighter component and useful gas species. Decomposition of large organic molecules takes place at temperature ranging from 1000 to 1300 °C, if the tar-laden gas is allowed some residence time is this temperature range. High-temperatures can be generated by (i) using high-temperature gasifiers (ii) heating the gas stream via heat exchangers (iii) introducing air or O₂ downstream of gasifier and (iv) using energy-efficient radio-frequency [31]. Many decomposition and chemical reactions take place simultaneously during thermal cracking. Figure 13 shows one representative scheme where toluene and naphthalene get cracked into lighter species that take part into more reactions. Higher temperature and longer residence time are known to promote thermal cracking [32].

Auto-thermal cracking or cracking in the presence of steam and hydrogen has been studied by many researchers to gain better understanding of tar cracking routes for the stable secondary and tertiary tar species. Thermal cracking effectively starts at a temperature level of 700 °C [33], but most of the tertiary species remain stable even up to a temperature of 900 °C [7]. In the temperature range of 900–1300 °C, conversion of most of them nears completion. Most often, in theoretical model studies as well as in experimental investigations, few single-ring or two-ring model aromatic tars are considered for analysis. They include naphthalene, phenol, toluene, benzene, pyrine, xylene. [3, 34, 35].

Among the most used model tars (including benzene, which is considered as an intermediate product in the conversion of other single-ring derivatives and PAHs),

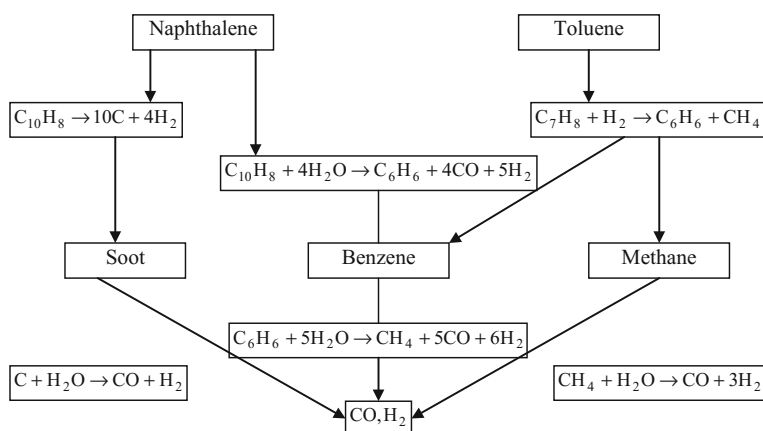


Fig. 13 Representative cracking steps for toluene and naphthalene [31]

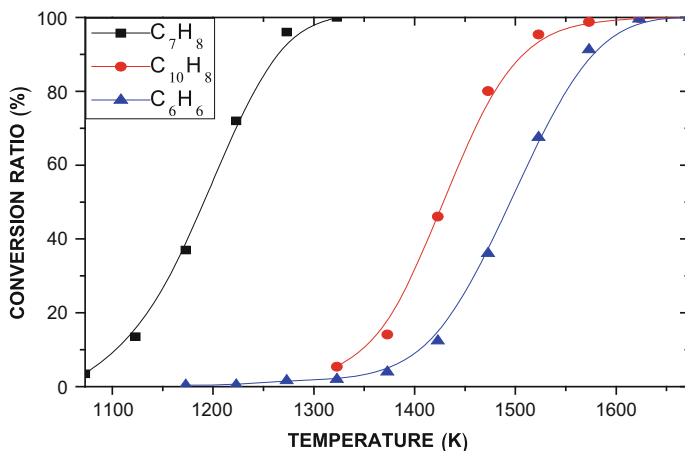


Fig. 14 Reactivity of model tars: benzene, toluene and naphthalene [34]

toluene (C₇H₈) shows higher reactivity at a comparatively lower temperature range (800–1000 °C), while naphthalene (C₁₀H₈) and benzene (C₆H₆) are found to remain stable even beyond 1000 °C (Fig. 14).

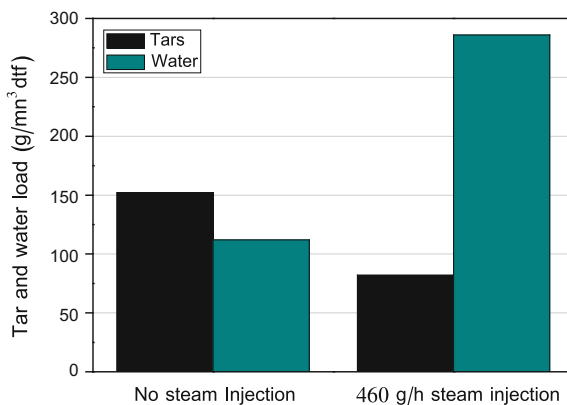
Studies with naphthalene suggest that thermal cracking at high-temperature often leads to generation of soot [34]. However, addition of H₂ and resorting to steam reforming could arrest this high-temperature soot formation and convert tars into CO, CO₂, CH₄ and H₂ [36, 37].

5.2 Steam Reforming

Steam reforming (STR), often considered under thermal cracking (in the absence of any catalyst activity), is another effective way of converting tars into non-condensable gas species. H₂ and CO are liberated as hydrocarbon reforming proceeds. Steam-to-carbon ration and reaction temperature are the two major influencing parameters in steam reforming. Use of in situ steam reforming by direct injection steam into gasifier bed has also been found to yield considerable tar conversion (Fig. 15, [30]).

Studies suggest steam reforming effectively destroys the stable tars at elevated temperature, enhancing carbon conversion to permanent gas species (CO, CO₂ and H₂) and improving the cleaned producer gas calorific value. Figure 16 shows relative temperature sensitivities of the reforming reactions involving the representative tars, viz. benzene, toluene and naphthalene [3]. Toluene conversion is occurring at comparatively lower range of temperature (800–950 °C), while benzene remaining mostly unaffected till 1100 °C.

Fig. 15 Producer gas tar content with and without steam injection [30]



Catalytic steam reforming (CSR) seeks to achieve tar conversion at lower temperature (below 900 °C). Ni and alumina are the common catalyst base materials. Poisoning of the catalyst is an issue. Metal catalyst (Ni) is very sensitive to the presence of S-species in the gas stream. In a mixed tar catalytic conversion experiment carried out at 850 °C, reported by NREL [38], established that Ni catalyst could effectively destroy species like phenol, cresol, naphthalene, phenanthrene, toluene and benzene (Table 8, [38]).

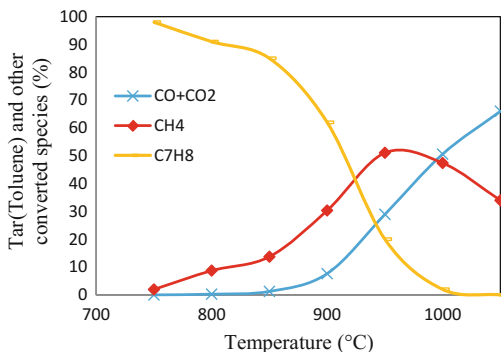
5.3 Partial Oxidation

Partial oxidation is another means of tar cracking. Oxidization with limited air is allowed which maintains high gas temperature and destroys considerable amount of tars (to the extent of 98–99% at 900 °C, [39, 40]). Most often, a catalytic partial oxidation (CPO) is preferred to promote desired reactions. A combination of catalytic partial oxidation and reforming could effectively convert tars even in medium-temperature range (Rhyner [28], see Fig. 12), making the processed gas suitable for fuel cell application.

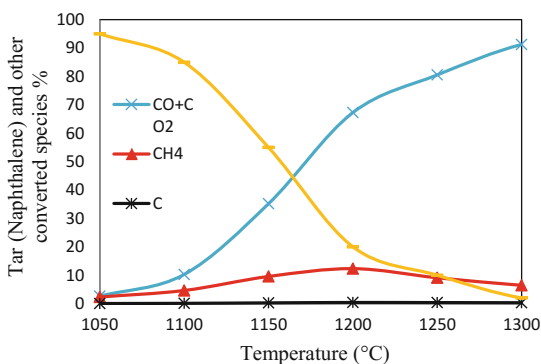
5.4 Catalytic Conversion

Catalytic tar decomposition is an effective route for conversion of tars at temperatures below 900 °C. The catalyst can be employed in the gasification reactor itself, in which case in situ tar conversion occurs as soon as they are formed in the reactor. The reactor design and its temperature and flow characteristics (or residence time) largely influence the extent of conversion. Fast catalyst de-activation is a major disadvantage. External reformer has the advantage of controlled-temperature

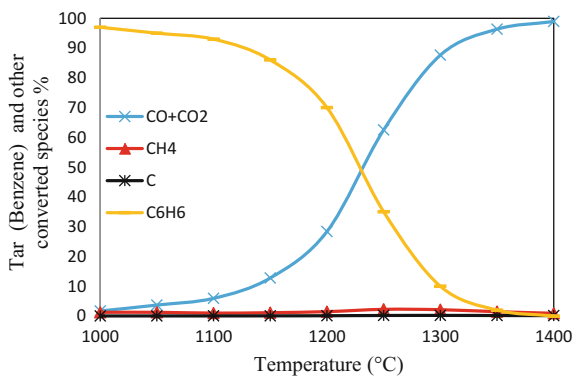
Fig. 16 Effect of temperature on tar conversion in steam reforming



(a) Steam reforming of Toluene (C_7H_8)



(b) Steam reforming of Naphthalene ($C_{10}H_8$)



(c) Steam reforming of Benzene

Table 8 Tar concentrations (ppmv) before and after Ni catalyst bed [38]

	Benzene (78)	Toluene (92)	Phenol (94)	Cresol (108)	Naphthalene (128)	Anthracene/ phenanthrene (178)	Total
Inlet	1035	375	340	125	250	50	2175
Outlet	505	110	55	0	30	0	700

operation of catalytic reactor. Non-metallic catalyst materials for tar decomposition like dolomites, zeolites and calcites could be employed in gasification reactors. They are relatively cheaper and perform well in contaminated gas. Metal catalysts, such as, Ni, Mo, Co, Pt and Ru in pure form or as mixtures supported on silica-alumina or zeolite base, have been used for tar decomposition [7, 30]. Sometimes, a combination of catalyst materials is used. A catalyst combination using NiMo/Al₂O₃ and dolomite has been reported to significantly promote toluene conversion in the temperature range of 650–50 °C. Dolomite catalyst has been found to promote benzene cracking significantly, reaching 40% at 950 °C and 80% at 1000 °C, while in the absence of catalyst material benzene conversion is only about 4% at 900 °C [7]. An elaborate review of the recent advances in catalytic tar conversion and comparative assessment of various catalyst materials could be found in Xu et al. [7]. In a recent study, using a catalytic candle filter (Ni and MgO) along with a catalytic dual fluid bed gasifier (Fe/Olivine bed catalyst), 80% tar reduction could be noted at the catalytic candle filter in the temperature range of 750–850 °C [41].

6 Conclusion

Tars are undesirable by-products of biomass gasification, posing threats to downstream components and energy conversion equipment. Their generation and gradual transformation are influenced by a number of parameters. Depending on the tolerance levels of the application equipment or final energy conversion process, tar cleaning and tar conversion systems need to be designed and implemented. While several cleaning options, having different levels of effectiveness, are available, they lead to separation of hydrocarbon contents leading to loss of fuel calorific value. Employing suitable tar conversion system could effectively destroy harmful tars, converting them to usable permanent gas species and improving product gas heat value. This chapter summarized technologies of gas cleaning employed in biomass gasification-based systems. Tar removal and tar conversion remained the main focus of discussion while issues related to other contaminants were also covered. Both traditional low-temperature cleaning system and hot gas clean-up systems were covered in detail. The process of tar formation during gasification as well as the processes employed in tar cracking and tar conversion has been elaborated so as to give the reader a clearer understanding of the issues involved in the selection of the gas-cleaning equipment. As could be seen, hot gas clean-up is the most desired

solution as it offers efficient conversion of tars and traces gas impurities, retaining the heat in the raw gas. New methods and approaches are increasingly being proposed and tried in order to upgrade the hot gas clean-up technology, making it suitable for implementation in high-efficiency energy conversion systems employing gas turbines and fuel cells.

References

1. Antonopoulos IS, Karagiannidis A, Gkouletsos A, Perkoulidis G (2012) Modelling of a downdraft gasifier fed by agricultural residues. *Waste Manage* 32:710–718
2. Marias F, Demarthon R, Robert-arnouil JP (2016) Modeling of tar thermal cracking in a plasma reactor. *Fuel Process Technol* 149:139–152
3. Bhandari PN, Kumar A, Bellmer DD, Huhnke RL (2014) Synthesis and evaluation of biochar-derived catalysts for removal of toluene (model tar) from biomass-generated producer gas. *Renew Energy* 66:346–353
4. del Alamo G, Hart A, Grimshaw A, Lundstrøm P (2012) Characterization of syngas produced from MSW gasification at commercial-scale ENERGOS Plants. *Waste Manage* 32:1835–1842
5. Arena U (2012) Process and technological aspects of municipal solid waste gasification. A review. *Waste Manage* 32:625–639
6. Milne TP, Evans RJ (1998) Biomass gasifier tar: their nature, formation and Conversion, NREL/TP-570-25357
7. Xu C, Donald J, Byambajav E, Ohtsuka Y (2010) Recent advances in catalysts for hot-gas removal of tar and NH₃ from biomass gasification. *Fuel* 89:1784–1795
8. Wolfesberger U (2009) First test run and tar analyses of a low temperature biomass pilot plant. Master thesis. Vienna University of Technology
9. Rabou LP, Zwart RW, Vreugdenhil BJ, Bos L (2009) Tar in biomass producer gas, the energy research centre of the Netherlands (ECN) experience: an enduring challenge. *Energy & Fuels* 23(12):6189–6198
10. Pedersen K, Malmgreem-Hansen B, Petersen P (1996) Catalytic cleaning of hot gas filtration. Biomass for Energy and the Environment. In Proceedings of 9th European Bioenergy Conference, Copenhagen, Denmark, June pp 24–27
11. Branca C, Giudicianni P, Di Blasi C (2003) GC/MS characterization of liquids generated from low-temperature pyrolysis of wood. *Industrial & Engineering Chemistry Research* 42(14): 3190–3202
12. Sikarwar VS, Zhao M, Clough P, Yao J, Zhong X, Memon MZ, Shah N, Anthony EJ, Fennell PS (2016) An overview of advances in biomass gasification. *Energy Environ Sci* 9:2939–2977
13. Sansaniwal SK, Pal K, Rosen MA, Tyagi SK (2017) Recent advances in the development of biomass gasification technology: A comprehensive review. *Renew Sustain Energy Rev* 72:363–384
14. Evans RJ, Milne TA (1987a) Molecular characterization of the pyrolysis of biomass. *Energy & Fuels* 1(2):123–138
15. Elliott DC (1988) Relation of reaction time and temperature to chemical composition of pyrolysis oils. ACS Symposium Series 376, *Pyrolysis Oils from Biomass*. E.J. Soltes and T.A. Milne (Eds), Denver, CO. April 1987
16. Evans RJ, Milne TA (1987c) An Atlas of Pyrolysis-Mass Spectrograms for Selected Pyrolysis Oils. Internal report. Golden, CO: Solar Energy Research Institute
17. Baker EG, Brown MD, Elliott DC, Mudge LK (1988) Characterization and Treatment of Tars from Biomass Gasifiers. Denver, CO: AIChE 1988 Summer National Meeting, pp 1–11

18. Evans RJ, Milne TA (1997) Chemistry of Tar Formation and Maturation in the Thermochemical Conversion of Biomass. In Developments in thermochemical biomass conversion, A.V. Bridgwater and D.G.B. Boocock (Eds). London: Blackie Academic & Professional, 2:803–816
19. Hassler PH, Nussbaumer T (1999) Gas cleaning for IC engine applications from fixed bed biomass gasification. *Biomass and Bioenergy*, 16(6):385–395
20. Stevens DJ (2001) Hot gas conditioning: recent progress with larger-scale biomass gasification systems. NREL report no SR-510-29952
22. Boerrigter H, Rauch R (2005) Syngas production and utilisation, Handbook of biomass gasification. Biomass Technology Group (BTG), The Netherlands
23. Fjellerup JS, Ahrenfeldt J, Henriksen UB, Gøbel B (2005) Formation, decomposition and cracking of biomass tars in gasification. DTU report
24. Reed TB, Das A (1998) Handbook of biomass downdraft gasifier engine systems. Biomass Energy Foundation Press, USA. ISBN 1-890607-00-2
25. Baker EG, Brown MD, Moore RH, Mudge LK, Elliott DC (1986) Engineering analysis of biomass gasifier product gas cleaning technology. Richland, WA: Battelle Memorial Institute, Biofuels and Municipal Waste Technology Division, PNL-5534
26. Brandin J, Tunér M, Växjö IO (2011) Small scale gasification: gas engine CHP for biofuels. Lund Publication
27. Chuah TG, Sibanda V, Knight P (2003) Gas cleaning at high temperatures using rigid ceramic filters. *Adv Powder Technol* 14(6):657–672
28. Rhyner U (2013) Reactive hot gas filter for biomass gasification. Dissertation for the degree of doctor of sciences, ETH Zurich
29. Turco M, Ausiello A, Micoli L (2016) The effect of biogas impurities on SOFC. Treatment of biogas for feeding high temperature fuel cells (edited volume). *Green Energy and Technology*, pp 137–149
30. Nagel FP, Ghosh S, Pitta C, Schildhauer TJ (2011) Biomass integrated gasification fuel cell systems—concept development and experimental results. *Biomass Bioenergy* 35(1):354–362
31. Din ZD, Zainal ZA (2016) Biomass integrated gasification—SOFC systems: technology overview. *Renew Sustain Energy Rev* 53:1356–1376
32. Houben M (2004) Analysis of tar removal in a partial oxidation burner (PhD). Eindhoven: Eindhoven University of Technology
33. Fagbemi L, Khezami L, Capart R (2001) Pyrolysis products from different biomasses: application to the thermal cracking of tar. *Applied energy* 69(4):293–306
34. Jess A (1996) Mechanisms and kinetics of thermal reactions of aromatic hydrocarbons from pyrolysis of solid fuels. *Fuel* 75(12):144–1448
35. Barman NS, Ghosh S, De S (2012) Gasification of biomass in a fixed bed downdraft gasifier—A realistic model including tar. *Bioresource Technology* 107:505–511
36. Ximena A (1989) Huttinger KJ Steam gasification of naphthalene as a model reaction of homogeneous gas/gas reactions during coal gasification. *Fuel* 68:1300–1310
37. Morf P, Hasler P, Nussbaumer T (2002) Mechanisms and kinetics of homogeneous secondary reactions of tar from continuous pyrolysis of wood chips. *Fuel* 81:843–853
38. Carpenter D, Ratcliff M, Dayton D (2002) Catalytic steam reforming of gasifier tars: On-Line monitoring of tars with a transportable molecular-beam mass spectrometer; Milestone Completion Report (No. NREL/TP-510-31384). National Renewable Energy Lab., Golden, CO.(US)
39. Brandt P, Henriksen UB (1996) Decomposition of tar in pyrolysis gas by partial oxidation and thermal cracking. In 9th European Bioenergy Conference, Elsevier pp 1336–1340
40. Houben MP, De Lange HC, Van Steenhoven AA (2005) Tar reduction through partial combustion of fuel gas. *Fuel*, 84(7):817–824
41. Garcia-Labiano F, Gayan P, Diego LF, Abad A, Mendiara T, Adanez J (2016) Tar abatement in fixed bed catalytic filter candle during biomass gasification in a dual fluidized bed. *Appl Catal B* 188:198–206

Part II
Experiments, Modeling and Numerical
Simulations of Gasification

Measurement Techniques: Cold Flow Studies

Premkumar Kamalanathan and Rajesh Kumar Upadhyay

Abstract It has been realized in recent decades that a proper investigation of gasification reactor requires the detailed information over the entire flow field, as well as time, at multiple scales. Such detailed information needs the use of sophisticated measuring techniques with capability to provide the required information over the entire flow field, as well as time, at multiple scales. Aside from the mean velocities and volume fractions, information about the flow fluctuations or dynamics (quantified in terms of cross-correlations and auto-correlations) is also desirable. In addition, it is preferable if such techniques are amenable to automation to reduce extensive human involvement in the data collection process. While such data are “stand-alone” sets of information, which can be used for design and scale-up strategies, it also provides information that is crucial to establish the validity of conventional models like phenomenological flow models describing residence time distribution (RTD), as well as more recent and sophisticated models like those based on computational fluid dynamics (CFD). In fact, it almost seems imprudent to validate CFD predictions on overall holdup and flow rates, because these spatial integrals of point properties are simply averages of a complete flow field that a CFD code is designed to and claims to compute. Thus, fair validation must involve validation at multiple scales, for which one needs experimental information also at multiple scales (and not just spatial and temporal averages). Several experimental techniques have been reported in past to quantify the flow field in gas–solid gasification reactors, with each technique having its own advantages and disadvantages. In this chapter, details of pressure, solid velocity, solid fraction, and RTD measurement techniques will be presented. Techniques will be divided majorly in two types, invasive and non-invasive. The postprocessing methods for each technique, advantages, and limitations will be discussed. Finally,

P. Kamalanathan · R. K. Upadhyay (✉)
Department of Chemical Engineering, Indian Institute of Technology,
Guwahati, Assam, India
e-mail: rkupadhyay@iitg.ac.in

P. Kamalanathan
e-mail: kpkkra@gmail.com

some of the recent findings on gas–solids circulating fluidized bed using radioactive particle tracking (RPT) technique will be discussed in detail to explain the use of the experimental techniques for design and scale-up of these reactors.

1 Introduction

Gasification process has been known from the nineteenth century, however got momentum for the past few decades due to the improvement over efficiency of the process and environmental concerns. Competitiveness of gasification process compared with the combustion in the carbon capture and gasification as a route to convert coal to other products drives the recent growth. Gasification at the industrial scale is carried out in moving bed, entrained, bubbling, and circulating fluidized bed. Breault [4] reported the commercially available technologies essentially involves any of the above contacting. Usually, the heat required for the gasification is generated in part of the reactor itself, and rest of the reactor is designed to have gasification reaction. The amount of conversion depends on the heat transport and flow properties of gasification agent, bed material (in fluidized beds), and fuel (coal or biomass).

Gasification reactor essentially involves contact of two or more phases where reactions happen. Reactor design and scale-up need thorough knowledge of the reactor; however, gasification reactors are complex and interactions of different phases present in the reactor are not well understood, particularly their ever-evolving transition along the reactor.

Investigation of such complex reactor demands the use of sophisticated measuring techniques with capability to provide the required information over the entire flow field, both global (time averaged) and local, at multiple scales [14]. Aside from the mean velocities and volume fractions, information about fluctuations is also needed. While such data are “stand-alone” sets of information and can be directly used to develop design and scale-up strategies, it also provides information that is crucial to establish the validity of phenomenological flow models and CFD models. A fair validation of CFD models must involve validation at multiple scales, for which one needs experimental information also at multiple scales (and not just spatial and temporal averages). This chapter describes the techniques for the measurement of hydrodynamics in gasifier at cold flow conditions with emphasis on the principal challenges in the implementation. The techniques are divided into pressure measurement, solid velocity measurement, volume fraction measurement of solids, and solid RTD measurement. This chapter does not attempt to cover all the aspects of the techniques. However, it gives the overall perspective and advantage and drawbacks of each technique which will enable the reader to choose the suitable technique based on the data required for their own applications, reactor

size, and operating conditions. Further investigation of gas–solid CFB based on radioactive particle tracking is discussed to demonstrate the depth of the information obtained from such sophisticated measurement techniques.

2 Pressure Measurement

For several decades, the pressure drop measurement is used, which is being simple, can be measured with ease, and can be applied at any conditions and chiefly applied to most of the industrial conditions. Pressure measurement is a straightforward measurement, and all it need is to proper positioning of the probe and precaution to avoid solid blockage of the probe. There are various kinds of pressure transducers available commercially which can measure differential or absolute pressure at high frequencies. Time-averaged measurements from two different planes are used for measuring the pressure drop between two different heights. Pressure drop measurements can be related to the solid holdup neglecting the solid and gas stress on the wall, as shown below

$$\varepsilon_g(\rho_p - \rho_g)g = -\frac{dP}{dx} \quad (1)$$

Such pressure drop measurements are used to find the solid holdup. In circulating fluidized bed gasifier, several pressure ports distributed along the length of the riser can be used to find the variation in solid holdup as a function of height. In bubbling and turbulent fluidized bed gasifiers, pressure difference between bed section and freeboard region gives the possibility to estimate the bed height if the average bulk density of the bed is known. Further, solid holdup itself gives the fair idea of the flow regime. However, in the transition zones and closely related zones, this flow regime demarcation may not give clear picture. Pressure fluctuations can also be used as tool for demarcation of the flow regime and gives better picture than the pressure drop measurements [45]. Recently, time series analysis of pressure fluctuations is used to characterize the dynamics of system under investigation. van Ommen et al. [91] listed the time domain and frequency domain analysis of pressure fluctuation data to characterize the system.

Pressure is a global measurement, and any change in the dynamics (bubble breakup and coalescence, clusters, etc.) changes the shear stresses, in turn pressure. However, pressure probes can only provide averaged information inside the bed. Hence, it is almost impossible to find the cause of the pressure change. For example, in turbulent or bubbling bed gasifier, pressure fluctuation can be caused because of the bubble breakup and coalescence and bubble formation at the distributor. In circulating fluidized bed gasifier, the formation of meso-scale meta-stable structures (commonly known as clusters), chocking, solid agglomeration, gas fluctuations, etc., can cause the pressure fluctuation. Further, local shear

stress may not be sensible along the column especially in the case of large-diameter columns [89]. In such cases, pressure fluctuations are measured locally instead of normally followed wall measurements. Such pressure probe measurement interferes with the gas/bubble flow behavior in the beds if the diameter of the probe is high or a purge flow is applied. Small probes and constant purge flow are often used to minimize the interference with the flow [28, 57, 89]. However, such probes can be easily damaged.

3 Solid Velocity Measurement Techniques

Velocity measurement technique can be classified as invasive and non-invasive technique. In invasive techniques, a probe is inserted inside the vessel to measure the flow field. The presence of a foreign element inside the vessel disturbs the flow field at the point of measurement itself due to the blockage of flow path, though the thickness of the probe is very small (sometimes in order of few μm). Further, the presence of solid particles, which are moving at relatively higher velocity (\sim few m/s), can damage the probe. However, due to the ease of application to obtain local values and relatively low cost, invasive techniques are widely used. Measurement techniques which are not intrusive and do not affect the flow are called as non-invasive techniques. Here in this chapter, we are not attempted to cover all the velocity techniques. The latest techniques which are widely used in the local measurements and validation of CFD model are focused.

3.1 *Optical Fiber Probe*

Optical fiber probes, pitot tube, extraction probe, and hot wire anemometry are the commonly used invasive techniques. Except optical fiber probes, other techniques are bulky and thus disturb the flow considerably. Pitot tube and extraction probe measure mixture properties and/or require separation of phases to obtain the solid velocity [48]. Optical fiber probe can be used to measure both velocity and solid volume fraction. It works based on the light reflection by the solids. Intensity of reflected light depends on the solid concentration, size, and material properties of solids [10, 95]. In the literature, different types of optical fiber probes are used which primarily differ in number of fibers used for receiving and transmitting light signal. One such three-fiber optical probe is shown in Fig. 1. For velocity measurement, time taken by the solids to travel between two receiving probes is measured. Cross-correlation is used to find the time traveled between the two probe points by assuming constant solid concentration of measured solids between the two points.

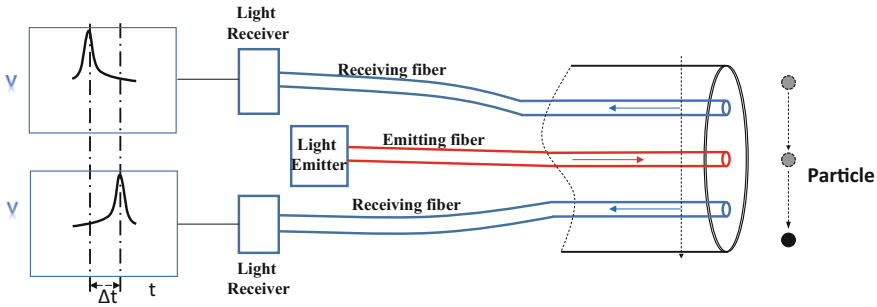


Fig. 1 Schematic of three fiber optical probe

$$R_{xy} = \frac{1}{T} \int_0^T v(t)g(t + \tau) \tag{2}$$

Time lag corresponding to the maximum correlation is considered as likely the time taken by the particle to travel between the probes. For better measurement of particle velocities, probe diameter should be small. If the diameter of probe is in the order of 1.5–2 mm, reflection measured by the receiving probe is of group of particles. Hence, in this case, cross-correlation will have preference for the solid clusters and individual particle velocity is missed. Further if the distance between the probe points is high or acquisition frequency is quite low, then particle may travel in the lateral direction leading to the disparities in the measurement. Hence, the probe must be compact and aligned in the direction of flow. To overcome the above limitations, five-point optical fiber probe was used in circulating fluidized bed (CFB) by Zhu et al. [106] and others. Typical size of a five-point optical fiber probe is of 200 μm. This helps in acquiring signal from a single or a group of smaller number of particle depending upon particle size. Velocity values are accepted only when the velocity evaluated by both pairs of fibers falls within the tolerance limit. This minimizes the error and increases the reliability of probe.

The optical probe can be used in pilot or real-scale plants. However, an extensive calibration is needed to measure the particle velocity. Further, the estimated solid velocity is strongly influenced by the gas flow in case of circulating fluidized bed and by rising bubbles in case of bubbling bed.

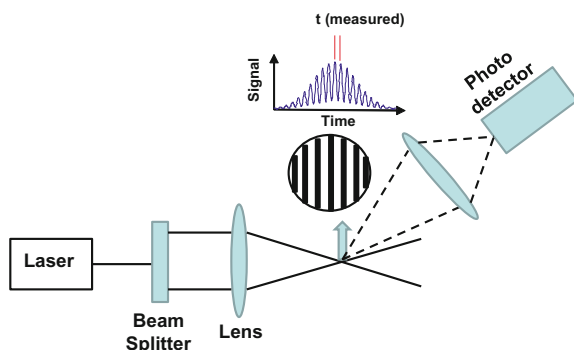
Laser Doppler velocimetry (LDV), positron emission particle tracking (PEPT), particle image velocimetry (PIV), radioactive particle tracking (RPT) are the widely used non-invasive techniques for local velocity measurement. Even though these non-invasive techniques exist for a long time, it has been found limited use in gasifier for the past two decades. Each of these techniques is briefly explained below.

3.2 Laser Doppler Velocimetry (LDV)

In LDV, velocity of a moving object is found by illuminating it using laser light and measuring the Doppler shift in the frequency of the light scattered by the moving element. Doppler effect is defined as the change in the frequency of light or sound, which is observed when the source, observer, or both is in motion. This change is proportional to the distance between the source and observer. With increase in the distance observed frequency decreases while frequency increases with decrease in the distance. In LDV experiments, for the light source, particle acts as a moving observer and which in turn acts as a moving source for the detector/receiver. Light scattered by the seeded particles is proportional to the velocity of the particle. In case of gasifier, solids are used as the seeded particles. These solids can be the same solids as used in gasifier or can be a very tiny particle which should have similar flow properties as of the gasifier solids. LDV technique can be operated in dual beam mode or fringe mode. Fringe mode is more commonly used. In fringe mode, two laser beams are used to form a measurement volume as shown in Fig. 2. Due to the interference of two different beams of same amplitude and frequency, alternating bands called fringes are formed. Fringe spacing is a function of angle between incident beams and wavelength of the beam. When the particle passes through the measurement volume, change in the frequency is observed in the detector, called as Doppler bursts. Velocity is calculated from the fringe spacing and time (from Doppler bursts). In the basic setup of LDV, velocity calculated is independent of the direction. To obtain the directional velocity, one of the beam frequencies is shifted, thereby creating fringe motion in the predefined direction. 3D components of velocity are measured with increased number of probes. Volumes formed of three laser beams are used for this purpose.

LDV is a well-established technique for velocity measurement in single phase flow [22] and has advantage over competing non-invasive techniques as no tedious calibration is required. The spatial (~ 0.1 mm) and temporal resolution of LDV is

Fig. 2 Schematic of LDV setup



quite high, but the major problem in the use of LDV for gasifier is the scattering caused by discrete phase (particularly when solids of different sizes are present in the flow which is the most common situation in any gasifier) which should not be misinterpreted as signal. Thus, no matter what the chosen wavelength of the laser, there is always a high probability of the light being scattered by the dispersed entities of the corresponding dimension, rendering the system opaque to the corresponding light (or laser). This problem gets more severe with high holdup or dispersed phase volume fractions (greater than 5%). For this reason, LDV can be reliably used only in restricted conditions of low holdup. Further, large size of solids can cut multiple fringes; at the same time to overcome this problem, a dedicated postprocessing schemes are required.

Advantages of LDV technique are:

1. Spatial and temporal resolution is very high
2. Calibration is not required

Disadvantages of LDV techniques are:

1. Due to scattering of light, volume fraction more than 5% cannot be used
2. Transparent investigation zone is necessary
3. Optical arrangement is tedious
4. Provide point measurement

For further reading on LDV technique, readers can refer Durst et al. [22], Zhang [104], Chaouki et al. [14], and Zhang et al. [103], Pantzali et al. [60, 61] for studies using LDV on gas–solid CFB.

3.3 Particle Image Velocimetry (PIV)

Particle image velocimetry is also an optical-based technique. However, PIV measurements are for field values where all the values in the predefined area can be measured. In PIV, seeded particles are photographed at sufficiently short interval whose subsequent images give the movement of the seeded particle within that interval. Typical PIV system consists of laser light, image recorder, and image processing software (Fig. 3). Laser lights are used to form laser sheet. Laser sheet illuminates the tracer particles in the imaging field. To avoid blurring of image, illumination duration of light should be short enough that the particles/tracers are frozen for the duration of imaging [68]. Pulsed lasers are used for illumination. Since the pulsed lasers operate at a fixed frequency, more than one laser is used to obtain the desired interval of pulse train. Using mirrors, lights are adjusted to form laser sheet at the desired region. The light scattered by the tracer particles is recorded by cameras such as charge-coupled device (CCD) or complementary metal oxide semiconductor (CMOS). The CCD sensors are more sensitive and less noisy;

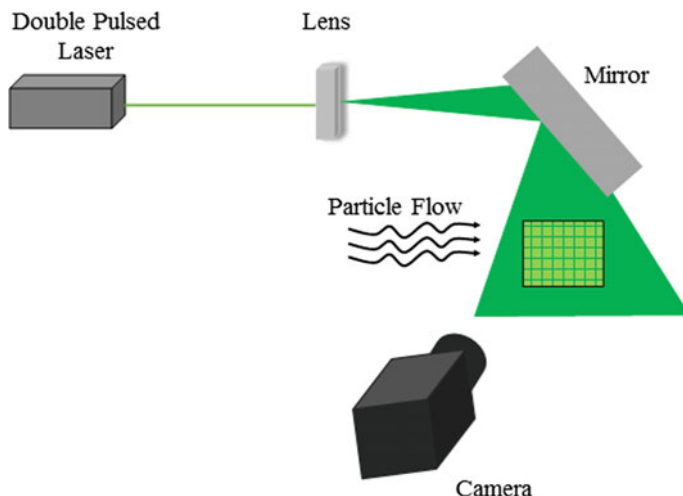


Fig. 3 Schematic of PIV measurement principle

however, CMOS sensors are faster. From the subsequent images, particle displacements are obtained which are subsequently used to measure the velocity. To measure the complete flow field, several seed particles are tracked; however, it is not possible to measure the displacement of each seed particle. Therefore, each image is divided into a small cell area called as interrogation cell. The cell size depends upon many factors like the intended resolution of measurement, quality of image, and desired accuracy. Previously, an auto-correlation algorithm was employed to analyze the images and find the displacement of the seed particles in a cell. However, this method had a difficulty in determining the direction of the velocity vector in the cell uniquely. Keane and Adrian [43] have reported a cross-correlation algorithm to analyze the image and find the displacement in the cell. Thereafter, several authors have used methods like cross-correlation, adaptive correlation to find the displacement [15, 20, 36, 70].

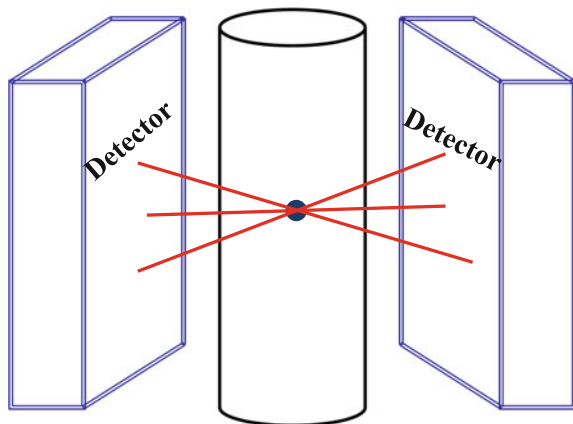
Typically, 2D planar PIV is mostly used. Recently, 3D volumetric PIV is also introduced to measure all the three components of the velocity. Major issues in PIV include its inability to measure in the high volume fraction systems and matching refractive index at the different interfaces. Further, temporal resolution is limited. Recently, high-speed particle image velocimetry (HSPIV) is used to overcome the temporal resolution limitation, which has a sampling rate up to 1 million/s. Still the local measurements inside the virtually opaque system are a challenge. Few PIV studies on CFB use specially designed borescope to overcome this limitation [31, 85]. However, use of borescope which is placed locally at different locations to measure the velocity field in the region of interest makes the technique intrusive. Interested readers can refer He et al. [37], Xu and Zhu [97], Yang and Zhu [102], etc., for investigation using PIV technique on gas–solid CFB.

3.4 Positron Emission Particle Tracking (PEPT)

Positron emission particle tracking (PEPT) is a radiation-based non-invasive technique. Annihilation occurs when the positron and electron collide, producing two anti-parallel gamma rays of equal energy. PEPT involves detecting the pair of gamma rays from the same annihilation and uses multiple such instances for finding the position of the tracer. Typically, ^{18}F , ^{61}Cu , ^{66}Ga radionuclides are used to prepare tracer, which is similar to the phase of interest. Position-sensitive gamma-ray cameras are used. Cameras are placed on either side of the column as shown in Fig. 4. Earlier, gas-filled multiwire proportional chambers were used as detectors; however, with recent developments, NaI (Tl) and BGO are used for scintillation in the positron camera. Positron cameras having surface of $0.59 \times 0.47 \text{ m}^2$ are used in University of Birmingham [13, 64]. A single tracer particle, which emits positron, is introduced into the system. Positron emitted by tracer annihilates with the electron present in the material surrounding the tracer which produces two back-to-back gamma rays, representing the line passing through the tracer. Multiple such lines of resolution are used for position reconstruction, by triangulation. In theory, two such lines are enough for reconstruction. However, in practice, about 50 such lines are used. This is because many of the events detected may be corrupt due to the Compton scattering and/or two detected gamma rays may not originated from the same annihilation event. These corrupted events are removed before finding the position by triangulation. The detectors at both ends are operated in coincidence with resolving time of 7 ns [63]. Thus, events recorded within this resolving time can be considered from same annihilation.

Recently, Yang et al. [100, 101] have reported a new algorithm for simultaneous tracking of multiple tracer particles. In this approach, standard PEPT algorithms are used to reconstruct the position of one tracer by discarding the events corresponding to other tracer particles. Then the discarded data is re-examined and used to find second tracer particle location and so on. This algorithm works reasonably well till

Fig. 4 Schematic of PEPT measurement principle [62]



the tracer particles did not come close to each other. In earlier PEPT studies, ^{22}Na (half-life of 2.6 year) and ^{18}F (half-life of 110 min) were used as tracer particles. The major disadvantage of ^{22}Na is that positron emission is always accompanied by the emission of a γ -ray of energy 1257 keV. The PEPT camera in such a case is not able to distinguish this γ -ray photon from the 512 keV annihilation γ -ray photon, whose transmission is key to the success of the experimental measurement. ^{18}F is convenient to produce, and also it is possible to produce a tracer particle having diameter 60 μm . However, ^{18}F has major drawback that it cannot be used in aqueous medium as the attached fluoride rapidly leaches back into the solution. Recently, ^{61}Cu (half-life 3.4 h) and ^{66}Ga (half-life 9 h) have used as a tracer particle.

Spatial accuracy of 1 mm is reported for the speed of 1 m/s [79]. However, the temporal resolution is in the order of milliseconds [13]. The major advantage of PEPT technique is that it does not require pre-calibration. However, limited energy of the gamma rays produced due to annihilation (512 keV), and cost is the major drawback of this technique which makes it of limited use. Further with change in the attenuation of the system, spatial and temporal resolution varies as the corrupted event increases with attenuation of the system.

3.5 *Radioactive Particle Tracking (RPT)*

RPT is a radiation-based non-invasive technique like PEPT. In RPT, motion of a single gamma-ray-emitting tracer particle is tracked using series of scintillation detectors placed around the system of interest (Fig. 5). The intensity of radiation emitted by tracer particle is recorded by each detector. Recorded counts are a unique function of distance between tracer particle and detector, solid angle, attenuation, and time of acquisition. Since the solid angle and attenuation changes with the position in the system, calibration is required. In calibration, tracer is kept at known positions, and counts recorded on each detector for this known position are noted down. Similarly, a distance count map is generated for all the detectors used in the measurement for all the locations inside the column of interest at “in situ” condition. The accuracy of RPT measurement depends on accuracy of calibration step. The position of tracer particle is reconstructed during the actual experiments by comparing the counts recorded by each detector during the experiments with counts recorded during the calibration. Thus, Lagrangian position time series of the tracer particle is obtained. Time differencing between two successive particle positions yields the instantaneous velocities as a function of time and position (Lagrangian velocities). If one visualizes an imaginary grid that conforms precisely to the system geometry (much like a grid used in CFD calculations), then for every occurrence of the tracer particle in any given cell within this grid, a “snapshot” of the Lagrangian velocity associated with that occurrence may be ascribed to that phase within that cell. After many such occurrences have

Fig. 5 Photograph of RPT setup



occurred during successive sojourns of the tracer particle in that specific cell, ensemble averaging of all these instantaneous velocity occurrences can be performed. Over the whole time span of the experiment, repeating the process over all cells conforming to the system geometry yields the ensemble-averaged velocity flow map. The difference between the time-averaged velocity field and instantaneous velocities (associated with all the occurrences discussed above) yields the instantaneous fluctuation velocity field. From this information, a rich database of flow quantities such as kinetic energies of the turbulence, Reynolds stresses, dispersion coefficients, and other parameters that represent the prevailing flow regimes and flow characteristics is evaluated [74, 86, 88]. Beside these quantities, several other parameters such as diffusion, auto-correlation coefficient, Hurst components, time-of-flight, and RTD can also be calculated [74]. In some instances, dynamic time series analysis of RPT data has been presented as a potential method to distinguish flow regimes in multiphase reactors [8, 11, 25]. The flowchart for RPT data processing is shown in Fig. 6.

The tracer particle used in experiments should be identical to the phase of interest whose velocity is to be mapped. In case of tracking solid phase, size, shape, and density of the tracer particle should be same as of the solids present in the system. In case of liquid, tracer particle should be neutrally buoyant. NaI (TI) is the

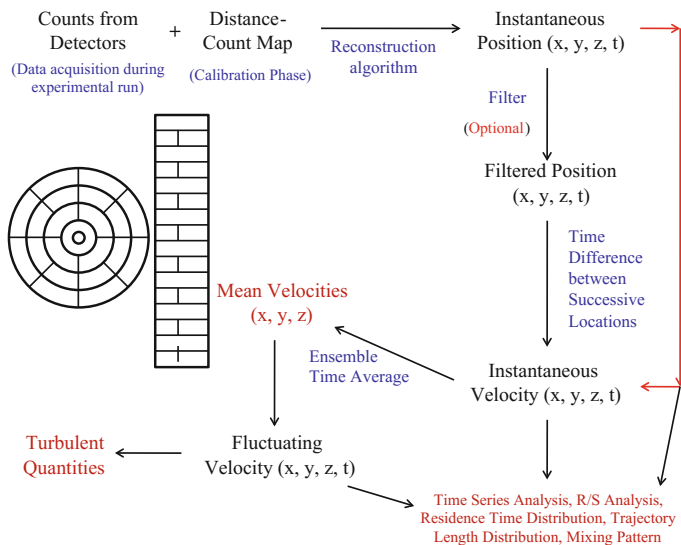


Fig. 6 Flowchart of RPT data processing

most commonly used scintillation detectors because of the cost factor; others like BGO are also in use. In principle, to obtain a position in three dimension, minimum four detectors are required. However, due to the statistical nature of gamma-ray emission and to cover region of interest, more than four detectors are used.

Spatial resolution less than 1.0 mm at 50 Hz is reported [86–88]. Temporal resolution up to 200 Hz is reported [7]. Versatility, scalability, and portability are the major advantage of the RPT technique which allows the use of RPT technique for any system (gas–liquid, gas–solids, liquid–solids, and gas–liquid–solids) at any scale (laboratory and pilot plant scale) of any dimension (from few cm to few m range). However, requirement of calibration at in situ condition is the major drawback of the technique which limits the application of the technique at high pressure and high temperature environment. However, few authors [69, 75] have implemented RPT at relatively high pressure and temperature and have shown that fundamentally this technique is also applicable in these environments. However, such applications are quite a few in the literature.

3.6 *Magnetic Particle Imaging (MRI)*

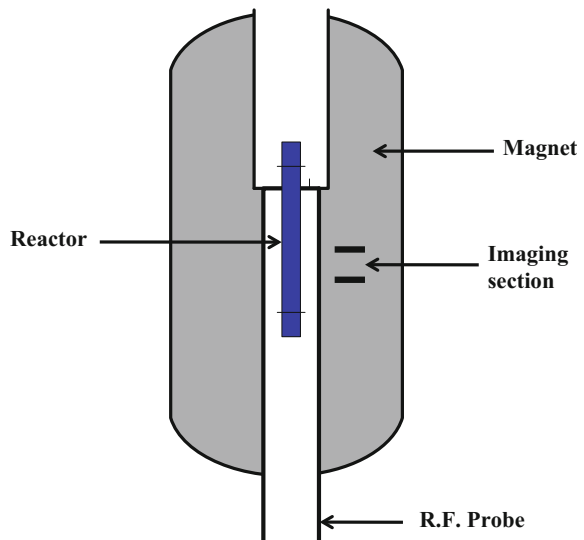
The use of MRI technique to study multiphase flow began in late 1980s and early 1990s. In this technique, a large and very strong magnet (around 5 T or more strength) is concentrically placed around the vessel of interest to generate a strong magnetic field. A radio wave antenna is used to send the signal and then receive it

back. In this technique, the phase velocity is measured by imaging spatial variation in magnitude of magnetization. A lump of spin (which is a fundamental quantity tagged to elementary particles that constitute all matter) is tagged with a radio frequency (RF) excitation at a certain time, and its relaxation is imaged through later times. Thus, the velocity is calculated by the displacement of the spins over the two successive excitations and the relaxation rate of spin vector [9, 29, 30, 53, 67, 76, 77]. Figure 7 shows the schematic diagram of an MRI setup. This is a single technique in which velocity distribution, phase holdups, and spatial mapping of chemical constituent of multiphase flows can be measured in one measurement.

In the literature, two main approaches are used for velocity imaging in multiphase flows with MRI. These two classes of strategies for MRI-based flow imaging are time-of-flight and phase-shift techniques. The “time-of-flight” method is similar to the classical tracer experiment in which displacement of tagged spins is detected during the time between initial excitation and signal measurement. This method produces excellent one-dimensional velocity profiles of the flow [9, 29, 30]. Phase-shift method uses some other unique aspects of MRI imaging related to detection of spin.

The spatial resolution of this technique is very high (of the order of few micrometers). The major drawback of this technique is that it requires very high density magnetic field which demands a very high power source, hence the cost of this technique is very high. Also the power sources must be reliable, uninterrupted, and without voltage fluctuations, so that the strength of the electromagnet, and hence the induced magnetic field, is maintained during the entire span of the experiment. Mainly for this reason, thus far MRI has been attempted only in small-sized (64 mm internal diameter and 550 mm height) vessels [78].

Fig. 7 Schematic diagram of MRI imaging



It is clear that all the techniques discussed in Sect. 3 have their own problems, but more importantly are very effective and accurate in certain limited set of conditions or applications. For example, MRI imaging which is arguably the most sophisticated of these techniques is limited to small-sized vessels owing the requirements of a very high magnetic field strength. On the other hand, a modest pressure probe or optical fiber probe is cheap and versatile in permitting its use in almost all kinds of vessels, including industrial scale vessels. Naturally, owing to its invasive nature as well as inherent limitations of the instrument, high accuracy is not always assured. In many cases, very high accuracy is also not required, for instance in an industrial reactor only an idea of velocity field is more than sufficient to tune the operating conditions. However, for fundamental investigations of reactor behavior, velocity field (mean field as well as fluctuations) can be best done with techniques such as MRI, PEPT, and RPT for fluidized bed gasifier. Further, for circulating fluidized bed gasifier, PIV and LDA can also be used beside RPT and PEPT depending upon the local solid holdup. LDA can be used in CFB where solid holdup is below 5%. Borescope-aided PIV is used to study the visually opaque regions of CFB. PEPT and MRI are almost ruled out for pilot plant and industrial scale setup. Further in the case of dusty environments, all the optical-based methods require extra care on postprocessing and/or calibration to increase the signal-to-noise ratio.

In summary, one must ask the important question as to what one wants from a velocity measurement technique. This would lead us to a “wish list” and based on this wish list, one should choose the suitable technique for velocity measurement.

For further reading on the velocity measurement techniques and its applications in different gas–solid reactors, readers can refer Nieuwland et al. [56], Chouki et al. [14], Sun and Yan [84].

4 Solid Fraction Measurement Techniques

In gasifier, the distribution of the phases (gas and solids) typically varies both in time and space. These variations in gas–solid distribution have a strong influence on the performance of the gasifier. Therefore, it is critical to precisely measure the gas–solid distribution for better design, scale-up, and operation of gasifier. Several measurement techniques have been used in the literature to measure the gas–solid distribution in gasifier. Some of the key techniques which are widely used are discussed in this section. Similar to velocity measurement, volume fraction measurement techniques are also classified as invasive and non-invasive techniques. Invasive techniques that have been majorly used are capacitance probe [80, 81, 95], optical fiber probe [17, 21, 50], and pressure transducers [28, 24] (Gibilaro et al. 1988). Among the non-invasive techniques, tomographic techniques (electrical capacitance tomography, positron emission tomography, X-ray and gamma-ray tomography) are most commonly used. The details of pressure probe measurement technique for global

measurements are already discussed in Sect. 2. Hence, in this section, other invasive and non-invasive techniques for local measurements will be discussed.

4.1 Capacitance Probe

The capacitance probe is an invasive technique to measure the solid concentration or bed voidage. Kunii et al. [44] and Geldart and Kelsey [27] has used plate type capacitance probe to measure the voidage in gas–solids fluidized bed as shown in Fig. 8a. The technique uses the fact that the dielectric constant of solid and fluidizing gas are quite different and permittivity of a gas–solid mixture is a strong function of the solid concentration. Hence, temporal variation of the solid concentration at the capacitor in gasifier or in any gas–solid medium causes a change in the capacitance which results in a proportional DC voltage change with time. The change in DC voltage can be measured and calibrated in terms of solid concentration at the probe. Therefore, by measuring the capacitance of these plates as a function of time, time-resolved solids concentration between the plates can be obtained. It should be noted that a pre-calibration curve between the changes in DC voltage with solid concentration is required for the calculation of solid concentration in fluidizing medium, which poses a major challenge in the use of capacitance probe. Further, the dimensions of the plate type capacitance probe were relatively high. Werther and Molerus [95] have shown that such probe can significantly change the dynamics of the bed at the point of measurement itself. They have developed a needle-type capacitance probe to measure the solid concentration

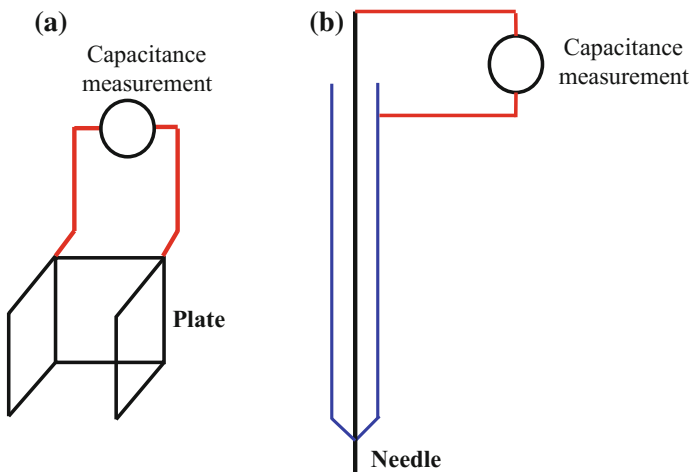


Fig. 8 Schematic diagram of **a** plate type, **b** needle capacitance probe

which had much smaller dimensions compared to plate type probe. In the needle probe, needle works as one pole of capacitor (sensing electrode) while the metal body of the probe works as other pole (ground electrode) to complete the circuit as shown in Fig. 8b. Soong et al. [83] have introduced guard electrode which surrounds the needle (sensor) electrode. It has been found that guard electrode reduces most of the background electric field disturbance and makes the data more accurate and reproducible. Most of the commercial vendor sells the capacitance probe with guard electrode. However, pre-calibration is still needed for reconstructing the phase distribution, and accuracy of the measurement depends upon the calibration. Several authors have used different calibration methodology. Hage and Werther [32] have suggested methodology for the calibration of capacitance probe in gas–solid system which is most commonly used. In this methodology, they have measured the voltage output from capacitance probe for only gas (without solid) and fixed bed of known solid concentration. By using these values, they have proposed a correlation between the measured output voltage at operating condition and solid concentration as given in Eq. 3.

$$C_s = C_{pb} \frac{V - V_g}{V_{pb} - V_g} \quad (3)$$

where C_{pb} is solid concentration at packed bed condition, V is the measured voltage output at actual operating condition, V_{pb} is voltage output at packed bed condition, V_g is voltage output for only gas, and C_s is solid concentration for measured voltage output at actual condition.

The major issue associated with the capacitance probe is to define the measuring volume which depends upon the system type and operating condition. Further, capacitance probe performance is sensitive to humidity, temperature, particle diameter, and particle shape which changes the dielectric constant and makes it more difficult to define the measuring volume. In gasifier, size, shape, and temperature of the bed changes with time and along the bed height (more prominently for circulating fluidized bed) which makes the accuracy of capacitance probe more vulnerable.

4.2 Optical Fiber Probe

Similar to capacitance probe, optical fiber probe is also an invasive technique. The optical fiber probes are widely used in gas–solid system because of their low cost, simplicity, and ease of postprocessing. The principle of the technique is already discussed in Sect. 3 for velocity measurement. For solid fraction measurement, mainly two types of optical probes are used: reflection or backscatter probe and transmission-type probe. In reflection probe, emission and detection fibers are placed at the same side while in transmission probe they face each other and

separated by a short distance. Defining the measuring volume in backscattering probe is difficult as it depends on solid concentration. For a dilute system, light can travel a good distance before it meets with reflecting particle, while in dense system this distance will be much shorter. Transmission probe can overcome this issue where measuring volume is fixed between emission and detection probe. However, the backscattering-type probe is more compact and hence less intrusive compared to transmission probe [41]. Most of the work reported on optical probe uses reflection/backscattering-type probe. Similar to capacitance probe, calibration is essential in optical fiber probe for the measurement of solid concentration. This poses major problem as it is very difficult to have a homogeneous gas–solid mixture in fluidized bed over a wide range of solid concentration. Several methods can be found in the literature for the calibration of optical probe in gas–solid system. Hartge et al. [35] immersed probe in a liquid–solid homogeneous fluidized bed of known solid concentration and then in a gas–solid packed bed of known solid concentration. A calibration curve or chart is prepared by using different concentration of solids in liquid–solid fluidized bed. Cutolo et al. [18] used solid feed hopper for feeding the solids at different concentrations through the pipe and plotted the known concentration as a function of voltage. Lischer and Louge [49] have developed a rigorous model for calculating the reflectivity of a group of particles in front of the fiber. Some authors have used capacitance probe for calibrating the optical probe. A detailed review on calibration methods for optical fiber probe for solid volume fraction can be found in Xu et al. [98].

4.3 Electrical Capacitance Tomography (ECT)

Electrical capacitance tomography is a non-invasive measurement technique which works on the same principle as of the capacitance probe. It also utilizes the basic facts that the dielectric constant of solids and gas used in gasifier or in any gas–solid bed is quite different. The only difference from the capacitance probe is that in ECT electrodes are mounted on the outer periphery of the wall and do not disturb the flow. A typical schematic of ECT setup is shown in Fig. 9a. Several electrodes are

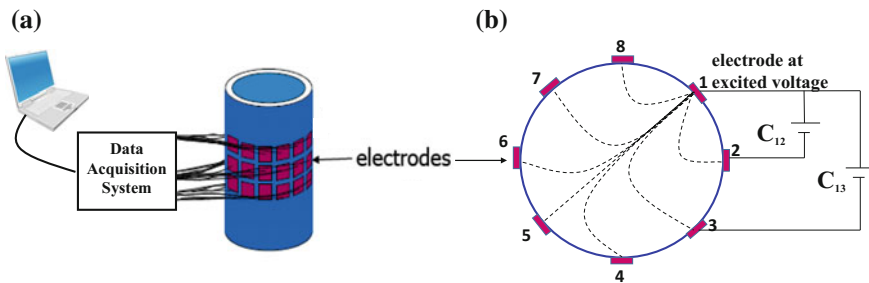


Fig. 9 a Schematic diagram of ECT setup. b Measurement method of ECT [88]

used to cover the entire cross section of the bed to provide full three-dimensional pixel-wise distribution of solids and gas in the bed. In ECT, generally 8, 12, or 16 electrodes, based on column diameter and resolution required, are used. The electrodes are excited one by one by providing a voltage to one particular electrode and maintaining other electrode at reference potential (as shown in Fig. 9b). The capacitance value between the excited electrode and other electrodes is collected. Similarly, other electrodes are excited, and capacitance values are noted down. Hence, a total $n(n - 1)/2$ measurements are performed for n number of electrodes used in the experiment. The permeability distribution in the bed is calculated by using these measured capacitance values. The governing equations to be solved are:

$$\nabla \varepsilon(x, y) \nabla \phi = 0 \quad (4)$$

$$C_{ij} = \frac{1}{\Delta V_{ij}} \oint_A \varepsilon(x, y) \nabla \phi \, dA \quad (5)$$

Here, $\varepsilon(x, y)$ is the permittivity distribution in the measuring plane, ϕ is the electric potential field, C_{ij} is the measured capacitance between electrodes i and j , ΔV_{ij} is the applied voltage difference between the excited electrode and other electrode over the pair ij , and A is the surface area of the electrode. The phase distribution is directly related with the permeability distribution.

Image reconstruction based on “so-called” inverse problem (determining the permeability distribution from capacitance measurement) possesses the major challenge and limits the accuracy of the measurement. Various schemes are used in the literature to solve this inverse problem. Algebraic reconstruction technique [71], model-based reconstruction method [39], linear back projection [23], iterative linear back projection [99] are among the few. Linear back projection (LBP) is most widely used algorithm as it is less computational expensive and can provide real-time image which is the major advantage of the ECT technique over the other tomographic method. However, this algorithm provides blurred image and shows a smoothing effect on the sharp transitions between the different dielectric constants. The sensitivity of this algorithm is localized and high only near the electrode and deteriorates when moved far from the electrodes. Iterative LBP minimizes this problem; however, it is computationally costly and prevents real-time imaging. Warsito and Fan [93] have proposed a new algorithm—an analog neural network multicriteria optimization image reconstruction technique (NN-MOIRT) which gives better image resolution.

4.4 Gamma-Ray and X-Ray Tomography

Gamma-ray and X-ray tomography have been used for investigation of gas–solid systems for the past three decades. The continuous development of gamma and X-ray technique is mainly due to the medical imaging. Basically, gamma-ray and

X-ray tomography are based on the transmission tomography principle which uses the fundamental property of matter to attenuate the light. Both X-ray and gamma ray are the electromagnetic radiation, when it is passed through the attenuating medium; the intensity of emitted beam reduces. The reduction in the intensity of emitted beam is given by Beer Lambert law as follows,

$$\frac{I}{I_0} = e^{-\int \mu_l dl} \quad (6)$$

where μ_l is the effective mass attenuation coefficient of the medium, I , I_0 are the intensities of transmitted and emitted beams, l is the transmission length. Effectively, effective mass attenuation coefficient can be calculated from the both emitted and detected intensity if the length of the transmission is known. However, this effective mass attenuation coefficient calculated gives the line-averaged values not the point values. For measurements of solid fraction in gas–solid system, these kinds of line-averaged values are used by several authors, as it is non-invasive and simple to measure and usually called as densitometry (first generation tomography). In densitometry technique, detector and collimated source are placed in line in such a way that the detector center and source center are collinear. The investigation system is placed in between the source and detector. To obtain the mass attenuation coefficient, the individual attenuation coefficients of the phases are obtained by measuring the intensity of the transmission at the empty bed, packed bed, and at actual operating conditions. From the mass attenuation coefficients, chordal average volume fraction can be computed as follows:

$$\mu_l = \mu_s \varepsilon_s + \mu_g \varepsilon_g \quad (7)$$

$$\varepsilon_g + \varepsilon_s = 1 \quad (8)$$

where μ_g and μ_s are the individual mass attenuation coefficients of the gas and solid. From the densitometry technique, chordal averaged values are obtained. To obtain radial values, Abel transformation is used by researchers, considering the distribution as axisymmetric. This kind technique can be applied for two-phase systems and also for three-phase systems by using additional radiation source [86].

Even though simple, densitometry technique cannot be applied everywhere, to obtain reliable radial distribution as most of the gas solid systems are not azimuthally symmetric. Therefore, similar to medical imaging, computed tomography uses multiple such projection. The projections may be parallel, fan beam, or conical. Instead of single detectors, multiple detectors are used. The fan beam projections are more popular compared to the other projections. The schematic of fan beam projection is given in Fig. 10. The source and detectors are traversed around the column to obtain multiple projections. To obtain the volume fraction distribution, mass attenuation coefficient to be obtained as function of the position.

From the intensity ratio, obtaining the mass attenuation is an inverse problem. Analytical technique like Radon transform, filter back projection is fastest technique;

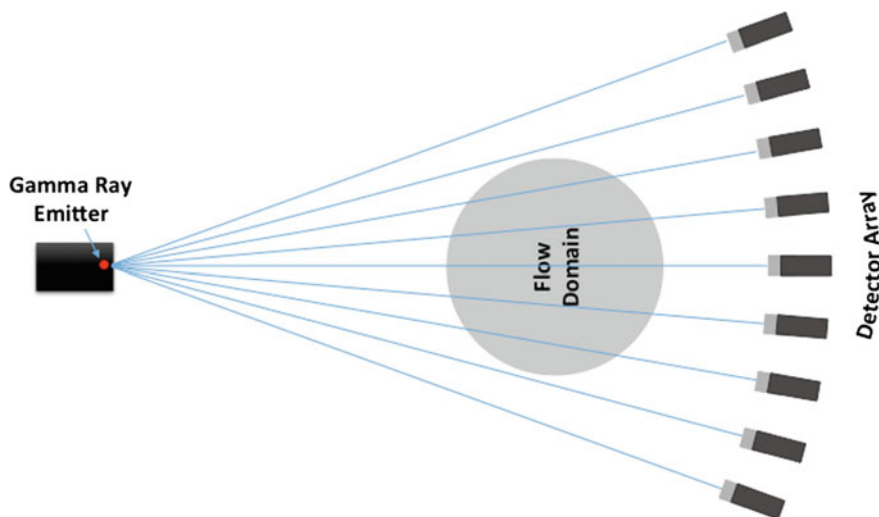


Fig. 10 Schematic of fan beam projection used in X-ray and gamma-ray tomography

however, they are limited by accuracy for multiphase systems. Computationally intensive iterative techniques like algebraic reconstruction techniques are widely used. Expectation minimization (EM) algorithm is introduced to obtain the better image construction for transmission tomography by redefining the problem as maximum likelihood estimate optimization problem [47]. Kumar [46] compared the filter back projection, algebraic reconstruction technique, and expectation minimization technique for multiphase systems and concluded that EM algorithm gives better estimate. O’Sullivan and Benac [58] reformulated EM algorithm as double minimization problem. Varma et al. [92] compared the alternative minimization (AM) and EM algorithm for multiphase systems using gamma-ray tomography and concluding that the AM gives better image reconstruction.

Both X-ray and gamma ray use very similar principles and reconstruction algorithms. X-ray cannot be used for those conditions where high attenuated medium or walls are present. However, gamma-ray tomography can be used in those conditions too. X-ray is safer than gamma ray. The above techniques give better spatial resolution at the cost of time resolution. The time resolution is very poor, and time-averaged imaging is usually obtained. Johansen et al. [40] used multiple gamma sources and multiple detectors bunch to get better time-resolved images in the range of milliseconds, however it compromising the spatial resolution. Hori et al. [38] used multiple X-ray tubes which are switched to obtain the temporal resolution up to 2000 frame per second. Hampel et al. [33] used electron beam in limited view to produce X-rays instead of using multiple X-ray tubes, thus obtaining the temporal resolution up to 7 kHz.

The techniques discussed in this section have their own advantages and disadvantages. Till date no technique available, which can provide very high temporal and spatial resolution and is easy to handle. Intrusive probes are cheaper and can be

used at any scales. However, they can change the phase distribution at the point of measurement itself. Further, based on their measurement principles, these probes can cause unique challenges. Capacitance probe is very sensitive to temperature and relative humidity. Any change in these two parameters can change the accuracy of the pre-calibrated measurement. In gasifiers, both the parameters can frequently change based on the reactor type and feed. Optical fiber probes can be used at industrial scale, and it provides high temporal resolution. However, the spatial resolution is very low, and determining the measurement volume itself is a measure issue which can change the solid concentration profile.

Non-invasive techniques do not disturb the flow; however, they generally require higher cost and difficult to handle due to inverse nature of problem. ECT temporal resolution is very high, but it gives poor spatial resolution. Applying ECT at large-diameter system is very difficult due to limited number of electrodes which further lower down the spatial resolution. Gamma-ray tomography can be used at industrial scale system, but it provides time-average solid distribution due to poor temporal resolution. However, spatial resolution of gamma-ray and X-ray tomography is good. The radiation is also a cause of concern and hence requires proper handling and safety gadgets, which increase the cost of the system. Further details on techniques and applications of these techniques on gas–solid beds can be found in Nieuwland et al. [56], Chaouki et al. [14], van Ommen and Mudde [90], Sun and Yan [84].

5 Residence Time Distribution

RTD studies are widely used to find non-idealities in the flow of the fluid inside the reactor. The technique can be used at any scale and for both cold and hot flow condition. The solids or fluid elements in gasifier flow through different path, thus take different time to exit the reactor. RTD is a probability density function $E(t)dt$ which gives the fraction of elements leaving the system that remained in the system for the time between t and $t + dt$. RTD can be applied to any conserved entity in a flow system [55]. Tracer which represent phase of the interest is injected at the inlet and concentration of the tracer at the outlet is measured with respect to time to obtain RTD. Modeling of RTD distribution is as important as measuring the RTD; however, this is beyond the scope of this chapter. Nauman and Buffham [54], Nauman [55], Gao et al. [22] give the review of RTD models available.

Several methods are used to measure the RTD depending upon phase of interest and system. Bader et al. [2] used NaCl chemical as tracer for the measuring the solid RTD. Tracers are injected with the aid of compressed air. Samples are recovered isokinetically and washed, and conductivity of the solution is determined. The concentration of the NaCl is obtained from the conductivity meter. Some of the commonly used chemical tracers are NaCl, KCl, NaOH, BaCl₂ salt, etc. [2, 72, 82, 105]. Colored tracer is used as tracer and detected using CCD video and image analysis. Bi et al. [3] used orange-colored lignite pellets and image recording to find the residence time distribution in binary solid circulating fluidized bed.

Radioisotope-based tracer is also used by researchers to study the solid RTD [1, 65] where bed material is labeled with the radioactive material and irradiated. Ambler et al. [1] used ^{68}Ga as radioactive material and labeled the sand particle by evaporation of milking solution with EDTA. Usually in gasifier, tracer particles are injected by pulse injection with the pressurized air. Sodium iodide scintillation detector is used to detect the concentration of the tracer at the outlet which is proportional to the counts detected. All the above techniques are disruptive to the flow. Other techniques, which are non-disruptive, overcome the injection disadvantages. Mostly they are optical based or radioactive based. Wei et al. [94] and Harris et al. [34] used phosphorescent tracer in the experiments. These particles emit radiation following exposure to light. In the inlet plane, tracers are activated using flashlight. Light-detecting photomultiplier tube (PMT) is used for detecting the tracers. Single radioactive particle is used by few researchers to quantify the RTD [6, 42]. A single radioactive particle which is similar to the bed material is tracked continuously using scintillation detectors. To obtain reliable distribution, experiments are carried for long hours to obtain the sufficient number of particle tracks. Most of the studies investigated the bed materials, there are few studies conducted to investigate the RTD of fuel particles (coal). Pant et al. [59] investigated pilot scale gas–solid fluidized gasifier using ^{198}Au labeled coal particles.

Axial and radial gas dispersion are studied in fluidized bed/circulating fluidized beds using gas tracers [2, 51, 66, 96]. For gas tracing, helium, hydrogen, propylene, propane, ethane, carbon dioxide are widely used as tracers in literature. Photo-ionization detector, infrared detectors, thermal conductivity detector, flame ionization detector are used for detection. Radioactive tracers like ^{41}Ar are also used [66]. Cents et al. [12] used ultrasound for the detection of the helium tracer in gas–solid fluidized bed without disturbing the flow.

6 Application of Radioactive Particle Tracking: Case Study of CFB

CFB is one of the commercial gasifier technology available, which is also the least understood reactor due to the complex interactions of gas–solid, solid–solid, and solid–wall. High-velocity circulating fluidized beds are recommended for the gasification operations to achieve low residence time and high throughput. Pressure drop is the most studied variable in CFB to understand the global solid holdup. However, pressure drop studies do not give information on the local hydrodynamics and fluctuations. Such local informations are needed for modeling and understanding of CFB, especially in case of partial reactions like gasification. To obtain such local hydrodynamics and fluctuations, advanced measurement techniques are needed. RPT technique is chosen to demonstrate the use of advanced measurement technique and depth of information which can be obtained from such technique. Most of the advanced technique has the similar capabilities of producing detailed information which can be used to understand the physics in addition as a catalyst to the development and validation of CFD.

In this section, RPT technique is used to study the solid motion, local velocity field, and solid turbulent properties in high-velocity gas–solid CFB. In CFB, gas and solids flow concurrently upward in the riser and solids are separated in the cyclones and fed back to the riser. Experiments are conducted in the riser of 0.05 m diameter and length of 3.2 m. Investigations are conducted in the region of 1.2–2.0 m. Detectors are arranged strategically around the investigation zone. Figure 5 shows the photograph of riser and detectors placed around the riser. Measurement principles are previously explained in the RPT section, and data processing is given in the flowchart in Fig. 6. Glass beads of mean size - 500 μm and density - 2500 kg/m^3 are used as the solid phase, and air is used as the gas phase. Scandium 46 impregnated in glass beads is irradiated and used as tracer in this study. Further details of the experiments can be found elsewhere [42]. Results are given for the operating condition of U_g - 7 m/s and G_s - 110 $\text{kg/m}^2\text{s}$.

In RPT, a single solid particle is tracked continuously which is similar to the Lagrangian tracking of solids. For an ergodic system, the large number of independent individual trajectories is equal to the single circulation of the large number of particles. Solid particles follow torturous path. Each such path can be tracked in RPT whenever the particle passes through the investigation zone. Lagrangian track gives idea about whether the flow has the large number of internal circulations, the predominant flow direction, flow path, and the preference region. For example, Fig. 11 shows one such Lagrangian track of the solid particle in the x-z, y-z, r-z, and r- θ plane. Figure shows the solid motion is chaotic. It can be seen that solid particle travels predominantly in the axial direction and relatively less motion is observed in the radial direction. There are instances where internal circulations are observed; however, those instances are very less in occurrences. Very few techniques, like RPT and PEPT, have such capability to infer the data in terms of Lagrangian movement. These kinds of Lagrangian information is really needed to study the local solid mixing. Degaleesan [19] and Roy [73] evaluated the local mixing in terms of the solid diffusivity similar to the concept of fluids in Bubble column and liquid–solid riser. Bhusarapu [5] and Kamalanathan [42] evaluated local mixing in gas–solid CFB in terms of solid diffusivity. It is inferred that the solid particle sometime accelerates and sometimes decelerates. Deceleration of the solid particle may be due to the solid–solid interactions and cluster formation.

Instantaneous velocity of the solid particle is obtained from the Lagrangian particle position by time differentiation. From the Lagrangian velocities, Eulerian information is obtained by forming the virtual grid. Whenever the particle moves through the grid, the velocity vector is assigned to the particular cell according to the midpoint of the velocity vector. The arithmetic average of the all velocities over each cell gives the ensemble-averaged velocity in that particular grid.

$$\langle v_q(i,j,k) \rangle = \frac{1}{N(i,j,k)} \sum_{n=1}^{N(i,j,k)} v_q(i,j,k) \quad (9)$$

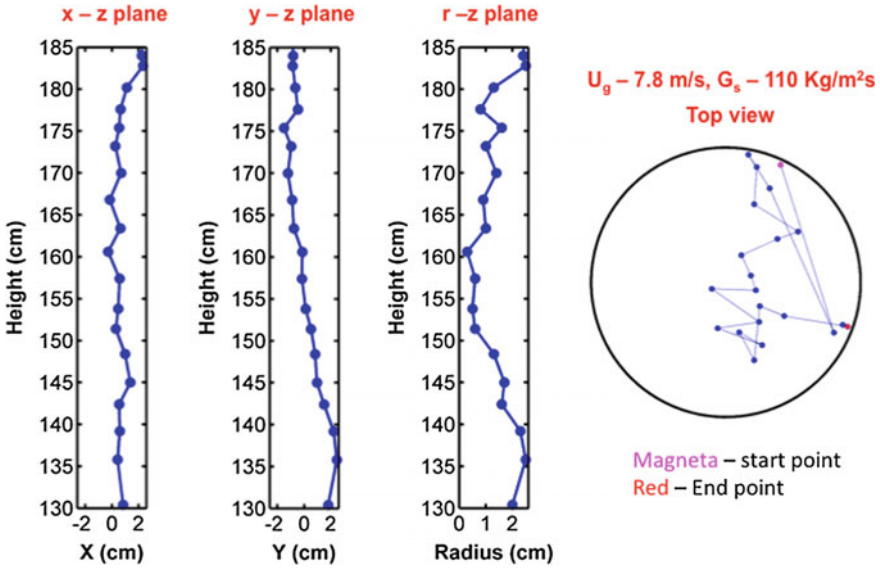


Fig. 11 Typical position map of single trajectory in different planes

PDF of instantaneous velocities in each cell gives the distribution/spread. Such information is useful for the development and validation of CFD model. Thus, validating the CFD simulations not just mean but at the level of the fluctuations. One such instance of axial velocity distribution is shown in Fig. 12 at different radial positions. It can be seen that such distributions are high near the wall and low near the center. Occurrence of negative velocities in the center is relatively low, and near the wall it is high. Negative velocities of the solid might be due to the formation of clusters. Occurrence of negative velocities can be related to the occurrence of the clusters. However, all the clusters might be not necessarily form the negative velocity since it depends on the size and shape of the clusters. It is well known that the cluster formation changes the dynamics of CFB both at axial and

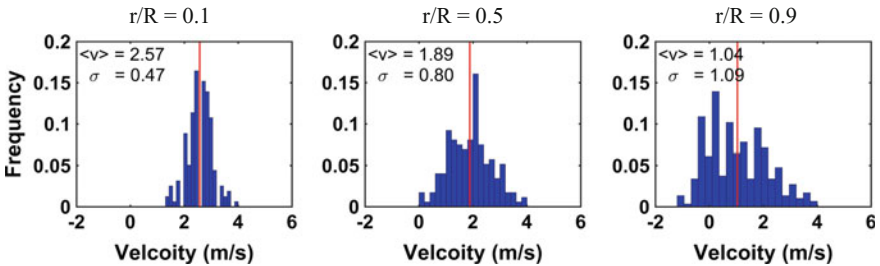


Fig. 12 PDF of axial instantaneous velocities at theta plane = 0° at height of H = 1.4 m

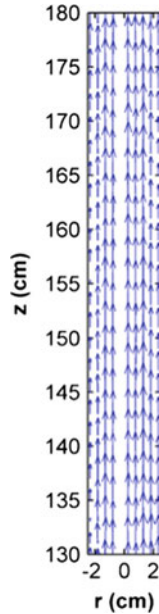


Fig. 13 Mean velocity vector plot at plane of 0–180°

radial positions in CFB as confirmed by various studies [52, 19]. Cluster formation in the riser is confirmed by the photographic studies of Kamalanathan [42].

Figure 13 shows the velocity vector plot. Velocity vector plot gives qualitative information about the overall flow pattern. It can be inferred from the plot that the most of solids flow upward and radial directed motion is negligible. The mean velocity vector plot does not show any downward motion, and also velocity near the wall is relatively less than the center. Similar vector plots can be plotted in any planes and highly useful to understand the flow pattern. Such plots in all the planes gave very similar vector plots confirming the axisymmetric flow.

Ensemble-averaged velocities in the axial and radial direction are shown in Fig. 14 at different heights. Mean axial solid velocities are high in the center and low near the wall. The gradient of mean axial velocity along the radial direction increases. Further with increase in the height, the change in the mean axial solid velocity is 10% or less. Thus, flow can be considered as developed. Compared with the radial mean velocity, the flow is predominately in the axial direction. Further, the radial mean axial velocity at all the reported heights is negligible. Similar observations have been made for azimuthal velocity too. All the mean axial solid velocities are positive. However, it does not mean that there is no negative velocities, in the mean sense the flow is upward. PDF of the instantaneous velocities clearly shows that negative velocities are observed all along the column. Thus, this kind of detailed analysis is required to disseminate the local information.

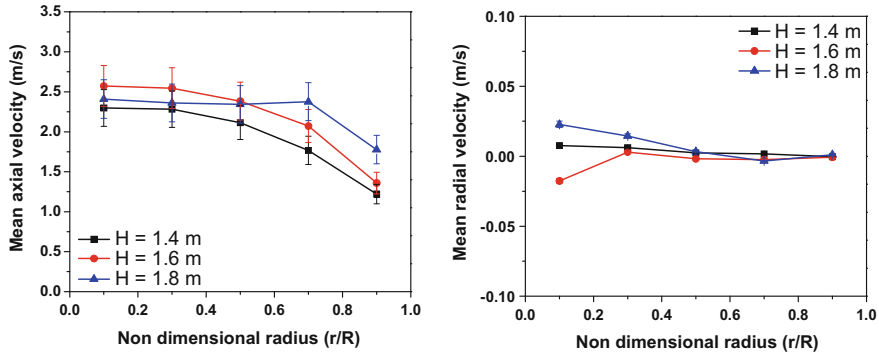


Fig. 14 Azimuthally averaged mean axial velocities at different heights

Fluctuating and turbulent solid motion are quantified using the second-order moments of velocity. From the instantaneous velocities and ensemble-averaged velocity, the fluctuating RMS velocity can be calculated as follows

$$v'_q(i, j, k) = v_q(i, j, k) - \langle v_q(i, j, k) \rangle \quad (10)$$

$$\langle v_q \rangle^{RMS} = \sqrt{\langle v_q'^2 \rangle} \quad (11)$$

Further, Reynolds stresses are obtained as

$$\tau_{qs} = \rho_p \langle v'_q(i, j, k) v'_s(i, j, k) \rangle \quad (12)$$

Figure 15 shows the axial and radial RMS velocities at different height. With increase in the height, there is no significant change in the axial and radial RMS velocities. Axial RMS velocities are order of magnitude higher than the radial RMS velocities. Thus, fluctuations are primarily in the flow direction. Axial RMS fluctuations are high near the wall and low in the center. High fluctuations might be due to the high occurrences of cluster formation near the wall, and solid–solid interactions near the wall are high due to the high volume fraction compared with the center of the column. Information on RMS fluctuations is increasingly important in the fast reactions and mass transfer controlled reactions as local fluctuations play major role in the conversion. In addition to that, such information is needed for the validation of advanced CFD simulations. Solid mean velocity and solid fluctuations profile are contrary to each other. Thus, the governing phenomena of mean velocity and fluctuations are different.

Normal and shear Reynolds stress can be obtained as shown in Fig. 16. Normal Reynolds stresses are significant; however, other shear stresses are negligible. Thus, confirming the flow is anisotropic. Radial shear stress is very less due to the high momentum of the particle in the axial direction as the flow is predominantly in axial direction.

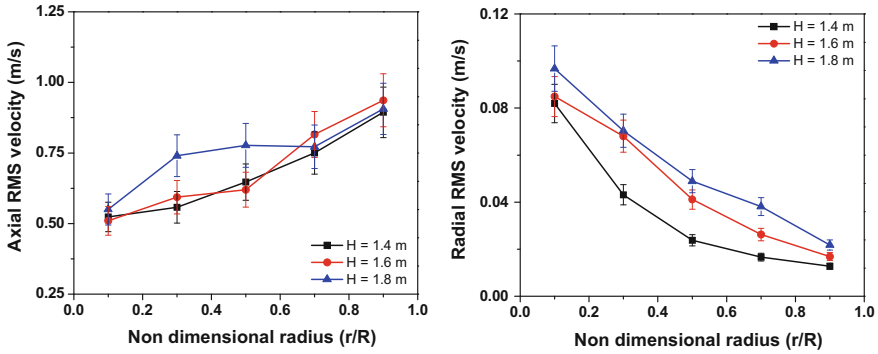


Fig. 15 Azimuthally averaged RMS velocities at different heights

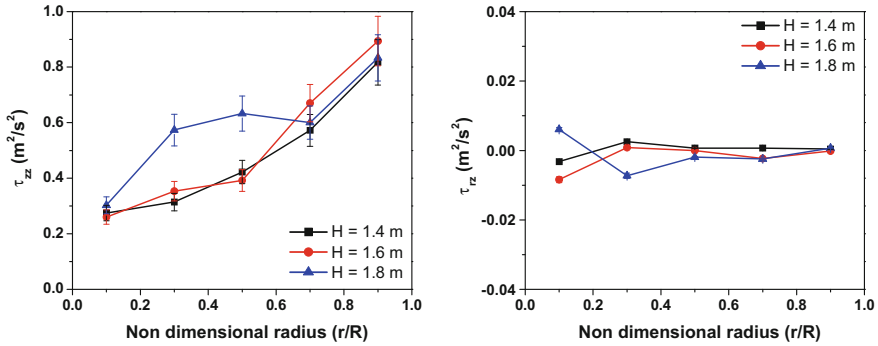


Fig. 16 Azimuthally averaged Reynolds stresses at different heights

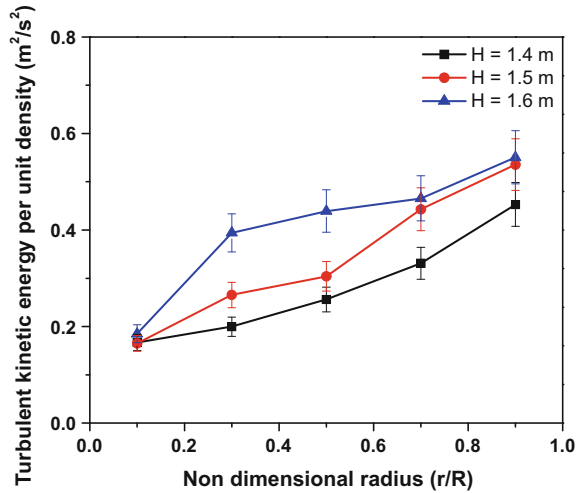
Turbulent kinetic energy can be inferred as the energy available for the dissipation. Fluctuating turbulent kinetic energy per unit mass is sum of the normal components of the Reynolds stress can be computed as

$$KE = \frac{1}{2} \rho_p [\langle v_r'^2 \rangle + \langle v_\theta'^2 \rangle + \langle v_z'^2 \rangle] \tag{13}$$

Figure 17 shows the turbulent kinetic energy at different heights. Fluctuating turbulent kinetic energy available is two orders of magnitude less than the kinetic energy available. Thus, it can be inferred that the energy available for the dissipation is negligible.

Similar information can be drawn for different operating condition and at different scales, which are shown by Kamalanathan [42]. Combined with advanced CFD models, this information can greatly help in developing the detailed understanding of such complex system, which can lead to better design and scale-up of gas–solid system.

Fig. 17 Azimuthally averaged turbulent kinetic energy at different heights



References

1. Ambler PA, Milne BJ, Berruti F, Scott DS (1990) Residence time distribution of solids in a circulating fluidized bed: experimental and modeling studies. *Chem Eng Sci* 45(8):2179–2188
2. Bader R, Findlay J, Knowlton TM (1988) Gas/solid flow patterns in a 30.5-cm-diameter circulating fluidized bed riser. In: Basu P, Large JF (eds) *Circulating fluidized bed technology II*. Pergamon, Oxford, pp 123–137
3. Bi J, Yang G, Kojima T (1995) Lateral mixing of coarse particles in fluidized beds of fine particles. *Trans Inst Chem Eng* 73:162–167
4. Breault RW (2010) Gasification processes old and new: a basic review of the major technologies. *Energies* 3(2):216–240
5. Bhusarapu S (2005) Solid flow mapping in gas-solid risers. DSc thesis, Washington University, USA
6. Bhusarapu S, Al-Dahhan MH, Dudukovic MP (2004) Quantification of solids flow in a gas-solid riser: single radioactive particle tracking. *Chem Eng Sci* 59:5381–5386
7. Bhusarapu S, Al-Dahhan MH, Duduković MP (2006) Solids flow mapping in a gas-solid riser: Mean holdup and velocity fields. *Powder Technol* 163:98–123
8. Bhusarapu S, Cassanello M, Al-Dahhan MH, Dudukovic MP, Trujillo S, O'Hern TJ (2007) Dynamical features of solids motion in gas-solid risers. *Int J Multiph Flow* 33:164–181
9. Callaghan PT (1991) *Principles of nuclear magnetic resonance microscopy*. Clarendon Press, Oxford
10. Caloz YP (2000) Experimental investigation of local solids fluid dynamics in different industrial-scale circulating fluidized beds with optical probes. PhD thesis, Swiss Federal Institute of Technology, Zurich
11. Cassanello M, Larachi F, Marie-Noelle M, Guy C, Chaouki J (1995) Experimental characterization of the solid phase chaotic dynamics in three-phase fluidization. *Ind Eng Chem Res* 34(9):2971–2980
12. Cents AHG, Kersten SRA, Brilman DWF (2003) Gas-Phase RTD Measurement in Gas and Gas-Solids Reactors Using Ultrasound. *Ind Eng Chem Res* 42:5506–5515
13. Chan CW, Seville J, Yang Z, Baeyens J (2009) Particle motion in the CFB riser with special emphasis on PEPT-imaging of the bottom section. *Powder Technol* 196:318–325

14. Chaouki J, Larachi F, Dudukovic MP (1997) Noninvasive tomographic and velocimetric monitoring of multiphase flows. *Ind Eng Chem Res* 36(11):4476–4503
15. Chen RC, Fan LS (1992) Particle image velocimetry for characterizing the flow structure in three-dimensional gas-liquid-solid fluidized beds. *Chem Eng Sci* 47:3615–3622
16. Chew JW, Hays R, Findlay JG, Knowlton TM, Reddy Karri SB, Cocco RA, Hrenya CM (2012) Cluster characteristics of Geldart Group B particles in a pilot-scale CFB riser. II. Polydisperse systems. *Chem Eng Sci* 68:72–81
17. Cui H, Chaouki J (2004) Effects of temperature on local two-phase flow structure in bubbling and turbulent fluidized beds of FCC particles. *Chem Eng Sci* 59(16):3413–3422
18. Cutolo A, Rendima I, Arena U, Marzocchella A, Massimilla L (1990) Optoelectronic technique for the characterization of high concentration gas-solid suspension. *Appl Opt* 29:1317–1322
19. Degaleesan S (1997) Fluid dynamic measurements and modeling of liquid mixing in bubble columns. DSc thesis, Washington University, St. Louis
20. Delnoij E, Kuipers JAM, van Swaaij WPM, Westerweel J (2000) Measurement of gas-liquid two-phase flow in bubble columns using ensemble correlation PIV. *Chem Eng Sci* 55:3385–3395
21. Du B, Warsito W, Fan LS (2003) Bed nonhomogeneity in turbulent gas-solid fluidization. *AIChE J* 49(5):1109–1126
22. Durst F, Melling A, Whitelaw JH (1981) Principles and practice of laser Doppler anemometry. Academic press, London
23. Dyakowski T, Edwards RB, Xie CG, Williams RA (1997) Application of capacitance tomography to gas–solid flows. *Chem Eng Sci* 52:2099–2110
24. Fan LT, Ho TC, Hiraoka S, Walawender WP (1981) Pressure fluctuations in fluidized bed. *AIChE J* 27:388–396
25. Fraguio MS, Cassanello MC, Larachi F, Chaouki J (2006) Flow regime transition pointers in three-phase fluidized beds inferred from a solid tracer trajectory. *Chem Eng Process Process Intensif* 45:350–358
26. Gao X, Wu C, Cheng Y, Wang L, Li X (2012) Experimental and numerical investigation of solid behavior in a gas–solid turbulent fluidized bed. *Powder Technol* 228:1–13
27. Geldart D, Kelsey JR (1972) The use of capacitance probes in gas fluidised beds. *Powder Technol* 6(1):45–50
28. Geldart D, Xie HY (1992) The use of pressure probes in fluidized beds of group a powders. In: Potter OE, Nicklin DJ (eds) *Fluidization VII*. Engineering Foundation, New York, USA, pp 749–756
29. Gladden LF (1994) Nuclear magnetic resonance in chemical engineering: principles and applications. *Chem Eng Sci* 49:3339–3408
30. Gladden LF, Alexander P (1996) Applications of nuclear magnetic resonance imaging in process engineering. *Meas Sci Technol* 7:423–435
31. Gopalan B, Shaffer F (2013) Higher order statistical analysis of Eulerian particle velocity data in CFB risers as measured with high speed particle imaging. *Powder Technol* 242:13–26
32. Hage B, Werther J (1997) The guarded capacitance probe—a tool for the measurement of solids flow patterns in laboratory and industrial fluidized bed combustors. *Powder Technol* 93:235–245
33. Hampel U, Speck M, Koch D, Menz H-J, Mayer H-G, Fietz J, Hoppe D, Schleicher E, Prasser H-M (2005) Experimental ultra fast X-ray computed tomography with a linearly scanned electron beam source. *Flow Meas Instrum* 16:65–72
34. Harris AT, Davidson JF, Thorpe RB (2003) Particle residence time distributions in circulating fluidised beds. *Chem Eng Sci* 58:2181–2202
35. Hartge EU, Rensner D, Werther J (1988) Solids concentration and velocity patterns in circulating fluidized beds. In: Basu P, Large JF (eds) *Circulating fluidized bed technology II*. Pergamon, Oxford, pp 165–180

36. Hassan YA, Blanchat TK, Seeley CH Jr, Canaan RE (1992) Simultaneous velocity measurements of both components of a two-phase flow using particle image velocimetry. *Int J Multiph Flow* 18:371–395
37. He Y, Deen NG, Annaland MVS, Kuipers JAM (2009) Gas–solid turbulent flow in a circulating fluidized bed riser: experimental and numerical study of monodisperse particle systems. *Ind Eng Chem Res* 48(17):8091–8197
38. Hori K, Fujimoto T, Kawanishi K (1996) Application of cadmium telluride detector to high speed X-ray CT scanner. *Nucl Instrum Methods A* 380–397
39. Isaksen O (1996) A review of reconstruction techniques for capacitance tomography. *Meas Sci Technol* 7:325–337
40. Johansen GA, Froystein T, Hjertaker BT, Olsen O (1996) A dual sensor flow imaging tomographic system *Meas. Sci Technol* 7:297–307
41. Johnsson H, Johnsson F (2001) Measurements of local solids volume-fraction in fluidized bed boilers. *Powder Technol* 115(1):13–26
42. Kamalanathan P (2016) Investigation of gas solid circulating fluidized bed at two scales using experimental and numerical techniques. PhD thesis, IIT Guwahati, India
43. Keane RD, Adrian RJ (1992) Theory of cross-correlation analysis of PIV images. *Appl Sci Res* 49:191–215
44. Kunii D, Yosmda K, Hmxta J (1967) The behaviour of freely bubbling fluidized beds. In: *Proceedings of the international symposium on fluidization*, 243, Eindhoven
45. Kunii D, Levenspiel O (1991) *Fluidization engineering*, 2nd edn. Butterworth-Heinemann, Stoneham
46. Kumar S (1994) Computed tomographic measurements of void fraction and modeling of the flow in bubble columns. PhD thesis, Florida Atlantic University, USA
47. Lange K, Carson R (1984) EM reconstruction algorithms for emission and transmission tomography. *J Comput AssistTomogr* 8:306–316
48. Ligrani PM, Singer BA, Baun LR (1989) Miniature five-hole pressure probe for measurement of three mean velocity components in low-speed flows. *J Phys E: Sci Instrum* 22:868–876
49. Lischer OJ, Louge MY (1992) Optical fiber measurements of particle concentration in dense suspensions: calibration and simulation. *Appl Optics* 31:5106–5113
50. Liu J, Grace JR, Bi X (2003) Novel multifunctional optical-fiber probe: II. Development and validation. *AIChE J* 49(6):1405–1420
51. Mahmoudi S, Seville JPK, Baeyens J (2010) The residence time distribution and mixing of the gas phase in the riser of a circulating fluidized bed. *Powder Technol* 203(2):322–330
52. Manyele SV, Pärssinen JH, Zhu J (2002) Characterizing particle aggregates in a high-density and high-flux CFB riser. *Chem Eng J* 88:151–161
53. Muller CR, Davidson JF, Dennis JS, Fennell PS, Gladden LF, Hayhurst AN, Mantle MD, Rees AC, Sederman AJ (2007) Rise velocities of bubbles and slugs in gas-fluidised beds: ultra-fast magnetic resonance imaging. *Chem Eng Sci* 62:82–93
54. Nauman EB, Buftham BA (1983) *Mixing in continuous flow systems*. Wiley, NY
55. Nauman EB (2008) Residence time theory. *Ind Eng Chem Res* 47:3752–3766
56. Nieuwland JJ, Meijer R, Kuipers JAM, van Swaaij WPM (1996) Measurements of solids concentration and axial solids velocity in gas-solid two-phase flows. *Powder Technol* 87(2):127–139
57. Nijenhuis J, Korbee R, Lensselink J, Kiel JHA, van Ommen JR (2007) A method for agglomeration detection and control in full-scale biomass fired fluidized beds. *Chem Eng Sci* 62:644–654
58. O’Sullivan JA, Benac J (2007) Alternating minimization algorithms for transmission tomography. *IEEE Trans Med Imaging* 26:283–297
59. Pant HJ, Sharma VK, Goswami S, Samantray JS, Mohan IN, Naidu T (2014) Residence time distribution study in a pilot-scale gas -solid fluidized bed reactor using radiotracer technique. *J Radioanal Nucl Chem* 302:1283–1288

60. Pantzali MN, Lozano Bayón N, Heynderickx GJ, Marin GB (2013) Three-component solids velocity measurements in the middle section of a riser. *Chem Eng Sci* 101:412–423
61. Pantzali MN, De Ceuster B, Marin GB, Heynderickx GJ (2015) Three-component particle velocity measurements in the bottom section of a riser. *Int J Multiphase Flow* 72:145–154
62. Parker DJ, Dijkstra AE, Martin ITW, Seville JPK (1997) Positron emission particle tracking studies of spherical particle motion in rotating drums. *Chem. Engng. Sci.* 52:2011–2022
63. Parker DJ, Forster RN, Fowles P, Takhar PS (2002) Positron emission particle tracking using the new Birmingham positron camera. *Nucl Instrum Meth A* 477:540–545
64. Parker DJ, Fan X (2008) Positron emission particle tracking—application and labelling techniques. *Particology* 6:16–23
65. Patience GS, Chaouki J, Grandejean BPA (1990) Solids flow metering from pressure drop measurement in circulating fluidized beds. *Powder Technol* 61:95–99
66. Patience GS, Chaouki J (1993) Gas phase hydrodynamics in the riser of a circulating fluidized bed. *Chem Eng Sci* 48:3195–3205
67. Powell RL (2008) Experimental techniques for multiphase flows. *Phys Fluids* 20:040605-1–040605-22
68. Prasad AK (2000) Particle image velocimetry. *Curr Sci* 79:51–60
69. Rados N, Shaikh A, Al-Dahhan MH (2005) Solids flow mapping in a high pressure slurry bubble column. *Chem Eng Sci* 60:6067–6072
70. Reese J, Fan LS (1994) Transient flow structure in the entrance region of a bubble column using particle image velocimetry. *Chem Eng Sci* 49:5623–5636
71. Reinecke N, Mewes D (1994) Resolution enhancement for multi-electrode capacitance sensors. In: *Proceedings of European concerted action on process tomography, Oporto*, pp 50–61
72. Rhodes MJ, Zhou S, Hiram T, Cheng H (1991) Effects of operating conditions on longitudinal solids mixing in a circulating fluidized bed riser. *AIChE J* 37:1450–1458
73. Roy S (2000) Quantification of two-phase flow in liquid-solid risers. PhD thesis, Washington University, USA
74. Roy S, Kemoun A, Al-Dahhan MH, Dudukovic MP (2005) Experimental Investigation of the Hydrodynamics in a Liquid-Solid Riser. *AIChE J* 51:802–835
75. Sanaei S, Mostoufi N, Radmanesh R, Sotudeh-Gharebagh R, Guy C, Chaouki J (2010) Hydrodynamic characteristics of gas-solid fluidization at high temperature. *Can J Chem Eng* 88:1–11
76. Sederman AJ, Johns ML, Bramley AS, Alexander P, Gladden LF (1997) Magnetic resonance imaging of liquid flow and pore structure within packed beds. *Chem Eng Sci* 52:2239–2250
77. Sederman AJ, Johns ML, Alexander P, Gladden LF (1998) Structure-flow correlations in packed beds. *Chem Eng Sci* 53:2117–2128
78. Sederman AJ, Gladden LF (2001) Magnetic resonance imaging as a quantitative probe of gas-liquid distribution and wetting efficiency in trickle-bed reactors. *Chem Eng Sci* 56:2615–2628
79. Seville JPK, Ingram A, Parker DJ (2005) Probing processes using positrons. *Chem Eng Res Des* 83:788–793
80. Sharma AK, Tuzla K, Matsen J, Chen JC (2000) Parametric effects of particle size and gas velocity on cluster characteristics in fast fluidized beds. *Powder Technol* 111(1–2):114–122
81. Shi TM, Xie CG, Huang SM, Williams RA, Beck MS (1991) Capacitance-based instrumentation for multi-interface level measurement. *Meas Sci Technol* 2:923–933
82. Smolders K, Baeyens J (2000) Overall solids movement and solids residence time distribution in a CFB-riser. *Chem Eng Sci* 55:4101–4116
83. Soong CH, Tuzla K, Chen JC (1993) Identification of particle clusters in circulating fluidized bed. In: Avidan AA (ed) *Proceedings of 4th international conference on circulating fluidized beds*. Somerset, USA, pp 615–620
84. Sun J, Yan Y (2016) Non-intrusive measurement and hydrodynamics characterization of gas–solid fluidized beds: a review. *Meas Sci Technol* 27:112001

85. Tartan M, Gidaspow D (2004) Measurement of granular temperature and stresses in risers. *AIChe J* 50:1760–1775
86. Upadhyay RK (2010) Investigation of multiphase reactors using radioactive particle tracking. PhD thesis, IIT Delhi, India
87. Upadhyay RK, Roy S, Pant HJ (2012) Benchmarking Radioactive Particle Tracking (RPT) with Laser Doppler Anemometry (LDA). *Int J Chem React Eng* 10:1–14
88. Upadhyay RK, Pant HJ, Roy S (2013) Liquid flow patterns in rectangular air-water bubble column investigated with radioactive particle tracking. *Chem Eng Sci* 96:152–164
89. van Ommen JR, van der Schaaf J, Schouten JC, van Wachem BGM, Coppens M-O, van den Bleek CM (2004) Optimal placement of probes for dynamic pressure measurements in large-scale fluidized beds. *Powder Technol* 139:264–276
90. van Ommen JR, Mudde RF (2008) Measuring the gas-solids distribution in fluidized beds—a review. *Int J Chem React Eng* 6:1–29
91. van Ommen JR, Sasic S, van der Schaaf J, Gheorghiu S, Johnsson F, Coppens MO (2011) Time-series analysis of pressure fluctuations in gas-solid fluidized beds—a review. *Int J Multiph Flow* 37:403–428
92. Varma R, Bhusarapu S, O’Sullivan JA, Al-Dahhan MH (2008) A comparison of alternating minimization and expectation maximization algorithms for single source gamma ray tomography. *Meas Sci Technol* 19(015506):1–13
93. Warsito W, Fan LS (2001) Network based multi-criterion optimization image reconstruction technique for imaging two-and three-phase flow systems using electrical capacitance tomography. *Meas Sci Technol* 12:2198–2210
94. Wei F, Wang Z, Jin Y, Yu Z, Chen W (1994) Dispersion of lateral and axial solids in a concurrent down flow circulating fluidization. *Powder Technol* 81:25–30
95. Werther J, Molerus O (1973) The local structure of gas fluidized beds. II: The spatial distribution of bubbles. *Int J Multiph Flow* 1:123–138
96. Werther J, Hartge EU, Kruse M (1992) Radial gas mixing in the upper dilute core of a circulating fluidized bed. *Powder Technol* 70:293–301
97. Xu J, Zhu JX (2012) A new method for the determination of cluster velocity and size in a circulating fluidized bed. *Ind Eng Chem Res* 51:2143–2151
98. Xu G, Liang C, Chen X, Liu D, Xu P, Shen L, Zhao C (2013) Investigation on dynamic calibration for an optical-fiber solids concentration probe in gas-solid two-phase flows. *Sensors* 13(7):9201–9222
99. Yang WQ, Spink DM, York TA, McCann H (1999) An image reconstruction algorithm based on Landweber’s iteration method for electrical-capacitance tomography. *Meas Sci Technol* 10:1065–1069
100. Yang Z, Parker DJ, Fryer PJ, Bakalis S, Fan X (2006) Multiple-particle tracking an improvement for positron particle tracking. *Nucl Instrum Meth A* 564:332–338
101. Yang Z, Fryer PJ, Bakalis S, Fan X, Parker DJ, Seville JPK (2007) An improved algorithm for tracking multiple, freely moving particles in a positron emission particle tracking system. *Nucl Instrum Meth A* 577:585–594
102. Yang J, Zhu J (2014) A novel method based on image processing to visualize clusters in a rectangular circulating fluidized bed riser. *Powder Technol* 254:407–415
103. Zhang M, Qian Z, Yu H, Wei F (2003) The solid flow structure in a circulating fluidized bed riser/downer of 0.42-m diameter. *Powder Technol* 129:46–52
104. Zhang Z (2010) LDA application methods. Springer, Heidelberg
105. Zheng CG, Tung YK, Li HZ, Kwauk M (1992) Characteristics of fast fluidized beds with internals. In: Proceedings of the 7th engineering foundation conference on fluidization. Brisbane, Australia, pp 275–283
106. Zhu J, Li G, Qin S, Li F, Zhang H, Yang Y (2001) Direct measurements of particle velocities in gas—solids suspension flow using a novel five-fiber optical probe. *Powder Technol* 115:184–192

Cavity Models for Underground Coal Gasification

Preeti Aghalayam

Abstract Underground coal gasification is an in situ coal utilization technique that has immense potential as a future clean coal technology. UCG possesses a number of advantages including the ability to use deep and unmineable coals. The most important component of UCG is the underground “cavity”—which serves as a chemical reactor with rich interplay of kinetics and transport. Field and laboratory-scale experiments have revealed several interesting features of the UCG cavity. Modeling studies on the UCG cavity involve fundamental models and CFD simulations. In this chapter, we will discuss various experiments and models of UCG cavities, with a focus on the effects of reaction chemistry and thermomechanical spalling on cavity evolution.

1 Underground Coal Gasification

Underground coal gasification is a clean coal technology proposed for future applications in various parts of the world. It consists of the in situ reaction of coal deposits in order to release combustible product gas—which can subsequently be used in various applications. The technique affords several advantages—primarily, it allows the utilization of deep coal deposits (up to 1 km under the surface of the earth) and minimizes the environmental impacts of coal mining and transport. Some of the challenges of UCG include the potential of surface subsidence and aquifer contamination. UCG has had a long history—for instance, the Angrenskaya shallow coal mine in Uzbekistan, UCG was used to produce domestic heating gas on a sustained basis for several decades since the late 1950s [1]. At present, several worldwide projects are at various stages of development.

P. Aghalayam (✉)

Department of Chemical Engineering, Indian Institute of Technology
Madras, Chennai 600036, India
e-mail: preeti@iitm.ac.in

© Springer Nature Singapore Pte Ltd. 2018

S. De et al. (eds.), *Coal and Biomass Gasification*, Energy, Environment,
and Sustainability, https://doi.org/10.1007/978-981-10-7335-9_8

207

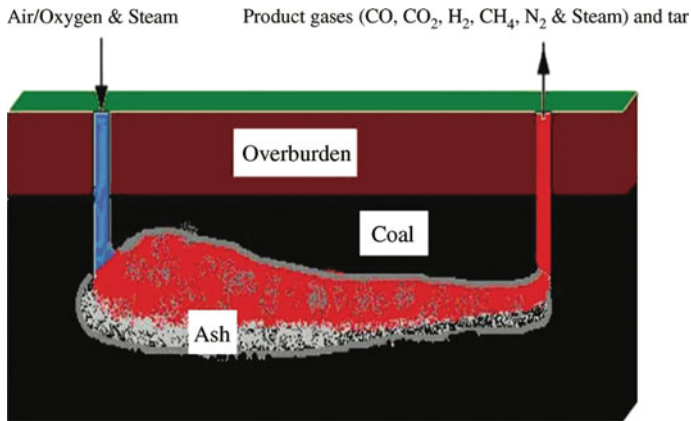


Fig. 1 Schematic of UCG [3]

1.1 The UCG Technique

In UCG, first a vertical injection borehole is dug from the surface to the bottom of the coal seam. Next, a production borehole is created at a prescribed distance from injection. The main challenge in UCG is to find a means of connecting the injection and production boreholes. Directional drilling techniques are employed in order to provide the initial horizontal connection. Reactant gases (air, oxygen, and steam) are injected, and an ignition protocol is used, in order to kick start the various chemical reactions that constitute UCG. As the reactions proceed and coal and char are consumed, a cavity is created underground near the point of injection. The underground cavity grows with time, and the combustible gases generated by the reactions are captured above ground at the production well. The typical operating conditions of UCG are—30–50 bars (for a coal seam ~300–500 m deep) and 500–1000 °C outlet temperatures depending slightly on the nature of the coal [2]. Figure 1 presents a simple schematic of this complex underground process.

1.2 Worldwide Practice of UCG

While there are a number of advantages of UCG, a widespread commercialization of the technique is not yet evident. Considerable success has, however, been enjoyed in Angrenskaya [1] in Uzbekistan and Chinchilla [4] in Australia. Nevertheless, there are a number of blocks on the road to the commercialization of UCG [5]. The potential of UCG in adding to the energy mix, particularly for coal-rich countries such as India, cannot be underemphasized [6].

Some of the early studies on UCG at the field-scale were undertaken in the USA at the Lawrence Livermore National Laboratories [7, 8]. An analysis of the potential

of CCS in conjunction with UCG has been analyzed [2]. In recent times, the activities in India [6], Bangladesh [9], Canada [10], and Poland [11] are noteworthy.

The early practice of UCG was limited to shallow mines, and the product gas used mostly for domestic heating purposes [1], whereas the current proposals regarding UCG cover a wide variety of coals and lignites and propose uses for the product gas ranging from hydrogen production, Fischer–Tropsch synthesis, electricity generation, and polygeneration [2, 12], in various parts of the world.

1.3 Chemical Reactions in UCG

Several chemical reactions occur (simultaneously) in UCG—including both heterogeneous and homogenous ones. It has been clearly shown in simulations that the experimental determination of reaction kinetics for specific coals is required [13]. The first important event is the drying of the wet coal—and most of the UCG models consider this drying step as a reaction, as well [14]. Next, the pyrolysis of the coal to release volatiles and leave behind reactive char is to be considered. The stoichiometry of the pyrolysis reaction depends on the ultimate analysis of coal and char and can be determined in prior calculations [14]. The rate expressions for pyrolysis of some of the coals of interest in UCG are specified in the literature [15, 16]. Likewise, the char oxidation has been studied and rate expressions provided [14, 16–19] for various coal chars. The steam and CO₂ gasification reactions are possibly the most important in UCG and have been studied experimentally [17, 20, 21], albeit only for a handful of coals from this viewpoint. Handy tabulations of quantitative reaction rate expressions and kinetic parameters for all the reactions for a handful of specific coals are reported in [12, 14, 16], while an optimization routine to “up-scale” kinetics determined at atmospheric pressure to the higher pressures which are relevant to UCG, is demonstrated in [19], treating coal as pure carbon as a first approximation.

1.4 Mathematical Modeling of UCG

In practice, UCG is extremely complex, and procuring experimental evidence regarding controlling phenomena is difficult. The high-temperature sequence of gas and solid–gas reactions occurs deep under the earth’s surface, and the distances between the injection and production wells can be hundreds of meters, precluding the possibility of developing large databases of temperature and reactant composition information. Apart from the scale of the problem, the safety aspects such as runaway reactions, aquifer contamination, and roof collapse render field-scale experiments of UCG very challenging indeed.

The role of mathematical modeling in providing a basis encouraging investments in UCG at a chosen site, and for making predictions of both product gas quality and process economics, is vital. Extensive research on the development of mathematical tools particularly applicable to UCG is being conducted [3]. The models for UCG broadly focus on fundamentals (determination of intrinsic kinetics or mass and heat transport effects); process modeling (providing expected compositions and calorific value of the product gas under at various operating conditions); and economics (e.g., predicting the cost of UCG generated electricity on a per Btu basis; or comparing cost of H₂ production per Kg from UCG).

Kinetic studies that provide the reaction rate parameters for the pyrolysis, oxidation, steam gasification, and CO₂ gasification of various chars are important first steps in modeling of UCG. For example, extensive studies of the Wyodak coal in the USA have been undertaken earlier [14] and useful data on kinetic constants provided [12]. Some information regarding a lignite from the Falkirk mine in the USA is also available [17]. Extensive studies on Indian coals and lignites have been recently conducted [16, 20], and samples from proposed UCG sites in Poland are analyzed [21]. Interesting developments regarding the pressure dependence of the kinetic parameters are provided as well [19, 22] in the literature.

Predictive process models for UCG incorporate fundamentals, such as kinetics of chemical reactions in UCG, provide quantitative details regarding expected product gas composition and other features. One-dimensional models that treat the “UCG reactor” as a packed bed reactor have provided analyses of several coals from India and the USA [13, 14]. A more advanced pseudo-one-dimensional model incorporates cavity aspects and predicts the product gas compositions, and their dependence on various factors including pressure and intrinsic coal reactivity [23]. On the other hand, plant-wide and reservoir models have been recently developed that tackle the entire UCG operation including the various associated unit operations and provide another viewpoint about the UCG process [24–26]

Another focal point in modeling for UCG has been regarding economics. Although these models are under development at this point, with extensive discussions on the various associated costs [6, 27] of UCG, it is evident that it is important to analyze the cost of UCG product gas on a local basis. The Canadian scenario is explored in [10, 28], and potential of UCG in fertilizer production in Bangladesh is presented in [27]. Other economic analyses for USA [29]; India [6]; Poland [30], and Bulgaria [31] target various aspects related to the costs of UCG.

One of the unique features of UCG is the formation and growth of the underground cavity. It has been shown in several studies that the nature of the cavity (in terms of size, porosity, conductivity, growth rate, and so on) can have a direct impact on the performance of UCG [16, 32]. The cavity “sub-model” has been under study for the past several decades, and the rest of this chapter will focus particularly on the UCG cavity, which can be considered as a chemical reactor.

2 Cavity Models for UCG

The earliest inclination of the importance of the UCG cavity was obtained in the field-scale studies conducted in the USA by the Lawrence Livermore National Laboratory [7]. In a series of experiments termed the “Large Block Experiments,” large sections of coal at a chosen site were gasified and the product gas composition were analyzed. Upon cooling, the blocks were extracted and studied. A hemispherical dome-shaped cavity was observed, and it was hypothesized that the chemical reactions of UCG occur within and on the roof of this cavity [8]. Furthermore, the nature of the coal, including its porosity, carbon, ash, and moisture content, was found to affect the cavity significantly [8].

2.1 Laboratory Demonstration of UCG (Micro-UCG)

The shape and evolution of the UCG cavity have recently been examined in detail in a series of laboratory-scale experiments, for an Indian coal from a proposed UCG site [33, 34]. The laboratory technique that mimics the UCG process, albeit on a small scale, is termed “Micro-UCG.” Figure 2 shows the experimental setup that is used. The original details of UCG are retained as feasible. Vertical boreholes are created in a ~15 cm coal block and further connected at the bottom by a horizontal borehole. An ignition protocol utilizing LPG is implemented. Detailed experiments varying the composition of the injected reactant gases (O₂ and steam) are performed, and the developed UCG cavity examined at the end of the experiment.

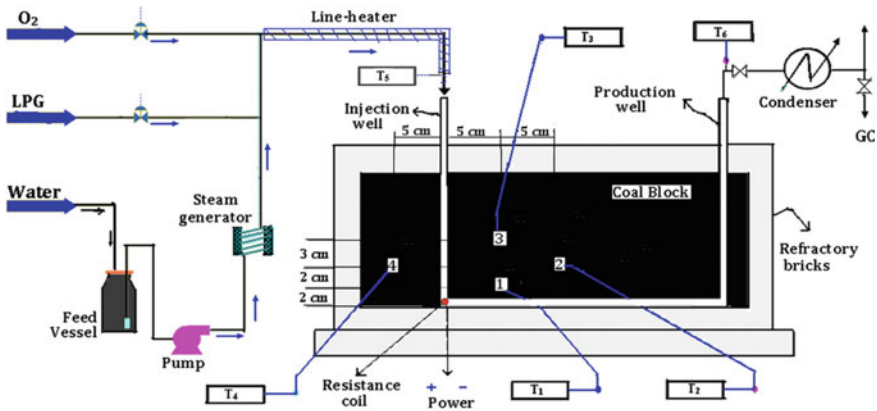


Fig. 2 Schematic of the micro-UCG experiment [33]

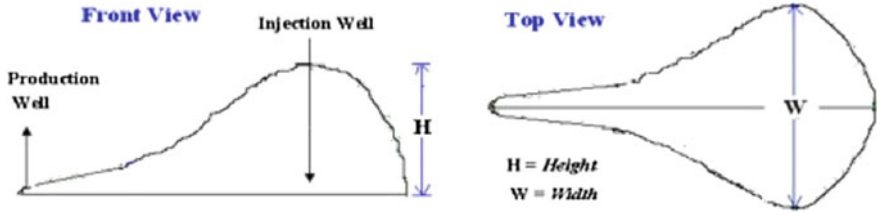


Fig. 3 A generalized picture of the UCG cavities from micro-UCG experiments [33]

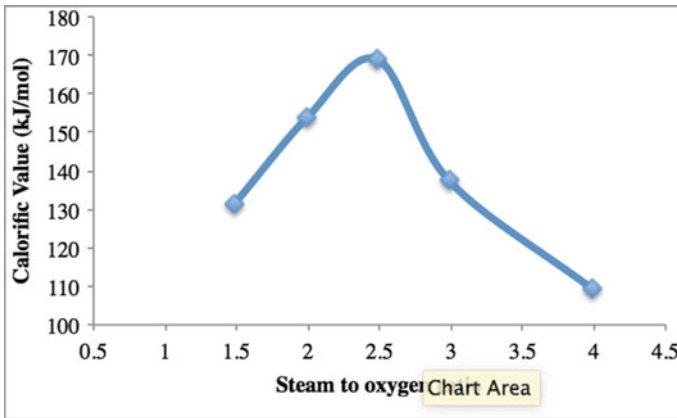


Fig. 4 Variation in the calorific value of the product gas with the inlet steam to oxygen ratio indicates an optimum value (from [34])

Some of the important conclusions from the Micro-UCG experiments are—the UCG cavity has a hemispherical dome which is more or less symmetric around the injection point; it also has a long tail that extends toward the production borehole; the growth of the cavity is more in the vertically upward direction than the downward one; and the distance between the injection and production wells affects the size and shape of the cavity. Furthermore, the growth rate of the UCG cavity is found to be more in case of steam gasification (i.e., when steam/oxygen mixtures are used as a reactant medium) than in combustion (i.e., when pure oxygen is used as the reactant medium), possibly due to the thermomechanical spalling of coal from the cavity roof and kinetic effects. Figure 3 presents a generalized picture of the micro-UCG cavities that were developed in this work. The calorific value of the product gas is measured in this work, and the results shown in Fig. 4. It is seen clearly that the inlet steam to oxygen ratio has a significant impact on the quality of the product gas in micro-UCG [34].

2.2 Experiments and Simulations of Thermomechanical Spalling

As the temperature in the UCG cavity rises, and the reactant gases diffuse into the porous network of coal at the top of the cavity, it is expected that they dislodge pieces of coal from the block and that these pieces fall on to the floor of the cavity. The tendency for spalling is likely to be a unique property of each coal.

In well-designed laboratory-scale experiments using an Indian hard coal and a soft lignite (with high moisture content), it has been demonstrated that only the latter has a high tendency for spalling [18]. Figure 5 is a picture of the heater plate at the bottom of the coal block that was subjected to high temperature (700 °C) and a reactive atmosphere for 18 h. Spalled pieces of the lignite, which have dislodged from the coal block and fallen on to the floor of the UCG cavity are observed in this case. In an earlier study, similar conclusions were drawn—one of three studied coal samples demonstrated loosened char and ash on the cavity floor while the others did not [8], demonstrating that spalling characteristics can vary significantly from coal to coal.

In a related experiment, the quantitative aspects of spalling of the high moisture Indian lignite have been tackled [35]. The experimental setup is a simple one involving a block of the lignite suspended in an UCG-like environment and connected to a load cell in order to monitor its weight as a function of time. Figure 6 shows a schematic of the experimental setup used in this work. The weight of the block varies continuously due to the chemical reactions of UCG but presents discontinuities due to the discrete spalling events. These are well captured in the experiment, and spalling rates in the range 2–26 kg/m²/h are observed for the various samples. The heterogeneity in preexisting cracks and other weak points in the blocks lead to the variation in the spalling rates, in repeated experiments.

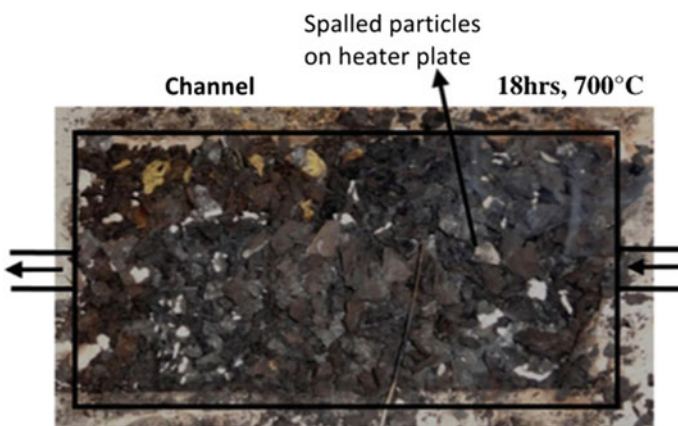


Fig. 5 Evidence of thermomechanical spalling in a laboratory experiment on a high moisture lignite [18]

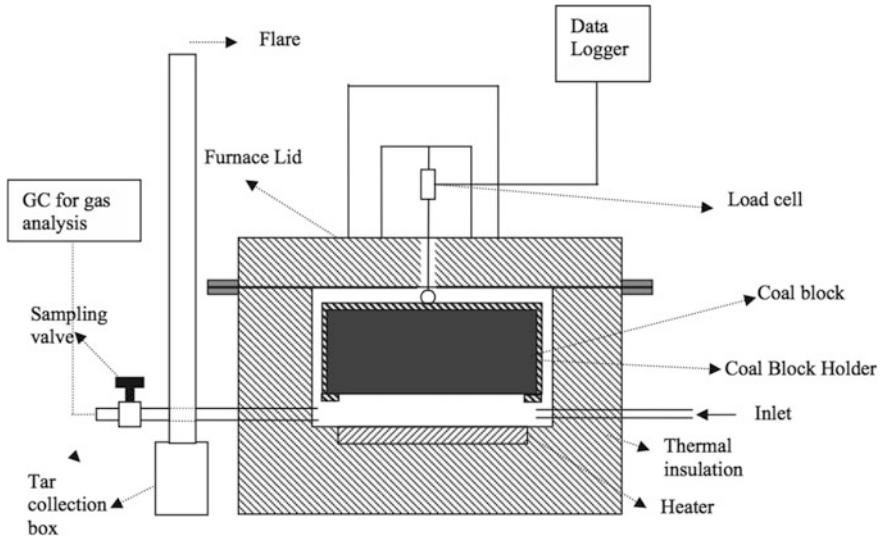


Fig. 6 Schematic of the laboratory setup used to measure quantitative spalling rates [35]

Modeling of thermomechanical spalling and inclusion of the effect of spalling on UCG was first undertaken in the 1980s [36]. A one-dimensional model incorporated spalling using two parameters—a critical length (into the coal seam at the roof of the cavity) and critical temperature (at which spalling events occur). The variation of the roof temperature was tracked as a function of time. The discrete spalling events were identified, and it was concluded that overall, the growth rate of the cavity is mostly driven by the mass transport of oxygen to the roof.

Analysis of the influence of thermomechanical spalling on cavity shape, size, and growth rate is demonstrated in a series of 3-D simulations that present a realistic picture of the UCG cavity [37]. In this work, gasification of underground coal, formation and evolution of the cavity, and reactant gas flow patterns are modeled using a combination of two modules—one that tackles the flow equations and the other spalling of coal and/or rock layers. Char oxidation is the only reaction considered though the framework is flexible enough for the introduction of other reactions as well. The spalled coal that falls into the cavity void is assumed to be immediately gasified. The permeabilities of the ash, coal, and rock layers are assumed at different values. The spalling rate is assumed to be a constant, and different values for the rate are examined in parametric studies.

The results of these simulations demonstrate that a high spall rate leads to rapid upward growth of the cavity toward the rock, with steep coal walls. Furthermore, an ash layer of low permeability on the bottom of the cavity leads to significant bypassing of reactant gases and in general, inefficient gasification. A symmetrical cavity around the injection point is observed when an initial linkage between injection and production wells is created [37], which is consistent with the experimental and other observations of other studies on UCG cavities.

Recent analysis of spalling improves upon the earlier results, and a complete quantitative method for incorporating the phenomena into cavity modeling and simulations is developed [16]. This model, which tackles both the prediction of cavity growth and product gas compositions, is described later in some detail.

2.3 Flow and Transport in UCG Cavities

Another important aspect of UCG models is the velocity contours of the reactant gases in the cavity space. This involves the flow patterns in the void space as well as in the porous network of the rubble/roof of the cavity. It has been demonstrated that the effects of mass transport of reactant gases to the cavity roof and associated effects can control UCG performance significantly [38], and thus, it is important to model the nature of flow of reactant gases in the UCG cavity well.

A two-dimensional axisymmetric model that represents the UCG cavity is studied to determine the importance of heat and mass transport on chemical reactions [38]. CFD modeling assuming a cylindrical shaped cavity, with an ash bed region in the bottom and void space on top, is undertaken. Oxidation and CO₂ gasification reactions are incorporated as boundary conditions, and the coal is assumed to be pure carbon. Contours of temperature and reactant gas mass fractions in the cavity are obtained in this study and indicate the importance of heat and mass transport in capturing UCG performance.

A systematic model of the UCG cavity is proposed in [39]. In this work, the impact of non-ideal flow patterns in the UCG cavity is analyzed using a compartment modeling approach. First, four channel shapes/sizes are chosen based on earlier literature. CFD simulations are performed in order to determine reactant gas flow patterns in these cavities. The results of the CFD simulations are used to determine residence time distribution curves. The RTD curves are then used to develop a compartment model—i.e., combination of ideal reactors that approximately represents the flow in the cavity. Figure 7 depicts the proposed compartment model for the UCG cavity and consists of several perfectly stirred reactors, a recycle stream, dead volume, and a plug flow reactor. The model is general enough to be valid for all the four cavity sizes (representing the UCG cavity on different days since the inception of UCG). ASPEN-based simulations using the proposed compartment model are performed, and reasonable results for the homogeneous water gas shift reaction shown.

Although this work represents a significant advancement in the modeling of the reactant gas flow patterns in the UCG cavity, it has a handful of disadvantages as well. For one, the phenomenon of thermomechanical spalling is not included here. As seen in Sect. 2.2, this can be a very important aspect governing cavity growth and product gas compositions. Furthermore, four fixed cavity sizes are chosen for analysis and the evolution in cavity shape/size is not included. Finally, the model predictions do not tackle the heterogeneous reactions of coal gasification.

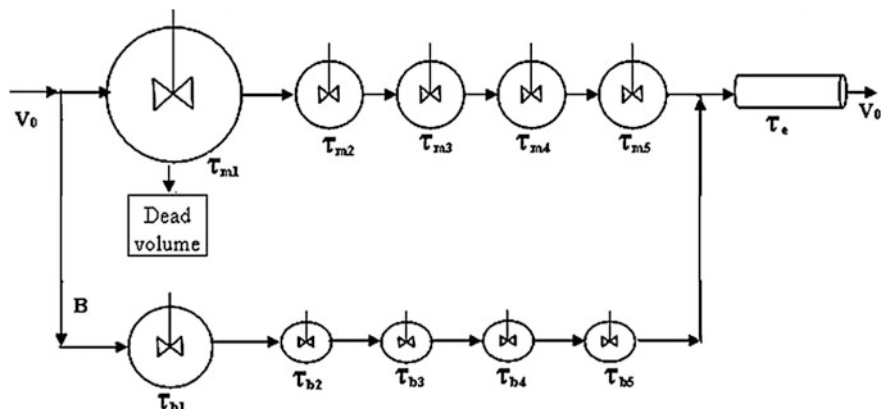


Fig. 7 Compartment model consisting of perfectly stirred reactors, dead volume, a bypass stream, and a plug flow reactor proposed to represent flow in an UCG cavity [39]

Nevertheless, this is a good cavity model and the use of combinations of ideal reactors is a handy technique to save on the computational expense associated with UCG simulations.

2.4 Product Gas Composition Prediction in Cavity Models

The cavity models for prediction of product gas compositions generally use idealized flow patterns [13, 14, 23, 40] or involve expensive CFD simulations that cannot be easily combined with reaction chemistry [41]. A recent series of articles presents one way of overcoming these challenges, using the technique of compartment modeling [16, 32]. The requirement of a computational tractable UCG model that captures kinetics, spalling effects, and flow patterns of the reactant gases in the cavity is well met in this work. The UCG cavity is divided into rubble, void, and roof zones, and different properties are envisaged in each case. The overall UCG phenomenon is divided into two phases—in phase I, the coal cavity grows due to reaction and spalling, in the vertical direction, ultimately reaching the overburden [16]; whereas in phase II, the outflow channel, that connects the injection borehole to the production borehole, grows [32]. The two phases will typically occur simultaneously in UCG processes although in case of coals with high spalling rates, they may occur sequentially.

As described in Sect. 2.3, the reactant gas flow patterns in the various zones of the cavity model are examined using CFD simulations as in other work [39] and translated into a simplified sequence of ideal flow reactors, i.e., a compartment model [16, 32]. The main components of the compartment model proposed in phase I are a hemispherical radial PFR representing the rubble zone, and a CSTR that represents the void space in the cavity. In phase II, the compartment model consists mainly of CSTRs in series for both for the rubble and the void zones.

Coal drying, pyrolysis, char oxidation, steam, and CO₂ gasification are incorporated via kinetic rate expressions developed in an earlier experimental paper for an Indian lignite [20]. Mass transport effects are included as well. The most interesting aspect of this cavity model is the inclusion of a discrete spalling component, based on laboratory-scale experimental observations [35] on Indian lignite, which are described in Sect. 2.2. The two parameters used to model spalling are the critical roof temperature and volume of coal (lignite in this case) spalled, which are taken as 900 °C and 0.002 m³, respectively, based on the experiment. When the roof temperature reaches the critical value, the prescribed volume of coal spalls and falls on to the floor of the cavity. The temperature of the roof then immediately lowers, and the volume of the radial PFR representing the rubble zone is updated suitably. The form of the spalling model used here is similar to earlier work [37]; however, the parameters are evaluated from specific laboratory-scale experiments, and this represents a good advancement.

Thus, the cavity model accounts for the complex flow patterns in the UCG cavity in addition to reaction kinetics and spalling effects. All the parameters of the model are particular to the coal under consideration and have been determined in earlier studies on the same. The comparison of the results of modeling simulations of “early stage UCG” (phase I) with earlier micro-UCG experiments [34] is reasonable. The product gas composition, total volume of coal consumed, and size of the UCG cavity that is measured in the experiments are predicted well in the simulations. Table 1 shows a comparison of the two.

Assuming that the growth of the cavity in the vertical direction occurs *before* the growth of the outflow channel (i.e., the two phenomena occur sequentially) and a predictive model is developed in a subsequent article [32] for the entire duration of UCG. The article is capable of predicting the observations in terms of gas calorific value very well. It is particularly relevant that the time taken for the UCG activity to “end”—i.e., the time at which all the coal that can be gasified is consumed—agrees well between the simulations and experiments. However, the model assumptions are valid only in case of high spalling coals and thus may not be universally applicable.

This comprehensive cavity model represents a giant leap in UCG model predictions and covers most of the important aspects. But, reaction kinetics and spalling parameters are not generalizable and need to be evaluated via independent experiments for each coal of interest. While the intrinsic kinetics from experiments of thermal analysis and so on can be utilized (possibly, after correcting for the higher pressure that can exist in UCG [19]), scale effects can be dominant in case of spalling and experimental information on spalling parameters has to be obtained

Table 1 Comparison of results of the cavity model with experimental data

Parameter	Experiment [34]	Simulation [16]
Calorific value (kJ/mol)	160	157
Total volume of coal consumed (cm ³)	1000	1120

from field-scale studies as possible. Furthermore, an experimental database of both laboratory and pilot-scale studies is required in order to validate cavity models, before extensive predictions of expected product gas compositions can be made. The importance of such predictive models can, however, not be underemphasized.

2.5 Growth of UCG Cavities

An important aspect of UCG is the rate of growth of the UCG cavity. It is generally believed that a significant component of cavity growth occurs due to thermomechanical spalling events. Using a one-dimensional mathematical model, the cavity growth rate for a generalized, semi-infinite coal block was obtained [42] in early studies.

In a systematic study, the cavity growth in all three dimensions has been obtained in the micro-UCG experiments described above in Sect. 2.1 [34]. The results, depicted in terms of the volume of the cavity as a function of time, are qualitatively consistent with the earlier simulations though a quantitative comparison is not viable as the growth rate is not obtained as a function of temperature in this experiment. Figure 8 shows the linear increase in the cavity volume as a function of the time of the experiment. It is seen that the size and rate of growth of the gasification cavity are higher than that of the combustion cavity.

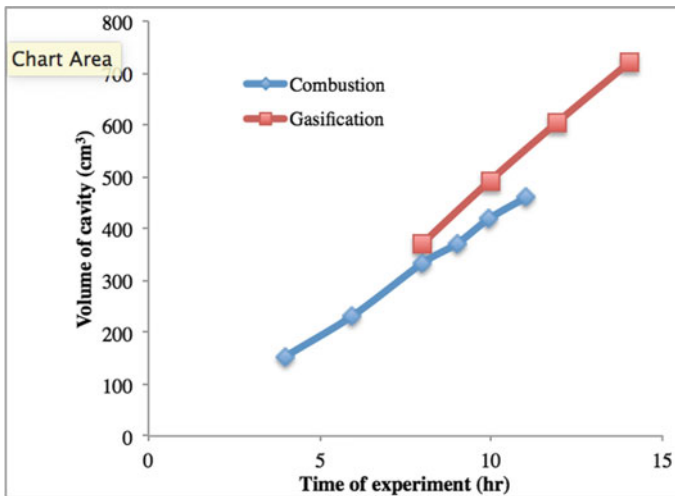


Fig. 8 Variation of the UCG cavity volume as a function of time in micro-UCG experiments (from [34])

The rate of growth of the UCG cavity is estimated in cavity model simulations for Indian lignites, which demonstrate a high rate of spalling, at $54 \text{ cm}^3/\text{mole}$ of gas fed [16], using a quantitative model based on various experiments on the chosen coal sample. This is in reasonable agreement with the experimental study described above.

3 Future Prospects

Recent advancements in mathematical modeling and laboratory-scale experiments on underground coal gasification provide the promise for a bright future for UCG. Several coal-rich countries including India are actively pursuing studies in UCG as a future clean coal technology that can add significantly to the energy mix of the country. Although there are issues related to public perceptions and government regulations regarding UCG, the scientific community has shown remarkable resilience in pursuing the topic. The various research studies in open literature represent the focus and commitment toward ensuring safe, efficient, and productive practice of UCG, particularly in deep-seated coal mines that are not currently accessible by mining techniques. The technological developments required for UCG are all at a mature stage, and it can be expected that the technique will emerge as an effective means of utilization of coal in the future.

Experiments on UCG are expensive and complicated, and the protocols are as yet not well established. The correspondence between results from laboratory-scale studies and larger field-scale experiments has to be explored further. In the meantime, the role of mathematical modeling and simulation studies in determining the feasibility of UCG in various proposed coal mines is vital. UCG cavity modeling is the most important component of this exercise, and the rich literature on this topic is a testament to this. Three-dimensional simulations performed at scale, incorporating specific kinetics, spalling and flow pattern information for a proposed pilot-scale study, and validated against experimental data from the same, are hopefully realizable in the near term future!

Acknowledgements I am grateful to my colleagues Prof. Sanjay Mahajani and Anuradda Ganesh for the several years of discussions on UCG that we have had. I would also like to express my gratitude to ONGC, IRS, Ahmedabad, and the several research scholars who have worked very hard on unraveling the myriad mysteries hidden in this rich topic.

References

1. Olness D (1982) The Angrenskaya underground coal gasification station. LLNL Publ.
2. Friedmann SJ, Upadhye R, Kong FM (2009) Prospects for underground coal gasification in carbon-constrained world. *Energy Proc* 1(1):4551–4557
3. Aghalayam P (2010) Underground coal gasification: a clean coal technology, vol 5

4. Blinderman MS, Saulov DN, Klimenko AY (2008) Forward and reverse combustion linking in underground coal gasification. *Energy* 33(3):446–454
5. Shackley S, Mander S, Reiche A (2006) Public perceptions of underground coal gasification in the United Kingdom. *Energy Policy* 34(18):3423–3433
6. Khadse AN (2015) Resources and economic analyses of underground coal gasification in India. *Fuel* 142:121–128
7. Hill RW, Thorsness CB (1982) Large block experiments in underground coal gasification. LLNL Publ.
8. Creighton JR, Thorsness CB (1981) Laboratory scale simulation of underground coal gasification: simulation and theory. LLNL Publ.
9. Sajjad M, Rasul MG (2015) Prospect of underground coal gasification in Bangladesh. *Proc Eng* 105:537–548
10. Olateju B, Kumar A (2013) Techno-economic assessment of hydrogen production from underground coal gasification (UCG) in Western Canada with carbon capture and sequestration (CCS) for upgrading bitumen from oil sands. *Appl Energy* 111:428–440
11. Bielowicz B, Kasiński JR (2015) The possibility of underground gasification of lignite from Polish deposits. *Int J Coal Geol* 139(1):191–205
12. Uppal AA, Bhatti AI, Aamer E, Samar R, Khan SA (2015) Optimization and control of one dimensional packed bed model of underground coal gasification. *J Process Control* 35:11–20
13. Khadse AN (2006) Reactor model for the underground coal gasification (UCG) channel reactor model for the underground coal gasification (UCG) channel. *Int J Chem React Eng* 4
14. Thorsness CB, Grens EA, Sherwood A (1978) A one-dimensional model for in-situ coal gasification. LLNL Publ.
15. Campbell JH (1978) Pyrolysis of subbituminous coal in relation to insitu gasification. *Fuel* 57:217–224
16. Samdani G, Aghalayam P, Ganesh A, Sapru RK, Lohar BL, Mahajani S (2016) A process model for underground coal gasification—Part-I: Cavity growth. *Fuel* 181:690–703
17. Mann MD, Knutson RZ, Erjavec J, Jacobsen JP (2004) Modeling reaction kinetics of steam gasification for a transport gasifier. *Fuel* 83(11–12):1643–1650
18. Bhaskaran S, Ganesh A, Mahajani S, Aghalayam P, Sapru RK, Mathur DK (2013) Comparison between two types of Indian coals for the feasibility of underground coal gasification through laboratory scale experiments. *Fuel* 113:837–843
19. Kariznovi M, Nourozieh H, Abedi J, Chen Z (2013) Simulation study and kinetic parameter estimation of underground coal gasification in Alberta reservoirs. *Chem Eng Res Des* 91(3):464–476
20. Mandapati RN, Daggupati S, Mahajani SM, Aghalayam P, Sapru RK, Sharma RK, Ganesh A (2012) Experiments and kinetic modeling for CO₂ gasification of indian coal chars in the context of underground coal gasification. *Ind Eng Chem Res* 51:15041–15052
21. Iwaszenko S (2015) Using Mathematica software for coal gasification simulations—selected kinetic model application. *J Sustain Min* 14(1):21–29
22. Roberts DG, Harris DJ (2000) Char gasification with O₂, CO₂ and H₂O: Effects of pressure on intrinsic reaction kinetics. *Energy Fuels* 14:483–489
23. Perkins G, Sahajwalla V (2008) Steady-state model for estimating gas production from underground coal gasification. *Energy Fuels* 22(6):3902–3914
24. Verma A, Olateju B, Kumar A, Gupta R (2015) Development of a process simulation model for energy analysis of hydrogen production from underground coal gasification (UCG). *Int J Hydrogen Energy* 40(34):10705–10719
25. Andrianopoulos E, Korre A, Durucan S (2015) Chemical process modelling of underground coal gasification and evaluation of produced gas quality for end use. *Energy Proc* 76:444–453
26. Seifi M, Abedi J, Chen Z (2014) Application of porous medium approach to simulate UCG process. *Fuel* 116:191–200
27. Nakaten N, Islam R, Kempka T (2014) Underground coal gasification with extended CO₂ utilization—an economic and carbon neutral approach to tackle energy and fertilizer supply shortages in Bangladesh. *Energy Proc* 63:8036–8043

28. Verma A, Kumar A (2015) Life cycle assessment of hydrogen production from underground coal gasification. *Appl Energy* 147:556–568
29. Kelly KE et al (2016) Underground coal thermal treatment as a potential low-carbon energy source. *Fuel Process Technol* 144:8–19
30. Burchart-Korol D, Krawczyk P, Czaplicka-Kolarz K, Smoliński A (2016) Eco-efficiency of underground coal gasification (UCG) for electricity production. *Fuel* 173:239–246
31. Nakaten N, Schlüter R, Azzam R, Kempka T (2014) Development of a technical-economic model for dynamic calculation of COE, energy demand and CO₂ emissions of an integrated UCG-CCS process. *Energy* 66:779–790
32. Samdani G, Aghalayam P, Ganesh A, Sapru RK, Lohar BL, Mahajani S (2016) A process model for underground coal gasification—Part-II growth of outflow channel. *Fuel* 181:587–599
33. Daggupati S et al (2010) Laboratory studies on combustion cavity growth in lignite coal blocks in the context of underground coal gasification. *Energy* 35(6):2374–2386
34. Daggupati S et al (2011) Laboratory studies on cavity growth and product gas composition in the context of underground coal gasification. *Energy* 36(3):1776–1784
35. Bhaskaran S et al (2015) Experimental studies on spalling characteristics of Indian lignite coal in context of underground coal gasification. *Fuel* 154:326–337
36. Britten JA, Thorsness CB (1989) Model for cavity growth and resource recovery during underground coal gasification. *Situ* 13(1–2):1–53
37. Biezen ENJ, Molenaar J, Bruining J (1995) An integrated 3D model for underground coal gasification. In: Society of Petroleum Engineers annual technical conference. Dallas, U.S.A.
38. Perkins G, Sahajwalla V (2007) Modelling of heat and mass transport phenomena and chemical reaction in underground coal gasification. *Chem Eng Res Des* 85:329–343
39. Daggupati S et al (2011) Compartment modeling for flow characterization of underground coal gasification cavity. *Ind Eng Chem Res* 50(1):277–290
40. Park KY, Edgar TF (1987) Modeling of early cavity growth for underground coal gasification. *Ind Eng Chem Res* 26:237–246
41. Nitao JJ et al (2011) Progress on a new integrated 3-D UCG simulator and its initial application. In: Proceedings of international Pittsburgh coal conference
42. Perkins G, Sahajwalla V (2005) A mathematical model for the chemical reaction of a semi-infinite block of coal in underground coal gasification. *Energy Fuels* 19(8):1679–1692

Gasification of Mixed Biomass: Analysis Using Equilibrium, Semi-equilibrium, and Kinetic Models

Debarshi Mallick, Buljit Buragohain, Pinakeswar Mahanta
and Vijayanand S. Moholkar

Abstract Biomass gasifiers with capacities exceeding 1 MW have large biomass consumption, and mixture of biomasses need to be used as feedstock in these gasifiers. In this chapter, we have presented a review of our studies in gasification of biomass blends using approaches of non-stoichiometric equilibrium, semi-equilibrium, and kinetic models. Initially, gasification of biomass mixtures has been assessed using thermodynamic equilibrium and semi-equilibrium (with limited carbon conversion) model employing Gibbs energy minimization. Influence of operating parameters such as equivalence ratio, temperature of gasification, and composition of the biomass mixture has been evaluated using two criteria, viz net yield and LHV of the producer gas. Interestingly, optimum operating conditions for all biomass mixtures have been established as equivalence ratio ~ 0.3 and gasification temperature ~ 800 °C. The kinetic model analysis of gasification of biomass based on a circulating fluidized bed gasifier. A series of chemical reactions was considered for obtaining complete mass balance. Although the profiles of molar composition, net yield and LHV of the

D. Mallick · P. Mahanta

Department of Mechanical Engineering, Indian Institute of Technology Guwahati,
Guwahati 781039, Assam, India
e-mail: debarshi@iitg.ernet.in

P. Mahanta

e-mail: pinak@iitg.ernet.in

B. Buragohain · P. Mahanta · V. S. Moholkar (✉)

Center for Energy, Indian Institute of Technology Guwahati, Guwahati 781039,
Assam, India
e-mail: vmoholkar@iitg.ernet.in

B. Buragohain

e-mail: buljit@gimt-guwahati.ac.in

V. S. Moholkar

Department of Chemical Engineering, Indian Institute of Technology
Guwahati, Guwahati 781039, Assam, India

B. Buragohain

Department of Mechanical Engineering, Girijananda Chowdhury Institute
of Management and Technology, Azara, Guwahati 781017, Assam, India

© Springer Nature Singapore Pte Ltd. 2018

S. De et al. (eds.), *Coal and Biomass Gasification*, Energy, Environment,
and Sustainability, https://doi.org/10.1007/978-981-10-7335-9_9

producer gas predicted by kinetic model matched with equilibrium models qualitatively, significant quantitative difference was evident. The processes of char gasification and tar oxidation have slow kinetics that adversely affects the carbon conversion in the riser of the circulating fluidized bed gasifier.

Keywords Gasification • Equivalence ration • LHV • Equilibrium model
Semi-equilibrium model • Kinetic model

1 Introduction

Global consumption of energy has been greatly increased in recent years due to industrial development, economy, and population growth. Fossil fuels are the most common energy sources used in the world. Combustion of these fossil fuels produces large amount of CO₂ which contributes to greenhouse effect and global warming [1]. These issues have made substitution of conventional fuels with alternate fuel sources that are renewable, sustainable, and environmentally friendly. Unless we give a serious thought toward the renewable energy, the problem of energy crisis cannot be resolved. Renewable energy sources can reduce our dependence on fossil fuels and help us to reduce greenhouse gas emissions. So, there is an immediate need for harnessing the large potential of renewable energy sources in a planned and strategic way in order to diminish the gap between demand and supply of required energy, and at the same time avoiding issues of climate change risk. Among all renewable resources of energy, biomass is the only carbon source which can be converted to solid, liquid, and gaseous product through various thermochemical conversion processes [2]. Biomass is the fourth largest source of energy in the world after coal, petroleum, and natural gas and provides about 14% of the world's energy consumption [3]. Hence, extensive abundance of biomass has been widely recognized as the potential to supply larger amounts of useful energy with fewer environmental impacts compared to fossil fuels [4].

There are three thermochemical routes to extract energy from biomass, viz. pyrolysis, combustion, and gasification. Gasification is a thermochemical process that converts organic- or fossil-based carbonaceous materials into combustible gases, liquid, and tar. The combustible gases mainly contain methane, hydrogen, carbon monoxide, carbon dioxide and nitrogen. In order to enhance efficiency of gasification process, various types of gasifiers have been developed, viz. updraft gasifier, downdraft gasifier, cross-draft gasifier, bubbling fluidized bed gasifier, circulating fluidized bed gasifier, entrained flow gasifier. Amongst them, fluidized bed gasification is one of the promising technologies to extract energy from biomass, as it has distinct merits such as excellent mixing, fuel flexibility, thermal as well hydrodynamic uniformity, effective temperature control, higher efficiency and better control of solid and gas flow.

In order to analyze the performance of fluidized bed gasification as a function of process parameters, several models have been developed by different researchers. These models can be broadly classified in two categories, viz. thermodynamic

equilibrium modeling and kinetic modeling. The equilibrium modeling approach is independent of the gasifier type, as it does not consider the hydrodynamic and other process conditions of gasification. Depending on procedure of determining the product composition of gasification process, the equilibrium model may be further classified as the stoichiometric equilibrium model and non-stoichiometric equilibrium model. The stoichiometric equilibrium models are based on reactions that occur between the chemical species involved in the process, while, non-stoichiometric models are based on elemental balance between the reactants and products at given conditions of temperature and pressure. The kinetic models of gasification usually consider the hydrodynamic behavior of gasification system coupled with the reaction kinetics. Kinetic modeling is physically most realistic approach. Though, many limitations of these models in terms of proper and reliable operational data restrict their wide applicability.

The chapter tries to give a comprehensive overview of the different mathematical models viz. equilibrium, semi-equilibrium, and kinetic models of biomass gasification using a circulation fluidized bed gasifier as basis. Three representative biomasses, which are available in India [5] viz. sawdust, rice husk, and bamboo dust have been selected for the present study. The important parameters such as temperature of gasification, equivalence ratio that influence the quality, and yield of the producer gas resulting from biomass gasification [6, 7] have been briefly discussed.

2 Biomass Gasification Models

The gasification processes essentially involve complex chemical reactions, partial oxidation, char gasification, conversion of tar and hydrocarbons, and the water–gas shift reaction. These complex processes are coupled with sensitivity of the product distribution to the heating rate and residence time in the gasifier. Reliable data and information on these aspects are required for development of mathematical models. The main objectives in development of the gasification models are: (1) study of the various thermochemical processes during the gasification of the biomass and (2) to obtain the influence of input variables, such as equivalence ratio, moisture content, air/fuel ratio, fuel gas composition and yield, and the calorific value of the fuel gas. Simple thermodynamic gasification models are based on the final conditions of temperature and pressure in the gasifier that dominates the chemical equilibrium. More rigorous models take into account various zones in the gasifier, with different temperature ranges, that are associated with different steps of the overall gasification process.

Kinetic models essentially provide the information on kinetic mechanisms to describe the conversion during biomass gasification, which is very important in designing, evaluating, and improving gasifiers. The kinetic models are very precise and detailed but are computationally intensive [8].

The kinetic rate models always contain some constraints that limit their applicability to various systems. On the other hand, thermodynamic equilibrium models, which are independent of gasifier design, are more appropriate for studies on the

influence of the most essential process parameters such as temperature of gasification and equivalence ratio. During the chemical equilibrium condition, the reacting systems are at its most stable composition, and a condition is determined when the entropy of the system is maximized; however, Gibbs free energy is minimized. In practical situation, thermodynamic equilibrium may not be achieved even at comparatively high operation temperatures [9].

Aspen Plus is the simplest possible model which incorporates the main gasification reactions and the gross physical characteristics of the gasification reactor. It is a problem-oriented software used to facilitate the calculation of chemical, physical, and biological processes. It can be applied to describe the processes involving solids, vapor, and liquid streams. The Aspen Plus process simulator is prepared with a large property data bank having the various stream properties required to model the material streams in a gasification unit, with an allowance for the addition of in-house property data. Aspen Plus simulator is basically used to simulate coal conversion processes viz indirect coal liquefaction processes [10], methanol synthesis [11], integrated coal gasification combined cycle power plants [12], compartment fluidized bed coal gasifiers [13], atmospheric fluidized bed combustor processes [14], coal hydrogasification processes [15], and coal gasification simulation [16]. Though, the effort that has been made on biomass gasification with the use of Aspen Plus simulator is less extensive.

The artificial neural networks (ANN) have been comprehensively applied in the fields of pattern recognition, function approximations, signal processing, and process simulation. ANN incorporates the non-mechanistic, non-equilibrium modeling for biomass gasification [17].

2.1 Equilibrium Model for Biomass Gasification

The equilibrium model is a useful tool for optimization of gasifier in terms of gasifier operating conditions. It can be applied to both moving as well as fluidized bed gasifiers. This approach of mathematical modeling is independent of the reactor type and not limited to a specified range of operating conditions. The equilibrium models are classified as stoichiometric and non-stoichiometric on the basis of algorithm used for Gibbs energy minimization. The stoichiometric model needs a defined reaction mechanism which incorporates all chemical reactions and the different species involved at gasification temperature. On the other hand, in non-stoichiometric approach, no need of a particular reaction mechanisms or species is involved during numerical simulation. It is based on the elemental composition obtained from ultimate analysis [18]. In non-stoichiometric equilibrium approach [19], the elemental composition is obtained using Gibbs energy minimization using numerical methods without specifying the possible reactions taking place. The stoichiometric equilibrium model is based on the species which are present in the largest amounts having the lowest value of free energy of formation.

The equilibrium models are developed on the basis of following assumptions [20]:

1. The process occurs at steady state. The reactor is implicitly considered to be zero dimensional.
2. The gasifier is isothermal at equilibrium condition.
3. Reaction rate is fast enough and residence time is sufficient to reach equilibrium condition.
4. Gases except H_2 , CO , CO_2 , and CH_4 , N_2 and H_2O are negligible.
5. Char contains only solid carbon.
6. Ash residue is negligible.
7. The product gas is at the gasifier temperature.
8. All the gases obey the ideal gas law.
9. Potential and kinetic energies are negligible.
10. Tars are not modeled.

The equilibrium model shows great disagreement under some circumstances due to presence of large number of assumptions. At relatively low gasification temperature, this model overestimates H_2 and CO yields and the underestimation of CO_2 , methane, tars, and chars [18].

Several authors have applied thermodynamic equilibrium approach (stoichiometric and non-stoichiometric models) for biomass gasification [21–27]. Zainal et al. [21] have modeled the biomass gasification process using stoichiometric thermodynamic equilibrium approach. They studied the effect of gasification temperature and the moisture content on the composition of the producer gas using different types of biomass materials. Similarly, Alderucci [22] has also studied biomass gasification with steam and CO_2 as gasification medium using the equilibrium model. Jarunghammachote and Dutta [23] developed the thermodynamic equilibrium model based on the equilibrium constant for predicting the composition of producer gas. To improve the results of the model, the authors have used the coefficients for correcting the equilibrium constant of the water–gas shift reaction and the methane reaction. The predicted results obtained from the modified model were found to match satisfactorily with the experimental results reported by Jayah et al. [24]. Schuster et al. [25] investigated biomass gasification using equilibrium model using steam as the gasifying agent in a fluidized bed gasifier. The study reported that the prediction of gas yield and LHV was in the range of the measured results; however, the CH_4 content in the product gas was overestimated though, it was not significantly influence the overall efficiency of the system. Li et al. [26] applied a non-stoichiometric equilibrium model (minimization of Gibbs free energy) to predict the fuel gas composition for a circulating fluidized bed coal gasifier. Jarunghammachote and Dutta [27] studied the non-stoichiometric equilibrium model for gasification in different types of bed. The study reported significant deviation from the experimental data, especially for the prediction of CO and CO_2 concentration. The author has modified the model to consider the effect of carbon conversion and observed the improved results closer to the experimental data. However, this model could not give results with high accuracy for the spouted-bed gasification process. The modified model predicted higher heating

values compared to experimental due of the overprediction of the CO content in the fuel gas.

Relative to stoichiometric equilibrium models, less number of papers have been published on application of non-stoichiometric models for biomass gasification. Different algorithms for Gibbs energy minimization have been applied by different researchers in these non-stoichiometric models. Most commonly used Gibbs energy minimization algorithms include STANJAN [28], RAND [29], CANTERRA, and SOLGASMIX [30].

We present below the summary of our research on gasification of biomass mixtures in a circulating fluidized bed gasifier using non-stoichiometric equilibrium model. Using this model, an attempt has been made to assess the principal characteristics of the producer gas, viz. yield of gas (per unit wt of biomass mixture), H_2 and CO content of the gas, and the LHV of the gas. For the simulations, FACT-SAGE software that employs the algorithm SOLGASMIX has been used. The equations of Gibbs free energy minimization and the solution algorithm in details are available in the original paper by Buljit et al. [31] and Eriksson [32], respectively. For the gasification of mixture of biomass (binary mixture of any two of the three biomasses viz. sawdust, bamboo dust and rice husk in three proportions in weight percent as 25–75%, 50–50% and 75–25%), four representative temperatures, viz. 700, 800, 900, and 1000 °C and three equivalence ratios, viz. 0.2, 0.3, and 0.4 are chosen for the simulations.

The result shows that net producer gas yield increases with equivalence ratio (ER) from 0.2 to 0.4. For the mixtures of rice husk and bamboo dust, the total gas yield is essentially independent of the mixture composition. However, when sawdust content increases in the mixture, the gas yield slightly increases due to the higher carbon content in sawdust compared in the biomass. Figure 1a, b describes the trends of net producer gas yield resulting from gasification of rice husk/sawdust (RH + SD) and bamboo dust/sawdust (BD + SD) mixture, respectively, for different gasification temperature and ER. For a specified gasification temperature, the H_2 content of the producer gas decreases with ER for all biomass mixtures. For ER = 0.2 and up to 900 °C, the H_2 content shows an increasing trend and thereafter decreases. No particular trend can be seen for hydrogen with constituents of the biomass mixture. Carbon monoxide content in the producer gas also decreases with ER at a specified temperature. For biomass mixtures comprising sawdust, the CO content increases with the proportion of sawdust in the mixture clearly due to higher carbon content of sawdust than rice husk and bamboo dust. For a given gasification temperature, the LHV reduces with increasing air ratio as the major combustible gases, viz. H_2 and CO decreases with ER, but the LHV increases with gasification temperature for a given ER. The LHV values for any combination of ER and gasification temperature are higher for biomass mixture containing sawdust than the corresponding rice husk/bamboo dust mixture. The net thermal energy content of producer gas is also higher for mixtures containing sawdust and varies directly with the proportion of the sawdust content in the mixture. Figure 2a, b describes the trends of lower heating values resulting from gasification of rice husk/sawdust (RH + SD) and bamboo dust/sawdust (BD + SD) mixture, respectively, for different ER and gasification temperature.

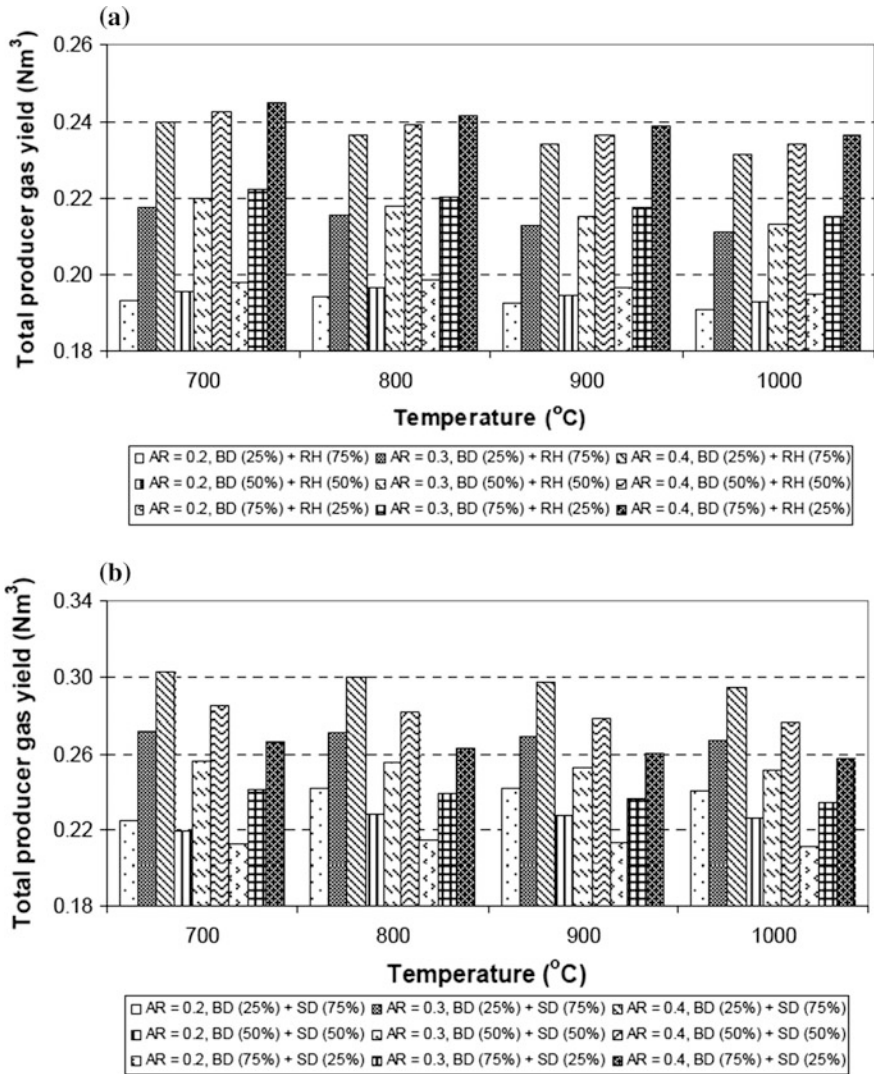


Fig. 1 Variation in total producer gas yield for **a** Rice husk (RH) and Sawdust (SD) **b** Bamboo dust (BD) and Sawdust (SD) mixture for different ER and gasification temperature using equilibrium method (adopted from Buragohain et al. [31])

2.2 Semi- or Quasi-Equilibrium Model for Biomass Gasification

The equilibrium models are useful tools for preliminary assessment of gasification characteristics of different biomass feedstocks. However, due to significant difference between actual operating conditions and the assumptions in the equilibrium

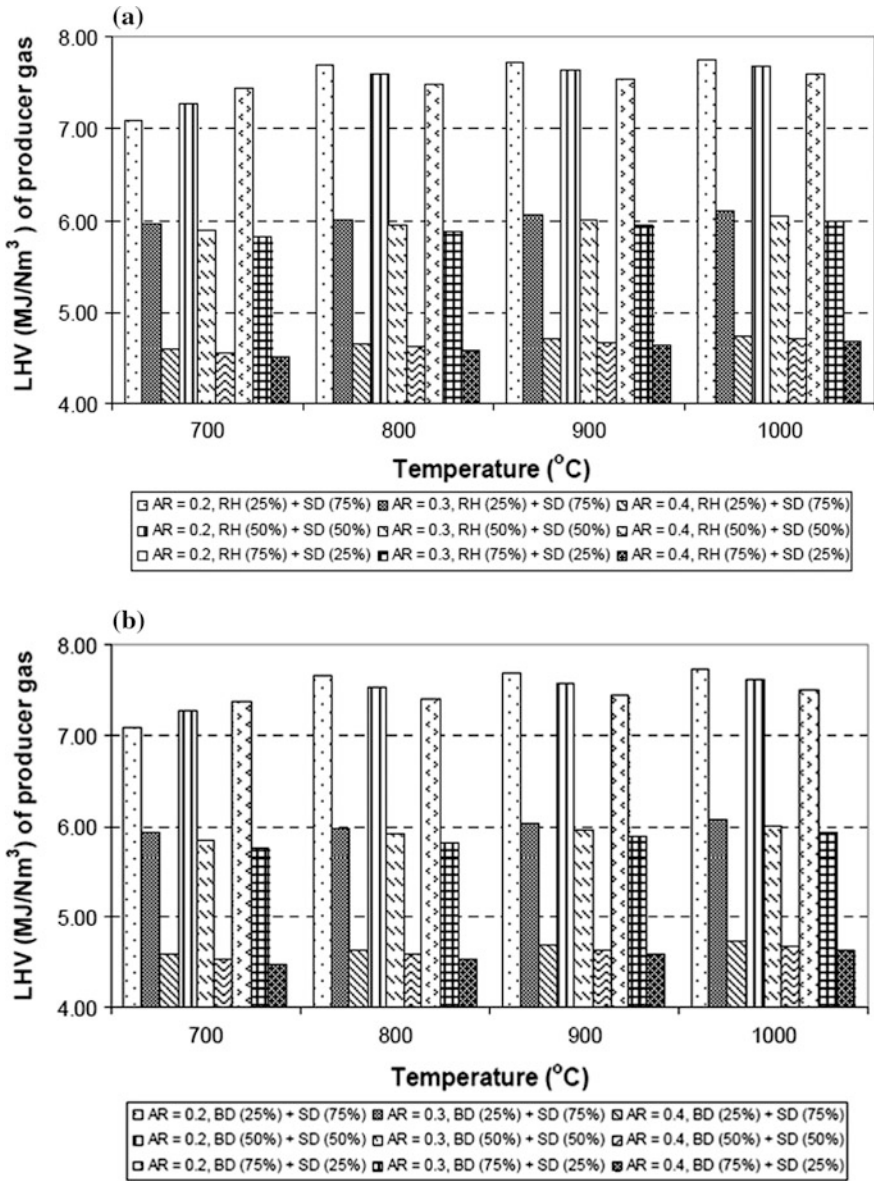


Fig. 2 Variation in LHV of producer gas for **a** Rice husk (RH) and Sawdust (SD) **b** Bamboo dust (BD) and Sawdust (SD) mixture for different ER and gasification temperature using equilibrium method (adopted from Buragohain et al. [31])

model, these models cannot predict quantitatively accurate results for all operating conditions. Major limitation of equilibrium model is that gasification reactions are mostly influenced by kinetics and mass transfer, and thus, some reactions

(especially with solid phase reactants) do not reach equilibrium condition [18]. As mentioned earlier, thermodynamic equilibrium models do not require any knowledge of the mechanisms of transformation. Furthermore, they are independent of the reactor and not limited to a specified range of operating conditions. The equilibrium model is valuable as they predict the thermodynamic limits of the gasification reaction system. Thus, in order to describe the behavior of gasifiers more accurately, modifications have been made to equilibrium models.

The semi- or quasi-equilibrium approach accounts for the deviation from the equilibrium reactions, and hence, has improved accuracy in predicting the producer gas composition [33]. In this approach, the equilibria of the reactions defined in the model are evaluated at a temperature, which is lower than actual process temperature. For fluidized bed gasifiers, the average bed temperature can be used as the process temperature, while for downdraft gasifiers, the outlet temperature at the throat exit should be used as the process temperature. Till now, few researchers have addressed the thermodynamic equilibrium approach for biomass gasification in air/steam fluidized bed gasification. Ngo et al. [34] have developed the quasi-equilibrium three-stage gasification model to investigate the effects of gasification temperature and steam fuel ratio on the producer gas composition, carbon conversion, char residue, gas yield, lower heating value, and H_2 to CO molar ratio, in a dual circulating fluidized bed gasifier. The model included three stages, viz. biomass pyrolysis, char–gas reaction, and gas-phase reaction, where empirical equations are involved to take into account the deviation from theoretical equilibrium reactions. The model was validated with the experimental data obtained for biomass steam gasification. The study reported that the producer gas compositions predicted by the model had a reasonable agreement with experimental data. The prediction accuracy of the quasi-equilibrium model would be improved, if tar formation and cracking in the pyrolysis stage were also considered. Bacon et al. [35] have reported quasi-equilibrium models for each independent chemical reaction. Kersten et al. [36] have developed quasi-equilibrium model for operating temperatures in the range 740–910 °C. The authors reported that the equilibrium of Boudouard reaction, water–gas shift reaction, and methane reaction should be evaluated at much lower temperatures for circulating fluidized bed gasifier. The author also reported that quasi-equilibrium approach appeared to be independent of process temperature in this temperature range. Kersten et al. [36] and Li et al. [18] have added empirical relations to their initial thermodynamic models to calculate the carbon conversion and the yield of CH_4 . The use of these correlations was limited only for the reactors developed by authors, and not for all reactors in general.

Our simulation results using quasi-equilibrium model are deviated from the results of equilibrium models discussed earlier. It was observed that the LHV and net yield of the producer gas (per unit biomass feed) reduced for semi-equilibrium model compared to equilibrium model. Hydrogen and carbon monoxide content of the fuel gas composition also reduced as compared to the equilibrium conditions. These two parameters, viz. H_2 and CO contents and LHV, showed direct variation with the extent of carbon conversion.

Similar studies have been reported by Melgar et al. [37]. The authors have observed that with the reduction in ER, the CO and CO₂ content in the product gas increases. Furthermore, Melgar et al. [36] have reported higher CH₄ content in product gas at relatively low ER and gasification temperature. Schuster et al. [38] have stated the leveling off of LHV of product gas at gasification temperatures beyond 800 °C. All of these findings in previous literature have agreed with simulations results of our study.

2.3 Kinetic Model for Biomass Gasification

The kinetic rate model describes the char reduction process using kinetic rate expressions obtained from experiments that permit better simulation of the experimental data for practical conditions in which the residence time of gas and biomass is relatively short. Another facet of this approach that makes it physically more realistic is that the kinetic reaction scheme is coupled to the hydrodynamics of the system. The major limitation of kinetic model is availability of reliable data and other parameters of the gasifier system. The first limitation of the kinetic modeling is availability of precise kinetic constants over a wide range of pressure and temperature. Second limitation is in terms of coupling of hydrodynamics of the gasifiers and kinetics of reaction scheme by identification and quantification of proper linkages between the two. These models involve various physical aspects of the gasification system, viz. gas–solid and solid–solid transport coefficients, velocities of various phases and residence time distribution. These features make the model system precise and more error-prone.

Modeling of the biomass gasification with conventional reaction kinetics approach is an arduous and complicated task due to large variation in composition, structure, reactivity, and physical reactivity of the chars, and very large number of chemical reactions that occur simultaneously. Therefore, kinetic models with “lumped” approach have been employed, in which conversion of biomass as a whole has been considered—instead of conversion of individual components of lignin, cellulose, or hemicellulose. The char gasification with the slowest kinetics is the controlling step in biomass gasification.

There are numeral approaches for modeling the complex pyrolysis process of biomass and the most common of them can be classified into two major categories viz. model fitting and model free. To investigate the kinetics of the decomposition process, thermogravimetric analysis (TGA) that uses Arrhenius rate expression is often used. In the model-fitting method, different models are fit to the experimental data and the model giving the best statistical fit is selected as the model from which the activation energy (E_a) and frequency factor (A) are evaluated. In model-free method, the degree of conversion for a reaction is assumed to be constant and therefore the reaction rate solely depends on the reaction temperature. Both approaches of kinetic analysis of biomass pyrolysis, viz. model-free approach (such as Kissinger method, Kissinger-Akahira-Sunose method, Flynn-Wall-Ozawa

method, Friedman method) and model-fitting approach (such as Distribution of Activation Energy Method, Coats-Redfern method) have limitations. Model-fitting methods are applied to extract a single set of Arrhenius parameters for an overall process and are not capable to show this type of complexity in the solid-state reactions. The most important limitation of this method is its inability to uniquely select appropriate reaction model. The model-free methods simply “postpone” the consideration of an appropriate conversion function until an estimate of the kinetic parameters (E_a and A) is calculated. Furthermore, iso-conversional or model-free methods are unsuitable for those reaction schemes containing competing reactions, where the net rate of reaction depends on changes in temperature.

Issues with the conventional methods of determining kinetic factors

Conventional techniques for determination of kinetic parameters use thermogravimetric analyzer (TGA) data for analysis. However, as noted previously, this approach has several limitations and issues. Due to these limitations, the values of the kinetic parameters of frequency factor (A) and activation energy (E_a) for gasification of similar biomasses reported by different authors show high inconsistency, with variation of several orders of magnitude. Recent papers by Li et al. [38] and Campbell et al. [39] have addressed these issues and have proposed new alternate approaches for the analysis of TGA data for accurate determination of kinetic parameters. Main limitations of the conventional TGA data analysis techniques, as reported by Li et al. [38] and Campbell et al. [39] are as follows:

- (i) TGA data may contain noise, which can get magnified in the differential approach of analyzing data. This problem can be obviated (to some extent) by use of integral methods for data analysis. The temperature integral does not have any analytical solution [40, 41] and needs to be solved numerically. The numerical methods have several approximations and truncations that introduce large errors in the results.
- (ii) Large number of chemical reactions occurs during pyrolysis of biomass—either in series or parallel. In this situation, the kinetic parameters of one reaction can get influenced by other reaction. In addition, heat and mass transfer effects (such as diffusion, heat transfer, adsorption, desorption) associated with the system in which pyrolysis is conducted also affect the kinetic parameters.
- (iii) The three kinetic parameters in the Arrhenius model (kinetic constant, activation energy, and frequency factor) are interrelated, and hence, should be determined simultaneously. Rigorous determination of these parameters requires exact knowledge of reaction mechanism, which may not be known in most cases. In view of this limitation, shortcut methods involving model-free approach determine only two parameters, viz. Arrhenius constant and activation energy, which is error-prone. The apparent activation energy of the overall pyrolysis process may vary with conversion and temperature.
- (iv) Fit TGA data to Arrhenius kinetics also has problems of kinetic compensation effect (KCE), in which error in value of one of the parameters in the

triplet (k , A , E_a) can be compensated by shift in another parameter. The kinetic compensation effect is manifested in terms of an isokinetic temperature, at which all reactions belonging to same “compensation set” have same kinetic rate constant [42]. The numerical errors in data processing lead to large discrepancies in kinetic data, as reported in literature [43, 44]. The overall result of these issues is that most of the TGA generated kinetic data is of empirical nature—without much physical meaning.

Campbell et al. [39] have proposed a quantitative method based on the parameter “optimization indicator” (Ω) for determining whether trends in activation energy versus char conversion are error derived (for single model reaction), or whether it is an artifact (for multi-model reactions). Errors in TGA data mostly occur due to deviation of actual experimental procedure from the standard (i.e., heating rates <10 °C/min, and sample mass <10 mg). Samples with large mass, large heating rates, low purge gas rate and thick sample result in thermal gradients during decomposition, self-cooling and mass transfer effects. The optimization indicator proposed by Campbell et al. helps in identification of unsuitable data for kinetic analysis. Campbell et al. [39] have demonstrated the use of Ω as indicator for TGA data containing non-kinetic influences related to experimental variables such as heat and mass transfer. Optimization indicator (Ω) can be used for eliminating suspect TGA data. Thus, use of Ω as an indicator for reconcilability and quality of gathered data is an efficient tool for determination of activation energy.

Numerous researchers have focused on kinetic models of biomass gasification: Wang and Kinoshita [45], Giltrap et al. [46], Chen [47], Jayah et al. [25], and Babu and Sheth [48]. Wang and Kinoshita [45] have proposed kinetic model based on the mechanism of surface reactions in the reduction zone assuming a given residence time and reaction temperature of gasifier. The model developed by Giltrap et al. [46] for the reduction zone of fixed bed gasifier predicted the composition of the producer gas under steady-state condition. The precision of the model is limited by the data availability in the initial conditions at the top of the reduction zone. The author did not consider the pyrolysis and cracking because the possible pyrolysis products, reactions, and intermediate products would make the model more complex. The model produced reasonable agreement with the experimental results for all components of the producer gas, however, this model over predicts the concentration of CH_4 . Chen [47] developed a kinetic model to estimate the length of the gasification zone and the diameter of the reactor and analyzed the dependence of the reactor’s performance on operating parameters, viz. moisture content, particle size, air temperature, and gasifier load. Chen’s model consisted of three different stages. The first stage estimates the air/fuel ratio required for a specific operating condition. First part of the model is used as input in the second stage, where the drying, pyrolysis, and combustion zones are all lumped together. The output from the lumped zone, which calculated the concentrations and temperatures, is then used as input in third part of the model that predicts temperature profile along gasification zone, gas composition, conversion efficiency, and the length of the gasification zone at any given time interval. An important limitation of Chen’s

model was overestimation of the temperature of gas emerging from “lumped” zone due to an unrealistic low estimation of heat loss and the omission of CO and H₂ in the pyrolysis gas. To overcome these deficiencies, Jayah et al. [25] introduced modifications to the reactor with a variable cross section rather than constant gasification zone diameter. Giltrap’s model [46] has been modified by Babu and Sheth [48] suggesting an exponentially varying char reactor factor (CRF) for better prediction of the temperature profile in the reduction reaction zone of gasifier. The model was simulated using a finite difference method to determine temperature and composition profiles in the reduction zone. The model predictions had good agreement with experimental data of Jayah et al. [25].

For simulation of biomass gasification in circulating fluidized bed in our study [49], the reaction scheme is integrated with volume as an independent variable with Runge–Kutta 4th order–5th order adaptive step size methods. The kinetic model comprised of scheme of 13 known chemical reactions (both homogeneous and heterogeneous) among various species resulting from pyrolysis of biomass. The kinetic constants for the reactions were obtained from literature and are depicted in Table 1. Three types of biomasses, viz. rice husk, bamboo dust and sawdust, were considered for simulations. For the kinetic model, 12 simulation sets for each biomass with permutation combination of three equivalence ratios, two gasification temperatures and two reaction volumes, viz. 0.0486 and 0.081 m³ is considered. Summary of simulations of biomass gasification using this kinetic model is given below.

Carbon monoxide and hydrogen produced during pyrolysis stage of gasification show sharp reduction with increasing ER. Nonetheless, H₂ and CO content of pyrolysis gas shows increasing trend with increasing pyrolysis temperature.

Extent of CO₂ content in pyrolysis gas was rather insensitive to gasification temperature. The CO₂ content of pyrolysis gas varied directly with the ER and inversely with the temperature of gasification. The tar content of the pyrolysis gas gradually reduced with increasing temperature. However, in the later stages of gasifier, tar content of the producer gas reduced rather slowly, due to slow kinetics of tar oxidation. In fact, the tar content of the producer gas remained nearly constant from pyrolysis zone till exit of the gasifier. Among the three biomasses used as feedstock, as compared to rice husk and bamboo dust, reduction in the weight fraction of sawdust char was higher. The degree of char gasification increased with ER and the fractional gasification of char reduced with temperature for a particular ER and gasification volume. The gas yield decreased with increasing ER for given gasifier volume and temperature and increased marginally with gasification temperature.

LHV of the producer gas was found to be increase with gasification temperature for given ER and reactor volume. However, it decreased with ER for a given gasification temperature and reactor volume. For a given air ratio and gasification temperature, the LHV decreased with increasing reactor volume. For ER = 0.3 and 0.4, the LHV of producer gas from rice husk was almost independent of gasification temperature and reactor volume. For ER = 0.2 and gasification temperature = 800 °C, the LHV of producer gas shows a drastic tenfold increase compared to the LHV at 700 °C for same ER. Figure 3a, b describes the trends in LHV of the producer

Table 1 Scheme of reactions in the kinetic model along with rate expressions [49]

Sr. no	Reaction	Rate expression (either kg/s or kmol/m ³ -s, as applicable)	Ref.
Heterogeneous reactions of char gasification			
1	$(1 + \beta_c) C + \left(1 + \frac{\beta_c}{2}\right) O_2 \rightarrow \beta_c CO + CO_2$ $C + 0.85O_2 \rightarrow 0.3CO + 0.7CO_2$	$r_1 = -\frac{dW}{dt} = 2.268 \times 10^7 \times \exp\left(\frac{-8559}{T}\right) W_p [O_2]$ (kg/s) ($\beta_c = 0.43$)	[50]
2	$C + H_2O \rightarrow CO + H_2$	$r_2 = -\frac{dW}{dt} = \frac{6692 \times \exp\left(\frac{-15516}{T}\right) \times W_p \times [H_2O]}{1 + 3.16 \times 10^{-2} \exp\left(\frac{5620}{T}\right) [H_2O] + 5.36 \times 10^{-3} \exp\left(\frac{2193}{T}\right) \times [H_2] + 8.25 \times 10^{-5} \exp\left(\frac{11359}{T}\right) [CO]}$ (kg/s)	[51]
3	$C + CO_2 \rightarrow 2CO$	$r_3 = -\frac{dW}{dt} = \frac{1.3692 \times 10^9 \left(\frac{-32235}{T}\right) \times W_p \times [CO_2]}{1 + 6.6 \times 10^{-2} [CO_2] + 0.12 \exp\left(\frac{3865}{T}\right) \times [CO]}$ (kg/s)	[51]
4	$C + 2H_2 \rightarrow CH_4$	$r_4 = -\frac{dW}{dt} = \frac{66.92 \times \exp\left(\frac{-15116}{T}\right) \times [H_2] \times W_p}{1 + 3.16 \times 10^{-2} \exp\left(\frac{5620}{T}\right) [H_2O] + 5.36 \times 10^{-3} \exp\left(\frac{2193}{T}\right) \times [H_2] + 8.25 \times 10^{-5} \exp\left(\frac{11359}{T}\right) [CO]}$ (kg/s)	[50]
Homogeneous reaction among gaseous species			
5	$CO + H_2O \rightleftharpoons CO_2 + H_2$	$r_5 = \frac{-d[CO]}{dt} = 2.78 \times 10^3 \times \exp\left(\frac{-1510.7}{T}\right) [CO][H_2O] - \frac{[CO_2][H_2]}{0.0265 \exp\left(\frac{2938.5}{T}\right)}$ (kmol/m ³ · s)	[52]
6	$CO + 0.5 O_2 \rightarrow CO_2$	$r_6 = \frac{-d[CO]}{dt} = 3.25 \times 10^{10} \exp\left(\frac{-15098}{T}\right) [CO][O_2]^{1/2} [H_2O]^{1/2}$ (kmol/m ³ · s)	[53]
7	$CH_4 + \frac{3}{2} O_2 \rightarrow CO + 2H_2O$	$r_7 = \frac{-d[CH_4]}{dt} = 5 \times 10^{11} \exp\left(\frac{-24157}{T}\right) [CH_4]^{0.7} [O_2]^{0.8}$ (kmol/m ³ · s)	[53]
8	$CH_4 + \frac{1}{2} O_2 \rightarrow CO + 2H_2$	$r_8 = \frac{-d[CH_4]}{dt} = 4.4 \times 10^{11} \exp\left(\frac{-15098}{T}\right) [CH_4]^{1/2} [O_2]^{5/4}$ (kmol/m ³ · s)	[54]
9	$CH_4 + H_2O \rightarrow CO + 3H_2$	$r_9 = \frac{-d[CH_4]}{dt} = 3 \times 10^8 \times \exp\left(\frac{-15098}{T}\right) [CH_4][H_2O]$ kmol/m ³ · s	[54]
10	$H_2 + \frac{1}{2} O_2 \rightarrow H_2O$	$r_{10} = \frac{-d[H_2]}{dt} = 5.183 \times 10^{13} T^{3/2} \exp\left(\frac{-3420}{T}\right) [H_2]^{3/2} [O_2]$	[54]
11	$C_2H_6 + \frac{5}{2} O_2 \rightarrow 2CO + 3H_2O$	$r_{11} = \frac{-d[O_2]}{dt} = 2.281 \times 10^{11} \exp\left(\frac{-20131}{T}\right) T^{0.5} [C_n H_m][O_2]$	[55]
12	$C_2H_4 + 3 O_2 \rightarrow 2CO_2 + 2H_2O$	$r_{12} = \frac{-d[C_2H_4]}{dt} = 4 \times 10^{11} \exp\left(\frac{-24200}{T}\right) [C_2H_4]^{0.7} [O_2]^{0.8}$	[56]
13	$CH_{0.85}O_{0.17} (Tar) + 0.68 O_2 \rightarrow 0.75 CO + 0.25 CO_2 + 0.28 H_2O$	$r_{13} = \frac{-d[Tar]}{dt} = 1.264 \times 10^{13} \exp\left(\frac{-24200}{T}\right) [Tar][O_2]$	[56]

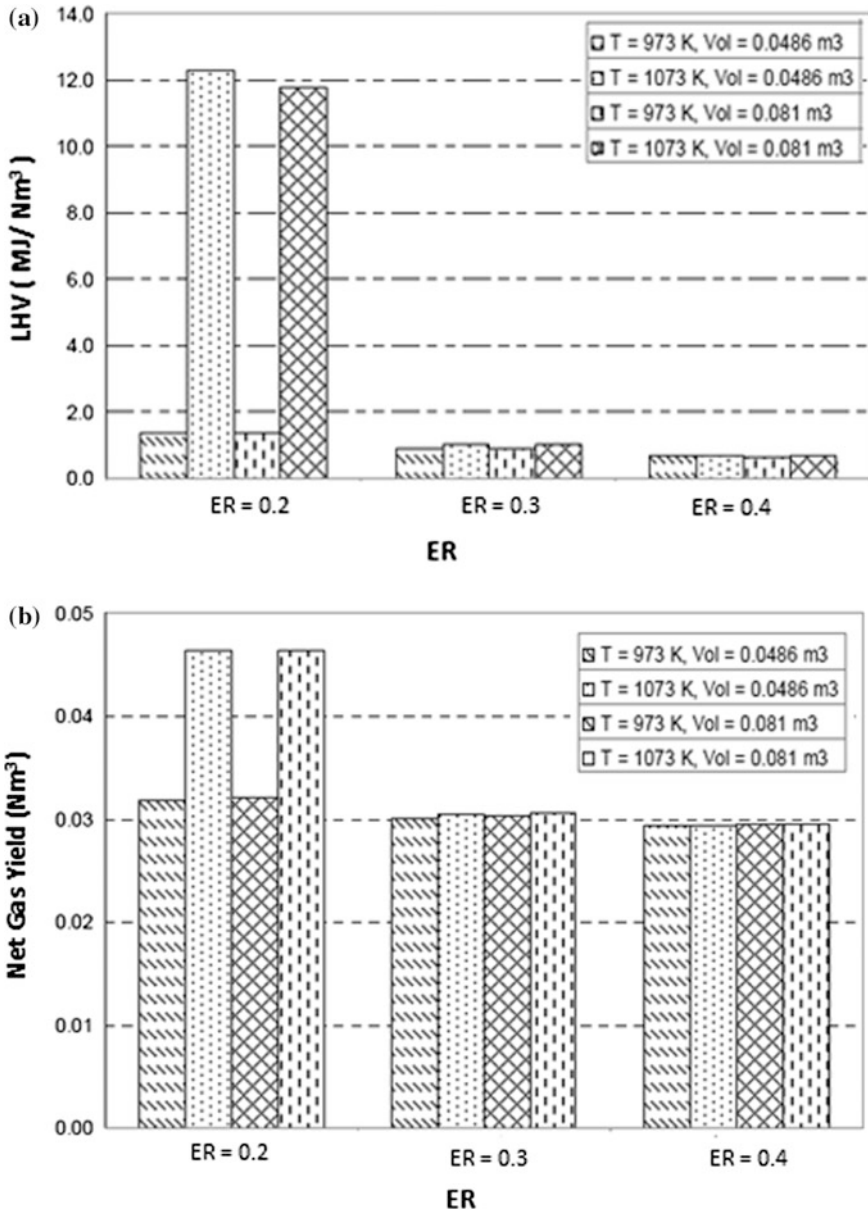


Fig. 3 Simulation results of biomass gasification with kinetic models: **a** Variation of LHV of the producer gas; **b** Net gas yield with ER for rice husk under different gasifying conditions (adopted from Buragohain et al. [49])

gas and net producer gas yield resulting from gasification of rice husk, respectively, calculated using kinetic model under different gasifying conditions. Comparing among rice husk and bamboo dust, higher gas yield is observed for sawdust obviously due higher carbon and least ash content. Higher LHV of producer gas for sawdust (than rice husk) under similar gasifying conditions is also attributed to higher carbon content of sawdust, which results in higher CO content of producer gas.

3 Conclusions

Several models have been developed for gasification of biomass, viz. kinetic, equilibrium, and artificial neural networks. The kinetic model predicts the progress and product composition at different positions along a reactor, whereas an equilibrium model predicts the maximum possible yield of a desired product from a reacting system. The equilibrium models are computationally less intensive compared to kinetic models. However; these models do not give quantitatively accurate results due to several assumptions that are not obeyed under practical conditions. The semi-equilibrium approach accounts for the deviation from the equilibrium conditions, and thus, improves the quantitative accuracy of the prediction of producer gas composition. The potential for power generation from gasifier can be estimated on the basis of yield and LHV of the producer gas achieved from gasification of biomass (either individual or mixture). In this chapter, an attempt has been made to present a comparison of equilibrium, semi-equilibrium and kinetic models for biomass gasification. The equilibrium and semi-equilibrium models predicted the characteristics of the producer gas that is insensitive to gasification temperature, whereas the kinetic model revealed greater sensitivity of producer gas characteristics toward gasification temperature at low equivalence ratios. As a whole, a relative analysis of the equilibrium, semi-equilibrium and kinetic models has highlighted the potential of these models to represent biomass gasification process. This chapter could be a useful source of information for design and optimization of large-scale biomass gasifiers using biomass (individual)/biomass mixtures as feedstocks.

References

1. Escobar J, Lora E, Venturini O, Yanez E, Castillo E, Almazan O (2009) Biofuels: environment, technology and food security. *Renew Sustain Energy Rev* 13:1275–1287
2. Demirbas A (2008) Biofuels sources, biofuel policy, biofuel economy and global biofuel projections. *Energy Convers Manag* 49:2106–2116
3. Saxena R, Adhikari D, Goyal H (2009) Biomass-based energy fuel through biochemical routes: a review. *Renew Sustain Energy Rev* 13:167–178

4. Maniatis K, Guiu G, Riesgo J (2002) The European commission perspective in biomass and waste thermochemical conversion. In: Bridgwater AV (ed) *Pyrolysis and gasification of biomass and waste, Proceedings of an Expert Meeting*, pp 1–18
5. Biomass Atlas of India (2017) Combustion gasification and propulsion laboratory. Indian Institute of Science, Bangalore. <http://cgpl.iisc.ernet.in>. Accessed 20 May 2017
6. Gumz W (1950) *Gas producers and blast furnaces: theory and methods of calculations*. Wiley
7. Desrosiers R (1981) Thermodynamics of gas-char reactions. In: Reed TB (ed) *Biomass gasification—principles and technology*. Noyes Data Corporation
8. Sharma AK (2008) Equilibrium and kinetic modelling of char reduction reactions in a downdraft biomass gasifier: a comparison. *Sol Energy* 52:918–928
9. Nemtsov DA, Zabaniotou A (2008) Mathematical modeling and simulation approaches of agricultural residues air gasification in a bubbling fluidized bed reactor. *Chem Eng J* 143:10–31
10. Barker RE (1983) ASPEN modeling of the tri-state indirect-liquefaction process. Oak Ridge National Laboratory, Oak Ridge, USA
11. Kundsens RA, Bailey T, Fabiano LA (1982) Experience with ASPEN while simulating a new methanol plant. *AIChE SympSer* 78:214
12. Phillips JN, Erbes MR, Eustis RH (1986) Study of the off-design performance of integrated coal gasification. In: *Combined cycle power plants, computer aided engineering of energy systems, vol 2. analysis and simulation, Proceedings of the winter annual meeting of the American Society of Mechanical Engineers*
13. Yan HM, Rudolph V (2000) Modeling a compartmented fluidized bed coal gasifier process using ASPEN PLUS. *Chem Eng Commun* 183:1–38
14. Douglas PL, Young BE (1990) Modelling and simulation of an AFBC steam heating plant using ASPEN/SP. *Fuel* 70:145–154
15. Backham L, Croiset E, Douglas PL (2003) Simulation of a coal hydrogasification process with integrated CO₂ capture. *Combust Can* 3A(4)
16. Lee HG, Chung KM, Kim C, Han SH, Kim HT (1992) Coal gasification simulation using ASPEN PLUS. In: *US–Korea joint workshop on coal utilization technology*, pp 447–474
17. Brown D, Fuchino T, Marechal F (2006) Solid fuel decomposition modelling for the design of biomass gasification systems. In: Marquardt W, Pantelides C (eds) *Proceedings of the 16th European symposium on computer aided process engineering and 9th international symposium on process systems engineering*, pp 1661–1666
18. Li XT, Grace JR, Lim CJ, Watkinson AP, Chen HP, Kim JR (2004) Biomass gasification in a circulating fluidized bed. *Biomass Bioenergy* 26:171–193
19. Mathieu P, Dubuisson R (2002) Performance analysis of a biomass gasifier. *Energy Convers Manag* 43:1291–1299
20. Loha C, Gu S, Wilde JD, Mahanta P, Chatterjee PK (2014) Advances in mathematical modeling of fluidized bed gasification. *Renew Sustain Energy Rev* 40:688–715
21. Zainal ZA, Ali R, Lean CH, Seetharamu KN (2001) Prediction of performance of a downdraft gasifier using equilibrium modeling for different biomass materials. *Energy Convers Manag* 42(12):1499–1515
22. Alderucci V (1994) Thermodynamic analysis of SOFC fueled by biomass derived gas. *Int J Hydrogen Energy* 19(4):369–376
23. Jarungthammachote S, Dutta A (2007) Thermodynamic equilibrium model and second law analysis of a downdraft waste gasifier. *Energy* 32:1660–1669
24. Jayah TH, Aye L, Fuller RJ, Stewart DF (2003) Computer simulation of a downdraft wood gasifier for tea drying. *Biomass Bioenergy* 25:459–469
25. Schuster G, Löffler G, Weigl K, Hofbauer H (2001) Biomass steam gasification: an extensive parametric modeling study. *Bioresour Technol* 77:71–79
26. Li X, Grace JR, Watkinson AP, Lim CJ, Ergudenler A (2001) Equilibrium modeling of gasification: a free energy minimization approach and its application to circulating fluidized bed coal gasifier. *Fuel* 80:195–207

27. Jarungthammachote S, Dutta A (2008) Equilibrium modeling of gasification: Gibbs free energy minimisation approach and its application to spouted bed and spout-fluid bed gasifiers. *Energy Convers Manag* 49:1345–1356
28. Reynolds WC (1986) The element potential method for chemical equilibrium analysis: implementation in the interactive program STANJAN. Technical Report, Stanford University, Stanford, USA, p 48
29. Smith WR, Missen RW (1982) Chemical reaction equilibrium analysis: theory and algorithms. Wiley, New York
30. Eriksson G (1975) Thermodynamic studies of high temperature equilibria—XII: SOLGAS-MIX, a computer program for calculation of equilibrium composition in multiphase systems. *Chem Scr* 8:100–103
31. Buragohain B, Mahanta P, Moholkar VS (2011) Investigations in gasification of biomass mixtures using thermodynamic equilibrium and semi-equilibrium models. *Int J Energy Environ* 2(3):551–578
32. Eriksson G (1975) Thermodynamic studies of high temperature equilibria—XII: SOLGAS-MIX, a computer program for calculation of equilibrium composition in multiphase systems. *Chem Scr* 8:100–103
33. Gómez-Barea A, Leckner B (2013) Estimation of gas composition and char conversion in a fluidized bed biomass gasifier. *Fuel* 107:419–431
34. Ngo SI, Nguyen TDB, Lim Y, Song BH, Lee UD, Choi YT, Song JH (2011) Performance evaluation for dual circulating fluidized-bed steam gasifier of biomass using quasi-equilibrium three-stage gasification model. *Appl Energy* 88:5208–5220
35. Bacon DW, Downie J, Hsu JC, Peters J (1982) Modeling of fluidized bed wood gasifiers. In: Overend RP, Milne TA, Mudge LK (ed) *Fundamentals of thermochemical biomass conversion*. Elsevier, London, pp 717–732
36. Kersten SRA, Prins W, Van der Drift A, Van Swaaij WPM (2002) Interpretation of biomass gasification by “quasi”-equilibrium models. In: *Proceedings of the twelfth European conference on biomass for energy, industry and climate protection*, Amsterdam, Netherland
37. Melgar A, Perez JF, Laget H, Horillo A (2007) Thermochemical equilibrium modeling of a gasifying process. *Energy Convers Manag* 48:59–67
38. Li X, Grace JR, Bi X, Campbell JS (2016) A new pyrolysis model based on generalized extreme value (GEV) distributions and its application to lignocellulosic biomass. *Fuel* 184:211–221
39. Campbell JS, Grace JR, Lim CJ, Mochulski DW (2016) A new diagnostic when determining the activation energy by the advanced iso-conversional method. *Thermochim Acta* 636:85–93
40. Lyon RE (1997) An integral method of non-isothermal kinetic analysis. *Thermochim Acta* 297:117–124
41. Tang W, Liu Y, Zhang H, Wang C (2003) New approximate formula for Arrhenius temperature integral. *Thermochim Acta* 408:39–43
42. Galwey AK, Brown ME (1997) Arrhenius parameters and compensation behaviour in solid-state decompositions. *Thermochim Acta* 300:107–115
43. Brown ME, Maciejewski M, Vyazovkin S, Nomen R, Sempere J, Burnham A, Opfermann J, Strey R, Anderson HL, Kemmler A, Keuleers R, Janssens J, Desseyn HO, Li CR, Tang B, Roduit B, Malek J, Mitsuhashi T (2000) Computational aspects of kinetic analysis: Part A: the ICTAC kinetics project—data, methods and results. *Thermochim Acta* 355:125–143
44. Galwey AK (2003) Eradicating erroneous Arrhenius arithmetic. *Thermochim Acta* 399:1–29
45. Wang Y, Kinoshita CM (1993) Kinetic model of biomass gasification. *Sol Energy* 51(1):19–25
46. Giltrap DL, McKibbin R, Barnes GRG (2003) A steady state model of gas-char reactions in a downdraft gasifier. *Sol Energy* 74:85–91
47. Chen JS (1987) Kinetic engineering modelling of co-current moving bed gasification reactors for carbonaceous material. Dissertation, Cornell University, New York
48. Babu BV, Sheth PN (2006) Modeling and simulation of reduction zone of downdraft biomass gasifier: effect of char reactivity factor. *Energy Convers Manag* 47(15–16):2602–2611

49. Buragohain B, Chakma S, Kumar P, Mahanta P, Moholkar VS (2013) Comparative evaluation of kinetic, equilibrium and semi-equilibrium models for biomass gasification. *IJEE* 4(4):581–614
50. Liu H, Gibbs BM (2003) Modeling NH_3 and HCN emissions from biomass circulating fluidized bed gasifiers. *Fuel* 82:1591–1604
51. Luo CH, Aoki K, Uemiya S, Kojima T (1998) Numerical modeling of a jetting fluidized bed gasifier and the comparison with the experimental data. *Fuel Process Technol* 55(3):193–218
52. Biba V, Macak J, Klose E, Malecha J (1978) Mathematical model for the gasification of coal under pressure. *Ind Eng Chem Process Des Dev* 17:92–98
53. Jensen A, Johnsson JE, Andreies J, Laughli K, Read G, Mayer M, Baaumann H, Bonn B (1995) Formation and reduction of NO_x in pressurized fluidized bed combustion of coal. *Fuel* 74(11):1555–1569
54. Jones WP, Lindstedt RP (1988) Global reaction schemes for hydrocarbon combustion. *Combust Flame* 73:233–249
55. Zimont VL, Trushin YM (1969) Total combustion kinetics of hydrocarbon fuels. *Combust Explos Shock Waves* 5(4):391–394
56. Corella J, Sanz A (2005) Modeling circulating fluidized bed biomass gasifiers. A pseudo-rigorous model for stationary state. *Fuel Process Technol* 86(9):1021–1053

Numerical Modelling of Fluidized Bed Gasification: An Overview

Saurabh Gupta, Sminu Bhaskaran and Santanu De

Abstract An overview of the computational fluid dynamics (CFD) modelling techniques used to study multiphase reacting flow in fluidized bed reactors is presented in this chapter. Research in fluidized bed gasifiers has gained momentum in recent years due to their various industrial applications. Experimental investigation of such intricate process requires sophisticated and expensive measuring techniques. Moreover, it is very difficult to capture essential process details of these systems by available experimental methods. On the other hand, numerical simulation offers a viable approach to experimental investigations. The numerical simulations not only offer a better insight into the complex gas–solid flow dynamics, but it also carries paramount importance in the design and optimization of fluidized bed systems. The present chapter primarily focuses on the CFD modelling fundamentals and their application pertaining to fluidized bed reactors. Detailed description of gas–solid flow modelling and chemical reaction kinetics is given separately.

Keywords Fluidized bed gasification • Discrete element method
Multiphase particle-in-cell method • Two-fluid model • Particle-laden flows

Nomenclature

ε	Volume fraction
ρ	Density (kg/m^{-3})
u	Velocity (ms^{-1})
P	Pressure (Pa)
R	Universal gas constant ($\text{Jkmol}^{-1}\text{K}^{-1}$)

S. Gupta • S. Bhaskaran • S. De (✉)
Department of Mechanical Engineering,
Indian Institute of Technology Kanpur, Kanpur, India
e-mail: santanu80@gmail.com

S. Gupta
e-mail: sgamubesu@gmail.com

S. Bhaskaran
e-mail: sminub@gmail.com

T	Temperature (K)
Y	Mass fraction
τ	Stress tensor (Pa)
μ	Viscosity ($\text{kgm}^{-1}\text{s}^{-1}$)
g	Acceleration due to gravity (ms^{-2})
Re	Reynolds number
d/D	Diameter (m)
C_D	Drag coefficient
θ_s	Granular temperature (ms^{-2})
e	Coefficient of normal restitution
λ	Bulk viscosity ($\text{kgm}^{-1}\text{s}^{-1}$)
H	Enthalpy (J)
h	Heat transfer coefficient ($\text{W/m}^2\text{K}$)
Nu	Nusselt number
Pr	Prandtl number
A	Area (m^2)
m/M	Mass (kg)
F	Force (N)
Γ	Torque (N-m)
V	Volume (m^3)
c_p	Specific heat at constant pressure ($\text{m}^2/\text{s}^2\text{K}$)
c_v	Specific heat at constant volume ($\text{m}^2/\text{s}^2\text{K}$)
ς	Thermal conductivity ($\text{Wm}^{-2}\text{K}^{-1}$)
k	Reaction rate constant
M_w	Molecular weight
t	Time (s)

Subscripts

g	Gas phase
s/p	Solid/particle phase
l	Laminar
t	Turbulent
i	ith species

1 Introduction

Fluidized bed gasification is a complex physical process which involves particle-laden flow with chemical reactions, heat transfer and mass transfer processes occurring simultaneously. Gasification in fluidized bed reactors is a focus of research since last few decades as it offers high degree of solid mixing along with several other advantages. Although developments in fluidized bed gasification

technology are being pursued since many years, there is lack of complete understanding of such a complicated process. Primarily, laboratory-scale models and pilot-scale plants are built to study the essential aspects of the process before realization of the industrial plants. Due to highly complex nature of the process, scale-up operation of the reactor is not straightforward and relies on empirical data input.

Of late, computational fluid dynamics (CFD) has emerged as an alternative to understand the aspects of fluidized bed gasification which are not possible to examine with experiments such as local flow patterns, temperature and species distributions in the reactor. Numerical simulations can be very useful in the optimization and modification of the reactor design. Numerical models aided with empirical data are invoked in the governing equations of the multiphase reacting flow to model different processes taking place within the reactor. Empirical sub-models provide closure to the macro-scale simulations and predict particle-particle interactions (collisions), gas-particle interactions (drag), chemical kinetics, small-scale turbulence and turbulence-chemistry interactions. These sub-models are developed for individual processes in particular operating conditions and extended to gasification systems where these processes interfere with each other. The bottleneck of numerical simulations is the correct implementation of these numerical models in order to obtain trustworthy results. However, as of now CFD codes for multiphase reacting flows are not matured adequately so that they can be confidently utilized for design and optimization. Apparently, it is not possible that a single simulation method can account for all length and timescales. Therefore, a multi-scale approach is more suited where large-scale processes are resolved and the effect of small scales is modelled.

Gas-solid flows can be modelled by two approaches: Eulerian-Eulerian (EE) approach, where both phases are treated as continuum and typically governed by a Navier-Stokes-type equation and the Eulerian-Lagrangian (EL) approach, where the solid phase is represented by discrete particles and their motion is computed by solving Newton's second law of motion. Eulerian-Lagrangian-based direct numerical simulation method can resolve all scales ranging from micrometres to several metres but is limited to only small-scale systems owing to their very high computational cost. The present modelling of gas-solid flow is limited to EE-based two-fluid model (TFM) and EL-based models, discrete element method (DEM), multiphase particle-in-cell (MP-PIC) method. TFM employs a continuum description for both the solid and gas phase and uses empirical correlations to model the gas-solid interactions. Main advantage of this approach is its affordable computational cost, whereas disadvantage is that the detailed realistic information of particle-particle and particle-gas interactions cannot be obtained. On the other hand, EL-based models identify discrete character of the particles and can provide critical information of flow physics. Main drawback of these methods is that they become computationally expensive with high particle loading; hence, their application is restricted to the fundamental research of flow physics in small-scale systems. Chemical reaction sub-models of gasification and associated processes

such as drying, pyrolysis and combustion are invoked in the governing equations of gas–solid flow to account for gasification process in fluidized bed reactors.

Large number of reactions occurs in the gasification system, and it is not possible to calculate all the reactions simultaneously so a reduced reaction mechanism is adopted which includes only major conversion reactions. A comprehensive numerical model of fluidized bed gasification process is built which is based on the description of the dynamic behaviour of multiphase flow, heat and mass transfer, and chemical kinetics. Consequently, it is an extremely challenging task to make such CFD model which can generate reliable results. This chapter aims to provide a review of the various CFD modelling approaches applied to solid fuel gasification in fluidized bed reactor.

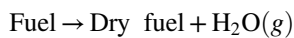
The remainder of the chapter is organized as follows. In Sect. 2, modelling of chemical kinetics of various processes of gasification, such as drying, devolatilization, char conversion and homogeneous reactions, is discussed. Fluid dynamics modelling pertaining to fluidized bed reactors is presented in Sect. 3 covering the Eulerian–Eulerian approach-based two-fluid model and Eulerian–Lagrangian approach-based models, namely discrete element method and multi-phase particle-in-cell method. Applications of gas–particle reaction modelling for the fluidized bed gasification systems are also summarized. In these two sections, the mathematical formulation used for gas–particle flow and chemical reactions and their coupling is explained. Finally, conclusions along with future directions are summarized in Sect. 4.

2 Gasification Kinetics Modelling

Gasification of solid fuels consists of four processes, drying, devolatilization, combustion and gasification. Drying occurs between temperatures 100–150 °C where moisture contained in the fuel converts into vapour. In devolatilization or pyrolysis, dry solid fuel transforms into char, volatile gases and tar. The subsequent gasification process includes chemical reactions among volatile gases, gasification agent and char at high temperatures. Chemical reaction sub-models of gasification process are integrated with fluid dynamics and heat transfer equations to construct an inclusive model to carry out CFD simulations.

2.1 Drying

Drying is the evaporation of the fuel moisture from the raw fuel.



In the literature, drying process is usually modelled in two ways. In the first approach, drying is modelled as a chemical reaction and its rate is determined by Arrhenius expression [1, 2]:

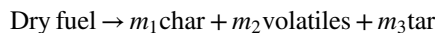
$$\text{Moisture} \rightarrow^k \text{Steam}$$

$$k = A e^{\left(-\frac{E}{RT}\right)} (1 - \varepsilon_g) \rho_s X \quad (1)$$

Here, k is the reaction rate constant which is a function of activation energy (E), pre-exponential factor (A), mass fraction of solid species (X) and absolute temperature (T). In the second approach, drying can be assumed to occur instantaneously at the feeding location and moisture in gaseous form is directly added to the other fuel components; therefore, no explicit model for drying is used. Gerber et al. [3] added 10% moisture by weight in gaseous form with the remaining fuel at the inlet entering at the temperature of 150 °C. Drying may also be modelled as an isothermal evaporation process, and it may be described by a lumped method at the evaporation temperature with the following rate expression [4]: $\dot{r}_{evap, H_2O} = \frac{(T - T_{evap}) m c_p}{\Delta H_{evap} \delta t}$, where T_{evap} , δt and ΔH_{evap} are the evaporation temperature, the time step used and heat of vapourization, respectively.

2.2 Devolatilization

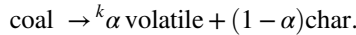
After all the moisture content present in the fuel particle evaporates, devolatilization process takes place. Devolatilization or pyrolysis is a complex thermo-chemical process which includes several reactions accompanied by heat and mass transfer. During this stage, the solid fuel particle undergoes thermal decomposition without oxidation. There are three main components produced during pyrolysis of carbonaceous fuels: volatile gases (H_2 , CO , CO_2 , H_2O , CH_4 , etc.), tar and remaining solid residue, char, i.e. fixed carbon and ash.



where m is the mass fraction and sum of mass fractions of all product species is unity. In the most simplified model of pyrolysis, it is regarded that drying and devolatilization occur instantaneously at the feeding location and devolatilization products enter the reactor [5]. The volatile matter constitutes several species but an empirical formula may be formed on the basis of proximate and ultimate analysis which is used to determine stoichiometric coefficient for pyrolysis products [6]. Ash refers to the inorganic residue which is considered as an inert compound. Tar contains heavier molecular gaseous species and is condensable below a certain value of temperature and concentration. On the other side, tar can undergo cracking when the reactor is maintained at a sufficiently high temperature. It can be further

cracked into light gasses in presence of catalysts such as dolomite/olivine. Tar conversion process is not very well understood for the numerical model development [7].

In general, kinetic models of biomass pyrolysis process can be grouped into two main categories: single-step reaction and multi-step reactions. Single-step devolatilization model is based on empirical models which correlate the volatile release rate to volatile matter yield and particle temperature. The simplest model for pyrolysis is based on the global reaction rate [8], where it is assumed that the pyrolysis rate is proportional to the amount of volatile matter left in the particle:

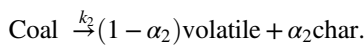
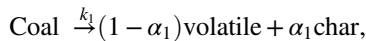


Here, α is mass stoichiometric coefficient. First-order reaction rate may be used:

$$\frac{dm}{dt} = k(m_\infty - m). \quad (2)$$

In the above expression, m and m_∞ are time dependent volatile mass and total volatile yield at $t = \infty$, respectively. Arrhenius reaction rate expression is used to determine the reaction rate constant, $k = A e^{(-E_i/RT)}$. Major drawback of this model is that the final volatile matter yield (m_∞) is considered as constant which may not be true in case of actual process.

Two-step parallel reaction model estimates that the kinetics constants such as activation energy and pre-exponential factor are not constant for entire temperature range in the reactor. Therefore, two-step model includes two parallel reactions occurring into two different temperature ranges contrary to single-step models, which consider constant value of the kinetic parameters in the whole temperature range. Multi-step kinetic mechanisms with distributed activation energies are able to describe competitive reactions occurring during the devolatilization process. An empirical model based on two competing overall reactions is proposed by Kobayashi [9]:



Rate constants are given by Arrhenius expression, $k_i = A_i e^{(-E_i/RT)}$. Total volatile yield can be found out by the following expression [9]:

$$\int_0^t (\alpha_1 k_1 + \alpha_2 k_2) e^{\int_0^t (\alpha_1 + \alpha_2) dt}. \quad (3)$$

It is assumed that devolatilization takes place only in the dense zone, and volatile distribution is uniform along the reactor. While modelling tar, it is a common practice to assume pyrolysis products free of tar [10]. In some studies, tar is

represented by some aromatic hydrocarbon (C_6H_6 , etc.) [11, 12] or it is considered as an inert heavy cyclic hydrocarbon [4] which does not take part in reaction. Gerber et al. [3] divided pyrolysis into two different steps: primary pyrolysis and secondary pyrolysis. Primary pyrolysis is related to the thermal degradation of feedstock into char, volatile gases and primary reactive tar which was modelled by single-step lumped model. The thermal cracking of primary tar is called as secondary pyrolysis which produced an inert tar along with other gaseous components. This process was represented by a first-order kinetic model [13], $r_{cracking} \rightarrow \vartheta_i 10^{4.98} e^{-\left(\frac{93}{RT}\right)} \rho_{tar}$, where ρ_{tar} is the density of the tar in the gas stream and ϑ_i is the stoichiometric coefficients of secondary pyrolysis products.

Pitt [14] introduced the concept of multi-step kinetic modelling and assumed the occurrence of a large number of independent, first-order parallel reactions during the pyrolysis process with the same pre-exponential factor and different activation energies. Variation in activation energies is characterized by a continuous distribution function (distributed activation energy model). More complex multi-step reaction mechanism has been proposed recently by Sommariva et al. [15], where they modelled coal as an aromatic cluster connected by bridges, side chains and functional groups on peripheral positions. Using three different grades of reference coal for characterization of the devolatilization process, Sommariva et al. [15] approximated the coal model as a linear combination of the thermal degradation of the reference coals. Their pyrolysis kinetic model with 30 reactions predicted the thermal degradation of different coals in a wide range of operating conditions. Other mathematical models have been published describing the pyrolysis of a coal particle [16, 17].

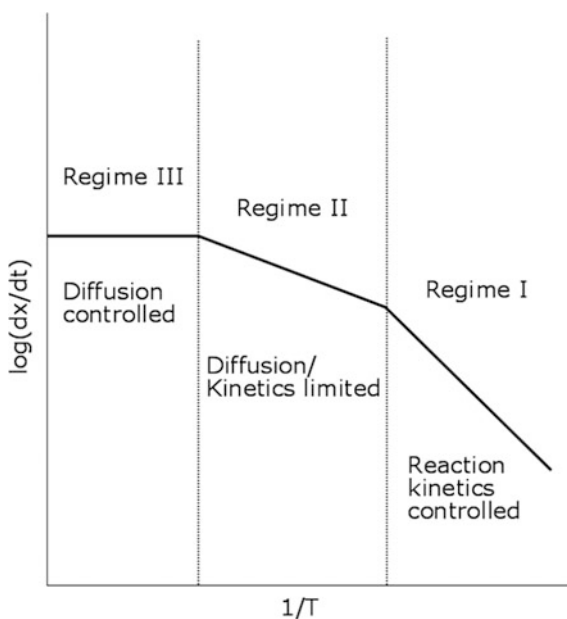
Above-mentioned first-order and two-step kinetic models are empirical; therefore, they are limited in their use to a particular coal and operating conditions. Comprehensive network type models are most advanced mathematical models which can predict volatile release rate and the species composition during pyrolysis process for a wide range of operating conditions and coal ranks. These models use a statistical network approach to explain the macro-molecular chemical structure of the parent coal and its devolatilization action. Coal is considered as a matrix of aromatic clusters connected by bridges. Pyrolysis is assumed to be depolymerization process in which large molecular structure breaks into smaller fragments and these fragments are later subjected to other conversion processes. Statistical network models like FG-DVC, FLASHCHAIN, chemical percolation devolatilization (CPD) model are the most popular ones. These models include network modelling, coal structure characterization, depolymerization reactions, cross-linking reactions and formation of non-condensable gas, tar and char. More information about these models may be found in Refs. [18–20]. Due to their complexities, network models are not implemented in the CFD codes directly but are useful to generate the input data for yields and kinetic rates in devolatilization CFD sub-models [21].

2.3 Char Conversion

Char is the residue remained after devolatilization process. Char converts into different gaseous components at temperature above than 700 °C, and an inert product ash remains after complete conversion of char. Char conversion is an intricate process which involves diffusion of gases such as O₂, CO₂, H₂O, H₂ from surrounding atmosphere to the outer surface and into the porous interior of char particle. Gasification model contains a set of reactions of char and its intermediate products which can be endothermic and exothermic in nature. Reactivity of char can be divided into three regimes based on the temperature range as shown in Fig. 1 [22]. At high operating temperature, reaction rate is much higher than the bulk diffusion rate; thus, char conversion rate is mainly controlled by bulk diffusion (Regime III). In moderate temperature range, when the diffusion rate becomes comparative to the chemical reaction rate, both the reaction kinetics and the diffusion rate determine the char conversion rate (Regime II). In Regime I, which occurs at low temperatures, reaction kinetics is the rate determining step.

Primarily, char conversion models can be divided into surface-based and intrinsic models. In surface-based models, reaction is assumed to occur at the surface of the particle whereas in intrinsic type models, the reaction takes place on pore surfaces within the particle interior. In most of the numerical studies, a simplified approach is adopted in which the heterogeneous reactions take place at the reacting char particle surface. ‘One-film’ and ‘two-film’ models serve as the most basic strategies to model heterogeneous reactions taking place at the surface of a

Fig. 1 Temperature dependency of reaction rate



chemically reacting char particle [23]. In both models, char particle is assumed to be impermeable to gas-phase species. The ‘one-film’ model assumes that the char oxidation reaction takes place at the particle surface and produces CO and CO₂. This model is extended to gasification reactions, where the flame location is assumed to be located at the particle surface. Char and volatile reactions supposedly occur at the particle surface with formation of H₂O, CO and CO₂ as main products. Carbon dioxide oxidizes carbon at a slower rate than oxygen. When oxygen is depleted at the surface, carbon dioxide acts as the carbon conversion agent. The ‘two-film’ model assumes that a deoxidization reaction, $C + CO_2 \rightarrow 2CO$, occurs at the particle surface. Carbon monoxide diffuses outward and reacts with oxygen to form carbon dioxide at the ‘flame sheet,’ $CO + \frac{1}{2}O_2 \rightarrow CO_2$. This reaction is assumed to be infinitely fast so both CO and O₂ concentrations become zero at the flame sheet. Therefore, two gas films are recognized: one at the particle surface and the other at the detached flame sheet. In gasification reaction model, when flame is not located at the particle surface, the volatile matter and product of surface reactions react at the flame sheet. Time rate of change of mass of carbonaceous particle is modelled [24] by the homogeneous model, $\frac{dm}{dt} = -km$, where the kinetic constant, k , is a function of particle surface temperature and determined from Arrhenius reaction rate expressions. In most of the cases, surface temperature is not known and it is obtained by solving energy equation of the particles. Gerber et al. [4] modelled char particle decomposition during wood gasification process as:

$$\frac{dm_{char}}{dt} = -(k_{H_2O} + k_{O_2} + k_{CO_2})m_{char} + k_{char}m_{wood}.$$

Here, the first and second terms on the r.h.s. are due to consumption and production of char, respectively. The general char reaction model, kinetic diffusion limited rate (KD) model [25], considers combined effect of char kinetics and diffusion limited rates. It uses kinetics-controlled equation at low particle temperature while diffusion-controlled equation at higher particle temperature. So, heterogeneous reactions between char and gases (O₂, H₂O, CO₂) can be characterized by a global reaction scheme based on the reaction kinetics and the diffusion rate and this model is applied to calculate heterogeneous reaction rate constant (k):

$$k = \frac{6V_c P_i \epsilon_s}{d_p} \left[\frac{1}{k_a} + \frac{1}{k_d} \right]^{-1}. \quad (4)$$

Here, V_c is the volume of the char, P is the partial pressure of the i th reactant species and d_p is the granular diameter. Diffusion rate (k_d) can be defined as, $k_d = \frac{Sh D_{gs} M_{w,c}}{RT_s d_p}$. Sherwood number (Sh) is a function of Reynolds and Schmidt number, $Sh = 2 + 6Re^{1/2} Pr^{1/3}$. D_{gs} is the mass diffusion coefficient, $D_{gs} = \frac{8.34 \times 10^{-6} T^{1.75}}{P}$. The kinetic rate constant (k_a) is calculated from the Arrhenius

expression. Combining diffusion and kinetic rate, char conversion rate can be expressed as [26],

$$\frac{dm_{C-i}}{dt} = -A_p P_i \left[\frac{1}{k_a} + \frac{1}{k_d} \right]^{-1}.$$

Here, m_{C-i} is the mass of char remained in the particle during reaction of char with gasifying species i , and A_p is the particle surface area.

Surface-based models consider grains as non-porous and do not take care of internal char properties. The random pore model proposed by Bhatia and Perlmutter [27] considers the effect of char particle porosity distribution and surface area in kinetics–diffusion-controlled reaction systems. Their model provides more realistic picture and good agreement with experimental data especially for high-rank coals. Intrinsic models primarily assume that char combustion takes place in internal pores of particle. Char burnout kinetic (CBK) model [28, 29] is regarded as the most comprehensive model which is applicable for a wide range of coal. It comprises different sub-models which account for morphological changes in char structure. These sub-models are invoked in diffusion and reaction rate constants. Carbon burnout kinetics–gasification (CBK/G) model [30] was developed mainly for gasification process and predicts the gasification rate, particle temperature, variation in particle diameter, density at a gas temperature and partial pressures of the oxidizing agents. CBK/G includes a combined oxidation/gasification mechanism involving the three surface reactions for char oxidation used in carbon burnout kinetics–extended model (CBK/E) plus four reactions for gasification by CO_2 , H_2O , CO and H_2 . This model is specifically designed for char burnout prediction and fly ash carbon content.

Various gasification reaction mechanisms are used by researchers in the literature, and the following global heterogeneous reactions are considered as important among them.

$\text{C} + \text{O}_2 \rightarrow \text{CO}_2$	R1
$\text{C} + \text{CO}_2 \rightarrow 2\text{CO}$	R2
$\text{C} + \text{H}_2\text{O} \rightarrow \text{CO} + \text{H}_2$	R3
$\text{C} + 2\text{H}_2 \rightarrow \text{CH}_4$	R4
$\text{C} + 0.5\text{O}_2 \rightarrow \text{CO}$	R5

R1 is the oxidation reaction which is exothermic and faster than other reactions. Boudouard (R2) and water–gas (R3) reactions are endothermic in nature, whereas methanation (hydrogasification) reaction (R4) is the slowest one and exothermic. R5 is a combustion reaction which occurs in oxygen deficient environment.

These reactions may be arranged based on their rate constants:

$$k_{\text{C} + \text{O}_2} \gg k_{\text{C} + \text{H}_2\text{O}} > k_{\text{C} + \text{CO}_2} \gg k_{\text{C} + \text{H}_2}.$$

Reactive fuel particle shrinks as the char–gas chemistry consumes solid fuel. Without considering the effect of particle size reduction on the trajectory followed by particle on its way out of the reactor, char entrainment will not be accurately predicted [31]. Shrinking is modelled by the unexposed-core model/shrinking core model and the exposed-core model/ash-segregated model [32]. In shrinking core model, it is assumed that reactions take place at the particle surface surrounded by ash. Reactant gases diffuse through the surrounding layer of product gases and inert ash in order to reach the core. In the exposed-core model or ash-segregated model, it is assumed that ash dissociates from the particle surface as soon as it forms. Therefore, particle surface is always exposed to the surrounding gas environment. Exposed-core model is largely used in CFD modelling due to its simplicity [33]. In order to incorporate shrinking of the solid particles, an expression relating radius of solid particle to mass of the particle keeping particle density constant is used by Bruchmüller et al. [34], $R = \left(\frac{3m_p}{4\pi\rho_p}\right)^{1/3}$. In constant shrinkage model, it is assumed that the particle shrinks up to some portion of the original particle volume during pyrolysis and gasification until it gets out of the reactor irrespective of heating rate [4].

2.4 Homogeneous Reactions

During devolatilization, light gases such as CO₂, H₂O, H₂, CO, light hydrocarbons (C_aH_b) and other hydrocarbons (C_aH_bO_c) further react with oxygen or peruse their own reaction mechanisms. The released volatile gases react with oxidizing/gasifying agent or with each other. These reactions are termed as homogeneous reactions. A detailed reaction mechanism for homogeneous gasification reactions does not exist. Furthermore, a comprehensive chemical mechanism will require solving large number of species transport equations which is computationally expensive. Therefore, a reduced reaction mechanism is often considered which includes only important chemical reactions. Conservation equations of species mass fractions are given by a common form,

$$\frac{\partial}{\partial t}(\rho_g \epsilon_g Y_{g,i}) + \nabla(\rho_g \epsilon_g u_g Y_{g,i}) = -\nabla(\epsilon_g J_{g,i}) + (\epsilon_g R_{g,i}) + R_{s,i}, \quad (5)$$

where $J_{g,i}$, $R_{g,i}$, $R_{s,i}$ are the diffusion flux, the net rate of production of i th homogeneous species and the heterogeneous reaction rate, respectively. Gas-phase properties are obtained from the computed mass fractions of the gaseous species. Homogeneous reactions do not alter the net mass or enthalpy content of gas mixture. Turbulence influences heat and mass transfer rates in the reactor significantly. Rate of homogeneous reaction is determined by combined effect of turbulent mixing and chemical reaction. The overall rate can be computed by only mixing rate or by combination of two methods. As an example, finite-rate/ eddy-dissipation

model calculates both the Arrhenius and eddy-dissipation reaction rates. The minimum of these two rates is taken as the net reaction rate [11]:

$$k_{hom} = \min(k_{Ar}, k_{EBU}),$$

where k_{hom} is homogeneous reaction rate constant, k_{Ar} is Arrhenius reaction rate constant and k_{EBU} is the turbulent mixing rate calculated by eddy break-up model:

$$k_{EBU} = A \frac{\varepsilon}{K} \min\left(\frac{Y_{R,i}}{S_{R,i}}, B \frac{Y_{P,j}}{S_{P,j}}\right).$$

Here, Y is the mass fraction, S is the stoichiometric coefficient of reactants/products, k is the turbulent kinetic energy and ε is the rate of dissipation of turbulent kinetic energy. Also, A and B are the model constants.

Primarily, the following homogeneous reactions are considered as important besides several other reactions:

$\text{CO} + \frac{1}{\varphi} \text{O}_2 \rightarrow \left(\frac{2}{\varphi} - 1\right) \text{CO}_2 + 2\left(\frac{1}{\varphi} - 1\right) \text{CO},$	R6
$\text{H}_2 + \frac{1}{2} \text{O}_2 \rightarrow \text{H}_2\text{O},$	R7
$\text{CH}_4 + \text{H}_2\text{O} \rightarrow 3\text{H}_2 + \text{CO},$	R8
$\text{CO} + \text{H}_2\text{O} \rightarrow \text{CO}_2 + \text{H}_2.$	R9

Reactions R8 and R9 are the methane steam reforming reaction and water–gas shift reaction, respectively. Information about kinetic expressions and other reactions is available in Ref. [11, 35–37].

The gas phase is a multi-component mixture, which includes O_2 , CO_2 , CO , H_2 , H_2O , CH_4 , N_2 . Diffusion flux $J_{g,i}$ in the species transport equation is calculated using Fick's law,

$$J_{g,i} = -\left(\rho_g D_{m,i} + \frac{\mu_t}{Sc_t}\right) \nabla Y_{g,i}.$$

Here, Sc_t is the turbulent Schmidt number and $D_{m,i}$ is the diffusion coefficient for the i th species in the mixture.

3 Modelling of Particulate Flow in Fluidized Beds

Numerical simulations of the fluidized bed reactors are based on two approaches: Eulerian–Eulerian (EE) and Eulerian–Lagrangian (EL) approaches. In direct numerical simulation (DNS), governing equations are numerically solved without using any model. Flow in the fluidized bed reactors is usually turbulent in nature; therefore, in DNS one has to resolve all scales of turbulence on the computational

mesh, ranging from the smallest scale of dissipation, i.e. the Kolmogorov length scale up to the largest scale, i.e. the integral length scale. Therefore, the computational cost of DNS is very high. In an attempt to simulate a full-scale fluidized bed model, the computational resources required by DNS would exceed the capacity of the most powerful computers available recently. Numerical simulations of gas–solid flows in fluidized bed reactors are mainly limited to multi-scale methods, namely two-fluid model (TFM), discrete particle method (CFD-DPM) and multiphase particle-in-cell (MP-PIC) approach, where the former is an EE method and the last two methods are based on EL approach. In both EE and EL approaches, gas phase is treated as a continuum. In EE method, particles are also treated as continuum whereas in EL method, particles are recognized within the Lagrangian framework. Due to the continuum assumption of the particles in TFM, additional closure models are required to account for the particle–particle collisions and particle–gas interactions. Eulerian modelling offers a reasonable choice for computational modelling of real-scale fluidized bed systems since it is able to handle relatively large-scale systems with sufficient accuracy. Discrete element method does not require any closure laws as they calculate motion of each individual particle having different shapes/sizes by solving the Newton’s equation of motion on the particle scale. The detailed information such as particle trajectory and transient forces acting on individual particle can be attained. However, owing to the computational constraints, total number of particles that can be managed by this method is significantly lower compared to that encountered in actual fluidized bed reactors. Eulerian–Lagrangian-based MP-PIC approach uses a stochastic particle method to model the solid phase. It uses a concept of parcels which contain set of particles with same properties such as size, velocities, position, temperature, species mass fractions and density. Unlike CFD-DEM model which calculates collision force by direct particle contact, MP-PIC method models collision forces acting on particles as a spatial gradient. With the help of stochastic parcels, a large commercial system containing billions of particles can be simulated.

3.1 Two-Fluid Model (TFM)

EE approach is affordable from computational cost viewpoint yet effective method to model gas–solid flow. Main advantage of TFM is that it can characterize two-phase flow at relatively large scales, i.e. pilot or industrial scale, even though simultaneously retains the physics at smaller scale. In this model, both the gas phase and the solid phase are described as fully interpenetrating continuous fluids. A concept of phase volume fraction is introduced which is a continuous function of space and time. Volume of gaseous phase cannot be occupied by solid phase, and the sum of both phase volume fractions is unity. Both phases are governed by set of generalized Navier–Stokes equations. Chemical reaction kinetics is grid resolved, and reactions rates are computed for single particle properties such as particle diameter, density, temperature in a cell.

The mass conservation equation for gas and solid phases is given by,

$$\frac{\partial}{\partial t} (\varepsilon_g \rho_g) + \nabla \cdot (\varepsilon_g \rho_g \mathbf{u}_g) = \dot{S}_{gs}, \quad (6)$$

$$\frac{\partial}{\partial t} (\varepsilon_s \rho_s) + \nabla \cdot (\varepsilon_s \rho_s \mathbf{u}_s) = \dot{S}_{sg}. \quad (7)$$

Here, ε_g represents volume fraction of gaseous phase. \dot{S} is the rate of change of mass due to heterogeneous reactions pertaining to interphase mass transfer; $\dot{S}_{gs} = -\dot{S}_{sg} = \sum_j \sum_i M_{w,i} \gamma_i R_{i,j}$ where $M_{w,i}$, γ_i , $R_{i,j}$ are molecular weight of the i th species, stoichiometric coefficient and reaction rate, respectively. Due to interphase mass transfer, additional source terms are added into appropriate momentum and energy equations also. Density of the gas phase ρ_g is obtained from equation of state by assuming it as a mixture of ideal gases, $\rho_g = \frac{P_g}{RT} \left(\sum_{i=1}^n \frac{Y_i}{M_{w,i}} \right)^{-1}$.

Gas and solid phase momentum equations are expressed by similar expressions as,

$$\frac{\partial}{\partial t} (\varepsilon_g \rho_g \mathbf{u}_g) + \nabla \cdot (\varepsilon_g \rho_g \mathbf{u}_g \mathbf{u}_g) = -\varepsilon_g \nabla P_g + \nabla \cdot (\varepsilon_g \boldsymbol{\tau}_g) + f_{gs} + \varepsilon_g \rho_g \mathbf{g} + \dot{S}_{gs} \mathbf{u}_s, \quad (8)$$

$$\frac{\partial}{\partial t} (\varepsilon_s \rho_s \mathbf{u}_s) + \nabla \cdot (\varepsilon_s \rho_s \mathbf{u}_s \mathbf{u}_s) = -\varepsilon_s \nabla P_s + \nabla \cdot (\varepsilon_s \boldsymbol{\tau}_s) + f_{sg} + \varepsilon_s \rho_s \mathbf{g} + \dot{S}_{sg} \mathbf{u}_s. \quad (9)$$

The gas and solid phase stress tensors, $\boldsymbol{\tau}_g$, $\boldsymbol{\tau}_s$, are given by,

$$\boldsymbol{\tau}_g = - \left(\lambda_g - \frac{2}{3} \mu_g \right) (\nabla \cdot \mathbf{u}_g) \mathbf{I} - \mu_g \left((\nabla \mathbf{u}_g) + (\nabla \mathbf{u}_g)^T \right), \quad (10)$$

$$\boldsymbol{\tau}_s = \left\{ -P_s + \left(\lambda_s - \frac{2}{3} \mu_s \right) (\nabla \cdot \mathbf{u}_s) \right\} \mathbf{I} + \mu_s \{ (\nabla \mathbf{u}_s) + (\nabla \mathbf{u}_s)^T \}. \quad (11)$$

The bulk viscosity λ_g is usually set to zero for gases, and the dynamic viscosity of gas phase is expressed as the sum of laminar and turbulent viscosities, $\mu_g = \mu_{g,l} + \mu_{g,t}$. The gas-phase turbulent viscosity, $\mu_{g,t}$, is determined from the turbulence model. In Reynolds-averaged Navier–Stokes (RANS) equations approach, $k-\varepsilon$ turbulent model is often used to calculate turbulent stresses. In $k-\varepsilon$ model, gas-phase turbulent viscosity $\mu_{g,t}$ is obtained in terms of turbulent kinetic energy, k , and its dissipation rate ε ; $\mu_{g,t} = \rho_g C_\mu \frac{k^2}{\varepsilon}$. Additional transport equations for k and ε are solved. More details about this model are available in Ref. [38]. Large eddy simulation (LES) resolves the large eddies within the flow field and models the small eddies by using a sub-grid scale model (SGS). This model is more accurate than RANS and computationally cheaper than DNS. In LES, the sub-grid scale viscosity ($\mu_{g,t}$) is modelled by Smagorinsky model [39],

$\mu_{g,t} = \rho_g (C_t \Delta)^2 \sqrt{S} S$ where, C_t is the sub-grid scale eddy coefficient, S is the strain tensor and $\Delta = (\Delta x \Delta y \Delta z)^{1/3}$ is used as the length scale.

Last term in momentum equations of both the phases represents the momentum transfer due to interphase mass exchange. Drag term (f) which evolves due to gas–solid phase interactions can be represented as $f_{sg} = \beta(u_g - u_s) = -f_{gs}$. Drag becomes zero if slip velocity ($u_g - u_s$) between gas and solid velocity is non-existent. Three models are widely used for interphase momentum transfer coefficient (β).

Syamlal et al. model [40]:

$$\beta = \frac{3}{4} C_D \left(\frac{Re_s}{u_{r,s}} \right) |u_s - u_g| \frac{\varepsilon_s \varepsilon_g \rho_g}{u_{r,s}^2 d_s} \quad , \quad C_D = \left(0.63 + \frac{4.8}{\sqrt{Re_s / u_{r,s}}} \right)^2, \quad (12)$$

Gidaspow model [41]:

$$\beta = \left\{ \begin{array}{ll} 150 \frac{(1-\varepsilon_g)^2}{\varepsilon_g} \frac{\mu_g}{d_s^2} + \frac{1.75 \rho_g |u_s - u_g| (1-\varepsilon_g)}{d_s}, & \varepsilon_g < 0.8 \\ \frac{3}{4} C_D \frac{\rho_g |u_s - u_g| \varepsilon_g (1-\varepsilon_g)}{\varepsilon_g^{2.65}}, & \varepsilon_g \geq 0.8 \end{array} \right\}, \quad (13)$$

$$C_D = \left\{ \begin{array}{ll} 24 \left(\frac{1 + 0.15 (\varepsilon_g Re_s)^{0.687}}{Re_s \varepsilon_g} \right) & \text{if } Re_s < 1000 \\ 0.44 & \text{if } Re_s \geq 1000 \end{array} \right. \quad (14)$$

$$\text{Where, } Re_s = \frac{\rho_g |u_s - u_g| d_s}{\mu_g}$$

Energy-minimization multi-scale (EMMS) model [42]:

$$\beta = \left\{ \begin{array}{ll} 150 \frac{(1-\varepsilon_g)^2}{\varepsilon_g} \frac{\mu_g}{d_s^2} + \frac{1.75 \rho_g |u_s - u_g| (1-\varepsilon_g)}{d_s}, & \varepsilon_g < 0.74 \\ \frac{3}{4} C_D \frac{\rho_g |u_s - u_g| \varepsilon_g (1-\varepsilon_g)}{d_s} \omega, & \varepsilon_g \geq 0.74 \end{array} \right\}, \text{ where} \quad (15)$$

$$\omega = \left\{ \begin{array}{ll} -0.5760 + \frac{0.0214}{4(\varepsilon_g - 0.7463)^2 + 0.0044}, & 0.74 \leq \varepsilon_g \leq 0.82 \\ -0.0101 + \frac{0.0038}{4(\varepsilon_g - 0.7789)^2 + 0.0040}, & 0.82 \leq \varepsilon_g \leq 0.97 \\ -31.8295 + 32.8295 \varepsilon_g, & \varepsilon_g > 0.97 \end{array} \right\}. \quad (16)$$

Appropriate closures relations provided by the kinetic theory of granular flow are used to model effective solid phase pressure P_s , effective solid phase shear viscosity μ_s and bulk viscosity λ_s . These models are discussed in the next section.

3.2 Kinetic Theory of Granular Flow

In the EE approach, the solid phase is regarded as a continuum. Kinetic theory of granular flow is employed to model the properties of solid phase such as shear viscosity, bulk viscosity, solid pressure. Instantaneous particle velocity U_s can be divided into a mean velocity component u_s and a fluctuating component u'_s . The mean velocity component is computed by solving momentum transport equation of solid particles, and fluctuation velocity is modelled by means of kinetic theory of granular flow (KTGF) [43]. The local and instantaneous fluctuations are accounted for Brownian motion of granular particles. KTGF is analogous to kinetic theory of dense gases [44] and associates the fluctuating velocity to a pseudo-granular temperature of particles, $\frac{3}{2}\theta_s = \frac{1}{2}\langle u'_s u'_s \rangle$, where $u'_s = U_s - u_s$.

Stresses are generated due to the interaction between gas-solid particles, solid-solid particle and solid particles-wall. Granular temperature for solid phase which is equivalent to the thermodynamic temperature is calculated by solving a transport equation of kinetic energy of the solid fluctuations:

$$\frac{3}{2} \left[\frac{\partial}{\partial t} (\epsilon_s \rho_s \theta_s) + \nabla \cdot (\epsilon_s \rho_s \theta_s u_s) \right] = \left(-\nabla P_s \bar{\bar{I}} + \bar{\bar{\tau}}_s \right) : \nabla u_s + \nabla \cdot (\kappa_s \nabla \theta_s) - \gamma_s + \varphi_s + D_{gs}. \quad (17)$$

First term on the r.h.s. accounts for production of fluctuation energy which includes solid pressure and shear stress tensor. I is a unit tensor. The second term on the r.h.s. is the diffusion of energy fluctuations due to temperature gradient, γ_s is the dissipation of fluctuating energy due to collisions, φ_s is the exchange of fluctuating energy between the phases and D_{gs} is the rate of energy dissipation due to transfer of gas phase fluctuations to the particle phase fluctuations.

Different approaches are available in the literature for modelling of the diffusion coefficient, κ_s [40, 41, 45]. Expressions suggested by Syamlal et al. [40] and Gidaspow [41] are widely used. The diffusion coefficient proposed by Gidaspow [41] is

$$\kappa_s = \frac{150 d_s \rho_s \sqrt{\pi \theta_s}}{384 (1+e) g_0} \left[1 + \frac{6}{5} (1+e) \epsilon_s g_0 \right] + 2 \rho_s \epsilon_s^2 d_s (1+e) g_0 \sqrt{\frac{\theta_s}{\pi}}, \quad (18)$$

whereas Syamlal et al. [40] proposed:

$$\kappa_s = \frac{15 d_s \rho_s \epsilon_s \sqrt{\pi \theta_s}}{4(41-33\eta)} \left[1 + \frac{12}{5} \eta^2 (4\eta-3) \epsilon_s g_0 + \frac{16}{15\pi} (41-33\eta) \eta \epsilon_s g_0 \right], \quad (19)$$

where, $\eta = \frac{1}{2}(1+e)$.

The dissipation of fluctuating energy due to collisions is modelled as [45]:

$$\gamma_s = \frac{12(1 - e^2)g_0}{d_s\sqrt{\pi}}\rho_s\varepsilon_s^2\theta_s^{3/2}. \tag{20}$$

Once the granular temperature is known, the solid pressure P_s , solid shear viscosity μ_s and the solid bulk viscosity λ_s may be obtained. The solid bulk viscosity λ_s , which is a measure of viscous effect due to compression and expansion of voids, is modelled as follows [41]:

$$\lambda_s = \frac{4}{3}\varepsilon_s^2\rho_s d_s g_0(1 - e)\left(\frac{\theta_s}{\pi}\right)^{1/2}. \tag{21}$$

The KTGF expresses the solid’s shear and bulk viscosity, the pressure in terms of the solid’s volume fraction ε_s , the coefficient of normal restitution for particle collision and the granular temperature θ_s . The solid pressure represents the normal force due to particle interactions and is derived by Gidaspow [43] as:

$$P_s = (1 + 2(1 + e)\varepsilon_s g_0)\rho_s \varepsilon_s \theta_s. \tag{22}$$

g_0 , the radial distribution function, yields the probability of collisions; the equation given by Bagnold [46] is mostly used:

$$g_0 = \frac{3}{5}\left[1 - \left(\frac{\varepsilon_s}{\varepsilon_{s,max}}\right)^{1/3}\right]^{-1}. \tag{23}$$

Here, $\varepsilon_{s,max}$ is the maximum solid volume fraction for a random packing. Equation of solid shear viscosity derived by Gidaspow (32) is given as:

$$\mu_s = \frac{4}{5}\varepsilon_s\rho_s d_s g_0(1 + e)\sqrt{\frac{\theta_s}{\pi}} + \frac{10\rho_s d_s \sqrt{\pi\theta_s}}{96(1 + e)\varepsilon_s g_0}\left[1 + \frac{4}{5}g_0\varepsilon_s(1 + e)\right]^2. \tag{24}$$

A frictional component of viscosity can also be included to account for the viscous-plastic transition that occurs when particles of a solid phase reach the maximum solid volume fraction. If the frictional viscosity is included in the calculation, expression derived by Schaeffer et al. [47] can be used,

$$\mu_{s,fr} = \frac{P_s \sin\varphi}{2\sqrt{I_{2D}}}, \tag{25}$$

where φ is the angle of internal friction and I_{2D} is the second invariant of the deviatoric stress tensor. More details on KTGF can be found out in [43].

Energy equation for both gaseous and solid phases individually is solved to take care of heat transfer between phases, viscous dissipation and work done due to compression or expansion of gases and radiative heat transfer.

$$\frac{\partial}{\partial t} (\varepsilon_g \rho_g H_g) + \nabla (\varepsilon_g \rho_g \vec{u}_g H_g) = \frac{d(\varepsilon_g P_g)}{dt} + \vec{T}_g : \nabla \varepsilon_g \vec{u}_g - \nabla (\varepsilon_g q_g) + S_{gs} H_s + Q_{gs} + S_{gr}, \quad (26)$$

$$\frac{\partial}{\partial t} (\varepsilon_s \rho_s H_s) + \nabla (\varepsilon_s \rho_s \vec{u}_s H_s) = \frac{d(\varepsilon_s P_s)}{dt} + \vec{T}_s : \nabla \varepsilon_s \vec{u}_s - \nabla (\varepsilon_s q_s) + S_{sg} H_s - Q_{gs} + S_{sr}. \quad (27)$$

First term on the right-hand side is the work term due to volume fraction change, second term is the viscous dissipation and third term is the heat flux. $S_{gs} H_s$ and $S_{sg} H_s$ account for enthalpy exchange between two phases due to heterogeneous reactions. The heat exchange between two phases can be expressed as $Q_{gs} = h_{gs} (T_g - T_s)$, where the heat transfer coefficient between the gas and solid phase is $h_{gs} = \frac{Nu_s \varepsilon_g A_s}{d_s}$. Nusselt number is obtained using an empirical correlation for granular flows [48]:

$$Nu = \left(7 - 10\varepsilon_g + 5\varepsilon_g^2\right) \left(1 + 0.7Re_s^{0.2} Pr^{\frac{1}{3}}\right) + \left(1.33 - 2.4\varepsilon_g + 1.2\varepsilon_g^2\right) Re_s^{0.7} Pr^{\frac{1}{3}}. \quad (28)$$

The above expression is applicable for the range of void fraction $0.35 \leq \varepsilon_g \leq 0.65$ and Reynolds number up to 10^5 . Here, Pr is the Prandtl number of the gas phase. Heat transfer due to radiation needs to be included in the energy equation due to high-temperature operation of the fluidized bed systems. In sparse particle regions such as in circulating fluidized beds, the radiative heat transfer can contribute to substantial fraction of the overall heat transfer coefficient. Although when particle loading in the reactor is very high, such as bubbling fluidized beds, the radiative heat transfer can be neglected compared to other modes of heat transfer [49]. P-1 model and Rosseland model are computationally cheaper and are mostly employed in the modelling of combustion and gasification systems. Discrete ordinates model and discrete transfer radiation model are certainly more efficient models but rarely used due to their high computational expense. More details on these models can be found in Ref. [50].

Eulerian–Eulerian model has been utilized to study various aspects of fluidized bed gasification on pilot and laboratory scales. Flow characteristics at high pressure and temperature in a spout fluidized bed coal gasifier have been investigated using TFM [51, 52]. Yu et al. [11] developed a 2D model based on TFM coupled with chemical reaction kinetics to study the bubbling fluidized bed coal gasification. Using a chemical mechanism consisting 15 species and 11 elementary reactions, they found that the gas composition at exit agreed reasonably well with the experimental data for Colombia coal. Wang et al. [10] extended TFM coupled with

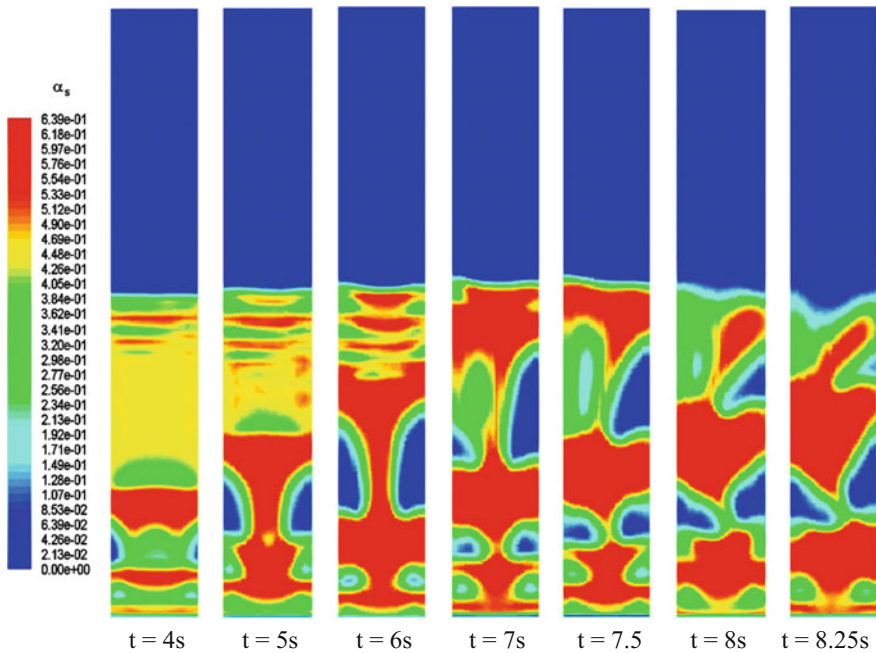


Fig. 2 Time evolution of particle concentrations (Reprinted from [10], with permission from Elsevier)

reaction kinetics to three-dimensional numerical simulations of coal gasification in a fluidized bed gasifier (Fig. 2). The exit gas compositions are found to be consistent with those obtained from experiments. Effects of different parameters on gas–solid flow patterns, profiles of gas velocities, particle velocities and gas composition have been examined, which are otherwise not possible to obtain experimentally.

Effects of limestone calcination on the hydrodynamic behaviour, temperature and reaction distributions in a bubbling bed coal gasifier have been examined using numerical simulations [12]. The numerical predictions yield reasonably good agreement with experimental results. Gasification of wood and char in a two-dimensional bubbling fluidized bed reactor has been investigated using TFM, and the effects of initial bed height, wood feeding rate and reactor throughput on the tar yield are examined [3]. Three-dimensional simulations of biomass gasification in a circulating fluidized bed (CFB) reactor have been carried out, where the impacts of turbulence models, radiation model, water–gas shift reaction (WGSR) and equivalence ratio (ER) on the gasification process have been thoroughly investigated [53]. Xue and Fox [54] simulated wood gasification in a 2D laboratory-scale-fluidized bed gasifier and reported effect of air/biomass mass flow ratio, reactor temperature and biomass moisture content on gas composition and product yields at the exit of the gasifier. A variable particle density model is used to

calculate the particle drag, instead of a constant particle density assumption. Numerical simulations revealed that biomass particle conversion is faster and particle flow accelerates along the reactor. Full loop simulations are carried out to analyse the hydrodynamics and chemical kinetics in a 2D dual-bed gasifier [55]. The product gas composition and temperature are found to be consistent with the experimental results. Wang et al. [56] examined suitability of energy-minimization multi-scale (EMMS) drag model on the hydrodynamics in dual-fluidized bed gasifier. Several other studies [57–66] may be found in the literature which validated satisfactory performance of TFM in predicting fluid dynamics and chemical kinetics of gasification.

3.3 Discrete Element Method

Discrete element method (DEM) is an Eulerian–Lagrangian approach-based model. It identifies discrete character of particles. Gas-phase equations are solved on Eulerian grid which is at least an order of magnitude larger than the particle size. Solid phase is composed of individual discrete particles, and their individual movement is governed by Newton's second law of motion. The interparticle interaction and particle interaction with gas and wall may be modelled based on hard sphere or soft sphere models.

3.4 Hard Sphere Model

In the hard sphere collision model, particles interact through binary collision where contact occurs at a point and no overlapping is allowed. During elastic collisions, momentum remains conserved and is assumed to be instantaneous, pairwise additive. Particles are in free flight motion in between collisions. During the simulation, collisions are processed in the order of their occurrence. Major drawback of this model is that it is incapable to handle multiple collisions occurring simultaneously. Therefore, in particle-dense flows, this model becomes inefficient because multiple collisions are to be processed at the same instance which leads to crashing of the model. Coefficient of restitution is employed to calculate the energy dissipation if the collisions are not fully elastic which can be found out readily by experiments. Hard sphere model is computationally cheaper and most suitable for dilute granular flows where intermediate collision time is large [67].

Before the collision, system is described by translational and rotational velocity components of particles, whereas relative velocity characterizes the system during the collision. Hoomans et al. [68, 69] proposed hard sphere approach considering only impulsive force as interaction forces. The particles' state, before and after the

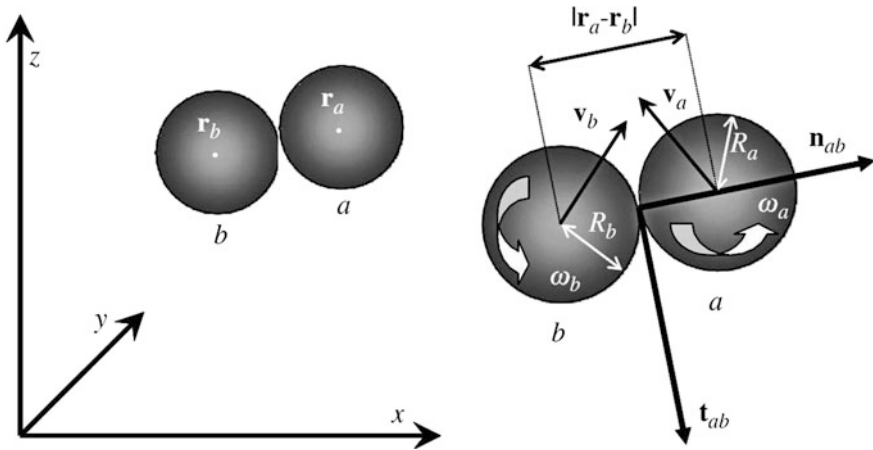


Fig. 3 Scheme of the collision between two particles (Reprinted from [67], with permission from Elsevier)

collision, is depicted in Fig. 3. For a binary collision between two rigid spheres a and b, the relative velocity at the contact point can be defined as:

$$\vec{u}_{ab} = (\vec{u}_a - \vec{u}_b) - (R_a \vec{\Omega}_a + R_b \vec{\Omega}_b) \times \vec{n}_{ab}, \tag{29}$$

Here, $\vec{u}, \vec{\Omega}, R$ are translation velocity, rotational velocity and radii of the particles prior to collision. The normal (\vec{n}_{ab}) and tangential (\vec{t}_{ab}) unit vectors are defined as:

$$n_{ab} = \frac{r_a - r_b}{|r_a - r_b|}, \quad t_{ab} = \frac{\vec{u}_{ab,0} - n_{ab}(\vec{u}_{ab,0} \cdot n_{ab})}{|\vec{u}_{ab,0} - n_{ab}(\vec{u}_{ab,0} \cdot n_{ab})|},$$

Superscript ‘0’ denotes pre-collision velocities.

Relative velocity after collision can be obtained by applying Newton’s second and third laws to binary collision of two spheres,

$$m_a(\vec{u}_a - \vec{u}_{a,0}) = -m_b(\vec{u}_b - \vec{u}_{b,0}) = J, \tag{30}$$

$$\frac{I_a}{R_a}(w_a - w_{a,0}) = \frac{-I_b}{R_b}(w_b - w_{b,0}) = n_{ab} \times J, \tag{31}$$

which gives

$$\vec{u}_{ab} - \vec{u}_{ab,0} = \frac{7J - 5n_{ab}(J \cdot \vec{n}_{ab})}{2m_{ab}}. \tag{32}$$

Here, J is the impulse vector and the reduced mass is $m_{ab} = \left(\frac{1}{m_a} + \frac{1}{m_b}\right)^{-1}$. During particle–wall collision, m_b is set as infinity, and $m_{ab} = m_a$. In order to close the above system of Eqs. (29–32), the following relationships are used for the spherical particles,

$$\vec{u}_{ab} \cdot \vec{n}_{ab} = -e_n(\vec{u}_{ab,0} \cdot \vec{n}_{ab}), \quad (33)$$

$$|\vec{u}_{ab} \times \vec{n}_{ab}| = -\mu(\vec{u}_{ab} \cdot \vec{J}), \quad (34)$$

$$\vec{u}_{ab} \times \vec{n}_{ab} = -\beta_0(\vec{u}_{ab,0} \times \vec{n}_{ab}), \quad (35)$$

where e_n , μ , β_0 are the coefficients of normal restitution ($0 < e_n < 1$), dynamic friction ($\mu \geq 1$) and tangential restitution ($0 < \beta_0 < 1$). Thus, normal component of the impulse vector can be written as $J_n = -(1 + e_n)m_{ij}(\vec{u}_{ij,0} \cdot \vec{n}_{ij})$.

Tangential component J_n is found out by identifying sliding or sticking nature of collisions.

$$J_t = \left\{ \begin{array}{ll} -\frac{2}{7}(1 + \beta_0) \times m_{ab}(\vec{u}_{ab,0} \cdot \vec{t}_{ab}) & \text{if } \mu J_n \geq -\frac{2}{7}(1 + \beta_0)m_{ab}(\vec{u}_{ab,0} \cdot \vec{t}_{ab}) \\ -\mu J_n & \text{if } \mu J_n < -\frac{2}{7}(1 + \beta_0)m_{ab}(\vec{u}_{ab,0} \cdot \vec{t}_{ab}) \end{array} \right\}. \quad (36)$$

The above Eq. (36) illustrates sticking- and sliding-type collisions, respectively. The total impulse vector is obtained by addition of two components: $J = J_n n_{ab} + J_t t_{ab}$. More details can be found out in Ref. [68].

3.5 Soft Sphere Model

In the soft sphere model, particle motion is governed by Newton's law and interaction between particles is considered in the form of contact forces. In the presence of only contact forces, the particle velocity can be calculated as:

$$m_a \frac{du_a}{dt} = \sum \vec{F}_{\text{contact}, a}. \quad (37)$$

Here, subscript 'a' stands for the particle under consideration. Velocity after collision can be computed by particle deformation theory [70], and contact time during collision is determined by elastic properties of particle. This approach allows multiple contacts at the same time, hence makes it suitable for dense particle systems. This model is used where solid volume fraction of particle phase is high and momentum transport due to particle interaction cannot be neglected. The calculation of the contact force between particles is quite complex so a simplified

model called ‘linear spring and dashpot model’ given by Cundall & Strack [71] is used to solve contact mechanics (Fig. 4). The contact forces are modelled as the function of relative velocity and particle overlap, where the spring and dashpot simulate the deformation and damping effects, respectively.

Contact forces can be divided into tangential and normal components,

$$\vec{F}_{contact,a} = \sum_j (\vec{F}_{ab,n} + \vec{F}_{ab,t}) \tag{38}$$

$\vec{F}_{ab,n}$ and $\vec{F}_{ab,t}$ are the normal and tangential components of the contact force between particles a and b . The normal component can be represented as $\vec{F}_{ab,n} = -k_n \delta_n \vec{n}_{ab} - \eta_n \vec{u}_{ab,n}$. In the expression, the first part represents the elastic deformation and the second part represents viscous dissipation. k_n is the normal spring stiffness, and $\vec{u}_{ab,n}$ is the normal relative velocity. The normal overlap can be calculated as $\delta_n = R_a + R_b - |r_b - r_a|$

The position vectors of sphere a and b are r_a, r_b , and the damping coefficient is

$$\eta_n = \begin{cases} \frac{-2 \ln e_n \sqrt{m_{ab} k_n}}{\sqrt{\pi^2 + \ln^2 e_n}} & \text{if } e_n \neq 0 \\ 2\sqrt{m_{ab} k_n} & \text{if } e_n = 0 \end{cases} \tag{39}$$

Tangential component of the contact forces is obtained by using the friction collision law, which is based on the equation of Coulomb friction,

$$\vec{F}_{ab,t} = \begin{cases} -k_t \delta_t - \eta_t \vec{u}_{ab,t}, & \text{if } |\vec{F}_{ab,t}| \leq \mu |\vec{F}_{ab,n}| \\ -\mu |\vec{F}_{ab,n}| \vec{t}_{ab}, & \text{if } |\vec{F}_{ab,t}| > \mu |\vec{F}_{ab,n}| \end{cases} \tag{40}$$

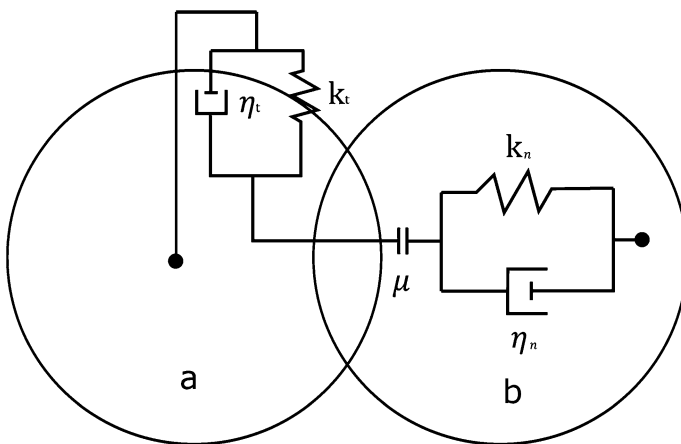


Fig. 4 Spring–slider–dashpot collision model [71]

Here, k_t, δ_t, η_t are the tangential stiffness, displacement and damping coefficient, respectively. Tangential relative velocity is $\vec{u}_{ab,t} = \vec{u}_{ab} - \vec{u}_{ab,n}$, and the tangential damping coefficient is:

$$\eta_t = \begin{cases} \frac{-2\ln\beta_0\sqrt{\frac{2}{7}m_{ab}k_t}}{\sqrt{\pi^2 + \ln^2\beta_0}} & \text{if } \beta_0 \neq 0 \\ 2\sqrt{\frac{2}{7}m_{ab}k_t} & \text{if } \beta_0 = 0 \end{cases}, \tag{41}$$

Here, β_0 is the friction coefficient. The tangential displacement coefficient is:

$$\delta_t = \begin{cases} \delta_{t,0}H + \int_{t_0}^t u_{ab,t}dt & \text{if } |F_{ab,t}| \leq \mu|F_{ab,n}| \\ \frac{\mu}{k_t}|F_{ab,n}|t_{ab} & \text{if } |F_{ab,t}| > \mu|F_{ab,n}| \end{cases}, \tag{42}$$

H is the rotation matrix here. The normal spring stiffness (k_t) is chosen arbitrarily, provided that the maximum extent of overlap between contacting particles is less than 1% of particle diameter at any time step. Torque acting on a ‘a’th particle due to particle–particle contacts is calculated by $\Gamma_{C,i} = \sum_b (r_a n_{ab} \times F_{ab,t})$ where n_{ab} denotes the unit vector from the centre of particle a to that of particle b. It is a time-driven model, and computational time step should be considerably less than contact time between particles. More detailed discussion can be found out in van der Hoef et al. [72, 73].

Main advantage of this method is that the desired thermo-chemical properties such as the size and shape of individual particles can be defined, and hence, the critical information regarding particle trajectory and particle interactions can be obtained accurately. Discrete element method (DEM) provides more realistic way to simulate gas–solid flow, but with increase in population of discrete particles, it becomes computationally expensive. Due to this reason, very few studies are carried out on reactor-level gasification systems. Ash and bed particles are modelled as inert medium and leave the gasification system without taking part in any reactions, whereas char particles undergo successive physical and chemical changes during processes such as heating, drying, pyrolysis and gasification. Therefore, both inert and reactive particles are governed by flow dynamics conservation equations but reaction chemistry affects only char particles.

Each particle’s movement is tracked individually based on the forces and torque acting on them. Gravity, drag, pressure gradient and collision force are considered as the effective forces acting on the solid particles. The movement of an i th particle having mass m_i and volume V_i in the system can be calculated using Newton’s second law,

$$m_i \frac{du_i}{dt} = m_i \frac{d^2r_i}{dt^2} = m_i g - V_i \nabla P_g + \frac{V_i \beta}{1 - \epsilon_g} (u_g - u_i) - \sum_{j=1}^k F_{c,ij}. \tag{43}$$

Here, the velocity is v_i and the position vector of the i th particle is r_i . The third term on the right side represents drag force exerted by gas on the particles.

Interphase momentum transfer coefficient, β , is modelled by the drag models discussed in Sect. 3.1. Last term on the right-hand side denotes sum of all contact forces on a particle upon colliding with j th entity (other particles or walls). The angular momentum of the i th particle may be calculated as:

$$I_i \frac{dw_i}{dt} = \sum_{j=1}^n \Gamma_{t,ij} + \Gamma_{r,ij}. \quad (44)$$

Here, I_i is the moment of inertia and $\Gamma_{t,ij}$ and $\Gamma_{r,ij}$ denote the torque developed by tangential forces and the rolling friction, respectively.

Gas-phase transport equations are solved on Eulerian grid, and gas-phase interaction with solid particles is resolved at computational grid. Particles are treated as source or sink in the gas-phase momentum equations. Gas-phase hydrodynamics is calculated by solving volume-averaged Navier–Stokes equations with addition of a void fraction term, ε_g [74].

$$\frac{\partial}{\partial t} (\varepsilon_g \rho_g) + \nabla \cdot (\varepsilon_g \rho_g u_g) = \dot{S}_{gs}, \quad (45)$$

$$\frac{\partial}{\partial t} (\varepsilon_g \rho_g u_g) + \nabla \cdot (\varepsilon_g \rho_g u_g u_g) = -\varepsilon_g \nabla P - \nabla \cdot (\varepsilon_g \tau_g) - S_p + \varepsilon_g \rho_g g. \quad (46)$$

Void fraction ε_g is calculated as $\varepsilon_g = 1 - \frac{\sum_{i=1}^n V_{i,t}}{V_{cell}}$ where $V_{i,t}$ is the volume of i th particle in the cell. On the right-hand side of Eq. (45) is the source term which is the sum of mass transfer of a species, from solid phase to the gas phase due to drying, devolatilization, heterogeneous reactions, etc. Two-way coupling between the gas phase and the particles is enforced via the source term S_p in the momentum equation (Eq. (46)) of the gas phase. The source term arises due to the reaction to the drag experienced per unit volume by a particle which is computed as:

$$S_p = \frac{1}{V_{cell}} \int \sum_{i=1}^{n_p} \frac{V_i \beta}{(1 - \varepsilon_g)} (u_g - u_i) D(r - r_i) dV. \quad (47)$$

Here, n_p is the total number of particles in the current cell, and the distribution function D distributes the reaction force acting on the gas phase to the Eulerian grid. The volume of the smallest computational cell for the fluid should be much larger than the volume of a particle.

Energy balance equation for the particle may be written as:

$$m_i C_{p,i} \frac{dT_i}{dt} = \sum_j^{n_p} Q_{ij} + h_i A_i (T_i - T_g) + Q_{i,rad} + Q_{i,react}. \quad (48)$$

Here, A_i is the surface area of the particle, h_i is the heat transfer coefficient, T_i is the temperature of particle and T_g is the temperature of the gas phase. Heat transfer

coefficient h_i can be calculated as $h_i = \frac{Nu \epsilon_g}{d_i}$ where Nu is the Nusselt number, $Nu = 2 + 0.6Re_p^{1/2}Pr^{1/3}$ [75]. First term on the r.h.s. represents conduction heat exchange between particles; $Q_{i,rad}$ is the particle-surrounding radiative heat transfer and can be calculated as $Q_{i,rad} = \sigma_{SB} \epsilon_p A_p (T_p^4 - T_{surr}^4)$. Here, σ_{SB} is the Stefan–Boltzmann constant and ϵ_p is the particle emissivity. Surrounding emissivity can be assumed unity, and T_{surr} is the surrounding temperature and can be computed by taking average of particle temperature on the bed [33]. $Q_{i,react}$ is the heat transfer due to chemical reactions that i th particle undergoes. $Q_{i,react} = -\frac{dm_i}{dt} \Delta H_{react,i}$. $\Delta H_{react,i}$ is the heat of reaction of the heterogeneous reaction, whereas time rate of change of particle mass $\frac{dm_i}{dt}$ can be obtained by heterogeneous chemistry. Energy equation for inert particle is similar to Eq. (48) except the $Q_{i,react}$ term which is zero in this case.

Gerber et al. [4] coupled gasification kinetics model involving drying, particle shrinkage, pyrolysis and gasification with linear spring–dashpot discrete element method (DEM) to model particle motion. Around 12,000 perfectly spherical charcoal particles were used. A zero-dimensional particle conversion model for thermo-chemical conversion of reacting particles was used, where reactions occur at the particle surface and products leave at particle surface temperature.

Though DEM illustrates particle motion in greater detail, very few studies are available covering CFD-DEM simulations of fluidized bed gasification. This may be due to the requirement to simulate large number of particles in gasification systems. Due to this, DEM is restricted to fundamental investigations of the particle-laden flows. Tsuji et al. [76] coupled DEM method with Navier–Stokes equations and simulated a spouting bed.

Oevermann et al. [77] and Gerber et al. [4] investigated the effect of wood feeding rate on exhaust gas compositions and temperature in a laboratory-scale bubbling fluidized reactor. Spring damper collision model was used to model collision. Detailed chemical reaction mechanism including transient heat-up, drying, particle shrinkage, pyrolysis, gasification and tar cracking was used. In their model, pyrolysis was defined as a two-step process. Volatile gases, tar, charcoal were the products formed during primary pyrolysis, whereas secondary pyrolysis involved tar decomposition into gaseous products and an inert tar, which was considered stable in gasifier operating conditions. A zero-dimensional lumped model was used to represent drying, pyrolysis and gasification processes. Numerical results reported an increase in the concentrations of CO and H₂ with an increase in wood feed rate, whereas the amount of CO₂ in the product gas was found to be nearly independent of the wood feed rate. Yang et al. [78] employed the CFD-DEM coupling approach to investigate the gas–solid hydrodynamics and in the spout-fluid bed with two interconnected chambers. They analysed solid circulation, spouting evolution and spout-annulus interface by solving time-averaged governing equations. Soft sphere approach-based linear spring and dashpot model was utilized to determine the interparticle contact forces. Tangential collision force was limited by the Coulomb’s friction law in occurrence of sliding between particles.

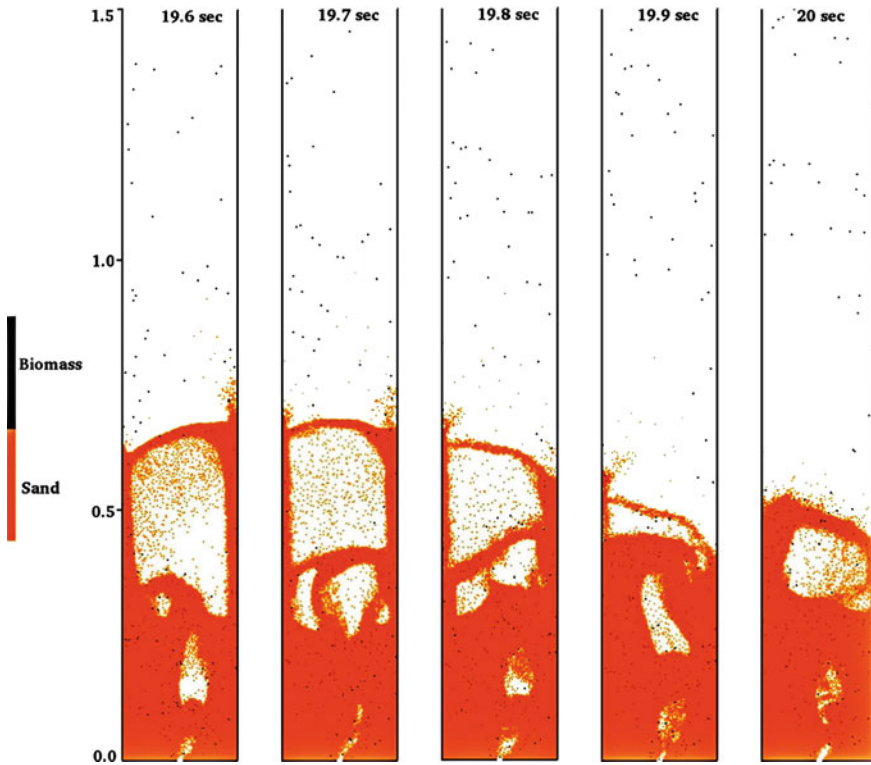


Fig. 5 Time evolution of particle flow patterns in CFD-DEM (Reprinted from [26], with permission from Elsevier)

Geng et al. [79] simulated char combustion in a bubbling fluidized bed of inert sand. They adopted the shrinking particle model to describe char combustion process in which particle density was taken to be constant whereas its diameter decreases. They included ash inhibition effect in their char conversion model in which surrounding sand particles does not let char particles react with CO which was the only product species considered. At low temperature, CO diffused away from char particles without any reaction whereas at high temperatures CO oxidized to CO₂. They concluded that their model described the effects of bed temperature, oxygen concentrations and gas superficial velocities more effectively.

Ku et al. [26] studied the effect of reactor temperature, steam/biomass mass ratio and biomass feed position on biomass gasification in a fluidized bed reactor using 40,000 spherical sand particles (Fig. 5). Devolatilization rate was modelled using a single-step first-order Arrhenius reaction. CH₄ was the only hydrocarbon considered whereas neglecting other hydrocarbon species. The char consumption rate included the effects of both diffusion and kinetic rates. Reaction chemistry was represented by two heterogeneous reactions and two homogeneous reactions. Results showed that increasing temperature aided the H₂ and CO yield in

endothermic reactions. H_2 and CO_2 yields increased, whereas CO yield decreased with the increase of steam/biomass mass ratio. Using a coupled CFD-DEM model, Liu et al. [80] investigated combustion of char and propane in a fluidized bed reactor. The model predicted that gaseous fuel reduced the char combustion rate, and this effect was more distinct at higher bed temperatures. Recently, Wang et al. [81] examined the effect of two different arrangements of cyclone on the gas–solid flow dynamics in order to scale up circulating fluidized bed (CFB) reactor using coupled CFD-DEM. A total number of 900,000 particles having a constant diameter and a constant density were tracked in the flow domain. Several other studies based on CFD-DEM model [82–86] have been published recently, primarily focusing on flow characterization and comparison with TFM but full loop three-dimensional simulations with realistic particle loading is not carried out yet.

3.6 MP-PIC Method

CFD-DEM provides detailed information about particle phase such as particle trajectories, particle–particle and particle–fluid interactions; therefore, it caters more realistic approach to model granular flows. Main disadvantage with this method is that the particle-laden flows having particle volume fraction more than 5% becomes computationally expensive [87]. On the other hand, TFM has been used for large-scale simulations extensively by various researchers to investigate fluidized bed systems because of its less computational cost. Multiphase particle-in-cell (MP-PIC) method treats particle phase as continuum yet contains its discrete character. Solid phase is represented by computational particles which constitute number of particles with identical properties such as particle diameter, velocity, density, volume and position. Individual particle properties are mapped to the Eulerian grid by using interpolation functions to get the continuum particle properties on grid. Particles dynamics and chemical reaction kinetics are resolved on the grid cell using mapped particle properties. Fluid phase properties are updated back from grid to the individual particles. This has enabled the MP-PIC method to be utilized as a particle–fluid solver that can tackle particle loading range from dilute to dense and various particle size distributions.

The dynamics of the particulate phase is explained using a particle probability distribution function $f(x_p, u_p, m_p, T_p, t)$ where x_p is the particle location, u_p is the particle velocity, m_p is the particle mass and T_p is the particle temperature. Particles may have different sizes and densities. The particle distribution can be updated by solving a Liouville equation [88, 89] for the particle distribution function f .

$$\frac{\partial f}{\partial t} + \frac{\partial(fu_p)}{\partial x_p} + \frac{\partial(fA_p)}{\partial u_p} = \frac{f_D - f}{\tau_D}. \quad (49)$$

The term on the right-hand side is the collision damping term, and it represents damping of particle velocity fluctuations generated due to particle collisions. τ_D is the collision damping time and is proportional to the time between particle collisions. f_D is the PDF for the local mass-averaged particle velocity and can be obtained by $f_D = [\int f du_p] \delta(u_p - \bar{u}_p)$ where $\bar{u}_p = \frac{\int f m_p u_p dm_p du_p}{\int f m_p dm_p du_p}$.

The particle distribution function integrated over velocity and mass gives the probable number of particles per unit volume at location x and time t in the interval du_p, dm_p . The continuum mass and momentum equations of the particulate phase on the Eulerian grid can be obtained by taking moments of PDF f and integrating over the mass, velocity and temperature coordinates.

The particle acceleration term a_p is defined as:

$$\frac{du_p}{dt} = \beta(u_g - u_p) - \frac{\nabla P}{\rho_p} - \frac{\nabla \tau_p}{\varepsilon_p \rho_p} + g + \frac{u_p - \bar{u}_p}{\tau_D}, \tag{50}$$

where ε_p is the solids volume fraction; β is the interphase momentum transfer coefficient which is a function of the particle size, velocity, position and time; τ_p is the solids contact stress. The particle stress gradient is difficult to be calculated for each particle in a dense flow; therefore, it is modelled as a spatial gradient on the Eulerian grid and interpolated back to particles. Particle–particle collisions are computed by the particle normal stress, τ_p . The continuum particle stress model in which the off-diagonal elements of the stress tensor are neglected is used which is an extension of the model given by Harris and Crighton [90], $\tau_p = \frac{P_s \varepsilon_p^b}{\max[\theta_{cp} - \theta_p, \varepsilon (1 - \theta_p)]}$. The constant P_s has units of pressure, and θ_{cp} is the particle volume fraction at close packing. Value of constant b is taken between 2 and 5. Value of ε is of the order of 10^{-7} . Thus, the particle stress relies only on the concentration of particles while neglecting the size and velocity of particles.

The solids volume fraction can be calculated as:

$$\varepsilon_p = \iiint f \frac{m_p}{\rho_p} dm_p du_p dT_p. \tag{51}$$

The gas volume fraction can be found out by $\varepsilon_g = (1 - \varepsilon_p)$. Mass source term in the gas continuity equation can be derived as

$$\dot{S}_{gs} = - \iiint f \frac{dm_p}{dt} dm_p du_p dT_p. \tag{52}$$

where $\frac{dm_p}{dt}$ is rate of change of particle mass producing gases by chemical reactions.

The interphase momentum transfer rate per unit volume, f , on the fluid phase is

$$f = - \iiint f \left\{ m_p \left[D_p (u_g - u_p) - \frac{\nabla p}{\rho_p} \right] + u_p \frac{dm_p}{dt} \right\} dm_p du_p dT_p. \quad (53)$$

The equation of particle motion is written as $\frac{dx_p}{dt} = u_p$. The temperature is assumed to be constant in the particle interior, and any temperature gradient is neglected. Also, it is assumed that there is no chemical reaction occurring inside the particle. Lumped model of particle temperature equation can be expressed as:

$$c_V \frac{dT_p}{dt} = \frac{\zeta_g Nu_g}{m_p 2r_p} A_p (T_g - T_p) + Q_{rad,p}, \quad (54)$$

where c_V is the specific heat of the particle material, T_p is the particle temperature, Nu_g is the Nusselt number for heat transfer in the fluid to the particle, r_p is the particle radius and ζ_g is the fluid thermal conductivity.

Interphase heat transfer from particle to fluid phase is given by

$$Q = \iiint f \left\{ m_p \left[D_p (u_g - u_p)^2 - c_V \frac{dT_p}{dt} \right] - \frac{dm_p}{dt} \left[H_p + \frac{1}{2} (u_g - u_p)^2 \right] \right\} dm_p du_p dT_p, \quad (55)$$

where H_p is particle enthalpy. The term $(u_g - u_p)^2$ is negligible in low Mach number flows.

In the MP-PIC method, cell-averaged chemical kinetics is used to model chemistry. Average properties of the particle phase are used to calculate chemical reaction rates in each grid cell. Mass, momentum and energy are transferred between solid and gas phases based on heterogeneous chemistry. Individual transport equations are solved for each gas species in the gaseous phase, and the cumulative gas-phase properties are computed from the mass fractions of the constituting gas mixture.

Snider et al. [87] extended MP-PIC modelling to simulate reacting phenomena in a three-dimensional coal gasifier. They used cell-averaged chemistry to incorporate reaction mechanism in their gasification model. Rate of change of mass of individual particles was related to molar concentration rate change of solid carbon which was based on the assumption that the rate of solid carbon consumption is proportional to the volume of particles, $\frac{dm_p}{dt} = \frac{\varepsilon_g Mw_c}{\rho_p \varepsilon_p} m_p \frac{d[C(s)]}{dt}$ where Mw_c is the molecular weight of carbon and $\frac{d[C(s)]}{dt}$ is rate of change of molar concentration of solid carbon. Contrary to Eulerian assumption, average properties of particle phase such as particle temperature, particle diameter were computed by interpolating individual particle's properties to the grid. Rate of reaction depends on average properties which vary due to local particle distribution from cell to cell. Drying and

devolatilization were assumed instantaneous, and moisture and volatile matter were added to mixture of carbon and ash at the feeding location. Change in mass of particles depends on solid mass consumption/production rate in heterogeneous reaction chemistry. Gasification reaction mechanism was defined by set of total five homogeneous and heterogeneous reactions. Chemical reactions were modelled by Arrhenius law and take the form of ordinary differential equations. The energy conservation equation of the fluid phase was coupled with energy transfer from the solid phase. They found out uniform temperature distribution in the fluidized bed except at fuel feed location owing to combustion heat release. The model over-predicted the concentrations of H_2O , H_2 , N_2 , CO_2 in outlet product gas stream.

Abbasi et al. [91] examined the flow patterns, local particle velocities, particle solid fractions and gas composition in the gasifier feeding section using MP-PIC approach. The MP-PIC model predicted early signs of suspension choking in the gasifier feeding section. Xie et al. [35] investigated coal gasification in a pilot fluidized bed gasifier using MP-PIC model. The flow patterns, particle species, reaction rate and gas composition distribution, carbon consumption were scrutinized under different operating conditions. Instead of defining any complex heterogeneous reaction mechanism at the particle surface, total consumption rate of particles was expressed by global reaction rates. A set of twelve reactions was used to describe gasification reaction chemistry in the reactor with assumptions of instantaneous drying and devolatilization at the coal feeding location. Predicted gas compositions at the outlet were found to be in good agreement with experimental data.

Loha et al. [92, 93] studied biomass gasification in a fluidized bed reactor using MP-PIC scheme-based commercial code BARRACUDA [94]. At a constant steam–biomass ratio, the concentrations of H_2 , CO , CH_4 increased whereas CO_2 concentration decreased with increasing temperature. It was asserted that the high temperature facilitates the steam gasification and Boudouard reactions (Fig. 6). The product gas compositions were found to be in agreement with the experimental results. Chen et al. [95] investigated gas–solid flow in a circulating fluidized bed (CFB) riser using Geldart A and B particles. It was reported that TFM simulations with the EMMS drag model gave more accurate results than the MP-PIC simulations though MP-PIC scheme was able to detect the effect of realistic particle size distributions in CFB risers. Discrepancies in numerical results with experiments were mainly attributed to the drag force models used in MP-PIC simulations, i.e. Richardson et al. model [96] and the Stokes model [97] which were basically developed for a single particle in gas flow and do not include solids concentration effect. Recently, Zhang et al. [98] studied bed-to-wall heat transfer between an immersed vertical heat tube and bed materials in a gas–solid fluidized bed. Predicted radial and axial profiles of heat transfer coefficients at different superficial gas velocities are found to be in good agreement with experimental results. Several other numerical studies based on MP-PIC approach are available in Refs. [99–101].

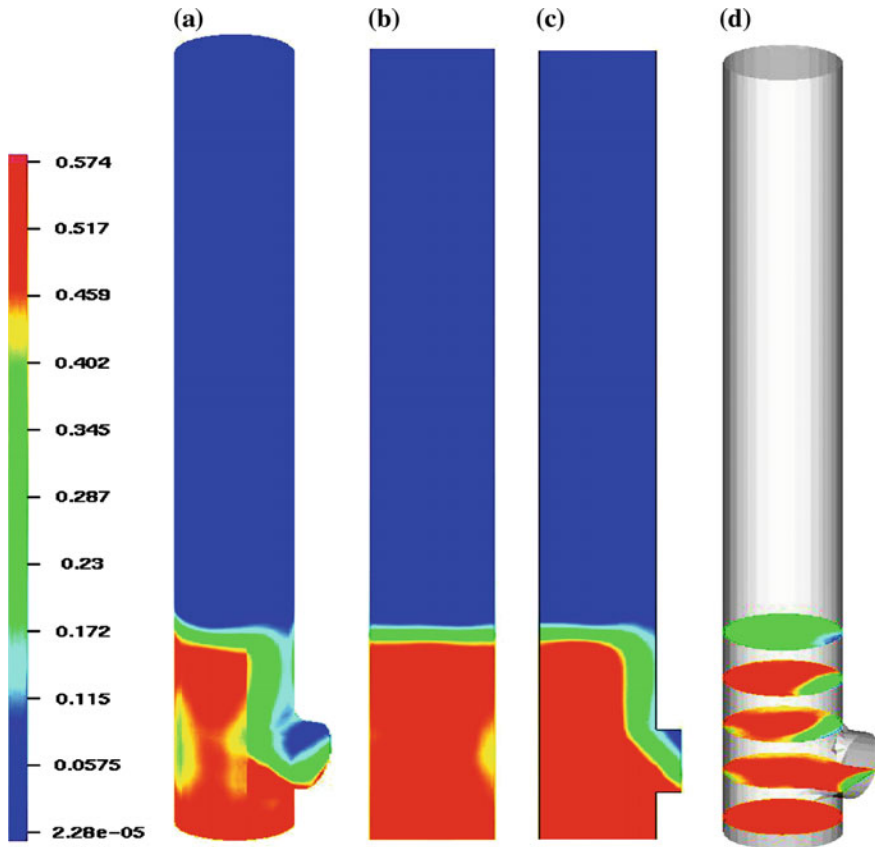


Fig. 6 Time-averaged solid volume fraction in **a** entire geometry, **b** X–Z plane, **c** Y–Z plane and **d** cut planed along the height (Reprinted from [92], with permission from Elsevier)

4 Conclusions

In this chapter, an overview of the CFD modelling strategies used to study fluidized bed gasifiers is presented. Despite significant efforts by researcher community, it is not possible to obtain in-depth qualitative as well as quantitative results with available experimental measurement techniques [102]. Computer-aided models are developed in an attempt to gain better understanding of gas–solid reacting flow encountered in fluidized beds. The integrated model of fluidized bed gasification incorporates particle interactions, hydrodynamics of dense gas–particle flow, turbulence, heat and mass transfer, radiation, particle shrinkage, pyrolysis, as well as homogeneous and heterogeneous chemical reactions. Numerical simulations made it possible to obtain finer insight which is otherwise very difficult to be determined experimentally. It is reasonable to resolve or model all length and timescales in

order to get complete information about the flow; however, due to computational cost constraints, fully resolved discrete particle methods such as direct numerical solution, lattice Boltzmann methods, are only limited to small particle population systems. In view of this, multi-scale modelling approach is developed in which macro-scale flow-governing equations are resolved and small-scale details are modelled using suitable closure approximations. EE model, such as TFM, being computationally efficient has been successfully utilized in large-scale numerical simulations but modelling of the industrial scale units is still problematic with present computational resources. Industrial scale systems can be simulated using a larger grid size, which cannot capture the structures at smaller scales [103]. TFM models solid phase as pseudo-fluid phase, and KTGF provides empirical closures for interaction forces and constitutive relations for solid phase properties. Main disadvantage of TFM is that KTGF is not capable to model poly-disperse fluidized systems as it has no provision to describe particle mixing and segregation rates in a quantitative manner. TFM uses representative average particle size obtained from experiments in simulations. Separate transport equations need to be solved for particles having different size and type; therefore, it is not possible to model wide distributions of particles. Also, it is not yet feasible to monitor variation in particle size due to attrition, agglomeration and localized chemical reaction rates. CFD-DEM and MP-PIC models consider solid phase as discrete particles. MP-PIC can handle full three-dimensional laboratory-scale systems containing millions of particles, whereas CFD-DEM is restricted to systems containing few thousands particles [104]. Gas–solid drag relations can be further improved by accounting particle heterogeneity and mobility which can be derived from fully resolved DPM simulations. With the advancement in computational resources, it is anticipated that the resolved DPM methods will be able to tackle densely packed fluidized systems which will improve the closure relations used in multi-scale models. In near future, it does not appear to be acceptable employing CFD-DEM for the simulation of large scale containing realistic number of particles. Collision force models used in CFD-DEM such as spring-dashpot model are derived for static, homogeneous mono-disperse spheres [74], yet they are applied to locally inhomogeneous and non-static systems. Furthermore, a more comprehensive reactive model needs to be developed. Heat-up, drying and pyrolysis are highly complex processes, and sub-models used are very simplified which certainly affect the accuracy of the numerical results. In most of the computational studies, particles are assumed to be spherical, which is not true for biomass particles like rice straw, wood. Variation in particle attributes such as density, porosity, composition and shape due to different processes occurring in the reactor is not accounted in the current modelling approaches. Owing to the computational convenience, a reduced chemical reaction model is adopted so efforts are required for the completeness of chemical reaction models. Each reaction is governed by a rate coefficient fitted with empirical data input which is obtained by conducting respective reaction in a specific operating condition. It is not recommended to blend rate constants acquired from different sources; however, in the absence of relevant chemistry available for gasification, unrelated reaction kinetics is used. In present scenario, fluidized bed gasification

modelling is very simplified and based on several simplifying assumptions so more realistic and accurate models need to be developed in order to address underlying physical and chemical processes. Lastly, there is an acute need to develop experimental techniques so that accuracy of CFD models can be validated.

Acknowledgements The authors would like to acknowledge joint financial support from Ministry of Human Resource and Development and Ministry of Coal under the IMPRINT initiative by Government of India (Project No: MHRD /ME /2016408B, Title: Development of pressurized dual fluidized bed gasifier for high-ash Indian coal).

References

1. Syamlal M, Bisset L (1991) METC Gasifier advanced simulation (MGAS) model, U.S. department of energy office of fossil energy, Morgantown energy technology center P.O. Box 880, Morgantown, West Virginia 26507-0880
2. Bryden KM, Ragland KW, Rutland CJ (2002) Modeling thermally thick pyrolysis of wood. *Biomass Bioenergy* 22(1):41-53
3. Gerber S, Behrendt F, Oevermann M (2010) An Eulerian modeling approach of wood gasification in a bubbling fluidized bed reactor using char as bed material. *Fuel* 89(10):2903-2917
4. Gerber S, Oevermann M (2014) A two dimensional Euler-Lagrangian model of wood gasification in a charcoal bed-Part I: model description and base scenario. *Fuel* 115:385-400
5. Bukur DB, Amundson NR (1981) Fluidized bed char combustion diffusion limited models. *Chem Eng Sci* 36(7):1239-1256
6. Silaen A, Wang T (2010) Effect of turbulence and devolatilization models on coal gasification simulation in an entrained-flow gasifier. *Int J Heat Mass Transf* 53(9):2074-2091
7. Gómez-Barea A, Leckner B (2010) Modeling of biomass gasification in fluidized bed. *Prog Energy Combust Sci* 36(4):444-509
8. Badzioch S, Hawksley PG (1970) Kinetics of thermal decomposition of pulverized coal particles. *Ind Eng Chem Process Des Dev* 9(4):521-530
9. Kobayashi H, Howard JB, Sarofim AF (1977) Coal devolatilization at high temperatures. In: Symposium (international) on combustion, vol 16, no 1. Elsevier, pp 411-425
10. Wang X, Jin B, Zhong W (2009) Three-dimensional simulation of fluidized bed coal gasification. *Chem Eng Process* 48(2):695-705
11. Yu L, Lu J, Zhang X, Zhang S (2007) Numerical simulation of the bubbling fluidized bed coal gasification by the kinetic theory of granular flow (KTGF). *Fuel* 86(5):722-734
12. Armstrong LM, Gu S, Luo KH (2011) Effects of limestone calcination on the gasification processes in a BFB coal gasifier. *Chem Eng J* 168(2):848-860
13. Radmanesh R, Chaouki J, Guy C (2006) Biomass gasification in a bubbling fluidized bed reactor: experiments and modeling. *AIChE J* 52(12):4258-4272
14. Pitt GJ (1962) The kinetics of the evolution of volatile products from coal. *Fuel* 41:267-74
15. Sommariva S, Maffei T, Migliavacca G, Faravelli T, Ranzi E (2010) A predictive multi-step kinetic model of coal devolatilization. *Fuel* 89(2):318-328
16. Maffei T, Frassoldati A, Cuoci A, Ranzi E, Faravelli T (2013) Predictive one step kinetic model of coal pyrolysis for CFD applications. *Proc Combust Inst* 34(2):2401-2410
17. Anthony DB, Howard JB (1976) Coal devolatilization and hydrogasification. *AIChE J* 22(4):625-656

18. Fletcher TH, Kerstein AR, Pugmire RJ, Grant DM (1990) Chemical percolation model for devolatilization: 2. temperature and heating rate effects on product yields. *Energy Fuels* 4 (1):54–60
19. Niksa S, Kerstein A (1991) Flashchain theory for rapid coal devolatilization kinetics. 1. Formulation. *Energy Fuels* 5(5):647–665
20. Solomon PR, Hamblen DG, Carangelo RM, Serio MA, Deshpande GV (1988) General model of coal devolatilization. *Energy Fuels* 2(4):405–422
21. Vascellari M, Arora R, Pollack M, Hasse C (2013) Simulation of entrained flow gasification with advanced coal conversion submodels. Part I: Pyrolysis. *Fuel* 113:654–669
22. Smoot LD, Smith PJ (2013) *Coal combustion and gasification*. Springer Science and Business Media
23. Turns SR (2006) *An Introduction to Combustion*, 2nd edn, McGraw-Hill
24. Mermoud F, Salvador S, Van de Steene L, Golfier F (2006) Influence of the pyrolysis heating rate on the steam gasification rate of large wood char particles. *Fuel* 85(10):1473–1482
25. Baum MM, Street PJ (1971) Predicting the combustion behaviour of coal particles. *Combust Sci Technol* 3(4):231–243
26. Ku X, Li T, Løvås T (2015) CFD–DEM simulation of biomass gasification with steam in a fluidized bed reactor. *Chem Eng Sci* 122:270–283
27. Bhatia SK, Perlmutter DD (1980) A random pore model for fluid-solid reactions: I. Isothermal, kinetic control. *AIChE J* 26(3):379–386
28. Hurt R, Sun JK, Lunden M (1998) A kinetic model of carbon burnout in pulverized coal combustion. *Combust Flame* 113(1–2):181–197
29. Hurt RH, Calo JM (2001) Semi-global intrinsic kinetics for char combustion modeling. *Combust Flame* 125(3):1138–1149
30. Liu GS, Niksa S (2004) Coal conversion submodels for design applications at elevated pressures. Part II. char gasification. *Prog Energy Combust Sci* 30(6):679–717
31. Gräbner M, Ogriseck S, Meyer B (2007) Numerical simulation of coal gasification at circulating fluidised bed conditions. *Fuel Process Technol* 88(10):948–958
32. De Souza-Santos ML (2004) *Solid fuels combustion and gasification: modelling, simulation, and equipment operations*. CRC Press
33. Zhou H, Flamant G, Gauthier D (2004) DEM-LES simulation of coal combustion in a bubbling fluidized bed Part II: coal combustion at the particle level. *Chem Eng Sci* 59 (20):4205–4215
34. Bruchmüller J, van Wachem BGM, Gu S, Luo KH, Brown RC (2012) Modeling the thermochemical degradation of biomass inside a fast pyrolysis fluidized bed reactor. *AIChE J* 58(10):3030–3042
35. Xie J, Zhong W, Jin B, Shao Y, Huang Y (2013) Eulerian-Lagrangian method for three-dimensional simulation of fluidized bed coal gasification. *Adv Powder Technol* 24 (1):382–392
36. Hurt RH, Calo JM (2001) Semi-global intrinsic for char combustion modeling. *Combust Flame* 125:1138–2114
37. Čejně F, Hernandez JP (2002) Modeling and simulation of coal gasification process in fluidized bed. *Fuel* 81:1687–1702
38. Jones WP, Launder B (1972) The prediction of laminarization with a two-equation model of turbulence. *Int J Heat Mass Transf* 15(2):301–314
39. Smagorinsky J (1963) General circulation experiments with the primitive equations: I the basic equations. *Mon Weather Rev* 91:99–164
40. Syamlal M, Rogers W, O'Brien TJ (1993) *MFIX documentation theory guide*. U.S. Department of Energy, Office of Fossil Energy Technical Note
41. Gidaspow D (1994) *Multiphase flow and fluidization: continuum and kinetic theory description*. Academic Press
42. Yang N, Wang W, Ge W, Li J (2003) CFD simulation of concurrent-up gas–solid flow in circulating fluidized beds with structure-dependent drag coefficient. *Chem Eng J* 96:71–80

43. Ding J, Gidaspow D (1990) A bubbling fluidization model using kinetic theory of granular flow. *AIChE J* 36(4):523–538
44. Chapman S, Cowling TG (1970) *The mathematical theory of non-uniform gases*, 3rd ed. Cambridge University Press
45. Lun CKK, Savage SB, Jeffrey DJ, Chepurnity N (1984) Kinetic theory for granular flow: inelastic particles in Couette flow and slightly inelastic particles in a general flow field. *J Fluid Mech* 140:223–235
46. Bagnold RA (1954) Experiments on a gravity-free dispersion of large solids spheres in a Newtonian fluid under shear. *Proc. Roy. Soc. A* 225:49–63
47. Schaeffer DG (1987) Instability in the evolution equations describing incompressible granular flow. *J Diff Eq* 66:19–50
48. Gunn D (1978) Transfer of heat or mass to particles in fixed and fluidised beds. *Int. J Heat Mass Transf* 21:467–476
49. Basu P (2006) *Combustion and gasification in fluidized beds*. CRC Press
50. Bakul CEJ, Gershtein VY, Xianming L (2001) *Computational fluid dynamics in industrial combustion*. CRC Press, New York
51. Zhong W, Zhang M, Jin B, Yuan Z (2007) Flow behaviors of a large spout-fluid bed at high pressure and temperature by 3D simulation with kinetic theory of granular flow. *Powder Technol* 175(2):90–103
52. Zhong W, Yu A, Zhou G, Xie J, Zhang H (2016) CFD simulation of dense particulate reaction system: approaches recent advances and applications. *Chem Eng Sci* 140:16–43
53. Liu H, Elkamel A, Lohi A, Biglari M (2013) Computational fluid dynamics modeling of biomass gasification in circulating fluidized-bed reactor using the Eulerian-Eulerian approach. *Ind Eng Chem Res* 52(51):18162–18174
54. Xue Q, Fox RO (2014) Reprint of: Multi-fluid CFD modeling of biomass gasification in polydisperse fluidized-bed gasifiers. *Powder Technol* 265:23–34
55. Manchasing C, Kuchonthara P, Chalermssinsuwan B, Piumsomboon P (2013) Experiment and computational fluid dynamics simulation of in-depth system hydrodynamics in dual-bed gasifier. *Int J Hydrogen Energy* 38(25):10417–10430
56. Wang X, Lei J, Xu X, Ma Z, Xiao Y (2014) Simulation and experimental verification of a hydrodynamic model for a dual fluidized Bed gasifier. *Powder Technol* 256:324–335
57. Zhang N, Lu B, Wang W, Li J (2010) 3D CFD simulation of hydrodynamics of a 150 MW e circulating fluidized bed boiler. *Chem Eng J* 162(2):821–828
58. Seo MW, Nguyen TD, Lim YI, Kim SD, Park S, Song BH, Kim YJ (2011) Solid circulation and loop-seal characteristics of a dual circulating fluidized bed: experiments and CFD simulation. *Chem Eng J* 168(2):803–811
59. Nguyen TD, Seo MW, Lim YI, Song BH, Kim SD (2012) CFD simulation with experiments in a dual circulating fluidized bed gasifier. *Comput Chem Eng* 36:48–56
60. Xueyao W, Zhengzhong M, Jing L, Xiang X, Yunhan X (2013) Numerical simulation for the loop seal in the circulating fluidized bed and experimental validation. *Appl Therm Eng* 52(1):141–149
61. Guan Y, Chang J, Zhang K, Wang B, Sun Q (2014) Three-dimensional CFD simulation of hydrodynamics in an interconnected fluidized bed for chemical looping combustion. *Powder Technol* 268:316–328
62. Liu H, Cattolica RJ, Seiser R, Liao CH (2015) Three-dimensional full-loop simulation of a dual fluidized-bed biomass gasifier. *Appl Energy* 160:489–501
63. Luo K, Wu F, Yang S, Fang M, Fan J (2015) High-fidelity simulation of the 3-D full-loop gas–solid flow characteristics in the circulating fluidized bed. *Chem Eng Sci* 123:22–38
64. Cheng Y, Thow Z, Wang CH (2016) Biomass gasification with CO₂ in a fluidized bed. *Powder Technol* 296:87–101
65. Guan Y, Chang J, Zhang K, Wang B, Sun Q, Wen D (2016) Three-dimensional full loop simulation of solids circulation in an interconnected fluidized bed. *Powder Technol* 289:118–125

66. Zi C, Sun J, Yang Y, Huang Z, Liao Z, Wang J, Yang Y, Han G (2017) CFD simulation and hydrodynamics characterization of solids oscillation behavior in a circulating fluidized bed with sweeping bend return. *Chem Eng J* 307:604–620
67. Deen NG, Annaland MVS, Van der Hoef MA, Kuipers JAM (2007) Review of discrete particle modeling of fluidized beds. *Chem Eng Sci* 62(1):28–44
68. Hoomans BPB, Kuipers JAM, Briels WJ, Van Swaaij WPM (1996) Discrete particle simulation of bubble and slug formation in a two-dimensional gas-fluidised bed: a hard-sphere approach. *Chem Eng Sci* 51(1):99–118
69. Hoomans BPB, Kuipers JAM, Van Swaaij WPM (2000) Granular dynamics simulation of segregation phenomena in bubbling gas-fluidised beds. *Powder Technol* 109(1–3):41–48
70. Hertz H (1881) On the contact of elastic bodies. *J für die reine und angew Mathe* 92:156–171
71. Cundall PA, Strack OD (1979) A discrete numerical model for granular assemblies. *Geotechnique* 29(1):47–65
72. Van der Hoef MA, Ye M, van Sint Annaland M, Andrews AT, Sundaresan S, Kuipers JAM (2006) Multiscale modeling of gas-fluidized beds. *Adv chem Eng* 31:65–149
73. van der Hoef MA, van Sint Annaland M, Deen NG, Kuipers JAM (2008) Numerical simulation of dense gas-solid fluidized beds: a multiscale modeling strategy. *Annu Rev Fluid Mech* 40:47–70
74. van der Hoef MA, van Sint Annaland M, Kuipers JAM (2004) Computational fluid dynamics for dense gas–solid fluidized beds: a multi-scale modeling strategy. *Chem Eng Sci* 59(22):5157–5165
75. Kunii D, Levenspiel O (1991) *Fluidization Engineering* (Series in Chemical Engineering), 2nd edn. Butterworth-Heinemann, Stoneham, MA
76. Tsuji Y, Kawaguchi T, Tanaka T (1993) Discrete particle simulation of two-dimensional fluidized bed. *Powder Technol* 77(1):79–87
77. Oevermann M, Gerber S, Behrendt F (2009) Euler–Lagrange/DEM simulation of wood gasification in a bubbling fluidized bed reactor. *Particuology* 7(4):307–316
78. Yang S, Cahyadi A, Sun Y, Wang J, Chew JW (2016) CFD–DEM investigation into the scaling up of spout-fluid beds via two interconnected chambers. *AIChE J* 62(6):1898–1916
79. Geng Y, Che D (2011) An extended DEM–CFD model for char combustion in a bubbling fluidized bed combustor of inert sand. *Chem Eng Sci* 66(2):207–219
80. Liu D, Chen X, Zhou W, Zhao C (2011) Simulation of char and propane combustion in a fluidized bed by extending DEM–CFD approach. *Proc Combust Inst* 33(2):2701–2708
81. Wang S, Luo K, Hu C, Fan J (2017) CFD-DEM study of the effect of cyclone arrangements on the gas-solid flow dynamics in the full-loop circulating fluidized bed. *Chem Eng Sci*
82. Bellan S, Matsubara K, Cheok CH, Gokon N, Kodama T (2017) CFD-DEM investigation of particles circulation pattern of two-tower fluidized bed reactor for beam-down solar concentrating system. *Powder Technol* 319:228–237
83. Le Lee J, Lim EWC (2017) Comparisons of Eulerian–Eulerian and CFD-DEM simulations of mixing behaviors in bubbling fluidized beds. *Powder Technol*
84. Nikolopoulos A, Stroh A, Zeneli M, Alobaid F, Nikolopoulos N, Ströhle J, Karellas S, Epple B, Grammelis P (2017) Numerical investigation and comparison of coarse grain CFD–DEM and TFM in the case of a 1 MW th fluidized bed carbonator simulation. *Chem Eng Sci* 163:189–205
85. Carlos Varas AE, Peters EA, Kuipers JAM (2017) Computational Fluid Dynamics–Discrete Element Method (CFD–DEM) Study of Mass-Transfer Mechanisms in Riser Flow. *Ind Eng Chem Res* 56(19):5558–5572
86. Xu Y, Li T, Musser J, Liu X, Xu G, Rogers WA (2017) CFD-DEM modeling the effect of column size and bed height on minimum fluidization velocity in micro fluidized beds with Geldart B particles. *Powder Technol*
87. Snider DM, Clark SM, O'Rourke PJ (2011) Eulerian-Lagrangian method for three-dimensional thermal reacting flow with application to coal gasifiers. *Chem Eng Sci* 66(6):1285–1295

88. Andrews MJ, O'rourke PJ (1996) The multiphase particle-in-cell (MP-PIC) method for dense particulate flows. *Int J Multiph Flow* 22(2):379–402
89. Snider DM (2001) An incompressible three-dimensional multiphase particle-in-cell model for dense particle flows. *J Comput Phys* 170(2):523–549
90. Harris SE, Crighton DG (1994) Solutions, solitary waves and voidage disturbances in gas-fluidized beds. *J Fluid Mech* 266:243
91. Abbasi A, Ege PE, De Lasa HI (2011) CFPD simulation of a fast fluidized bed steam coal gasifier feeding section. *Chem Eng J* 174(1):341–350
92. Loha C, Chattopadhyay H, Chatterjee PK (2014) Three dimensional kinetic modeling of fluidized bed biomass gasification. *Chem Eng Sci* 109:53–64
93. Loha C, Gu S, De Wilde J, Mahanta P, Chatterjee PK (2014) Advances in mathematical modeling of fluidized bed gasification. *Renew Sustain Energy Rev* 40:688–715
94. Llc C (2009) Barracuda: computational particle fluid dynamics. CFPD-software, Albuquerque, NM
95. Chen C, Werther J, Heinrich S, Qi HY, Hartge EU (2013) CFPD simulation of circulating fluidized bed risers. *Powder Technol* 235:238–247
96. Richardson JF, Davidson P, Harrison D (1971) *Fluidization*. Academic Press, London and New York
97. White FM (1991) *Viscous fluid flow*. McGraw-Hill, New York
98. Zhang Y, Wei Q (2017) CFPD simulation of bed-to-wall heat transfer in a gas-solids bubbling fluidized bed with an immersed vertical tube. *Chem Eng Process* 116:17–28
99. Shi X, Wu Y, Lan X, Liu F, Gao J (2015) Effects of the riser exit geometries on the hydrodynamics and solids back-mixing in CFB risers: 3D simulation using CFPD approach. *Powder Technol* 284:130–142
100. Liang Y, Zhang Y, Li T, Lu C (2014) A critical validation study on CFPD model in simulating gas–solid bubbling fluidized beds. *Powder Technol* 263:121–134
101. Wang Q, Yang H, Wang P, Lu J, Liu Q, Zhang H, Wei L, Zhang M (2014) Application of CFPD method in the simulation of a circulating fluidized bed with a loop seal Part II—investigation of solids circulation. *Powder Technol* 253:822–828
102. Yang GQ, Du B, Fan LS (2007) Bubble formation and dynamics in gas–liquid–solid fluidization—a review. *Chem Eng Sci* 62:2–27
103. Agrawal K, Loezos PN, Syamlal M, Sundaresan S (2001) The role of meso-scale structures in rapid gas-solid flows. *J Fluid Mech* 445:151–185
104. Snider DM (2007) Three fundamental granular flow experiments and CFPD predictions. *Powder Technol* 176(1):36–46

Entrained Flow Gasification: Current Status and Numerical Simulations

Mayank Kumar

Abstract Entrained flow gasification is perhaps the most adopted gasification technology around the world. Most of the IGCC deployments around the world have chosen entrained flow gasification as the coal conversion technology. It offers high temperatures, high mass throughput, low amount of tars and oils in the flue gas stream, and high carbon conversion efficiencies. The drawbacks of this technology include frequent maintenance of critical equipment such as wall refractory and injectors. This chapter focuses on both the commercial aspects, in terms of worldwide deployment and operational experience, and the technical aspects of entrained flow gasification. The technical discussion is centered on the computational fluid dynamics modeling, owing to the deep complexity inherent in the turbulent fluid mechanics of these systems. There is a dedicated discussion on the char consumption model, including the heterogeneous kinetics, as well since it plays a key role in determining the sizing and overall design of the gasifier.

Keywords Gasification • Entrained flow gasification

Nomenclature

\dot{m}_p	char consumption rate (kg/s)
P_g	reactant partial pressure (atm)
t	time (s)
k_d	rate constant for diffusion
k_s	rate constant for kinetics
A_0	external surface area of the particle (m ²)
A_d	diffusion constant
d_p	particle diameter (m)

M. Kumar (✉)
Department of Mechanical Engineering,
Indian Institute of Technology Delhi, Delhi, India
e-mail: kmayank@mech.iitd.ac.in

T_g	gas temperature (K)
P	total gasifier pressure (atm)
R	universal gas constant (J/mol-K)
k_{dash}	ash diffusion constant
ε	ash voidage fraction
r_p	instantaneous radius of the shrinking core (m)
R_p	fixed radius of the char-ash complex (m)
Ψ	structure parameter for the particular coal/char type
S	instantaneous total internal reactive area of the porous char (m ² /g)
S_0	initial internal reactive area (m ² /g)
A	instantaneous surface area of the shrinking core (m ²)
m_{po}	original char mass in the particle (kg)
k_1, k_2, k_3	Arrhenius type constants
η	effectiveness factor
ν_o	stoichiometric coefficient for the particular gasification reaction
D_e	internal particle diffusivity (m ² /s)
G	local irradiation (W/m ²)
k_a	absorption coefficient (m ⁻¹)
I_b	black-body intensity (W/m ² -sr)
$\Phi(\vec{s}, \vec{s}')$	scattering phase function
N_p	number of particles
ε_p	particle emissivity
q_{in}	radiative flux at the wall (W/m ²)
q_{out}	emitted heat flux from wall (W/m ²)
ε_w	wall emissivity
T_w	wall temperature (K)
I_{out}	radiative intensity leaving the wall (W/m ² -sr)

Abbreviations

CFD	Computational fluid dynamics
CWS	coal-water slurry
PHICCOS	Phase-inversion-based coal-CO ₂ slurry
CCS	<i>carbon capture and sequestration</i>
IGCC	Integrated gasification combined cycle
ASUs	Air separation units
EOR	Enhanced oil recovery
OSEF	Oxygen-staged entrained flow
OMB	opposed multiburner
ODE	ordinary differential equations
SCM	<i>shrinking core model</i>

RPM	<i>random pore model</i>
LH	Langmuir–Hinshelwood
PDE	partial differential equations
MFF	moving flame front
RTE	radiative transport equation
FVM	finite volume method
DOM	Discrete ordinates method
LES	Large eddy simulations

1 Introduction

Gasification has seen a recent upsurge in popularity owing to environmental concerns as well as a renewed interest in coal-to-chemicals conversion. Entrained flow gasifiers are the technology of choice in this gasification revolution for many countries around the world. The reasons are manifold, including high carbon conversion efficiencies, high mass throughputs, compact reactor sizes, and scalability to higher pressures. The distinguishing features of entrained flow gasifiers are the high-temperature slagging operation, small particle residence times (of the order of seconds), and micron-sized (10–150 μ) pulverized feedstock requirement.

The basic design of the entrained flow gasifier can be gauged from the various commercial gasifiers depicted in Fig. 1. The feedstock is fed into the gasifier, along with the carrier gas, via axial or radial/tangential injectors in an up-flow or down-flow configuration. The powdered coal is entrained with the gas as it is converted in the presence of gasifying agents such as oxygen, carbon dioxide, and steam. The key technological challenges in entrained flow gasification include rather frequent injector and refractory wear owing to the high temperatures, and issues with slag handling, especially for the high-ash-content coals. Understanding char structural evolution, heterogeneous kinetics, transport processes within the coal particle and the boundary layer, and turbulent two-phase reacting flows are a few of the problems that confront design engineers as they tackle these technological challenges. This chapter will provide an overview of the aforementioned aspects of entrained flow gasification and delve into a literature review of the recent modeling efforts toward gaining a better understanding of the physicochemical processes inside an entrained flow gasifier. A survey of the key projects employing entrained flow gasifiers around the world is also provided. Readers should note that a basic familiarity with the general process of coal gasification is assumed in the sections that follow.

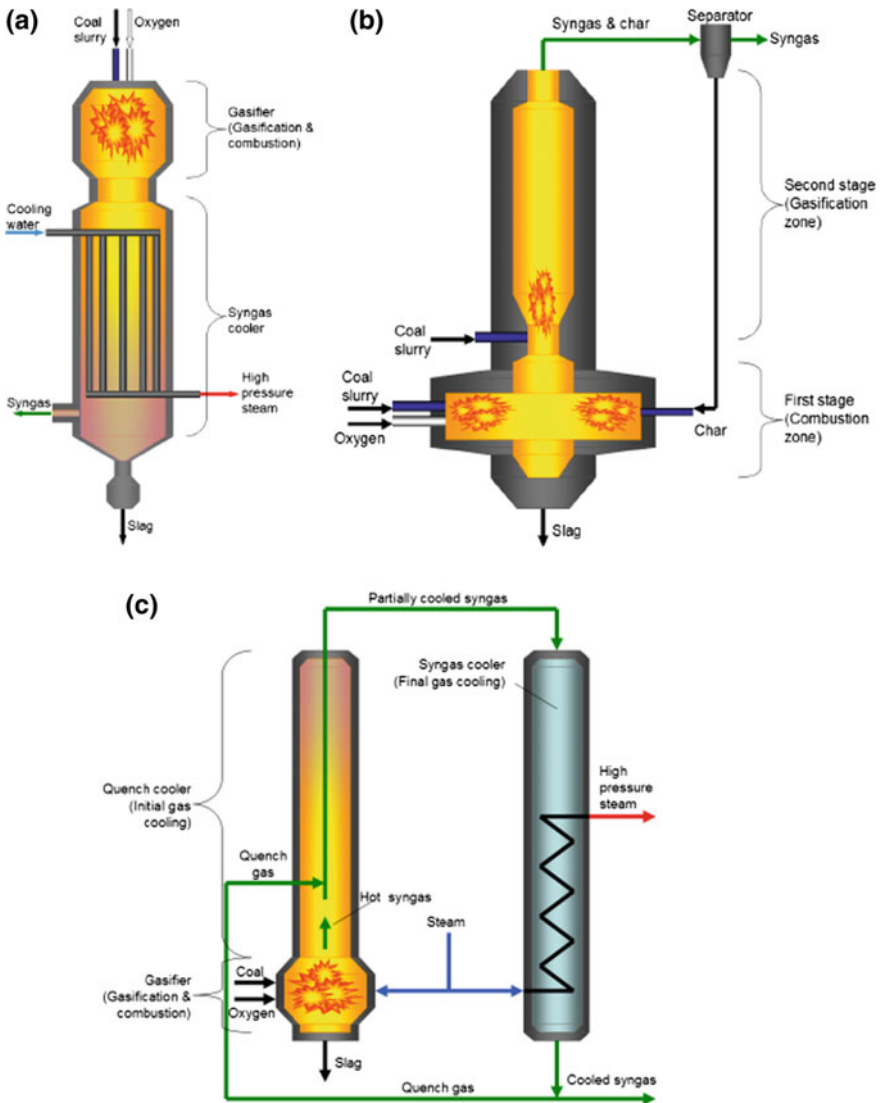


Fig. 1 a GE (radiant), b CoP E-GAS, and c SCGP (Shell) gasifiers

2 Commercial Entrained Flow Gasifiers

A variety of commercial entrained flow gasifier designs is available in market today. Table 1 lists some of the most frequently deployed gasifiers around the world. They include the General Electric (GE), Shell, Mitsubishi Heavy Industries (MHI), Siemens, CB&I E-Gas, and the PRENFLO gasifier. Some of the

Table 1 Major commercial entrained flow gasifier designs [1]. Acronyms: RL—refractory lining, MW—membrane wall, WW—water-cooling wall

Manufacturer	Coal feeding	Oxidant	Wall	Flow-direction
SHELL	Dry	O ₂ -blown	RL and MW	Up
SIEMENS	Dry	O ₂ -blown	RL/MW	Down
CB&I E-GAS	Slurry	O ₂ -blown	RL	Up
PRENFLO PSG	Dry	O ₂ -blown	MW	Up
PRENFLO PDQ	Dry	O ₂ -blown	MW	Down
GE (Texaco)	Slurry	O ₂ -blown	RL	Down
MHI	Dry	Air-blown	MW	Up
ECUST	Slurry/Dry	Air/O ₂ -blown	RL/MW/WW	Down
HCERI	Dry	O ₂ -blown	WW	Up
MCSG	Slurry	O ₂ -blown	Not known	Down
Tsinghua OSEF	Slurry	O ₂ -blown	MW/WW	Down

indigenously developed gasifiers in China also have significant deployment, albeit within the country, and will be discussed in Sect. 2.2.1.

Most of the entrained flow gasifiers can be operationally classified into the following categories, as also shown in Table 1:

- 1. Dry fed versus slurry fed:** The MHI, Siemens, Shell, and PRENFLO gasifiers use dry feeding of powdered coal, whereas the GE, E-Gas, ECUST, and Tsinghua OSEF gasifiers operate on coal-water slurry (CWS) feed. Coal-water slurry is prepared by wet grinding the coal in a rod mill [2]. Coal is delivered by a conveyer into the rod mill feed hopper. The coal has to be grounded to the right particle size and size distribution in order to form a stable coal/water slurry at optimum slurry solids concentration, which is typically about 60–65% by weight [2]. Slurry feed has the disadvantage of losing a portion of the produced sensible heat on the vaporization of the slurry. Consequently, a higher percentage of oxygen is needed in order to attain the desired temperatures in the gasifier, resulting in a lower overall plant efficiency. CWS feeding is especially uneconomical for low-rank coals that already contain significant amount of moisture. Dry feeding system is preferred for the high moisture content coals. The dry feed systems use a lock hopper operating in a batch mode, intermittently charging coal fines into the pressurized gasifier via staged opening and closing of valves on the top and bottom of the pressure vessel [2]. Lock hoppers as used in the dry-coal fed gasifiers are costly and bulky equipment with complex valve systems that have to provide a gas-tight block in a dusty atmosphere [3]. Consequently, the lock-hopper system operates at lower pressures as compared to the CWS feed, resulting in a lower thermodynamic efficiency for the overall

plant. The practical pressure limit for lock hoppers is about 50 bars, whereas for CWS pumps the pressure could, in principle, be as high as 200 bar [3].

In effect, the choice of the coal feeding system depends upon the properties of the available feedstock as well as the requirements driven by the overall plant operating conditions. Alternative feeding strategies are also being developed in order to get over the disadvantages of both the feeding approaches described above. A phase-inversion-based coal-CO₂ slurry (PHICCOS) feeding system has been proposed that takes advantage of the availability of super-critical CO with liquid-like properties [4]. It operates at ambient temperature, without the use of lock hoppers and can achieve very high pressures. Furthermore, the feeding system inherently reduces the moisture and ash content of the feedstock, which makes it especially attractive for low-rank and high-ash coal.

2. **Air-blown versus oxygen-blown:** The majority of the present-day commercial entrained flow gasifiers are oxygen-blown. The air-blown MHI gasifier is a notable exception. Coal-water slurry feed systems have to typically go with oxygen-blown gasifiers in order to generate sufficient sensible heat for the evaporation of the slurry water. Moreover, oxygen-blown operation results in an undiluted stream of carbon dioxide as the effluent making the process amenable to carbon capture and sequestration (CCS). There are other advantages of oxygen-blown operation as well, namely:
 - a. Reduction in the gasifier size and all other equipment by at least 75% owing to the absence of nitrogen in the stream
 - b. Reduction in the total amount of heat lost in the flue gas
 - c. Facile removal of pollutants from the flue gases owing to their enhanced partial pressure
 - d. Latent heat of condensation can be recovered by opting for pressurized operation, as discussed next
 - e. Significant reduction in the formation of the oxides of nitrogen
3. **Refractory wall-lining versus Membrane wall versus Water-cooled wall:** Moving to membrane wall or water-cooled wall offers the advantage of not having the peak reactor temperature limited by the refractory material.
4. **Pressurized versus atmospheric pressure operation:** Although gasifiers conventionally used to operate at atmospheric pressure, present-day entrained flow designs are invariably pressurized, operating up to 40 bars and beyond. Pressurization considerably reduces the reactor size across the plant and is also beneficial for the removal of pollutants owing to their resultant higher partial pressure. The pressurized flue gas stream provides for a plant that is 'capture-ready' for CO₂ sequestration. Moreover, pressurized oxy-coal combustion has the advantage of recovering much of the latent heat of vaporization of the water vapor in the flue gas, resulting in an increase of several percentage points in the plant efficiency. This is because the elevated flue gas pressure raises the dew point and the available latent enthalpy in the flue gases [5].

2.1 IGCC Demonstration Projects

Integrated gasification combined cycle (IGCC) plants combine high-pressure coal gasification with combined cycle power generation, i.e., employing gas turbine to burn the produced syngas along with a steam turbine as the bottoming cycle. IGCC projects are often accompanied with air separation units (ASUs) and oxygen-blown gasifiers so that a pure stream of carbon dioxide can be captured from the flue gases and buried deep below the earth, or used for enhanced oil recovery (EOR), the process being termed as carbon capture and sequestration (CCS). IGCC with CCS was until recently hailed as a major solution to the global environmental challenge of curbing the CO₂ emissions from coal plants. Almost all of the IGCC demonstration projects around the world have been conducted using entrained flow gasification technology. The list of some of the major IGCC projects to-date, starting from the 1980s, is provided in Table 2.

However, the development of IGCC as the pioneering clean-coal technology has suffered recent drawbacks. Some of the later IGCC demonstration plants have run into legal issues with their respective states' key consumer groups related to their ever-increasing operating costs and low availability. For example, Duke Energy's Edwardsport plant was originally slated to cost \$1.9 billion, but the costs had risen to \$3.5 billion in 2016 [7]. Under a settlement reached in the January of the same year, Duke Indiana agreed to refund customers \$87.8 million and also agreed to provide \$500,000 to fund solar installations. The plant was often operating at less than 50% of its capacity after going commercial in 2013 [7].

The Kemper County IGCC project was a first-of-a-kind electricity plant to employ gasification and the capability to capture and store CO₂ emissions, although

Table 2 Commercial-size IGCC plants using entrained flow gasification [6]

Project name and location	Gasification technology	MW (gross)	Startup date
Cool water, Mojave, CA, US	Texaco (GE)	120	1984
SEP-Demkolec, Buggenum, Netherlands	Shell	253	1994
Wabash River, West Terre Haute, IN, US	Destec	296	1995
Tampa Electric, FL, US	Texaco (GE)	312	1996
ELCOGAS, Puertollano, Spain	Krupp-Uhde PRENFLO	335	1997
ISAB Energy, Sicily, Italy	Texaco (GE)	512	2001
Sarlux, Sardinia, Italy	Texaco (GE)	548	2000
API Energia, Falconara, Italy	Texaco (GE)	280	2001
Duke Energy, Edwardsport, IN, US	GE	618	2013
GreenGen, Tianjin, China	HCERI	250	2018 (Est)
Nakoso IGCC, Nagasaki, Japan	MHI	540	2020 (Est)

based on the fluidized-bed technology for the low-rank Mississippi lignite. Again, the problems hampering the Kemper IGCC project were symptomatic of the other recent IGCC demonstration projects in the US and Europe. Since IGCC with carbon capture is not yet a proven technology, many of the design specs often need changes, delaying the project. One design flaw miscalculated pipe thickness, length, quantity, and metallurgy. After these changes were made, additional changes needed to be done to support structures [8]. The problems get compounded when dealing with high-ash coals—for example, clinker formation is often encountered on the gasifier walls. Nonetheless, Kemper IGCC started generating electricity from gasified lignite from early 2017 [9].

GreenGen is another significant IGCC with carbon-capture project, envisioned by the China Huaneng group along with the Mississippi-based Peabody Energy, and located in Tianjin, China. The project plans to use a novel entrained flow gasifier designed by the Thermal Power Research Institute (TPRI) in Xi'an, China [10]. Apart from generating power, the plant is also slated to supply heat and syngas to neighboring chemical plants. However, the GreenGen project also has been beset by multiple delays in its 10-year history and was scaled back [11].

2.2 Entrained Flow Gasification for Coal-to-Chemicals

With the solar tariffs going southward for some time in the past and expected to follow the same trend in the foreseeable future, it is going to be tougher for IGCC to make economic sense. Coal-to-chemicals, on the other hand, can be the thing of the future—at least for countries like China and India.

2.2.1 Developments in China

Coal is recognized as a significant part of China's energy strategy going forward. The GE, Shell, Siemens are some of the international origin gasifiers that have been used in China since the 1980s. Moreover, the Chinese Government actively supports coal gasification-related research programs at universities and research institutions. As a result, seven major Chinese universities, corporations, and institutes have successfully commercialized a number of different indigenous gasifier designs. These gasifiers and gasification technologies are being used in over 100 different projects [12]. Most of the gasifiers are employed for coal-to-chemicals projects, including production of ammonia, methanol, dimethyl ether, liquid fuels, hydrogen. Two of the most popular gasifiers are briefly described below:

A. East China University of Science and Technology (ECUST) Gasifier

The ECUST gasifier employs the so-called opposed multiburner (OMB) gasification technology developed at ECUST. The gasifier features four burners located

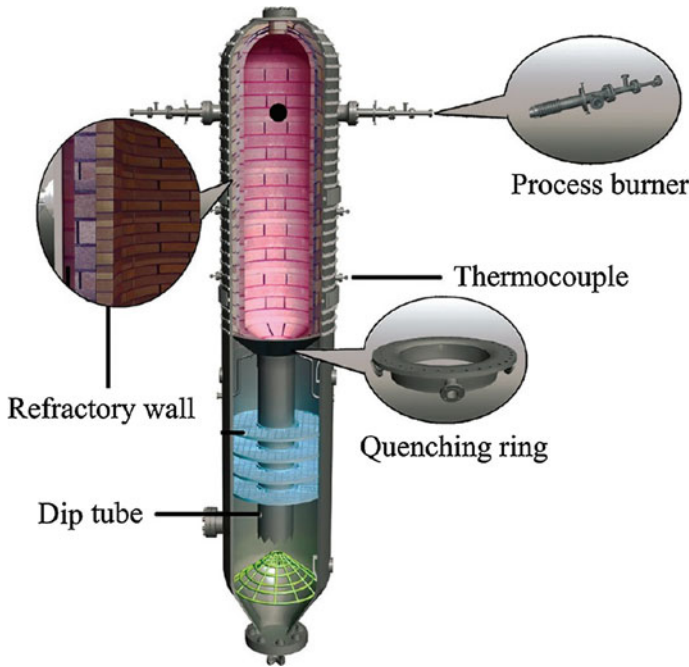


Fig. 2 ECUST opposed multiburner (OMB) slurry gasifier [13]

around the top of the gasifier spaced at 90° intervals from each other forming two pairs of opposed burners. This configuration permits equal, flexible control of large amount of coal slurry, and the impinging flow facilitates mixing of reactants [2]. This is an oxygen-blown gasifier with both dry and wet feeding possible. Thirty-one coal projects have been identified in China that utilize an estimated total of 88 ECUST OMB gasifiers having coal feeding capabilities ranging from 750 to 3000 tons per day [2] (Fig 2).

B. Tsinghua OSEF Gasifier

The oxygen-staged entrained flow (OSEF) gasifier is a product of the R&D conducted at the Tsinghua University’s Institute of Thermal Engineering. As the name suggest, the gasifier employs staged addition of oxygen which has been reported to enhance the life of the main burner [2]. The gasifier utilizes coal slurry feed in a membrane-wall design, which is reported to result in increased flexibility in coal feedstocks, operational stability, high-pressure gasification, and reduced capital costs [12]. As of 2013, sixteen projects had been licensed using the OSEF gasifier.

A recent review study of the Chinese coal utilization activity established that currently eight international and seven Chinese licensors of coal gasification technology have successfully commercialized their operations [12].

2.2.2 Developments in India

Coal gasification developments in India have been greatly subdued when compared to the frenzy in China. At the same time, there is the realization that coal-to-chemicals might be a better coal utilization strategy than coal-to-power via IGCC [14]. There are only a couple of projects worthy of mention at this point. The first one is the Reliance Industries Limited (RIL) petcoke gasification project, which is a part of its refinery complex in Jamnagar, often stated as the largest in the world. The plant uses ten units of E-GAS entrained flow gasifiers to convert blends of petcoke and imported coal into syngas. The syngas is used to power existing refinery heaters and gas turbines, produce hydrogen for the refinery and carbon monoxide for a new acetic acid plant [15].

The country's maiden fertilizer project based on coal converted to syngas has been recently kicked off after some delay at Talcher, Orissa. The plant would utilize Shell's entrained flow gasification technology and is slated to gasify a mix of high-ash local coal with as much as 25% petcoke [16]. The project is a joint venture between several public sector companies in the coal and fertilizers sector. It should be noted that indigenous gasification technology development is significantly muted in India, as compared to China.

3 Modeling Entrained Flow Gasification

The design of coal combustion and gasification systems has long been an experience-based enterprise. However, the advent of supercomputing has opened up options to create high-resolution and high-fidelity models of the various stages of the coal utilization process. In particular, modeling of the entrained flow gasifier requires understanding of a wide range of physicochemical phenomena including heterogeneous chemistry, mechanics of turbulent swirling flows, turbulence-chemistry interactions, radiative heat transfer, reaction and transport within the porous char particle. A detailed CFD model of entrained flow gasification is indeed what is needed to capture these phenomena in the requisite detail. The CFD model attempts to capture this detail through relevant submodels and their coupling. The modular structure of a CFD model, along with the interactions between various modules, is represented in the block diagram in Fig. 3 [17]. It is important to carefully construct and validate the most important building blocks of the integrated model in order to accurately predict some of the overall metrics of gasifier performance, like fuel conversion and syngas composition.

The gas-phase is typically solved using the discretized mass, momentum, energy, and species conservation equations. The approach is pretty generic, having been successfully implemented multiple times in gasification CFD modeling

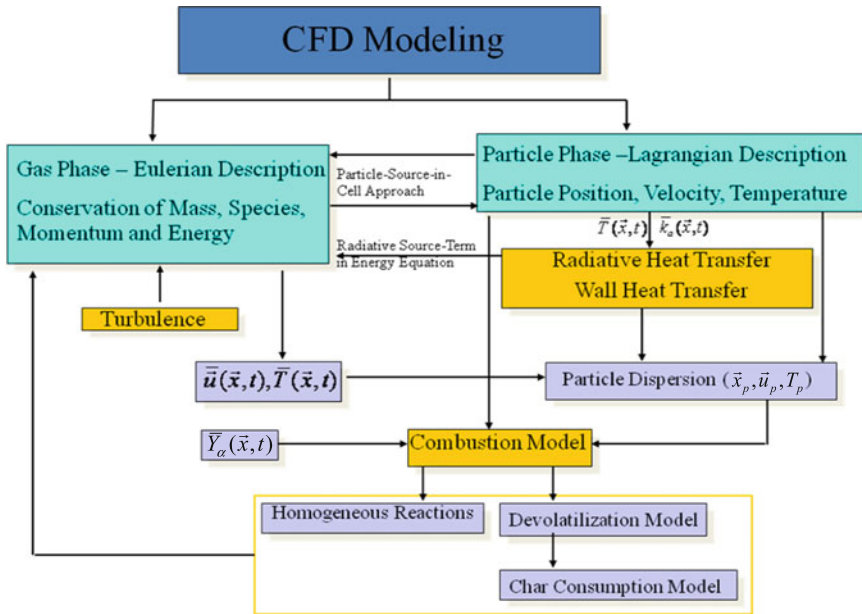


Fig. 3 Block diagram representing components of a CFD model of entrained flow gasification and their interactions [17]

[18–25] and does not need re-iteration. While the gas-phase is solved in a Eulerian fashion, the particle-phase lends itself better to the lagrangian tracking methodology. Many of the details of the particle solution approach are quite specific to entrained flow coal gasification, and therefore need special treatment. These details are described in the next section. Apart from the particle-phase model, radiation heat transport is another physical model that is quite important to construct accurately while modeling entrained flow gasification, and is therefore described briefly in Sect. 3.2.

3.1 Particle-Phase Modeling Methodology

A representative number of ‘computational’ particles is tracked through the domain, and the inter-phase exchange terms are tracked as the particles cross individual Eulerian cells. These exchange terms are then added to the gas-phase conservation equations to model the impact of the particles on the gas-phase. This is termed as the particle-source-in-cell approach [26].

The lagrangian modeling of the particle phase merits some attention. The governing equations for mass, momentum, energy along with the commonly used correlations for drag and Nusselt number are provided in Table 3. Equation (1)

Table 3 Particle-phase conservation equations

Mass	$\frac{dm_p}{dt} = \frac{dm_{C-O_2}}{dt} + \frac{dm_{C-CO_2}}{dt} + \frac{dm_{C-H_2O}}{dt} + \frac{dm_{devol}}{dt} + \frac{dm_{vapor}}{dt}$ (1)
Momentum	$\frac{du_p}{dt} = F_D(u - u_p) + \frac{g_i(\rho_p - \rho)}{\rho_p} + F_i$ (2)
Drag	$C_D = a_1 + \frac{a_2}{Re_p} + \frac{a_3}{Re_p^2}$, $Re_p = \frac{\rho d_p u - u_p }{\mu}$, $F_D = \frac{18\mu C_D Re_p}{\rho_p d_p^2}$ (3)
Energy	$Q_G = \frac{dm_{C-O_2}}{dt} H_{C-O_2} + \frac{dm_{C-CO_2}}{dt} H_{C-CO_2} + \frac{dm_{C-H_2O}}{dt} H_{C-H_2O}$ $m_p c_p \frac{dT_p}{dt} = h_p A_0 (T - T_p) + \frac{\varepsilon_p A_0}{4} (G - 4\sigma T_p^4) + Q_G$ (4)
Nusselt number	$Nu = \frac{h_p d_p}{k_g} = 2.0 + 0.6 Re_p Pr^{1/3}$ (5)

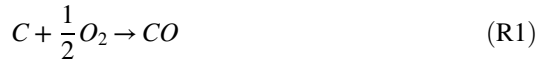
denotes that the net rate of change of the particle mass is given by summing up the contributions from the water vapor loss and devolatilization, as the particle enters the high-temperature environment, followed by the contributions from the heterogeneous combustion and gasification reactions. The energy equation is also of note—it stipulates that the net rate of change of the particle internal energy is arrived at by accounting for the heat loss through forced convection and radiation along with the heats of reaction associated with the individual gasification reactions. Note that the treatment of convective heat loss is tailored to prevent forming a system of coupled ODEs to solve for the particle temperature and burning rate. More elaborate treatments can be found [27, 28] that lead to the solution of coupled ODEs at each particle-phase iteration or time-step.

3.1.1 Devolatilization

As discussed in the preceding section, the coal particle first releases moisture and volatiles as a result of temperature rise following injection in the gasifier. A popular model used to describe the devolatilization rate is the CPD model [29], which predicts the rates based on the band-energies and crosslinking in the lattice structure of the parent coal. This model predicts the amount of volatiles released, but the volatile species composition is not specified. The same is true for other models such as the two-competing rates Kobayashi model [30], which empirically determines the devolatilization rates through two different relations at high and low temperatures. However, knowledge of the total devolatilization rates is not sufficient in the context of coupled CFD simulations; a quantitative description of the devolatilization product composition is also needed. The devolatilization product composition determines the reactions and hence the temperature in the near-burner region and the product composition at the gasifier exit. Experimental studies, specific to the coals of interest, such as Ref. [31] are needed to determine the total volatile yield and product composition as a function of the heating rates, temperatures, and times.

3.1.2 Char Consumption

Following devolatilization and vapor loss, coal particles lose mass via the heterogeneous reactions, as described by Eq. (1). This loss of fixed-carbon by the particle via reaction with gas-phase reactants, namely O_2 , CO_2 , H_2O is referred to as ‘char consumption’ in this chapter.



Char consumption is a cumulative effect of three separate physical and chemical processes: diffusion through the boundary layer and char porous structure, heterogeneous kinetics, and char structure/surface area evolution. The overall process can be represented as a resistance network comprised of kinetic and diffusion resistances. The resultant char consumption rate, \dot{m}_p , due to heterogeneous reaction with a gas-phase reactant of partial pressure P_g , where m_p is the particle mass and t is the time, is given by [32, 33]

$$\dot{m}_p = \frac{P_g}{\frac{1}{k_d} + \frac{1}{k_s}} \quad (6)$$

$$k_d = A_0 \cdot A_d \left(\frac{T_g}{2000} \right)^{0.75} / (P d_p) \quad (7)$$

where k_d and k_s are the rate constants for diffusion and kinetics, respectively. P_g is the bulk partial pressure of the particular gas-phase reactant, such as O_2 , CO_2 , or H_2O . A_0 is the external surface area of the particle. The diffusion constant A_d depends on the particular gasification reaction being considered. d_p is the particle diameter and T_g is the gas temperature. P is the total gasifier pressure and R is the universal gas constant.

Equation (6) can be interpreted in a variety of ways, depending upon the particular description of the kinetics coupled with the surface area evolution via the parameter k_s . For example, if heterogeneous reaction is assumed to occur only at the external surface of the particle, Eq. (6) represents a kinetics/diffusion *fixed-core model*, which is the default char consumption model in Fluent. The model is schematically depicted in Fig. 4. These models have routinely been used in CFD simulations of entrained flow gasification [18, 19, 21]. The reaction surface is assumed to be at a fixed radius, coinciding with the original surface area, A_0 . The model typically employs nth order Arrhenius kinetics, with $n = 1$, to model k_s .

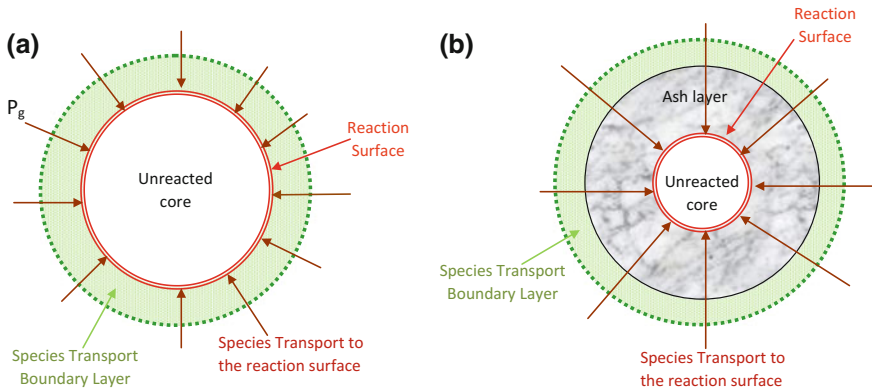


Fig. 4 Schematic of **a** kinetics/diffusion fixed-core model, and **b** shrinking core model (SCM)

$$k_s = A_0 \cdot A_s \exp(-E_s/RT) \quad (8)$$

The *shrinking core model* (SCM) [23] is a more accurate alternative that has been used to model char consumption in entrained flow gasification [20, 24, 25]. Apart from the Arrhenius kinetics and the film diffusion effects, the model accounts for the reduction in the char core radius as conversion proceeds. The effect of diffusion through the surrounding ash layer is also incorporated. The reaction occurs at the surface of the inner shrinking core. The resulting char consumption rate is given by

$$\dot{m}_p = \frac{P_g}{\frac{1}{k_d} + \frac{1}{k_s (r_p/R_p)^2} + \frac{1}{k_{dash} \left(\frac{R_p}{r_p} - 1\right)}} \quad (9)$$

$$k_{dash} = k_d \varepsilon^{2.5} \quad (10)$$

k_{dash} is the ash diffusion constant. ε is the voidage of the ash layer, defined as the ratio of the void space to the total volume in the ash specimen. r_p is the instantaneous radius of the shrinking core. R_p is the fixed radius of the char-ash complex, same as the original radius of shrinking core. A schematic of the SCM is shown in Fig. 4.

The *random pore model* (RPM) [34] offers a more detailed treatment of the reactive surface area during char conversion than SCM. The evolution of the internal surface area during char conversion is expressed as

$$\frac{S}{S_0} = (1-x) \sqrt{1-\psi \ln(1-x)} \quad (11)$$

where x is the conversion fraction and ψ is the structure parameter for the particular coal/char type. S is the instantaneous total internal reactive area (cm^2/g) of the porous char particle as opposed to the external surface area used by the previous models. S_0 is the initial internal reactive area. The expression is derived by employing detailed physics of the evolution of the porous structure of a reacting char particle and should be contrasted with the shrinking core model, which gives a surface area evolution of the form $\frac{A}{A_0} = (1-x)^{2/3}$, where A is the instantaneous surface area of the shrinking core. Coupling surface area evolution using RPM with Arrhenius kinetics, the kinetics parameter k_s can be represented as:

$$k_s = m_{po} S \cdot A_s \exp(-E_s/RT) \quad (12)$$

where m_{po} is the original char mass in the particle. In the next section, more accurate descriptions of heterogeneous reaction, than Arrhenius kinetics, are discussed. Lately, RPM is being increasingly used in entrained flow gasification CFD studies to describe particle structural evolution [17, 22, 35, 36].

3.1.3 Heterogeneous Kinetics

An outstanding lacuna in much of the entrained flow gasification CFD literature is that Arrhenius rate expressions are still being employed to model the kinetics, even at elevated pressures. It is generally accepted that the n th order equation may be inaccurate in modeling the pressure-dependence of gasification kinetic rate expressions and gasification kinetics are better represented by Langmuir–Hinshelwood (LH) type rate expressions for char- CO_2 and char- H_2O reactions [37–41] For char- CO_2 reaction, the LH kinetic rate, R_{LH} , can be expressed as:

$$R_{LH} = \frac{k_1}{1 + k_2 P_{\text{CO}_2} + k_3 P_{\text{CO}}} \quad (13)$$

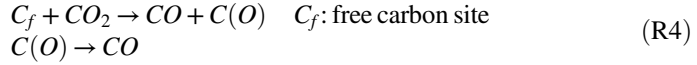
where k_1 , k_2 , k_3 are Arrhenius-type constants. Similar equations are written for the char- O_2 and char- H_2O reactions. In conjunction with the RPM, the char consumption rate for the char- CO_2 reaction, assuming complete kinetic control, can be written as

$$\dot{m}_p = k_s P_g = R_{LH} m_{po} S P_g \quad (14)$$

It is also useful to write the char consumption rate under complete diffusion control.

$$\dot{m}_p = P_g k_d \quad (15)$$

The formulation in Eq. (13), after extensive derivation [42] is consistent with the following reaction steps:



Since the LH mechanism accounts for the fundamental heterogeneous kinetic processes of adsorption and desorption, the LH-type rate expression is found to be better for the gasification reactions than an nth order Arrhenius-type rate expression. The gasification rate for char- CO_2 reaction, when experimented upon in the kinetics-limited regime at temperatures up to 1500 K, has been found to increase with the partial pressure of CO_2 up to a point and then remain constant. An LH-type relation models such behavior much better than an nth order one. The $k_3 P_{CO}$ term in (13) pertains to the inhibition in the gasification reaction due to saturation of the char activated surface by CO at high CO partial pressures.

Several variations of the LH mechanism exist in the literature, aimed toward capturing the physics of the heterogeneous reactions better. For example, in one study a modified nth order LH relation was observed to perform better than the first-order LH relation [43].



$$R_{C-O_2} = \frac{k_{ads} P_{O_2, s}^n}{1 + (k_{ads}/k_{des}) P_{O_2, s}^n} \quad (16)$$

Here n can be thought of as the order of the adsorption step in reactions (R6).

More sophisticated rate expressions are also available [38, 39] referred to as the semi-global models, which take into account, to various degrees, the possible adsorption and desorption sub-steps of intermediate complexes for the particular heterogeneous reactions. For example, in Ref [38].

$$\begin{aligned} R_{C-CO_2} &= - \frac{k_7 k_4 P_{CO_2}}{k_7 + \gamma k_4 P_{CO_2} + \gamma k_4' P_{CO} + k_4 P_{H_2O} + k_6' P_{H_2}} s^{-1} \\ R_{C-H_2O} &= - \frac{k_7 k_6 P_{H_2O}}{k_7 + \gamma k_4 P_{CO_2} + \gamma k_4' P_{CO} + k_4 P_{H_2O} + k_6' P_{H_2}} s^{-1} \end{aligned} \quad (17)$$

Very few researchers working on CFD modeling of entrained flow gasification have employed the LH-type relations [16, 35]. A possible reason is the absence of the relevant kinetics data for the particular coal—since performing the requisite experimentation and fitting the data to LH kinetics are more involved and rarer to find in the open literature as compared to simple Arrhenius kinetics.

The discussion so far still ignores the pore diffusion effects within the particle and assumes a constant reactant concentration inside the particle. The model could be improved to include pore diffusion effects by incorporating an effectiveness factor η ,

derived by solving a reaction–diffusion equation within the particle [44] and coming up with a correction factor. In spherical coordinates, η can be expressed as:

$$\eta = \frac{1}{\theta} \left(\frac{1}{\tanh(3\theta)} - \frac{1}{3\theta} \right) \tag{18}$$

$$\theta = \frac{r_p}{3} \sqrt{\frac{\nu_o k_1}{2D_e} \frac{k_2 P_g}{1 + k_2 P_g} (k_2 P_g - \ln(1 + k_2 P_g))^{-1/2}}$$

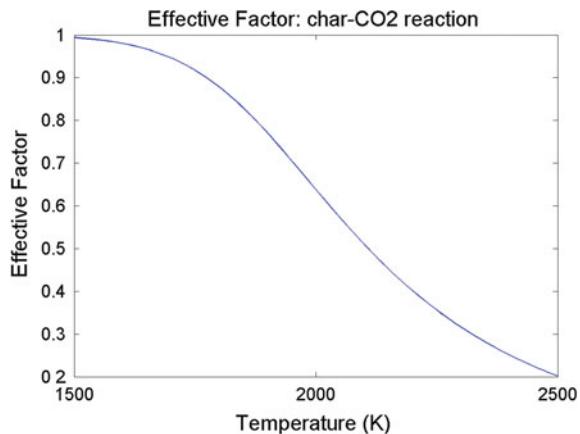
where k_1, k_2 are the corresponding constants in the LH reaction rate expression (13), ν_o is the stoichiometric coefficient for the particular gasification reaction, and D_e is the internal particle diffusivity.

There are several references in the literature to this kind of pore diffusion correction [45, 46] essentially by researchers investigating single particle gasification. Again very few studies to-date have incorporated the impact of this effectiveness factor calculation on CFD modeling of entrained flow gasification [17, 35]. Figure 5 shows the variation of η for char-CO₂ reaction with reaction temperature for a particle of mean diameter in our gasifier. η varies from 0.2 to 1 as generally reported in the literature [45, 46].

3.1.4 Single Versus Two-Film Model of Char Burning

With regard to modeling the transport and homogeneous reactions within the boundary layer of the char particle, broadly two approaches are found in the literature. The first approach, namely the single film model described by Eqs. (6)–(8), is routinely employed in gasification studies in the literature [18–22, 47, 48] As depicted in Fig. 6a, the single film model [49] assumes that although CO and O₂ are present simultaneously in the boundary layer around the particle, they do not react with each other. CO and O₂ are allowed to react only after they diffuse out of the boundary layer. To the contrary, the double-film model [49], as shown in Fig. 6b,

Fig. 5 Variation of effectiveness factor with temperature [17]



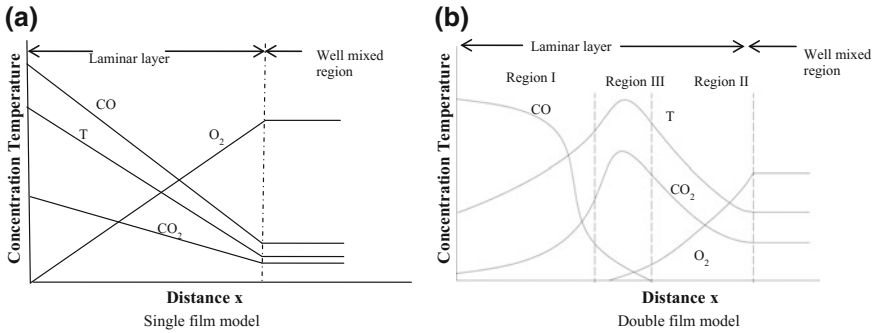


Fig. 6 a Single film and b double-film models of char consumption [49]

allows CO and O₂ to react in a diffusion flame in the boundary layer to yield CO₂ which then diffuses on one side toward the particle and on other side into the well-mixed region.

The most accurate method of predicting char consumption rate would involve solving the complete set of reaction–diffusion equations throughout the particle and into the boundary layer. Such calculations [17] indicate that reality is much closer to the double film than the single film model, as indicated in Fig. 7. The results indicate that homogeneous reactions do occur in the boundary layer and there seems to be a flame-zone outside the particle where both CO and O₂ mol fractions tend to

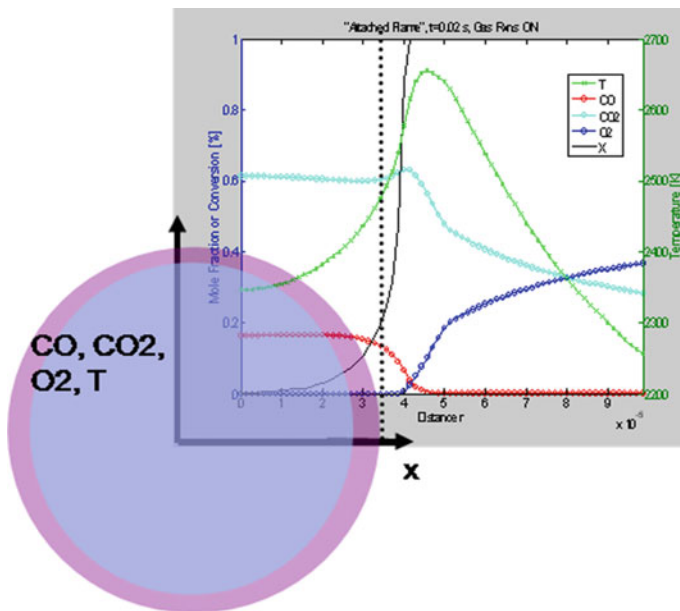


Fig. 7 Continuous film model [17]

zero and the temperature profile attains a peak. However, the double-film model has not been employed in CFD models of combustion or gasification because, depending on the assumptions, it requires the solution of a system of coupled algebraic equations, if not coupled PDEs. Solving PDEs for each tracked particle can be computationally prohibitive for well-resolved CFD model of any commercial or pilot-scale gasifier.

However, using a set of simplifying assumptions, Zhang et al. [50, 51] have proposed the moving flame front (MFF) model of char consumption, reducing the set of governing equations such that it can be adapted to CFD model without significant computational expanse. The location of the flame sheet, where oxidation of CO occurs in the boundary layer, and consequently the char consumption rate can be evaluated as explicit functions of various kinetic and diffusion rates involved. The key assumption involves neglecting the gasification reaction with CO₂ in presence of oxygen since the oxidation reaction with O₂ is much faster. The location of flame sheet dynamically adjusts so that equilibrium is approached at the fastest possible rate. The expressions for the net burning rate and location of the flame front are too complicated [51] to be presented here but can be incorporated into custom codes or into commercial solvers using user-defined subroutines.

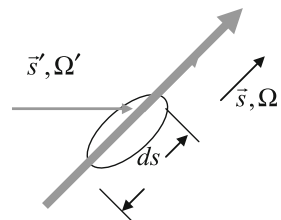
3.2 Radiative Heat Transport in Entrained Flow Gasifiers

Radiation is the primary mode of heat transport in furnaces such as entrained flow gasifiers, where the length scale is of the order of 1 m [52]. For example, the CFD simulations of the MHI gasifier in Ref [17] predicted that radiation flux is greater than 60% of the total power received by the wall. In effect, radiation significantly impacts the overall heat transfer process, hence the fluid dynamics and the reaction rates, and is also critical in solving the particle temperature via Eq. (4).

The radiative transport equation (RTE) (19, Fig. 8) needs to be solved in order to provide the irradiation term, G , in the particle energy Eq. (4), and to also close the radiation term in the gas-phase energy balance.

$$\frac{dI}{ds} = -(k_a + k_s)I + k_a \frac{\sigma T_b^4}{\pi} + \frac{k_s}{4\pi} \int_{4\pi} \Phi(\vec{s}, \vec{s}') I(\Omega') d\Omega' \tag{19}$$

Fig. 8 Radiative transfer equation



This equation is derived for a pencil beam of radiation traveling in a direction \vec{s} , with local intensity $I(\vec{x}, \Omega)$. k_s is the scattering coefficient, k_a is the absorption coefficient, I_b is the black-body intensity, and $\Phi(\vec{s}, \vec{s}')$ is the scattering phase function from a direction \vec{s}' to the direction \vec{s} of the beam of interest.

G is the local irradiation defined in terms of I as:

$$G = \int_{4\pi} I(\Omega') d\Omega' \quad (20)$$

In a two-phase reacting flow situation like entrained flow gasification, k_a and k_s include contributions from both gas and particle phases. However, in such an optically thick medium as the entrained flow gasifier, contribution from the particle-phase far outweighs that from the gas-phase [17]. While the weighted-sum-of-gray-gases method is used to evaluate gas-phase radiative constants, the particle-phase values can be expressed in terms of the number of particles N_p within a control volume (ΔV), particle emissivity, ε_p , and particle external surface area, A_0 , as follows:

$$k_p = \sum_p \varepsilon_p A_0 \frac{N_p}{\Delta V} \quad (21)$$

$$k_{sp} = \sum_p (1 - \varepsilon_p) A_0 \frac{N_p}{\Delta V} \quad (22)$$

where k_p and k_{sp} are the contributions of the particle phase to the absorption and the scattering coefficients, respectively, and the summation is conducted over all the particles present in the control volume. Thus, the same intensity field calculated via Eq. (19) contains all the information of radiation due to the gas-phase as well as the particle-phase emission, absorption, and scattering. This is quite different from the conservation equations of mass, momentum, species, and energy which are written separately for the gas-phase and the particle phase.

The 'finite volume method' (FVM) for radiation, or the discrete ordinates method (DOM) is typically used to solve the radiative transport Eq. (19) in conjunction with a CFD model. In FVM, the RTE, which is fundamentally derived along a beam of radiation, is adapted to the finite volume formulation. The adaptation is achieved by writing the RTE for M (say) discrete directions for each control volume. Subsequently, we have M -coupled transport equations for the directional radiative intensities I^m . These transport equations are solved through the domain along with the rest of the gas-phase transport equations.

3.2.1 Radiative Heat Transfer at the Wall

As mentioned in the previous section, radiative heat transport is expected to be a significant portion of the total wall heat flux in entrained flow gasifiers. The incident

radiative flux at the wall, q_{in} , is an important output of the RTE solution and is evaluated through a first moment of radiative intensity as follows:

$$q_{in} = \int_{\vec{s} \cdot \vec{n} > 0} (\vec{s} \cdot \vec{n}) I(\Omega) d\Omega \quad (23)$$

where \vec{n} is the outward wall normal. The emitted heat flux from wall, q_{out} , can be calculated as:

$$q_{out} = \sigma \varepsilon_w T_w^4 + (1 - \varepsilon_w) q_{in} \quad (24)$$

$$I_{out} = \frac{q_{out}}{\pi}$$

where ε_w is the wall emissivity, T_w is the wall temperature, and I_{out} is the radiative intensity leaving the wall. I_{out} is used as the boundary condition in the solution of RTE. For a gray wall ($\varepsilon_w < 1$), the emitted radiation depends on the incoming radiation which in turn depends on the calculated intensity field available only after solving the RTE. Hence in the presence of gray walls, the solution is inevitably iterative.

3.3 Application of the CFD Model

The complete CFD model constructed by integrating the various submodels can subsequently be utilized to perform sensitivity analysis in order to ascertain the impact of various operating conditions as well as to validate the choice of the particular submodel over the competing ones. The latter aspect is elaborated here by taking the example of the turbulence model. Subsequently, the utility of a validated CFD model in predicting the optimal operating of an entrained flow gasifier is discussed.

3.3.1 Impact of the Turbulence Model

The choices available within the RANS methodology include the standard k- ε , realizable k- ε , standard k- ω , SST k- ω , RNG k- ε , and the RSM models among others. There is no clear consensus yet within the gasification modeling community as to which RANS model performs the best. This is perhaps owing to the heuristic nature of these models. For example, one study found the standard k- ε , SST k- ω , and the RSM to give consistent and similar results for a generic two-stage entrained flow gasifier, whereas the standard k- ω and the RNG k- ε models deviated from the consistent trends [53]. Even within the three models that gave consistent results, there were noticeable differences in their predictions above and below the coal injector.

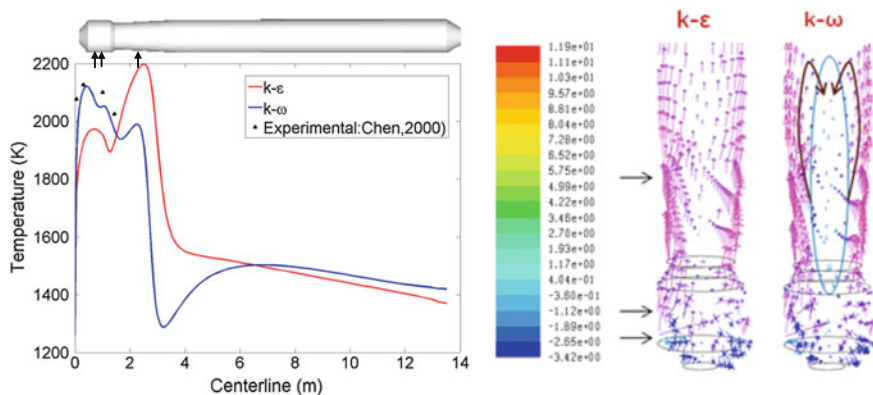


Fig. 9 Comparison of the standard $k-\epsilon$ and the SST $k-\omega$ turbulence models. Note the small, but negative velocities predicted along the gasifier axis by the SST $k-\omega$ model

Another study reported the SST $k-\omega$ to perform better than the standard $k-\epsilon$, realizable $k-\epsilon$, and the standard $k-\omega$ counterparts in modeling the pilot-scale two-stage MHI gasifier [17]. The SST $k-\omega$ matched the experimental data along the gasifier centerline better than others and was successful in predicting the expected recirculation zone along the gasifier centerline. The results are shown in Fig. 9.

Large eddy simulations (LES) are expected to provide better results of the gasification process and their usage is expected to increase in the future owing the growing access to supercomputing facilities. For example, Abani et al. [54], compared LES and RANS result while modeling the BYU laboratory scale gasifier and reported significant differences in mixing, combustion and gasification characteristics between the two models. Near nozzle mixing was over-predicted by the RANS models and resulted in shorter combustion zones. While the RANS models were satisfactory in predicting the broader axial variation along the gasifier, it performed poorly compared to the LES in predicting the measured radial variation of species mole fractions. LES captured the various unsteady structures across all gasifier zones, as expected.

3.3.2 Sensitivity Studies on the Gasifier Performance

Multiple studies exist in the literature where a model of entrained flow gasification has been validated from experimental data and applied toward optimization of the gasifier performance by means of sensitivity studies on the influential parameters. Chen et al. [55]. Applied their gasification model to an air-blown two-stage gasifier and concluded that devolatilization and char oxidation reactions are responsible for almost 80% of the total carbon conversion, while the gasification reactions with steam and CO_2 account for the rest. They also reported the air ratio (i.e., air feed rate as compared to the stoichiometric requirement) to have a significant impact on

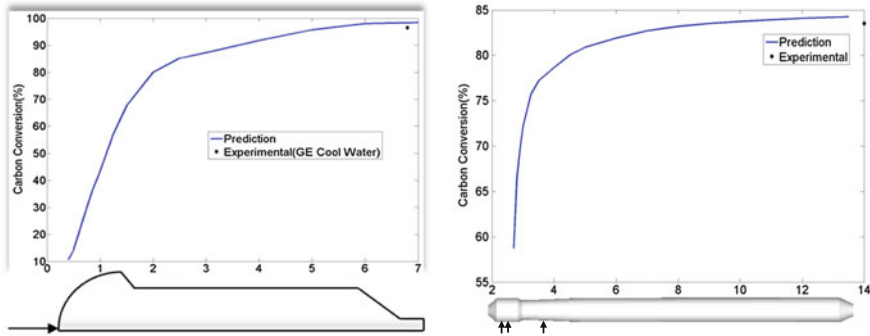


Fig. 10 Comparison of the standard $k-\epsilon$ and the SST $k-\omega$ turbulence models. Note the small, but negative velocities predicted along the gasifier axis by the SST $k-\omega$ model

the exit gas composition, and posited that there exists a best air ratio for each coal depending upon the composition and heating value of the particular coal.

Another two-stage entrained flow gasifier, but with opposed multiburners (OMB) ECUST design, was simulated and the impact of coal and air burners (OMB) ECUST design, was simulated and the impact of coal and air burners (OMB) ECUST design, was studied [56]. It was found that optimal gasifier performance resulted when oxygen or coal are injected at the upper level at greater than or equal to 50% of the total feed rate. Furthermore, both the exit flue gas temperature and the species mole fractions can be suitably controlled by altering the injection staging.

Kumar et al. used CFD simulations to predict potential hot spots near the gasifier walls or the burners [17]. The information from simulations can then be used to design gasifiers with reduced refractory or injector failure. The same study showed that CFD simulations can help decide the optimal gasifier length for the range of coals and operating conditions under consideration. For example, the gasifier in Fig. 10a is shown to utilize its length much more effectively than the gasifier in Fig. 10b which is oversized since most of the carbon conversion is achieved with the first half of its length. Since the CFD simulations of entrained flow gasification also invariably track particle trajectories, including their structural evolution under carbon conversion, they can also predict the optimal particle size for maximum carbon conversion [17].

4 Conclusions

1. Entrained flow gasification is the most widely deployed gasification technology around the world, especially when it comes to IGCC.
2. Entrained flow gasification is also heavily deployed toward the coal-to-chemicals conversion route, especially in China.

3. Computational Fluid Dynamics (CFD) simulations are the most suited for understanding entrained flow gasifiers owing to the complex interactions with turbulence, particle dispersion, heat transfer, and heterogeneous chemistry.
4. Sufficiently detailed models of char consumption, surface area evolution, and heterogeneous kinetics are necessary to ensure predictive accuracy of the integrated CFD model.
5. The integrated and validated CFD model can be used to conduct optimization studies on key gasifier design and operating parameters such as injection staging, air-fuel ratio, reactor length, operating pressure, and temperature.

References

1. Wang T, Stiegel GJ. Integrated gasification combined cycle (IGCC) technologies. Woodhead Publishing
2. NETL website
3. Steynberg A, Dry M. Fischer-Tropsch technology, vol 152
4. Botero C, Field RP, Herzog HJ, Ghoniem AF (2013) Coal-CO slurry feed for pressurized gasifiers: slurry preparation system characterization and economics. *Energy Procedia* 37:2212–2223
5. Hong JH, Chaudhry G, Brisson JG, Field RP, Gazzino M, Ghoniem AF (2009) Analysis of oxy-fuel combustion power cycle utilizing a pressurized coal combustor. *Energy* 34(9):1332–1340
6. Tavoulareas ES, Jozewicz W. Multipollutant emission control technology options for coal-fired power plants. DIANE Publishing
7. <http://www.utilitydive.com/news/indiana-regulators-approve-settlement-for-dukes-edwardsport-coal-plant/425254/>. Accessed 5 Sep 2017
8. <http://spectrum.ieee.org/energywise/energy/fossil-fuels/kemper-county-and-the-perils-of-clean-coal-technology>. Accessed 5 Sep 2017
9. <http://www.elp.com/articles/2017/02/kemper-county-igcc-power-plant-makes-electricity.html>. Accessed 5 Sep 2017
10. <https://www.technologyreview.com/s/411393/china-closes-the-clean-coal-gap/>. Accessed 5 Sep 2017
11. <https://www.technologyreview.com/s/537696/fixing-chinas-coal-problem/>. Accessed 5 Sep 2017
12. Coal Gasification in China: A Study Report, US-China Energy Center, West Virginia University
13. <http://cornerstonemag.net/development-of-coal-gasification-technology-in-china/>. Accessed 5 Sep 2017
14. <http://economics.times.indiatimes.com/industry/indl-goods/svs/metals-mining/coal-gas-can-help-lower-import-bill-by-10-bn-in-5-yrs-coal-secretary-susheel-kumar/articleshow/57478524.cms>. Accessed 5 Sep 2017
15. <http://www.modernpowersystems.com/features/featuregasifier-projects-and-igcc-the-big-picture-4188432/>. Accessed 5 Sep 2017
16. <http://www.dnaindia.com/business/report-fertiliser-from-coal-project-kicks-off-shell-to-provide-technology-to-psu-jv-2472845> Accessed 5 Sep 2017
17. Kumar M (2011) Multiscale CFD simulations of entrained flow gasification. PhD thesis, Massachusetts Institute of Technology

18. Brown BW, Smoot LD, Smith PJ, Hedman PO (1988) Measurement and prediction of entrained-flow gasification processes. *AIChE J* 34:435–446
19. Chen C, Horio M, Kojima T (2000) Numerical simulation of entrained flow coal gasifiers. Part I: modeling of coal gasification in an entrained flow gasifier. *Chem Eng Sci* 55:3861–3874
20. Choi Y (2001) Numerical study on the coal gasification characteristics in an entrained flow coal gasifier. *Fuel* 80:2193–2201
21. Fletcher D (2000) A CFD based combustion model of an entrained flow biomass gasifier. *Appl Math Model* 24:165–182
22. Watanabe H, Otaka M (2006) Numerical simulation of coal gasification in entrained flow coal gasifier. *Fuel* 85:1935–1943
23. Wen CY, Chaung TZ (1979) Entrainment coal gasification modeling. *Ind Eng Chem Proc Des Dev* 18:684–695
24. Govind R, Shah J (1984) Modeling and simulation of an entrained flow coal gasifier. *AIChE J* 30:79–92
25. Vamvuka D, Woodburn ET, Senior PR (1995) Modeling of an entrained flow coal gasifier 1. Development of model and general predictions. *Fuel* 74:1452–1460
26. Crowe CT, Sharma MP, Stock DE (1977) The particle-source-in-cell method for gas and droplet flow. *J Fluids Eng* 99:325–332
27. Law CK (2010) *Combustion physics*. Cambridge University Press
28. Turns SR (1996) *An Introduction to combustion*. McGraw-Hill
29. Grant DM, Pugmire RJ, Fletcher TH, Kerstein AR (1989) A chemical model of coal devolatilization using percolation lattice statistics. *Energy Fuels* 3:175–186
30. Kobayashi H, Howard JB, Sarofim AF (1976) Coal devolatilization at high temperatures. *Proc Combust Inst* 411–425
31. Tomita A, Xu W (1987) Effect of coal type on the flash pyrolysis of various coals. *Fuel* 66:627–631
32. Smith IW (1982) The combustion rates of coal chars: a review. In: *Nineteenth symposium (international) on combustion*, pp 1045–1065
33. Wu Y, Zhang J, Smith PJ, Zhang H, Reid C, Lv J, Yue G (2010) Three-dimensional simulation for an entrained flow coal slurry gasifier. *Energy Fuels* 24:1156–1163
34. Bhatia SK, Perlmutter DD (1980) A random pore model for fluid-solid reactions: I. Isothermal, kinetic control. *AIChE J*
35. Vascellari M, Arora R, Hasse C (2014) Simulation of entrained flow gasification with advanced coal conversion submodels. Part 2: char conversion. *Fuel* 118:369–384
36. Jeong H, Seo DK, Hwang J (2014) CFD modeling for coal size effect on coal gasification in a two-stage commercial entrained-bed gasifier with an improved char gasification model. *Appl Energy* 123:29–36
37. Roberts DG, Harris DJ (2006) A kinetic analysis of coal char gasification reactions at high pressures. *Energy Fuels* 2314–2320
38. Liu G, Niksa S (2004) Coal conversion submodels for design applications at elevated pressures. Part II. Char gasification. *Prog Energy Combust Sci* 30:679–717
39. Muhlen HJ, Heek KH, Juntgen H (1985) Kinetic studies of steam gasification of char in presence of H₂, CO₂ and CO. *Fuel* 64:944–949
40. Weeda M, Abcouver HH, Kapteijn F, Moulijn JA (1993) Steam gasification kinetics and burn-off behavior for a bituminous coal derived char in the presence of H₂. *Fuel Process Technol* 36:235–242
41. Lussier MG, Zhang Z, Miller DJ (1998) Characterizing rate inhibition in steam/hydrogen gasification via analysis of absorbed hydrogen. *Carbon* 36:1361–1369
42. Koenig PC, Squires RG, Laurendeau NM (1986) Char gasification by carbon dioxide. *Fuel* 65:412–416
43. Murphy JJ, Shaddix CR (2006) Combustion kinetics of coal chars in oxygen-enriched environments. *Combust Flame* 144(4):710–729

44. Bischoff KB (1965) Effectiveness factors for general reaction rate forms. *AIChE J* 11:351–355
45. Liu G, Rezaei HR, Lucas JA, Harris DJ, Wall TF (2000) Modelling of a pressurised entrained flow coal gasifier: the effect of reaction kinetics and char structure. *Fuel* 79:1767–1779
46. Hong J, Hecker WC, Fletcher TH (2000) Modeling high-pressure char oxidation using langmuir kinetics with an effectiveness factor. *Proc Combust Inst* 28:2215–2223
47. Chen C, Horio M, Kojima T (2001) Use of numerical modeling in the design and scale-up of entrained flow coal gasifiers. *Fuel* 80:1513–1523
48. Liu XJ, Zhang WR, Park TJ (2001) Modelling coal gasification in an entrained flow gasifier. *Combust Theor Model* 5:595–608
49. Caram HS, Amundson NR (1997) Diffusion and reaction in a stagnant boundary layer about a carbon particle. *Ind Eng Chem Fundam* 16:171–181
50. Zhang M, Yu J, Xu X (2005) A new flame sheet model to reflect the influence of the oxidation of CO on the combustion of a carbon particle. *Combust Flame* 143:150–158
51. Zhang MC, Yu J, Zhang J, Qi YF (2007) An improved moving flame front model for combustion of a carbon particle with finite-rate heterogeneous oxidation and reduction 2 improved MFF model 3 limiting cases. *Energy Eng*
52. Viskanta R, Menguc MP (1987) Radiation heat transfer in combustion systems. *Prog Energy Combust Sci* 13:97–160
53. Silaen A, Wang T (2010) Effect of turbulence and devolatilization models on coal gasification simulation in an entrained-flow gasifier. *Int J Heat Mass Transf* 53(9):2074–2091
54. Abani N, Ghoniem AF (2013) Large eddy simulations of coal gasification in an entrained flow gasifier. *Fuel* 104:664–680
55. Chen C, Horio M, Kojima T (2000) Numerical simulation of entrained flow coal gasifiers. Part II: effects of operating conditions on gasifier performance. *Chem Eng Sci* 55(18):3875–3883
56. Unar IN, Wang L, Pathan AG, Mahar RB, Li R, Uqaili MA (2014) Numerical simulations for the coal/oxidant distribution effects between two-stages for multi opposite burners (MOB) gasifier. *Energy Convers Manag* 86:670–682

Advanced Numerical Methods for the Assessment of Integrated Gasification and CHP Generation Technologies

Ahmed M. Salem, Umesh Kumar, Ainul Nadirah Izaharuddin,
Harnek Dhani, Tata Sutardi and Manosh C. Paul

Abstract The chapter gives an overview of new techniques developed and used in coal, biomass and waste materials gasification. All of the above-mentioned materials have similar properties for hydrocarbon content. As a consequence, most of them are used for power and heat generation through gasification technology. The chapter discusses advanced kinetic as well as computational fluid dynamics (CFD) modelling schemes valid for a wide range of coal and biomass materials using a downdraft gasifier. The models show validated results with experimental data. Underground coal gasification (UCG) is also discussed, modelled and verified to some extent. Applications leading to the combined heat and power (CHP) generation from syngas produced through the gasification of such feedstocks are presented.

Nomenclature

Upper Case Letters

- A Pre-exponential factor (s^{-1})
- C Concentration (mol/m³)
- D Diameter (m)

A. M. Salem · U. Kumar · A. N. Izaharuddin · H. Dhani · T. Sutardi · M. C. Paul (✉)
Systems, Power & Energy Research Division, School of Engineering, University of Glasgow,
Glasgow G12 8QQ, UK
e-mail: Manosh.Paul@glasgow.ac.uk

A. M. Salem
e-mail: a.salem.2@research.gla.ac.uk

U. Kumar
e-mail: Umesh.Kumar@glasgow.ac.uk

A. N. Izaharuddin
e-mail: a.binti-izaharuddin.1@research.gla.ac.uk

H. Dhani
e-mail: Harry.Dhani@glasgow.ac.uk

T. Sutardi
e-mail: t.sutardi.1@research.gla.ac.uk

<i>E</i>	Energy (kJ/mol)
<i>H</i>	Enthalpy (kJ/mol)
<i>K</i>	Kinetic constant (s^{-1})
<i>M</i>	Molecular mass (kg/mol)
<i>P</i>	Pressure (Pa)
<i>GH</i>	Hearth Load ($Nm^3/(h\ m^2)$)
<i>T</i>	Temperature (K)
<i>R</i>	Net rate of formation ($mol\ m^{-3}s^{-1}$)
<i>V</i>	Volume (m^3)
<i>W</i>	Power (W)

Lower Case Letters

c_p	Specific heat at const. pressure ($J\ mol^{-1}\ K^{-1}$)
<i>m</i>	Mass (kg)
<i>n</i>	No. of moles (mol)
<i>r</i>	Reaction rate ($mol\ m^{-3}s^{-1}$)
<i>t</i>	Time (s)
<i>v</i>	Velocity (ms^{-1})
<i>y</i>	Composition fraction
<i>z</i>	Height (m)
h_s	Heat source ($W/m^2\ K$)
k_i	Reaction rate coefficient for reaction <i>i</i>
p_{ij}	Rate exponent of reacting species
J_i	The flux of species <i>i</i>
<i>YY</i>	Mass stoichiometric coefficient

Abbreviations

<i>B</i>	Biomass
<i>C</i>	Char
<i>MC</i>	Moisture content (%)
<i>A/F</i>	Air-to-fuel ratio
<i>ER</i>	Equivalence ratio
<i>CRF</i>	Char reactivity factor
<i>HR</i>	Heating rate ($K\ s^{-1}$)
<i>G</i>	Gases
Nm^3	Normal cubic metre
<i>py</i>	Pyrolysis

Subscripts

<i>d</i>	Drying
<i>f</i>	Fuel

g Gases
i Species
l Liquid
th Thermal

Greek Letters

ρ Density
 \sum Summation
 Δ Change in state
 β Temperature exponent
 τ_{ij} Stress tensor
 Γ_i Fick diffusion coefficients
 δ Kronecker delta
 ρg_i Gravitational body force
 μ Viscosity (kg/m s)
 σ Turbulent Prandtl number

1 Introduction

The world is continuously looking for new alternative sources for energy production that are clean, sustainable and renewable. Biomass, which is considered to be one of the most promising alternatives for fossil fuels nowadays, can be converted into gaseous, liquid and solid fuels for generating energy. Additionally, biomass does not contribute to the greenhouse effects as it is CO₂ neutral, which is an advantage against fossil fuels; and besides, it is a renewable source of energy. Therefore, researchers are working for energy production using biomass [1].

The most common use of biomass for energy is direct combustion, followed by gasification, carbonisation and pyrolysis [1]. Biomass gasification is considered to be one of the most promising techniques to convert solid fuels into useful gaseous fuels, which could be widely used in many industrial applications such as in power generation and internal combustion engines for various means of transportations.

Gasification is a thermochemical process that converts a solid form of fuels into a gaseous fuel at temperatures around 900 °C. It produces carbon monoxide (CO), hydrogen (H₂) and small amounts of methane (CH₄) as desired products with other undesired gases like nitrogen (N₂), carbon dioxide (CO₂) and other hydrocarbons (HC). Alternative feedstocks such as municipal solid waste (MSW) including food waste generated by every household, office, hotel, shop, school and other institutions can also be used for gasification.

Every year, we waste more food, consume more energy and contribute to global warming. The coming decades are crucial in reducing greenhouse gas emissions whilst reducing our dependency on dirty fossil fuels. Clean generation of energy

from farming waste is becoming ever more as approximately 1.3 billion tonnes of food are wasted every year globally equating to roughly 33% of the food produced for human consumption [2]. Over the last century, greenhouse gases produced from anthropological activities are the single largest driver of climate change [3]. As the global population grows exponentially so does our need for basic resources such as food, water and electricity. The global population is estimated to rise from approximately 6.5 billion to 10 billion by 2050 [4]. Over the next 30 years, the global energy demand is expected to increase by an astonishing 56% [5]. Challenging times lie ahead for the next generation in reducing our dependency on fossil fuels and utilising our waste. A promising technology under development to generate a clean source of energy from agricultural waste is gasification. Gasification is not a new technology; it has been about for many years. One of the most common applications of gasification dates back to the 1940s when the British public modified automobiles to run on gasifiers due to the shortage of petrol caused by WW2.

Gasification of biomass is playing a key role in reducing greenhouse gas emissions worldwide. In 2013, the supply of bioenergy was 57.7 EJ—10% of the global energy supply. From 2012 to 2013, the world biogas production output increased by 5.5% reaching 59 billion m³ [6]. Underground coal gasification (UCG) technology used to produce gaseous fuel and/or a wide range of chemical syntheses directly from the coal seam has also seen progress over the years [7]. Combining gasification with CHP (combined heat and power) generation gives great potential to produce electrical and thermal power onsite, completely decentralized from the main grid.

CHP generates power and simultaneously utilises the heat given off as a by-product in the process of power generation. Typically, for conventional power generation, heat generated from the production of electricity is normally wasted through dumping via the atmosphere. Power stations all over the world operate in this way; large cooling towers dissipate heat to the atmosphere and as a consequence, power stations have lower efficiencies than CHP stations. By strategically using the waste heat, CHP plants reach higher efficiencies, upwards of 80% in comparison to gas-fired power stations where typical efficiencies are around 40–50% [8]. CHP plants export heat energy in the form of steam and hot water. The export of heat or even cooling is used typically in local buildings and factories for industrial and residential purposes. Conventional power stations export electricity over the national grid where the electricity is distributed all over the country. Power losses in distributing electricity cannot be avoided, with typical power losses ranging from 7 to 9% [9]. Since CHP is generated locally, the technology is not susceptible to losses from distribution and, therefore, proves advantageous over conventional power generation and distribution. Distribution of electricity and heat locally proves more efficient and advantageous over conventional power generation and distribution. As a result, CHP plants can achieve higher overall efficiency in comparison to its counterparts.

Figure 1 illustrates the process of producing energy from biomass/waste which is fed into a gasifier to produce syngas. Syngas is then combusted to produce power through an internal combustion engine. Designing the most suitable gasifier for the

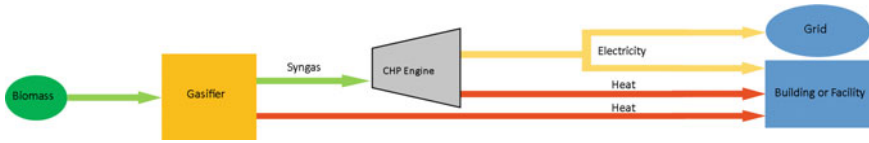
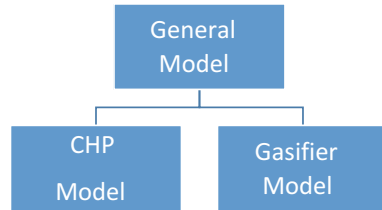


Fig. 1 Energy from biomass/waste process through gasification and CHP

Fig. 2 Structure of the general model



required thermal and electrical load depends upon many factors such as the feedstock, moisture content, equivalence ratio and the efficiency of the CHP engine.

A technical model was developed at the University of Glasgow to determine the gasifier dimensions and syngas quality for the University CHP system. Figure 2 illustrates the functionality of the technical model. The general model consists of two submodels combined. One of the submodels is the gasification model; the other is the CHP model. By combining both models, we are able to determine the physical dimensions of the gasifier required to power any CHP engine for any type of biomass waste. The model also gives a detailed analysis of the producer gas and concentrations. The model allows for analysis of any biomass waste specific to any geographic location in the world. By entering the ultimate analysis of the feedstock and the required thermal and electrical power outputs into the model, the model then generates the optimum gasifier design and predicted syngas quality in addition to the tar content and heating values.

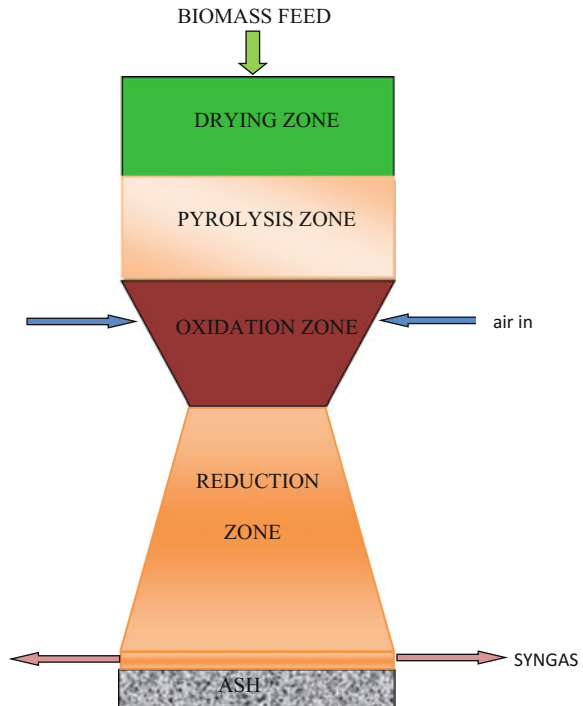
2 Gasification CHP Model Development

2.1 Kinetic Modelling for Biomass Gasification

Biomass gasification occurs through the four main steps: drying, pyrolysis, oxidation and gasification/reduction as illustrated in the schematic drawing of a downdraft gasifier in Fig. 3. Biomass is fed from the top of the downdraft gasifier into the drying zone, air is fed into the oxidation zone for the combustion process, and then the product gas is driven from the down of the gasifier. The ash is collected at the bottom.

Modelling biomass gasification is a favourable technique that can simulate gasifier design, output parameters, working conditions, etc. It is understood that a

Fig. 3 Schematic view of a downdraft gasifier



pure thermodynamic model cannot predict the product gas from a gasifier because it gives an over prediction for higher heating value (HHV) and H_2 output, also a lower amount of CO with a higher amount of CH_4 [10]. Altafini et al. [11] presented a kinetic model taking into account that the reduction reactions are generally slower than the oxidation reactions by several orders of magnitudes. The way to measure these effects is driven through the reaction rates which are the key for identifying the reaction formations and rates. Using high temperatures in reduction, the equilibrium model products may deviate from reality because of depending on the kinetic constant variations which affect gas composition. Thus, kinetic models are more suitable and accurate to predict the gas composition in a gasifier.

Previous kinetic and equilibrium models reported to have some limitations. For example, Budhathoki [12] introduced a model based on the combination between the kinetic approach for reduction zone and thermodynamic equilibrium for other zones. This model was compared with other experimental works for wood biomass and was found to be in a good agreement for the gas composition except for methane in which it gave higher prediction rates. Ratnadhariya and Channiwala [13] proposed a new model for modelling biomass gasification. It is composed of three different zones, in which drying and pyrolysis is the first zone followed by the combustion and reduction zones. The model is a combined system consisting of the stoichiometric model with assumptions for the pyrolysis and oxidation zones for predicting the output gas. This model provides the operating range for the woody

biomass materials. Dejtrakulwong and Patumsawa [14] built a four-zone kinetic model and studied the effect of moisture content and air-to-fuel ratio on the temperature and height of each zone, which is useful in the gasifier design evaluation.

Additionally, kinetic models presented in the published literatures have further limitation and shortage in reporting some details like biomass variety, tar formation and optimum working conditions. For instance, Budhathoki [12] reported that his model is only valid for wood biomass material, and it does not take into account any tar formation and higher hydrocarbons. Several other researchers (e.g. see [15–17]) only discussed the effect of changing biomass moisture content on producer gas heating value and showed that higher moisture content reduces the heating value. However, they did not show any possible effect on residuals and tar content. Further, they did not discuss the effect of other working parameters such as the equivalence ratio. While a thermochemical equilibrium model developed by Vaezi et al. [18] predicts biomass gasification of different biomass materials with effect of moisture content and air-to-fuel ratio on the producer gas heating value, again this study excludes tar content and discussion on the producer gas quality.

A four-zone integrated kinetic model was built, and the model allows investigation of the effect of moisture content and air-to-fuel ratio on the temperature and height of each zone, which is useful in gasifier design evaluation [19, 20]. This kinetic model for the first time incorporates the effect of height of the reduction zone on the concentration of different species of product gas as predicted. The model also provides useful information for the full design of a downdraft gasifier based only on a desired thermal power. Modelling involves an integration of the four zones (Fig. 3), and the thermochemical kinetic processes associated with the main zone are explained in the following sections.

2.1.1 Drying Model

The drying zone receives heat from oxidation which leads to an increase of the temperature. The initial temperature is supposed to be 298 K; however, when the temperature reaches 368 K, the vaporisation of the moisture content starts until it reaches 473 K as mentioned by Dejtrakulwong and Patumsawa [14]. At this temperature, the pyrolysis begins automatically, thus the devolatilisation of biomass occurs [14]. The rate at which the drying reaction taking place is determined as, [14, 21],

$$r_d = K_d \cdot C_{H_2O,l} \quad (1)$$

$$K_d = A_d \exp\left(\frac{-E_d}{RT_d}\right) \quad (2)$$

where the constants used in the drying model are summarised in Table 1.

Table 1 Data for the drying model [14]

A_d (s^{-1})	K_d (s^{-1})	E_d (kJ/mol)	T_d (K)
5.13×10^6	0.1652	88	400

2.1.2 Pyrolysis Model

Biomass after drying first decomposes into volatiles and char, and then these components further react with each other to form char and volatiles again, as shown in Fig. 4.

The kinetic rate equations for the devolatilisation process are written as [23]

$$\frac{dC_B}{dt} = -K_1 C_B^{n_1} - K_2 C_B^{n_1} \tag{3}$$

$$\frac{dC_{G1}}{dt} = K_1 C_B^{n_1} - K_3 C_{G1}^{n_2} C_{C1}^{n_3} \tag{4}$$

$$\frac{dC_{C1}}{dt} = K_2 C_B^{n_1} - K_3 C_{G1}^{n_2} C_{C1}^{n_3} \tag{5}$$

$$\frac{dC_{G2}}{dt} = K_3 C_{G1}^{n_2} C_{C1}^{n_3} = \frac{dC_{C2}}{dt} \tag{6}$$

where

$$K_1 = A_1 \exp\left[\left(\frac{D_1}{T}\right) + \left(\frac{L_1}{T^2}\right)\right] \tag{7}$$

$$K_2 = A_2 \exp\left[\left(\frac{D_2}{T}\right) + \left(\frac{L_2}{T^2}\right)\right] \tag{8}$$

$$K_3 = A_3 \exp\left[\left(-\frac{E}{RT}\right)\right] \tag{9}$$

The values of A , D and L for Eqs. (7), (8) and (9) are illustrated in Table 2. The following initial conditions are used for solving the coupled ordinary differential equations (3)–(9):

At $t = 0$, $C_B = 1$ and $C_{G1} = C_{C1} = C_{G2} = C_{C2} = 0$.

Fig. 4 Biomass devolatilisation [22]

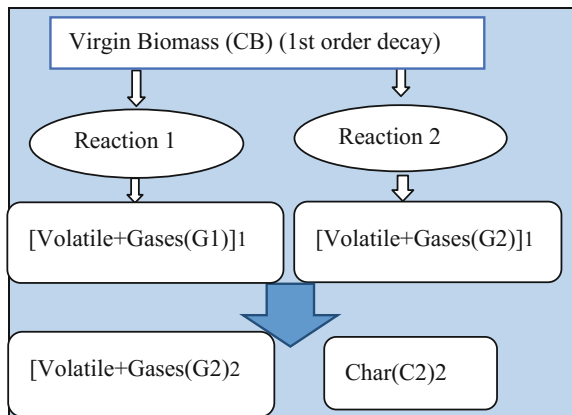


Table 2 Parameters of the pyrolysis model [22, 23]

R	A (s ⁻¹)	D (K)	L (K ²)	E (kJ/mol)
1	9.973 × 10 ⁻⁵	17254.4	-9061227	
2	1.068 × 10 ⁻³	10224.4	-6123081	81
3	5.7 × 10 ⁵			

Babu and Chaurasia [23] determined the optimum parameters for pyrolysis through a wide range of heating values and temperatures during isothermal and non-isothermal processes and found that the optimum conditions for non-isothermal process are as stated in Table 3. Optimum parameters ensure that all biomass successfully converted into volatiles and char, and final concentration of virgin biomass left is less than 0.03.

While they showed that the optimum temperature for pyrolysis is 1259 K, the temperature is still very high to handle before oxidation, and this will require a higher temperature in the oxidation zone plus specific design materials for the gasifier. As a consequence, we choose a temperature of 873 K to start with as the pyrolysis process is very slow, below 773 K as reported by Dejtrakulwong and Patumsawa [14]. The volatiles are assumed to be CO, CO₂, CH₄, H₂, H₂O and tar. The importance of this part is that it gives the final concentration of char and volatiles; after which the concentration of char is known at the end of devolatilisation and is used for the next step in which the volatiles concentration is predicted.

Sharma [24] introduced a model to predict the percentage composition of volatiles and considered a one-step model for the biomass pyrolysis as follows



where $C_aH_bO_d$ represents biomass, x is the concentration of different species of pyrolysis products in mol, $C_6H_{6.2}O_{0.2}$ is the tar chemical formula as considered by many researchers; see, e.g. [24]. The mass fraction (Y/Y) empirical relations used are:

$$\frac{Y_{CO}}{Y_{CO_2}} = \exp\left(-1.845 + \frac{7730.3}{T} - \frac{5019898}{T^2}\right) \quad (11)$$

$$\frac{Y_{H_2O}}{Y_{CO_2}} = 1 \quad (12)$$

$$\frac{Y_{CH_4}}{Y_{CO_2}} = 5 \times 10^{-16} \times T^{5.06} \quad (13)$$

Table 3 Optimum values of non-isothermal pyrolysis [23]

T (K)	HR (K/s)	Time (s)	n_1	$n_2 = n_3$
1259	51	9.53	1	1.5

2.1.3 Oxidation Model

The oxidation zone supplies the required heat for drying and pyrolysis. Oxidation also requires air to complete. If this air is less than the stoichiometric amount, the gasification (reduction) process will take place to produce syngas. The oxidation process taking place through the chemical reactions is illustrated in Tables 4 and 5. Pyrolysis products are oxidised in an order that depends on the reaction rate [24] as follows:

- Oxidation of all the hydrogen completes first (R1).
- Oxidation of CO then takes place (R2).
- If oxygen still remains, it will oxidise methane from pyrolysis (R3).
- And if more oxygen is available, it will oxidise tar and char according to their reaction rates (R4 and R5).

An energy balance is made for the combustion stage to determine the oxidation temperature based on

$$\sum X_i \cdot (h_f + C_p \cdot \Delta T)_{pyrolysis\ products} = \sum X_i \cdot (h_f + C_p \cdot \Delta T)_{combustion\ products} + Q_{loss} \quad (14)$$

The heat loss is mentioned in the oxidation zone only as it is higher in temperature than other zones, and the overall heat loss, as pointed out in [26], is assumed to be 10% of the product of equivalence ratio and HHV. The same energy balance principle is made for the pyrolysis and reduction zones.

Table 4 Oxidation reactions ([24, 25])

R	Reaction	A_j	E_j/R
1	$H_2 + 0.5O_2 \leftrightarrow H_2O$	1.6×10^9	3420
2	$CO + 0.5O_2 \leftrightarrow CO_2$	1.3×10^8	15106
3	$CH_4 + 1.5O_2 \leftrightarrow CO + 2H_2O$	1.585×10^9	24157
4	$C_6H_{6.62}O_{0.2} + 4.45O_2 \leftrightarrow 6CO + 3.1H_2O$	2.07×10^4	41646
5	$C + 0.5O_2 \leftrightarrow CO$	0.554	10824

Table 5 Rate expressions for the oxidation reactions ([24, 25])

R	Reaction rate (mol m ⁻³ s ⁻¹)
1	$r_{H_2} = A_1 T^{1.5} \exp\left(-\frac{E_{co}}{RT}\right) \cdot [C_{co2}][C_{H_2}]^{1.5}$
2	$r_{co} = A_2 \exp\left(-\frac{E_{co}}{RT}\right) \cdot [C_{co}][C_{o_2}]^{0.25}[C_{H_2O}]^{0.5}$
3	$r_{CH_4} = A_3 \exp\left(-\frac{E_{CH_4}}{RT}\right) \cdot [C_{o_2}]^{0.8}[C_{CH_4}]^{0.7}$
4	$r_{tar} = A_4 T \cdot P_A^{0.3} \cdot \exp\left(-\frac{E_{tar}}{RT}\right) \cdot [C_{o_2}][C_{tar}]^{0.5}$
5	$r_C = A_5 \exp\left(-\frac{E_{char}}{RT}\right) \cdot [C_{o_2}]$

2.1.4 Reduction Model

The change in mole fractions of any gas species at the reduction zone along the distance z (reduction height/length) is determined by Dejtrakulwong and Patumsawa [14];

$$\frac{dn_x}{dz} = \frac{1}{v} \left(R_x - n_x \frac{dv}{dz} \right) \quad (15)$$

The reactions considered for the reduction zone are illustrated in Table 6, and the reaction rates r_i are in Table 7.

Velocity, temperature and pressure variations along the reduction zone are obtained through the solution of the following differential equations [27]

$$\frac{dv}{dz} = \frac{1}{\sum_i n_i C_{pi}} \left[\frac{\sum_i n_i C_{pi} \sum_i R_i}{n} - \frac{\sum_i r_i \Delta H_i}{T} - \frac{dP}{dz} \left(\frac{v}{T} + \frac{v \sum_i n_i C_{pi}}{P} \right) - \sum R_i C_{pi} \right] \quad (16)$$

$$\frac{dT}{dz} = \frac{1}{v \sum_i n_i C_{pi}} \left[\sum r_i \Delta H_i - v \frac{dP}{dz} - p \frac{dv}{dz} - \sum R_i C_{pi} T \right] \quad (17)$$

$$\frac{dP}{dz} = 1183 \left(\frac{\rho_{gas}}{\rho_{air}} v^2 \right) + 388.19v - 79.896 \quad (18)$$

Table 6 Reduction reactions [27, 28]

R	Reactions	A (1/s)	E (kJ/mol)
1	Boudouard $C + CO_2 \leftrightarrow 2CO$	36.16	77.39
2	Water-gas $C + H_2O \leftrightarrow CO + H_2$	1.517×10^4	121.62
3	Methane formation $C + 2H_2 \leftrightarrow CH_4$	4.189×10^{-3}	19.21
4	Steam reforming $CH_4 + H_2O \leftrightarrow CO + 3H_2$	7.301×10^{-2}	36.15

Table 7 Rate expressions for the reduction reactions [27, 28]

R	Reaction rates ($\text{mol m}^{-3} \text{s}^{-1}$)
1	$r_1 = A_1 \exp\left(-\frac{E_1}{RT}\right) \cdot \left(y_{CO_2} - \frac{y_{CO}^2}{K_{eq,1}}\right)$
2	$r_2 = A_2 \exp\left(-\frac{E_2}{RT}\right) \cdot \left(y_{H_2O} - \frac{y_{CO} y_{H_2}}{K_{eq,2}}\right)$
3	$r_3 = A_3 \exp\left(-\frac{E_3}{RT}\right) \cdot \left(y_{H_2}^2 - \frac{y_{CH_4}}{K_{eq,3}}\right)$
4	$r_4 = A_4 \exp\left(-\frac{E_4}{RT}\right) \cdot \left(y_{CH_4} y_{H_2O} - \frac{y_{CO} y_{H_2}^3}{K_{eq,4}}\right)$

2.2 CFD Modelling

Computational fluid dynamics are powerful numerical techniques widely used in multiphase reacting flow modelling. Two techniques are usually available in literature namely Eulerian–Eulerian and Eulerian–Lagrange. In the Eulerian–Eulerian technique, the gas phase is considered as a continuum and properties of solid phase are calculated by the kinetic theory of granular flow. This technique, however, does not recognise the discrete behaviour of the solid phase so it may be inapplicable in modelling flows with a distribution of particle size and types. While in the Eulerian–Lagrange technique, the gas phase is considered as continuous and the solid is treated as a discrete phase. Each solid particle is tracked in the time domains and space by directly integrating the equations of motion while accounting for the interactions with the continuous phase. In this technique, the collisions of particles are described by hard and cold sphere approaches. The Eulerian–Lagrangian technique has been used extensively by many researchers to simulate coal combustion and biomass gasification in the literature [29–32]. The conservation governing equations for the discrete phase model [33] utilised in the biomass gasifier are summarised below.

Momentum balance:

$$\frac{\partial \vec{u}_s}{\partial t} = F_D(\vec{u} - \vec{u}_s) + \frac{\vec{g}(\rho_s - \rho)}{\rho_s} \quad (19)$$

where $F_D(\vec{u} - \vec{u}_s)$ is the drag force per unit solid particle mass and

$$F_D = \frac{18\mu C_D \text{Re}}{24\rho_s d_s^2} \quad (20)$$

Here, μ is the viscosity of the fluid, Re is the Reynolds number, ρ is the gas phase density, ρ_s is the density of the solid, \vec{u} is the gas phase velocity, \vec{u}_s is the solid phase velocity, d_s is the diameter of solid particle

The Reynolds number is defined as:

$$\text{Re} = \frac{\rho d_s |\vec{u}_s - \vec{u}|}{\mu} \quad (21)$$

Inert heating and cooling:

$$m_s c_s \frac{dT_s}{dt} = \varepsilon_s A_s \sigma (T_s^4 - T_s^4) + h A_s (T - T_s) \quad (22)$$

where m_s , is the mass of solid particle, c_p is the heat capacity of the solid particle (J/kg K), A_s is the surface area of the solid particle (m^2), T is the temperature of the

gas phase (K), h , is the convective heat transfer coefficient ($\text{W/m}^2 \text{K}$), ε_p is the particle emissivity, T_R is the radiation temperature.

Two competing rates (Kobayashi) model:

$$\frac{m_v(t)}{(1-f_{w,0})m_{p,0}-m_a} = \int_0^t (\alpha_1 R_1 - \alpha_2 R_2) \exp\left(-\int_0^t (R_1 - R_2) dt\right) dt \quad (23)$$

$$R_1 = A_1 e^{-\left(\frac{E_1}{RT_p}\right)}, \quad R_2 = A_2 e^{-\left(\frac{E_2}{RT_p}\right)}$$

$m_v(t)$ is the volatile mass at time t , $m_{p,0}$ is the initial of solid at injection, α_1 , α_2 are the yield factors, m_a is the ash content in the particle.

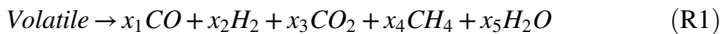
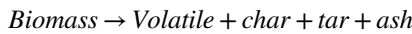
Heat transfer during the devolatilisation process:

$$m_p c_p \frac{dT_p}{dt} = h A_p (T - T_p) + \frac{dm_p}{dt} h_{fg} + \varepsilon_p A_p \sigma (T_R^4 - T_p^4) \quad (24)$$

Heat transfer during the char combustion process:

$$m_p c_p \frac{dT_p}{dt} = h A_p (T - T_p) + f_h \frac{dm_p}{dt} H_{reac} + \varepsilon_p A_p \sigma (T_R^4 - T_p^4) \quad (25)$$

The break-up approach for volatile was developed in the work [34] assumes that the volatile from the biomass consists of carbon, hydrogen, oxygen, nitrogen and sulphur. Volatile matters from biomass are first converted into the gas phase species. A gas phase volatile break-up reaction (R1) is used to convert this gaseous volatile to other gas phase species like CO, H₂, CO₂, CH₄ and H₂O.



$$\sum_i x_i = 1$$

To calculate the stoichiometric coefficient of reaction R1 volatile break-up approach is used [35]. Stoichiometric coefficients x_1 , x_2 , x_3 , x_4 and x_5 for the species are calculated from the molecular weights and mass fractions of these species. Using this approach, a script is developed to calculate the stoichiometric coefficients of the volatile break-up reaction and incorporate this reaction to the gasification simulation in ANSYS Fluent v15 [34]. Homogeneous gas phase reaction is modelled using Eddy dissipation model, and heterogeneous reaction is modelled using a multiple surface reaction model in ANSYS Fluent v15. All the homogeneous and heterogeneous reactions are listed in Tables 6 and 7.

3 Feedstock Characterisation and Results

The feedstocks analysed for the purposes of this research are based on Scottish agricultural waste sourced through the 'Farm Waste Utilisation' project [36]. A total of 462,000 hectares of oil seeds and cereals were grown in Scotland in 2016 [37]. Scotland's main cereal crop is barley, over a quarter million hectares of barley were grown and just over a hundred hectares of wheat for the year 2016 [37]. 28% of the barley grown in the UK is grown in Scotland of which 35% of the barley grown is used for malting and 55% is used for animal feed. Scotland has approximately 30,000 hectares of oats and oilseed rape. For the year 2015, Scotland farmers produced approximately one million tonnes of wheat and 1.9 million tonnes of barley. Furthermore, Scotland farms over 12% of the land used to grow cereal in the UK. There are two types of barley sown: one is sown in autumn (winter barley) and the other is sown around March or April (spring barley). Spring barley accounts for 80% of the barley crop produced in the Scotland [37]. Recoverable straw that can be used as biomass produced from UK farms typically ranges from 2.75 to 4 t/h depending upon crop type [38]. In 2007, the total produced over the UK was estimated at 11 million tonnes [38]. The straw is most commonly used for animal feed, livestock bedding or ploughed back into the field as fertilizer.

Figure 5 illustrates the HHV and tar content for all the feedstock analysed. The results show the effects of varying the feedstock on the HHV and tar content produced. It can be seen that wheat straw has the largest HHV. The HHV is dependent on the moisture content of the feedstock. In this case, the moisture content of the wheat straw is 5.9%, the lowest moisture content compared to other feedstocks. Feedstock's with a lower moisture content result in higher values of CO and H₂, as a result, the HHV increases. As the moisture content increases the energy required to remove the moisture is not recoverable and can be seen as lost energy. As a direct result, the heating value is lower due to the energy losses which stem from removing moisture. On the contrast, barley straw has the lowest HHV due to high moisture content of the feedstock. Furthermore, the tar content produced is highest for barley and lowest for wheat. This is due to the fact that the moisture content is directly related to the amount of tar the system produces. In order to reduce the tar content, the moisture content must be reduced by means of drying the feedstock before gasification. It was reported in [19] that a decreasing the moisture content from 20 to 5% results in a decrease of 18–26%.

Figure 6 illustrates the concentration of syngas for the various feedstock tested. From the water-gas shift reaction, an increase in moisture of the feedstock and the presence of CO produces H₂. As a result, an increase in the H₂ content of the gas results in a greater production of CH₄ from direct hydrogenation [11]. Although the concentration of hydrogen and methane has increased as a result of a higher moisture content, the gain does not counterbalance in the loss in energy due to reduced CO produced in the syngas and ultimately as a result, syngas with a lower HHV is produced from feedstocks with higher moisture contents. The HHV is lower due to the reduced CO content of the syngas. As a result, the lost energy is

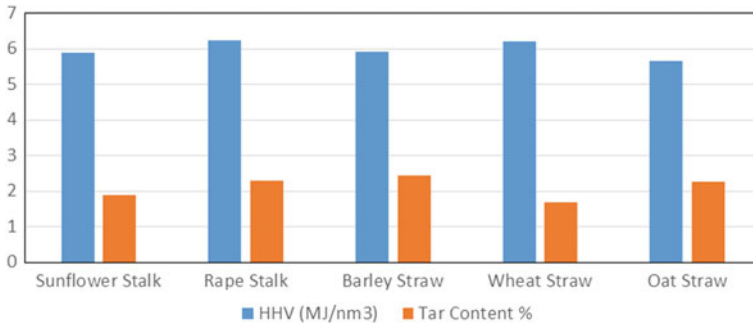


Fig. 5 Feedstock HHV and tar content

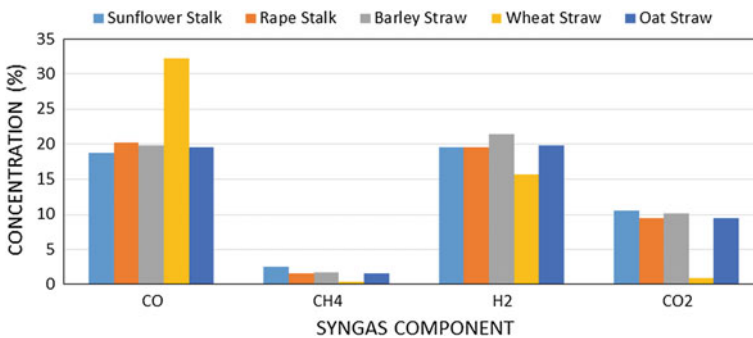


Fig. 6 Concentration of syngas for simulated feedstock

not recuperated from the amount of methane produced and hence gives a product gas with a lower HHV. From Fig. 6, it can clearly be seen that since wheat has a lower moisture content than other feedstocks, the result is a syngas with a higher CO composition with lower CH₄ and H₂, respectively. On the contrast, Barley straw has a lower CO concentration than wheat straw with larger quantities of CH₄ and H₂, respectively.

Figure 7 illustrates the fuel feed rate of the gasifier for given power outputs of the CHP engine. It can be seen that a gasifier with a wheat straw feedstock would require the least amount of feed in comparison to the other feedstocks. To power an engine at 25% load (e.g. 1173 kW thermal and 809 kW electrical), the gasifier would require 411 kg of wheat straw per hour. Wheat straw, in this case, is the most optimal feedstock due to its properties; it has the highest HHV compared to other feedstocks and thus the engine would require less feedstock in comparison to other feedstock.

A wide range of biomass materials (38% ≤ C ≤ 52%, 5.5% ≤ H ≤ 7%, and 36% ≤ O ≤ 45%) have also been tested with various working conditions to validate the model as presented in Fig. 8. The results of the producer gases show a

fairly good agreement with other experimental results, which prove the ability of the kinetic model operating under different working conditions for a wide range of biomass composition. Tar formation is also taken into account which, however, was not discussed by previous numerical models clearly. Figure 9 represents the contour profile of the various gas species during the gasification of rubber wood.

A thermochemical equilibrium model of gasification containing the global chemical equation [41] is adopted and by combining this with the exergy analysis of MSW, overall optimum conditions of gasification, varying the moisture content (MC), gasification temperature and equivalence ratio (ER) is presented in Fig. 10. The figure shows the optimum value of the producer gases at various exergy limitations, at 100%, 95%, 90% and 85%, respectively. Based on the limitation value of exergy, the optimum value of the moisture content is reported to be at the range of 0–10%, temperature 1108–1145 K and equivalence ratio 0.26–0.37 in the MSW gasification.

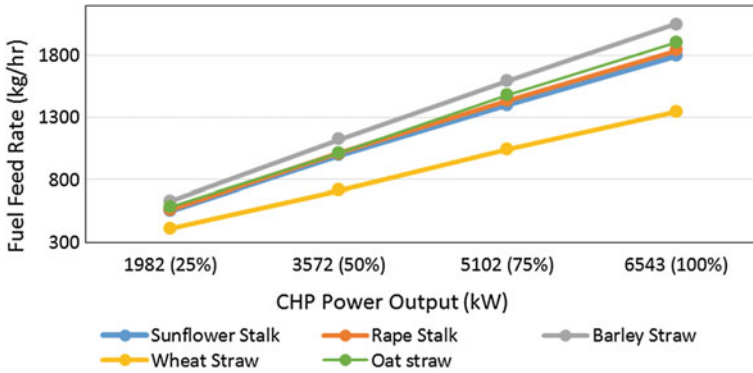


Fig. 7 Fuel feed rate of gasifier/power output

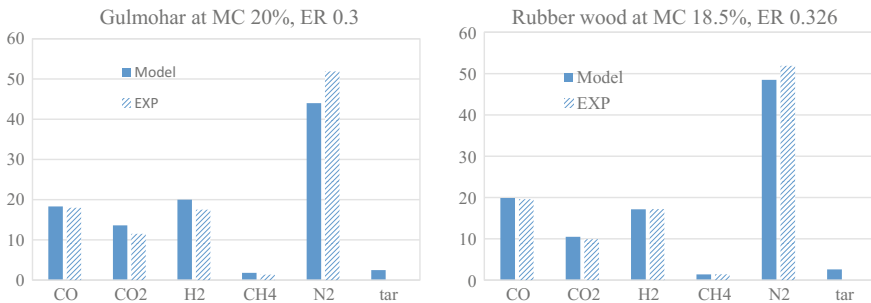


Fig. 8 Comparison for gas volumetric composition between the present work and other experimental work for same (feedstock, ϕ and MC), Rubber wood [39] and Gulmohar [40]

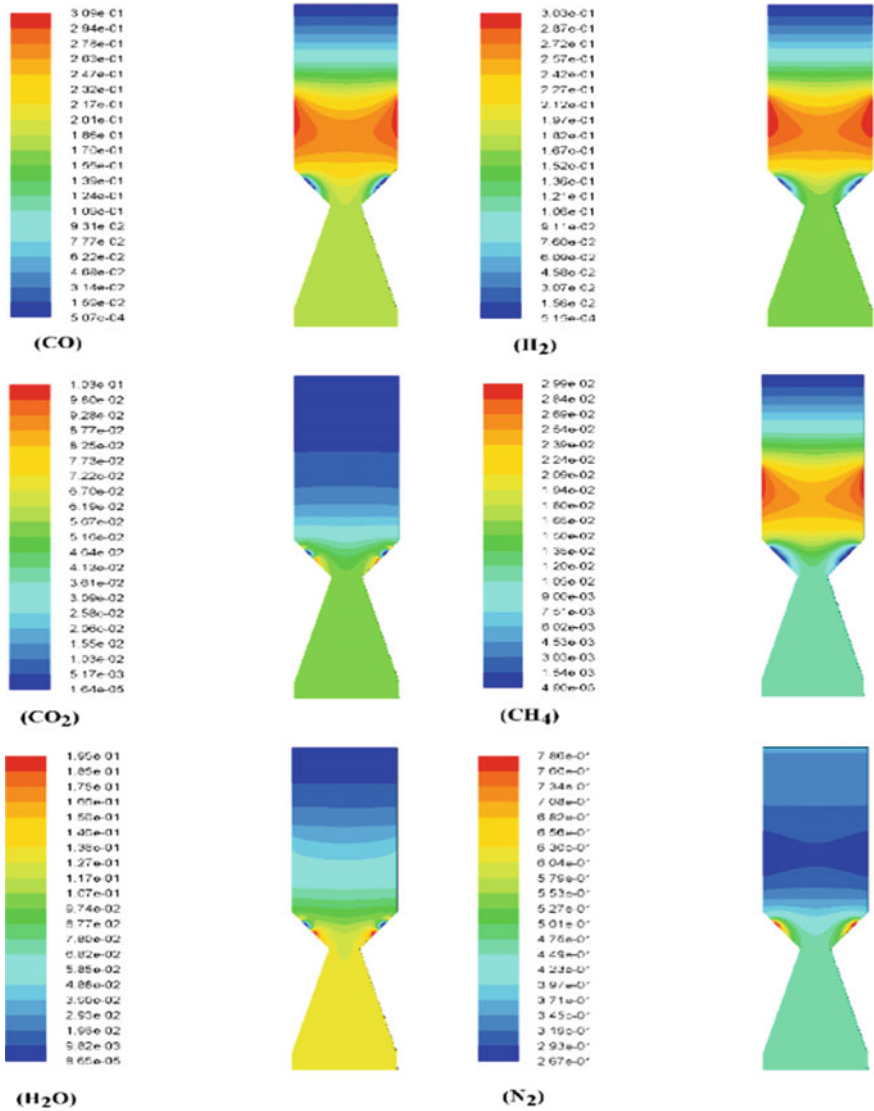


Fig. 9 Simulated various gas composition in downdraft gasifier

4 UCG Process Modelling

The main processes involved during the coal gasification are devolatilisation/pyrolysis, combustion/oxidation and reduction. In the UCG application, these mechanisms occur in the seam coal surface, and the research at the University of Glasgow is currently focused on the numerical modelling of surface reactions based

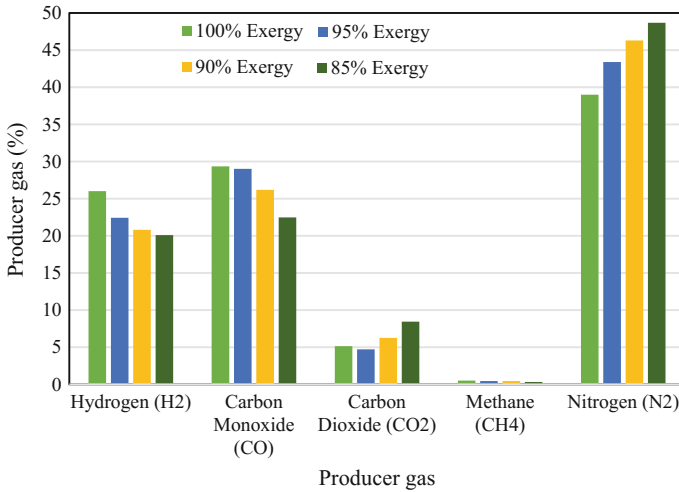


Fig. 10 Overall optimum conditions of moisture content range at 0–10%, temperature range at 1108–1145 K and equivalence ratio range at 0.26–0.37

on a coal (PSOC 1451) particle injected in a cylindrical reactor illustrated in Fig. 11 [42, 43].

The contour plot of furnace/reactor temperature presented in Fig. 12 indicates the oxidation process occurring dominantly, reaching the maximum of temperature of ~ 2100 K at 10 s. The temperature then gradually decreases due to the reduction of oxygen concentration which is replaced by the appearance of CO_2 concentration. After a time of 20 s, the reduction phase has started and at the time of 105 s it is a totally reduction zone. The further description of this behaviour can also be seen in the profile of oxygen and CO_2 in the reactor.

From Fig. 13a, the appearance of O_2 by the time is decreasing until at some point it disappears. This decrease is caused by its reaction with coal particle, producing CO and CO_2 , which is supported by Fig. 13b where the concentration of CO_2 is presented. The reduction of magnitude of CO_2 especially in the hot zone area, as seen in the contour plot of Fig. 13b, indicates its reaction with char and H_2O thus results in the production of other syngas products such as CO , H_2 and CH_4 presented in Fig. 14. These formations occur in the reduction stage/zone.

In order to establish a correlation of the reaction process at each zone with the syngas formation, the product gases are monitored with time and presented in Fig. 14. Each zone of gasification in the UCG application has its specific behaviour while producing the gas products as can be seen in Fig. 14. Along the reactor, the O_2 concentration decreases but in contrast CO_2 increases. In the same process, from the time 0–50 s, the H_2O increases and after 50 s, it then decreases. However, after

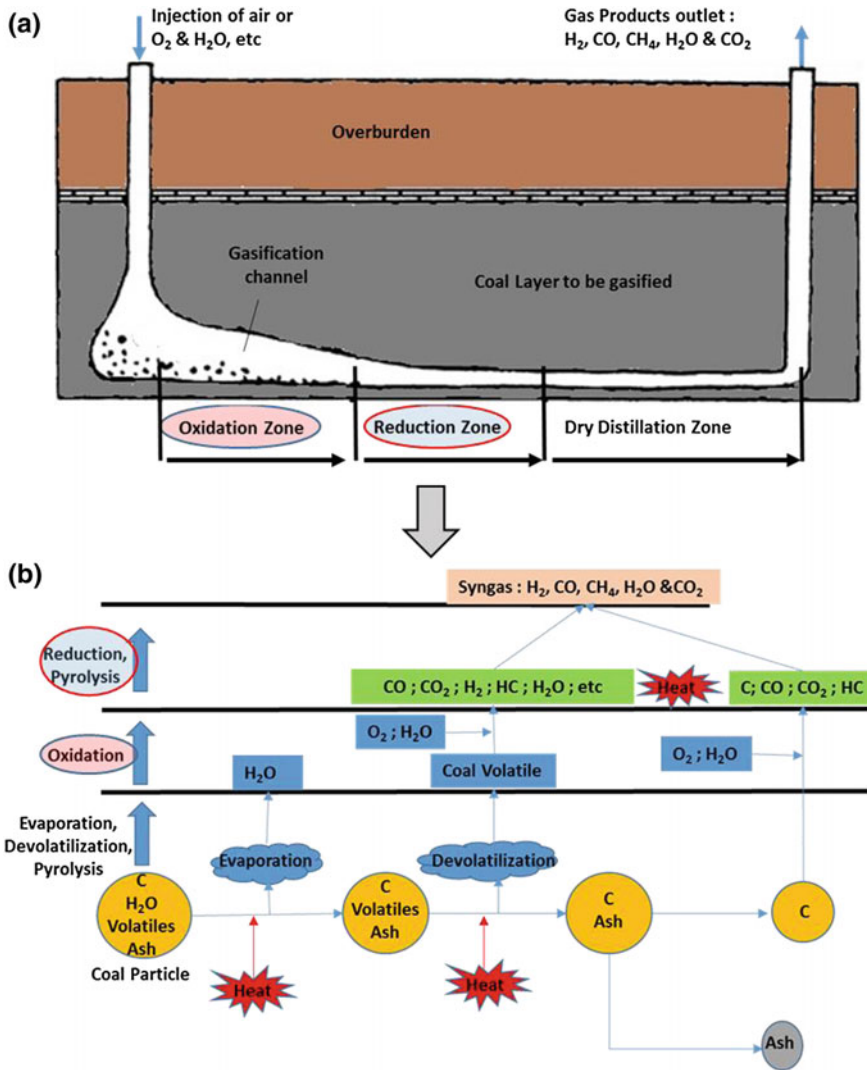


Fig. 11 Illustration of gasification in a seam coal in UCG [7] and b coal particle

50 s, the H₂ production increases slightly faster than it did before. Further, as seen in the figure, the area of the reduction zone in the furnace is larger after 50 s than the oxidation zone, thus correlating with the H₂ production as a consequence of the more H₂O reduction after this time. The same occurs for the others syngas products, thus increases the syngas products as it is expected.

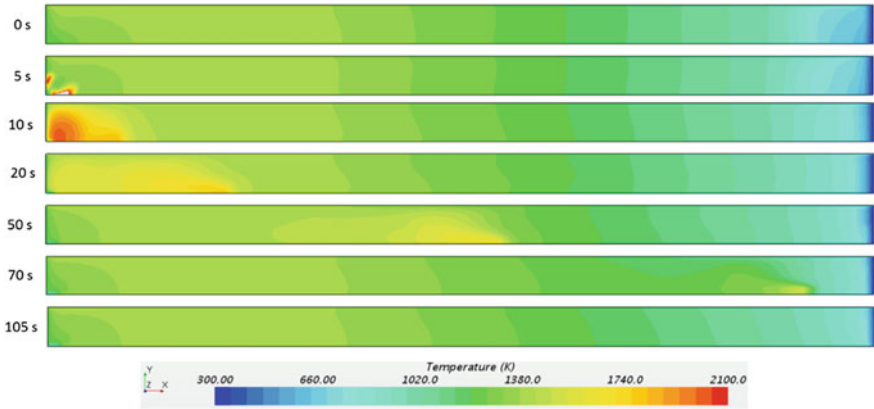


Fig. 12 Contour plot of temperature in the reactor

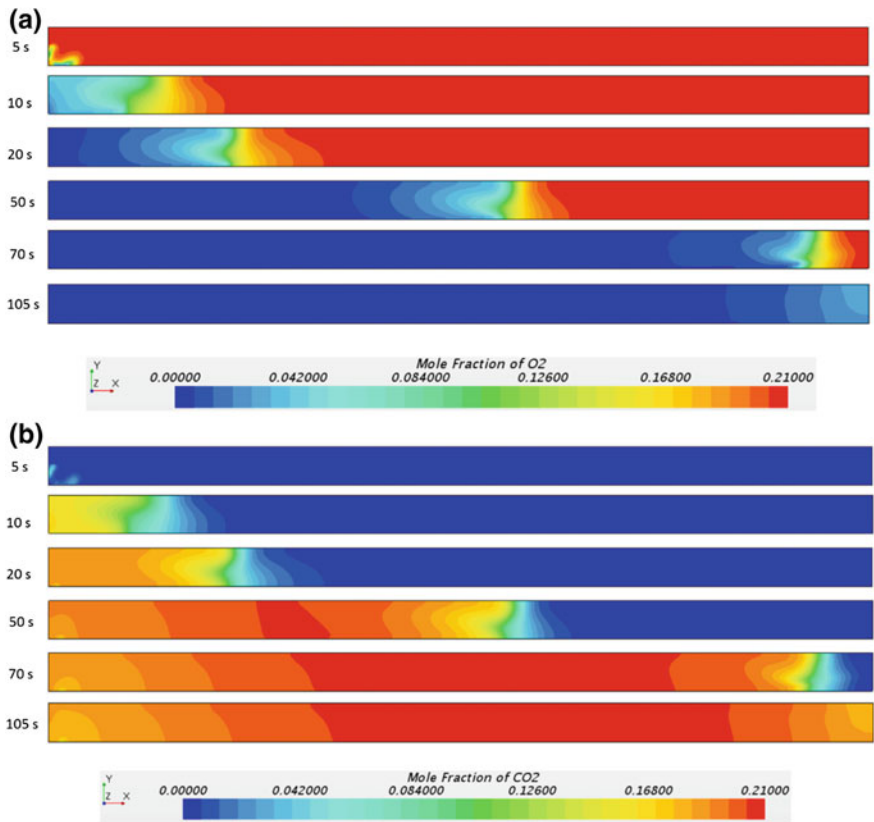


Fig. 13 Contour plots of a O₂ and b CO₂ in the furnace reactor

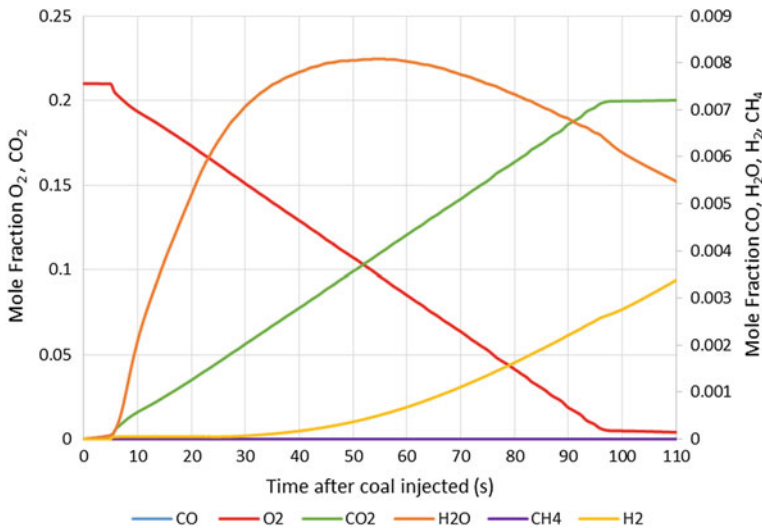


Fig. 14 Gas production profile of coal particle gasification

5 Conclusion

The chapter gives an overview of new modelling approaches used for coal, biomass and waste gasification. Kinetic work presents a four-zone kinetic model for a downdraft gasifier in which the gasification products are determined using a novel approach that includes an optimum length of the reduction zone. It gives accurate results for producer gas composition, tar content and gives also predictions for dimensions of a downdraft gasifier. Previous models never combined altogether in one work. Finally, the results from this model were used to test wide range of biomass materials to conclude the optimum working conditions and ideal feedstocks that give a higher yield of syngas with a lower tar content. Key design parameters for a downdraft gasifier are mentioned and its effect on working conditions is discussed using current model. A two-dimensional (2D) numerical model has been developed to run side by side with the kinetic model to simulate the rubber wood gasification in a downdraft gasifier using Eulerian–Lagrange computational fluid dynamics (CFD) model.

Based on the kinetic model developed, a Simulink model for an integrated gasifier and CHP model has been developed with the aim of predicting the most optimum gasifier design and syngas concentrations based on Scottish agricultural waste. The model incorporates a CHP engine that currently provides Glasgow University campus with heat and electricity. The model is able to predict the most adequate gasifier design and syngas quality for the based on the ultimate analysis of the feedstock and the electrical and thermal load required from the CHP engine.

An equilibrium numerical model of municipal solid waste (MSW) has been developed to simulate producer gas output in a downdraft gasifier under various working conditions. Finally, a coal particle model of gasification has been developed in order to give better understanding of chemical reactions process and the syngas formation. This model can be used to describe how the syngas formation in the oxidation or reduction zone as it occurs in the UCG application.

Acknowledgements Financial support for the research work presented in this chapter is received from the Innovate UK (132362, TS/N011686/1), Interface Food and Drink (IFD0190) and University of Glasgow KE Fund (GKE100). AMS, ANI and TS also thank, respectively, the British Embassy in Egypt and The Egyptian Cultural Affairs and Missions Sector, the Malaysian Government Majlis Amanah Rakyat (MARA) and the Ministry of Research and Higher Education (KEMENRISTEKDIKTI) Republic of Indonesia, for supporting their postgraduate research study at the University of Glasgow.

References

1. Basu P (2013) Biomass gasification, pyrolysis, and torrefaction. In: Practical design and theory, 2nd edn, Academic Press, Amsterdam
2. Climate Change (2013) The physical science basis, intergovernmental panel on climate change
3. United Nations Department of Economic and Social Affairs (2004) World population to 2300. United Nations, Department of Economic and Social Affairs, New York
4. EIA (2012) International energy statistics database. www.queia.gov/ies
5. WBA (World Bioenergy Association) (2016) WBA global bioenergy statistics
6. http://data.worldbank.org/indicator/EG.ELC.LOSS.ZS?end=2014&locations=GB&start=1960&view=chart&year_high_desc=false
7. Bhutto AW, Bazmi AA, Zahedi G (2013) Underground coal gasification: from fundamentals to applications. *Prog Energy Combust Sci* 39(1):189–214
8. Serranoa C, Monederoa E, Lapuertab M, Porteroa H (2011) Effect of moisture content, particle size and pine addition on quality parameters of barley straw pellets. *Fuel Process Technol* 92(3):699–706
9. Katak R, Chutia RS, Mishra M, Bordoloi N, Saikia R, Bhaskarb T (2015) Recent advances in thermochemical conversion of biomass. Amsterdam, Netherlands, pp 31–64
10. Li XT, Grace JR, Lim CJ, Watkinson AP, Chen HP, Kim JR (2004) Biomass gasification in a circulating fluidized bed. *Biomass Bioenergy* 171–193
11. Altafini CR, Wander PR, Barreto RM (2003) Prediction of the working parameters of a wood waste gasifier through an equilibrium model. *Energy Convers Manag* 44:2763–2777
12. Budhathoki R (2003) Three zone modeling of downdraft biomass gasification: equilibrium and finite kinetic approach. MSC thesis, University of Jyväskylä
13. Channiwala SA, Ratnadhariya JK (2009) Three zone equilibrium and kinetic free modeling of biomass gasifier—a novel approach. *Renew Energy* 34(4):1050–1058
14. Dejtrakulwong C, Patumsawa S (2014) Four zones modeling of the downdraft biomass gasification process: effects of moisture content and air to fuel ratio. *Energy Procedia* 52:142–149
15. Zainal ZA, Ali R, Lean CH, Seetharamu KN (2001) Prediction of performance of a downdraft gasifier using equilibrium modeling for different biomass materials. *Energy Convers Manag* 42(12):1499–1515

16. Dutta A, Jarunthammachote S (2007) Thermodynamic equilibrium model and second law analysis of a downdraft waste gasifier. *Energy* 32:1660–1669
17. Koroneos C, Lykidou S (2011) Equilibrium modeling for a downdraft biomass gasifier for cotton stalks biomass in comparison with experimental data. *J Chem Eng Mater Sci* 2(4):61–68
18. Vaezi M, Fard MP, Moghiman M (2007) On a numerical model for gasification of biomass materials. In: 1st WSEAS international conference on computational chemistry, cairo, egypt. 29–31 Dec 2007
19. Salem AM, Paul MC (2016) An integrated kinetic model for a downdraft gasifier based on a novel approach. *Int J Adv Sci Eng Technol* 4(3):182–185
20. Salem AM, Paul MC (2017) Integrated kinetic modelling and design for downdraft gasifiers based on a novel approach. *Biomass Bioenergy* (under revision)
21. Roy PC, Chakraborty N (2009) Modelling of a downdraft biomass gasifier with finite rate kinetics in the reduction zone. *Int J Energy Res* 833–51
22. Koufopanos CA, Maschio G, Lucchesit A (1989) Kinetic modelling of the pyrolysis of biomass and biomass components. *Can J Chem Eng* 67
23. Babu BV, Chaurasia AS (2003) Modeling, simulation and estimation of optimum parameters in pyrolysis of biomass. *Energy Convers Manag* 44:2135–2158
24. Sharma AK (2011) Modeling and simulation of a downdraft biomass gasifier 1. Model development and validation. *Energy Convers Manag* 52:1386–1396
25. Tinaut FV, Melgar A, Pérez JF, Horrillo A (2008) Effect of biomass particle size and air superficial velocity on the gasification process in a downdraft fixed bed gasifier. An experimental and modelling study. *Fuel Process Technol* 89:1076–1089
26. Bridgewater R, Shand A (1984) Fuel gas from biomass: status and new modeling approaches. In: *Thermochemical processing of biomass*, pp 229–254
27. Giltrap DL, McKibbin R, Barnes GRC (2003) A steady state model of gas-char reactions in a downdraft biomass gasifier. *Sol Energy* 74:85–91
28. Kinoshita CM, Wang Y (1993) Kinetic model of biomass gasification. *Solar Energy* 51 (1):19–25
29. Armin Silaen TW (2010) Effect of turbulence and devolatilization models on coal gasification simulation in an entrained flow gasifier. *Int J Heat Mass Transf* 53:2074–2091
30. Chan MC (2000) Numerical simulation of entrained flow coal gasifier—Part II: Effects of operating conditions on gasifier performance. *Chem Eng Sci* 55:3875–3883
31. Chan MC (2000) Numerical simulation of entrained flow coal gasifiers—Part I: Modeling of coal gasification in an entrained flow gasifier. *Chem Eng Sci* 55:3861–3874
32. Chen CJ (2012) Numerical investigation on performance of coal gasification under various injection patterns in an entrained flow gasifier. *Appl Energy* 100:218–228
33. ANSYS Inc (2013) ANSYS 15 fluent theory guide, Canonsburg, PA 15317
34. Kumar U, Salem AM, Paul MC (2017) Investigating the thermochemical conversion of biomass in a downdraft gasifier with a volatile break-up approach. In: 9th international conference on applied energy (ICAE2017), Cardiff, UK
35. Janajreh MS (2013) Numerical and experimental investigation of downdraft gasification of wood chips. *Energy Convers Manag* 65:783–792
36. Paul MC (2016–2017) Farm waste utilisation: robust thermal engineering approach for generating energy from wastes. <http://www.combgen.gla.ac.uk/index.php?id=news&post=common-interest-group-on-farm-waste-utilisation>
37. The National Non-Food Crops Centre, National and regional supply/demand balance for agricultural straw in Great Britain
38. McKendry P (2002) Energy production from biomass (part 3): gasification technologies. *Biores Technol* 83(1):55–63
39. Jayah TH, Aye L, Fuller RJ, Stewart DF (2003) Computer simulation of a downdraft wood gasifier for tea drying. *Biomass Bioenergy* 45:459–469

40. Dutta PP, Pandey V, Das AR, Sen S, Baruah DC (2014) Down draft gasification modelling and experimentation of some indigenous biomass for thermal applications. *Energy Procedia* 54:21–34
41. Mendiburu AZ, Carvalho JA, Coronado CJR (2013) Thermochemical equilibrium modeling of biomass downdraft gasifier: stoichiometric models. *Energy* 66:1–13
42. Sutardi T, Paul MC, Karimi N, Younger PL (2017) Identifying kinetic parameters for char combustion of a single coal particle. In: *Proceeding of the European combustion meeting, Dubrovnik, Croatia, 18–21 April 2017*
43. Sutardi T, Paul MC, Karimi N, Younger PL (2017) Numerical modelling for process investigation of a single coal particle combustion and gasification. In: *Proceedings of the World Congress on Engineering, vol II. London 5–7 July 2017, pp 946–951. ISBN:978-988-14048-3-1*

Transient Cold Flow Simulation of a Fast Fluidized Bed Fuel Reactor for Chemical Looping Combustion

Ramesh K. Agarwal, Mengqiao Yang and Subhodeep Banerjee

Abstract Circulating fluidized bed (CFB) in chemical looping combustion (CLC) is a novel carbon capture technology which offers great advantage for high efficiency and low cost. To obtain a thorough understanding of the hydrodynamics behavior inside the reactors as well as CLC process, numerical simulations are conducted. Computational fluid dynamics (CFD) simulations are performed with dense discrete phase model (DDPM) to simulate the gas–solid interactions. CFD commercial software ANSYS Fluent is applied for the simulations. Two bed materials of different particle density and diameter, namely the molochite and Fe100, are used in studying the hydrodynamics and particle behavior in a fuel reactor corresponding to the experimental setup of Haider et al. at Cranfield University in U.K. Both the simulations reach satisfactory agreement with the experimental data concerning both the static pressure and volume fraction at various heights above the gas inlet inside the reactor. It is found that an appropriate drag law should be used in the simulation depending on the particle size and flow conditions to obtain accurate results. The simulations demonstrate the ability of CFD/DDPM to accurately capture the physics of CFB-based CLC process at pilot scale which can be extended to industrial-scale applications.

Keywords Chemical looping combustion · Circulating fluidized bed DDPM · Cold flow simulation · Solid volume fraction · Molochite

1 Introduction

In 1896, Arrhenius was the first to quantify the contribution of CO₂ to the greenhouse effect and analyze the relationship between long-term variations in climate and the concentration of CO₂ [1]. Since the 1970s, fossil fuels have dominated the

R. K. Agarwal (✉) · M. Yang · S. Banerjee
Washington University in St. Louis,
1 Brookings Drive, St. Louis, MO 63130, USA
e-mail: rka@wustl.edu

© Springer Nature Singapore Pte Ltd. 2018
S. De et al. (eds.), *Coal and Biomass Gasification*, Energy, Environment,
and Sustainability, https://doi.org/10.1007/978-981-10-7335-9_13

fuel markets for power generation worldwide; today, 39% more oil, 107% more coal, and 131% more natural gas are used in the world compared to that in 1980 [2]. Greenhouse gas produced from fossil fuels combustion absorbs infrared thermal radiation from solar energy thus leads to an increase in the atmospheric average temperature causing global warming. The resulting changes due to global warming in the rain patterns, melting of polar ice caps, and rising sea levels will sharply affect the human and animal habitats and ecosystems. Although some renewable energy such as wind, solar, geothermal, tide, and ocean waves, as well as nuclear energy can alleviate the global warming effects since they are emissions-free, their industrial use is still very limited due to their relatively higher cost and low efficiency; however, this situation is likely to change in the next decade. Since the fossil fuels are predicted to maintain their position as the dominant energy source in the near future [3], development of techniques for carbon capture from power plants and other industrial processes emitting CO₂ and its sequestration and utilization has become the focus of modern research in combustion technology.

In recent years, chemical looping combustion (CLC) has been put forward as a next-generation CO₂ capture technology which shows great promise for low cost and high efficiency. To avoid direct contact between fuel (gas or coal particles) and oxygen, this technology employs metal oxide solids as the oxygen carrier (OC). Gaseous fuel is injected into the fuel reactor, and then it is oxidized by the OC to initiate combustion; the reduced OC is then transferred to an air reactor and is re-oxidized by air; finally, the re-oxidized OC is transported back to the fuel reactor to complete a looping process. In this way, H₂O and CO₂ produced in the fuel reactor are completely separated from the air and no extra separation process is required for capture of pure CO₂ compared to the traditional carbon capture technologies such as post-combustion capture or oxy-fuel combustion which requires separation of oxygen from air resulting in 12–20% increase in energy requirements [4]. The performance of a CLC system significantly depends on the choice of an oxygen carrier; the ideal oxygen carrier should have high conversion and reaction rates as well as nontoxic behavior [5]. The application of solid fuels such as biomass or coal in CLC has also attracted great attention, and several injection methods have been put forward. One method is to inject coal into syngas and obtain a fully gasified fuel mixture which is subsequently injected into the fuel reactor [6]. From a CLC perspective, using pre-gasified coal in the fuel reactor is essentially identical to using gaseous fuel. Another method, coal-direct chemical looping combustion (CD-CLC), aims to inject pulverized coal into the fuel reactor where it devolatilizes and is gasified before reacting with the OC [7]. For CLC systems, the fuel reactor configurations, such as the moving bed, packed bed, bubbling bed, or fast fluidized bed, also have an influence on the system behavior as well as its performance. The fast fluidized bed, which was first introduced by Yerushali et al. is the concentration of this paper [8]. The fast fluidized bed can generate a region in which the solid–gas relative slip velocity changes rapidly. Many researchers have studied the gas velocities and slip velocities in the fast fluidization regime [9]. Compared to the packed bed and bubbling bed, the fast fluidized bed produces greater gas–solid contact, which leads to a higher fuel conversion rate [8]. However,

the major difficulty lies in its inability to accurately control the circulation and solid transfer rates. In this paper, CFD cold flow simulations are conducted to understand the hydrodynamics inside a fast fluidized bed.

Majority of the CLC studies have been performed by conducting small-scale experiments in a laboratory. There are very few pilot-scale CLC plants and hardly any large-scale industrial plants. Due to the high cost associated with industrial-scale CLC projects, computational fluid dynamics (CFD) simulations can provide a much cheaper alternative to study their detailed hydrodynamics, chemistry, and performance [10]. However, even though laboratory-scale and pilot-scale studies of CLC are mostly investigated, numerical simulations using CFD have been rarely mentioned. By selecting different modeling approaches, simulations of multiphase flows of granular solid and gas systems with different fluidized beds can be performed. The two-fluid model or Eulerian–Eulerian considers both the gas and solid phase as interpenetrating continua, and the mass, momentum, and energy equations are calculated by averaging the particle variables over an appropriate region with constitutive relations for the solid phase obtained from the kinetic theory of granular flow, which is an extension of the classical kinetic gas theory. By using the two-fluid model, the work of Ding and Gidaspow [11] shows great agreement for a bubbling bed simulation. The Eulerian–Eulerian approach requires less computational resources and is often used for pilot and industrial-scale modeling [12]. However, its disadvantage is that due to treatment of the solid phase as a continuous phase; it cannot trace the dynamic behavior of particles. The Eulerian–Lagrangian approach, also known as discrete element method (DEM), however, treats the gas as a continuous phase and the solids as discrete particles that are tracked individually. However, due to the limitation of computational resources, DEM models are typically limited to small-scale applications with the number of particles normally constrained to around 1 million [13]. To avoid this limitation, the dense discrete phase model (DDPM) has been put forward [14]. DDPM no longer explicitly tracks the details of particle–particle and particle–wall collisions but employs a force to represent the details of the collisions; this approach thus accelerates the simulation. Since DDPM can implement the realistic particle distribution and track the discrete nature while maintaining a lower computational cost than DEM [15], it is an ideal modeling approach for simulation of a pilot-scale CLC project.

In a cold flow experiment conducted at Cranfield University in UK, Haider et al. [16] mention encountering the problem of controlling the solids transfer and circulation rates inside the fuel reactor. By employing the numerical simulation, the cause of this problem can be thoroughly investigated. Given the large number of particles involved in the experiment and the level of accuracy desired, DDPM is well-suited for this simulation. In this paper, CFD simulation of the multiphase flow using DDPM is conducted and compared with the experimental data of Haider et al. [16]. Additional simulations are also conducted using different bed materials, and the hydrodynamic behavior at various bed heights is investigated. The aim of this paper is to demonstrate the capability of DDPM simulation in modeling a

pilot-scale fast fluidized bed and lay the foundation for large-scale simulations using solid fuel in industrial-scale modeling of CLC system.

2 Modeling Approach for DDPM Simulation

In this paper, a CFD simulation software, ANSYS Fluent version 14.5 [17, 18], is employed in the modeling work. In Fluent, the dense discrete phase model (DDPM) formulation assumes that the solid phase is sufficiently dilute, so that the effects of the particle volume fraction on the gas phase and the particle–particle interactions can be neglected; it requires that the volume fraction of solid phase should be constrained to within 12% [18]. Since no chemical reactions are considered in this cold flow simulation, only the mass and momentum conservation equations are considered to compute the gas phase flow field.

The gas phase is treated as a continuous phase, and the mass conservation (continuity) equation can be represented as

$$\frac{\partial}{\partial t} (\alpha_f \rho_f) + \nabla \cdot (\alpha_f \rho_f u_f) = 0 \quad (1)$$

where α_f , ρ_f , and u_f represent the local volume fraction, the density, and the velocity of the fluid phase, respectively. The conservation of momentum equation is written as

$$\frac{\partial}{\partial t} (\alpha_f \rho_f u_f) + \nabla \cdot (\alpha_f \rho_f u_f u_f) = -\alpha_f \nabla p_f - \nabla \cdot \bar{\bar{\tau}}_f + \alpha_f \rho_f \mathbf{g} - R_{sg} \quad (2)$$

where p_f , $\bar{\bar{\tau}}_f$, and \mathbf{g} represent the fluid pressure, the fluid shear stress tensor, and the acceleration due to gravity respectively, and R_{sg} is the transfer of fluid momentum to the solid phase.

For an Newtonian fluid, the shear stress tensor $\bar{\bar{\tau}}_f$ is given by

$$\bar{\bar{\tau}}_f = \mu_f \left[\left(\nabla u_f + \nabla u_f^T \right) - \frac{2}{3} \nabla \cdot u_f \bar{\bar{I}} \right] \quad (3)$$

For the solid phase, the trajectory of the particles is obtained from the force balance given by

$$\frac{\partial u_s}{\partial t} = \mathbf{g} \frac{(\rho_f - \rho_s)}{\rho_s} + F_D (u_f - u_s) + F_{KTGF} \quad (4)$$

The terms on the right-hand side in Eq. (4) are forces due to gravity, interphase drag, and particle collisions, respectively. The drag coefficient F_D is

$$F_D = \frac{18\mu_f C_D Re_p}{\rho_p d_p^2} \frac{C_D Re_p}{24} \quad (5)$$

where d_p represents particle diameter; C_D represents the drag coefficient; and Re_p represents the Reynolds number, which is defined as

$$Re_p = \frac{\rho_f d_p |u_f - u_p|}{\mu_f} \quad (6)$$

The drag coefficient used in this work is from the drag model of O'Brien and Syamlal [19] because it corrects for the terminal velocity, which is the minimum required velocity to lift the particle moving out of the bed and thus is a significant index for characterizing the motion of a fluidized bed.

$$C_D = \left(0.63 + \frac{4.8}{\sqrt{Re_p/v_{r,p}}} \right)^2 \quad (7)$$

where $v_{r,p}$ represents the terminal velocity correction given by

$$v_{r,p} = 0.5 \left(A - 0.06Re_p + \sqrt{(0.06Re_p)^2 + 0.12Re_p(2B - A) + A^2} \right) \quad (8)$$

$$A = \alpha_f^{4.14} \text{ and } B = \begin{cases} 0.8\alpha_f^{1.28} & \text{if } \alpha_f \leq 0.85 \\ \alpha_f^{2.65} & \text{if } \alpha_f > 0.85 \end{cases}$$

In the DDPM approach, the force due to particle collisions is obtained from the particle pressure predicted using the kinetic theory of granular flows given by

$$F_{KTGF} = -\nabla \cdot \bar{\bar{\tau}}_s \quad (9)$$

3 Simulation of Fast Fluidized Bed with Molochite as Bed Material

In this section, a coupled CFD/DDPM model of a fast fluidized bed is applied with molochite as the bed material. The simulation offers an understanding of the pressure and volume fraction distribution at different bed heights. To simplify the simulation, the current work only considers the fuel reactor section of the Cranfield pilot-scale advanced capture technology (PACT) circulating fluidized bed reactor and maintains a constant circulating solids mass flow corresponding to the experimental conditions by utilizing a constant solids injection. The geometry and mesh of the fuel reactor are presented in Fig. 1. The geometry is a 1:1 scale model

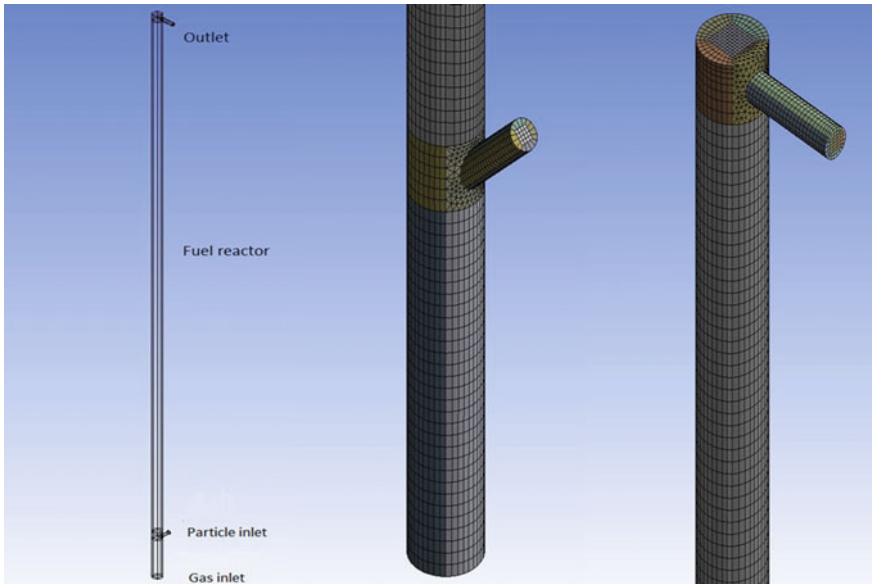


Fig. 1 Geometry and mesh in the upper and lower part of the fuel reactor of Haider et al. [16]

derived from the PACT reactor [16]. The riser height is 7.3 m with an interior diameter of 0.1 m, and the diameters of the particle inlet and outlet pipes are 0.04 m. The mesh including 107578 computational cells is generated such that the solution is mesh independent. A second-order upwind numerical scheme provides an accurate and stable solution.

The molochite particles used in this simulation have a density of $1,400 \text{ kg/m}^3$ and average diameter of 519 μm . To further reduce the computational cost, the work implements the parcel concept to simplify and accelerate the simulation process [20]. One parcel stands for a cluster of particles with the same intensive properties as the individual particles. The mass and volume of the parcels are adopted during the calculations instead of those of the individual particle. The parcel diameter is set at 0.002 m which is slightly less than the minimum numerical cell size required so that a total of 178,265 parcels are initially employed in the entire system. The key modeling parameters for this DDPM simulation are given in Table 1.

This simulation is conducted using ANSYS Fluent v.14.5 [17, 18]. The total simulation lasts for around 300 physical hours due to the large number of particles. The pressure and velocity distributions are monitored at several different height-inlet, 0.4, 0.45, 0.68, 0.75, 3.05, 5.0, 5.9, and 6.2 m. Prior to the start of the simulation, 178,265 particles are released into the fuel reactor and are totally settled down for 0.5 s so that the kinetic energy of the particles becomes negligible and the particles can be randomly distributed. This settled particle bed is considered as the initial condition for the simulation. Then, the gas inlet boundary condition is set to

Table 1 Key modeling parameters for the fast fluidized bed simulation with molochite as bed material

Particle diameter	0.000519 m (519 μm)
Parcel diameter	0.002 m
Particle density	1,400 kg/m^3
Primary phase material	Air
Discrete phase material	Molochite
Gas inlet boundary condition	Velocity inlet at 2.55 m/s
Particle inlet boundary condition	Wall; particle injection at 3.2 $\text{kg/m}^2/\text{s}$
Outlet boundary condition	Pressure outlet
Drag model	Syamlal–O’Brien [19]
Numerical scheme	Phase-coupled simple
Discretization scheme	Second-order upwind
Time step	Fluid: 1×10^{-3} s, particle: 1×10^{-4} s

inject the fluidizing gas from the bottom of the riser at 2.55 m/s. Meanwhile, the mass flux at the particle inlet is set at 3.2 $\text{kg/m}^2/\text{s}$, which corresponds to the solids circulation rate of Haider et al. [16]. The particle velocities and distributions are monitored at 1 s intervals, which are shown in Fig. 2.

From Fig. 2, the fast fluidization regime inside reactor is clearly evident. Once gas is injected, the settled bed of particles experiences a sudden lift force and the particles begin to move upward. The leading particles cluster reaches the top of the reactor at around 17 s where they exit the fuel reactor (the rest of the circulating fluidized bed system is not considered in the present simulation). To further investigate the circulation condition, the particle mass flow rate at the outlet, averaged over 0.5 s intervals, is shown in Fig. 2. From Fig. 3, few particles escape the fuel reactor from the start of the simulation at a discontinuous rate. A continuous stream of particles begins to exit the fuel reactor at around 17 s, as shown by the particle tracks in Fig. 2. From this time to the end of the simulation, the mass flow at the outlet was almost stable at around 0.002 kg/s . This is of the same order as the particle injection rate of 0.004 kg/s used in the simulation to represent the continuous particle recirculation in the experiment of Haider et al. [16]. Hence, a stable circulating system has been successfully achieved in the simulation. The slightly lower outlet mass flow is due to a slightly reduced initial particle loading compared to the experimental condition.

Since it is the pressure gradient that drives the particles movement in the reactor, it is necessary to investigate the pressure trend. Time variations of the static pressure at height of 0 m (gas inlet), 0.4 m, 0.68 m, and 5.9 m are shown in Fig. 4. As soon as the gas is injected, it immediately experiences resistance from the particle bed that causes a significant spike in static pressure detected by the inlet monitor. As the gas moves through the bed, the pressure spike is still evident at different heights simultaneously but at a reduced magnitude. With time, the particles in the bed begin to move upward by the pressure buildup leading to decrease in

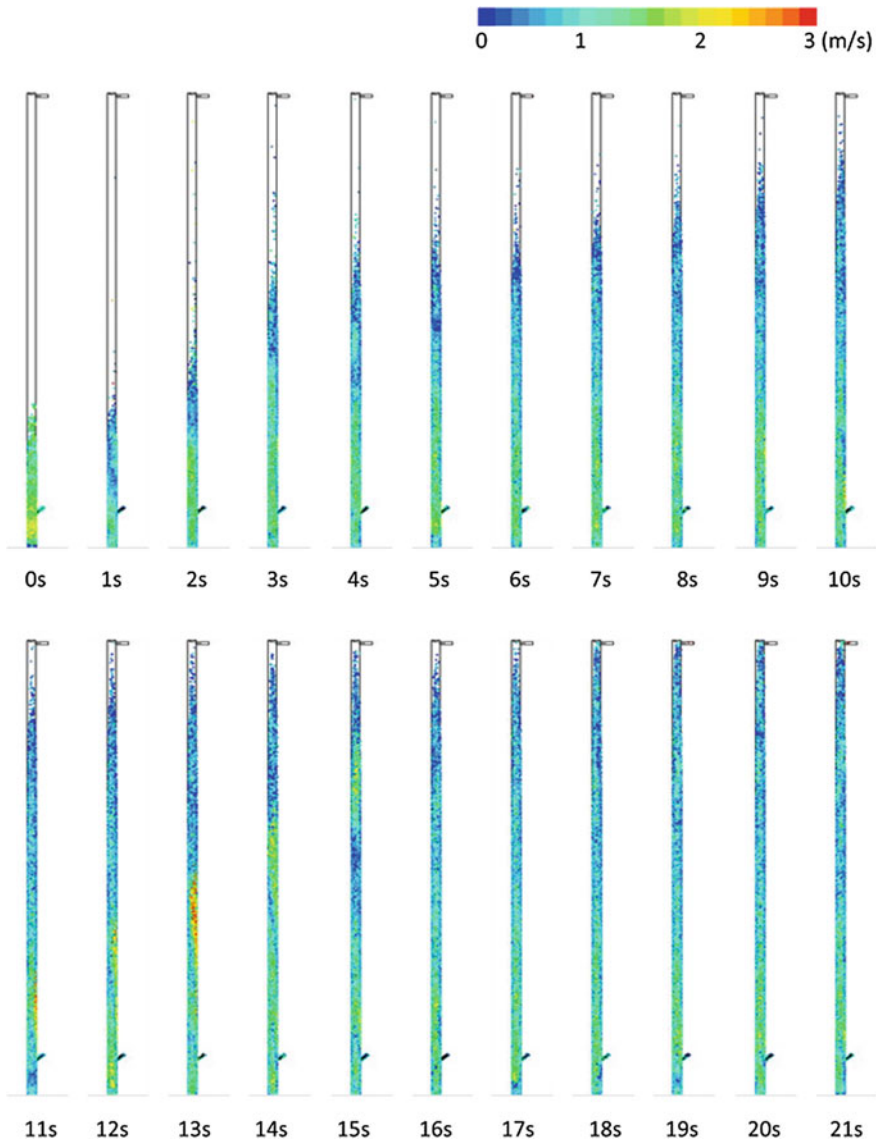


Fig. 2 Particle tracks colored by velocity magnitude for the fast fluidized bed simulation with molochite

the pressure at the inlet and increase in higher planes. At 5.9 m near the top of the bed, there is minimal effect on the pressure because of the movement of particles. The pressures in the bed stabilize after around 5 s when the fast fluidization regime is fully developed.

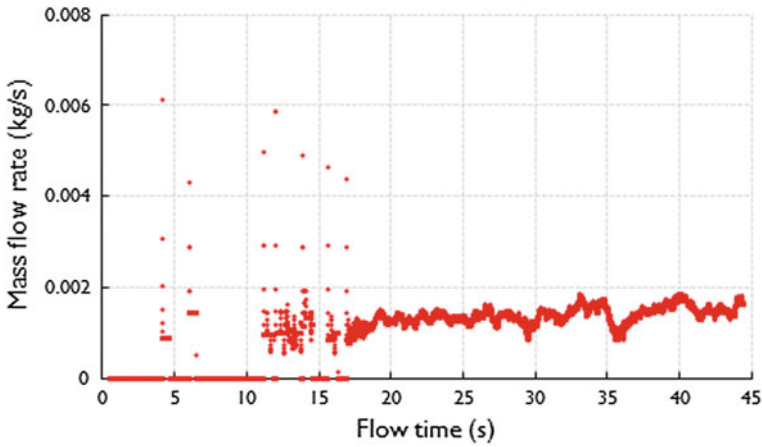


Fig. 3 Time variation of outlet mass flow rate for the fast fluidized bed simulation with molochite

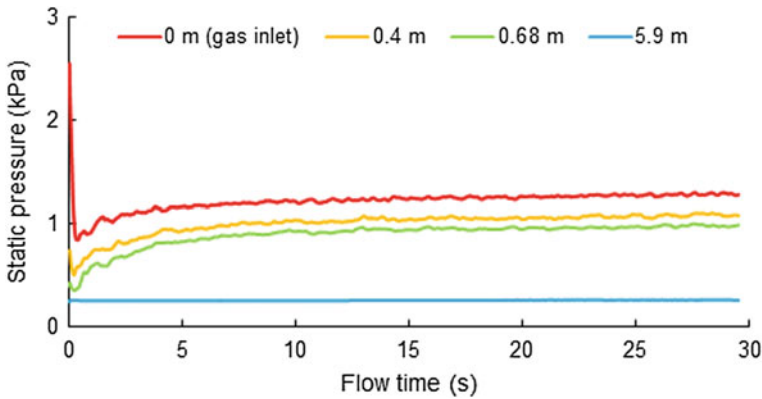


Fig. 4 Time variation of static pressure at various heights for the fast fluidized bed simulation with molochite

The solids volume fractions at different heights are also investigated and are shown in Fig. 5. From 0.5 s, the volume fraction at the bottom experiences a large value due to the gathered initial particles as a result of momentum transfer and particles movement, and the particles at lower height are driven to the top of the reactor. Higher heights at 0.4 and 0.75 m experience the volume increment in the following period with a decreasing magnitude. For example, at 0.5 s, volume fraction at bottom is monitored at 0.48, but the volume fractions at 0.4 and 0.75 m remain zero until 0.77 and 1.12 s, when both of these planes experience a volume fraction increment of 0.2 and 0.16, respectively. Afterward, the volume fractions at various heights decrease and tend to remain unchanged after several seconds, which indicate a stable particle distribution in the reactor.

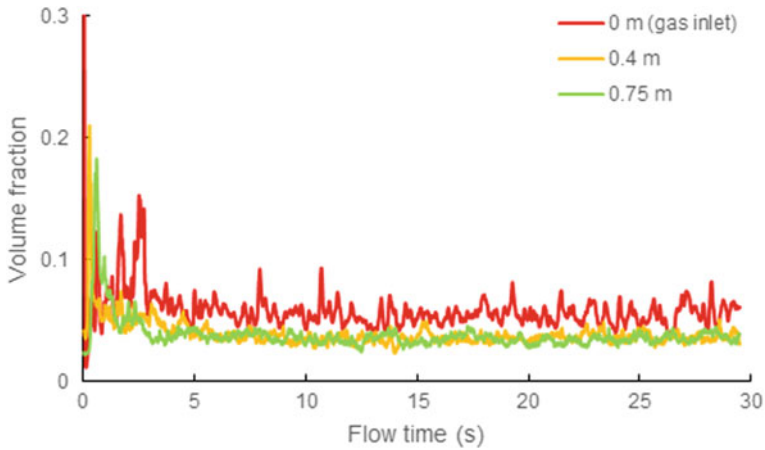


Fig. 5 Time variation of volume fraction at various heights for the fast fluidized bed simulation with molochite

The stable time-averaged pressures at various heights along the fuel reactor are shown in Figs. 6 and 7 and are compared with the experimental data from Haider et al. [16]. From Fig. 6, the simulation pressure matches with the experimental data both in trend and magnitude except at the gas inlet. The discrepancy in the pressure at the bottom (gas inlet) can be explained as the consequence of different initial process used in the simulation which is different from the experiment. In the experiment, the particles are released from a narrow tunnel throughout, whereas in the simulation, the particles are injected directly from the bottom and are allowed to

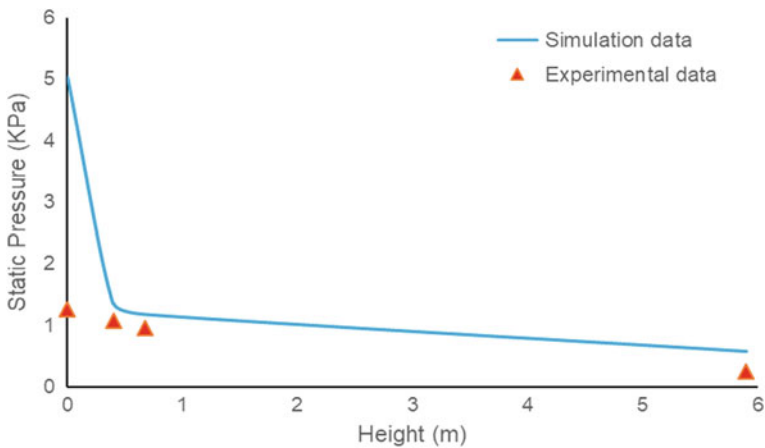


Fig. 6 Comparison of pressure variation at various heights for the fast fluidized bed simulation with molochite

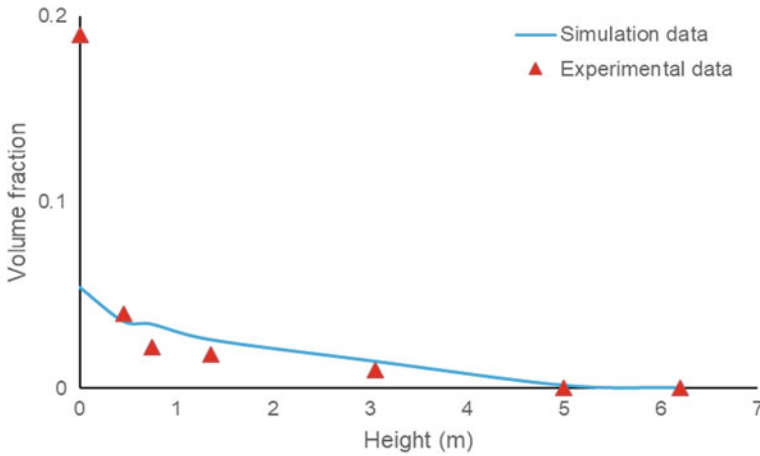


Fig. 7 Comparison of volume fraction at various heights for the fast fluidized bed simulation with molochite

settle for 500 ms prior to gas injection. The influence of the initialization decays along the height of the reactor, and pressure data at higher planes are consistent with the experimental results. An obvious pressure gradient is observed in Fig. 6, which highlights the crucial role that pressure plays in the particle circulation in the fast fluidized bed. The plot of the volume fraction in Fig. 7 also displays a gradient along the height, which can be considered as the main reason for the pressure gradient in Fig. 6. The discrepancy between the simulation and the experiment at the gas inlet is also evident in Fig. 7 due to the difference in the initialization process in the simulation and the experiment.

4 Simulation of Fast Fluidized Bed with Fe100 as Bed Material

The multiphase simulation results in Sect. 3 demonstrate that the CFD/DDPM simulations capture the flow and particles hydrodynamics of low-density bed materials quite well. In this section, a higher density material is considered to determine how the performance of fast fluidized bed depends on the material density. In this simulation, the bed particles are Fe100 with a diameter of 6×10^{-5} m (60 μ m) and a density of 5,818 kg/m³. It should be noted that although the Syamlal–O’Brien drag law [19] used in Sect. 4 works well for large diameter, low-density particles like molochite, it does not provide accurate results for the fine Fe100 particles considered in this section. Therefore, a more general drag law due to Gidaspow [21] is employed which is well-suited for both the packed and dilute portions of the fast fluidized bed system to capture accurately the hydrodynamic

behavior. The gas injection rate is maintained at 2.55 m/s as in Sect. 3, and all other modeling parameters are kept the same as in Table 1. For the initialization process, 178,265 particles are released into the riser which are settled down for 500 ms. By keeping the parcel diameter the same, the computational cost for Fe100 simulation does not increase a lot. The particle velocities and distributions are inspected at 0.01 s intervals, and the particle tracks and mass flow rate at the outlet are given in Figs. 8 and 9, respectively.

Figure 8 shows that the finer Fe100 particles require less travel time compared to molochite; the leading particles cluster reaches the top of the fuel reactor at 1.25 s.

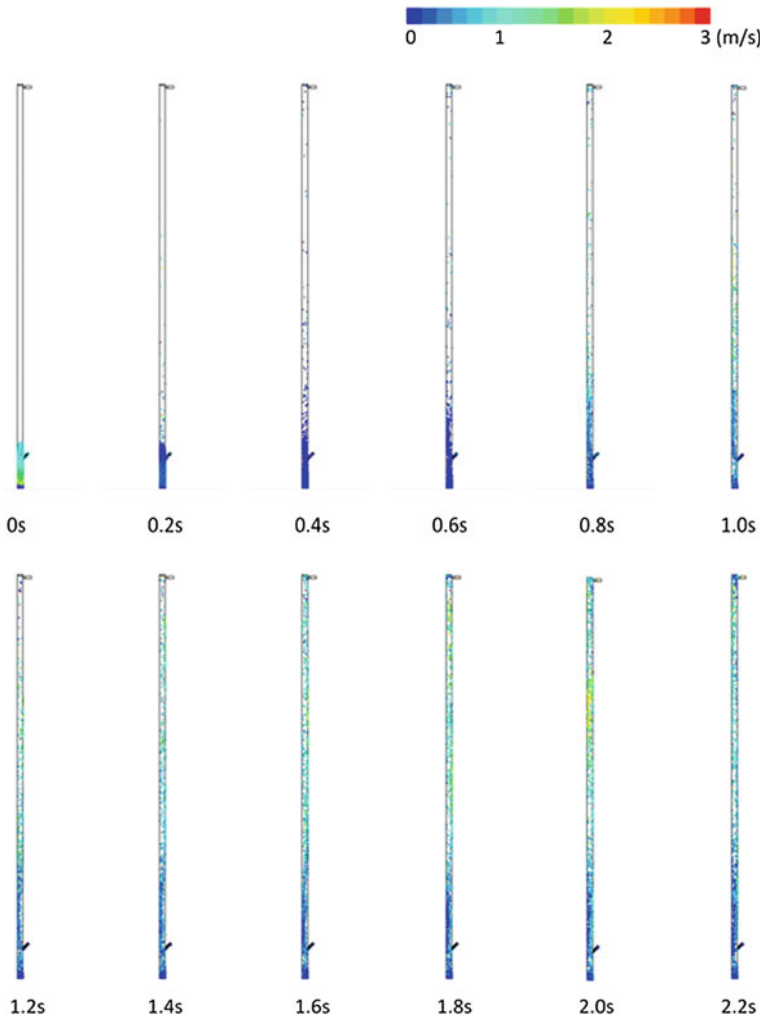


Fig. 8 Particles tracks colored by velocity magnitude for the fast fluidized bed simulation with Fe100

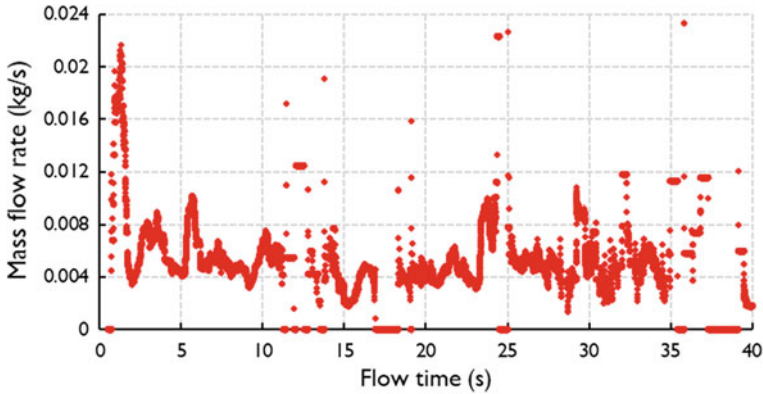


Fig. 9 Time variation of outlet mass flow rate for the fast fluidized bed simulation with Fe100

Given the smaller diameter, the Fe100 particles are less likely to collide with one another when moving through the reactor and thus reach the top earlier. From the particle tracks shown in Fig. 9, it can be observed that the particles outflow does not demonstrate continuous behavior. The use of the Gidaspow drag law [21] could be one possible reason. Although the Gidaspow drag law shows a wide applicability for various fluidized bed systems, it may not represent the physical behavior for this specific situation; thus, further improvement to the particle drag law is recommended. The discontinuity in the particles outflow could also be attributed to the relatively coarse mesh at the outlet, a constraint imposed by the available computational resources. However, the average mass flow rate remains nearly stable from 30 s onwards, consistent with a stable circulation condition as observed in the experiment [16].

The pressure distributions at different heights are displayed in Fig. 10. Similar to the case in Sect. 3 with molochite as bed material, it is clear that a pressure gradient exists in the fuel reactor. However, in this case, the pressure at the bottom of the reactor experiences unsteady behavior due to the irregular and uncertain movement and collisions of the large number of fine Fe100 particles. At higher planes, the pressure is relatively stable due to the reduced particle concentration. Particle volume fractions at various heights are shown in Fig. 11. The volume fraction at the bottom of the reactor is unsteady: It increases gradually for the first 12 s and then oscillates irregularly up to 30 s, which also corresponds to the observed pressure changes in Fig. 10. This is reasonable since the variation in the static pressure is caused by the presence of particles. After 30 s, the bottom volume fraction achieves relatively stable behavior. In addition, the particles behavior at the bottom only slightly affects the volume fraction at higher planes due to the small number of particles transferred. To validate the fast fluidized bed simulation with Fe100, comparisons of pressure and volume fraction between the simulation and experiment [16] are given in Figs. 12 and 13, respectively. The results of simulation match the experiment data both in trend and magnitude except for differences at the

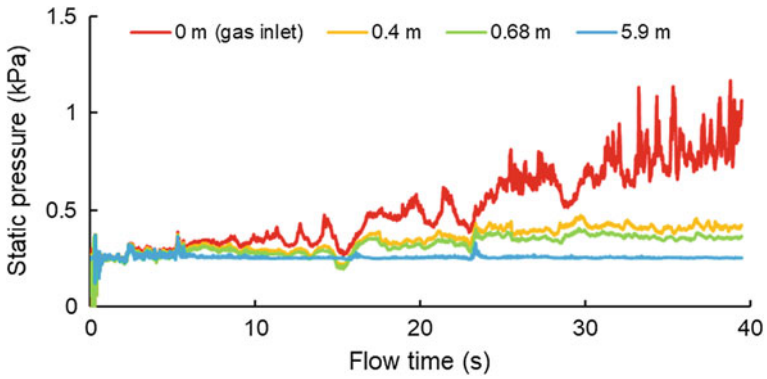


Fig. 10 Time variation of static pressure at various heights for the fast fluidized bed simulation with Fe100

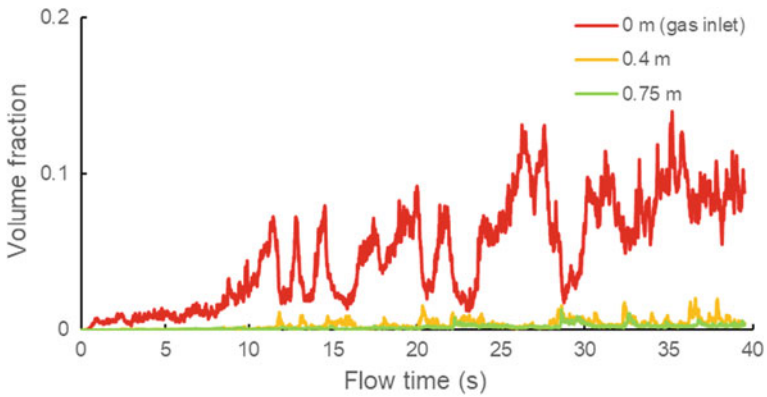


Fig. 11 Time variation of volume fraction at various heights for the fast fluidized bed simulation with Fe100

inlet plane. Similar behavior was observed in the simulation with molochite in Sect. 3 and can be explained again due to the different initial processes employed in the experiment and the simulation.

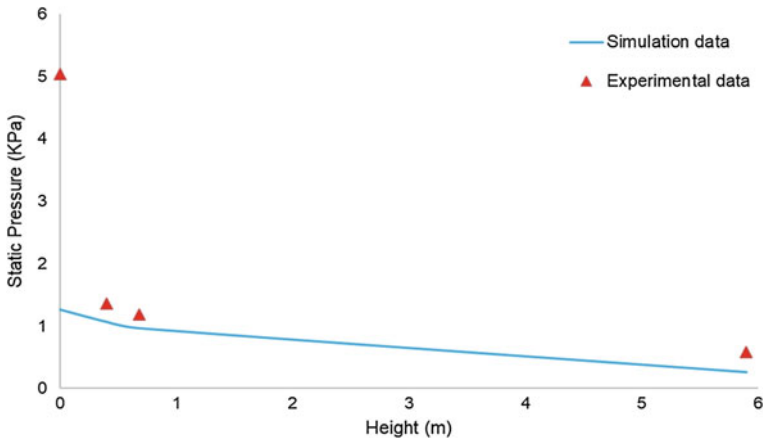


Fig. 12 Comparison of pressure variation at various heights for the fast fluidized bed simulation with Fe100

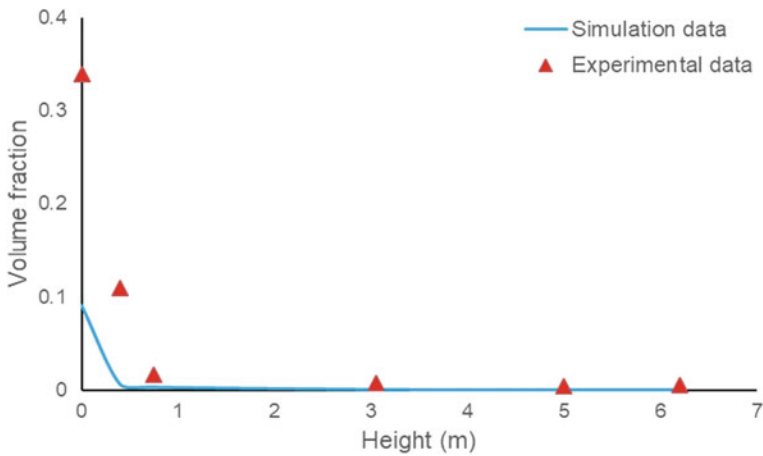


Fig. 13 Comparison of volume fraction at various heights for the fast fluidized bed simulation with Fe100

5 Conclusions

In this work, CFD/DDPM cold flow simulations of a fast fluidized bed fuel reactor are carried out by using ANSYS Fluent. The first simulation using molochite as a bed material showed great agreement with the experimental data obtained by Haider et al. [16] at Cranfield University in UK. The results showed that proper initial particle distribution and circulating mass flow rate are required to achieve the complete and stable circulation condition and to obtain the correct relationship

between the static pressure and the volume fraction in the fuel reactor. Drag law plays an important role in obtaining accurate simulations; Syamlal–O’Brien drag law was found to be appropriate for this simulation given the particle size. To explore the applicability of DDPM for a high-density and small diameter bed material, a simulation using Fe100 as bed material was conducted which showed acceptable results compared to the experimental data. Gidaspow’s drag law was found to be more suitable for this simulation. The multiphase simulations in this paper demonstrate that the CFD/DDPM modeling is suitable for simulation of the gas and particles hydrodynamics of a fast fluidized bed CLC fuel reactor. Future work should focus on developing a particle initialization scheme that can more accurately represent the experimental condition prior to the start of the simulation as well as improving the drag laws for various flow conditions.

References

1. Arrhenius S (1896) On the influence of carbonic acid in the air upon the temperature of the ground. *Philos Mag J Sci* 41:237–276
2. Epstein A (2014) Moral case for fossil fuel. Penguin Group (USA) LLC, New York
3. UEI Administration (2010) International energy outlook 2010. US Department of Energy, Washington, DC
4. Lyngfelt A, Leckner B (1999) Minisymposium in CO₂ capture and storage. In: Technologies for CO₂ separation. Gothenburg
5. Mattisson T, Lyngfelt A (2001) Capture of CO₂ using chemical-looping combustion. In: First biennial meeting of the Scandinavian-Nordic section of the combustion institute, Goteborg, Sweden
6. Banerjee S, Agarwal RK (2015) Transient reacting flow simulation of spouted fluidized bed for coal-direct chemical looping combustion with different Fe-based oxygen carriers. *Appl Energy* 160:553–560
7. Gnanaprasasam NV, Reddy BV, Rosen MA (2009) Hydrogen production from coal using coal direct chemical looping and syngas chemical looping combustion systems: assessment of system operation and resource requirements. *Hydrogen Energy* 34(6):2606–2615
8. Yerushalmi J, Turner DH, Squires AM (1976) The fast fluidized bed. *Ind Eng Chem Res* 15:47–53
9. Zou L, Guo Y, Chan C (2008) Cluster-based drag coefficient model for simulating gas-solid flow in a fast fluidized bed. *Chem Eng Sci* 63(4):1052–1061
10. Jung J, Gamwo IK (2008) Multiphase CFD-based models for chemical looping combustion process: fuel reactor modeling. *Powder Technol* 183(3):401–409
11. Ding J, Gidaspow D (1990) A bubbling fluidization model using kinetic theory of granular flow. *AIChE* 36(4):523–538
12. Almstedt A, Enwald H (1999) Fluid dynamics of a pressurized fluidized bed: comparison between numerical solutions from two-fluid models and experimental result. *Chem Eng Sci* 54(3):329–342
13. Ghaboussi J, Barbosa R (1990) Three-dimensional discrete element method for granular materials. *Numer Anal Methods Geomech* 14(7):451–472
14. Cloete S, Johansen S, Popoff MB (2010) Evaluation of a Lagrangian discrete phase modeling approach for resolving cluster formation in CFB risers. In: International conference on multiphase flow, Leipzig, Germany

15. Chen X, Wang J (2014) A comparison of Two-fluid model, dense discrete particle model and CFD-DEM method for modeling impinging gas-solid flows. *Power Technol* 254:94–102
16. Haider SK, Duan L, Patchigolla K, Anthony E (2016) A hydrodynamic study of a fast-bed dual circulating fluidized bed for chemical looping combustion. *Energy Technol* 4(10):1254–1262
17. ANSYS (2012) ANSYS fluent user's guide. ANSYS Inc, Canonsburg, PA
18. ANSYS (2012) ANSYS fluent theory guide. ANSYS Inc, Canonsburg, PA
19. Syamlal M, O'Brien T (1989) Computer simulation of bubbles in a fluidized bed. *AIChE Symp Ser* 85:22–31
20. Patankar N, Joseph D (2001) Modeling and numerical simulation of particulate flows by the Eulerian-Lagrangian approach. *Multiphase Flow* 27(10):1659–1684
21. Gidaspow D (1992) *Multiphase flow and fluidization*. Academic Press, San Diego, CA

Part III
Integration of Renewable Energy and
Utilization of Wastes

Sustainability Assessment of the Biomass Gasification Process for Production of Ammonia

Pratham Arora, Andrew Hoadley and Sanjay Mahajani

Abstract Any technology needs to be environmentally sustainable to be successful. The biomass gasification technology is often perceived to be carbon neutral. However, these perceptions need to be confirmed using a rigorous life-cycle assessment (LCA). This chapter presents a sustainability assessment of the biomass gasification technology for the production of ammonia. Conventional ammonia production that is based on hydrocarbon feedstock is known to be energy-intensive and tends to make a substantial contribution to the global greenhouse gas emissions. Therefore, an environmentally benign feedstock in the form of biomass is proposed as an alternative. Biomass, when used as a feedstock for ammonia production, is expected to yield a considerable reduction in environmental impacts. This chapter undertakes a cradle-to-gate life-cycle assessment (LCA) for ammonia production from biomass through the gasification route. Three different biomass feedstocks, namely wood, straw, and bagasse, are compared for their environmental sustainability by using different environmental indicators. Furthermore, these feedstocks are modeled for cultivation in three different geographical regions. The results suggest that different biomass feedstocks and geographical regions have their own niche environmental advantages. The global warming potential (GWP) for the straw-based ammonia production was found to be close to natural gas-based ammonia production. Contrariwise, 78% reduction in GWP compared to natural gas-based ammonia production is noticed when bagasse is used as a feedstock for ammonia production.

P. Arora (✉)

The Energy and Resources Institute (TERI), Delhi, India
e-mail: pratham.arora@teri.res.in

A. Hoadley

Department of Chemical Engineering, Monash University, Melbourne, Australia
e-mail: andrew.hoadley@monash.edu

S. Mahajani

Department of Chemical Engineering, Indian Institute of Technology Bombay, Mumbai, India
e-mail: sanjaym@iitb.ac.in

© Springer Nature Singapore Pte Ltd. 2018

S. De et al. (eds.), *Coal and Biomass Gasification*, Energy, Environment, and Sustainability, https://doi.org/10.1007/978-981-10-7335-9_14

Keywords Biomass gasification • Life-cycle assessment (LCA)
Global warming potential (GWP) • Ammonia production

1 Introduction

At the 2015 United Nations Climate Change Conference or COP 21, 174 nations committed themselves for combatting climate change. To achieve the target of limiting global warming to less than two degrees Celsius ($^{\circ}\text{C}$) compared to preindustrial levels, nations are encouraging cleaner alternatives for already established processes [14]. Biomass, an abundant renewable resource, is often projected as an alternate to conventional fuels. By the application of different thermochemical conversion routes, biomass can be converted into syngas, bio-oil, and char. These products can be used to replace fossil fuels in a wide range of activities ranging from heat and power applications to production of chemicals. The products from thermochemical conversion of biomass are often considered carbon neutral based on the fact that any emissions from biomass-based processes would subsequently be absorbed for future production of biomass. However, these assumptions need to be supported by a rigorous life-cycle assessment (LCA).

Biomass is a scattered resource and requires an effective supply chain management for its use in a large-scale plant. Hamelick et al. [6] have reported that the energy requirements for transport of biomass feedstock range from 1.2 to 1.3 $\text{MJ}_{\text{primary}}/\text{MJ}_{\text{delivered}}$ for different European countries. Depending upon the country's energy mix, this energy may be supplied by fossil fuels or renewable energy sources. Consequently, the CO_2 emissions associated with the supply chain would be critical in establishing the sustainability of any biomass-based process. Roder et al. [11] have estimated the greenhouse gas (GHG) emissions associated with electricity generation from forest and sawmill residues. Their study predicts that depending upon the supply chain the GHG emissions range from 132 to 1330 g CO_2 eq./kWh electricity produced. The lower values correspond to an emission reduction of 80% when compared to fossil fuels, whereas the higher value surpasses the emissions by fossil fuel route by more than 70%. Thus, a LCA is indispensable for estimating the emission reductions resulting from any biomass-based process.

The present chapter demonstrates the use of LCA for predicting the viability of ammonia production from syngas through the gasification route. Ammonia forms the backbone of the nitrogen-based fertilizer industry. The average global energy consumption from the production of ammonia is estimated to be 52.6 $\text{MJ}/\text{t NH}_3$ [10]. Natural gas supplies 70.7% of this energy consumption, and the remaining is supplied by oil and coal. The use of fossil fuels is inherently coupled with GHG emissions. Biomass gasification can yield hydrogen-rich syngas, which on conditioning can act as a suitable feedstock for ammonia production. The flowsheet for ammonia production from biomass is shown in Fig. 1. The basic flowsheet starts with biomass gasification. The chapter considers the use of dual fluidized bed gasifier based on the syngas requirements and the scale of operation. The syngas

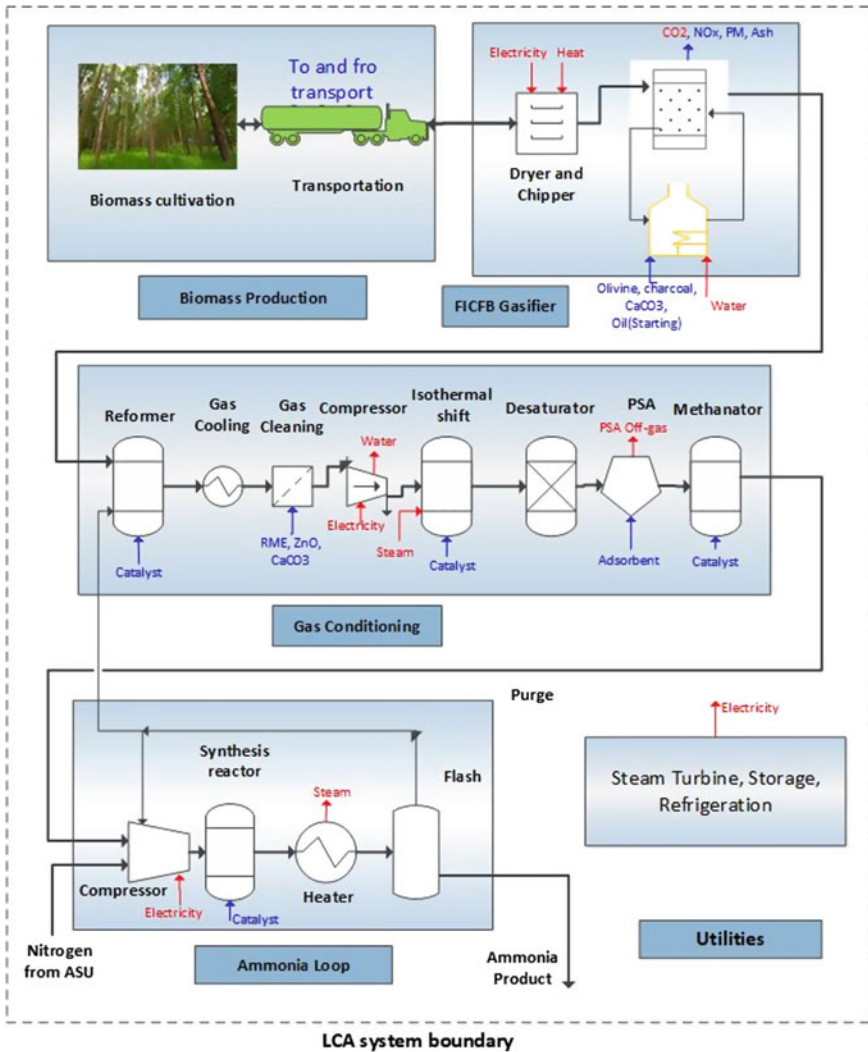


Fig. 1 Biomass-to-ammonia process system boundary

produced is cleansed of impurities and particulates. The syngas is also reformed as it contains a considerable amount of methane. Thereafter, the shift reaction is employed to convert carbon monoxide to carbon dioxide. The syngas is then stripped of carbon dioxide using a pressure swing adsorption (PSA). A methanator is then used for removal of any trace carbon monoxide and carbon dioxide. Finally, the syngas enters into a high-pressure ammonia loop which leads to the production of pure ammonia. The details of the complete process are reported elsewhere [1]. Three different biomass feedstocks, namely wood, straw, and bagasse that were

grown in Australia, India, and Brazil, respectively, were compared for their potential for ammonia production. The three biomass feedstocks selected differ on the basis of chemical and physical properties as well as supply chain. The wood feedstock is sourced from eucalyptus plantation as an energy crop. Straw is a primary residue available in the agricultural fields after the harvesting season. Bagasse is a secondary residue available at sugar mills during the sugar-crushing season. The feedstocks were selected to understand the effect of composition of biomass and the supply chain on the environment.

2 Methodology

The environmental impacts of the biomass-to-ammonia process were estimated using the LCA framework. This framework involves four major steps [9]:

1. determining the goals and scope of the LCA;
2. compiling an inventory of energy and mass inputs and outputs across all relevant life-cycle stages;
3. evaluating relevant environmental impacts that are associated with the life-cycle inputs and outputs; and
4. interpreting the results, which will lead to a more informed decision making and improvement of results.

These four mandatory stages are governed by ISO norms [9]. The stages are presented in Fig. 2.

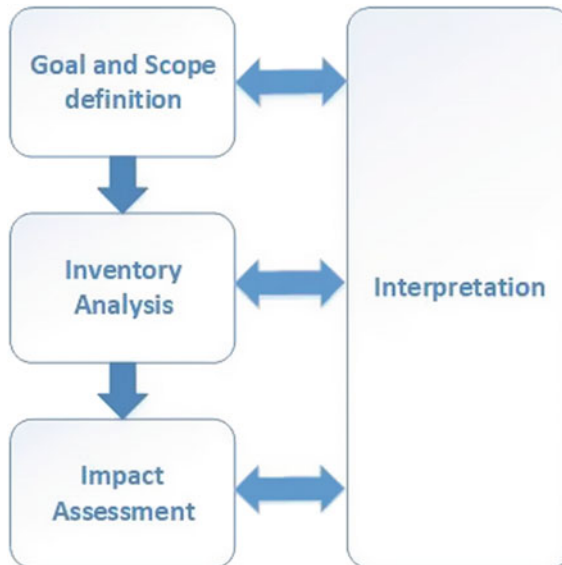


Fig. 2 LCA framework

The goal and scope definition step is used to state the intended applications of the study, the audience of the study, and the methods (and assumptions) that are undertaken. In the life-cycle inventory (LCI) analysis, all the mass and energy flows in the different process stages are tabulated. The inventories are characterized in the impact assessment stage in order to predict various midpoint and endpoint impacts. Any additional results are evaluated in the interpretation stage to predict the impacts of the process, while stating the limitations and providing future recommendations. The flows between the different LCA stages suggest that the whole process requires several iterations to reconcile the goals, data requirements, available inventories, impact categories, and characterization models.

The goal and scope definition step provides the necessary details and transparency that make an LCA study useful to its intended audience. The goal of this chapter is to identify the environmental “hot spots” in the life cycle of ammonia production from a biomass feedstock through the gasification route. Another important decision to be made is the choice between attributional and consequential LCA. An attributional LCA describes the emissions within the system boundary based on the inputs and outputs. A consequential LCA aims to describe the change in environmental emissions by the introduction of a product in a surrounding environment. An example of the consequential LCA can be the effect on food supply systems as a result of land use for bioenergy. The main characteristics of both the approaches are listed in Table 1 [13]. The LCA study in this chapter will focus on the attributional LCA of the biomass-to-ammonia process. The selection of the functional unit is another important parameter. The purpose of the functional unit is to quantify the identified functions in a more precise manner, which will facilitate mathematical analysis. A functional unit serves as a reference to which the inputs and outputs of our life-cycle system are normalized. The present chapter has adopted a functional unit of production of 1 kg of ammonia from biomass feedstock. This choice of the functional unit was made to facilitate a comparison between the present chapter and other studies on ammonia production.

The biomass-to-ammonia flowsheet was modeled in ASPEN Plus simulation software (Aspen Technology Inc., [3]). ASPEN Plus is a process modeling software for conceptual design, simulation, and optimization of chemical engineering

Table 1 Overview of consequential and attributional LCA [13]

Characteristic	Attributional LCA	Consequential LCA
Synonym	Status quo	Change-oriented
Data	Average historical	Marginal future
Knowledge required	Physical mechanisms	Physical and market mechanisms
Functional unit	Represents static situation	Represents change in volume
System boundaries	Static processes	Affected processes by change in demand
System expansion	Optional	Obligatory
Quality	Sensitive to uncertainties	Higher sensitivity to uncertainties

operations. A gasifier model proposed by Arora et al. [2] has been utilized for modeling the gasifier. This model had the ability to predict the syngas output from the gasification of three different biomass feedstocks, namely wood, straw, and bagasse. The conditioning of syngas for ammonia production was also modeled in ASPEN Plus. The ASPEN Plus model provided the heat and mass balance for the three biomass-to-ammonia process flowsheets corresponding to three different biomass feedstocks.

A cradle-to-gate LCA study was carried out with the help of MS Excel worksheets for different biomass-to-ammonia process variants. The LCI data were extracted from the ASPEN Plus flowsheets for the biomass-to-ammonia process as well as the ecoinvent databases [15]. The ASPEN Plus flowsheets provided the material and energy balances for major process unit operations. Ecoinvent databases were used to supply data for background processes such as biomass cultivation, transportation, electricity production. A summary of the mass and energy flows that were considered in the LCA is reported in Table 2. A system boundary for the biomass-to-ammonia process is shown in Fig. 1. Figure 1 displays all the major process stages and the inputs and outputs (from both nature and the techno-sphere, that is, man-made world) that are considered in the LCA. Except for biomass production, all the other stages have been modeled in ASPEN Plus. CO₂ emissions and intake during cultivation have been treated as carbon cycles. CO₂ emissions that originate from biomass have been termed as biogenic and have not been considered in the analysis.

Inventory analysis was performed based on a model that was developed by Heijungs and Suh [7]. This approach utilized matrix algebra to reconcile the various unit process inventories imported from ASPEN Plus and the ecoinvent databases. The LCA considers a total of nineteen hundred different types of emissions that are a result of different unit processes. Each unit process is represented by a matrix column; the rows indicate the process inputs and the outputs including the emissions. The matrix columns that represent different unit processes together form the process matrix, M . The process matrix is divided into a technology matrix (A) that represents the mass and energy flows among unit processes and an intervention matrix (B) that represents flows from and into the environment such as CO₂ emissions. The combined inventories for all the relevant processes are combined to form a technology matrix and an intervention matrix as shown in Eq. 1.

$$M = \begin{pmatrix} A \\ B \end{pmatrix} \quad (1)$$

The final output from the complete process is represented by vector, m . The vector m may be further divided into two vectors: Vector, d , which represents the functional unit or the intended process output for normalizing all process flows, and vector, g , which represents the total process emissions that are a result of normalized process flows (Eq. 2).

Table 2 Summary of mass and energy flows that were considered in the LCA of the biomass-to-ammonia process

LCI elements considered	Process stage	Reference quantity
Wood/straw/bagasse production	Biomass production	From ASPEN Plus model
Biomass transportation	Biomass production	100 km transport for wood and straw feedstock
Electricity	Gasification, compression, refrigeration and steam turbines	From ASPEN Plus model
Infrastructure	Whole plant	5.79×10^{-6} p/Nm ³ syngas (Ecoinvent database)
Silica sand	Gasification	9.5 kg/t biomass
Fuel (Natural gas)	Gasification	0.16 MJ/t biomass
Charcoal	Gasification	5.35 kg/t biomass
Calcium carbonate	Gasification	5.76 kg/t biomass
Fly ash disposal	Gasification	9.71 kg/t biomass
Bottom ash	Gasification	From ASPEN Plus model
Reforming catalyst	Reforming	From ASPEN Plus model
Dolomite	Reforming	From ASPEN Plus model
Fuel (natural gas)	Reforming	From ASPEN Plus model
Rape methyl ester	Gas cleaning	3.95 kg/t biomass
Sodium hydroxide	Gas cleaning	0.16 kg/t biomass
Sulfuric acid	Gas cleaning	2.78 kg/t biomass
Zinc oxide	Gas cleaning	0.51 kg/t biomass
Shift catalyst	Shift reactor	From ASPEN Plus model
Adsorbent	PSA	From ASPEN Plus model
Methanation catalyst	Methanator	From ASPEN Plus model
Synthesis catalyst	Synthesis reactor	From ASPEN Plus model
Wastewater	Gasification and desaturator	From ASPEN Plus model
Fly ash disposal	Gasification	60% to incineration and 40% to landfill
Auxiliary transport (chemicals, catalysts, adsorbents, and bed material)	Whole process	100 km by road and 600 km by rail

(continued)

Table 2 (continued)

LCI elements considered	Process stage	Reference quantity
Landfill (Waste chemicals, catalysts, adsorbents and bed material)	Waste disposal	From ASPEN Plus model and correlations
Landfill transportation	Waste disposal	10 km by road

$$m = \begin{pmatrix} d \\ g \end{pmatrix} \quad (2)$$

The relationship between the technology matrix (A) and the final demand vector (d) can be established with the help of a scaling vector, s , as shown in Eq. 3. Since both the technology matrix and the final demand matrix would be known, the scaling vector can be calculated using Eq. 4.

$$As = d \quad (3)$$

$$s = A^{-1}d \quad (4)$$

The scaling vector is then used to calculate the process emissions pertaining to the intended process output or the functional unit (Eq. 5).

$$g = Bs \quad (5)$$

To summarize, the technology matrix is solved for a particular process configuration (or the selected functional unit) and the related intervention matrix gives the relevant emissions for the same process configuration (or the selected functional unit). The multi-functionality of the unit processes has been solved by using system-expansion (substitution) methodology. This methodology involves adding stand-alone unit processes to simplify algebraic operations in matrices.

The environmental emissions that are calculated for the complete process are used in the life-cycle impact assessment (LCIA). According to ISO standards [9], LCIA consists of both mandatory and optional elements. They can be summarized as:

- Selection of impact categories, category indicators, and characterization models that correspond to the goal and the scope of the LCA.
- Assignment of elementary flows in the inventory to the selected impact categories. This is also known as classification.
- Calculation of category indicator results. This is also known as characterization.
- Normalization of the category indicator results relative to some reference value.
- Sorting of the impact categories in the order of their importance to some particular decisions. This is called grouping.

- Data quality analysis for understanding of the reliability of the collection of indicator results.

Among these steps, the last three, which are normalization, grouping, and data quality analysis, are optional. When selecting impact categories, it is important to understand the difference between midpoints and endpoints (Fig. 3). The main difference lies in the extent of the cause and effect chain that is considered. This can be understood with the help of an example. CFC-11 is an ozone depleting chemical which can cause destruction of the ozone layer and result in the thinning of this layer over certain parts of the earth. This can lead to higher rates of skin cancer and eye damage in exposed humans, crop damage on exposed land, and degradation of plastics, resulting from a greater amount of ultraviolet light reaching the earth. These final consequences are known as the endpoint impacts as they are the ultimate consequence of the emission. The midpoint indicator would be stratospheric ozone depletion because it is a common stressor which leads to different endpoint impacts. All the emissions that contribute to an impact category must be converted to a common unit, which is known as a category indicator, for example, the CO₂ equivalent for global warming potential. Different characterization models may be employed for the conversion of emissions to a particular category indicator.

According to IPCC [8], the environmental impacts can be divided into global ones such as global warming, acidification and local ones such as soil quality,

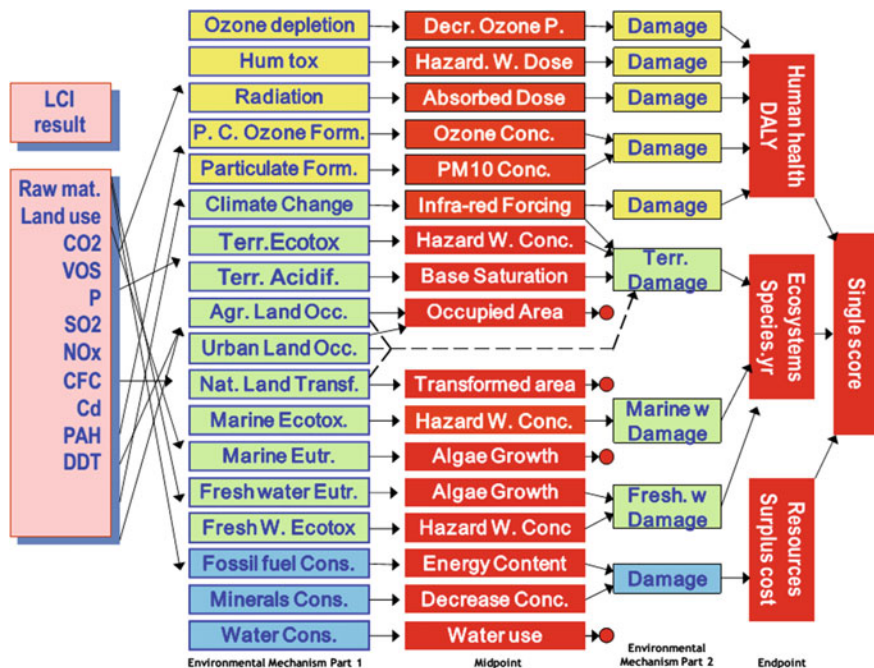


Fig. 3 ReCiPe methodology (reprinted from Goedkoop et al. [5])

Table 3 Overview of different LCA perspectives [12]

	Individualist	Hierarchist	Egalitarian
Vision on nature	Considers nature robust	Considers nature tolerant	Considers nature vulnerable
Level of knowledge	Only considers certain (proven) effects	Considers likely effects	Considers all known effects
Time horizon	Emphasizes present and short-term effects	Balanced time perspective	Current and future effects are considered equal
Vision on society	Economic output is market driven	Developments within limits of nature	Equality and social driven
Manageability	Adaptive management style	Preventive and comprehensive management style	Controlling and limited management style

biodiversity. Recent LCA studies use standard LCIA methods such as ReCiPe, EDIP, LIME, TRACI (Curran [4]). These impact assessment methods may be limited to endpoint or midpoint indicators or might predict both. In LCA, for impact categories that are based on midpoints, relationships between emissions and environmental stressors are often well established. Alternately, impact categories that are based on specific endpoints require extensive observations, risk analyses, and data to relate them to emissions of different substances. Thus, the use of midpoint indicators is more common.

The chapter uses the ReCiPe impact assessment methodology [5]. This methodology predicts eighteen midpoint indicators and three endpoint indicators, which are based on the LCI data. The impact categories and the category indicators for the ReCiPe methodology are shown in Fig. 3 [5].

Further, each of these midpoint and endpoint indicators can be predicted based on three different perspectives, namely individualist, hierarchist, and egalitarian. The assumptions undertaken in these perspectives are presented in Table 3 [12]. This chapter utilizes the hierarchist perspective, which is based on common policy principles. Additionally, since the hierarchist perspective is widely used, it would assist in the comparison of the LCA results and different LCA studies.

The LCA results that were calculated from the MS Excel-based framework were validated against the results that were generated by the commercial LCA software Simapro. An error of less than two percent was noticed between the two results.

3 Results and Discussion

A cradle-to-gate LCA for the different variants of the biomass-to-ammonia process has been performed. The mass and energy balance for the three flowsheets utilizing different biomass feedstocks is shown in Table 4. The three flowsheets resulted in

Table 4 Material and energy balance for the biomass-to-ammonia process

	Wood	Straw	Bagasse
Feed (kg/h)	5000	5000	5000
Syngas yield (kg/h)	6500.89	6614.88	6176.33
Electricity production (MW)	1.84	2.02	1.67
Electricity required from grid (MW)	1.89	1.88	1.86
Ammonia production (kg/h)	2703.68	2640.23	2411.24

different syngas yields as well as final ammonia yield, for similar feedstock input (on mass basis). The different ammonia yields are attributed to the difference in composition of the feedstocks considered as well as the extent of gasification. Furthermore, the production of different amounts of char for the three feedstocks alters the steady-state temperature profile of the dual fluidized bed gasifiers. This in turn alters the electricity generation, a considerable proportion of which is generated from the cooling of gasification flue gas. Electricity is mainly required for the compression of syngas. In the proposed flowsheet, syngas is compressed before the shift reactor and then again before the ammonia synthesis loop. The electricity produced from flue-gas cooling is not sufficient to meet the compression electricity requirement. The balance electricity, thus, needs to be imported from the grid.

The LCA results for the eighteen midpoint indicators are shown in Table 5. The LCA results have also been compared with the LCA of conventional ammonia production utilizing natural gas feedstock. In conventional ammonia production, natural gas is reformed to produce hydrogen-rich syngas which can be conditioned to react with nitrogen and produce ammonia. One of the most crucial midpoint indicators is the global warming potential (GWP). The GWP for the biomass-to-ammonia process varies considerably for the three biomass feedstocks. It is lowest for bagasse feedstock associated with Brazil and highest for straw feedstock available in India. The major contributors to the GWP are presented in Fig. 4. Electricity import from the grid is the major contributor to the GWP for all the feedstocks. The contribution of the electricity import from the grid to the total GWP differs for the three flowsheets based on the country's energy mix. The GWP linked to electricity production is 1.06, 1.51, and 0.28 kg CO₂ eq./kWh of electricity production for Australia, India, and Brazil, respectively. In India, the electricity production is primarily coal based and high CO₂ emissions are associated with it. In Brazil, on the other hand, hydel power and biomass-based power have considerable contribution to the total power generation. The results also predict that straw production has more emissions linked to it when compared to wood production and bagasse production. The inventories point out that the emissions related to straw production can mainly be attributed to the use of fertilizers. Charcoal and rape methyl ester (RME) are used for cleaning the syngas downstream the gasifier. In the bagasse-to-ammonia flowsheet, the ammonia production plant is assumed to be near the sugar mill. Thus, the transportation of biomass is omitted for the bagasse-based ammonia production.

Table 5 LCIA for the biomass-to-ammonia process

Impact category	Unit	Natural gas-to-ammonia	Wood-to-ammonia	Straw-to-ammonia	Bagasse-to-ammonia
Climate change	kg CO ₂ eq	1.90E+00	1.19E+00	1.72E+00	4.44E-01
Ozone depletion	kg CFC-11 eq	2.22E-07	2.25E-08	7.83E-08	2.80E-08
Terrestrial acidification	kg SO ₂ eq	8.26E-03	6.33E-03	1.16E-02	3.91E-03
Freshwater eutrophication	kg P eq	1.33E-04	5.37E-05	5.61E-04	9.34E-05
Marine eutrophication	kg N eq	4.00E-04	1.76E-04	6.12E-03	4.78E-04
Human toxicity	kg 1,4-DB eq	4.02E-01	3.32E-01	7.07E-01	3.13E-01
Photochemical oxidant formation	kg NMVOC	3.73E-03	4.50E-03	5.37E-03	2.35E-03
Particulate matter formation	kg PM10 eq	2.44E-03	1.91E-03	4.61E-03	1.09E-03
Terrestrial ecotoxicity	kg 1,4-DB eq	3.02E-04	5.00E-04	2.72E-02	3.98E-03
Freshwater ecotoxicity	kg 1,4-DB eq	1.61E-02	3.43E-03	3.16E-02	1.84E-02
Marine ecotoxicity	kg 1,4-DB eq	1.30E-02	3.08E-03	2.49E-02	1.53E-02
Ionizing radiation	kBq U235 eq	7.69E-02	3.78E-04	6.55E-02	3.24E-02
Agricultural land occupation	m ² a	1.67E-02	2.22E+00	1.84E-01	2.45E-01
Urban land occupation	m ² a	4.09E-03	5.15E-02	2.12E-02	2.61E-03
Natural land transformation	m ²	4.77E-04	2.02E-04	1.84E-04	1.96E-04
Water depletion	m ³	5.48E-02	3.56E-03	3.15E-02	3.46E-02
Metal depletion	kg Fe eq	8.19E-02	5.40E-02	5.98E-02	4.30E-02
Fossil depletion	kg oil eq	8.38E-01	2.77E-01	4.26E-01	1.02E-01

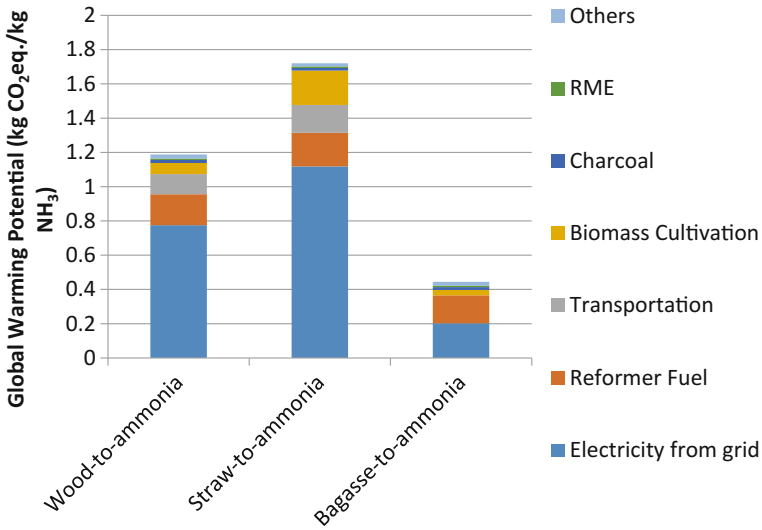


Fig. 4 Global warming potential (GWP) for the biomass-to-ammonia process

Different factors contributed to the ozone depletion potential of the three feedstocks (Fig. 5). The ozone depletion potential of the wood feedstock results mainly from transportation and wood cultivation. In the case of the straw feedstock, the major contributors to the ozone depletion potential were straw cultivation,

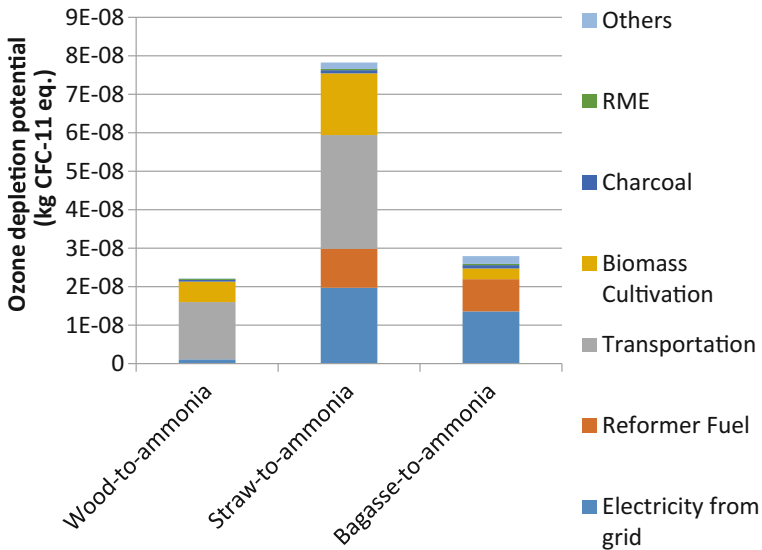


Fig. 5 Ozone depletion potential for the biomass-to-ammonia process

transportation, and electricity production. Electricity production and syngas reformer fuel were the main contributors to the ozone depletion potential in the bagasse feedstock. However, the ozone depletion potential process is much lower for the biomass-to-ammonia process when compared to conventional natural gas-based ammonia production.

The high acidification and eutrophication potential for straw is attributed to coal-based electricity production in India. The terrestrial ecotoxicity for the biomass-to-ammonia process stems mainly from biomass cultivation, whereas electricity production and biomass cultivation are the major contributors to the freshwater ecotoxicity. The majority of photochemical oxidant formation, particulate matter formation, and ionizing radiation resulted from electricity consumption, biomass cultivation, and transportation. The water depletion potential of bagasse (which comes from the cultivation of sugarcane which has a high water requirement) is similar to other biomass feedstocks, namely wood and straw. This can be understood by the allocation of water requirement among various products of sugarcane cultivation. Bagasse as a waste material would not normally have the water allocated to it. Thus, a mere 1.5% of the total inputs to the sugarcane cultivation are attributed to bagasse production. Additionally, agricultural land occupation is very high for the wood-based ammonia production process. While straw and bagasse are residues from agricultural and industrial processes, separate land would be required for cultivation of wood as a dedicated energy crop. The midpoint indicators can be combined into a single score endpoint indicator by normalizing all the impact categories. Single score endpoint results for different process variants that were normalized using world average emissions are shown in Fig. 6.

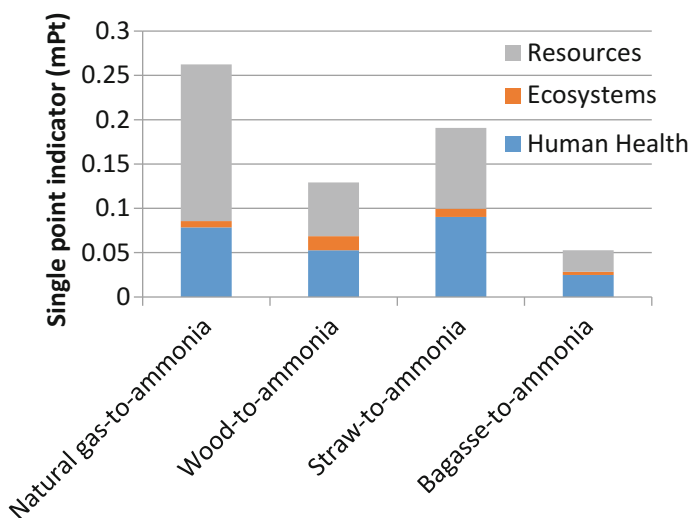


Fig. 6 Endpoint single point indicator for the biomass-to-ammonia process

These results highlight the potential of LCA in understanding the sustainability aspects of renewable energy systems. The single score endpoint indicators confirm the environmental superiority of the biomass-to-ammonia production when compared to conventional fossil fuel-based ammonia production. Conventional natural gas-based ammonia production not only affects the human health by the release of harmful emissions but also depletes the limited fossil fuel reserves. The single score indicator for the straw feedstock is largely attributed to electricity consumption. The results for the GWP and the ozone depletion potential underline the variation experienced in LCA results, when the feedstock and the process configurations are changed. The electricity consumption from the grid was found to be a major contributor to many impact categories. The key to a sustainable biomass-to-ammonia process is the reduction in the import of electricity from the grid.

This chapter relies upon ecoinvent databases for the majority of LCI data. The assumptions adopted in this chapter are consistent with the assumptions adopted by the ecoinvent database. Since the ecoinvent database primarily focuses on the European conditions, some of the assumptions in the LCA might not translate to real impacts. One example is the assumption that fly ash that is generated in the gasification process will be disposed of by municipal incineration, which is based on the ecoinvent database. This incineration of fly ash is responsible for ~ 50% of the emissions that lead to human toxicity. This practice of incineration of fly ash was not found to be common in the geographical locations that are considered in this chapter. The human toxicity potential can, possibly, be reduced to half if the fly ash is disposed of in landfills or recycled for construction applications. Even if the fly ash is incinerated, the ecoinvent database would appear to treat all fly ash in a similar manner, such that fly ash that results from coal combustion is considered to be identical to fly ash from biomass gasification.

Another important aspect of the LCA is the selection of inventories. This chapter utilizes ecoinvent inventories that are normalized for Australian conditions, in the wood-to-ammonia scenario. For the straw-to-ammonia scenario, only the electricity production inventory was available for India. World average inventories were utilized for all the other process inputs and outputs. In the bagasse-to-ammonia scenario, inventories were available for bagasse production and electricity production in Brazilian conditions. The remaining process inputs and outputs were modeled using world average inventories. Since, electricity was found to be the chief contributor to the GWP and to the single score endpoint indicator, the assumptions mentioned above are expected to yield reliable results in comparison with ammonia production from three different feedstocks. The scope of available LCI data for different world regions is expected to increase in the future. This enhancement of LCI data would further assist in a rigorous comparison on the basis of LCA. Thus, this chapter may be used as an example for a thorough analysis of any biomass-based system. Different biomass feedstocks, process configurations, and geographical regions have their own advantages.

4 Conclusions

This chapter highlights the advantages of LCA, for predicting the viability of ammonia production from syngas through the gasification route. A cradle-to-gate LCA for the different variants of the biomass-to-ammonia process has been performed. 78% reduction in GWP compared to natural gas-based ammonia production is noticed when bagasse is used as a feedstock for ammonia production. This is attributed to renewables-based electricity production and the absence of transportation for the bagasse feedstock in Brazil. GHG-intensive electricity production and straw production in India make the GWP of the straw-to-biomass process similar to the GWP of the fossil fuel-based ammonia production. The GWP of the wood-to-ammonia process, which was modeled for Australian conditions, was midway between straw and bagasse. The single score endpoint indicators confirm the reduction in emissions that result from the biomass-to-ammonia process when compared to conventional fossil fuel-based ammonia production. The methodology can be employed as an example in the development of different sustainable chemical production processes.

References

1. Arora P, Hoadley AFA, Mahajani SM, Ganesh A (2016) Small-scale ammonia production from biomass: a techno-enviro-economic perspective. *Ind Eng Chem Res* 55(22):6422–6434. <https://doi.org/10.1021/acs.iecr.5b04937>
2. Arora P, Hoadley AFA, Mahajani SM, Ganesh A (2017) Compartment model for a dual fluidized bed biomass gasifier. *Chem Eng Res Des* 117:274–286. <https://doi.org/10.1016/j.cherd.2016.10.025>
3. Aspen Technology Inc. (2011) Aspen plus user models
4. Curran MA (2012) Life Cycle Assessment Handbook a Guide for Environmentally Sustainable Products. Wiley, Hoboken, NJ. <https://doi.org/10.1002/9781118528372>
5. Goedkoop M, Heijungs R, Huijbregts M, De Schryver A, Struijs J, van Zelm R (2009) ReCiPe 2008, a life cycle impact assessment method which comprises harmonised category indicators at the midpoint and the endpoint level
6. Hamelinck CN, Suurs RAA, Faaij APC (2005) International bioenergy transport costs and energy balance. *Biomass Bioenergy* 29(2):114–134. <https://doi.org/10.1016/j.biombioe.2005.04.002>
7. Heijungs R, Suh S (2002) The computational structure of life cycle assessment. Springer (Eco-Efficiency in Industry and Science). https://books.google.co.in/books?id=eAes3rhR_3kC
8. IPCC (2011) Special report on renewable energy sources and climate change mitigation. In: Edenhofer O, Pichs-Madruga R, Sokona Y, Seyboth K, Matschoss P, Kadner S, Zwickel T, Eickemeier P, Hansen G, Schlömer S, von Stechow C (eds). Cambridge University Press, United Kingdom and New York, NY, USA
9. ISO (2006) Environmental management - Life cycle assessment—principles and framework. citeulike-article-id:4482380
10. Kool A, Marinussen M, Blonk H (2012) LCI data for the calculation tool Feedprint for greenhouse gas emissions of feed production and utilization Dry Milling Industry. The Netherlands

11. Röder M, Whittaker C, Thornley P (2015) 'How certain are greenhouse gas reductions from bioenergy? Life cycle assessment and uncertainty analysis of wood pellet-to-electricity supply chains from forest residues'. *Biomass Bioenergy* 79:50–63. <https://doi.org/10.1016/j.biombioe.2015.03.030>
12. De Schryver AM (2011) Value choices in life cycle impact assessment. Radboud University. http://www.ru.nl/publish/pages/556452/2010deschryver_phdthesis_11jan2011.pdf
13. Singh A, Pant D, Olsen SI (eds) (2013) *Life cycle assessment of renewable energy sources*. Springer, London (Green Energy and Technology). <https://doi.org/10.1007/978-1-4471-5364-1>
14. UNFCCC (2015) Adoption of the Paris agreement. Proposal by the President, Paris climate change conference, Nov 2015, COP 21. doi:FCCC/CP/2015/L.9/Rev.1
15. Weidema BP, Bauer C, Hischier R, Mutel C, Nemecek T, Vadenbo CO, Wernet G (2011) Overview and methodology. Data quality guideline for the ecoinvent database version 3, Ecoinvent <http://www.pre-north-america.net/download/manuals/EcoinventOverviewAndMethodology.pdf>

Recent Advances in Power Generation Through Biomass and Municipal Solid Waste Gasification

Natarianto Indrawan, Ajay Kumar and Sunil Kumar

Abstract This review focuses on the fundamentals, recent technology development, environmental and economic analyses, and commercialization of power generation by gasification of municipal solid wastes (MSW) and biomass wastes for distributed power application. Design and operational factors affecting the performance and emission characteristics of power generation systems using syngas are reviewed. The performance characteristics include maximum power output, engine efficiency, and specific fuel consumption of various technologies. Emissions characteristics include levels of carbon dioxide (CO₂), carbon monoxide (CO), nitrogen oxides (NO_x), unburned hydrocarbon (HC), sulfur dioxide (SO₂), and polychlorinated dibenzo-p-dioxins and dibenzofurans (PCDD/PCDF). Large-scale system (>1 MW) is typically selected for power generation via MSW gasification, which is generally accomplished using plasma-based gasification followed by the use of internal combustion (IC) engines or gas turbines to achieve high efficiency. Plasma is preferred for treating MSW due to its unique capability to ionize materials, minimize tars, and improve syngas quality. Besides, co-gasification of MSW and biomass is also an alternative for power generation. Finally, techno-economic and life cycle analyses of power generation from plasma gasification system are summarized.

N. Indrawan
Environmental Science Program, Oklahoma State University (OSU),
Stillwater, OK, USA
e-mail: natarianto.indrawan@okstate.edu

N. Indrawan
Department of Mechanical Engineering, Institut Teknologi Nasional,
Bandung, Indonesia

A. Kumar (✉)
Biosystems and Agricultural Engineering Department, OSU, Stillwater, OK, USA
e-mail: ajay.kumar@okstate.edu

S. Kumar
CSIR - National Environmental Engineering Research Institute, Nagpur, India
e-mail: s_kumar@neeri.res.in

Keywords MSW • Biomass • Gasification • Syngas • Power generation
Emissions • Plasma

1 Introduction

With an increase in price of natural gas, gasification can take essential role in power production since clean energy from gasification can be harvested at a low cost and gasification is capable of using diverse types of feedstock such as biomass and MSW. Gasification allows the organic feedstocks to be in a limited oxygen environment inside the gasifier reactor in order to produce synthetic gas or syngas, which is a mixture of combustible gases such as carbon monoxide (CO), hydrogen (H₂), and methane (CH₄). Feedstocks such as biomass, agricultural residues, coal, and municipal solid waste (MSW) are commonly used [1]. As an illustration, recent natural gas price for industrial customers in China has reached to around 10–15 USD/MMBtu and is predicted to steadily increase in the coming years, while syngas production cost is approximately 5–6 USD/MMBtu [1, 2]. The increase in price of natural gas price is mostly contributed by the use of liquefied natural gas (LNG) in the natural gas pipeline networks that requires further processing for liquefaction and transportation at the receiving terminal that eventually increases the final cost, commonly known as landed price. The gasification process, through the use of local resources, such as biomass, coal, and MSW, can directly eradicate the necessity of pipeline network for delivering it to the end-customers.

The syngas can directly be utilized in an internal combustion engine and gas turbine to produce heat and electricity. Syngas energy content, when air is used as the gasifying medium, is approximately one-third compared to natural gas. Syngas energy content typically ranges from 4 to 15 MJ/Nm³, while natural gas energy content ranges from 35 to 40 MJ/Nm³ [3]. Although the energy content of syngas is considerably lower than that of natural gas, syngas provides several compensations. Syngas can be easily stored, transferred, and injected into natural gas pipeline network; syngas can be also further converted into several valuable chemicals, such as methanol, alkanes [4]. Moreover, syngas-operated engine provides an excellent performance for the power generation with minimum modification. The current development of the internal combustion engine has an output power range up to 6,500 kW and potentially brings a high return of the investment due to an increased efficiency, longer interval maintenance, lower noise level, and robust emission performance [5].

This chapter reviews power generation for distributed power application via biomass and MSW gasification and feeding 100% syngas into IC engine including gas turbines. Advantages and constraints such as system efficiency, modification requirement, and emission performances are discussed in detail. An economic assessment of power generation from MSW gasification is also presented.

2 Gasification Designs

To produce a high-quality and stable syngas that delivers high-power generation performance, selecting appropriate gasifier depending on requirements of feedstock and downstream equipment is critical. Each of the gasifiers has its unique operational characteristics including its advantages and disadvantages, (summarized in Table 1).

2.1 *Fixed-Bed Gasifier*

Fixed-bed gasifier can either be a downdraft or updraft. In downdraft gasifier, the biomass and syngas both move downward. The biomass is fed from the top, drops downward and reacts with the air or other gasifying agent, which is injected from another side of the reactor. Then, both producer gas (syngas) and solid products (ash and char) are formed and move down to the base of the reactor. In updraft gasifier, biomass is fed from the top and moves downward, but the gasifying agent is fed from the bottom of the reactor and moves upward to form syngas, which exits near the gasifier top (Table 1).

2.2 *Fluidized Bed Gasifier*

Fluidized bed reactors (FBGs) have been used for years in the gasification process because of their flexibility in accepting wide particle size, but their performance is limited due to low carbon conversion [6]. The gasification medium is fed in continuously from the bottom, while the feedstock is fed close to the bottom (reactor bed). The main advantage of FBGs is uniform distribution and mixing of feedstock with sand bed and gasifying agent, thereby reducing heat and mass transfer limitations. Generally, there are two main types of FBRs: the bubbling fluidized bed reactor (BFBG) and the circulating fluidized bed reactor (CFBG). Technically, CFBG is more preferred as it can handle large feed throughputs since it can recycle large amounts of solids [7], prevent the buildup of ash due to high operating temperature range (800–1000 °C), avoid the oxygen trap in the bubble, and, therefore, maintain high efficiency [8].

2.3 *Entrained Flow Gasifier*

The entrained flow gasifiers (EFGs) operate based on the co-current feed of the fine materials (typically less than 75 μm) and the gasification medium in the pressurized and turbulent-flow environment [9, 10]. Normally operated at temperatures of

Table 1 Characteristics of commercially available thermal technologies [8]

Parameters	Gasifier type		Bubbling fluidized bed	Circulating fluidized bed	Twin fluidized bed	Entrained flow bed	Plasma
	Downdraft	Updraft					
Design	Simple and proven with low investment cost	Proven but complex with high investment cost	Proven but complex with high investment cost	Circulating fluidized bed	Complex and high investment cost	Complex and high investment cost	Simple but high investment cost
Maximum fuel moisture (%)	25	60	55	55	11–25	15	N/A
Syngas LHV (MJ/Nm ³)	4.5–5.0	5–6	3.7–8.4	4.5–13	5.6–6.3	4–6	12–15
Tar (mg/Nm ³)	0.015–3.0	30–150	3.7–61.9	4–20	0.2–2	0.01–4	Negligible
Ash and particle	Low	High	High	High	High	Low	Negligible
Reaction temperature (°C)	700–1090		800–1000	800–1000	800–1000	1,200–1,600	>4,000
Syngas output temperature (°C)	700	200–400	800–1000		800–1000	>1260	
Admissible power (MWe)	Up to 1	Up to 10	1–20	2–100	2–50	5–100	1–50
Carbon conversion efficiency	High	High	High, loss of carbon in ash	High	High	High	Very high
Operational flexibility	Very limited. Any major change in process variable needs changes to the reactor design	Any	Accepts load less than the design load	Accepts load less than the design load	Accepts load less than the design load	Very limited	High
Hot gas efficiency (%)	85–90	90–95	89	89	90–95	80	90–95

Table 2 Proximate and ultimate analyses of MSW and biomass

Feedstock type (References)	MSW-1 [25]	MSW-2 [25]	MSW-3 [70]	Switchgrass [26]	Wood chips [71]	Red cedar [72]
Proximate (wt%, dry basis)						
Moisture content (wet basis)	51.7	44.0	20	7.69	7.50	10.39
Volatile matter	44.2	46.9	75.95	78.60	82.20	78.31
Fixed carbon	–	–	10.23	17.47	17.60	20.42
Ash	4.1	9.1	13.81	3.93	0.20	1.27
Ultimate (wt%, dry basis)						
Carbon, C	21.2	24.7	48.23	49.63	52.13	54.44
Hydrogen, H	3.0	3.3	6.37	5.72	6.36	5.80
Oxygen, O	23.1	18.3	28.48	40.37	41.23	38.28
Nitrogen, N	0.3	0.33	1.22	0.30	0.07	0.20
Sulfur, S	0.03	0.03	0.76	0.05	0.01	0.01
Lower heating value (MJ/kg)	6.80	9.10	16.30	16.49	20.17	18.44
Higher heating value (MJ/Kg)	7.14*	9.55*	20.20	17.73	21.24	19.69
Bulk density (kg/m ³)			1,051	91	660	122

*Note: calculated using $1.05 \times \text{LHV}$

1,200–1,600 °C and at pressures of 2–8 MPa [7, 11], the gasifier has short residence time and high carbon conversion (98–99.5%); therefore, it can produce tar-free syngas [9]. Due to their advantages, EFGs are the most commonly used for commercial gasification of coal [11]. The disadvantage of this gasifier is mostly related to the high operating temperature. Such high temperatures reduce burner and refractory life and require the use of expensive materials of construction as well as the use of high-temperature heat exchangers to cool the syngas [11].

2.4 Plasma Gasifier

Plasma gasifier is a relatively new method of gasification especially for using municipal solid waste (MSW). The plasma gasification was firstly introduced by Dr. Camacho in 1973 [12]. “Plasma” is defined as any gas with part of the atoms or molecules partly or fully ionized. Plasma is formed by running an electric current through a gas resulting in high temperature that breaks organic molecule, thus generating syngas. At the same time, melting of inorganic components (glass, metal, silicate, and heavy metals) gives rise to a slag that vitrifies on cooling. Plasma gasification typically operates at temperatures of over 5,000 °C [13]. Due to

unique characteristics and high complexity of MSW (properties compared in Table 2), plasma gasifier offers significant advantages including tar-free syngas, flexibility in accepting feedstocks including hazardous wastes, and high carbon conversion. Plasma gasifier can reduce up to 90% (volume basis) of the feedstock materials, making it a robust technology to reduce landfill area for disposing MSW [14]. However, drawbacks of this system mostly relate to its high capital cost, ranging from 5,000 to 13,000 USD/kW [14, 15], high process temperature compared to the conventional non-plasma gasifiers. Since it is a relatively new method for treating MSW, the technology is not well developed [14].

3 Syngas Properties

Performance of power generation through gasification is heavily dependent on syngas properties including gas composition, heating value, particulates, and tar contents.

3.1 Gas Composition

Gas composition affects the flame speed, ignition, knock characteristics, spark timing, and air-to-fuel ratio that are required to have an optimal engine performance [16]. Primary combustible portion of syngas includes carbon monoxide (CO), methane (CH₄), hydrogen (H₂), and small fraction of other hydrocarbons such as acetylene (C₂H₂), ethylene (C₂H₄), and ethane (C₂H₆). Non-combustible gases such as carbon dioxide (CO₂) and nitrogen (N₂) are also generally found in the syngas generated from biomass and MSW. Gaseous heavier hydrocarbon in the syngas can directly increase syngas energy content because heavier hydrocarbons, such as ethylene and ethane, have high energy content [17]. However, the process of producing heavier hydrocarbon of the syngas is impractical due to complex operating parameters in the gasification such as feedstock types, moisture content, reactor temperatures and pressure, gasification medium, residence time, and presence of bed catalyst [18]. Furthermore, high hydrogen content can increase efficiency of power production because hydrogen could improve cylinder pressure inside the combustion chamber, leading to an increase in thermodynamic efficiency of the internal combustion (IC) engine [19, 20]. High hydrogen content can also improve combustion temperature and flame speed inside the cylinder [21]. In addition, hydrogen potentially inhibits combustion knock during engine operation [22]. Syngas with high hydrogen content has also shown to reduce emissions of nitrogen oxides (NO_x), hydrocarbon (HC), and carbon monoxide (CO) [19]. Both N₂ and CO₂, normally available in syngas do not contribute to syngas energy content, but the presence of these gases, especially CO₂, might reduce the knocking tendency of the engine [23].

3.1.1 Effect of Feedstock Properties

In order to increase energy content of syngas, feedstock selection is crucial. Regardless of the feedstock type, homogeneous carbon-based material is highly preferred to generate CO and H₂. In contrary, the non-combustible components such as ash and metal do not contribute to the syngas generation. MSW/biomass converts into syngas with an efficiency of 80–95% [7, 24]. However, gasifying MSW is more challenging than biomass due to its diverse composition that includes plastic and metal. Typically, organics content such as paper and food waste are abundant (63–71%) in MSW (composition of MSW in the world and USA as shown in Fig. 1). Plastics are found in the range of 10–13%.

As commonly known, the higher the heating value of syngas is, the better the combustion, flame quality, and performance of the power generation will be. Due to high ash content of MSW, the syngas generated from MSW is low in energy content. With air as a gasification medium, syngas energy content (LHV) ranged from 4.0 to 7.0 MJ/Nm³ [24, 25]. The energy content can increase up to 10 MJ/Nm³ if oxygen is used as a gasification medium [24]. In comparison, biomass gasification typically generates syngas with energy content of 4–6 MJ/Nm³ and 10–15 MJ/Nm³ when air and oxygen is used, respectively [7]. To further increase syngas energy content, steam can be used as a gasification medium as steam does not dilute the syngas with nitrogen as air does [26] and steam promotes the reaction producing hydrogen, such as water–gas and water–gas shift reactions [8].

Composition of MSW varies widely depending on collection method, but in general MSW contains plastics and has relatively high ash content. Most plastics are considered suitable feedstock for gasification, because these are carbonaceous materials and are converted into syngas. With 100% polypropylene as feedstock resulted in syngas with the heating value (LHV) of 6–9 MJ/Nm³ and tar content of 2 g/Nm³ [27]. However, results might be different if other plastic components are

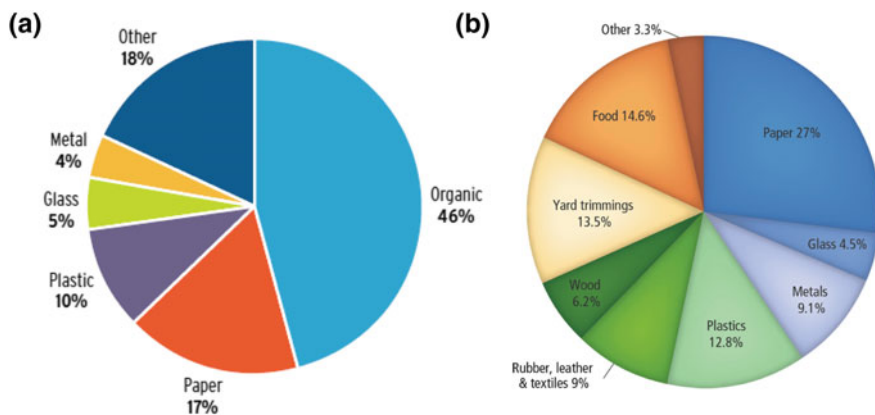


Fig. 1 Typical composition of MSW in the world (2009) [55] and in the USA (2013) [69]

used including polyethylene terephthalate (PET), high-density polyethylene (HDPE), polyvinyl chloride (PVC), low-density polyethylene (LDPE), polypropylene, polystyrene, polyethylene (PE), acrylonitrile butadiene styrene (ABS), polyamide (PA) or nylons, and polybutylene terephthalate (PBT) [28]. Chlorinated plastics, such as PVC, can result in dioxin if reaction environment is favorable. However, gasification typically generates syngas free from dioxin (PCDD) and furan (PCDF) [29, 30].

3.1.2 Effect of Gasification Medium/Oxidizing Agent

The gasification medium heavily effects composition and energy content of the syngas. Air is commonly used as gasification medium to reduce cost, but nitrogen, present in the air, dilutes the syngas and lowers the syngas heating value. Steam or oxygen gasification generates syngas with higher energy content, but adds to capital and operating costs. Steam also promotes hydrogen producing reactions including water–gas and water–gas shift reactions [8]. An oxygen/steam gasification produces syngas with hydrocarbon components (e.g., ethylene and ethane) only in the order of less than 5% [31], while steam gasification can produce heavier hydrocarbons up to 7% [32], leading to an increase in syngas energy content. Heavier hydrocarbons of the syngas could potentially increase greenhouse gas (GHG) emissions because of incomplete combustion [33]. Typically, syngas energy (LHV) of 4–6 MJ/Nm³, 10–12 MJ/Nm³, and 15.69 MJ/Nm³ was reported using air, oxygen, and steam, respectively, as gasifying medium [32, 34, 35]. If the oxygen is used to partially oxidize the feedstock to provide heat required for endothermic reactions, the process is typically termed as directly heated, while indirectly heated gasification needs external energy sources [35].

3.2 Tar Content and Removal Mechanism

Another property of syngas that is severely important to control for power production is its tar content. Tar is defined as the organics produced under thermal or partial oxidation (gasification) of any organic material and assumed to be largely aromatic [36]. Based on chemical solubility and condensability of different tar compounds, tars are classified into five: tar class I (GC undetectable), tar class II (heterocyclic), tar class III (light aromatic: 1 ring), tar class IV (light polycyclic aromatic hydrocarbons (PAH) compounds), and tar class V (heavy PAH compounds) [37]. Tars lead to an increase in corrosion, agglomerations, and fouling in the engine and pipes, as well as considered a health hazard [23]. Tars also are detrimental to catalysts used for syngas conversion and application in fuel cell [4]. For power generation, syngas tar content should not exceed 100 mg/m³ to ensure reliable operation and life of an engine [36].

Tar removal techniques are generally categorized into (a) primary removal techniques and (b) secondary removal techniques. Primary removal techniques refer to techniques that are employed inside the gasifier without the need of a secondary reactor. These include selection of gasifier design, optimization of gasification operating conditions, and addition of catalysts in the gasifier bed (called in-bed catalysts) [37]. Secondary tar removal techniques use a separate reactor to destruct and reform tars. Secondary tar cleaning techniques are divided further into dry, wet, catalytic, and thermal/hot gas cleaning system [37]. As tar removal is critical for commercialization of gasification-based technologies, environmental friendly but effective and robust techniques, such as biomass filter [38] and low-density energy of plasma cracking [39], are also being explored. For power production, reciprocating IC engines are relatively more tolerant of contaminants than gas turbines [35, 40]. The recommended limit of syngas tar content for reciprocating IC engine ranges from 10 to 100 mg/m³ [36, 40]. Robust gas filter and syngas cleaning system are essential before syngas can be injected into IC engines.

4 IC Engine

IC engine is economical for power generation applications as compared to the newer technologies (e.g., microturbines, fuel cells) due to the technology maturity, proven performance, rapid start-up and shutdown, relatively high efficiencies, and low costs [5]. Current generation efficiencies range from 30 to 37% (HHV), and current installed costs range from about \$1,000/kW to about \$700/kW for generation capacities between 100 and 5,000 kW [5]. With maintenance cost of 0.01–0.02 USD/kWh, this technology is highly preferred especially for distributed power generation application.

Theoretically, three operating parameters that affect the engine power are engine design, operating conditions, and fuel consumption. The mathematical equation describing that condition can be expressed as below [41]:

$$P_e = n \cdot i \cdot V_T \cdot \rho_{ia} \cdot \eta_v \cdot C \cdot F_{re} \cdot F_{sm} \cdot H_{ve} \cdot \eta_e \quad (1)$$

where P_e = the power output of the engine, kW; n = the number of engine revolutions per second, rev/s; i = the index that depends on the engine type (1 for 2-stroke engine and $\frac{1}{2}$ for 4-stroke engine); V_T = the engine displacement, m³; ρ_{ia} = the referenced air density, kg/m³ for intake manifold pressure and temperature; η_v = the engine volumetric efficiency; C = the volume correction factor, indicative of the volume occupied by the gaseous or vaporized fuel; F_{re} = the equivalence ratio in the engine admitted mixture; F_{sm} = the stoichiometric air-to-fuel ratio of engine intake mixture, kg of fuel per kg of air; H_{ve} = the energy content of the fuel, kJ/kg; and η_e = the effective efficiency. Thus, the parameters

affecting the engine are: (1) engine design, $K_d = i \cdot V_T \cdot \eta_v \cdot \eta_c$; (2) operating condition, $K_o = n \cdot \rho_{ia} \cdot F_{rc}$; and (3) fuel composition, $EFQ = C \cdot F_{sm} \cdot H_{ve}$.

Typically, the IC engine can be classified into natural gas engine, gasoline engine, compressed ignition (diesel) engine, and gas turbine. These engines are technically proven to run on syngas generated from gasification of biomass and MSW as described below.

4.1 Natural Gas Engine

Natural gas engine is one of the spark ignition (SI) engines. The three advantages of using natural gas engine, compared to gasoline and diesel engines, are that it produces lesser emissions (sulfur, nitrogen, and carbon dioxide), are less expensive, and are considerably more efficient. In addition, the natural gas engines do not produce a pungent odor [42]. Sridhar et al. [43] fed syngas with LHV of 4.9 MJ/m³ and density of 1.7 kg/m³ into 12.1 L, 4-stroke, six-cylinder, and 101 kW natural gas engine at 1,500 rpm of engine speed and compression ratio of 10. By modifying the carburetor, they found that the maximum brake power output, brake-specific fuel consumption, and engine (electrical) efficiency were about 60 kW, 5.06 kg/kWh and 24.7%, respectively. CO and NO_x emissions were 1.4–6.5 g/kWh and 0.7–2.5 g/kWh, respectively. Raman and Ram [34] fed 100% syngas with LHV of 5.6 MJ/m³ and density of 1.05 kg/m³ into six-cylinder, 100 kW natural gas engine running at engine speed of 1,500 rpm. The engine was adjusted to have compression ratio of 12 with air-to-fuel ratio of about 1.2. The tar content was reduced from 350 to 30 mg/m³ using a series of gas cleaning system equipment that included a venturi scrubber, chiller, fabric filter, and paper filter. The engine ran smoothly producing maximum power output of about 73 kW with the engine efficiency of about 21% and specific fuel consumption of about 3.21 kg/kWh. However, emissions performance was not reported. Tsiakmakis et al. [44] fed syngas generated from fluidized bed gasification of olive, peach, and grape kernel into a 4.7 kW, one-cylinder natural gas engine running at 3,400 rpm of engine speed with the compression ratio of 10, and air-to-fuel ratio of about 1.74. The syngas energy contents ranged from 4.52 to 6.96 MJ/Nm³, depending on the feedstock. Authors also used propane to increase the energy content of the syngas mixture up to about 23.73–24.4 MJ/m³. The maximum engine power output was 3.55–3.68 kW, depending on the feedstock with the engine efficiency in the range of 23.2–26.2%. The engine was not modified, and emission performance was not reported. Margaritis et al. [45] fed 100% syngas (containing 53.1–55% N₂, 23.6–24.1% H₂, 3.8–4.1% CH₄, 9.5–10.6% CO, and small fraction of O₂, with energy content of 5.65 MJ/Nm³) derived from downdraft gasification of olive kernel into six-cylinder 135 kW natural gas engine at 1,500 rpm engine speed and power setting of 70 kW. Tar and particulates from the syngas were removed using venturi scrubber, heat exchanger with chiller, a mist of eliminator, and a series of fine filters. A gas blower was also used to ensure stable flow of the syngas entering into

the gas engine. The cold gas and electric efficiency were 75% and 16.1%, respectively. However, air-to-fuel ratio as well as any operational issues were not reported. Henriksen et al. [46] tested a two-stage gasifier—the pyrolysis and char gasification taking place in separate reactors—with a 75 kW three-cylinder natural gas engine and observed stable operation producing power for approximately 410 h. The syngas had 6.2 MJ/Nm³ of energy content with 32–35% H₂, 28–30% N₂, 20% CO₂, 15–18% CO, and 2–3% CH₄. The maximum power output of the engine runs with natural gas, and 100% syngas was 25 kW and 20 kW, respectively; hence, 80% of de-rating factor was observed. The efficiency from gas to mechanical power (engine efficiency) was about 28%. During the operation, one of the cylinders did not ignite for several reasons.

4.2 Gasoline Engine

The gasoline engine is a type of SI engine. Shah et al. [47] tested a 5.5 kW gasoline engine running on 100% syngas reducing tars to about 14 mg/m³. The engine was modified by adding two air venturies in series to establish the flow of syngas from the storage tank to the air intake manifold. To run the engine on syngas, the engine was first cranked on gasoline and then the gasoline was turned off with the syngas supply being turned on simultaneously. The engine efficiency was about 19% with maximum brake power of 1.39 kW. CO emissions decreased by 30–96% when syngas was used compared to gasoline. The higher CO emission of gasoline might be because of the operation of the gasoline in rich conditions and higher carbon content of gasoline (88.7% w/w versus 16.9% w/w of syngas) [48]. However, syngas operation resulted in 33–167% higher CO₂ emission compared to gasoline. This can be attributed to higher conversion of CO to CO₂ during the syngas operation. The exhaust CO₂ was 10.6–13.1% for syngas operation and 4.9–8.1% for gasoline operation. There was no trend observed for HC emission—HC emission was found to be less than 40 ppm for almost all the load variation. This might be due to the very low HC (1.2–6.4%) in the syngas. Syngas operation resulted in 54–84% lower NO_x emission than the gasoline operation. The Zeldovich mechanism can be used to explain the lower NO_x emission from syngas. As LHV of syngas is lower (5.6 MJ/m³) than that of gasoline (44.4 MJ/kg), the temperature of combustion for syngas operation is lower, resulting in lower NO_x emission. Mustafi et al. [16] tested a gasoline-based engine using syngas with LHV of 15 MJ/m³. The specific fuel consumption was about 1 kg/kWh at 2,000 rpm. The maximum torque produced was 22 Nm (~16.22 lb-ft), which resulted in maximum brake power output of 4.61 kW. The HC emissions from syngas were very low (about 0–20 ppm) compared to those from gasoline (90–225 ppm) and from natural (20–106 ppm). CO₂ emissions from syngas were higher (19% v/v) compared to that from gasoline (15% v/v). CO emission was low, indicating complete combustion in the engine. However, syngas operation resulted in higher NO_x emission (~4500 ppm), compared to gasoline operation (~1500 ppm).

4.3 Compressed Ignition (Diesel) Engine

Diesel engine is a type of reciprocating IC engine, called compression ignition (CI) engine. However, in CI engine, air is compressed first, and then, the fuel is injected in the CI engine allowing the engine to design for high compression ratio. Several studies reported performance of diesel engine (with little modification) running on syngas. Homdoug et al. [49] tested the modified diesel engine running on 100% syngas. The modification to the engine included changes to the combustion chamber, reduction of compression ratio, mounting of ignition system in place of injector nozzle, and mounting of air–gas mixer. The tar content of the syngas (LHV of 4.64 MJ/m^3) was reduced using gas cleaning system to below 50 mg/m^3 . The highest engine efficiency attained was about 24% with the specific fuel consumption of 5.52 kg/kWh producing 3.5 kW at 1700 rpm . The compression ratio used was 14:1. CO, and HC emissions were in the range of 0.3–0.4% and 3.5–10 ppm, respectively. Sridhar et al. [43] also investigated performance of a modified 28 kW diesel engine running on syngas with tar content of about 60 mg/m^3 . A new carburetor was developed to ensure that the carburetor maintains the gas pressure close to that of air pressure, thereby ensuring that the air-to-fuel ratio is set irrespective of the total air–fuel flow rate. Homogeneity of the fuel and air mixture entering the engine was effected by long interconnecting duct along with a few bends (with a large diameter for keeping pressure losses to a minimum) between the gas carburetor and intake manifold. The maximum power achieved was 20 kW (engine efficiency of 27.6%, and de-rating of 20–30%) with the compression ratio of 17:1 and mixture energy density of 2.2 MJ/kg . The fuel-specific consumption was about 4.07 kg/kWh if the syngas density was assumed to be about 1.7 kg/m^3 . CO and NO_x emissions were in the range of 14.4–57.6 g/kWh and 0.1–0.7 g/kWh, respectively. Nataraj et al. [50] investigated a single-cylinder, 3.7 kW (at 1500 rpm) diesel engine with compression ratio of 17.5 running on 100% syngas (energy content of $5\text{--}5.6 \text{ MJ/m}^3$ and tar content below $50\text{--}60 \text{ mg/m}^3$). The maximum power output and engine efficiency were 2.96 kW and 18.9%, respectively. Engine modification, if any, was not reported. CO, NO_x , and HC emissions were in the ranges of 0.3–0.4%, 40–100 ppm, and 20–50 ppm, respectively. The summary of recent researches on these engines (natural gas, gasoline, and compressed ignition) is presented in Table 3.

4.4 Gas Turbine

The power plant based on advanced combined cycle gas turbine can offer gross thermal efficiency of 50–54% at HHV basis [51]. Recent advances in gas turbines have made these suitable to use syngas with low LHV ($7\text{--}12 \text{ MJ/Nm}^3$) [52]. However, gas turbines are generally very sensitive to gas quality and can only allow extremely low levels of contaminants including tar, alkali metals, sulfur, and

Table 3 Summary of engine power generation and emissions performance compared to previous works using 100% syngas

References	Gasification parameters										Engine parameters						Emission parameters						
	Type of biomass	Reactor type and capacity	Equivalent ratio, ER	Cold gas efficiency, %	Syngas LHV, MJ/Nm ³	Engine size, kW	Original fuel type	No. of cylinder	Rated speed, rpm	Modification performed	Bore x stroke, mm	Total displacement, L	Compression ratio (CR)	Air-Fuel ratio (AFR)	Max. Brake Power produced, kW	Specific Fuel Cons., kg/kWh	Engine Efficiency, %	HC	CO	NO _x	CO ₂	SO ₂	
[54]	Charcoal longan tree	Downraft, 5 to 6 kg/h	N/A	N/A	4.64	8.2	Diesel	1	1800	Changed combustion chamber to cavity	92 x 90	0.6	14	N/A	3.17	5.53	23.5%	3.5 to 10 ppm	03,000 to 4,000 ppm	N/A	N/A	N/A	N/A
[48]	N/A	Downraft, 75 kg/h	N/A	N/A	4.90	28	Diesel	3	1,500	SI engine, developed new carburetor	110 x 116	3.3	17	1.2 to 1.5	20	4.52	27.6%	N/A	14.4 to 57.6 g/kWh	0.1 to 0.7 g/kWh	N/A	N/A	N/A
[48]	N/A	Downraft, 75 kg/h	N/A	N/A	4.90	101	Natural gas	6	1,500	Carburetor adapted	130 x 152	12.1	10	1.2 to 1.5	60	5.06	24.7%	N/A	1.4 to 6.5 g/kWh	0.7 to 2.5 g/kWh	N/A	N/A	N/A
[52]	N/A	No gasifier	N/A	N/A	5.79 ^a	5.5	Gasoline	1	3,600	Two air venturis in series added	N/A	N/A	N/A	N/A	1.39	5.53	19% (electrical eff.)	N/A	45.3 to 51 g/kWh ^b	0.5 g/kWh ^b	254 g/kWh ^b	N/A	N/A

(continued)

Table 3 (continued)

References	Gasification parameters										Engine parameters					Emission parameters							
	Type of biomass	Reactor type and capacity	Equivalent ratio, ER	Cold gas efficiency, %	Syngas LHV, MJ/Nm ³	Engine size, kW	Original fuel type	No. of cylinder	Rated speed, rpm	Modification performed	Bore x stroke, mm	Total displacement, L	Compression ratio (CR)	Air-Fuel ratio (AFR)	Max. Brake Power produced, kW	Specific Fuel Cons., kg/kWh	Engine Efficiency, %	HC	CO	NO _x	CO ₂	SO ₂	
[16]	N/A	N/A	N/A	N/A	15.3	N/A	Gasoline	—	2,000	N/A	76.21 x 111.1	0.5	4.5:1 to 20:1	4.25:1	4.6	1.1	36%	0 to 20 ppm	N/A	4,500 ppm	N/A	190,000 ppp	N/A
[39]	Wood chips	Downdraft, 87 kg/h	0.35	88%	5.6	100	Natural gas	6	1,500	Fuel intake manifold, hydraulic governor	132 x 150	12.3	12	1.2	73	3.21	21%	N/A	N/A	N/A	N/A	N/A	
[56]	Sawdust, Sugarcane	Downdraft	N/A	N/A	4.4	100	Producer gas	N/A	1,500	None	N/A	N/A	N/A	N/A	98	4.9 to 5.7	24.3 to 28.2%	N/A	N/A	N/A	N/A	N/A	
[51]	Wood chips	Downdraft	N/A	N/A	6.2	N/A	Natural gas	3	N/A	None	N/A	N/A	N/A	N/A	20	3.5	28%	N/A	N/A	N/A	N/A	N/A	
[49]	Peach kernels	Bubbling fluidized bed	N/A	N/A	6.9	4.7	Natural gas	1	3,400	None	71.9 x 65.5	0.3	10	1.7	3.68	0.49	26.2%	N/A	N/A	N/A	N/A	N/A	
[55]	Rice bran oil methyl ester	Downdraft	N/A	N/A	5.60	3.7	Diesel	1	1,500	N/A	87.5 x 110	0.7	17.5	N/A	2.96	5.78	18.9%	20 to 50 ppm	3,000 to 4,000 ppp	40 to 100 ppp	N/A	N/A	

(continued)

Table 3 (continued)

References	Gasification parameters										Engine parameters					Emission parameters						
	Type of biomass	Reactor type and capacity	Equivalent ratio, ER	Cold gas efficiency, %	Syngas LHV, MJ/Nm ³	Engine size, kW	Original fuel type	No. of cylinder	Rated speed, rpm	Modification performed	Bore x stroke, mm	Total displacement, L	Compression ratio (CR)	Air-Fuel ratio (AFR)	Max. Brake Power produced, kW	Specific Fuel Cons., kg/kWh	Engine Efficiency, %	Total emission	HC	CO	NO _x	CO ₂
[28]	Switchgrass	Downdraft, 100 kg/h	0.25	68%	6 to 7	10	Natural gas	2	3,600	Air fuel intake	71.9 x 70.1	0.6	N/A	1.2 to 1.6	5	1.9	21.3% (electrical eff.)	0 to 262 ppm	4,000 ppm	21.5 to 32.5 ppm	75,000 ppm	429 to 768 ppm
[57]	MSW and Switchgrass (SG)	Downdraft, 100 kg/h	0.20	56 to 59%	6.4 to 6.8	10	Natural gas	2	3,600	Air fuel intake with two venturics	71.9 x 70.1	0.6	N/A	0.5 to 1.0	5	2 to 5	16.4 to 21.3% (electrical eff.)	0 to 256 ppm	0 to 8,825 ppm	0.8 to 26 ppm	14,667 to 69,333 ppm	22 to 119 ppm

Note: 1) Calculated, 2) Syngas LHV based on purchased based, 3) Calculated based on AFR 1.2

Table 4 Typical gas quality requirements for power generation [34–36, 40]

Parameter	Boiler	Internal combustion engine	Gas turbine
LHV (MJ/Nm ³)	>4	>4	>4
Particulate (mg/Nm ³)	None	<5–50	<5–7
Tars (mg/Nm ³)	None	<10–100	<100–500
Alkali metals (ppm)	None	<1–2	<0.2–1

chlorine compounds. General limits of contaminants are presented in Table 4 [35]. The use of a properly designed dual-fuel combustion system and their controls is key to achieving reliable and robust gas turbine operation using syngas generated from biomass and MSW [52].

An electrical efficiency of 31.5% was achieved by feeding syngas with LHV of 9–20 MJ/Nm³ that was generated from 2 × 80 MW CFB gasification of wood biomass (moisture of up to 37.5%) in Lahti Energia steam power plant of Valmet, Finland [53]. The CFB gasifier operated at 5–30 kPa and 750–900 °C using air as gasification medium, while the steam power plant was run on 120 bar and 550 °C. The plant achieved nearly 80% of operational availability in 2014 with no major maintenance issue including no indications of corrosion or erosion on the boiler tubes; tube manufacturing marking was still visible after 13,000 h of operation. However, a small amount of dust/slag in gas cooler, and thin dust layer in the boiler was visible [53].

5 Power Generation from Biomass and MSW Gasification

The power generation through gasification of biomass and MSW is promising throughout the world, especially in the areas that have abundant availability of unused biomass and solid wastes and are still not connected to the electrical grid. Biomass gasification has been known and used since the World War II, when approximately one million downdraft gasifiers were used to operate cars, trucks, boat, train, and electric generators in Europe [54]. On the contrary, the use of MSW in gasification is relatively new as MSW generation is projected to increase globally from 1.3 billion tons (1.2 kg per person per day) in 2012 to over 2.2 billion tons (1.42 kg per person per day) in 2025 [55]. Compared to current practices of incineration and landfill of MSW, gasification is considered superior from environmental perspectives as it can produce power without release of methane, dioxins, and furans (PCDD/PCDF) [29], can reduce the landfill area needed by over 88% [14], and produce non-leaching vitrified slag [30].

5.1 Co-gasification of Biomass and MSW for Power Generation

Co-gasification is defined as gasification of a mixture of biomass, waste, or coal to improve operational reliability and/or achieve low carbon footprint by reducing greenhouse gas (GHG) emissions [56]. Most reports on co-gasification are based on a mixture of biomass and coal since the majority of conventional power plants are steam-based coal power plant and adding biomass to replace some parts of coal can reduce GHG emissions. Co-gasification of biomass and MSW offers significant advantages as global MSW generation has been increasing by approximately 69.2 million tons per year [55]. MSW has become a public health hazard by contaminating soil, water, and air through leaching and biodegradation processes. As compared to coal and biomass, MSW can generate additional revenue from tipping fees that can make the process much more economical. Low operational cost of MSW gasification can be achieved by deploying gasification technologies (e.g., fixed-bed gasifiers) instead of high-power thermal plasma gasification that generally used for the gasification of wastes [30, 57].

Robinson et al. [58] reported the co-gasification of wood pellets and refused derived fuel (RDF) in gasification temperature of 725, 800, and 875 °C, with RDF ratio of 0, 25, 50, and 100 wt% and air as gasification medium and equivalent ratio of 0.29–0.31 in a bubbling fluidized bed gasifier. The tests resulted in a syngas with LHV of 4.9–5.7 MJ/Nm³, gasification efficiency of 48–58%, and tar content of 15–50 g/Nm³. However, agglomeration of ash was found at gasification temperature of 875 °C for all mixtures containing RDF that prevented the steady-state operation of gasifier.

Similarly, Ong et al. [59] conducted the co-gasification of wood chips and dried sewage sludge in a fixed-bed downdraft gasifier with sludge ratio of 0, 20, and 33 wt%. The tests generated syngas with LHV of 3.6–4.6 MJ/Nm³ and gasification efficiency of 63.2% at gasification temperature of 650–900 °C. However, the test could only use sludge at maximum ratio of 33 wt% due to agglomerated ash that leads to blockage of gasifier.

Narobe et al. [60] performed the co-gasification of wood pellets and plastics with plastics ratio of 0, 25, 75, and 100 wt% on 100 kW dual fluidized bed gasifier with steam as gasification medium (steam-to-carbon mass ratio of 2.3) and using olivine as heterogeneous catalyst. The experiment resulted in syngas with LHV of 16 MJ/Nm³ at plastic ratio of 75 wt% in gasification temperature of 850–900 °C and generated tar of 0.2–1.3 kg/h with syngas flow rate of 7–17 kg/h. Elevating plastics content in feed lowered syngas yield but increased fractions of ethane and ethylene and decreased CO₂ in syngas.

A co-gasification of switchgrass and MSW has recently been conducted at Oklahoma State University. The proximate and ultimate analysis of the feedstocks is summarized in Table 2 for MSW-3 and switchgrass. The ratio of MSW on the feedstock was varied from 0, 20, 40, and 60%. The gasification used downdraft

reactor with thermal capacity of 60 kW and equivalent ratio of 0.20; air was used as the gasification medium. The feedstock throughput was constantly maintained at 95 kg/h. The co-gasification resulted in the syngas energy content (LHV) of 6.47, 6.76, and 6.72 MJ/Nm³ and cold gas efficiency (CGE) of about 68, 59.4, and 58.6% for MSW ratio of 0, 20, and 40 wt%, respectively. The co-gasification produced stable and maximum power output of 5 kW at all MSW ratios (0, 20 and 40 wt%) using 10 kW natural gas SI engine and confirm system workability for off-grid power generation application. Details regarding this are provided elsewhere [61].

At large scale, co-gasification of MSW and bottom ash has been reported [25]. With the feedstock throughput of 251.8 ton/day and using oxygen rich air (36% oxygen) as gasification medium, the operating temperature inside the gasifier (combustion and melting zone) reached 1,000–1,800 °C and generated syngas with LHV of 4.4 MJ/Nm³. With the total plant capacity of 50 MW consisting of steam turbine and gas engine, total power output of the steam turbine and gas engines reached 9.0 and 1.6 MW, respectively, with cold gas and power generation efficiencies of 54.6 and 18.9%, respectively, and with the average power generation of 408 kWh/t-MSW [25]. The PCDD/PCDF in the flue gas was 0.0082 ng/Nm³, much lower than the local regulation of 0.05 ng/Nm³ [25].

5.2 MSW Gasification Using Plasma Technology

Among thermochemical treatment processes, gasification using thermal plasma (“known as plasma gasification”) seems one of the most appropriate and proven technologies to deal with various components of MSW. The comparison between plasma gasification and other thermochemical treatment processes is summarized in Table 5.

Generally, plasma technology can be classified into two groups: thermal or equilibrium plasma and non-thermal plasma [57]. The main characteristics of thermal plasma are the use of extremely high temperature, high intensity, non-ionizing, and high energy density radiation that can reach temperature of up to 20,000 °C. The main advantages of thermal plasma include high energy density and high temperature that allow high heat and reactant transfer rate, smaller footprint size of equipment, and rapid start-up and shutdown [62]. However, the major drawbacks include high electricity consumption (15–20% of power output of the plant [24]) and the need to replace electrode due to sputtering that increases the maintenance cost [63]. In comparison, non-thermal plasma (also known as “cold plasma”) has lower degree of ionization; thus, it is generated either at low pressure or at lower power, or in different pulsed discharge systems, requiring much less power consumption [57, 64]. Thermal plasma can be classified into four categories: direct current (DC) electric discharge, alternating current (AC), or transient arcs (e.g., lamps, circuit breakers, or pulsed arcs), radio frequency (RF) inductively

Table 5 Comparison between plasma gasification and other thermochemical technologies for MSW [24, 30, 37, 53, 74]

Parameters	Incineration	Conventional gasification	Pyrolysis	Plasma gasification
Process goal	To convert wastes into high-temperature flue gases	To convert wastes into syngas consisting primarily of CO, H ₂ , CH ₄	To convert wastes into mainly bio-oil and syngas	To convert wastes into high-quality syngas
Temperature (°C)	850–1200	550–900	500–800	>4000
Pressure	Atmospheric	Varies	Slight over atmospheric	Atmospheric
Fuel created	Not applicable	Syngas	Bio-oil and a small fraction of syngas (CO and H ₂)	Syngas
Emissions	SO ₂ , NO _x , HCl, PCDD/PCDF, particulates	H ₂ S, HCl, COS, NH ₃ , HCN, tar, alkali, particulates	H ₂ S, HCl, NH ₃ , HCN, tar, particulates	SO ₂ , NO _x , HCl, particulates
Ash	Is composed of ferrous metal, nonferrous metal, and inert materials	Is a vitreous slag that can be used as construction aggregate	Contains high carbon are disposed as industrial waste	Is an inert, non-hazardous and non-leaching glassy slag that can be used as construction aggregate
Gas cleaning system	Treatment is mandatory to meet the air pollution standard	Syngas must be cleaned before it can be used.	Syngas must be cleaned before it can be used	Complex syngas cleaning system is not required as tars, and other pollutants are vitrified in slag
Power generation efficiency	3–30%	14–35%	Not applicable	20–40%

coupled discharge, and microwave discharge. The non-thermal plasma can also be classified into several categories, which are corona discharge, pulsed corona discharge, dielectric barrier discharge, spark discharge, and atmospheric pressure plasma jet. The differences among these categories are discussed in more detail elsewhere [64]. A MSW plasma gasification with capacity of 300 ton/day using four 300 kW plasma torches operated in Utashinai, Japan, producing syngas with high CO and H₂. The syngas generated was used to produce steam for powering steam turbine producing 8 MW power. However, about half of total power output was used for the plant operation [65].

5.3 *Recent Commercialization of MSW Gasification for Power Generation*

Several power plants using plasma gasification, mostly using plasma torches that run on high temperature ($>4,000\text{ }^{\circ}\text{C}$), have been reported (summary of plants operating since the late 1990s is in Table 6). Among these plants, several have stopped operating due to inconsistent supply of feedstock or inefficient operation. However, many plants are operational and economically competitive because of their uniqueness of processing complicated MSW feedstock such as medical and hazardous wastes.

6 Environmental and Emissions Standards

The environmental pollutants produced during power generation through gasification of biomass and MSW are available either in three forms: (1) ash/slag, (2) fly ash/flue gas, and (3) engine emissions. Among the elemental pollutants generated (shown in Table 7), hazardous and lethal pollutant that are of major concern include PCDD/PCDFs and tar that can be significantly reduced by the limited oxidizing environment of gasification and robust syngas cleaning system.

Ash generated from biomass/MSW gasification must comply with pertinent standard. Leaching test and acid extraction are the common method used to measure potential to contaminate groundwater. Table 8 shows contaminants from gasification of a MSW power plant with capacity of 50 MW and associated standard [25].

Table 9 compares the emission performance of a biomass gasification power plant using steam cycle with emission standards. The plant used CFB gasifier and operated at 5–30 kPa and 750–900 $^{\circ}\text{C}$, while the steam power plant was run on 120 bar and 550 $^{\circ}\text{C}$. Among the emissions, NO_x emission was dominant ($\sim 161\text{ mg/Nm}^3$), but still under the EU and USA standards.

MSW gasification offers considerably high reduction of emissions as compared to incineration and landfill disposal with gas capture. MSW gasification generates only about 1 kg of CO_2 equivalent per kWh of generated power, while landfill with gas capture produces approximately 2.75 kg/kWh and incineration releases approximately 1.6 kg/kWh of power generated [66]. MSW gasification generates 31 g of NO_x and 9 g of SO_2 per ton of waste, while landfill releases 68 g of NO_x and 53 g of SO_2 per ton waste, and incineration generates more than 192 g of NO_x and more than 94 g of SO_2 per ton waste [66].

Table 6 List of power generation plants using plasma technology for using MSW

Plants	Descriptions	Status	Ref
The Maharashtra Enviro Power Ltd. ("MEPL") Plant located in Pune, India	Syngas is used to generate electricity. 40–60 waste streams including hazardous and medical waste with total capacity of 72 tpd are simultaneously treated. Approximately 1.6 MW of electricity is exported to the grid	In operation since 2008	WPC, Heberlein and Murphy [30, 75]
Tees Valley Plant located in northeast UK	With 1,000 tpd of feedstock, the Tees Valley project, owned by Air product, was the biggest plasma gasification power plant with total power output capacity of 2 × 50 MW. Two units of gasifier have been delivered to site on May 2013. Plasma torches were acquired from Westinghouse Plasma Corporation (WPC). The project cost reached 13,000 USD/kw. However, due to technical and economic difficulties, Air product suspended this project in 2016	Suspended since April 2016	WPC, Messenger [30, 76]
Eco-Valley Plant located in Utashinai, Japan	The plant, sponsored by Hitachi and Westinghouse Corporation, began operation in 2003 with total capacity of 165 tpd for treating MSW and auto shredder residue (ASR) (50:50 mixture) supplying 1.5 MW of electricity to the grid. Plasma torches operated at above 5,500 °C, and generated syngas with LHV and cold gas efficiency of around 11.9 MJ/Nm ³ and 79%, respectively. The electricity was produced through steam (Rankine) cycle. Torch power requirement is about 2.4% of the energy input, while syngas production is 78% of energy output	Ceased operation in 2013	Willis et al. [77]
Chengtou hazardous waste facility located in Shanghai, China	The plant, owned by GTS Energy, was built to treat 30 tpd of medical wastes and generated electricity using steam cycle	In operation since 2014	WPC [30]
Plasco Plant located in Ottawa, Canada	The plant treats 85 tpd of post-recycle MSW and generates 4 MW (net) of electricity using gas engine	In operation since 2008	Agon [75]
Morcenx Plant located in Morcenx, France	The technology provider is Europlasma. The plant runs on 100 tpd of industrial waste combined with 41 tpd of wood chips generating total electricity of nearly 12 MW and hot water of 18 MW using two plasma torches and the syngas generated is directly used to run gas engines	In operation since 2014	Agon [75]
Bijie Plant located in Bijie, China	The project, owned by Greenworld Energy Solutions Corp. (GES), is designed to treat 600 tpd of MSW generating 15 MW of electricity. WPC is the provider of plasma technology	Being prepared for commissioning	Agon [75]

Table 7 Possible elemental pollutants generated from the gasification of biomass and MSW and associated technologies to minimize the pollutants

Pollutant	Production precursor	Reduction method
<i>Major elements in ash and fly ash</i>		
Chlorine, Cl	Observed only in Fly ash/flue gas [25] due to feedstock (esp. MSW) containing chlorine	Flue gas desulfurization (FGD) technology: once-through (wet and dry) and regenerable (wet and dry) techniques [78]
Sulfur, S	Distributed in slag and flue gas (dominant), due to feedstock containing sulfur Together with oxygen, sulfur forms sulfur dioxide (SO ₂)	<i>Slag:</i> Cyclone and other ash/slag removal systems [25] <i>Flue gas:</i> Flue gas desulfurization (FGD) technology: once-through (wet and dry) and regenerable (wet and dry) techniques [2, 78]
Calcium, CaO	Distributed in slag and flue gas due to feedstock (esp. MSW) containing calcium [25]	Same as above
Silica, SiO ₂	Distributed in slag and flue gas due to feedstock (e.g., MSW) containing silica [25]	Same as above
Aluminum, Al ₂ O ₃	Distributed in slag and flue gas (slightly more dominant) [25] due to feedstock (esp. MSW) containing aluminum	Same as above
Sodium, Na ₂ O	Distributed in slag and flue gas [25] due to feedstock (esp. MSW) containing sodium	Same as above
Potassium, K ₂ O	Distributed in slag and flue gas (slightly more dominant) [25] due to feedstock (esp. MSW) containing potassium	Same as above
Magnesium, MgO	Distributed in slag and flue gas [25] due to feedstock (esp. MSW) containing magnesium	Same as above
<i>Heavy metals in ash and fly ash</i>		
Lead, Pb	Distributed in slag and fly ash/flue gas (majority) due to feedstock (esp. MSW) containing lead	<i>Slag:</i> Cyclone, ash/slag removal system [25] <i>Flue gas:</i> (1) Selective catalytic reduction (SCR) with flue gas desulfurization (FGD) [79] (2) Activated carbon injection (ACI) [79] (3) ACI with fabric filter (FF) [79] (4) Electrostatic precipitators (ESP) [79] (5) Baghouse filter [25]

(continued)

Table 7 (continued)

Pollutant	Production precursor	Reduction method
Ferrous, Fe	Distributed in slag (dominant) and flue gas, due to feedstock (esp. MSW) containing ferrous	Same as above
Copper, Cu	Distributed in slag (dominant) and flue gas, due to feedstock (esp. MSW) containing copper	<p><i>Slag:</i> Cyclone, ash/slag removal system [25]</p> <p><i>Flue gas:</i> (1) Selective catalytic reduction (SCR) with flue gas desulfurization (FGD) [79] (2) Activated carbon injection (ACI) [79] (3) ACI with fabric filter (FF) [79] (4) Electrostatic precipitators (ESP) [79]</p>
Zinc, Zn	Distributed in slag and flue gas (dominant), due to feedstock (esp. MSW) containing zinc	Same as for Fe and Pb
Mercury, Hg	Distributed in slag and flue gas, due to feedstock (esp. MSW) containing mercury	<p><i>Slag:</i> (1) Cyclone [80] (2) Ash/slag removal system</p> <p><i>Flue gas:</i> (1) Selective catalytic reduction (SCR) with flue gas desulfurization (FGD) [79, 80] (2) Activated carbon injection (ACI) [79] (3) ACI with fabric filter (FF) [79] (4) Electrostatic precipitators (ESP) [79] (5) Baghouse filter [25] (6) Spray dryer absorber/fabric filter [80]</p>
Nickel, Ni	Distributed in flue gas [81] due to feedstock (esp. MSW) containing mercury	<p>(1) Selective catalytic reduction (SCR) with flue gas desulfurization (FGD) [79, 80] (2) Activated carbon injection (ACI) [79] (3) ACI with fabric filter (FF) [79] (4) Electrostatic precipitators (ESP) [79] (5) Baghouse filter [25] (6) Spray dryer absorber/fabric filter [80]</p>

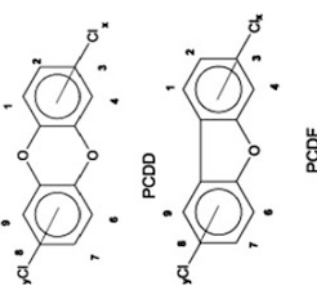
(continued)

Table 7 (continued)

Pollutant	Production precursor	Reduction method
Arsenic, As	Distributed in flue gas [81] due to feedstock (esp. MSW) containing mercury	Same as above
Cadmium, Cd	Distributed in flue gas [81] due to feedstock (esp. MSW) containing mercury	Same as above
<i>Engine emissions</i>		
Dust/particulates	Gasification process [25]	Cyclone, baghouse filter [25]
Carbon Dioxide, CO ₂	(1) Mostly due to the oxidation reactions of gasification [8]: 1. $\text{CO} + \frac{1}{2} \text{O}_2 \rightarrow \text{CO}_2$ 2. $\text{C} + \text{O}_2 \rightarrow \text{CO}_2$ 3. $\text{CH}_4 + 2\text{O}_2 \rightarrow \text{CO}_2 + 2 \text{H}_2\text{O}$ (2) The engine combustion 4. $\text{CH}_4 + \text{O}_2 \rightarrow \text{CO}_2 + \text{H}_2\text{O}$	<i>Primary method:</i> (1) The reduced use of coal as the input of gasification <i>Secondary method:</i> (2) CO ₂ sequestration: amine based sorbent [2] (3) Carbon capture
Sulfur Dioxide, SO ₂	A high-temperature combustion of the internal combustion (IC) engine converts sulfur in the fuel into SO ₂ and SO ₃ [82]	(1) Sulfur removal from the fuel (2) Flue gas desulfurization (FGD) technology: once-through (wet and dry) and regenerable (wet and dry) technique [78]
Nitrogen Oxides, NO _x	The high combustion of syngas/natural gas occurring at temperature higher than 1,200 °C following the Zeldovich mechanism develops the formation of NO _x [82]: $\text{N}_2 + \text{O} = \text{NO} + \text{N}$ $\text{N} + \text{O}_2 = \text{NO} + \text{O}$ $\text{N} + \text{OH} = \text{NO} + \text{H}$	(1) Selective catalytic reduction (SCR) method can be used prior to the stack [25] (2) Flue gas recirculation (FGR) [82] (3) Low NO _x burners (LNB) [82] (4) Combustion optimization [82] (5) Less excess air (LEA) [82] (6) Water/steam injection [82] (7) Air preheat reduction [82] (8) The use of ultra-low nitrogen fuel [82] (9) The use of non-thermal plasma reactor [82] (10) The use of oxygen instead of air [82]

(continued)

Table 7 (continued)

Pollutant	Production precursor	Reduction method
Carbon monoxides, CO	(1) Oxidation, water-gas and Boudouard reactions of gasification process [8]: 1. $C + \frac{1}{2} O_2 \rightarrow CO$ 2. $C + H_2O \rightarrow CO + H_2$ 3. $C + CO_2 \rightarrow 2CO$ (2) The incomplete combustion of the syngas engine	<i>From viewpoint of Gasification:</i> (1) Lowering the temperature of gasification [83]. However, high CO concentration is expected as it can increase the lower heating value (LHV) of the syngas <i>From viewpoint of engine operation:</i> The use of lean operation (high air-to-fuel ratio/AFR) [84]
PCDD/PCDFs	(1) Feedstock (esp. MSW) containing trace amount of chlorine [85–88], creates de novo synthesis, a reaction of the oxidative breakdown and transformation of macromolecular carbon structures to aromatic compounds [88–90] (2) Since PCDD has two oxygen atoms, and PCDF has one oxygen atom, a rich oxygen environment is preferred to accelerate the formation of PCDD/PCDFs [29, 88, 90] <div style="text-align: center;">  <p>PCDD</p> <p>PCDF</p> </div>	<i>Primary method (preventing the PCDD/PCDFs formation):</i> (1) Oxygen starving process such as gasification [29, 88–91] (2) Proper selection of raw materials, avoiding as possible the addition of chlorine into the process [88] (3) The use of inhibitor for preventing de novo synthesis such as triethanolamine [88]. Another is ammonia, however, it is not effective for large-scale plant [88, 90, 92–94] (4) Lowering hydrocarbon and dust emission [88] (5) Accelerated cooling of the flue gas into temperature of 600–200 °C [88, 95] <i>Secondary method (providing measures to limit the emission of PCDD/PCDFs to the atmosphere):</i> (1) Cyclone [95] (2) Electrostatic precipitator [95] (3) Baghouse filter, catalytic baghouse filter [95] (4) Flue gas desulfurization (FGD) technology: once-through (wet scrubber) [95] (5) Selective catalytic reduction (SCR) [95] (6) Dry absorption in resins (carbon particles dispersed in a polymer matrix) [95] (7) Adsorption with activated carbon or open hearth coke [95] (8) Fabric filter [95] (9) The use of entrained flow reactor [88, 95] (10) UV mediated dechlorination [85, 87], ionization device [88], and electron irradiation process [87]

(continued)

Table 7 (continued)

Pollutant	Production precursor	Reduction method
Hydrogen Fluoride, HF	Feedstock (esp. MSW) containing Fluoride [81]	<p>(11) Pulse corona-induced plasma [96]</p> <p>(12) Catalytic dechlorination through metal chloride [85]</p> <p>(13) Incineration above 1,200 °C [85]</p> <p>(14) Plasma gasification [97]</p> <p><i>Fly ash treatment (providing a safe handling of fly ash residues):</i></p> <p>(15) Thermal treatment at temperature >300 °C [87] using thermal treatment equipment such as electrical, oven, coke-bed melting furnace, rotary kiln with electric heater, sintering in LPG burning furnace, plasma melting furnace, etc. [87, 98]</p> <p>(16) Non-thermal plasma [87, 99–101]</p> <p>(17) Chemical reaction using metallic calcium in ethanol [87, 102]</p> <p>(18) Supercritical water oxidation (SCWO) [87]</p> <p><i>Flue gas:</i></p> <p>(1) Flue gas desulfurization (FGD) technology: once-through (wet and dry) and regenerable (wet and dry) technique [78]</p> <p>(2) Adsorbent (e.g., CaO) [97]</p>
<i>Tar in flue gas</i>	Thermal or partial oxidation regimes (gasification) of any organic material	<p>(1) Dry gas cleaning [37, 38]</p> <p>(2) Wet gas cleaning [26, 37]</p> <p>(3) Nickel-based catalyst catalytic cracking [37]</p> <p>(4) Non-nickel metal catalyst catalytic cracking [37]</p> <p>(5) Alkali metal catalyst catalytic cracking [37]</p> <p>(6) Basic catalyst catalytic cracking [37]</p> <p>(7) Acid catalyst catalytic cracking [37]</p> <p>(8) Activated carbon catalytic cracking [37]</p> <p>(9) Thermal cracking [37]</p> <p>(10) Plasma cracking [37]</p>

Table 8 Leaching and acid extraction test results of ash disposed from MSW gasification power plant [25]

Contaminants	Leaching test			Acid-extraction test	
	Measured	JIS standard	RCRA standard [103]	Measured	JIS standard
Cd	<0.001 mg/L	<0.01 mg/L	1.0 mg/L	<5 mg/kg	<150 mg/kg
Pb	<0.005 mg/L	<0.01 mg/L	5.0 mg/L	18 mg/kg	<150 mg/kg
Cr ⁶⁺	<0.02 mg/L	<0.05 mg/L	5.0 mg/L	<5 mg/kg	<250 mg/kg
As	<0.001 mg/L	<0.01 mg/L	5.0 mg/L	<5 mg/kg	<150 mg/kg
Total Hg	<0.0005 mg/L	<0.0005 mg/L	0.2 mg/L	<0.05 mg/kg	<15 mg/kg
Se	<0.001 mg/L	<0.01	1.0 mg/L	<5 mg/kg	<150 mg/kg
CN	–	–	–	<1 mg/kg	<50 mg/kg
F	–	–	–	172 mg/kg	<4000 mg/kg
B	–	–	–	260 mg/kg	<4000 mg/kg
Metal Fe	–	–	–	0.18 mg/kg	<1.0%
Ba	–	–	100 mg/L	–	–
Ag	–	–	5.0 mg/L	–	–

7 Economics of Power Generation from Plasma Gasification

Plasma gasification is one of the most promising thermal conversions of waste-to-energy (WtE) technologies. A number of plasma WtE projects were deployed throughout the world with varied capital cost depending upon the technology used. In UK, for instance, total waste processing capacity can reach over 978,000 tons per year in 2021 as a number of advanced waste gasification projects, mostly for power generation, are under construction including high-temperature plasma gasification (>4,000 °C) of Tees Valley that has a capital cost of around 13,000 USD/kW [15]. However, due to technical difficulty and hard economic return, the Tees Valley project has been discontinued since 2016. As comparison, an integrated biomass gasification combined cycle (IBGCC) power generation has a capital cost of 2,319 USD/kW that includes preparation of yard, gasifier, and supporting systems, and prime movers (gas turbine and steam turbine generator) and supporting systems [67]. Compared to other thermal processing technologies such as incineration, pyrolysis, and thermal plasma (high temperature), to date the gasification of biomass and MSW using air as gasification medium still exhibits greater economic return including lower construction cost and lower unit cost per generating capacity (based on a comparative analysis of commercial facilities at the scale of 250 tons per day (tpd) in the USA as shown in Table 10 [68]).

Table 9 Emission performance of 2×80 MW CFB gasifier steam power plant using wood biomass at Lahti Energia, Finland [53]

Emissions	Measured	EU standard [53, 104, 105]	US EPA standard [104, 105]
NO _x (mg/Nm ³)	161	200	264
SO ₂ (mg/Nm ³)	7	50	63
CO (mg/Nm ³)	<2	50	45
Dust (mg/Nm ³)	<2	10	11
HCl (mg/Nm ³)	<1	10	29
HF	<0.5	1	n.a
TOC	<1	10	n.a
PCDD/PCDF (ng/Nm ³)	<0.002	0.1	0.14
Mercury, Hg (mg/Nm ³)	<0.0001	0.05	0.06
Cd + TI (mg/Nm ³)	<0.0003	0.05	(Cd) 0.02 [106]
Sb + As + Co+ Cr + Cu + Mn+ Ni + Pb + V	<0.03 mg/ Nm ³	Total 0.5 mg/Nm ³	(Pb) 0.2 mg/dscm [106]

Note: dscm = dry standard cubic meter of stack gas

Table 10 Comparative economic analysis of thermal technologies for power generation from MSW [68]

Performance parameter	Incineration	Pyrolysis	Thermal plasma gasification	Air gasification for MSW
Capacity in solid waste tpd	250	250	250	250
Conversion efficiency (MWh/ton @ 8000BTU/lb)	0.7	0.3	0.4	0.9
Cost of construction (Rounded to \$10 MM)	60	40	100	30
Generating capacity MWh/Day	172	180	108	224
Unit cost US\$/kWh generating capacity	348	222	1000	125
Unit cost (US\$/Ton Capacity/day)	240	160	960	120

8 Conclusions

This book chapter reviews power generation from biomass and MSW through gasification for distributed power application. Gasification is a promising technology to reduce MSW carbon footprint, to generate electricity at remote locations utilizing local resources, and to support sustainable management of MSW. Running

100% syngas generated from biomass and MSW gasification into commercial engines, including gasoline, diesel, and natural gas engines, requires minimum modifications. However, wide commercialization of power production from gasification of biomass and MSW requires future development to address technical challenges, especially in removing syngas contaminants and increasing reliability and efficiency of advanced syngas to power conversion technologies, such as combined system with fuel cell and advanced gas turbine. Plasma gasification is another technology suitable for MSW utilization, but high capital and energy requirement is a barrier for its commercialization. The use of low-temperature plasma has potential to reduce the power requirement as non-thermal plasma is not considered energy or capital intensive. Economic feasibility of biomass/MSW gasification for power production appears more promising at medium scale than that at small or large scale [61]. However, compared to conventional methods such as incineration and landfills, gasification is still considered environmental friendly to reduce release of greenhouse gases and pollutants.

Acknowledgements This work was supported, in part, by Oklahoma Agricultural Experiment Station and Indonesia Endowment Fund for Education (LPDP).

References

1. Fair D (2015) Gasification—positioning for growth. In: Annual meeting 2016 of gasification technology council. Colorado Springs
2. Denton D (2015) Update on clean energy R&D projects and programs at RTI international. Gasification technology council, Arlington
3. EIA (2017) Natural gas. https://www.eia.gov/dnav/ng/ng_cons_heat_a_EPG0_VGTH_btucf_a.htm
4. Kumar A, Jones DD, Hanna MA (2009) Thermochemical biomass gasification: a review of the current status of the technology. *Energies* 556–581
5. Zogg R, Smutzer C, Roth K, Brodrick J (2007) Using internal-combustion engines for distributed generation. *ASHRAE Journal* 76–80
6. Tremel A, Becherer D, Fendt S, Gaderer M, Spliethoff H (2013) Performance of entrained flow and fluidised bed biomass gasifiers on different scales. *Energy Convers Manag* 69:95–106
7. McKendry P (2002) Energy production from biomass (part 3): gasification technologies. *Biores Technol* 83:55–63
8. Ruiz J, Juarez M, Morales M, Munoz P, Mendivil M (2013) Biomass gasification for electricity generation: review of current technology barriers. *Renew Sustain Energy Rev* 18:174–183
9. Phillips J (2006) Different types of gasifiers and their integration with the gas turbines. National Energy Technology Laboratory, Morgantown
10. Mahinpey N, Gomez A (2016) Review of gasification fundamentals and new findings: reactors, feedstock, and kinetic studies. *Chem Eng Sci* 148:14–31
11. Minchener AJ (2005) Coal gasification for advanced power generation. *Fuel* 84:2222–2235
12. Camacho SL (1973) Refuse converting method and apparatus utilizing long arc column forming plasma torches. U.S. Patent 3 779 182, December

13. Leal-Quir'os E (2004) Plasma processing of municipal solidwaste. *Braz J Phys* 34 (4B):1587–1593
14. Pourali M (2010) Application of plasma gasification technology in waste to energy—challenges and opportunities. *IEEE Trans Sustain Energy* 1(3):125–130
15. Cothran C (2015) Identifying likely late-stage UK WTE projects, Colorado springs. Gasification Technology Council, Colorado
16. Mustafi N, Miraglia Y, Bansal P, Elder S (2006) Spark-ignition engine performance with 'Powergas' fuel (mixture of CO/H₂): a comparison with gasoline and natural gas. *Fuel* 85:1605–1612
17. Khartchenko NV (1998) *Advance energy systems*. Taylor & Francis, Washington D.C
18. NNFCC (2009) *Review of technologies for gasification of biomass and wastes*. Ecolateral, London
19. Kahraman N, Ceper B, Akansu SO, Aydin K (2009) Investigation of combustion characteristics and emissions in a spark-ignition engine fuelled with natural gas-hydrogen blends. *Hydrog Energy* 34:1026–1034
20. Arroyo J, Moreno F, Munoz M, Monne C, Bernal N (2014) Combustion behavior of a spark ignition engine fueled with synthetic gases derived from biogas. *Fuel* 50–58
21. Korakianitis T, Namasivayam A, Crookes R (2011) Natural-gas fueled spark-ignition (SI) and compression-ignition (CI) engine performance and emissions. *Prog Energy Combust Sci* 89–112
22. Szwaja S (2009) Hydrogen rich gases combustion in the IC engine. *KONES Powertrain Transp* 447–454
23. Martinez JD, Mahkamov K, Andrade RV, Lora EES (2012) Syngas production in downdraft biomass gasifiers and its application using internal combustion engines. *Renew Energy* 1–9
24. Arena U (2012) Process and technological aspects of municipal solid waste gasification. A review. *Waste Manag* 32:625–639
25. Tanigaki N, Manako K, Osada M (2012) Co-gasification of municipal solid waste and material recovery in a large-scale gasification and melting system. *Waste Manag* 32:667–675
26. Indrawan N, Thapa S, Bhoi PR, Huhnke RL, Kumar A (2017) Engine power generation and emission performance of syngas generated from low-density biomass. *Energy Convers Manag* 148:593–603
27. Toledo JM, Azna MP, Sancho JA (2011) Catalytic air gasification of plastic waste (polypropylene) in a fluidized bed. part II: effects of some operating variables on the quality of the raw gas produced using olivine as the in-bed material. *Ind Eng Chem Res* 50:11815–11821
28. Sharuddin SDA, Abnisa F, Daud WMAW, Aroua MK (2016) A review on pyrolysis of plastic wastes. *Energy Convers Manag* 115:308–326
29. Jenkins S (2015) *Environmental advantages of gasification: public and agency awareness*. Colorado Springs, GTC, Colorado
30. WPC (2013) *Westinghouse plasma gasification is the next generation of energy from waste technology*. In: USEA annual meeting, Washington D.C.
31. Lv P, Yuan Z, Ma L, Wu C, Chen Y, Zhu J (2007) Hydrogen-rich gas production from biomass air and oxygen/steam gasification in a downdraft gasifier. *Renew Energy* 2173–2185
32. Hernandez J, Barba J, Aranda G (2012) Combustion characterization of producer gas from biomass gasification. *Global Nest* 14(2):125–132
33. Hagos FY, Aziz ARA, Sulaiman SA (2014) Trend of syngas as a fuel in internal combustion engines. *Adv Mech Eng* 1–10
34. Raman P, Ram N (2013) Performance analysis of an internal combustion engine operated on producer gas, in comparison with the performance of the natural gas and diesel engines. *Energy* 63:317–333
35. Belgiorno V, Feo GD, Rocca CD, Napoli R (2003) Energy from gasification of solid wastes. *Waste Manag* 23:1–15
36. Milne T, Evans R, Abatzoglou N (1998) Biomass gasifier "Tars": their nature, formation, and conversion. NREL, Golden

37. Anis S, Zainal Z (2011) Tar reduction in biomass producer gas via mechanical, catalytic and thermal methods: a review. *Renew Sustain Energy Rev* 15:2355–2377
38. Thapa S, Bhoi PR, Kumar A, Huhnke RL (2017) Effects of syngas cooling and biomass filter medium on tar removal. *Energies* 10(3):1–12
39. Van Heesch BE, Pemen GA, Yan K, van Paasen SV, Ptasinski KJ, Huijbrechts PA (2000) Pulsed corona tar cracker. *IEEE Trans Plasma Sci* 28(5):1571–1575
40. Baratieri M, Baggio P, Bosio B, Grigianti M, Longo G (2009) The use of biomass syngas in IC engines and CCGT plants: a comparative analysis. *Appl Thermal Eng* 3309–3318
41. Tinaut FV, Melgar A, Horrillo A, de la Rosa AD (2006) Method for predicting the performance of an internal combustion engine fuelled by producer gas and other low heating value gases. *Fuel Process Technol* 135–142
42. Basshuysen RV, Schafer F (2016) *Internal combustion engine handbook*, 2nd ed. SAE International
43. Sridhar G, Sridhar H, Dasappa S, Paul P, Rajan N, Mukunda H (2005) Development of producer gas engines. *Automob Eng* 219:423–438
44. Tsiakmakis S, Mertzis D, Dimaratos A, Toumasatos Z, Samaras Z (2014) Experimental study of combustion in a spark ignition engine operating with producer gas from various biomass feedstocks. *Fuel* 122:126–139
45. Margaritis NK, Grammelis P, Vera D, Jurado F (2012) Assessment of operational results of a downdraft biomass gasifier coupled with a gas engine. *Soc Behav Sci* 48:857–867
46. Henriksen U, Ahrenfeldt J, Jensen TK, Gøbel B, Bentzen JD, Hindsgaul C, Sørensen LH (2006) The design, construction and operation of a 75 kW two-stage gasifier. *Energy* 31:1542–1553
47. Shah A, Srinivisan R, To SDF, Columbus EP (2010) Performance and emissions of a spark-ignited engine driven generator on biomass based syngas. *Biores Technol* 101(12):4656–4661
48. Heywood J (1988) *Internal combustion engine fundamentals*. McGraw-Hill, New York
49. Homdoun N, Tippayawong N, Dussadee N (2015) Performance and emissions of a modified small engine operated on producer gas. *Energy Convers Manag* 94:286–292
50. Nataraj KM, Banapurmath N, Manavendra G, Yaliwal V (2016) Development of cooling and cleaning systems for enhanced gas quality for 3.7 kW gasifier-engine integrated system. *Int J Eng Sci Technol* 8(1):43–56
51. Phillips J (2015) Can future coal power plants meet CO₂ emission standards without carbon capture and storage? Electric Power Research Institute (EPRI), Palo Alto
52. Brdar RD, Jones RM *GE IGCC technology and experience with advanced gas turbines*. GE Power System, New York
53. Isaksson J (2015) *Commercial CFB gasification of waste and biofuels—operational experiences in large scale*. Gasification Technology Council, Colorado Springs
54. Reed TB, Das A (1988) *Handbook of biomass downdraft gasifier engine systems*. Solar Energy Res Inst, Golden, Colorado, p 140
55. Bank TW (2012) *What a waste: a global review of solid waste management*. Washington D. C., The World Bank
56. Farzad S, Mandegari MA, Görgens JF (2016) A critical review on biomass gasification, co-gasification, and their environmental assessments. *Biofuel Res J* 12:483–495
57. Gomez E, Rania DA, Cheeseema C, Wise DDM, Boccaccini A (2009) Thermal plasma technology for the treatment of wastes: a critical review. *J Hazard Mater* 161:614–626
58. Robinson T, Bronson B, Gogolek P, Mehrani P (2017) Air-blown bubbling fluidized bed co-gasification of woody biomass and refuse derived fuel. *Can J Chem Eng* 95:55–61
59. Ong Z, Cheng Y, Maneerung T, Yao Z, Tong YW, Wang C-H, Dai Y (2015) Co-Gasification of woody biomass and sewage sludge in a fixed-bed downdraft gasifier. *AIChE J* 61(8):2508–2521
60. Narobe M, Golob J, Klinar D, Francetic V, Likozar B (2014) Co-gasification of biomass and plastics: pyrolysis kinetics studies, experiments on 100 kW dual fluidized bed pilot plant and development of thermodynamic equilibrium model and balances. *Biores Technol* 162:21–29

61. Indrawan N, Thapa S, Bhoi PR, Kumar A, Huhnke RL (2017) Distributed power generation via co-gasification of municipal solid waste and biomass. In: Gasification and syngas technology council (GSTC) 2017. Colorado Springs
62. Ducharme C (2010) Technical and economic analysis of plasma-assisted waste-to-energy processes. Department of Earth and Environmental Engineering, Columbia University, New York
63. Ruj B, Ghosh S (2014) Technological aspects for thermal plasma treatment of municipal solid waste—a review. *Fuel Process Technol* 126:298–308
64. Fridman A (2012) Plasma chemistry. Cambridge University Press, New York
65. Heberlein J, Murphy AB (2008) Thermal plasma waste treatment. *J Phys D Appl Phys* 41: 1–20
66. Wilson B, Williams N, Liss B, Wilson B (2013) A comparative assessment of commercial technologies for conversion of solid waste to energy. *EnviroPower Renewable*, Boca Raton
67. EPA U (2007) Biomass combined heat and power catalog of technologies. Washington D. C., US EPA
68. Wilson B (2014) Comparative assessment of gasification and incineration in integrated waste management systems. *EnviroPower Renewable*, Boca Raton
69. EPA U (2016) Municipal solid waste. U.S. EPA, 29 March. <https://archive.epa.gov/epawaste/nonhaz/municipal/web/html/>. Accessed 2017
70. Bhoi P (2016) Sample identification: MSW. Hazen Research Inc, Golden
71. Patil KN, Huhnke RL, Bellmer DD (2006) Performance of a unique downdraft gasifier. In: ASABE annual international meeting. Portland
72. Bhoi PR, Huhnke RL, Kumar A, Thapa S, Indrawan N (2017) Scale-up of a downdraft gasifier system for commercial scale mobile power generation. *Renew Energy*
73. Pareek D, Joshi A, Narnaware S, Verma VK (2012) Operational experience of agro-residue Briquettes based power generation system of 100 kW capacity. *Int J Renew Energy Res* 2(3):477–485
74. Ryu C, Shin D (2013) Combined heat and power from municipal solid waste: current status and issues in south Korea. *Energies* 6:45–57
75. Agon N (2015) Development and study of different numerical plasma jet models and experimental study of plasma gasification of waste. Ghent University, Gent
76. Messenger B (2016) Air products to ditch plasma gasification waste to energy plants in teesside. In: *Waste management world*, 4 May. <https://waste-management-world.com/a/air-products-to-ditch-plasma-gasification-waste-to-energy-plants-in-teesside>. Accessed 24 June 2017
77. Willis KP, Osada S, Willerton KL (2010) Plasma gasification: lessons learned at Ecovalley WTE facility. In: *Proceedings of the 18th annual North American waste-to-energy conference*. Orlando
78. Taylor MR, Rubin ES, Hounshel DA (2005) Control of SO₂ emissions from power plants: a case of induced technological innovation in the U.S. *Technol Forecast Soc Chang* 72:697–718
79. EPA (2016) Mercury and air toxics standards: cleaner power plant. US EPA, 10 June. <https://www.epa.gov/mats/cleaner-power-plants>. Accessed 16 April 2017
80. Brown TD, Smith DN, O'Dowd WJ, Jr RAH (2000) Control of mercury emissions from coal-fired power plants: a preliminary cost assessment and the next steps for accurately assessing control costs. *Fuel Process Technol* 65–66:311–341
81. Zaman AU (2010) Comparative study of municipal solid waste treatment technologies using life cycle assessment method. *Int J Environ Sci Tech* 7(2):225–234
82. EPA (1999) Nitrogen oxides (NO_x), why and how they are controlled. US EPA, Research Triangle Park
83. Mountouris A, Voutsas E, Tassios D (2006) Solid waste plasma gasification: equilibrium model development and exergy analysis. *Energy Convers Manag* 47:1723–1737
84. Caton JA (2012) The thermodynamic characteristics of high efficiency, internal-combustion engines. *Energy Convers Manag* 58:84–93

85. Pereira MS (2004) Polychlorinated dibenzo-p-dioxins (PCDD), dibenzofurans (PCDF) and polychlorinated biphenyls (PCB): main sources, environmental behaviour and risk to man and biota. *Quim Nova* 27(6):934–943
86. Dyke P, Coleman P, James R (1997) Dioxins in ambient air, bonfire night 1994. *Chemosphere* 34(5–7):1191–1201
87. Kulkarni PS, Crespo JG, Afonso CA (2008) Dioxins sources and current remediation technologies—a review. *Environ Int* 34:139–153
88. Dopico M, Gómez A (2015) Review of the current state and main sources of dioxins around the world. *J Air Waste Manag Assoc* 65(9):1033–1049
89. Addink R, Olie K (1995) Role of oxygen in formation of polychlorinated dibenzo-p-dioxins/dibenzofurans from carbon on fly ash. *Environ Sci Technol* 29:1586–1590
90. Buekens A, Cornelis E, Huang H, Dewettinck T (2001) Fingerprints of dioxin from thermal industrial processes. *Chemosphere* 40:1021–1024
91. UCR (2009) Evaluation of emissions from thermal conversion technologies processing municipal solid waste and biomass. BioEnergy Producers Association, Los Angeles
92. Wielgosiński G (2011) The reduction of dioxin emissions from the processes of heat and power generation. *J Air Waste Manag Assoc* 61:511–526
93. Lundin L, Jansson S (2014) The effects of fuel composition and ammonium sulfate addition on PCDD, PCDF, PCN and PCB concentrations during the combustion of biomass and paper production residuals. *Chemosphere* 94:20–26
94. Lechtanska P, Wielgosinski G (2014) The use of ammonium sulfate as an inhibitor of dioxin synthesis in iron ore sintering process. *Ecol Chem Eng S* 21(1):59–70
95. UNEP (2008) Guidelines on best available techniques and provisional guidance on best environmental practices relevant to Article 5 and Annex C of the Stockholm convention on persistent organic pollutants. United Nations Environment Programme, Geneva
96. Yoshida K, Yamamoto T, Kuroki T, Okubo M (2009) Pilot-scale experiment for simultaneous dioxin and NO_x removal from garbage incinerator emissions using the pulse corona induced plasma chemical process. *Plasma Chem Plasma Process* 29:373–386
97. Kamińska-Pietrzak N, Smoliński A (2013) Selected environmental aspects of gasification and co-gasification of various types of waste. *J Sustain Mining* 12(4):6–13
98. Buekens A, Huang H (1998) Comparative evaluation of techniques for controlling the formation and emission of chlorinated dioxins/furans in municipal waste incineration. *J Hazard Mater* 62:1–33
99. Nifuku M, Horvath M, Bodnar J, Zhang G, Tanaka T, Kiss E, Woynarovich G, Katoh H (1997) A study on the decomposition of volatile organic compounds by pulse corona. *J Electrostat* 40, 41:687–692
100. Obata S, Fujihira H (1998) Dioxin and NO_x control using pilot-scale pulsed corona plasma technology. *Combust Sci Technol* 133:3–11
101. Zhou Y, Yan P, Cheng Z, Nifuku M, Liang X, Guan Z (2003) Application of non-thermal plasmas on toxic removal of dioxin-contained fly ash. *Powder Technol* 135–136:345–353
102. Mitoma Y, Egashira N (2004) Approach to highly efficient dechlorination of PCDDs, PCDFs, and coplanar PCBs using metallic calcium in ethanol under atmospheric pressure at room temperature. *Environ Sci Technol* 38:1216–1220
103. Ratafia-Brown J, Manfredo L, Hoffmann J, Ramezan M (2002) Major environmental aspects of gasification-based power generation technologies. US DOE, NETL, Morgantown
104. Themelis NJ (2006) Thermal treatment review. In: *Waste management world*, July–August, pp 37–45
105. Psomopoulos C, Bourka A, Themelis N (2009) Waste-to-energy: a review of the status and benefits in USA. *Waste Manag* 29:1718–1724
106. Lauber J, Morris ME, Ulloa P, Hasselriis F (2006) Comparative impacts of local waste to energy versus long distance disposal of municipal waste. In: *AWMA conference*. New Orleans

Solar-Assisted Gasification Based Cook Stoves

Ankur Kaundal, Satvasheel Powar and Atul Dhar

Abstract Indoor air quality is one of the prime concerns as it relates directly to the health of occupants. Detrimental pollutants from burning of solid fuels range from CO to NO, NO₂ and suspended particles containing polynuclear aromatic hydrocarbons pose serious threats to human lives. Incorporation of alternative means of heating and near-complete combustion of biomass feedstock would be a better solution to this problem. Gasification based natural draft and forced draft cook stoves are helpful in improving the wood utilization efficiency and reducing the harmful pollutants. The combustion unit of gasification based cook stove is equipped with the provision of primary and secondary air, which facilitates the combustion and makes near-complete utilization of feedstock practical. Thermal draft in the chimney, a control unit of overall process generates pressure difference which facilitates the incoming of primary as well as secondary air and sidewise keeps the flue gases moving. Utilization of solar heating for preheating the feedstock is another step for making the total process efficient. In this chapter, we will discuss the advantages and challenges of different cook stove designs and feasibility of incorporating the solar heating in them.

1 Introduction

According to Global Health Observatory data from WHO [1], around three billion people worldwide rely on biomass namely wood, crop residues, dung cakes, etc., to meet their day-to-day energy demands. Open fires and conventional cook stoves, which quite often are inefficient due to improper design, lead to the emission of harmful pollutants. Females and kids who are engaged to the hearth for longer durations are subjected to their detrimental effects. Smoke coming out of wood combustion consists of many harmful compounds, viz. NO_x, SO_x, CO, volatile organic compounds (VOC), particulate matter (PM), furans, and dioxins [2].

A. Kaundal · S. Powar (✉) · A. Dhar
School of Engineering, IIT Mandi, Mandi 175005, India
e-mail: satvasheel@gmail.com

© Springer Nature Singapore Pte Ltd. 2018
S. De et al. (eds.), *Coal and Biomass Gasification*, Energy, Environment,
and Sustainability, https://doi.org/10.1007/978-981-10-7335-9_16

403

Inhaling these compounds can put anyone on cardiovascular risks like cardiac arrhythmias, heart attacks, and other respiratory diseases [3–5]. Fine PM which gets inhaled quite easily may lead to the destruction of alveolar wall and disturb the lung functioning. All these effects though at snail's pace but due to chronic in nature they disturb the health of homies gradually and unluckily same is manifested years on.

Hence, it becomes essential to design the cook stove efficiently so as to have proper combustion of feedstock and simultaneous control over the emissions. Subsequent sections in this chapter will discuss the various aspects of combustion, the chemistry of wood burning, requisites for the efficient combustion, and various attempts which can improve the performance of domestic cook stoves.

2 History of Cook Stove and Biomass Burning

Biomass is a carbon-based organic material that quite often comes from plants and is supposed to be the oldest source of energy for household applications since our ancestors learned the secret of fire. Once upon a time when plants used to be alive, sun's energy during the process of photosynthesis gets stored in the plants in the form of carbohydrates [6]. When these carbohydrates in the form of starch and cellulose burn, chemical energy stored in them is released as heat. So, it can be stated that burning is the basic form of utilization of biomass energy. Ancient people started it with an open-hearth fire, and as the time progressed, subsequent modifications kept on taking place. Then three-stone cooking method or mud/clay stoves were developed, which went quite popular and are being used extensively even today. The manufacturing process is quite simple, and any of household members can fabricate it without any specific tool. But this combustion technique has some disadvantages, which can be enumerated as follows:

1. Due to the improper intake of air, wood combustion does not take place efficiently. Thus, to gain the same amount of heat output, more quantity of wood needs to be burnt.
2. Smoke escaping out of the combustion remains in the kitchen due to lack of specific ventilation, which gives birth to many respiratory disorders and leads to premature deaths.
3. Because of the improper design, heat of combustion is not utilized properly, and thus energy in fuel is wasted.
4. Because open flames keep on arising, working with such stove is little challenging. One needs to be extra careful to avoid any burns or scalds.

It was around 1970s when people started the intensive scientific research on the efficient working of domestic cook stoves [7, 8]. The phenomenon of flaming combustion related to wood burning began to study. New designs were developed using various input parameters such as required quantity of air for proper combustion, also the concepts of primary combustion and secondary combustion were

introduced. Today, we have several cook stove designs conforming to the norms issued by controlling authority, e.g., indoor air quality standards by WHO or acceptable limits set by any particular country's administration. The thermal efficiency of these cook stoves ranges from 26 to 34% with the natural draft and 36 to 41% with forced draft [9]. Furthermore, the complete combustion in these cook stoves has brought the emissions of CO, CO₂, and other pollutants under control. Emission of total particulate matter is also under acceptable limits. In short, these cook stoves have been proven to be better than their predecessors in multiple ways.

3 Chemistry of Wood Combustion

Ultimate analysis of wood shows the weight fraction of different elements present in it. The weight fraction of carbon in softwood ranges from 50 to 53% and same in hardwood ranges from 47 to 50% [10]. This variation is due to varying lignin and other extractable contents in wood. The percentage of hydrogen in almost every kind of timber is close to 6%. The weight percentage of oxygen ranges from 40 to 44%, and that of nitrogen from 0.1 to 0.2% [10] and sulfur content is as less as 0.1%.

The proximate analysis gives the content of water, tar, char, ash, etc., present in the wood. Combustible part of the wood is mainly made up of cellulose and lignin. Cellulose mainly breaks down to release volatile gases, whereas lignin breaks down to tar and char [11]. Cellulose and lignin are the organic compounds of carbon, hydrogen, and oxygen. The wood combustion is an indirect burning process, i.e., the flaming combustion is the result of reactions between oxygen and gases released from material and not the material itself. On the application of heat, wooden material releases gaseous components which show a high affinity toward oxygen to react and produce flames.

In the thermal decomposition of wood, pyrolysis of cellulose and hemicellulose both takes place quickly. Decomposition of lignin is comparatively more challenging as it needs higher temperature than former. In terms of energy requirement during pyrolysis, hemicellulose and lignin decomposition are endothermic in nature, whereas decomposition of cellulose is exothermic. The combustion process is the succession of pyrolysis, which is the thermal decomposition of cellulose. The entire structure of dry wood comprises of 45–50% cellulose. Shafizadeh [12] has shown the temperature dependency of cellulose pyrolysis, according to which pyrolysis in the temperature range less than 300 °C, release of gases in the form of CO₂, CO, and water vapors along with the formation of char take place. Whereas same in the temperature range above 300 °C, molecules are rapidly depolymerized to tarry pyrolyzate. Chemical structure of cellulose is shown in Fig. 1.

On the application of heat, cellulose starts breaking down. Product gases either retain in the material or come out. The entire combustion process is depicted in following three schematics. Figure 2a shows the wooden surface being exposed to the external heating. Figure 2b shows the decomposition of structure, where

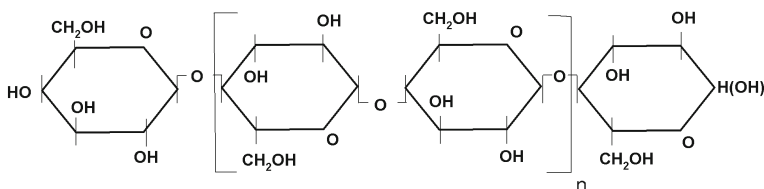


Fig. 1 Chemical structure of cellulose [13]

volatile components in the form of gases are released by the application of heat. Figure 2c shows the combustion process where these gases react with oxygen and generate more heat. The temperature due to this exothermic reaction is quite high so as to make it a luminous and flaming combustion. More heat on the surface accelerates the volatilization and continues the reaction. These processes can also be related in terms of temperature ranges in which they occur [15–17] as follow:

1. All loosely held moisture content evaporates in the temperature range of 100–170 °C.
2. Gases, viz. carbon monoxide, carbon dioxide, and condensable vapors spring up in the temperature range of 170–270 °C.
3. Reaction with oxygen and hence exothermic reaction starts at 270–280 °C, which can be manifested by a subsequent rise in temperature as heat generation keep on taking place.
4. Even without an external source of heat, this rise in temperature can be seen up to 400–450 °C. The maximum temperature of 600 °C can be witnessed by supplying external heat.

3.1 Phenomenon of Combustion in Cook Stoves

Any wooden biomass stores chemical energy, which is released as the result of the combustion process. Combustion is essentially a chemical reaction between pyrolyzed gaseous products and oxygen. The output of this reaction is manifested in the form of heat and high-temperature luminous flame. A pot can be brought to the direct contact of flame, and heat energy can be utilized. Combustion in domestic cook stoves is usually premixed and diffusion type in nature. In premixed combustion, feedstock and air are mixed before their entry into burning chamber or before the ignition in burning chamber. This air is known as the “primary air,” and along with the application of external heat, it is responsible for the release of pyrolysis gases. In short, this is known as primary combustion.

Rest of the air supplied during the process is “secondary air.” Oxygen present in the secondary air reacts with pyrolysis gases and results in “diffusion flame” [16]. Pyrolysis gases tend to rise from the wood surface that is why this flaming combustion is visible at a certain height from the wooden feedstock. We have yet another flame called “premixed flame,” which is present in primary combustion, but

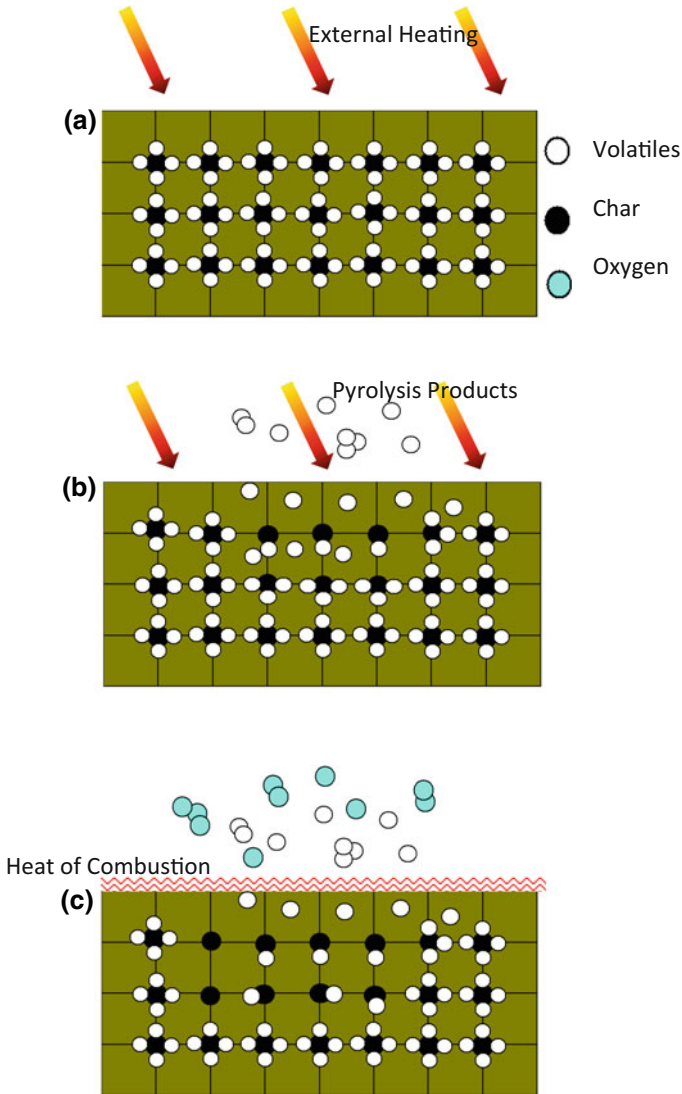


Fig. 2 a Surface exposed to external heating [14], b Pyrolysis products escaping out of surface [14], c Combustion: reaction between pyrolysis gases and oxygen [14]

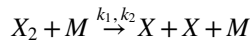
“diffusion flame” is remarkably dominant on the former one. It is the diffusion flame, which one sees during the combustion. Hence, the proper intake of primary and secondary air is remarkably important in efficient working of the cook stove. The quantity of air and the location where to feed it from are some parameters those need to be worked upon to make combustion an efficient one.

3.2 Chain Reactions

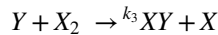
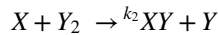
A chain reaction is a form of chemical reactions where the product of one reaction triggers other reactions to take place. Combustion of gaseous components is a chain reaction. Any chain reaction is characterized by three steps [17, 18]:

1. Initiation phase: In this phase, various chain carriers are formed as a result of the thermal decomposition in the presence of primary air. These may be atoms like H, O or free radicals like OH, CHO, and CH.

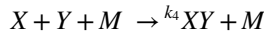
For a chemical reaction $X_2 + Y_2 \rightarrow 2XY$, chain initiation reaction is given by



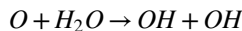
2. Propagation phase: These chain carriers react with molecules present on the reactant side and generate new chain carriers. The newly generated chain carriers follow the predecessors and continue the same. This promotes the reaction and propagation takes place. Chain propagation reaction with X and Y as free radicals is as follows:



3. Termination: Termination takes place by breaking the chain which happens either by eliminating the chain carrier from the reaction or by adsorption on another surface like container walls. Chain termination reaction is given as:



It is also possible that during the propagation stage more than one chain carriers are formed resulting in multiple further reactions at one time, known as chain branching, responsible for rapid combustion. Chain branching is characterized by the formation of two radicals from a reaction that consumes only one radical that will last till there is no trace of any reactant. Example of a chain-branching reaction is



4 Performance Analyses of Cook Stoves

There are certain parameters which can be used to assess the performance of a cook stove. At present there are some manufacturers having a good market, but whether their designs meet the standards or not hold substantial importance. Following are

the parameters along with descriptions, which one can rely on for the scientific performance specification of cook stoves.

4.1 Thermal Efficiency

Thermal efficiency in simple words is the ratio of output and input regarding heat gained and energy supplied, respectively. Energy supplied is in the form of the calorific value of wood. When wooden feedstock is subjected to combustion, chemical energy stored in it is released as heat. Utilization of this heat in some application is output. Attempts to minimize the heat loss to surroundings will be reflected by a consequent rise in thermal efficiency.

Thermal efficiency test starts with the identification of a number of outputs. For instance, a single pot stove will have one output. There might be some extra attachments like water heating coil inside the stove or any other thermic fluid heating coil. Any such modification will add to the number of outputs. One needs to be careful to consider all these while calculating the heat gain. Sometimes people sprinkle an easily combustible fluid on wooden feedstock, e.g., kerosene oil either to get an easy start or to accelerate the combustion. Energy content in terms of the calorific value of such oil must be added to the input energy supplied. Different wood samples have varying moisture content, which gives incorrect results if tested without monitoring. Moisture meter or any similar device can be used to continuously monitor the moisture percentage in wood. Samples under consideration shall be dried to attain same moisture content. This value is generally kept around 5% [19].

Assume the following notations for heating of water in a single pot.

m	= mass of water in pot (kg)
M	= mass of vessel with lid in (kg).
M_{fuel}	= mass of wooden feedstock consumed (kg)
CV_{fuel}	= calorific value of wood (kJ/kg)
M_k	= mass of kerosene oil used (kg)
CV_k	= calorific value of kerosene oil (kJ/kg)
T_1	= initial temperature of water ($^{\circ}\text{C}$)
T_2	= final temperature of water ($^{\circ}\text{C}$)
T_3	= final temperature of water in last pot at the end of combustion ($^{\circ}\text{C}$)
n	= total number of pots used
C_w	= specific heat of water (=4.186 kJ/kg/ $^{\circ}\text{C}$)
C_v	= specific heat of pot material

The thermal efficiency can be calculated from following formula:

$$\eta = \frac{[(n-1) \times (M \times C_v + m \times C_w) \times (T_2 - T_1)] + [M \times C_v + m \times C_w] \times (T_3 - T_1)}{(M_{fuel} \times CV_{fuel}) + (M_k \times CV_k)} \times 100$$

The first term in the numerator corresponds to first $(n - 1)$ pots, which are heated from temperature T_1 to T_2 , whereas the second term corresponds to n th pot, which is heated from T_1 to T_3 . The first term in denominator relates to energy content in wooden feedstock and the second one to that in kerosene oil.

Finally, power output rating which is the total energy gained per unit time is calculated as:

$$P = \frac{\dot{M} \times CV_{fuel} \times \eta}{3600 \times 100} \text{ (kW)}$$

where \dot{M} is consumption rate of wooden feedstock in (kg/h).

4.2 Tests for CO and CO₂ Emissions

Control over emissions in cook stove is highly important and can be yet another parameter to characterize a cook stove. Following methods can be employed for continuous measurement of CO and CO₂ emissions.

4.2.1 Multicomponent Gas Analyzer

Multicomponent gas analyzer is an infrared-based technique used to measure the concentration of various gases in a sample. The infrared beam emitted by a source is made to pass through the sample as a consequence of which signals are generated which relates to the optical energy coming out of the source and being transmitted through the sample. These signals are characterized by the optical wavelength and band pass [20]. These signals are manipulated and combined mathematically to determine the concentration of different species in the gas sample. This system measures the concentration of species in which absorption spectra is being overlapped.

4.2.2 Nondispersive Infrared

Nondispersive infrared or NDIR is one of the standard methods of measuring the carbon oxides, viz. CO and CO₂. All gas molecules have a tendency to rotate and vibrate at a certain particular frequency. These frequencies make unsymmetrical molecules to absorb light at specific wavelengths. When infrared light is thrown at a gas sample, each constituent will absorb some fraction of it. The constituent particles absorb the infrared whose wavelength is almost comparable to the size of a constituent. Employing an NDIR detector, rest of the wavelength can be measured. The difference between the amounts of projected infrared and that of non-absorbed

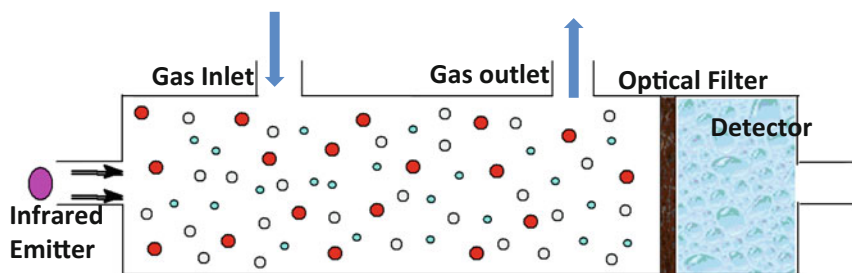


Fig. 3 Schematic of nondispersive infrared method

is proportional to the concentrations of constituents. In short the amount of absorbed infrared relates directly to the concentration of constituents [21]. Figure 3 shows the schematic diagram of NDIR [22] method.

4.3 Total Particulate Matter

Particulate matter is the constituent of air that is made up of quite small particles of harmful acids, chemicals, metal dust, soil, and other carcinogenic substances. Particulate matter is the propagator of cardiovascular, cerebrovascular diseases [23], and other respiratory disorders. So, the continuous monitoring of total particulate matter (TPM) holds substantial importance. The gravimetric method employed for the measurement of TPM consists of the cyclone with a 2.5μ particle size cutoff and one Pitot tube. This Pitot tube is used for the measurement of exhaust gas velocity which in turn helps to calculate the rate at which sample gas flows through the probe. Another important part of the system is filter paper usually polytetrafluoroethylene (PTFE) filter which is employed amid the way of flowing sample gas. The suspended PM gets deposit on the filter. The weight of filter before and after the flow is computed, and the difference between them gives the weight of PM present in flown quantity of sample gas [24]. Thereafter, total concentration of PM in the sample can be calculated as a weight change of filter paper divided by the volume of air flown by and is usually expressed in $\mu\text{g}/\text{m}^3$.

5 Current Status of Cook Stoves

Table 1 shows the concerning values of different cook stove models. The thermal efficiency of cook stoves labeled from A to K ranges from 26 to 38%, whereas same for L to Q ranges from 36 to 41%. The former type corresponds to natural draft cook stoves whereas later corresponds to the forced draft type cook stove. In forced draft type cook stoves, provision for external air supply is made either through a

blower or a fan. This simply shows that externally supplied air paves the way for improved combustion in the cook stove, and hence the thermal efficiency of later type is relatively higher than the former ones.

On the other hand, CO concentration in natural draft cook stoves is relatively higher than forced draft cook stoves. Least value for natural draft corresponds to cook stove labeled as D and is 0.1141 g/min whereas same goes as high as 2.95 g/min for cook stove K. If we look at the figures for forced draft, the range of CO concentration is 0.1015–0.497 g/min, which falls enough short than that for natural draft cook stoves.

Similarly, from available data, total particulate matter concentration in forced draft cook stoves falls below 23.214 mg/min mark whereas same for natural draft cook stoves ranges from 10.14 to 169.8 mg/min. The point to be noted here is that the traditional cook stoves without any dedicated draft lack the incoming of sufficient air, which is manifested through the poor emission control. The lower value of CO and TPM concentration in the cook stoves labeled from L to Q shows better combustion characteristics due to near-stoichiometric availability of oxygen. Hence, the thermal efficiency value for these cook stoves is relatively high.

6 Solar-Assisted Cook Stove

As discussed in Sect. 3, combustion is a two-stage phenomenon; the primary combustion comprises of the release of the gases on the application of heat and the secondary combustion, which is essentially the flaming combustion of already released gases. Preheating of the cook stove or preheating of the wooden feedstock through solar concentrators to release the volatile components is the proposed concept of “Solar-Assisted Gasification Based Cook Stove.”

Solar radiation possesses the densely packed huge potential of energy, the amount of which provided to the earth in just one hour is equivalent to what is consumed on earth in one entire year [28]. Solar concentrators are the devices which collect incoming solar radiations and direct it to a common focus either a point or a line. Solar irradiance at its origin, i.e., sun is around 63 MW/m² [29]. The average value of the solar radiation flux that reaches earth’s surface ranges between 200 and 1000 W/m². The concentrated radiation flux at the focus is multiple times of what was incident on the reflector. This multiplying factor is concentration ratio and is given in Table 2 for various collectors. Following table depicts the various types of solar collectors, corresponding concentration ratio, and temperature range that can be achieved.

Parabolic trough, cylindrical trough, and parabolic dish reflector have relatively high output temperature range. These collectors are not much complex and bulky and can be installed along with cook stoves, whereas Heliostat field collector, though features high concentration ratio and temperature range but requires too large space to install and lots of investment. This type is particularly suitable for commercial applications only.

Table 1 Current status of various available cook stoves

Label	Name of Cook Stove/ Manufacturer	Draft Type	Image	Thermal Efficiency (%)	CO (g/min)	TPM (mg/min)	Power Output (kW)	Ref.
A	Bio-Classic (Fuelwood) Front Feeding	Natural		26.01	0.406	28.19	1.49	[25]
B	Vikram Bio Super Chullah, Top Feeding	Natural		31.95	0.750	55.15	2.77	[25]
C	Adarsh Domestic	Natural		28.1	0.393	17.95	1.41	[25]
D	Chulika (Fuel-Wood)	Natural		29.77	0.114	10.14	0.74	[25]
E	Digvijay Chullah- Top Feeding	Natural		33.44	0.376	40.15	2.46	[25]
F	DB-II	Natural		33.57	0.372	24.79	2.20	[25]
G	EcoRecho Stove Gadgil Lab	Natural		32	0.730	–	–	[26]
H	Mirak Stove Gadgil Lab	Natural		28	0.760	–	–	[26]
I	Traditional Haitian Stove Gadgil Lab	Natural		24	1.080	–	–	[26]

(continued)

Table 1 (continued)

Label	Name of Cook Stove/ Manufacturer	Draft Type	Image	Thermal Efficiency (%)	CO (g/ min)	TPM (mg/ min)	Power Output (kW)	Ref.
J	Prakti Rouj stove Gadgil Lab	Natural		38	0.600	–	–	[26]
K	Wood Burning stove, Ordinary, Ghana	Natural		38	2.950	169.80	–	[27]
L	Oorja K3 Dlx	Forced		37.26	0.101	11.62	1.51	[25]
M	TERI SPF 0414S (Front Feed)	Forced		40.78	0.172	9.59	2.24	[25]
N	XXL Eco Chullah Stoves	Forced		36.52	0.135	6.69	1.98	[25]
O	Eco Chulha 2.5	Forced		39.28	0.497	23.21	3.37	[25]
P	Surya FDD	Forced		40.9	0.270	19.99	2.50	[25]
Q	TERI SPT 0314 Stove	Forced		40.81	0.183	12.32	1.46	[25]

Table 2 Concentration ratio and temperature range of various solar collectors [30]

Motion	Collector type	Absorber type	Concentration ratio	Temperature range (°C)
Stationary	Flat plate collector	Flat	1	30–80
	Evacuated type collector	Flat	1	50–200
	Compound parabolic	Tubular	1–5	60–240
Single-axis tracking	Linear Fresnel reflector	Tubular	10–40	60–250
	Parabolic trough collector	Tubular	15–45	60–300
	Cylindrical trough collector	Tubular	10–50	60–300
Two-axis tracking	Parabolic dish reflector	Point	100–1000	100–500
	Heliostat field collector	Point	100–1500	150–2000

Parabolic trough collector (PTC) is the compact structures with relatively less expensive technology and can be used to generate process heat up to 300 °C or sometimes little more than that. PTCs are fabricated by bending highly reflective metal sheet into a parabolic profile. The profile is the only important parameter in case of PTCs and needs to be taken care of. It must be designed so as to capture most of the incoming solar radiations and focus on the receiver tube, which is usually a metal black tube surrounded by a glass tube to avoid any heat loss to the ambient. PTCs can be extended to any length as per the suitability for a particular application. PTCs can be employed with single-axis tracking. If the collector is oriented in an east-west direction, it will track the sun from north to south [30]. It is also possible to do it just the other way round. Since PTC captures the radiations coming from the mouth of parabolic aperture, it can only use direct or beam radiations called as direct normal irradiance [29]. Diffuse radiations, which are deviated or scattered by clouds, dust particles, and other constituents are not of any utility to PTCs. Figure 4 shows installed parabolic trough collector.

Similarly, parabolic dish collector (PDC) has dish-type structure with point focus. Because of the very small area of the receiver, concentration ratio is quite large ranging from 100 to 1000. Temperature around 500 °C can be easily obtained in PDC. They need to be oriented so as to track along two axes for maximum efficiency. Thermal energy gained by the circulating fluid is further carried on for a particular application. Figure 5 shows installed parabolic dish-type collector.

Similarly, we have yet another category called Scheffler concentrator (SC), which is particularly suitable for cook stoves. This is quite similar to PDC, but the point focus is far away from the concentrator structure. That means while SC is located outside in sunlight, cooking pot can be placed inside the kitchen. This

concentrator is essentially a small lateral section of a big paraboloid. Temperature around 400 °C can be easily attained here. Hence, all kind of cooking, frying, etc., are possible (Fig. 6).

Fig. 4 Installed parabolic trough collector. *Image Courtesy: German Flabeg FE GmbH, Flabeg Research and Development Division*



Fig. 5 Installed parabolic dish collector *Image Courtesy: Solartron energy systems*



Fig. 6 Installed Scheffler concentrator [47]



6.1 Conceptual Designs for Incorporation of Solar Heat with Cook Stove

Following are some of the methods, which derive their concept from existing technologies and can be employed to use concentrated solar heat along with a cook stove:

6.1.1 Cook Stove Surrounded by a Jacket of Molten Salt

Use of molten salt as heat transfer fluid in solar collectors has been proposed by several researchers [31]. Commonly used synthetic oils can be used below 400 °C in various applications. According to Yang et al. [32, 33], molten salts can be used in the temperature range of 450–500 °C. A molten salt mixture of NaNO₃ and KNO₃ with 60:40 wt% has a melting point of 238 °C and can be used in solar collectors up to 565 °C [34]. Similar constituents with 50:50 wt% have a melting point of 220 °C and can be used in applications up to 550 °C [33]. The melting point is a little constraint because after sunset or during night time system will get choked after solidification of the mixture. Thermal storage system needs to be strong enough to cope with these requirements. Another alternative is to go with ternary mixtures of NaNO₃ and KNO₃ with other alkali and alkaline earth nitrates. For instance, a mixture of LiNO₃, NaNO₃, and KNO₃ in the ratio 30:18:53 of weight percentage melts at 120 °C [34]. Some binary mixture like 68% KNO₃ and 32% LiNO₃ has a melting point of 133 °C [35]. This temperature range is relatively easy to be managed with thermal storage system.

Herrmann et al. [36] discussed the storage system with nitrate salt inventory, nitrate salt storage, and oil-to-salt heat exchanger as the primary components. Heat energy can be interchangeably exchanged as per application requirement with high-pressure hot fluid on tube side and salt mixture on shell side [36] in shell and tube heat exchanger. Yang et al. [37] studied the design of molten salt receiver to enhance heat transfer and found that heat transfer Nusselt number of spiral tube is almost three times than that of a smooth tube. Grena et al. [38] studied linear Fresnel collector using molten nitrate salt and found 550 °C as the output temperature.

Furthermore, molten salt mixtures are quite cheap and environment-friendly [39]. Therefore, they can be used along with cook stoves. Figure 7 shows one similar concept in which parabolic trough heats up the molten salt mixture and same is circulated in a jacket surrounding the cook stove body. The heat of molten salt either preheats the combustion unit or preheats the wooden feedstock, so as to facilitate the release of volatile gases.

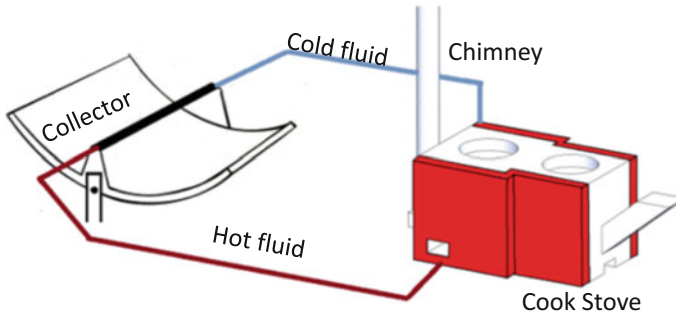


Fig. 7 Cook stove surrounded by a jacket of molten salt

6.1.2 Direct Heating Through an Optical Window

In direct method of heating, concentrated solar radiations are made to pass through a cavity onto the combustion chamber. This method does not require any intervening medium to exchange heat. Hence, efficiency and output temperature ranges are relatively higher in this method. According to Meng et al. [40] using curved quartz window and cup-shaped porous absorber, the peak temperature of 794 °C can be obtained under optimized conditions. Sarker et al. [41] investigated the use of recirculating metallic particles to enhance heat transfer and found that 10% metallic particle concentration in air can raise the temperature of air to 557 °C at an optimized flow rate. This temperature otherwise would be around 200 °C less in non-recirculating case. Kribus et al. [42] studied the geometric design of cavity and suggested truncated-cone-shaped cavity to achieve high transmission rates. Janajreh et al. [43] used the concept of a black body to absorb most of the radiations. Combustion chamber can be enclosed by an external enclosure having a hole or cavity. Solar radiations once entered through this cavity will remain entrapped because of multiple internal reflections and heat up the combustion chamber almost uniformly.

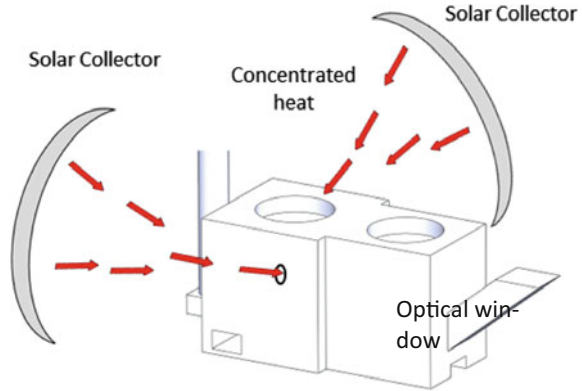
Steinfeld et al. [44] studied the optimum aperture size and optimum temperature. Following equation [44] can be used to deduce a relation between aperture radius and temperature attained.

$$T_{\max} = \left(\frac{\alpha IC}{\varepsilon \sigma} \right)^{0.25}$$

Here C is the mean flux concentration ratio within aperture radius r and is given by

$$C = \frac{P_{\text{aperture}}}{\pi r^2 I}$$

Fig. 8 Concentrated solar radiations through an optical window



$P_{aperture}$ is the amount of solar radiations intercepted by the aperture. α and ε are absorptivity and emissivity, respectively, and I is the direct normal irradiance.

Figure 8 shows the direct use of concentrated radiations with cook stove through an optical window. Radiations once made to pass through an optical window on the outer enclosure remain entrapped, and because of the minimum reradiation losses combustion chamber is heated up.

There are some other methods of carrying direct heating like the use of high heat capacity refractory honeycomb [45] on the outer enclosure. Concentrated radiations are focused on its surface, and resulting heat is slowly and uniformly diffused through it. Combustion chamber gets heat almost uniformly and paves the way for combustion process inside it. Scheffler concentrator is particularly suitable for this type of solar heating. Because the focus of concentrator is far away from the structure, so cook stove can be placed inside the kitchen, or any other suitable place and Scheffler concentrator is placed outside in the sun.

However, the addition of extra attachments with these cook stoves will impact the economics and people in rural and remote areas are not affluent enough to procure such stoves directly. But the improved features in these cook stoves can motivate them to adopt them. Rural people are often seen to believe the idea of contraction for maximizing the efficiency of their equipment. They need to be made aware of the improved features in solar-assisted cook stoves like increased efficiency, lesser amount of feedstock required. Furthermore, reduction in emission of harmful gases by making provision for proper natural or forced draft will also pave the way, which otherwise lead to chronic respiratory disorders. In short, it is going to be one time investment and leads to sustainable utility.

7 Summary and Outlook

According to World Energy Council report [46] out of total energy consumption in 2015 through various resources, the contribution of solar was just 0.45%. This indicates gross underutilization of available solar resources to us. Solar-assisted cook stove is an attempt to utilize solar heat in the day-to-day applications. As discussed earlier that wood combustion is an indirect one, i.e., it is not of wood and oxygen but between pyrolysis gases released from wood and oxygen. The release of these pyrolysis gases, i.e., primary combustion requires external heating. The subsequent portion of the feedstock is subjected to release these gases by the heat of already combusted feedstock. If concentrated solar heat is capable of performing this primary combustion either completely or partially, ample amount of feedstock can be saved. For the same amount of heat output from cook stove, the quantity of feedstock used would be less in the case of solar assistance. Removing the moisture present in wood through preheating by concentrated solar heat is yet another way to improve combustion characteristics. So it can be concluded that using concentrated solar heat in either way will improve the economics of domestic cook stove substantially.

References

1. Global Health Observatory (GHO) data, World Health Organization. Indoor Air Pollution. http://www.who.int/gho/phe/indoor_air_pollution/en/
2. Boman BC, Forsberg AB, Jarvholm BG (2003) Adverse health effects of ambient air pollution in relation to residential wood combustion in modern society. *Scand J Work Environ Health* 29(4):251–260
3. Bølling AK, Pagels J, Yttri KE, Barregard L, Sallsten G, Schwarze PE, Boman C (2009) Health effects of residential wood smoke particles: the importance of combustion conditions and physicochemical particle properties. *Part Fibre Toxicol* 6:29
4. Bart O, Broadwin R, Green S, Feng W-Y, Lipsett M (2006) Fine particulate air pollution and mortality in nine California counties: results from CALFINE. *Environ Health Perspect* 114(1):29–33. Web
5. Brook RD, Franklin B, Cascio W, Hong Y, Howard G, Lipsett M, Luepker R, Mittleman M, Samet J, Sidney C, Ira T (2004) Air pollution, and cardiovascular disease: a statement for healthcare professionals from the expert panel on population and prevention science of the American Heart Association. *Circulation* 109:2655–2671
6. Barker MA, Carr MD (1989) Photosynthesis—can our pupils see the wood for the trees? *J Biol Educ* 23:41–44
7. Grice JL (1971) Cook stove. United States Patent, Appl. No. 804,787, Primary examiner: Walter A. Scheel, Assistant examiner: Arthur O. Henderson, Patented 9 Mar 1971
8. Frelidenricli RG (1969) St, E. & Yorlt, N. 254 2/1968
9. Bureau of Indian Standard (2013) Portable bio-mass cook stove. ICS 97.040.20, IS 13152 (Part 1)
10. Ragland KW, Aerts DJ (1991) Properties of wood for combustion analysis. *Biores Technol* 37:161–168
11. Rowell RM Handbook of wood chemistry and wood composites, 2e, Chapter 6

12. Shafizadeh F (1982) Introduction to pyrolysis of biomass. *J Anal Appl Pyrol* 3:283–305
13. Anderson AB The composition and structure of wood. University of California, Forest Products Laboratory
14. Burning of Wood. <http://virtual.vtt.fi/virtual/innofirewood/stateofheart/database/burning/burning.html>
15. Mohan D, Pittman CU, Steele PH (2006) Pyrolysis of wood/biomass for bio-oil: a critical review. *Energy Fuels* 20:848–889
16. Basu P Biomass gasification and pyrolysis. In: Practical design and theory, Chapter 3
17. Zactruba J, Stonecypher L (2014) How much air is required to burn coal. In: Bright hub engineering, Dec 2014. <http://www.brighthubengineering.com/power-plants/20189-burning-coal-how-much-air-is-required/>
18. Burning wood for heating—the physics, physics of burning wood as a heating fuel. <http://mb-soft.com/public3/woodburn.html>
19. Portable solid bio-mass cookstove (Chulha). Bureau of Indian Standards. Doc:MED 04(1157) C, ICS 97.040.20, Feb 2013
20. Conlon B, Dittmar J (1990) US Patents, US4914719 A, Multiple component gas analyzer, April 1990
21. Non dispersive infrared (ND-IR) Spectroscopy. Specialty gases and specialty equipment. http://hiq.linde-gas.com/en/analytical_methods/infrared_spectroscopy/non_dispersive_infrared.html
22. Mendes LB, Edouard N, van Dooren HJ, Mosquera J (2015) NDIR gas sensor for spatial monitoring of carbon dioxide concentrations in naturally ventilated livestock buildings. *Sensors (Switzerland)* 15:11239–11257
23. Anderson JO (2012) Clearing the air: a review of the effects of particulate matter air pollution on human health. *J Med Toxicol* 8(2):166–175
24. Central Pollution Control Board, Kamyotra JS, Saha D (2011) Guidelines for the measurement of ambient air pollutants, vol 1, May 2011
25. Approved models of portable improved biomass cookstoves. <http://mnre.gov.in/file-manager/UserFiles/approved-models-of-portable-improved-biomass-cookstove-manufactures.pdf>
26. Lask K, Booker K, Han T, Granderson J, Yang N, Ceballos C, Gadgil A (2015) Performance comparison of charcoal cookstoves for Haiti: laboratory testing with water boiling and controlled cooking tests. *Energy Sustain Dev* 26:79–86
27. Obeng GY, Mensah E, Ashiagbor G, Boahen O, Sweeney DJ (2017) Watching the smoke rise up : thermal efficiency, pollutant emissions and global warming impact of three biomass cookstoves in Ghana, pp 1–14
28. Barlev D, Vidub R, Stroeve P (2011) Innovation in concentrated solar power. *Sol Energy Mater Sol Cells* 95(10):2703–2725
29. Fernáandez-García A, Zarza E, Valenzuela L, Perez M (2010) Parabolic-trough solar collectors and their applications. *Renew Sustain Energy Rev* 14:1695–1721
30. Kalogirou SA (2004) Progress in energy and combustion science 30:231–295
31. Kaundal A, Dhar A, Powar S (2017) Sustainable solid waste management through solar assisted gasification, paper no. 165. In: International conference on sustainable energy and environment challenges (SEEC-2017), Feb 2017
32. Yang Z, Garimella SV (2010) Thermal analysis of solar thermal energy storage in a molten-salt thermocline. *Sol Energy* 84(6):974–985
33. Hiroshi H, Yoshizawa Y, Suzuki A, Tamaura Y (2006) Study on design of molten salt solar receivers for beam-down solar concentrator. *Sol Energy* 80(10):1255–1262
34. Bradshaw RW, Meeker DE (1990) High-temperature stability of ternary nitrate molten salts for solar thermal energy systems. *Solar Energy Mater* 21(1):51–60
35. Zhao CY, Wu ZG (2011) Thermal property characterization of a low melting-temperature ternary nitrate salt mixture for thermal energy storage systems. *Sol Energy Mater Sol Cells* 95(12):3341–3346
36. Herrmann U, Kelly B, Price H (2004) Two-tank molten salt storage for parabolic trough solar power plants. *Energy* 29(5–6):883–893

37. Yang M, Yang X, Yang X, Ding J (2010) Heat transfer enhancement and performance of the molten salt receiver of a solar power tower. *Appl Energy* 87(9):2808–2811
38. Grena R, Tarquini P (2011) Solar linear fresnel collector using molten nitrates as heat transfer fluid. *Energy* 36(2):1048–1056
39. Kearney D, Herrmann U, Nava P, Kelly B, Mahoney R, Pacheco J, Cable R, Potrovitza N, Blake D, Price H (2003) Assessment of a molten salt heat transfer fluid in a parabolic trough solar field. *J Solar Energy Eng* 125(2)
40. Meng XL, Xia X-L, Sun C, Li X-L (2016) Optical transmission characteristics of concentrated solar rays in the vsr using cup-shaped porous absorber. *Proc Eng* 157:301–308
41. Sarker MRI, Saha M, Beg RA (2016) A concentrated solar cavity absorber with direct heat transfer through recirculating metallic particles, p 50040
42. Kribus A (1994) Optical performance of conical windows for concentrated solar radiation. *J Sol Energy Eng* 116(1):47
43. Janajreh I, Raza SS, Qudaih R, Talab I (2010) Solar Assisted Gasification: Systematic Analysis and Numerical Simulation. *Int J Thermal Environ Eng* 1(2):81–90
44. Steinfeld A, Schubnell M (1993) Optimum aperture size and operating temperature of a solar cavity-receiver. *Sol Energy* 50(1):19–25
45. Frosch RA (1981) Solar heated fluidized bed gasification system. United States Patent, Sept 22, 4290779
46. World Energy Council (2016) World energy resources 2016. <https://www.worldenergy.org/wp-content/uploads/2016/10/World-Energy-Resources-Full-report-2016.10.03.pdf>
47. Image Courtesy. Engineers Without Borders, Energy course at Imperial College London <http://www.sunspot.org.uk/ewb/>

Part IV
Advanced Technologies of Gasification

Dual Fluidized Bed Gasification of Solid Fuels

Sminu Bhaskaran, Saurabh Gupta and Santanu De

Abstract In dual fluidized bed gasification technology, the gasification/pyrolysis and combustion reactions are decoupled and conducted in two separate fluidized bed reactors connected by circulating inert or catalytic bed material. Hence, a nitrogen-free high-quality syngas is produced. The configuration obviates the need of a capital-intensive air separation unit. It is a complex reactor system, and the challenge lies in selecting appropriate bed material/catalyst, understanding flow patterns and heat transfer characteristics, and designing and operating such a system. This chapter reviews the basic concept, critical components, hydrodynamics, and process characteristics of this technology presenting the current state of the art.

Nomenclature

AER	Adsorption Enhanced Reforming
BFB	Bubbling Fluidized Bed
CFB	Circulating Fluidized Bed
CFM	Cold Flow Model
CV	Calorific Value
db	Dry basis
DFB	Dual Fluidized Bed
DFBG	Dual Fluidized Bed Gasifier
ECN	Energy Research Center of the Netherlands

S. Bhaskaran · S. Gupta · S. De (✉)
Indian Institute of Technology Kanpur, Kanpur 208016, UP, India
e-mail: sde@iitk.ac.in

S. Bhaskaran
e-mail: sminub@iitk.ac.in

S. Gupta
e-mail: saugupta@iitk.ac.in

FT	Fischer Tropsch
HDS	Hydrodesulfurization
PAH	Polycyclic Aromatic Hydrocarbons
SNG	Synthetic Natural gas
VTU	Vienna University of Technology (TU Wien)

1 Introduction

Gasification is a process of converting solid fuels (coal, biomass, or other carbonaceous feedstock) into a combustible gas (called synthetic gas or syngas) through a sequence of thermochemical reactions. Gasification has many industrial applications, e.g., power generation, production of liquid fuels and other useful chemicals.

The gasification involves several phenomena such as, the endothermic processes like drying, devolatilization and char gasification, the exothermic combustion of char and volatile hydrocarbons, and the transport of heat, mass, and momentum. If the endothermic and exothermic processes are conducted in a single fluidized bed, by injecting air and/or steam as gasification agents, the heat transfer between the sink (gasification) and the source (combustion) is direct. But, in such systems, the syngas produced is diluted with inert nitrogen present in air, and the resulting gas has lower calorific value. Nitrogen dilution may be avoided either by using pure oxygen as the gasification agent in place of air, or by physically separating the gasifier and the combustor using a dual fluidized bed system. The former option requires installation of air separation unit to produce high concentration of oxygen. In the latter option, the endothermic and exothermic processes are decoupled into two fluidized beds which are interconnected by circulating inert bed materials as a carrier of heat. The concept of DFBG process is depicted in Fig. 1. Between the above two approaches, the advantage of DFB gasifier is the production of high calorific value syngas without the need of capital-intensive air separation unit.

The research work on DFB gasifier can be categorized into cold flow studies and hot flow studies. The cold flow studies are used to investigate the hydrodynamic characteristics, whereas the hot flow studies are used to investigate the reactions and reactor performance of DFB gasifiers. In Sects. 2 and 3, the components of DFBG and the bed hydrodynamics are presented, respectively. Steam is usually used as the gasification agent in the DFB gasifier, which produces syngas without nitrogen dilution. The feedstocks for DFBG can be either coal, biomass, or even waste materials like plastics. The technical feasibility of different feedstocks is examined in Sect. 4.4. The bed material used in DFB system has mainly two functions: (1) to act as a heat carrier from the combustor to the gasifier and (2) to act as a carrier of unconverted char, which is dispersed in the bed material, from gasifier to combustor [7]. The commonly used inert bed material is silica sand due to its relatively better thermal properties and attrition resistance [35]. The details of different bed materials used in

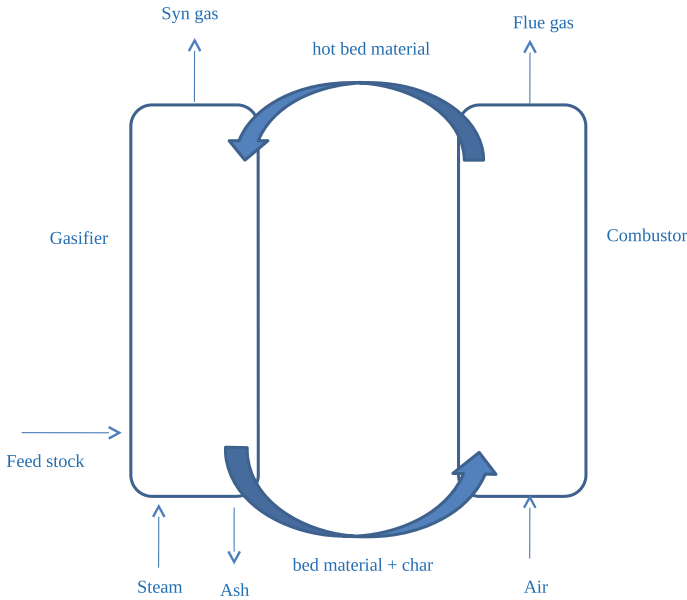


Fig. 1 Concept of dual fluidized bed gasification

DFBG are discussed in Sect. 4.3. Cleaning of tar and other impurities in the product gas for DFB gasifier are examined in Sects. 5 and 6. Section 7 concludes the chapter along with the discussion on future prospects of the technology.

2 Components of DFBG

The main components of DFBG are the fluidized beds, the gas–solid separators, and the connecting components. In DFBG, a low-velocity bubbling/turbulent bed is usually used for gasification, whereas high-velocity circulating bed or riser is used for char combustion [68]. Pure oxygen or steam is used as the fluidizing media in the gasifier, whereas air is usually used in the combustor. The combination of bubbling bed and high-velocity circulating bed (riser) ensures the solids movement between the beds [20]. Also, this combination ensures higher fuel residence time for slow gasification and tar reforming reactions compared to the combination where combustion takes place in bubbling bed and gasification in riser. In order to maximize the gasifier efficiency, the fuel allocation between the gasifier and the combustor should be optimized by proper hydrodynamic design (refer Sect. 3). At the exit of the riser, the solids need to be separated from the flue gas before it is circulated to the bubbling bed. Cyclones are usually used to separate solids from the gas. The solids are transferred between the two beds without the interchanging of gases by employing

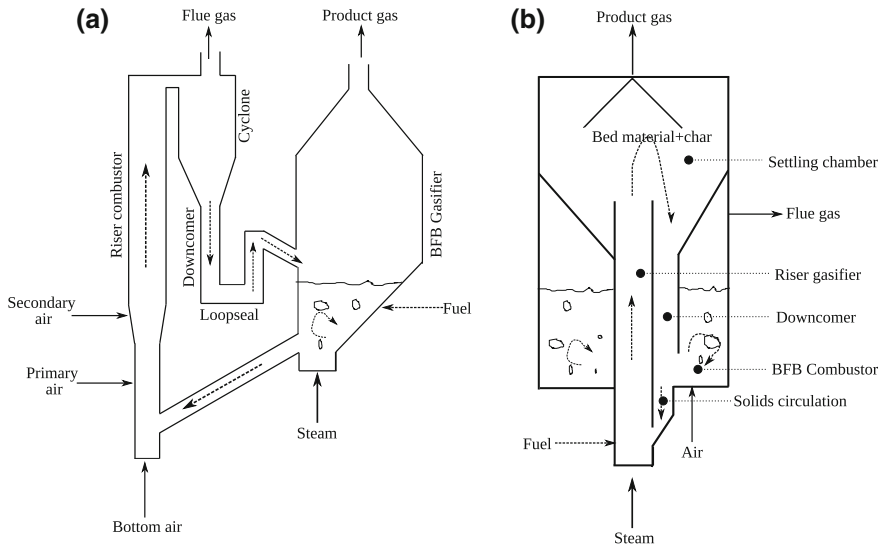


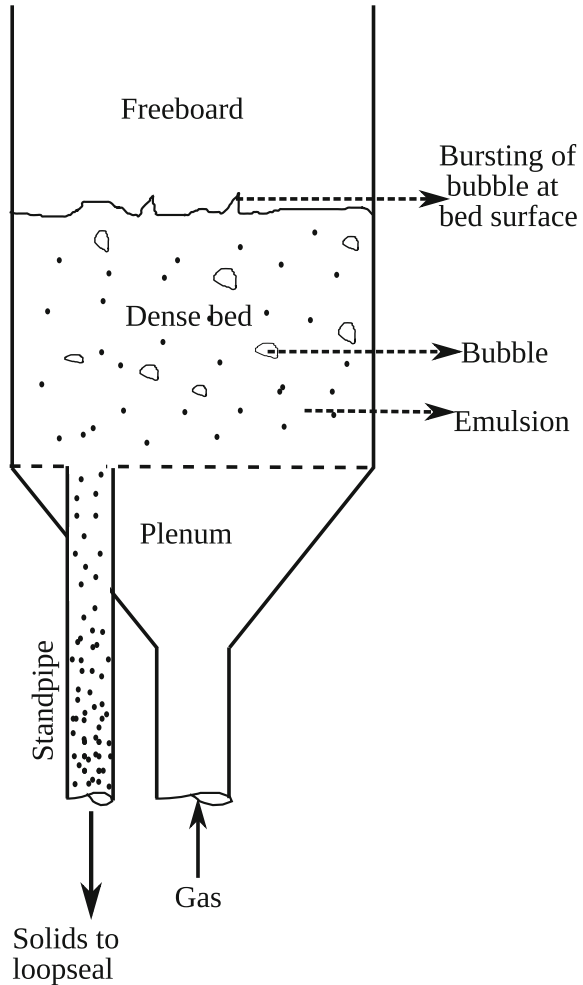
Fig. 2 Schematic of dual fluidized bed gasifier: **a** at VTU, Austria [49] and **b** Milena, ECN [41]

connecting components, e.g., mechanical valves or non-mechanical valves, such as, loop seals or L-valves. In DFB gasifier, non-mechanical valves are preferred over mechanical valves, since the former one work based on hydrodynamic principles without carrying any moving parts and hence experience less operational breakdowns. The schematic of two different DFBG designs are shown in Fig. 2. The number of loop seals can be one (either top or bottom) or two (top and bottom) depending on various designs. The bottom loop seal transfers solids from the bubbling bed to the riser, whereas the top loop seal transfers solids from the riser to the bubbling bed. The other components are standpipe and downcomer. The standpipe supplies solid materials from the bed to the loop seal at the bottom, whereas downcomer supplies solid materials from the solid–gas separator either directly to the bed or to the top loop seal. In this section, the features and working principles of each of these components are discussed.

2.1 Bubbling Fluidized Bed

A fixed bed of particles is incipiently fluidized, when a gradually increasing gas velocity reaches minimum fluidization velocity, U_{mf} . When the gas velocity is further increased, the extra gas flow in the form of *bubbles*. The portion of the bed outside the bubbles is called as *emulsion phase*. The bed comprising both emulsion phase and bubbles is known as *dense bed*. The bubbles are erupted at the surface of dense bed and flows into the space above it. This region is called as freeboard. Some-

Fig. 3 Gas–solid flow structure in a bubbling fluidized bed [5]



times, the bubbles entrain some solid particles into the freeboard. A further increase in gas velocity, especially in deep beds, causes formation of slugs or gas bubbles of size comparable to size of the bed. This is called as slugging. The next regime, upon increasing the gas velocity is turbulent bed, where the bubble and emulsion phase are violently agitated. The structure of bubbling fluidization regime is shown in Fig. 3. A detailed description of fluidization regimes may be referred in the literature [5, 22, 33].

In DFBB, the solid fuel is injected into the bubbling bed, and it gets dispersed into the bed material. The fluidization medium is steam. The solid particles experience up and down circulating motion, until it finds its way to the standpipe. Sometimes, the distributor plate is kept inclined to facilitate the movement of solids to the standpipe [31]. The gas mixing is characterized as complex two regions with near mixed flow

in emulsion phase and near plug flow in bubble phase and freeboard. The gas–solid contact is poor, if wider bubbles are present in the vessel [37].

2.2 Riser

The riser is operated under fast fluidization regime. The fast fluidization regime is defined as follows: The turbulent fluidization transforms into fast fluidization when the gas velocity is well above the transport velocity (U_{tr}) of the largest bed material. Beyond U_{tr} , solid particles fed to the bottom of a vertical vessel transverses it in fully entrained flow, and the concentration of the resulting suspension depends not only on the gas flow rate but also on the solid flow rate [69]. The solid flow rate should be sufficiently high to maintain a high solid concentration in the vessel. The main characteristics of fast fluidized bed are high slip velocity between the gas and solid, formation and disintegration of particle agglomerates, and dispersed plug flow gas mixing and near-perfect solid–solid mixing [5].

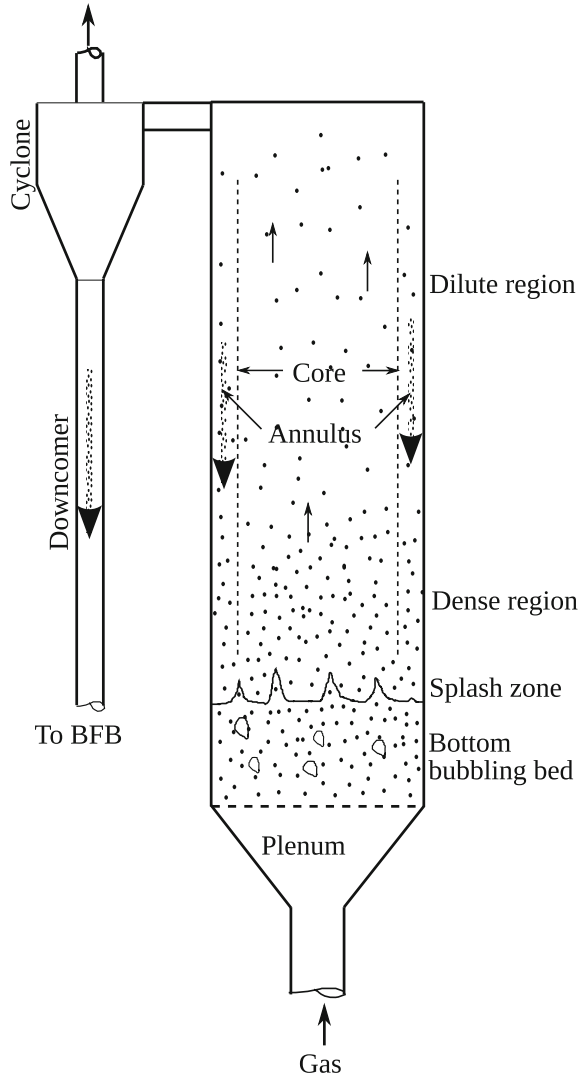
The hydrodynamics of fast fluidized bed (Fig. 4) is explained with core-annulus two-zone model, with upflow of gas and entrained solids in a dilute central core and down flow of dense strands or clusters in a thin annular region at the wall [21]. The solids are vertically distributed into two regions, a lower dense region with constant solid fraction and an upper lean region where the solid fraction falls exponentially with height toward the saturation carrying capacity of the gas. The boundary between the regions is highly diffused [34].

2.3 Gas–Solid Separators

Gas–solid separators are used in DFBG to separate the hot bed materials from the riser and play an important role to complete the circulation loop. The solids are separated from the gas by means of the following internal forces: inertial and/or centrifugal. There are mainly two types of separators: cyclones and inertial separators. Cyclones are the common devices in process industries and conventional power plants, as they are especially used to clean the exhaust gases from particulate matters. The cyclone installed in DFBG necessitates its operation under very high temperatures and solid concentration. The overall effect of temperature on cyclone is to reduce the collection efficiency, as the collection efficiency of cyclone is proportional to the square root of the solid–gas density difference and gas viscosity [5]. Internal refractory lining is provided to protect the wall from high temperature and to reduce the radiation and natural convection heat losses. Sometimes, the outer skin temperature would be still high, and in that case, water or steam jackets are provided for better thermal efficiency.

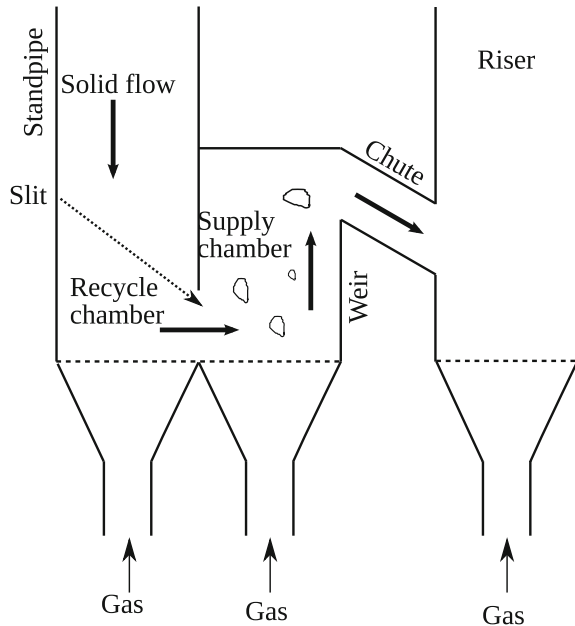
In inertial separators, the inertial forces on solids separate it from gases. The gas–solid suspension passes through an inlet nozzle and a series of obstacles, and changes

Fig. 4 Gas–solid flow structure in a circulating fluidized bed [22]



the flow direction frequently. The flow velocity of the suspension is reduced in the diverging nozzle (diffuser), reducing the solid-carrying capacity of the gas. The solid particles, because of its higher inertia, try to follow the original direction and are intercepted by the obstacle and fall down due to gravity (refer the settling chamber in Fig. 2b). The inertial separators are typically designed for coarse particles ($>10\text{--}20\ \mu\text{m}$) and are characterized by simple construction, low cost, and low pressure drop.

Fig. 5 Functioning of loop seal (Adapted from [6], with permission from Elsevier)

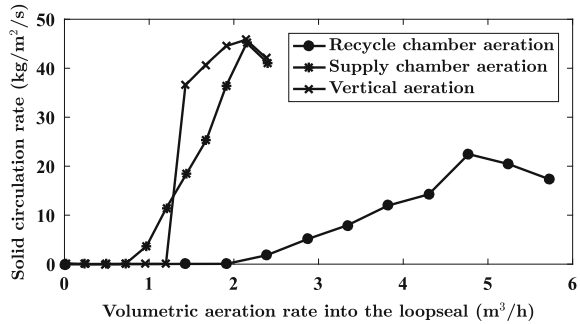


2.4 Non-mechanical Connecting Valves

Loop seals are the most commonly used non-mechanical connecting component. The function of the loop seal is to transfer the solids from the low-pressure region to the high-pressure region and at the same time prevent gas from short-circuiting through the low-pressure path. The solid movement is established by proper aeration of the valve, and the gas seal is obtained by ensuring appropriate amount of solids in the standpipe. The operation of loop seal is delineated by Basu and Butler [6], as shown in Fig. 5. The main parts of a loop seal are standpipe, supply chamber, recycle chamber, weir, and recycle pipe. The base of the standpipe acts as supply chamber, which has opening at least at one side. This opening connects to the recycle chamber through a horizontal passage. The recycle chamber has an opening at its top by using a weir, and this opening connects to an inclined recycle pipe. The recycle pipe extends to the bed.

The standpipe can be considered as a moving packed bed. Because of the opening at the supply chamber, the solids falls into the horizontal passage forming a slope. The angle of the slope is determined by the inter-particle frictional force (angle of repose). If air is injected perpendicular to the column (vertical aeration) and/or at the bottom of the supply chamber, the inter-particle frictional force is reduced and solids flow further in the horizontal passage toward the recycle chamber. The solids in the recycle chamber are fluidized in the bubbling regime causing the bed to expand beyond the weir. Thus, the solids flow over the weir into the recycle pipe.

Fig. 6 Variation of solid circulation rate with respect to loop seal aerations (Adapted from [53], with permission from Elsevier)



The gas sealing is achieved due to the pressure drop across the loop seal. The important feature of a loop seal is that the pressure drop across it is automatically adjusted against the pressure variations in the riser. This is possible due to the pressure drop characteristics of the packed bed in the standpipe. Hence, the aeration velocity in the supply chamber should not exceed the minimum fluidization velocity, otherwise the solids in the standpipe are fluidized, and any further increase in air flow will not increase the pressure drop across the standpipe.

The solids circulation rate in DFB system is directly varied by changing the loop seal aeration velocities, even though the gas velocity in the riser also influences the solid circulation rate. Seo et al. [53] studied the changes in the solid circulation rate against the different loop seal aeration velocities, such as supply chamber aeration velocity ($U_{g,sc}$), recycle chamber aeration velocity ($U_{g,rc}$), and vertical aeration velocity ($U_{g,vertical}$) by cold model experiments and numerical simulations. The results are shown in Fig. 6. The solid circulation can be effectively controlled by varying the loop seal aeration velocities. However, loop seal aeration cannot be increased beyond a certain limit, after which the pressure seal in the standpipe is broken. This defines the maximum operable velocity of the loop seal. Similarly, if the loop seal velocity is reduced below a certain value, the pressure drop across the standpipe falls below a value required to drive the solids.

Larsson et al. [36] reported the effect of the bed material properties on the aeration gas pathway in the loop seal. When low-density particles (2600 kg/m^3) are used, about 80–90% of the steam used for fluidization of a loop seal follows the direction of bed material, whereas only 65% (approximately) of the steam used for fluidization of the loop seal follows the direction of the bed material when high-density particles (3300 kg/m^3) are used. This forms a basis to calculate the effective steam-to-fuel ratio in the bubbling bed. The loop seal dynamics and gas carryover characteristics need to be studied further for its efficient design and control of solid circulation rate.

3 DFBB Hydrodynamics

The knowledge of hydrodynamics is a fundamentally important and common aspect in the modeling, design, and scale-up of DFBB. The main hydrodynamic parameters of interest in DFBB are bed geometry, bed material, fuel and gas residence times at different regions of the fluidized beds, gas–solid mixing efficiency, dispersion of char in bed material, gas dispersion in axial and radial directions, solid circulation rate, gas leakages in the reactors, etc. All these parameters depend on the complexity of flow within the reactors and loop seals [54]. The hydrodynamic measurements are very difficult or are expensive in industrial scale units under hot conditions. Hence, a cheap and convenient option to resemble the hydrodynamics of an actual plant is a scaled down cold flow model, operating at ambient conditions [9, 38]. The other features of cold flow model are easy handling, requirement of only minor experimental equipments, and possibility of visual observation of macroscopic flow structures [59]. The procedure followed for the hydrodynamic matching in the scaled down model is explained below.

Glicksman's scaling relationships for dynamic similarity of fluidized beds are the far most used scaling criteria which have proven its applicability to give satisfactorily agreement between hot fluidized rig and scaled down cold flow model (CFM) [18]. It sets a group of dimensionless numbers that should be matched while scaling down the hot fluidized bed. A full Glicksman criteria is found to be very difficult to follow because of very little freedom to fix the dimensions of CFM. Hence, researchers generally adopt simplified sets of Glicksman criteria, which give more freedom in choosing the scaling ratios [9, 46]. These criteria are applicable under high viscous dominated ($Re_p < 4-5$) or high inertia dominated limits (high Re_p) [17]. The new set is Froude number $\left(\frac{u_0^2}{gD}\right)$, the solids to gas density ratio $\left(\frac{\rho_p}{\rho_g}\right)$, the ratio of superficial gas velocity to minimum fluidization velocity or flow number $\left(\frac{u_0}{u_{mf}}\right)$, the reactor height to diameter ratio $\left(\frac{L}{D}\right)$, the dimensionless flux $\left(\frac{G_s}{\rho_p u_0}\right)$, the particle sphericity, and the dimensionless particle size distribution. Shrestha et al. [59] report a comprehensive list of scaling criteria used by different researchers.

An extensive review on cold flow models on DFB is given by Shrestha et al. [59]. Since, only a few hydrodynamic studies exist exclusively on DFBB, we extend our literature review to CFB studies to get useful insights. The major factors studied in cold flow experiments are pressure profile, solid circulation rate, and the hydrodynamic stability of the system. The most commonly used experimental technique to measure the solid circulation rate is as follows: The aeration at the non-mechanical valve is stopped abruptly at time zero, and the height of solids accumulation 'Δz' at the standpipe is noted against a given time interval, 't'. Then a rough approximation of the mass flux is given by, $m = \frac{\Delta z}{t} * \rho_b * A_{dc}$. But, care should be taken by optimally fixing the measurement interval, since solids removal from the riser may decay the riser pressure drop and may affect the steady operation of DFB system [38].

Karmakar and Datta [24] studied pressure profile and solid circulation rate in their cold model DFB setup, where the control of solids circulation between the fluidized beds is done with L-valves both at upper and lower positions. L-valve is another simple kind of non-mechanical valve. The pressure profile observed in their setup is shown in Fig. 7. The highest pressure drop is observed at the upper L-valve connecting cyclone and bubbling bed, followed by the lower L-valve connecting bubbling bed and riser. This proves the functionality of non-mechanical valve to make the solid circulation and gas seal, possible simultaneously. The effect of riser velocity on solid circulation rate, as observed, in their study is shown in Fig. 8. It is observed that the solid circulation strongly increases with riser velocity. They attributed this to the fact that the increase of upward drag force results in increase of net rising particle velocity. The strong coupling of solid circulation rate with riser velocity is also reported by other researchers [10, 32]. But there is a limit in the enhancement in solid circulation rate by the riser velocity, since solid circulation rate falls after reaching a maximum value while increasing the riser velocity. This is explained as follows: There is a saturation level in solid-carrying capacity of the gas for a particular bed material used. However, before attaining this saturation, the feed rate to the riser may act as a limiting factor. The feed rate to the riser is limited by the loop seal conditions and the high static pressure experienced at the riser [58]. After the

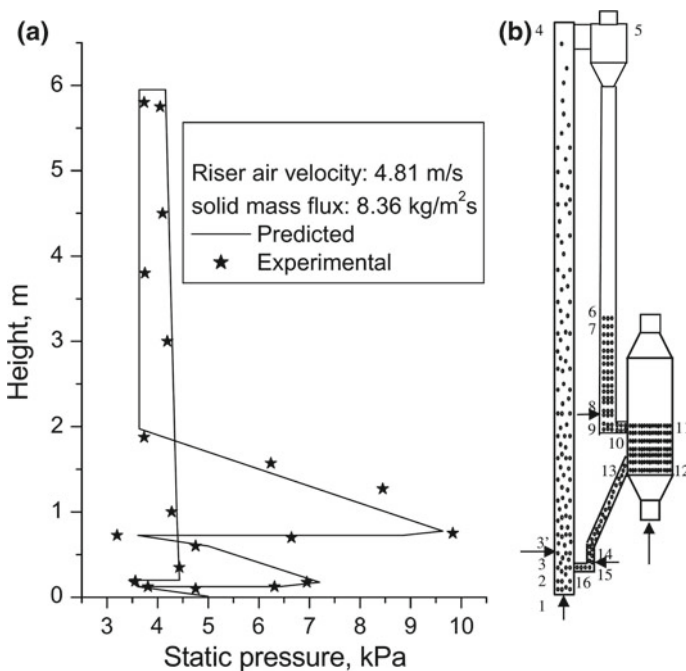
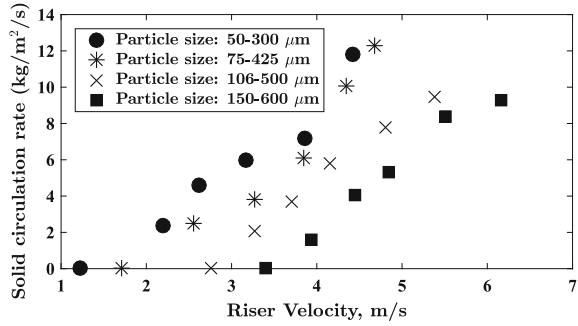


Fig. 7 **a** Pressure profile observed in a dual fluidized bed gasifier, **b** Schematic of the cold flow model with the arrows show the air flow direction (Reprinted from [24], with permission from Elsevier)

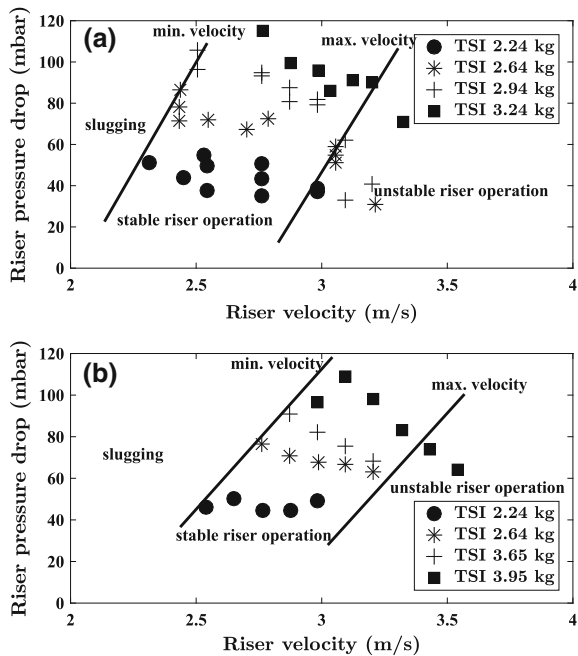
Fig. 8 Effect of riser velocity on solid circulation rate with different particle size (Adapted from [24], with permission from Elsevier)



feed rate to the riser is reduced, the solid holdup at the bubbling fluidized bed may increase at higher riser velocities. Lim et al. [39] caution the excessive increase in riser velocity, since it increases the chances of flue gas and air getting bypassed from riser to bubbling bed and increases the nitrogen dilution of product gas. It is found that gas velocity to BFB has negligible effect on solid circulation rate, but proper fluidization is required for smooth circulation [59].

Charitos et al. [10] investigated the stable operating region with two particle sizes (142 and 230 μm) by varying the riser velocity in the cold model of a calcium looping DFB, consisting of a loop seal for solid transport from BFB to riser. There are three regions of operation, as shown in Fig. 9. They are the region of stable riser

Fig. 9 Operational regions observed in a calcium looping dual fluidized bed with two different particle sizes: **a** 142 μm and **b** 230 μm (Adapted from [10], with permission from Elsevier)



operation bordered by a slugging region at lower velocities and a region of unstable riser operation at higher velocities. These minimum and maximum limits of stable operation increase with the total solid inventory (TSI) for both the particle sizes. It is found that above the maximum velocity the riser operation becomes unstable in a manner that there are undesirable sinusoidal fluctuations of pressure drops at different locations in the loop.

The knowledge of hydrodynamics is a prerequisite while designing the DFB gasification process. The mixing of fuel particles with bed material in BFB and its transport from BFB to riser determine the relative conversion of fuel in the gasifier and the combustor. The heat and mass transfer rates, and hence the overall reaction rate, are determined by the extent of gas–solid contact in the beds. The details of DFB gasification process and the effects of operating conditions and design parameters on gasifier performance are discussed in the next section.

4 DFBG Process

In this section, the existing literature on DFBG is reviewed from its process point of view, describing the syngas production, the quality of syngas, the favorable conditions to produce better quality syngas and the gas cleaning technologies. The theories of solid fuel gasification and combustion in the context of DFBG are explained shortly in the next paragraph. The details of kinetics and thermodynamics of gasification processes are given in [60] and [23].

When a biomass or coal particle is injected into the gasifier, it undergoes two distinct chemical processes; devolatilization of raw fuel and gasification of residual char. These two processes may undergo simultaneously, at high heating rate, or one after another, at low heating rate [60]. As the temperature of coal particle increases, by virtue of radiation and convective heat transfer from the hot sand particles, moisture is driven out in the initial stages, and devolatilization starts in a temperature range of 300–350 °C. The volatiles released undergo gas phase secondary cracking reactions and steam reforming reactions. The condensable hydrocarbons, which remain in the product gas even after these secondary pyrolysis reactions, are usually termed as tar. The tar content or its dew point should be minimized below a particular limit to avoid fouling issues in the downstream processing equipments of product gas. The devolatilization of coal generates a highly porous char structure. These hot char particles undergo gasification reactions with the volatiles expelling out from the solid fuel (internal gasification) and also with the steam injected. To maintain the heat balance, the circulating bed material transports portion of the char to combustor, where it undergoes combustion with the oxygen present in injected air. The oxygen molecules have to diffuse through the pores from the bulk phase to the reactive sites on the surface of porous char particles. There are three distinct regimes for the char reaction rate based on the reaction temperature: (i) around 300–500 °C, where the rate is influenced by intrinsic chemical reaction rate, (ii) around 500–800 °C, where the rate is influenced by both intrinsic reaction rate and pore diffusion limitations,

Table 1 Product gas compositions observed in different DFBG studies against the specified operating conditions

	VTU, Austria [20]	GoBiGas, Chalmer's University [3]	Milena, ECN [20]
Type of fluidized bed (gasifier/combustor)	BFB/CFB	BFB/CFB	CFB/BFB
Temperature, °C (gasifier/combustor)	900/1000	873/920	850/925
Power	8 MW _{th}	20MW _{biomethane}	0.8 MW _{th}
Bed material	Olivine	K ₂ CO ₃ activated olivine	Sand
Gas composition, vol %	H ₂ : 35–45 CO:20–30 CH ₄ :8–12 CO ₂ :15–25	H ₂ :39.9 CO:24.0 CH ₄ :8.6 CO ₂ :19.9	H ₂ :31 CO:27 CH ₄ :14 CO ₂ :22
Tar, g/Nm ³	1.5–4.5	20.5	40

and (iii) above 800 °C, where the rate is influenced by the limitation imposed by only external mass transfer. Because of the transport limitations, the heterogeneous reactions involving char are relatively slower, whereas the gas phase reactions are faster. The typical timescale for pyrolysis is about 10 s, whereas it can be several minutes for char gasification [70].

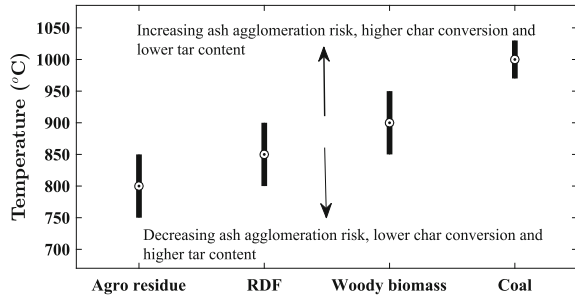
The typical product gas composition as observed at three different DFBG studies of different scales are tabulated in Table 1. The H₂ to CO ratio ranges from 1.4 to 1.6. The CV and H₂ composition of the syngas can be further improved by incorporating Adsorption Enhanced Reforming (AER) technology, where CaO is added to the bed material to selectively adsorb CO₂ present in the gasifier and transport it to the combustor.

4.1 Effect of Operating Conditions

The operating conditions which influence directly the product gas quality and yield in DFBG are temperature, pressure and steam-to-biomass ratio. The air flow rate to riser do not directly influence the product gas quality but should be fixed based on the design of fluidization regime, and it is usually in excess to stoichiometric amounts. If the riser temperature does not reach the required value, it may be necessary to inject additional fuel to the riser.

A higher gasifier temperature favors the endothermic reactions and increases the H₂ and CO contents. From the perspective of tar content, higher temperature enhances secondary tar cracking reactions and reduces tar content in the syngas [40]. But, practically, it is very difficult to go to higher temperature beyond 900 °C in gasifier, under DFBG operation. Also, the maximum temperature is usually limited by

Fig. 10 Operational temperature range for different feedstocks [14]



the melting temperature of ash present in the solid fuel, due to bed material agglomeration and associated problems. The effect of inorganic content on gasifier performance is explained in Sect. 4.4. The range of operational temperature for different feedstocks and the effect of higher and lower temperatures on the gasification process are shown in Fig. 10.

The pressurized gasifier offers economic advantages due to reduced gasifier size and reduced cost of product gas compression prior to chemical synthesis or burning the gas in gas turbine combustor. Besides this, high pressure operation has positive effect on the gasifier performance, especially for certain applications like generation of SNG. In general, with pressure, the carbon dioxide and methane yield increases, carbon monoxide yield decreases, and hydrogen and tar yield remain more or less constant [40, 63]. The changes in gas yield can be explained based on the changes in the gas phase reactions, like acceleration of water gas reaction kinetics and decrease in reforming of hydrocarbons (Le Chatelier principle). Especially, the increase of methane with pressure is linked to changes in secondary hydrocarbon reactions.

A higher steam-to-biomass ratio has a positive effect in gasifier performance in terms of higher hydrogen yield and lower tar yield. The value of steam-to-biomass ratio should account for the water content in biomass and generally ranges between 0.8 and 1.1 in DFBG [45]. The accurate measurement will account the split fraction of steam injected at the loop seal, between the gasifier and combustor. In DFBG, only less than 10% of steam injected take part in the process and the rest exit the gasifier unreacted [12]. So, an improved gasifier design with better steam utilization factor can enhance the positive effects of higher steam-to-biomass ratio.

4.2 Effect of Fuel Feed Location

There are generally two fuel feed locations to the bubbling bed of DFBG, viz. on the bed and in the bed. It is found that the fuel feed location influences the gasifier performance in terms of product gas composition, gas yield, and tar content. With on-bed fuel feeding, the major differences observed compared to in-bed fuel feeding are significantly higher CO content and lower H₂ content in the product gas, higher amount of product gas, and higher tar yields. Figure 11 shows the comparison of

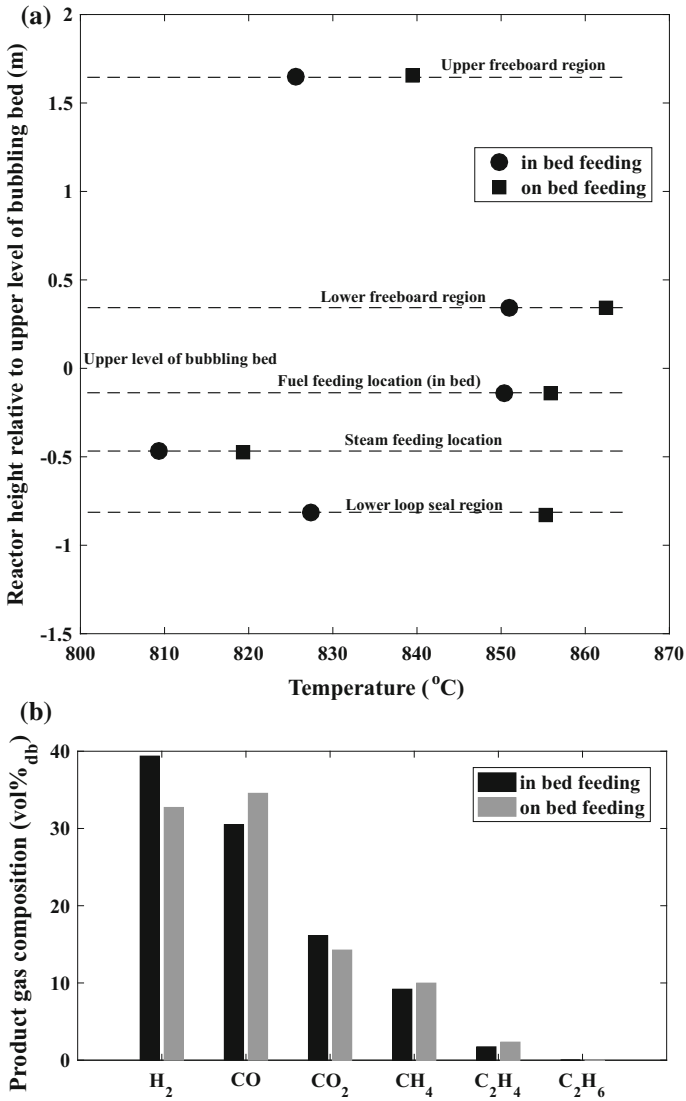


Fig. 11 Changes in temperature profile and product gas composition with respect to fuel feed locations (Adapted from [26], with permission from Elsevier)

product composition and gasifier temperature profile, between the two feed locations. When fuel feeding location is on the bed, the fuel meets the hot bed materials in the freeboard, and most of the pyrolysis process is completed there with higher heating rate. This results in product gas composition more similar to pyrolysis gas with higher tar content [19]. The gravimetric tar content increases from 1.5 to 9.7 g/Nm³, and product gas yield increases from 27.52 to 30.68 Nm³/h, when the fuel feed location is changed from in-bed to on-bed [65]. When the feed location is in bed, the fuel heating rate is lower and the pyrolysis gases are subjected to higher residence time in the gasifier and increased contact with catalytic bed materials. These factors favor the steam reforming reactions, increasing the hydrogen content and improving the utilization factor of steam.

In short, the on-bed feeding is favorable in terms of higher gas amount and gas calorific value, but not favorable in terms of gas quality due to higher tar content. So, the choice should be made according to the end use of product gas. For example, if the product gas is immediately used without cooling for heating applications, higher calorific value will be advantageous, but if the product gas is used for generation of synthetic fuels or gas turbine applications, the higher tar content will be problematic.

4.3 *Effect of Bed Materials*

As mentioned earlier, silica sand is the most generally used bed material in fluidized bed gasifiers mainly because of its thermal properties. Since silica sand does not exhibit catalytic activity toward fuel conversion reactions, it can be considered as a reference material in comparing the performance of different catalytically active bed materials. The use of active bed materials is attractive, especially due to the reduction of tar with in the gasifier and increase of total solid fuel conversion to syngas. The effects of bed material properties on fuel conversion can be summarized in terms of the thermal effect, the catalytic effect, the ash-enhanced catalytic effect, and the oxygen transport effect [7].

The thermal effect of bed material on fuel conversion is exerted based on the function of bed material as a heat source. For example, silica sand predominantly influences gasification process by its thermal effects. Presence of catalytic species present in the matrix of bed material crystals, e.g., Mg and Fe in Olivine ((MgFe)₂SiO₄), can exert catalytic effects on fuel conversion. Sometimes, calcination or heat treatment of olivine particles is done to increase the availability of active species on the surface of particles [11]. In situ calcination of bed material can also happen after around one week of gasifier operation [7].

The alkali and alkali earth metals present in the inorganic content of the fuel show catalytic activity toward the tar reaction and steam gasification of char [1, 42, 61]. The interaction of these metals with bed material species can inhibit or enhance its original catalytic activity. For example, Si reacts with the alkali to form stable silicates and inhibit the activity. Alternatively, alkali metals bond reversibly with the bed material, forming more active compounds. This effect is known as the

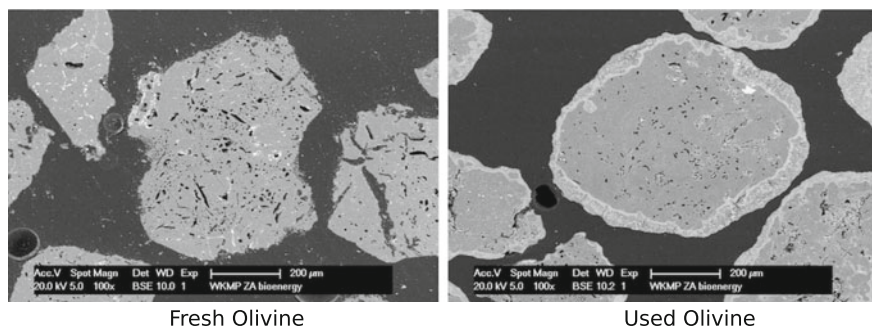


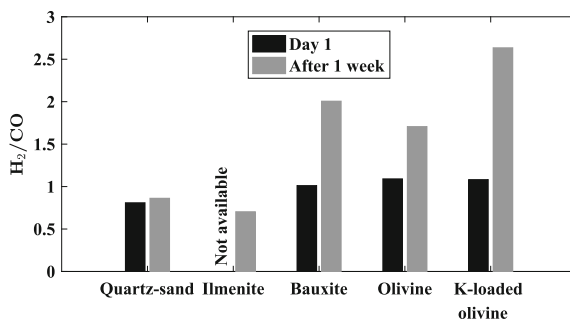
Fig. 12 Formation of layer on used olivine. Fuel is wood with an ash composition of 55% CaO (Reprinted with permission from [29]. Copyright (2011) American Chemical Society)

ash-enhanced catalytic effect by bed materials. By forming such reversible bonds, the active inorganic species present in ash are distributed throughout the DFB. Under certain conditions, over a longer run, the active inorganic species are coated on the bed material particle. This buildup of ash layer is the reason why certain bed material like olivine shows enhanced activity over a long run [30]. The energy-dispersive X-ray images of fresh and used olivine particles point to ash layer formation during a DFBG run as shown in Fig. 12. The variation of H_2/CO ratio (Fig. 13) and tar reduction (Fig. 14) after one week of operation is reported by Berdugo Vilches et al. [7].

As investigated in chemical looping combustion, the Fe content in the bed material can transport some oxygen from combustor to gasifier due to its cyclic oxidation and reduction. This oxygen can oxidize some part of the product gas and increase the char conversion in the gasifier. So, it is important to consider the effect of oxygen transport by the active bed materials while designing the DFBG process [2].

A comparison of product gas compositions observed in a DFBG while using different bed materials is given by Pfeifer et al. [45], as shown in Fig. 15. The bed materials considered for study are three natural minerals: silica sand, olivine, and limestone and two synthetic materials: Fe-supported olivine and Ni-supported olivine. The catalytic effect of olivine is evident here, and the changes in gas composition

Fig. 13 H_2/CO ratio on first day and after 1 week for different bed materials. Fuel-Wood pellets, Steam-to-fuel ratio = 0.8, Gasifier temperature=740–760 °C (Adapted with permission from [7]. Copyright (2016) American Chemical Society)



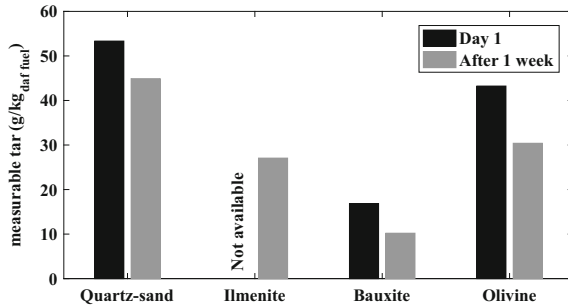


Fig. 14 Amount of tar in product gas on first day and after 1 week for different bed materials. BTX fraction not available for bauxite. Conditions same as that of Fig. 13 (Adapted with permission from [7]. Copyright (2016) American Chemical Society)

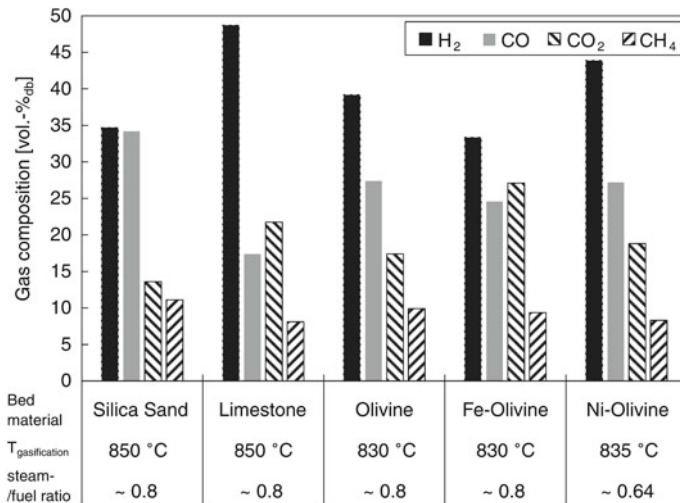


Fig. 15 Comparison on performance of different bed materials in terms of permanent gas compositions (Reprinted from [45], with permission from Springer)

are attributed to enhancement of shift reaction and increased conversion of hydrocarbons to CO and H₂ by steam reforming and dry reforming reactions [31]. Further, it can be seen that, with limestone significantly higher H₂ composition of 50% dry basis is achieved. It is attributed to the selective transport of CO₂ from gasifier to combustor by the CaO/CaCO₃ system via cyclic carbonation and calcination. It is recommended to use limestone as an additive to silica sand rather using as bed material due to higher attrition rates of limestone. Even CaO content as low as 0.1–0.2 kg/kg is sufficient to attain a gravimetric tar reduction by about 70–90% [52]. The addition of Ni to olivine further improves the performance of olivine as bed material in DFBG in terms of good permanent gas compositions and tar reduction upto two orders of magnitude [44].

4.4 Effect of Feedstocks

In many studies, the feedstock used in DFBG is wood pellets, mainly because of its favorable characteristics of low ash content (<1%). But other kinds of feedstocks are also tested for its technical feasibility with DFBG. They consist of agricultural residue (straw), coal (lignite and bituminous), waste sludge, plastics, and their blends. These feedstocks vary in their properties especially in terms of ash content, ash melting temperature, and volatile matter content, and hence in some extreme cases, special considerations should be given while designing the process. Schmid et al. [50] compared the effects of different biomass feedstocks on DFBG operation in their 100 kW test facility. The feedstocks considered are softwood pellets, hardwood chips, straw pellets, blended pellets of 40% straw and 60% wood, and sewage sludge pellets. The ash content is significantly high for sewage sludge and straw compared to wood. The ash melting point of 720 °C makes the fuel with 100% straw not suitable with DFBG operation because the temperature in gasifier or combustor usually crosses above 800 °C. Under such situations, fuel blending is a good strategy to generate feedstock with comfortable properties for gasifier operation. Figure 16 shows the gas composition, tar, dust, and char contents in the product gas observed for different feedstocks. The variation of product gas composition obtained with different feedstocks may be attributed to two factors: the changes in pyrolysis behavior due to variations in cellulose or lignin contents of the fuels, and/or the changes in catalytic activities of the inorganic components present in the ash. The high ash content of the sewage sludge results in a product gas loaded with more dust particles (inorganic fines) compared to other fuels. Schweitzer et al. [52] report that the main challenge in utilizing biogenic waste materials as feedstocks, is in handling of product gas impurities such as tar, NH₃, H₂S, and Cl. They studied steam gasification of sewage sludge and livestock manure in a 20 kW DFBG test facility, and not experienced bed agglomeration issues at a gasifier temperature of 820 °C.

Coal, as a feedstock for DFBG, is characterized by its lower reactivity, higher fixed carbon and ash contents, higher sulfur and nitrogen contents, and presence of fine particles, compared to biomass. The most popular technology for coal gasification is entrained bed technology, where the gasifier temperature is typically high in the order of 1600 °C. At this temperature, low reactivity of coal and its higher ash content are not problematic, because complete conversion is mostly achieved even in a single pass and the ash is recovered in the form of molten slag. But, as mentioned in the introduction of this chapter, entrained bed technology finds itself difficult to compete with combustion-based power production on economic basis, especially for low-rank coal. Hence, it is advantageous to widen the feedstock range of DFBG to coal, especially as a CCS enabled technology. Kern et al. [25] studied the feasibility of high-ash coal (31%_{db}) in DFBG, and the product gas composition is found to be relatively good. The interesting point to be noted in their study is that the carbon conversion in gasifier is only 36.41% as against the carbon conversion in entire DFBG of 93.13%. This is attributed to the lower volatile matter content and lower reactivity of coal. Due to the higher carbon allocation to combustor, it is not needed to inject

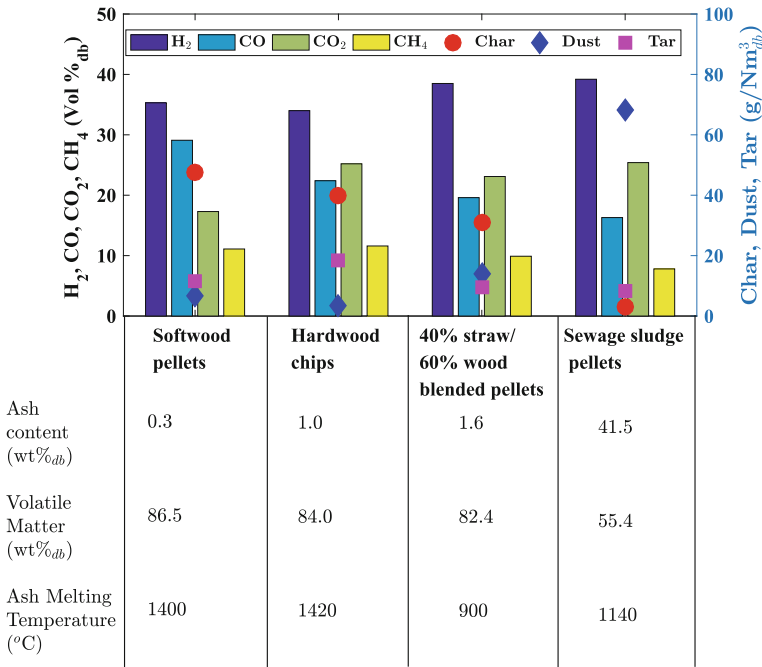


Fig. 16 Changes in product gas quality with different feedstocks [50]

additional fuel, unlike biomass as feedstock, to maintain the temperature. But the test is performed only for 8 h, and the effect of ash buildup on the gasifier operation is not characterized. The ash buildup can exert a positive impact on gasifier performance, if catalytically active species are present in ash, and under such condition, the bed material being injected to the reactor to make up the losses due to attrition can be gradually reduced in subsequent gasifier operation. However, it may also lead to bed material agglomeration problem, if the concentration of the species, which lowers the ash melting temperature, exceeds beyond a certain critical value.

DFBG also runs with plastic wastes, either as a stand-alone fuel [64] or on blending with biomass [66] or lignite [27]. The product gas is characterized with significantly high tar content in the range of 100 g/Nm³, when polymers are gasified in DFBG. The tar mainly consists of PAH and aromatics and also results in formation of tertiary tars on polymerization of tar components in the gas mixture [64]. Hence, it is necessary to further develop technologies to control or reduce the tar in product gas, when this kind of feedstocks are gasified.

5 Gas Cleaning

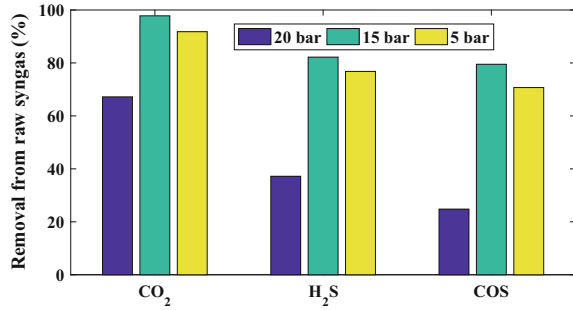
Purification and conditioning of product gas are unavoidable for almost all applications of syngas, except in direct combustion of product gas immediately after gasifier. The product gas needs to be processed to remove particulate matters, or-

ganic impurities (tar), and inorganic impurities like compounds of sulfur, nitrogen, chlorine, and any alkali/heavy metals. The extent of gas cleaning required depends on the downstream application of syngas. In general, more stringent conditions on minimum level of impurities in syngas are required for fuel or chemical synthesis compared to combustion of syngas in gas turbine combustion chamber or internal combustion engines, since the activity of the catalysts used in the synthesis process is very sensitive to small amounts of impurities. The level of impurities in the syngas depends on the type of gasification unit. Since DFBG operates at lower temperature under non-slagging condition, the syngas is relatively loaded with tar, dust, and unconverted carbon fines. Sulfur-based impurities (H_2S , COS , SO_2) and nitrogen-based impurities (NH_3 , HCN) depend on the sulfur and nitrogen contents in the feedstock. Hence, the gas cleaning technologies developed for high pressure and high temperature based entrained bed coal gasifiers are not suitable for atmospheric pressure and medium temperature based DFBG. A detailed description of different gas cleaning techniques is not under the scope of this chapter, and hence it is limited to couple of case studies related to DFBG (refer Sects. 5.1 and 5.2). Since tar handling and its reduction techniques directly affect the cold gas efficiency and product gas quality, a separate section is devoted to tar reduction (refer Sect. 6).

5.1 Fischer Tropsch Diesel from Syngas by Kim et al.

Kim et al. [28] employ a two-stage gas cleaning system in their integrated DFBG facility to produce Fischer Tropsch diesel. The first stage consists of conventional gas cleaning system to remove particulates and tar by cyclones, gravity-based dust collector, wet scrubber, and demister filter. By providing refractory lining, the temperature of raw gas is maintained, till it reaches the wet scrubber in order to prevent tar condensation and choking. The demister filter removes the entrained water droplets, condensed tar, and fine dust. Since the gasifier operates at atmospheric pressure, and the downstream physical absorption of impurities and FT synthesis operate at high pressure, the gas is compressed and stored to 6 MPa. The gas storage helps to smoothen the fluctuations, if any, in gas production. The gas enters second stage acidic gas removal stage where the impurities like CO_2 , H_2S , and COS are removed by RectisolTM process. The RectisolTM process uses chilled methanol as physical solvent to absorb acidic gases from syngas. The solubilities of acidic gases are favored by low temperature and high pressure conditions [55]. The typical absorption conditions used by Kim et al. [28] are $-30\text{ }^\circ\text{C}$ temperature and 2 MPa pressure. The methanol exiting the absorption tower is regenerated by flashing and N_2 stripping. The average removal efficiencies for CO_2 , H_2S , and COS observed in their study for an operational duration of 500 h are shown in Fig. 17. It is reported that the tar, if any remains in the syngas from the upstream cleaning stage, also gets dissolved in methanol.

Fig. 17 Removal of acid gas impurities from syngas by RectisolTM process [55]



5.2 Synthetic Natural Gas from Syngas by ECN

The energy research center of the Netherlands (ECN) employs OLGA tar removal technology in their synthetic natural gas production facility, which converts the syngas from MILENA dual fluidized bed gasifier [47]. The raw syngas first passes through a hot gas filter operating at 450 °C to remove the dust particles. Then the gas is directed to an oil-based gas scrubbing process, OLGA. The concept of OLGA is to selectively remove different classes of tar components from raw syngas, so that the dew point of tar is brought below the minimum temperature observed in the process chain. A classification of tar components for this purpose is given by Bergman et al. [8]. Hence, the key idea of OLGA process is to remove the tar-related problems (fouling), rather attaining a complete removal of all tar components [48]. In OLGA process, the tars are separated, first by condensation of heavy tars by cooling the gas from 450 °C to just above the water dew point and second by absorption of light tars. Since OLGA process is operated above the water dew point, there is no mixing of water and tar and hence a water treatment plant is not needed. An efficient cleaning system should not remove the permanent gases and light hydrocarbons such as methane, acetylene, or ethylene to any appreciable amount, so that the initial cold gas efficiency of the gasifier is maintained during the cleaning sequence, as the case with OLGA process. OLGA system is composed of a collector, absorber, and stripper. Heavy tars and particles are removed in the collector. The oil removes the light tar by absorption and is regenerated in stripper, by using N₂ as stripping medium. A simplified flow sheet of OLGA process is shown in Fig. 18. OLGA also removes other contaminants like thiophene and dioxins from the product gas, besides tar [71]. To remove water and aerosols, the gas passes through a cooler and a filter. Further sulfur removal is done in HDS system operating at 6 bar pressure. It consists of a CoMoO catalyst bed to convert organic sulfur to H₂S. The H₂S is later removed by adsorption on a ZnO bed. An extensive review on different gas cleaning technologies are seen in the literature [15, 43, 56, 57, 67].

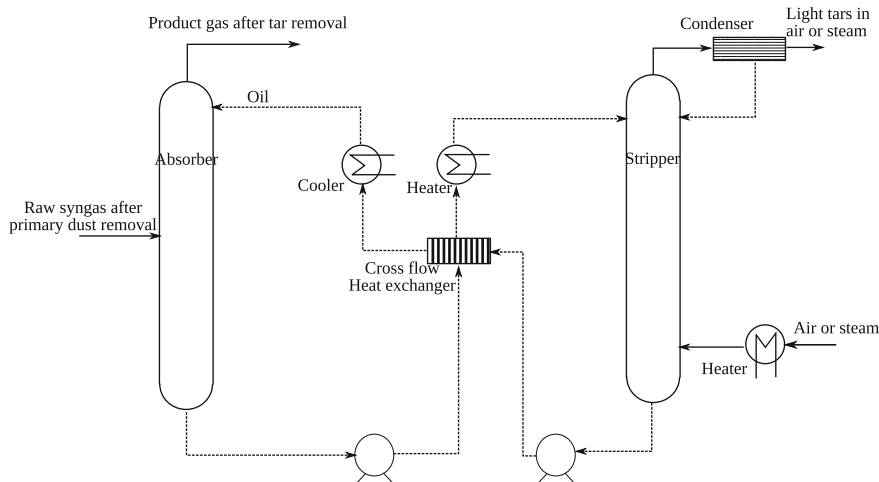


Fig. 18 A simplified flow sheet of OLGA process [71]

6 Tar Reduction

The presence of tar in the product gas is one of the main problems that restrict the commercialization of medium temperature gasification technologies like DFBG. The tar comprises of a wide spectrum of organic compounds, generally consisting of several aromatic rings. It does not pose any major problem in the process as long as it remains in the gas phase. But, if the temperature, anywhere in the syngas process chain falls below the dew point of tar, it initiates the fouling and this ultimately can result in malfunctioning or plugging of the equipment [71], leading to high maintenance cost and frequent operational shutdowns. The photograph of tar fouling in the pipeline and the equipment is shown in Fig. 19.

The methods to reduce tar content in the product gas are divided into two: primary methods and secondary methods. In primary methods, the higher organic compounds

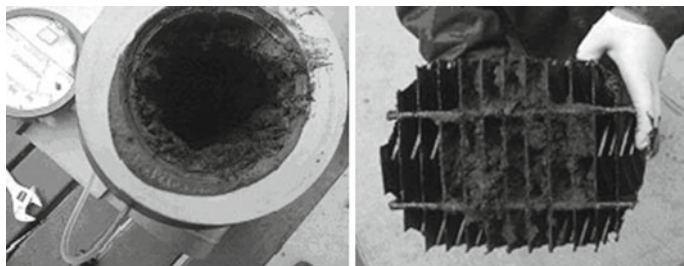
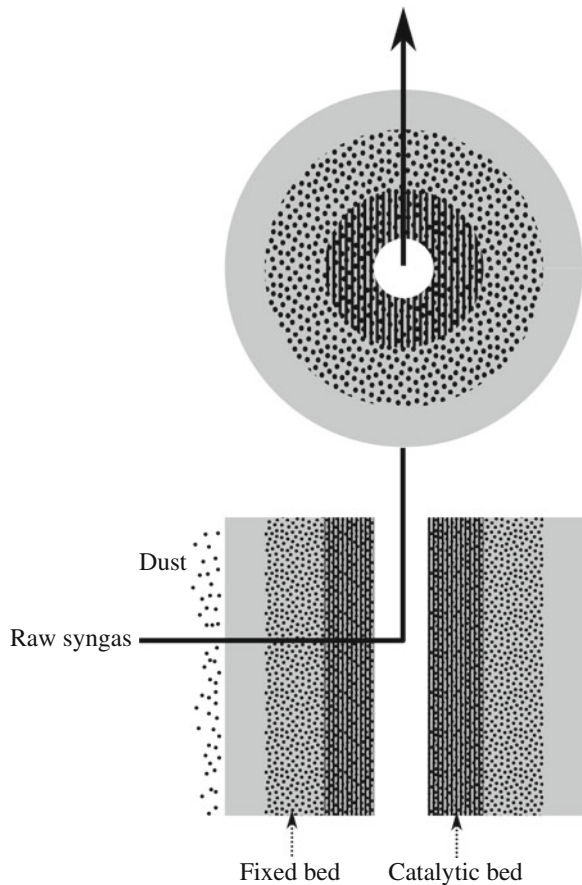


Fig. 19 Fouling of pipeline and equipment due to tar condensation (Reprinted from <http://www.thersites.nl/>, with permission from ECN, Netherlands)

are converted into permanent gas components or smaller organic compounds. They are generally applied with in the gasifier or immediately after the gasifier. The secondary methods comprise of the physical removal techniques of tar, such as water scrubbing, OLGA, RectisolTM, as we have seen in the last section. The primary methods are the most efficient, since the losses of primary heating value of solid fuel is minimum. The secondary methods are applied over and above the primary methods, if the latter is found incapable to achieve the target level of tar reduction.

The gasifier design and operation influence the tar conversion with in the gasifier. For example, the higher gas residence time in the hot region of gasifier results in lesser tar content because of the thermal cracking of higher hydrocarbons. Also, the use of catalytic bed materials reduces the tar content, as already explained in Sect. 4.3. Another novel method to reduce tar content is the installation of candle filters impregnated with reforming catalysts with in the freeboard of the gasifier. Figure 20 shows one such candle filter design. In the experimental facility used by Diego et

Fig. 20 Catalytic candle filter design for insitu tar reduction at the freeboard of bubbling fluidized bed (Adapted from [13], with permission from Elsevier)



al. [13], the candle filters are installed in a reactor just downstream to the gasifier of a DFBG, operating with Fe/olivine bed material. The tar content at the outlet of the candle filter is as low as $0.2 \text{ g/Nm}^3_{(db)}$. Naphthalene is found to be the major tar content at the outlet of the candle filter loaded with Ni catalyst, because it has highest resistance to cracking among the tar components detected [16]. Hence, Naphthalene can be considered as a model compound representing tar, especially in numerical simulation and design of secondary tar removal systems, under such conditions. The activity of the catalysts during continuous operation of the gasifier needs to be further assessed in order to determine its practical implications.

7 Summary and Future Prospects

From the ongoing discussions on various studies reported in this chapter, it is clear that there is no doubt on the technical feasibility of the DFBG process. But the major constraint for commercialization of DFBG plants is the lack of confidence on its economic feasibility. To date, all the DFBG studies are conducted at atmospheric pressure to the best of our knowledge. Numerical simulations show that the main auxiliary power consumption for integrated DFBG operation comes from product gas compression, during the downstream conversion of syngas [62]. Hence, a pressurized DFBG system will improve the net efficiency and also the gasifier capacity.

The steam utilization factor in DFBG is very low, as almost 90% of the steam injected to the gasifier exits unreacted [12]. This results in significant loss of heat and also increases the water treatment load when the tar mixes with water after condensation. The possibility of improved gasifier design for better utilization of steam needs to be investigated further. A gasifier design with better gas–solid contact and longer gas residence time inside the gasifier is expected to bring significant improvements. The next generation fluidized bed gasifier being developed at TU Wien, Austria, is a promising attempt in this regard. In this new design, the gasification reactor is subdivided into a lower bubbling fluidization zone and an upper turbulent fluidization zone, where the hot catalytic bed particles and product gas are in counter current movement [51].

Tar reforming is another important aspect for the further betterment of DFBG technology. Even though a superior gasifier design and use of catalytic bed materials reduce the tar content in the product gas, further conversion of tar and its secondary removal will be necessary especially for smooth downstream operation of gas turbine and synthetic fuel generation. The catalytic hot gas filter is a promising technology in terms of better thermodynamic efficiency, but needs to be further tested under real gasifier conditions. Further studies need to be conducted to explore fuel flexible operation of DFBG using different feedstocks, such as high-ash coals, biomass, waste plastic materials, and their blends.

Acknowledgements The authors would like to acknowledge joint financial support from Ministry of Human Resource and Development and Ministry of Coal under the IMPRINT initiative by Government of India (Project No: MHRD/ME/2016408B, Title: Development of pressurized dual fluidized bed gasifier for high-ash Indian coal)

References

1. Abu El-Rub Z, Bramer EA, Brem G (2004) Review of catalysts for tar elimination in biomass gasification processes. *Ind Eng Chem Res* 43(22):6911–6919. <https://doi.org/10.1021/ie0498403>
2. Alamia A, Thunman H, Seemann M (2016) Process simulation of dual fluidized bed gasifiers using experimental data. *Energy Fuels* 30(5). <https://doi.org/10.1021/acs.energyfuels.6b00122>
3. Alamia A, Larsson A, Breitholtz C, Thunman H (2017) Performance of large-scale biomass gasifiers in a biorefinery, a state-of-the-art reference. *Int J Energy Res*. <https://doi.org/10.1002/er.3758>
4. Basu P, Cheng L (2000) An analysis of loop seal operations in a circulating fluidized bed. *Chem Eng Res Des* 78(7):991–998. <https://doi.org/10.1205/026387600528102>
5. Basu P (2015) *Circulating fluidized bed boilers: design, operation and maintenance*. Springer International Publishing
6. Basu P, Butler J (2009) Studies on the operation of loop-seal in circulating fluidized bed boilers. *Appl Energy* 86(9):1723–1731. <https://doi.org/10.1016/j.apenergy.2008.11.024>
7. Berdugo Vilches T, Marinkovic J, Seemann M, Thunman H (2016) Comparing Active Bed Materials in a Dual Fluidized Bed Biomass Gasifier: Olivine, Bauxite, Quartz-Sand, and Ilmenite. *Energy Fuels* 30(6):4848–4857. <https://doi.org/10.1021/acs.energyfuels.6b00327>
8. Bergman PCA, Van Paasen SVB, Boerrigter H (2002) The novel OLGA technology for complete tar removal from biomass producer gas. In: *Pyrolysis and gasification of biomass and waste expert meeting*. Strasbourg, France
9. Bischi A, Langørgen Ø, Morin J-X, Bakken J, Ghorbaniyan M, Bysveen M, Bolland O (2012) Hydrodynamic viability of chemical looping processes by means of cold flow model investigation. *Appl Energy* 97:201–216. <https://doi.org/10.1016/j.apenergy.2011.12.051>
10. Charitos A, Hawthorne C, Bidwe AR, Korovesis L, Schuster A, Scheffknecht G (2010) Hydrodynamic analysis of a 10kWth Calcium Looping Dual Fluidized Bed for post-combustion CO₂ capture. *Powder Technol* 200(3):117–127. <https://doi.org/10.1016/j.powtec.2010.02.012>
11. Christodoulou Chr, Grimekis D, Panopoulos KD, Pachatouridou EP, Iliopoulou EF, Kakaras E (2014) Comparing calcined and un-treated olivine as bed materials for tar reduction in fluidized bed gasification. *Fuel Process Technol* 124:275–285. <https://doi.org/10.1016/j.fuproc.2014.03.012>
12. Corella J, Toledo JM, Molina G (2007) A review on dual fluidized-bed biomass gasifiers. *Ind Eng Chem Res* 46(21):6831–6839. <https://doi.org/10.1021/ie0705507>
13. de Diego LF, García-Labiano F, Gayán P, Abad A, Mendiara T, Adánez J, Nacken M, Heidenreich S (2016) Tar abatement for clean syngas production during biomass gasification in a dual fluidized bed. *Fuel Process Technol* 152:116–123. <https://doi.org/10.1016/j.fuproc.2016.05.042>
14. Devi L, Ptasinski KJ, Janssen FJJG (2003) A review of the primary measures for tar elimination in biomass gasification processes. *Biomass Bioenergy* 24(2):125–140. [https://doi.org/10.1016/S0961-9534\(02\)00102-2](https://doi.org/10.1016/S0961-9534(02)00102-2)
15. Dou B, Wang C, Chen H, Song Y, Xie B, Yujie X, Tan C (2012) Research progress of hot gas filtration, desulphurization and HCl removal in coal-derived fuel gas: a review. *Chem Eng Res Des* 90(11):1901–1917. <https://doi.org/10.1016/j.cherd.2012.04.009>
16. García-Labiano F, Gayán P, de Diego LF, Abad A, Mendiara T, Adánez J, Nacken M, Heidenreich S (2016) Tar abatement in a fixed bed catalytic filter candle during biomass gasification

- in a dual fluidized bed. *Appl Catal B: Environ* 188:198–206. <https://doi.org/10.1016/j.apcatb.2016.02.005>
17. Glicksman LR, Hyre M, Woloshun K (1993) Simplified scaling relationships for fluidized beds. *Powder Technol* 77(2):177–199. [https://doi.org/10.1016/0032-5910\(93\)80055-F](https://doi.org/10.1016/0032-5910(93)80055-F)
 18. Glicksman LR (1984) Scaling relationships for fluidized beds. *Chem Eng Sci* 39(9):1373–1379. [https://doi.org/10.1016/0009-2509\(84\)80070-6](https://doi.org/10.1016/0009-2509(84)80070-6)
 19. Gómez-Barea A, Ollero P, Leckner B (2013) Optimization of char and tar conversion in fluidized bed biomass gasifiers. *Fuel* 103:42–52. <https://doi.org/10.1016/j.fuel.2011.04.042>
 20. Göransson K, Söderlind U, He J, Zhang W (2011) Review of syngas production via biomass DFBGs. *Renew Sustain Energy Rev* 15(1):482–492. <https://doi.org/10.1016/j.rser.2010.09.032>
 21. Grace JR (1990) High-velocity fluidized bed reactors. *Chem Eng Sci* 45(8):1953–1966. [https://doi.org/10.1016/0009-2509\(90\)80070-U](https://doi.org/10.1016/0009-2509(90)80070-U)
 22. Grace JR, Knowlton TM, Avidan AA (1997) *Circulating fluidized beds*. Springer Netherlands. <https://doi.org/10.1007/978-94-009-0095-0>
 23. Higman C, van der Burgt M (2008) *Gasification*. Elsevier Inc
 24. Karmakar MK, Datta AB (2010) Hydrodynamics of a dual fluidized bed gasifier. *Adv Powder Technol* 21(5):521–528. <https://doi.org/10.1016/j.apt.2010.02.001>
 25. Kern S, Pfeifer C, Hofbauer H (2013a) Gasification of low-grade coal in a dual fluidized-bed steam gasifier. *Energy Technol* 1(4):253–264. <https://doi.org/10.1002/ente.201300009>
 26. Kern S, Pfeifer C, Hofbauer H (2013b) Gasification of wood in a dual fluidized bed gasifier: influence of fuel feeding on process performance. *Chem Eng Sci* 90:284–298. <https://doi.org/10.1016/j.ces.2012.12.044>
 27. Kern SJ, Pfeifer C, Hofbauer H (2013c) Cogasification of polyethylene and lignite in a dual fluidized bed gasifier. *Ind Eng Chem Res* 52(11):4360–4371. <https://doi.org/10.1021/ie303453e>
 28. Kim Y-D, Yang C-W, Kim B-J, Moon J-H, Jeong J-Y, Jeong S-H, Lee S-H, Kim J-H, Seo M-W, Lee S-B, Kim J-K, Lee U-D (2016) Fischer-tropsch diesel production and evaluation as alternative automotive fuel in pilot-scale integrated biomass-to-liquid process. *Appl Energy* 180:301–312. <https://doi.org/10.1016/j.apenergy.2016.07.095>
 29. Kirnbauer F, Hofbauer H (2011) Investigations on bed material changes in a dual fluidized bed steam gasification plant in güssing, Austria. *Energy Fuels* 25(8):3793–3798. <https://doi.org/10.1021/ef200746c>
 30. Kirnbauer F, Wilk V, Kitzler H, Kern S, Hofbauer H (2012) The positive effects of bed material coating on tar reduction in a dual fluidized bed gasifier. *Fuel* 95:553–562. <https://doi.org/10.1016/j.fuel.2011.10.066>
 31. Koppatz S, Pfeifer C, Hofbauer H (2011) Comparison of the performance behaviour of silica sand and olivine in a dual fluidised bed reactor system for steam gasification of biomass at pilot plant scale. *Chem Eng J* 175:468–483. <https://doi.org/10.1016/j.cej.2011.09.071>
 32. Kronberger B, Lyngfelt A, Löffler G, Hofbauer H (2005) Design and fluid dynamic analysis of a bench-scale combustion system with CO₂ separation/chemical-looping combustion. *Ind Eng Chem Res* 44(3):546–556. <https://doi.org/10.1021/ie049670u>
 33. Kunii D, Levenspiel O (1991) Fluidization and mapping of regimes. In: Kunii D, Levenspiel O (eds) *Fluidization Engineering* 2nd edn. Butterworth-Heinemann, Boston, pp 61–94. <https://doi.org/10.1016/B978-0-08-050664-7.50009-3>
 34. Kunii D, Levenspiel O (2000) The K-L reactor model for circulating fluidized beds. *Chem Eng Sci* 55(20):4563–4570. [https://doi.org/10.1016/S0009-2509\(00\)00073-7](https://doi.org/10.1016/S0009-2509(00)00073-7)
 35. Larsson A, Seemann M, Neves D, Thunman H (2013) Evaluation of performance of industrial-scale dual fluidized bed gasifiers using the chalmers 2–4 MW gasifier. *Energy Fuels* 27(11). <https://doi.org/10.1021/ef400981j>
 36. Larsson A, Thunman H, Ström H, Sasic S (2015) Experimental and numerical investigation of the dynamics of loop seals in a large-scale DFB system under hot conditions. *AIChE J* 61(11):3580–3593. <https://doi.org/10.1002/aic.14887>
 37. Levenspiel O (2002) G/S reactor models/packed beds, bubbling fluidized beds, turbulent fluidized beds and circulating (fast) fluidized beds. *Powder Technol* 122(1):1–9. [https://doi.org/10.1016/S0032-5910\(01\)00286-8](https://doi.org/10.1016/S0032-5910(01)00286-8)

38. Lim MT, Pang S, Nijdam J (2012) Investigation of solids circulation in a cold model of a circulating fluidized bed. *Powder Technol* 226:57–67. <https://doi.org/10.1016/j.powtec.2012.04.015>
39. Lim MT, Saw W-L, Pang S (2015) Effect of fluidizing velocity on gas bypass and solid fraction in a dual fluidized bed gasifier and a cold model. *Particuology* 18:58–65. <https://doi.org/10.1016/j.partic.2014.05.007>
40. Mayerhofer M, Mitsakis P, Meng X, de Jong W, Spliethoff H, Gaderer M (2012) Influence of pressure, temperature and steam on tar and gas in allothermal fluidized bed gasification. *Fuel* 99:204–209. <https://doi.org/10.1016/j.fuel.2012.04.022>
41. Van Der Meijden CM (2010) Development of the MILENA gasification technology for the production of Bio-SNG. PhD thesis, Eindhoven University of Technology
42. Nizhou A, Stanmore B, Sharrock P (2013) A review of catalysts for the gasification of biomass char, with some reference to coal. *Energy* 58:305–317. <https://doi.org/10.1016/j.energy.2013.05.057>
43. Paethanom A, Nakahara S, Kobayashi M, Prawisudha P, Yoshikawa K (2012) Performance of tar removal by absorption and adsorption for biomass gasification. *Fuel Process Technol* 104:144–154. <https://doi.org/10.1016/j.fuproc.2012.05.006>
44. Pfeifer C, Rauch R, Hofbauer H (2004) In-Bed catalytic tar reduction in a dual fluidized bed biomass steam gasifier. *Ind Eng Chem Res* 43(7):1634–1640. <https://doi.org/10.1021/ie030742b>
45. Pfeifer C, Koppatz S, Hofbauer H (2011) Steam gasification of various feedstocks at a dual fluidised bed gasifier: Impacts of operation conditions and bed materials. *Biomass Convers Biorefin* 1(1):39–53. <https://doi.org/10.1007/s13399-011-0007-1>
46. Pröll T, Rupanovits K, Kolbitsch P, Bolhàr-Nordenkamp J, Hofbauer H (2009) Cold flow model study on a dual circulating fluidized bed (DCFB) system for chemical looping processes. *Chem Eng Technol* 32(3):418–424. <https://doi.org/10.1002/ceat.200800521>
47. Rabou LPLM, Aranda Almansa G, Van Der Meijden CM, Van Der Drift A (2015) ECN system for methanation (ESME). 23rd European biomass conference and exhibition, no 1–4. Austria, Vienna
48. Rabou LPLM, Zwart RWR, Vreugdenhil BJ, Bos L (2009) Tar in biomass producer gas, the energy research centre of The Netherlands (ECN) experience: an enduring challenge. *Energy Fuels* 23(12):6189–6198. <https://doi.org/10.1021/ef9007032>
49. Schmid JC, Pfeifer C, Kitzler H, Proll T, Hofbauer H (2011) A new dual fluidized bed gasifier design for improved in situ conversion of hydrocarbons. In: International conference on polygeneration strategies. Vienna, Austria
50. Schmid JC, Wolfesberger U, Koppatz S, Pfeifer C, Hofbauer H (2012) Variation of feedstock in a dual fluidized bed steam gasifier influence on product gas, tar content, and composition. *Environ Prog Sustain Energy* 31(2):205–215. <https://doi.org/10.1002/ep.11607>
51. Schmid JC, Müller S, Hofbauer H (2016) First scientific results with the novel dual fluidized bed gasification test facility at TU Wien. In: 24th European biomass conference and exhibition . Amsterdam, The Netherlands, pp 842–846. <https://doi.org/10.5071/24thEUBCE2016-2CV.3.16>
52. Schweitzer D, Gredinger A, Schmid M, Waizmann G, Beirow M, Spörl R, Scheffknecht G (2017) Steam gasification of wood pellets, sewage sludge and manure: gasification performance and concentration of impurities. *Biomass Bioenergy*. <https://doi.org/10.1016/j.biombioe.2017.02.002>
53. Seo MW, Nguyen TDB, Lim YI, Kim SD, Park S, Song BH, Kim YJ (2011) Solid circulation and loop-seal characteristics of a dual circulating fluidized bed: experiments and CFD simulation. *Chem Eng J* 168(2):803–811. <https://doi.org/10.1016/j.cej.2011.01.041>
54. Seo MW, Suh YH, Kim SD, Park S, Lee DH, Song BH (2012) Cluster and bed-to-wall heat transfer characteristics in a dual circulating fluidized bed. *Ind Eng Chem Res* 51(4):2048–2061. <https://doi.org/10.1021/ie200649c>
55. Seo MW, Yun YM, Cho WC, Ra HW, Yoon SJ, Lee JG, Kim YK, Kim JH, Lee SH, Eom WH, Do Lee U, Bong Lee S (2014) Methanol absorption characteristics for the removal of H₂S

- (hydrogen sulfide), COS (carbonyl sulfide) and CO₂ (carbon dioxide) in a pilot-scale biomass-to-liquid process. *Energy* 66:56–62. <https://doi.org/10.1016/j.energy.2013.08.038>
56. Sharma SD, Dolan M, Park D, Morpeth L, Ilyushechkin A, McLennan K, Harris DJ, Tham-bimuthu KV (2008) A critical review of syngas cleaning technologies fundamental limitations and practical problems. *Powder Technol* 180(1):115–121. <https://doi.org/10.1016/j.powtec.2007.03.023>
 57. Sharma SD, Dolan M, Ilyushechkin AY, McLennan KG, Nguyen T, Chase D (2010) Recent developments in dry hot syngas cleaning processes. *Fuel* 89(4):817–826. <https://doi.org/10.1016/j.fuel.2009.05.026>
 58. Shrestha S, Ali BS, Jan BM, Hamid MDB, El Sheikh K (2015) Hydrodynamic characteristics in cold model of dual fluidized bed gasifiers. *Powder Technol* 286:246–256. <https://doi.org/10.1016/j.powtec.2015.04.082>
 59. Shrestha S, Ali BS, Hamid MDB (2016) Cold flow model of dual fluidized bed: a review. *Renew Sustain Energy Rev* 53:1529–1548. <https://doi.org/10.1016/j.rser.2015.09.034>
 60. Douglas Smoot L, Philip Smith J (1985) *Coal combustion and gasification*. Springer, US. <https://doi.org/10.1007/978-1-4757-9721-3>
 61. Sutton D, Kelleher B, Ross JRH (2001) Review of literature on catalysts for biomass gasification. *Fuel Process Technol* 73(3):155–173. [https://doi.org/10.1016/S0378-3820\(01\)00208-9](https://doi.org/10.1016/S0378-3820(01)00208-9)
 62. Tremel A, Becherer D, Fendt S, Gaderer M, Spliethoff H (2013) Performance of entrained flow and fluidised bed biomass gasifiers on different scales. *Energy Convers Manage* 69:95–106. <https://doi.org/10.1016/j.enconman.2013.02.001>
 63. Valin S, Ravel S, Guillaudeau J, Thiery S (2010) Comprehensive study of the influence of total pressure on products yields in fluidized bed gasification of wood sawdust. *Fuel Process Technol* 91(10):1222–1228. <https://doi.org/10.1016/j.fuproc.2010.04.001>
 64. Wilk V, Hofbauer H (2013) Conversion of mixed plastic wastes in a dual fluidized bed steam gasifier. *Fuel* 107:787–799. <https://doi.org/10.1016/j.fuel.2013.01.068>
 65. Wilk V, Schmid JC, Hofbauer H (2013) Influence of fuel feeding positions on gasification in dual fluidized bed gasifiers. *Biomass Bioenergy* 54:46–58. <https://doi.org/10.1016/j.biombioe.2013.03.018>
 66. Wilk V, Hofbauer H (2013b) Co-gasification of plastics and biomass in a dual fluidized-bed steam gasifier: possible interactions of fuels. *Energy Fuels* 27(6):3261–3273. <https://doi.org/10.1021/ef400349k>
 67. Woolcock PJ, Brown RC (2013) A review of cleaning technologies for biomass-derived syngas. *Biomass Bioenergy* 52:54–84. <https://doi.org/10.1016/j.biombioe.2013.02.036>
 68. Xu G, Murakami T, Suda T, Matsuzawa Y, Tani H (2006) The superior technical choice for dual fluidized bed gasification. *Ind Eng Chem Res* 45(7). <https://doi.org/10.1021/ie051099r>
 69. Yerushalmi J, Cankurt NT (1979) Further studies of the regimes of fluidization. *Powder Technol* 24(2):187–205. [https://doi.org/10.1016/0032-5910\(79\)87036-9](https://doi.org/10.1016/0032-5910(79)87036-9)
 70. Zhang J, Rongcheng W, Zhang G, Yao C, Zhang Y, Wang Y, Guangwen X (2013) Recent studies on chemical engineering fundamentals for fuel pyrolysis and gasification in dual fluidized bed. *Ind Eng Chem Res* 52(19):6283–6302. <https://doi.org/10.1021/ie303199g>
 71. Zwart RWR, der Drift A, Bos A, Visser HJM, Cieplik MK, Könemann HWJ (2009) Oil-based gas washing—flexible tar removal for high-efficient production of clean heat and power as well as sustainable fuels and chemicals. *Environ Prog Sustain Energy* 28(3):324–335. <https://doi.org/10.1002/ep.10383>

New Pathways in Clean Combustion of Biomass and Coal via Partial Gasification

H. S. Mukunda and Suresh Attanoor

Abstract This chapter addresses studies conducted on a new approach to clean combustion via gasification process progressing on the earlier work on packed bed reverse downdraft (REDS) combustion. The additional element is the development of continuous combustion device. The studies are aimed at the use of prepared (in terms of size and dryness) biomass in a broad range of densities (100 to 1000 kg/m³) in a newly conceived scalable combustion scheme. The range of power levels includes domestic demands (~ 1 kg/h), semi-industrial needs (3 to 20 kg/h), and larger industrial requirements (50 kg/h and more). System can deliver hot gases at a flame temperature from 1150 to 1200 °C. In domestic stoves, CO emissions are within the permissible limits (CO:CO₂ ratio of 0.006 ± 0.002) and PM2.5 emissions showed incremental steady values of a maximum of 30 µg/m³. An important aspect addressed here concerns the mode of assessment of efficiency and emissions from these stoves. It is suggested that recent expectations of domestic stove emissions need revision in favor of known concepts from other combustion devices. The second part is concerned with the use of coal of permitted ash content (of 21%, but up to 34%) sized to 2–8 mm for thermal applications and clean cold combustible gas applications. Studies on the flame propagation behavior in packed beds in REDS with air show rates about half of that with biomass. With air–steam mixtures, carbon conversion beyond 99% and avoidance of ash fusion are achieved. Operation of the bed with heated coal (~ 120 °C) and air up to 160 °C are considered beneficial to reduce the flaming time and char conversion times. The fixed bed studies provide inputs for evolution to mildly fluidizing strategy for complete conversion of coal without ash fusion.

H.S. Mukunda (✉) · S. Attanoor
Fire & Combustion Research centre, Jain University, Bengaluru, India
e-mail: hsm.cgpl@gmail.com

S. Attanoor
e-mail: sureshattanoor@gmail.com

1 Introduction

Biomass as a source of heat has been used for over several thousand years, even before coal became a source of energy. Its widespread availability has led to use more for fire (known as cooking fire classically) and not flame, the distinction between the two lying in the fact that in the case of fire, air for combustion enters in a free convective manner and in the case of flame, participation of air is controlled by design through the use of a fan or blower. Combustion of solid fuels has been practiced in the last hundred years with increased understanding of the processes. Coal as a fuel was brought in mostly for generating high pressure and high temperature steam that would run steam turbines to generate electricity. Since it is mined in select places, it is transported over distances to power stations distributed over various parts of countries. One of the differences between biomass and coal is that biomass that is grown widely and wastes are also widely distributed with intrinsic densities between 300 to 700 kg/m³ where as coal has much higher density of 1100–1400 kg/m³. Also biomass has ash content of a few percent, but coal has ash content varying from a few percent to as high as 40% (particularly those mined in India). Since transportation depends on liquid fossil fuels, it has been mandated in India legally to limit the ash content to less than 34% by coal beneficiation [17] to enable transportation to what is essential. In the case of biomass, it is particularly important to convert the potential disadvantage of the higher transportation cost associated with their lower density into an advantage by seeking arrangements for their use as much locally as possible.

Over a period of time, expectations have arisen on the clean combustion in domestic combustion systems (stoves) and industrial processes. In the case of domestic systems, limiting the emissions of both PM_{2.5} (particulate matter below 2.5 μm) and CO for combustion systems based on all fuels—gaseous, liquid, and biomass, has been the demand. For industrial systems, limiting the additional emissions of NO_x and SO_x is introduced for systems based on coal and mixed fuels. Mixing biomass wastes with coal has been aimed at limiting the emissions as required by the standards. Seeking higher combustion efficiency of combustion devices and heat transfer efficiency of heat utilization systems (cooking arrangements of high pressure boilers or other industrial arrangements) helps limit the emission of CO₂. The overall efficiency is measured in terms of kWh/kg fuel (typically 1 to 1.5 kWh/kg biomass or coal), larger values implying lower fuel consumption for generating the required energy—electrical or heat and thus lower emission of CO₂. Reduction in the raw fuel used to generate the same output implies reduction in all the emissions. However, these require careful control of combustion processes more difficult to achieve with solid fuels compared to liquid or gaseous fuels. The difficulty arises because fuel related shape, size, moisture fraction, and inorganic content (leading to ash) add additional features to be accounted for. *The most effective approach toward achieving greater efficiency and limiting emissions comes from gasification.*

The use of coal has always been in thermal power stations at several hundreds of MWe generation implying combustion systems at large throughputs (typically, a

hundred MWe generation system burns 60 to 70 tonnes per hour of coal). Reducing the emissions has been conceived through complex downstream clean-up units that can turn out to be very expensive. One strategy to reduce the emissions is to use the gasification approach. Since the conversion process leads to a gas throughput less than half of the burnt-gas throughput, treatment processes become more economical.

Gasification is a controlled process of thermochemical conversion that uses air (can also use oxy-steam oxidant for synthesis gas generation) with the first step leading to a raw or clean combustible gas and the next step involving combustion for heat or electricity generation in internal combustion engines. The process of gasification can be thought of as sub-stoichiometric combustion. When air enters a packed bed of sundry biomass pieces, on ignition, the fuel vapors burn with air to produce products called flaming pyrolysis products that generate a range of intermediate species. Significant amounts of CO_2 , CO , H_2 , and several complex hydrogenated compounds of carbon and hydrogen will get produced. These gases pass through a bed of hot charcoal in which the complex compounds will breakdown to simpler molecules that further react with carbon to produce a mixture of gases that when finally cooled and cleaned lead to a mixture having by volume, nearly equal amounts of CO and H_2 ($\sim 20\%$), and half of that as CO_2 ($\sim 10\%$) and rest nitrogen. This composition will be different if oxy-steam gasification is conducted. With fixed bed downdraft gasification systems, the arrangement of the packed bed will be such that the bed of biomass will later get converted to a bed of charcoal so that the pathway of the gas is consistent with the above description of biomass gasification process. Also when coal of 20 to 25% ash is gasified with air-steam mixture of the best proportions in a fixed bed, one can get a gas similar to air-biomass gasification. This is because coal at this ash fraction is more energetic than sundry biomass.

Depending on the application, it is possible to improve the quality of the combustible gas. When it comes to use in internal combustion engines, minimizing the fraction of most of particulates of all sizes and some higher hydrocarbons (from tens of ppm to a ppm or lower) is needed. Much early work on a novel ambient pressure-based open-top gasification technology for biomass in qualifying the gasification systems [8] for small- and medium-sized reciprocating engines with delivered power levels of 1 to 250 kWe [15] and a high pressure modification for small gas turbines of 30 kWe [16] have been reported. Considerable work on high pressure coal gasification systems have been reported extensively and the current status of the varieties of issues around it are described in the US department of Energy Web site [5].

While one would get an impression that large-scale gasification approaches are the more appropriate choice for current day needs of most countries including India, one challenging aspect concerns the large-scale introduction of solar photovoltaic power generation systems. These are being made cheaper for installation with a promise of much lower tariffs for the electricity generated. Whether this situation is short lived is less important than that it breaks into conventional investment planning processes that may not be very difficult to revive subsequently.

It is in this background that one needs to examine alternatives for the need of biomass and coal in future.

2 New Avenues for Biomass and Coal

It has been known over time that even downdraft biomass gasifiers have been used more for heat application than for electricity. One of the reasons is that the quality of gas demanded by turbocharged reciprocated engines is much higher than for naturally aspirated ones, and this is not easy to achieve. A simpler market to cater to is thermal applications at small to large throughputs and has been achieved significantly in many countries including India. Also as distinct from electricity generation which is pitted against the state in terms of electric supply, delivery of high grade heat (temperatures of 1000 to 1200 °C) through biomass or coal is pitted against fossil fuels—liquefied petroleum gas, high speed diesel, or furnace oil (fuel oil) and enjoys benefits of price of heat including amortization of investment costs being lower. This area has been green in several parts of India for over twenty years. However, over time, there have been challenges even here because the global reduction in the price of the fossil fuels and seeking less expensive solutions /it for delivery of heat from biomass or coal has become attractive in many areas of use. This is where the use of closely coupled gasification–combustion strategy makes much meaning.

Reverse downdraft (REDS) gasification system, otherwise also called top lit updraft (TLUD) is the first of such ideas when used with pellets of high density offers a clean and efficient cooking solution if the pellets are made available at affordable cost. Such a solution is a fire and forget strategy, albeit with moderate power control; it is a batch combustion process. The operational behavior has been characterized by [11–13]. A thorough and insightful investigation of the thermochemical processes and modeling of the operational behavior of biomass-based stoves has been dealt with by [18]. All these studies are limited to air as the oxidant and sized biomass pieces of varying density including pellets for the fuel bed. A very important inference from the studies is that one can achieve the best possible combustion process for solid fuels of various shapes and sizes. The basis of this inference is that the gasification process is a self-limiting thermal conversion process. Pieces of biomass actively involved in the conversion process in the fuel bed can neither generate more nor less than a mean value because the control is provided by heat flux back to the fuel. Greater volatilization demands greater flux than available and lower volatilization is enhanced because of the availability of larger gas phase heat flux controlled dominantly by the flow of air through the bed (superficial velocity discussed in [11, 18, 19]).

Evolution of these ideas into a continuous clean combustion system was tried through several approaches, and finally, it led to a horizontal ejector-based system [10] shown in Fig. 1. Fuel in terms of pieces smaller in size compared to the size of the fuel port (10 to 20 mm for a 1.5 kg/h domestic stove and larger sizes for larger systems) is fed periodically. The initial feed of about a third in height of the combustion zone is placed on the grate and lit using a small amount of kerosene, alcohol, or a gel fuel without the fan being switched on. This is because the air currents cause delayed ignition process. The jets of air maintained at speeds more than 10 m/s cause a low-pressure zone upstream and so, the gases generated due to the gasification

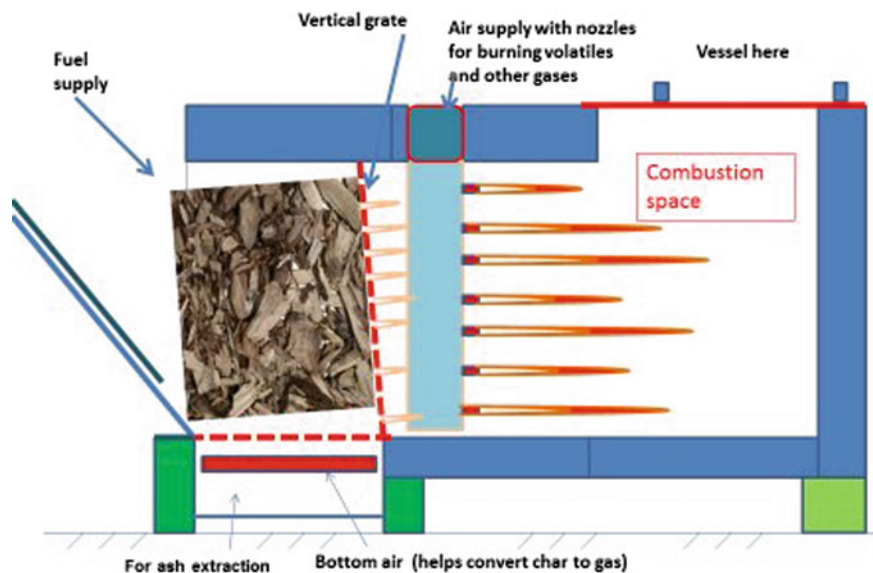


Fig. 1 Depiction of the principles of the horizontal ejector-based system also termed horizontal clean continuous combustion device

process are inducted into the combustion chamber where they burn with the air coming out of the ejector. Part of the air enters the bottom of the grate to help oxidize the carbon of the char left after volatilization. In the steady combustion process, two types of processes occur. The first type relates to the char that rests on the grate being converted to producer gas before entry into the combustion chamber because of the entrainment process. The second part relates to the top of the bed that has some biomass also releasing the volatiles. Part of these volatiles enter the combustion chamber directly due to air induction and burn up in the combustion zone. In view of the combined processes, the total process can be termed quasi-gasification process. The air induction process is such that a significant part of the unburnt gases from the fuel zone get mixed with the air before final combustion occurs much like in a flameless combustion system [7].

Full air supply can be turned on a few minutes after ignition. Then, the top of the fuel bed releases volatiles, and these burn up in the combustion space downstream after mixing with the ejector air that is introduced at speeds of 10 m/s or more through 3- to 4-mm-diameter holes. After about ten minutes during which period the fuel bed generates char over the grate, more fuel can be fed into the fuel space—to fill up the entire space. Allowing a small amount of space near the lip of the fuel port will permit a small amount of air induction. This artifice enables biomass fuels with varying CHNO composition to be burnt in a clean manner. The system will take 10 to 15 mins from ignition time to attain a steady combustion process.

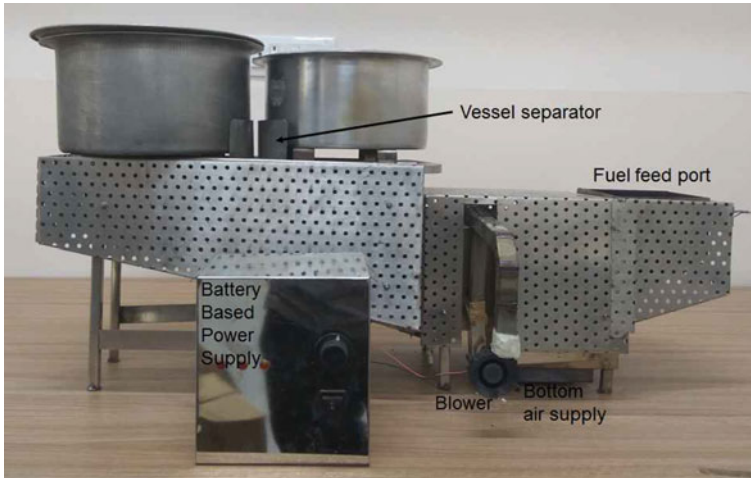


Fig. 2 The two-pan horizontal continuous clean combustion device (HC3D) for domestic use—1.5 kg/h with a 2 W blower operated with a rechargeable battery

The design has been realized at several throughputs—1 kg/h for a single-pan stove and 1.5 kg/h is a two-pan stove that can be seen in Fig. 2, 4 kg/h is a single-pan semi-industrial or larger scale cooking system, 12 to 200 kg/h for steam raising and other industrial applications. One key parameter that governs the design is the allowable mass fuel flux (kg/h m^2) with the reference area being the cross section of the combustion zone. This fuel flux is typically 100 to 300 kg/h m^2 . Larger values imply higher velocities through the entire zone, and this leads to more intense combustion, but larger particulate matter carry over. Thus for domestic applications, the flux must be set at the lowest and for industrial applications in which the hot gas path has opportunity to dump some particulate matter in other zones and allow for a clean exhaust, one can choose larger flux values. In one instance, the design for 20 kg/h has also handled 35 kg/h of pellet fuel.

Figure 3 shows the range of fuels that can be used in the stove. As can be noted from the figure, the packing densities of fuels that can be handled are very wide—from 100 to 700 kg/m^3 . Fuel costs have the same trend as density with lighter fuels being found more easily and the densification process adding to the cost of the fuel. Density of the fuel affects directly the periodicity of the fuel feed. The highest density fuel needs to be fed at nominal power perhaps once in an hour but the lower density fuels every ten minutes or so. Larger systems that are generally for industrial need will have automated feed system. The domestic system at 1 to 1.5 kg/h throughput is in a sense more difficult to be realized since the expectations are different. Clean combustion and continuous operation have to be coupled with reducing the initial cost of the device to ensure affordability of the community expected to benefit from it. Without automation, the limitation is that those who wish to use this device with



Fig. 3 Fuels that can be used in HC3D combustion systems: **a** cut tree droppings along with bark, packing density of 200 to 210 kg/m³, **b** casuarina chopped pieces, packing density of 240 to 280 kg/m³, **c** corncobs, packing density of 200 to 210 kg/m³, **d** cashew shell waste—90 to 100 kg/m³, **e** processed sawdust—cowdung balls, 60 to 80 kg/m³, **f** pellets of a mix of seasonal agro-residues, packing density = 600 kg/m³, ash content of all biomass ≤ 5%

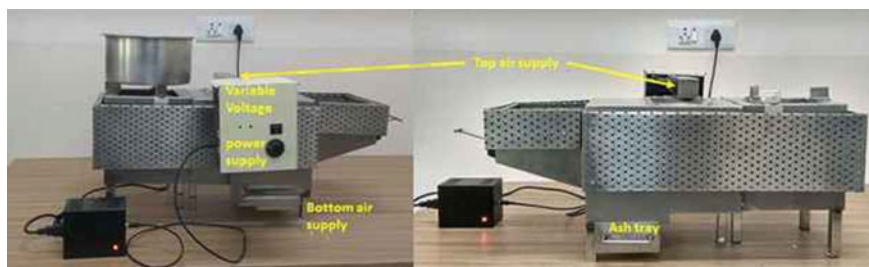


Fig. 4 The single-pan HC3D at 2.5 to 4 kg/h with a 12 W two-stage fan operated with a rechargeable battery

the low density fuel (that may be very cheap) will need to pay much larger attention to fuel feed.

While operational performance has been checked for all the fuels, select tests on efficiency and emission performance have been performed on 10% dry cut pieces of casuarina firewood.

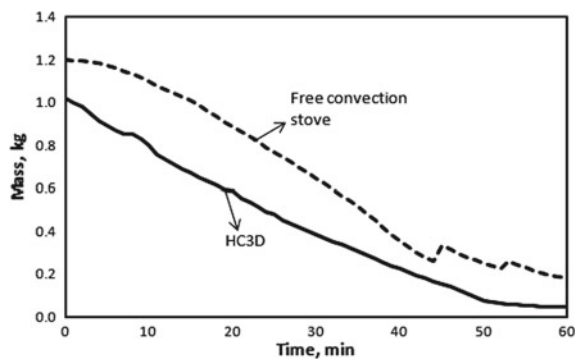
Figure 4 shows the views of a 3.5 kg/h system. In this system, fuel sizes up to 30 mm can be used. It has been also used for cashew shell waste in semi-industrial applications.

3 Efficiency or Flame Temperature as Performance Indicator

Whenever it comes to domestic stoves, water boiling efficiency has been chosen as the criterion to identify better stoves, classically called improved cookstoves. The question being brought up here is whether such an approach that has been adopted world over for over five decades is indeed correct. The issue arises because when the utilization efficiency is the combined effect of combustion efficiency and heat transfer efficiency. In order to combine these two for the purposes of standardization, flat-bottom vessels of specific sizes are prescribed for tests at specific power levels. Such an approach seems to be based on a consideration that combustion technology changes if any, only moderately because most combustion approaches were free convective based till the last decade. The combustion efficiency of such systems has been known to be poor, and energy balance studies show that unaccounted losses are about 30% [14]. These unaccounted losses are essentially due to incomplete combustion caused by large-scale free convective effects (Varun [18]). However, properly designed forced convection system can increase the efficiency by a factor of 2 or more and hence one can deliver more power for cooking. Larger cooking pots can be served with these devices at the same fuel consumption rate. If one were to look at combustion devices in gas turbine engines for instance, while combustion efficiency is still retained as one criterion for performance, a more appropriate one that affects the performance of the system is the temperature distribution at the exit of the combustor. This indicates to the possibility of separating the combustion efficiency from heat transfer efficiency. If one were to determine the temperature vs time in a zone where the flat-bottom vessel will be located at one or several locations across the combustor, one can obtain a very good estimate of the combustion efficiency. Plots of mass loss vs. time and combustor exit temperature from HC3D and a classical free-convective-based stove are set out in Figs. 5 and 6. The corresponding flame pictures from the two stoves are shown in Fig. 7.

As can be noted, HC3D demonstrates a near uniform temperature of $1050 \pm 50^\circ\text{C}$ whereas free convective stove shows fluctuating temperatures between $800 \pm 100^\circ\text{C}$.

Fig. 5 Comparison of mass loss versus time between a forced convection stove (HC3D) and a free-convection-based stove in the market



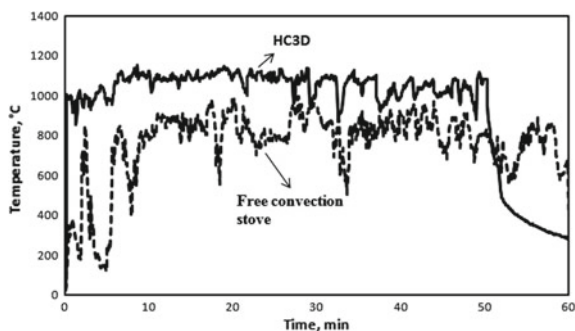


Fig. 6 Comparison of flame temperatures between a forced convection stove (HC3D) and a free-convection-based stove in the market



Fig. 7 Comparison between the flames behavior of a free convection stove and the single-pan forced convection single-pan stove (HC3D design)

The drop in temperature after 50 min with HC3D stove is due to the consumption of 1 kg of the biomass fed. As can be noted in Fig. 5, the mass has dropped to about 80 gms constituting the final char that takes time to get converted due to relatively inferior aero-thermal environment. In the case of free convection stove, this situation is caused some time later.

The difference in the thermal performance between the two cases is due to the fact that fuel generation and air supply are near uniform in HC3D, but widely varying temporally in the free convective stove. Smallest of wind currents around the stove can cause wide changes in the wall temperature-driven free convective ingestion of air into the combustion system. These are directly related to spatial and temporal variation of air-to-fuel ratio and the coupled volatilization variation due to fluctuating heat feed back. This is also the reason why laboratory tests and field tests show substantial differences; one should find much less difference in the case of forced convection stoves. These aspects have rarely been understood or acknowledged in the large cookstove literature. The more recently born global alliance on cookstoves

discusses a wide variety of issues surrounding clean cookstoves [1] with inadequate scientific inputs from solid fuel combustion science.

Based on these ideas, it appears that combustion efficiency and heat transfer efficiency can be decoupled also noting the fact that the use of the combustion system can be for cooking with a variety of vessels and of different diameters even in flat-bottom vessels. In fact, the vessel size dependence on the utilization efficiency has been brought out in [13] in which the efficiency improves by 10% if the diameter of the flat-bottomed vessel increases from 220 mm to 300 mm.

Varun [18] has made detailed studies on the heat balance on the REDS stove and shown that out of the input energy, 58% is the useful heat, 21% goes to lost in the flue gas, and 26% is stored in the body of the stove and lost to the environment.

4 Efficiency and Emissions

The results of efficiency measurements were made in a water boiling tests were made for 1 kg/h system with aluminum vessel of a 6 liter, 270 mm dia vessel using a conventional procedure. Similar tests were conducted for two-pan stove at 1.5 kg/h with aluminum vessels of 220 and 240 mm dia. Efficiencies of 35 to 38% have been measured for both these systems. Emission measurements of CO, CO₂, and NO_x have been made by using a hood arrangement and a flue gas analyzer (FGA 53X Indus system). Also spot mounted instruments were used to make measurements of ambient CO and PM (Optical sensor-based Airveda make with PM2.5 of 0 to 999 μg/m³ and PM10 of 0–1999 μg/m³ with relative errors of ± 10% and ± 10 μg/m³).

Complete combustion was assured through the measurements of temperature and oxygen in the direct exhaust stream. These showed values of temperature between 900 to 1100C and oxygen fraction between 4 and 6% in various experiments performed to clear the stove for other measurements. The measurements using hood need care in obtaining good estimates of the emissions. After a number of experiments with the hood, it was uncovered that to get better estimates of the data, it was useful to reduce the dilution of the hot gases to get lower levels of oxygen in the measured stream and hence better estimates of CO₂ fraction. The results of experiments on 1.5 kg/h two-pan stove that was run for one hour are as follows. Mass ratio, CO₂: Biomass was obtained as 1.75 ± 0.05. Measurement of CO gave CO:CO₂ mass ratio as 0.006 ± 0.0015 and total particulate matter (TPM) obtained from the difference in weight of the fine filter material as 22 ± 3 mg (note that this does not include PM2.5 emissions). Separate measurement of PM2.5 in the domestic and laboratory environment showed background values of 20 to 40 μg/m³ before and much after the experiment. During the experiment, the value went up to 200 μg/m³ during the light up period of a few minutes and dropped to 25 to 30 μg/m³ through rest of the duration. A suggestive estimate of the incremental PM2.5 is 30 μg/m³. This value is being indicated in this manner because the background PM2.5 in most of the Indian kitchens across the country, more particularly in the northern India is actually very much higher than these values [3], and the presence of a clean burning stove makes

little difference to the indoor PM_{2.5} levels (levels indicated in Balakrishnan et al. go up to 1000 $\mu\text{g}/\text{m}^3$).

The results of emissions can be expressed in other terms as well. CO produced in burning 1.5 kg in one hour can be expressed as $1500 \times 1.75 \times 0.006 \text{ g} = 15.75 \text{ g}$; it works out to 262 mg/min; it can also be expressed as 0.6 g/MJ of fuel energy. These results are correct to within 25%. Particulate matter (excludes PM_{2.5}) is 15 mg/kg fuel or 0.36 mg/min or 1 mg/MJ. Of these results, the scale-independent values are CO:CO₂ ratio, mg/MJ data and not the values in terms of emission per minute because this depends on the capacity of the stove (kg/h of burn rate). This is brought up specially because the recent trends in WHO guidelines [20] indicate to permitted emissions of CO and PM_{2.5} in terms of mg/min based on assumptions on air exchange rates in a standard kitchen. The essential problem with these guidelines is that the magnitudes limit indirectly the power rating of the stoves even for the low-emitting stoves. The power level at which the emissions can be met with will be one 0.65 kg/h stove. Family cooking in India occurs for an average of 5 members and needs two single-pan stoves of 650 to 750 g/h or two-pan stove of 1.5 kg/h for about an hour twice daily. This situation may not be universal but sufficiently general. Hence, limiting the emissions in terms of mg/min would artificially and unrealistically limit the cooking operations even with the best stoves. Hence, one option is to continue with the earlier guidelines that had longer time averages of 15 mins for some, 24 hours, and more for others. More appropriately, it appears that the standard guidelines in terms of scalable criteria are better—limiting to meaningful lower levels of CO:CO₂ ratio emissions of CO, PM in terms of mg/MJ, and PM_{2.5} in terms of $\mu\text{g}/\text{m}^3$. The subject of CO emissions has been discussed at length in earlier work on a variety of applications with gaseous fuel for domestic applications [2], and it is clear that CO:CO₂ ratio offers a generality for expecting clean combustion that can be applied even to biomass combustion systems.

On PM_{2.5}, since fine particulate matter is brought into the kitchen by the winds around, the more meaningful criterion for PM_{2.5} should be in terms of mg/m^3 . Also, because of movement of members inside the kitchen, a valid indicator for what will be inhaled is obtained from the local PM_{2.5} concentration.

A further point on the emissions of NO_x in biomass combustion systems is that at the flame temperatures of 1200°C, its generation is insignificant and with respect to SO_x, sulfur present in biomass is so low in most biomass that its generation is also insignificant.

Imposition of new WHO guidelines (in terms of mg/min) coupled with World Bank fiscal support system may actually work against any possibility of improving indoor air quality if the magnitude of cooking and the power of the stove(s) needed to meet the requirement are not factored into the guidelines.

5 Insights from Simple Experiments on Coal and High Density Biomass

Coal with varying ash fraction up to 40% has been used in combustors at particle sizes of 70 to 100 μm . Pulverizing coal to this fine size has been known to consume significant amounts of energy. Alternately, coal in larger sizes—typically upwards of 20 mm has been used in fluid bed combustion systems. Such a route has also been contemplated for gasification of coal. Issues of incomplete conversion of char in the coal as well ash fusion problems have been reported ([4]; Khadilkar [6]). Ash fusion is caused by the presence of potassium, sodium, and iron elements in coal but significantly encouraged by larger residence times and larger particle temperatures. On the other hand, shorter residence times lead to incomplete conversion. Based on these considerations, particle sizes of 3 to 8 mm have been considered as an alternate for gasification aimed at achieving near-complete conversion without ash fusion.

Since particle temperatures that matter in the conversion process depend on the flow of oxidizer rich gases around the particles, it was decided to adopt the packed bed approach like the reverse downdraft system (REDS) used for biomass (see Sect. 2) to understand the behavior of a packed bed of coal particles of the above size range. Figure 8 shows the schematic of the experimental setup. The reactor with 73 mm internal diameter and 170 mm length is made of 2-mm-thick mild steel shell insulated outside with alumino-silicate wool blanket. It has four thermocouples inserted laterally at a spacing of 34 ± 2 mm. Steam was generated in an electrically heated boiler to get steam at about 105 to 110°C and led through a valve to a mixing

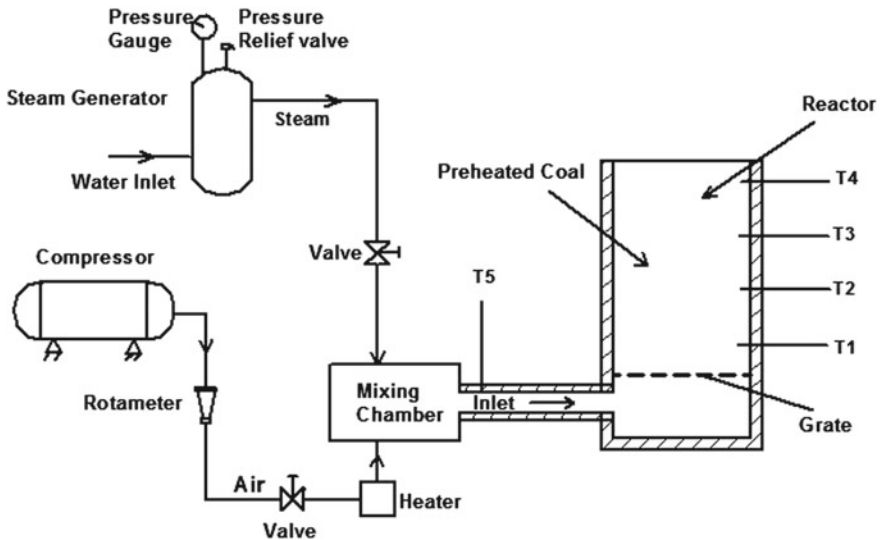


Fig. 8 Schematic of the apparatus for measuring flame propagation in packed bed of coal and wood pieces

Table 1 Performance behavior of biomass (wood and coconut shell pieces) and coal in REDS; Wd-o = wood in spheres, Cnut-sh = coconut shell pieces; coal size—see Fig. 10; Sup. vel = Superficial velocity m_{ini} = initial mass and m_{fin} = final mass

Property	Wd-o	Cnut-sh			Coal			Units
ρ_f	615	850			1250			kg/m ³
Size,	11	6–8			3, 8			mm
Moisture	10	10			7			%
Ash	1	1			21			%
Volatiles	74	74			29			%
Fixed carbon	15	15			43			%
	Air				Steam–air			
Sup. Vel	19	19	5.7	19	28	43.9	68	cm/s
T_{air}	28	155	140	150	155	170	170	°C
Fuel flux	155	470	126	728	960	800	604	kg/h m ²
m_{ini}	144	200	370	285	316	288	292	g
m_{fin}	2	2	81	61	75	70	62	g
\dot{r}	0.35	0.37	0.17	0.2	0.2	0.18	0.17	mm/s
$\rho_p \dot{r}$	300	311	212	250	250	225	212	kg/h m ²
ρ_{char}	185	342	800	736	729	777	711	kg/m ³
Steam fr.	–	–	–	–	–	0.29	0.31	–
Steam:air	–	–	–	–	–	0.25	0.27	–

chamber. Air heated to 150 to 180 °C in a separate arrangement was also led into the mixing chamber through a valve. This arrangement allowed the reactant stream to be monitored for its temperature (T_5) and led into the bottom of the reactor. The mixed hot gas stream would pass through the holes (2–3 mm dia) of a perforated stainless steel plate acting as a grate and pass through the bed. The coal used in these experiments had an ash content of 21%. The oxidants tested were air at ambient temperature and air or air–steam combination at temperatures of 130–150 °C. In actual experiments, wood spheres, coconut shell pieces, and sized coal whose proximate analysis set out in Table 1 are loaded into the reactor. On the top of test bed, fine pieces of biomass about 20 g were loaded. This was ignited with a sprinkle of kerosene, and after about a minute, bottom air was turned on to a specific superficial velocity. The system would acquire steady burning in about six minutes, and the conversion process lasted about 25 min.

The flame propagated downward in a direction opposite to the flow of the oxidant. After the flame reached the bottom during which period the coal would loose volatiles and the char left behind for the flame to get reversed. This phenomenon is the same as what would happen in the case of biomass. The bed height would continuously reduce due to volume reduction consequent upon the loss of volatiles and finally, with biomass, char would occupy 30% mass and similar height, with coal the

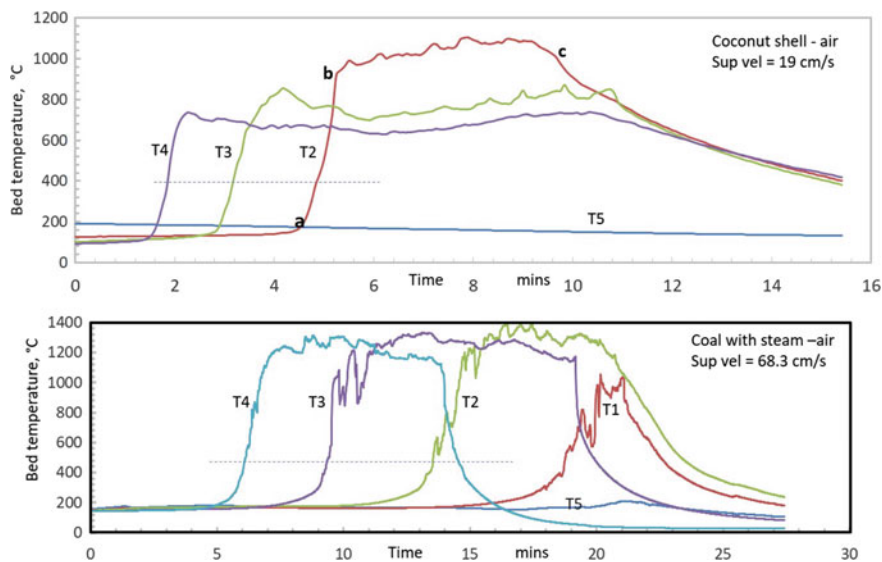


Fig. 9 Temperature vs. time at various locations in the packed bed

height reduction as well as weight reduction would be about 70%. The conversion of char would occur at near-constant temperature depending on the oxidant.

Initial experiments were conducted with ambient temperature coal and ambient air at superficial velocities between 5 and 6 cm/s. These showed that ash had fused into significant small lumps. It was argued that if coal was heated to a temperature below the point of significant evolution of volatiles, the conversion process time could be reduced. After tests, it was concluded that heating it 120 °C, there was significant evolution of volatiles and so it was decided that heating the coal to 100 °C would be satisfactory. Also air or air–steam mixtures would be maintained at higher temperatures up to 150 °C. Increase in superficial velocity with air increased the possibility of ash fusion. Peak temperatures would go up to 1600 °C, and this would inevitably lead to ash fusion problems. Therefore, it was decided to limit the peak temperatures by using air–steam mixtures. This would also enable gas composition to improve. Several experiments on this were also conducted. The fraction of steam in air–steam mixture was varied over a few tests. Broken coconut shell pieces and pellets of high density were also used in these experiments to see possible differences in the conversion behavior. Figure 9 shows the plots of temperature vs. time for experiments with coconut shell with air and coal with steam–air mixture. Point “a” is the start of the flame arrival at the location of the fuel, point “b” is the completion of the ignition process, and point “c” is the completion of the conversion process. Then onward there is a decay of temperature due to dominant cooling process caused by the flow of air through the system. Flame propagation rate can be estimated by the arrival of a specific isotherm at the different locations. The time difference between thermocouples at T4, T3, and T2 are 80 and 100 s. For distances between thermo-



Fig. 10 Coal pieces, hard ash (with some unconverted carbon), and soft ash found in the experiments

couples of 33 and 35 mm, we get propagation rates as 0.4 mm/s and 0.35 mm/s. An average value over the entire distance is 0.366 mm/s. A similar calculation for coal with steam at the conditions of the experiment shows the propagation rate as 0.17 mm/s. This implies that coal is much less reactive than biomass. Part of this feature is related to the fact that biomass has 75% volatiles whose conversion is due to gas phase reactions and coal that has 27% volatiles takes longer to convert because the solid char to gas conversion is slower.

The total conversion time for the mass introduced into the experiment for coal is 17 mins (1120 s) for the coal bed starting from thermocouple T4. This magnitude is 220 g. Thus, the mass conversion rate is 0.2 g/s. Each particle takes 0.4 s to get converted considering that each gram has on the average 13 pieces of mean size of $3\text{ mm} \times 8\text{ mm}$. This result is useful in the design of the reactor of a fluid bed kind. Table 1 provides the details and results of the experiments conducted on specific biomass and coal.

The results set out in this table have several features of interest. It is useful to recognize the well-known differences in density, volatile fraction, and ash content. The material that was left behind after the experiment on coal is about 21%, the measured ash fraction of the coal samples used. This implies that the conversion has been nearly complete. The regression rate at the superficial velocities considered here has remained nearly constant at around 0.18 ± 0.01 mm/s.

A very important inference from the experiments is that with air alone at higher superficial velocities, ash fusion appeared to be hard. It was inferred that this was related to peak temperatures going up to 1600 °C. However, with steam–air as the fluid, the temperatures were limited to 1300 °C with occasional peak touching 1400 °C as can be noted in Fig. 9. In these cases, the ash was soft even if packed and would break up when handled gently. Figure 10 shows the broken coal pieces used in the experiments, the hard fused ash in experiments with air at superficial velocity of 28 cm/s, and the broken soft ash from steam–air experiments at superficial velocity of 68 cm/s. At this condition, the bed appeared to be gently buoyant. The converted ash pieces would fly off from the reactor. Yet, the final condition was such that the process could not be sustained except as a batch process. It was inferred that it was

necessary to keep the particles separated so that ash fusion could be avoided. In fact, experiments with a reactor with increased height but with superficial velocity of 90 to 100 cm/s, the entire bed remained in an incipient fluidized condition.

6 Fluid Bed as an Extension of Packed Bed

A number of preliminary experiments were conducted to determine the operability of high density mildly fluidizing gasification systems for coal. These indicated that at superficial velocities of 1.2 to 1.4 m/s, the packed bed would be expanded by about 25% and as conversion proceeded, the lighter particles would in fact be thrown out. With an attached cyclone the hot gas bereft of particulate matter could be delivered. This system when attached to cooling and fine cleaning systems similar to those developed for biomass gasification systems (see [9]) would help getting engine consistent clean gas. Further work with respect to coal is a part of a separate document.

7 Summary

This chapter has addressed the work on a horizontal gasification-based combustion system for biomass for domestic and industrial applications. It is based on exploiting much of clean combustion that comes from reverse downdraft gasification strategy. The horizontal induced draft gasification-based approach is shown to lead to clean combustion over a range of throughputs from 1 to 200 kg/h. This scalability of the approach allows extension to even larger power levels.

The device emissions for domestic applications are indeed low as measured in terms of CO:CO₂ and total particulate matter as well as PM_{2.5}. It is suggested that efficiency is best assessed by separating combustion efficiency from heat transfer efficiency. Measuring the combustion system exit temperature profile and relating the delivered heat to the heat of combustion of the fuel will provide the combustion efficiency. The classical water boiling test with vessels similar to the ones used in practice will provide the overall efficiency. Improvements required on combustion and heat transfer can be separately addressed, a feature that has not been practiced in stove developments till now. Reduction in particulate emissions (including PM_{2.5}) can be achieved with lower throughput flux as the design parameter (of the order of 100 to 120 kg/h m²).

Conduct of flame propagation through packed bed of coal similar to REDS has indicated that the overall rate of conversion is much lower for coal than for biomass—about half the rate of biomass for 21% ash coal. While near-complete conversion has been possible with steam–air mixtures, prevention of ash fusion is possible in bubbling fluid bed operation with superficial velocities of 1.2 to 1.4 m/s enabling separation of particulate matter and extraction through an attached cyclone.

Acknowledgements The authors are grateful to the foundation for energy with advances sustainable technologies (FEAST) for permission to publish this paper and the authorities of Jain University for encouragement to work in this area. Patent has been filed in India, and PCT application has been filed on HC3D technology.

References

1. ACS, Alliance on cook stoves. <https://cleancookstoves.org/>
2. Advantica (2017) Combustion performance safety action levels for domestic gas appliances, Report R5205, 2002. <http://www.hse.gov.uk/gas/domestic/pdf/safetyactionlevels.pdf>, Also see <http://gb-gas.co.uk/gb-gasQuickReferenceGuide2016version2.pdf>
3. Balakrishnan K, Ghosh S, Ganguli B, Sambandam S, Bruce N, Barnes DF, Smith KR (2013) State and national household concentrations of PM_{2.5} from solid cookfuel use: results from measurements and modeling in India for estimation of global burden of disease. *Environment Health* 12:77
4. Hatt R (2017) Understanding boiler slag. <https://www.coalcombustion.com/pdf/PresentationsPDFs/Understandingboilerslag.pdf>
5. Intnet1 (2017) <https://energy.gov/fe/science-innovation/clean-coal-research/gasification>
6. Khadilkar AB, Rozelle PL, Pisupati SV (2015) Effect of heterogeneity in coal ash chemical composition on the onset of conditions favorable for agglomeration in fluid beds. *Energies* 8:12530–12545
7. Kumar S, Paul PJ, Mukunda HS (2002) Studies on a new high intensity low emission burner. In: *Proceedings of Combustion Institute*, vol. 29, pp 1131–1137
8. Mukunda HS, Paul PJ, Dasappa S, Shrinivasa U, Rajan NKS, Sharan H, Beuhler R, Hasler P, Kaufmann H (1994) Results of an Indo-Swiss programme for qualification, and testing of an 300 kW IISc-Dasag Gasifier. *Ener Sustain Dev* 1:46–49
9. Mukunda HS, Dasappa S, Paul PJ, Rajan, NKS., Shrinivasa U, Sridhar G, Sridhar HV (1997) Fixed bed gasification for electricity generation, Published in *Biomass Gasification and Pyrolysis: State of the Art and Future prospects*, Eds: Kaltschmitt K Bridgwater AV, CPL Press, UK
10. Mukunda HS (2015) New approach to clean combustion of solid fuels with varying properties, Internal report-01, FEAST, 2015; also see Progress report on the research, development and outreach on HC³D - 2015 to 2017. Both can be Accessed at www.feastenergy.com
11. Reed TB, Larson R (1996) A wood-gas stove for developing countries. *Energy for sustainable development* 3:34–37
12. Reed TB, Walt R, Ellis S, Das A, Deutch S (1999) Superficial velocity—the key to downdraft gasification. In fourth biomass conference of teh Americas, Oakland, USA, pp 343–356
13. Mukunda HS, Dasappa S, Paul PJ, Rajan NKS, Yagnaraman M, Ravikumar D, Deogaonkar M (2010) Gasifier stove—science, technology and outreach. *Curr Sci* 98:627–638
14. Sharma SK (1993) Improved solid biomass burning cookstoves, a development manual, Regional Wood energy development programme in Asia, Tech Report 44, FAO Field document
15. Sridhar G, Paul PJ, Mukunda HS (2001) Biomass derived producer gas as a reciprocating engine fuel—an experimental analysis. *Biomass Bioener* 21:61–72
16. Sridhar HV, Sridhar G, Dasappa S, Paul PJ, Mukunda HS (May 2007) On the operation of a high pressure biomass gasifier with gas turbine. In: 15th European Biomass conference & exhibition, Berlin, Germany
17. Zamuda CD, Sharpe MA (2007) A case for enhanced use of clean coal in India: an essential step towards energy security and environmental protection, Workshop on coal beneficiation and utilization of rejects, Ranchi, India, August 22–24, Accessed from https://www.fe.doe.gov/international/Publications/Coal_Beneficiation_Workshop/coal_beneficiation_paper_zamuda.pdf

18. Varunkumar S (2012) Packed bed gasification-combustion in biomass based domestic stoves and combustion systems, Ph. D Thesis, Indian Institute of Science
19. Varunkumar S (2013) Rajan NKS, Mukunda HS Universal flame propagation behavior in packed bed of biomass. *Combust Sci Technol* 185:1241–1260
20. WHO (2014) http://www.who.int/indoorair/guidelines/hhfc/recommendation_1/en/

Synergistic Effects in Gasification of Coal/Biomass Blends: Analysis and Review

Debarshi Mallick, Pinakeswar Mahanta and Vijayanand S. Moholkar

Abstract Electricity generation through coal–thermal route is one of the highest contributors to environment pollution through greenhouse gas emission, which has given rise to issue of climate change risk. Among different alternatives of renewable energy, an important source is biomass-based energy. Utilization of biomass for energy production in coal-fired power plants is essentially in terms of partial substitution of coal feed with biomass. Major challenge in this route is fluctuating supply and varying compositions of biomass. It can be overcome by adopting co-gasification technology (using mixed feed of biomass and low-grade coal) for power generation. In this chapter, we have presented a critical review and analysis of the literature in the area of co-gasification of biomass and coal. Analysis in this paper touches upon several facets of co-gasification process such as effect of biomass/coal ratio, the composition (proximate/ultimate analyses of biomass/coal), gasification media, temperature and heating rates on the gasification kinetics, producer gas composition, and yield. The synergistic effects between gasification of coal and biomass have been reviewed. The alkali/alkaline earth metal content in the ash of biomass catalyzes the kinetics of the gasification of coal char. However, if coal has high silica content, adverse reaction between silica and potassium oxides can deactivate the catalytic effect. Actual chemical mechanisms related to this synergy have also been described and discussed. Finally, a brief review of the literature on gasification of coal/biomass blends in bubbling/circulating fluidized bed gasifiers has also been presented.

D. Mallick · P. Mahanta

Department of Mechanical Engineering, Indian Institute of Technology Guwahati, Guwahati 781039, Assam, India

P. Mahanta · V. S. Moholkar

Center for Energy, Indian Institute of Technology Guwahati, Guwahati 781039, Assam, India

V. S. Moholkar (✉)

Department of Chemical Engineering, Indian Institute of Technology Guwahati, Guwahati 781039, Assam, India
e-mail: vmoholkar@iitg.ernet.in

Keywords Biomass • Coal • Co-gasification • Renewable energy
Synergistic effect

1 Introduction

The global demand for energy is on the rise, while the fossil fuel reserves, which are the major sources of primary energy, are limited and fast depleting. Presently, around 80% of the primary energy is obtained from conventional fossil fuels, viz. oil, natural gas, and coal [1]. Oil and natural gas have been the source of transportation fuel, while coal has been essentially utilized for electricity generation. However, the natural reserves of fossil fuels have been depleting fast. At the present rate of consumption, the oil and gas resources may not last for more than 50–60 years; whereas the coal may be available for another maximum 200 years [2]. Among the fossil fuel, coal meets 29% of global primary energy need and 39% of global electricity requirements [3]. Coal is the main commercial energy fuel in India, amounting to ~59% of installed electrical capacity in 2017 [4]. However, Indian coal is of low quality (due to high ash content) and low calorific value [5] and so it cannot be utilized efficiently. Another major concern associated with the usage of coal is the emissions. Fossil fuel combustion accounts for about 75% of total greenhouse gas (GHG) emissions, and combustion of coal alone accounts for 30–40% of the share of GHG from fossil fuels combustion [6, 7]. Hence, the coal utilization deserves special attention given the likelihood of continued use for electricity production. In this context, utilization of renewable energy sources in a planned and strategic way may serve as a potential approach to minimize the gap between demand and supply of required energy. Among all the sources of renewable energy, biomass is likely to become an important source owing to its availability worldwide in large amount. The utilization of biomass can reduce the CO₂ footprint to the environment. But the major challenge is the availability of a single type of biomass due to seasonal fluctuations, variations in organic compositions, and thermal conversion efficiency. However, implementation of co-gasification technology for power generation will benefit to overcome these challenges. This concept has received wide attention of researchers, and large amount of the literature has been published in this area. The basic idea underlying the co-gasification is synergistic effect of the alkali and alkaline earth metals present in the biomass for enhancing the gasification of the char resulting from coal pyrolysis. This synergistic effect not only enhances the energy efficiency of the process due to complete gasification of the feedstock, but also alters the composition of the producer gas resulting from the feedstock [8]. Another added advantage of this process is the reduction in tar content of producer gas, which makes the gas suitable for applications in engines. The most crucial merit of co-gasification is reduction of GHG emissions, ecofriendly, and also current utilization of low-grade coal.

This chapter touches upon several facets of co-gasification process, viz. the effect of operational parameters of biomass/coal ratio, the composition of biomass and coal, gasification media, equivalence ratio, temperatures of gasification and heating rates on the gasification kinetics, producer gas composition, and yield. In addition, the passive and active synergistic effects in co-gasification process are briefly discussed.

2 Composition of Coal and Biomass

The gasification behavior of carbonaceous material like coal and biomass is a major function of their compositions. The composition of carbonaceous material is evaluated in terms of proximate and ultimate analyses. Ultimate and proximate analyses of different coal and biomass species used as feedstock for gasification are summarized in Table 1. The major distinction between compositions of coal and biomass is in terms of the volatile matter, fixed carbon, and ash. Biomass contains more volatile matter, while coal has more fixed carbon. So, during co-gasification of coal and biomass blend, higher release of carbon-containing compounds is expected in comparison with gasification of coal alone. In general, H₂ content in biomass is more which makes it suitable as a blend to compensate the low H₂ content of coal. Biomass as gasification feedstock has the disadvantage of low energy density due to its high oxygen and moisture content, although it giving high hydrogen yield. Compared to coal, a relatively low sulfur and nitrogen contents of biomass imply a lower amounts of H₂S, NH₃, and HCN are expected during co-gasification. Different compositions of coal and biomass also affect the thermodynamic efficiency of the co-gasification process. Biomass usually contains higher O/C ratio, which is suitable for gasification as it enhances the reactivity at lower temperatures and also lowers the amount of oxygen required to be added for the process.

The ash content of coal is higher than biomass. Another interesting distinction between compositions of biomass and coal is in terms of the composition of ash. The ash in the coal primarily comprises of silica (SiO₂) and alumina, whereas the ash in biomass has significant quantities of alkali and alkaline earth metals (>40%), in the form of K₂O and CaO [9, 10]. The components of ash contents in biomass and coal are summarized in Table 2.

As compared to coal, the biomass has large oxygen content. On the contrary, coal has relatively higher carbon content than biomass. Another distinct difference between composition of coal and biomass is that coal has higher sulfur content (depending on the origin of coal). The nitrogen content of coal and biomass, however, is almost similar. Higher oxygen content of lignocellulosic biomass is attributed to its basic chemical structure. The biomass has “lignocellulosic composition” in that it has three main components, viz. cellulose, hemicellulose, and lignin. Cellulose is the linear polymer comprising glucose units linked by β-glycosidic linkages. The hydroxyl groups present in the cellulose impart it an ordered

Table 1 Ultimate and proximate analyses of different coal and biomass [8]

Biomass	Ultimate analysis (db.% w/w)					Proximate analysis (% w/w)					LHV (MJ/kg)
	C	H	O	N	S	Ash	VM	FC	M		
Rice husk	35.20	4.79	59.00	1.01	–	9.40	66.12	13.80	10.65	13.12	
Bamboo dust	43.45	5.49	50.74	0.33	–	2.68	70.83	15.62	10.87	14.85	
Wood sawdust	42.30	5.17	51.73	0.80	–	1.40	69.29	17.84	11.37	12.86	
Cedar wood	51.10	5.90	42.50	0.12	0.02	0.30	80–82	18–20	–	19.26	
Olive oil residue	50.70	5.89	36.97	1.36	0.30	4.60	76.00	19.40	9.50	21.20	
Rice straw	38.61	4.28	37.16	1.08	0.65	12.64	65.26	16.55	5.58	14.40	
Pine sawdust	50.54	7.08	41.11	0.15	0.57	0.55	82.29	17.16	–	20.54	
Spruce wood pellet	49.30	5.90	44.40	0.10	–	0.30	74.20	17.10	8.40	18.50	
Marc of grape	49.66	5.56	34.42	2.23	0.14	7.83	65.77	26.40	–	19.51	
Coffee husk	46.80	4.90	47.10	0.60	0.60	1.00	74.30	14.30	10.40	16.54	
Coffee ground	52.97	6.51	36.62	2.80	0.05	1.00	71.80	16.70	10.50	22.00	
Larch wood	44.18	6.38	49.32	0.12	–	0.12	76.86	14.86	8.16	19.45	
Grapevine pruning waste	46.97	5.80	44.49	0.67	0.01	2.06	78.16	19.78	–	17.91	
Jute stick	49.79	6.02	41.37	0.19	0.05	0.62	76–78	21–23	–	19.66	
Sugarcane bagasse	48.58	5.97	38.94	0.20	0.05	1.26	67–70	29–31	–	19.05	
Corn cob	40.22	4.11	42.56	0.39	0.04	2.97	71.21	16.11	9.71	16.65	
Peach stone	51.97	5.76	40.70	0.79	0.01	0.65	81.30	18.10	8.53	21.60	
Wheat straw	46.10	5.60	41.70	0.50	0.08	6.01	75.80	18.10	–	17.20	
Cotton stem	42.80	5.30	38.50	1.00	0.20	4.30	72.30	15.50	7.90	15.20	
Straw	36.55	4.91	40.70	0.55	0.14	8.61	64.98	17.91	8.50	14.60	
Camphor wood	43.43	4.84	38.53	0.32	0.10	0.49	72.47	14.75	12.29	17.48	
Beech wood	48.27	6.36	45.20	0.14	–	0.80	81.00	18.00	–	19.20	
Switchgrass	47.00	5.30	41.40	0.50	0.10	4.60	58.40	17.10	20.00	18.70	

(continued)

Table 1 (continued)

Biomass	Ultimate analysis (db.% w/w)				Proximate analysis (% w/w)				LHV (MJ/kg)	
	C	H	O	N	S	Ash	VM	FC		M
Petroleum coke	92.30	3.40	0.70	0.95	1.17	1.40	6.00	92.10	0.50	36.20
Lignite coal	44.66	3.66	13.90	1.0	0.21	18.42	35.17	28.27	18.4	18.05
Bituminous coal	74.73	4.43	13.68	1.02	0.19	4.08	36.95	56.90	2.07	28.05
Lean coal	66.05	3.25	2.53	1.17	0.19	25.30	20.65	53.15	0.92	24.14
Qunsam mine coal	80.30	5.50	12.60	0.9	0.70	12.90	38.80	49.10	4.20	26.99
Sub-bituminous coal	73.10	4.30	21.10	1.0	0.40	30.50	31.30	38.30	17.5	20.10
Indonesian coal	72.13	6.67	19.58	1.40	0.22	8.39	36.84	42.36	12.42	20.79
Anthracite coal	86.56	4.90	6.20	1.70	0.61	13.71	31.71	54.58	0.34	26.00
Shennu coal	70.35	4.56	10.53	1.04	0.55	9.19	28.51	58.52	3.78	27.08
Assam coal	61.37	5.27	28.18	0.94	4.24	10.0	40.50	47.50	2.00	22.55

Table 2 Ash composition analysis of biomass and coal (wt%) [8]

Fuel	SiO ₂	Al ₂ O ₃	CaO	Fe ₂ O ₃	K ₂ O	MgO	Na ₂ O	P ₂ O ₅	TiO ₂	SO ₃
Switchgrass (Manitoba, Canada)	52.50	2.10	6.40	0.30	20.30	6.50	1.60	5.00	0.02	2.60
Rice straw (Hubei Province, China)	51.99	0.91	7.68	0.84	17.61	2.33	0.96	2.49	0.04	6.50
Sawdust (Hubei Province, China)	16.47	6.50	24.89	4.57	7.76	5.56	12.84	2.42	0.58	7.64
Pine biomass (Statoil, Norway)	12.80	1.00	33.00	1.70	23.20	5.40	1.70	5.30	–	–
Sub-bituminous coal (Genesee, Alberta, Canada)	57.60	23.60	5.60	2.80	0.80	1.30	2.60	0.10	0.50	2.30
Lignite coal (Inner Mongolia, China)	65.79	14.73	4.33	2.67	1.71	1.44	1.04	0.97	0.50	6.67
Bituminous coal (NSW, Australia)	47.90	26.50	7.90	7.50	0.20	0.60	0.10	1.30	1.90	6.10
Lean coal (Inner Mongolia, China)	53.99	28.44	4.07	3.22	1.56	0.88	2.97	0.97	1.82	4.00

linear and crystalline structure due to intermolecular and intramolecular hydrogen bonds.

Hemicellulose is also a polymer with branched structure comprising pentose sugars (such as xylose) as monomer units. Other pentose sugars may also be present in the hemicellulose structure. These structural facets, heterogeneous in nature, result in relatively amorphous structure of hemicellulose, as compared to cellulose. Lignin is essentially an aromatic polymer comprising of three basic units, viz. p-coumaryl alcohol, coniferyl alcohol, and sinapyl alcohol. Lignin has hydrophobic and amorphous character, and the basic units of lignin linked to hemicellulose with covalent cross-linkages also result in embedding of cellulose fiber chains.

Coal does not have a well-defined structural composition like biomass. The principal organic components, which make up coal, are: maceral groups (vitrinite, liptinite and inertinite), inorganic minerals and moisture [11]. The hydrogen and oxygen contents of coal are very low, and the structure is very complicated and random. The grades of coal are decided by the carbon content. Higher carbon coals are essentially anthracite or bituminous coal, while lignite is relatively low-carbon-containing coal. Lignite coal has the highest oxygen content.

3 Catalytic Activity in Gasification

The key motive for co-gasification is the catalytic effect of alkali and alkaline earth metals in biomass on enhancing the gasification of char resulting from coal pyrolysis, which otherwise has slow kinetics. Coal ash has high silica (SiO_2) content, which is an efficient catalyst for cracking heavy hydrocarbon molecules. As compared to coal, pyrolysis of biomass results in significantly higher quantities of tar due to higher content of volatiles. SiO_2 in coal char can catalyze the thermal decomposition of these heavy hydrocarbons into lighter hydrocarbons such as methane or ethane. This results in enhancement of calorific value of the producer gas resulting from pyrolysis.

Inorganic materials that act as catalyst in coal gasification can be categorized in three groups, viz. alkali metals, alkaline earth metals, and transition metals. The catalytic effect is of relevance mainly for CO_2 and H_2O as gasifying agents [12]. From viewpoint of biomass/coal co-gasification, the catalytic effects of alkali and alkaline earth metals are relevant, as biomass is rich in these metals. Several authors have reported the catalytic activities of different alkali metal carbonates for gasification of pure graphite and coal char [13–15]. For gasification of Pittsburgh coal char, K_2CO_3 was the most active salt for both CO_2 gasification and H_2O gasification. The catalytic activity of the potassium also depended on the anion in the salt. Mckee [16] has reported that potassium carbonates, sulfates, and nitrates demonstrate better catalytic activity than silicates and halides. Alkali metal hydroxide also demonstrated comparable effects as carbonates in promoting CO_2 gasification and H_2O gasification. This result essentially points to necessity of presence of oxygen in the potassium salt anion for effective catalysis. Other similar

studies on steam gasification of lignite and sub-bituminous coal char [17–19] have also demonstrated the efficiency of potassium over other metal cations (such as Ca, Na, Fe, and Mg). Other factors influencing catalytic effect in gasification are temperature and pressure of gasification [20]. The catalytic effect of alkali metals is also a function of the physical location of gasification phenomenon (oxidation/reduction). Catalytic gasification via carbon loss from basal planes and steps of biomass particles results in formation of pits, which grow deeper and circular as the gasification proceeds. On the other hand, catalytic gasification from crystal edges produces channeling effect. The anisotropic component (e.g., carbon prismatic edges) of biomass is more susceptible to alkali-catalyzed gasification. The physical mechanism of the alkali catalysis is melting of the catalyst and absorption on the coal char particle.

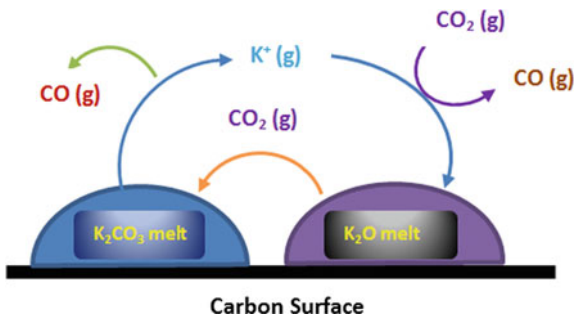
The alkaline earth metals are relatively less active in catalytic gasification, as compared to alkali metals. Calcium is reported to possess the highest catalytic activity for gasification among alkaline earth metals. The activation energies for catalytic reactions involving alkaline earth metal salt are higher than alkali metal salts. Among different salts of alkaline earth metals, the carbonates (i.e., CaCO_3) possess highest catalytic activity toward gasification. The catalytic effect of alkaline earth metal was more pronounced in the presence of CO/CO_2 mixtures than pure CO_2 . Presence of calcium reduces the inhibition effect of CO [18] on alkali metal catalysts. Moreover, calcium salts have lesser reactivity toward the coal minerals (viz. silica oxides) and are less prone to deactivation.

Catalyst activity partially depends on its dispersion properties. Potassium compounds are dispersed more easily compared to calcium compounds. Unlike calcium, potassium appears is able to diffuse through char and forms active gasification sites [21]. During CO_2 gasification, potassium carbonate is less mobile compared to steam gasification of coal [9]. It is reported that catalyst dissolving in the gasifying medium will help dispersion on the coal surface [21]. The catalytic activity of calcium reduces during gasification [22]; on the contrary, potassium is reported to maintain its activity, reflecting its relative mobility and ability to regenerate active sites.

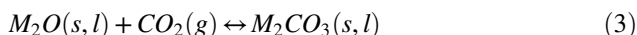
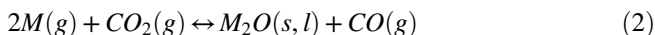
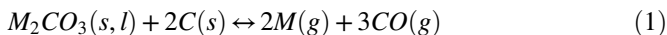
3.1 Chemical Mechanism of Alkali-Metal-Catalyzed CO_2 Gasification

Most of the published literature on mechanistic analysis of alkali metal catalysis has employed CO_2 as gasification medium for pure carbon or coal char. One of the earliest studies on understanding the mechanism of alkali-metal-catalyzed gasification of coal char was published by Mckee [16]. This study has suggested that alkali metal catalysis operates via oxidation–reduction sequence. First step in the physical mechanism proposed by Mckee [16] involves melting of K_2CO_3 followed by its deposition (in the form of thin film) on the surface and micropores in the char.

Fig. 1 Oxidation–reduction reaction pathways at the carbon/catalyst junction during CO₂ co-gasification. Adopted from Mallick et al. [8])



This facilitates contact between carbon and the catalyst. The molten film of K₂CO₃ acts as oxygen transfer medium between gasifying agent and char. The redox reactions in chemical mechanism proposed by Mckee [16] in alkali metal catalysis are as follows [12]:

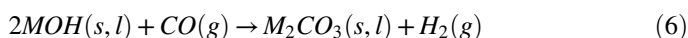
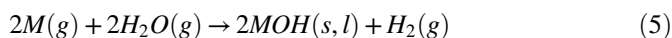
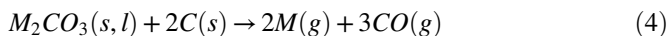


where *M* represents the alkali metal. The letters in the bracket indicate phase of the reactant (s—solid, l—liquid, and g—gas). The schematic of the reaction mechanism is depicted in Fig. 1 for potassium metal. It may be noted that overall reaction (or the resultant reaction) represented by Eqs. 1–3 is essentially the Boudouard reaction.

Among the three redox reactions listed above, the first reaction involving solid-phase reactants has the slowest kinetics and, thus, is the rate controlling step. Experimental observation of marked rise in rate of gasification at temperature (>1000 °C) higher than the melting point of carbonate supports the hypothesis proposed by Mckee [16].

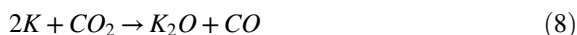
3.2 Steam Gasification of Char

Several authors have employed steam as the gasification medium for char. On a comparative basis, intrinsic kinetics of H₂O gasification of char and carbon was revealed to be much faster than CO₂ gasification. However, as far as catalytic effect of K₂CO₃ was concerned, the basic physical and chemical mechanisms with either H₂O or CO₂ as gasification medium were similar. Mckee and Chatterji [15] and Mckee [16] have proposed following elementary reactions for K₂CO₃-catalyzed steam gasification of carbon:

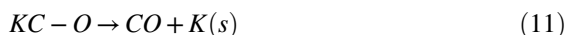
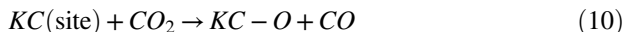


The overall reaction represented by Eqs. 4–6 is primary water–gas reaction. The rate determining step (or step with the slowest kinetics) among Eqs. 4–6 is Eq. 1 due to solid-phase reactants.

Kopyscinski et al. [23] have recently reported new mechanistic facets of the K_2CO_3 -catalyzed CO_2 gasification of ash-free coal. The redox reaction cycle of potassium proposed by Kopyscinski et al. [23] is as follows:



Mckee [16] has incorporated the redox cycle in localized sites where the carbon as well as catalyst can interact. As noted earlier, melting and deposition of K_2CO_3 on coal char generate a “KC” generalized site with proper potassium–carbon contact. The reaction scheme in this case is as follows:



The third reaction step, i.e., Eq. 12 which represents regeneration of the KC (site), requires mobility of part of potassium. On the basis of experimental results, the following mechanism has been proposed that involves $-CK$ and $-COK$ surface intermediates [23].

The new mechanism proposed by Kopyscinski et al. [23] essentially pointed nonexistence of K_2CO_3 under inert gas and gasification atmosphere at 700 °C. The schematic of the reaction mechanism is shown in Fig. 2. Two other important observations made by Kopyscinski et al. are as follows: (1) The oxygen bound in carbonate can be the gasification agent due to its mobility at ≥ 700 °C in the absence of CO_2 and (2) Under inert atmosphere (such as N_2), contact between ash-free coal and K_2CO_3 for extended period results in faster kinetics of gasification due to formation of potassium–carbon intermediate ($\sim K$) as a result of greater extent of catalyst reduction.

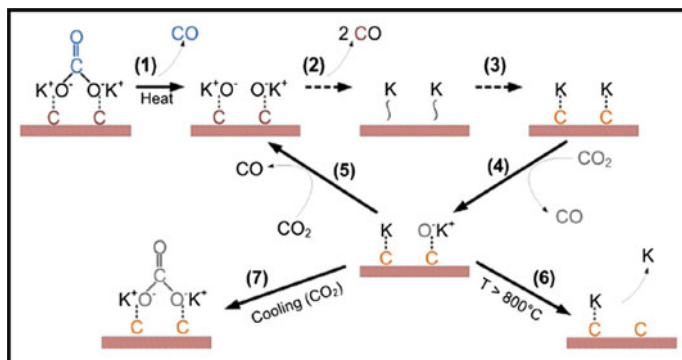


Fig. 2 Reaction scheme of K_2CO_3 on ash-free coal heated under N_2/CO_2 atmosphere. Adopted from Kopyscinski et al. [23]

4 Interaction of Coal/Biomass Blends: Synergistic Effect

A relatively new concept in coal gasification is the use of biomass and coal blends as feedstock. This concept has received wide attention of researchers, and large amount of the literature has been published in this area. Co-gasification of coal and biomass blends could be a bridge between energy production based on fossil and renewable fuels [24]. The basic idea underlying the co-gasification is synergistic effect of alkali and alkaline earth metal contents in the biomass for enhancing gasification of the char resulting from coal pyrolysis. This synergistic effect not only enhances the energy efficiency of the process due to complete gasification of the feedstock, but also alters the composition of the producer gas resulting from the feedstock. The addition of biomass lowers the CO_2 footprint. Another added advantage of this process is the reduction in tar content of producer gas, which makes the gas suitable for applications in engines.

The thermal decomposition of fuel is very essential to evaluate the performance of gasification processes. The pyrolysis is the initial stage of thermal conversion process of carbonaceous materials. So, a better knowledge of coal and biomass pyrolysis may be useful to predict the reactor performance in gasification process. Most of the co-gasification studies overlook the mechanisms by which coal/biomass blends interact and how coal and biomass gradually thermally degrade. Some pyrolysis results of coal and biomass blends have reported little or no synergy between the two fuels [25–29], whereas other authors have exposed substantial synergy [30–34].

4.1 Passive Synergistic Effect During Co-pyrolysis

Interactions of mineral matters and in individual components of biomass, when mixed with coal, need to be explained. The interparticle mobility of alkali metal

(potassium), in particular, allows transfer of the catalyst from a biomass to coal during co-pyrolysis. Therefore, biomass may provide an economical source of gasification catalysts to convert fossil fuels at relatively lower temperatures. In co-gasification of sub-bituminous coal with switchgrass, coal had high alumina and silica contents. These two components can react with potassium contents in the switchgrass ash to form potassium aluminosilicates (viz., KAlSiO_4 , KAlSi_3O_8) and inhibit gasification. The switchgrass/coal blends gasified relatively slowly than coal itself, which recommends that co-feeding biomass with coal char deactivates not only the potassium but also the other catalytic species present in coal [9]. The degree of synergistic effect essentially depends on several factors, viz. pyrolysis temperature, coal/biomass ratio, and composition of the feedstock.

Masandi et al. [35] pyrolyzed the switchgrass, pine sawdust, coal, fluid coke, and coal/biomass blends using TGA. Devolatilization of the biomass and coal portions of mixed samples occurred independently, i.e., without any significant synergy. Collot et al. [36] have observed that the degree of synergy was insignificant at temperature 850 and 950 °C during co-pyrolysis of Daw Mill coal and silver birch wood. However, Kajitani et al. [37] observed the synergistic effect at 850 and 950 °C in the thermogravimetric analyzer and 1200 °C in the drop tube furnace during co-gasification of bituminous coal and cedar bark. But, their analysis revealed no distinguished synergy at 1400 °C. The study reported by Yuan et al. [33] found that the synergy occurred only when coal/biomass mass ratio was 4:1, but for higher coal/biomass ratios (1:1 and 1:4) not only weakened the synergies but also reduced the gasification reactivity of the residual char. Synergistic effects of gasification of coal/biomass blends were also not clear from the work published by Moghtaderi et al. [27], Idris et al. [38], Meesri and Moghtaderi [26] using the TGA analysis. Masandi et al. [39] claimed that the alkali and alkaline earth metals present in biomass can undergo secondary reactions with minerals present in fossil fuel to form metal aluminosilicates compounds which hinder gasification reaction. Ding et al. [40] have reported co-pyrolysis study using cornstalk with three different types of coal, viz. Hulanbeier lignite coal, Shenmu bituminous coal, and Jincheng anthracite coal, in a high-pressure thermogravimetric analyzer. Inhibiting effect was observed due to the intimate contact and the formation of KAlSiO_4 with comparable gasification rate of biomass char and coal char.

Other authors like Vamvuka et al. [28], Garcia-Perez et al. [41], Jones et al. [42], and Pan et al. [29] have also reported no synergetic effect in the co-pyrolysis of the biomass/coal mixture, as each fuel decomposed independently and the total rate of weight loss equaled the sum of weight loss of each fuel.

4.2 Active Synergistic Effect During Co-pyrolysis

In spite of the lack of synergy in co-pyrolysis studies quoted above, other investigators have found synergy during coal/biomass pyrolysis. Synergistic effect

during pyrolysis of coal/biomass blends is due to the presence of high content of potassium in biomass char and the substantial discrepancy of gasification rate between biomass and coal char [40]. The mineral matters in biomass act as a catalytic agents supporting decomposition of coal/biomass blends by reducing the formation of char and favoring the formation of more volatile material [43].

Krerkkaiwan et al. [31] investigated the pyrolysis characterization of Indonesian coal (sub-bituminous), two types of biomass, viz. rice straw and *Leucaena leucocephala* wood, and blends of coal and biomass in a drop tube fixed bed reactor. The synergetic effect is observed in terms of higher gas yield and lower yield of tar and char, for coal/biomass ratio of 1:1. This positive synergetic effect could be described by the transferring of active OH and H radicals from the biomass to the coal and also the catalytic role of potassium from the biomass. Pyrolysis study reported by Yuan et al. [33] revealed that synergy occurred only when the mass ratio of coal and biomass was 4:1. However, higher coal/biomass ratios (1:1 and 1:4) not only weakened the synergies, but also reduced the gasification reactivity of the residual char. The positive synergy during co-gasification was more pronounced at higher biomass blending ratio (70 wt%) as reported by Oney et al. [44] and Gao et al. [45]. On the other way, Jeong et al. [46] have observed that synergy was remarkable for all coal/biomass ratios (4:1, 1:1, and 1:4) and increased as the amount of biomass increased in the blend. The co-pyrolysis study reported by Oney et al. [44] exposed substantial synergy in the fixed bed reactor, especially when the proportion of coal content in the blend was <33%. Brown et al. [47] performed an innovative study on catalytic gasification of coal char using switchgrass-derived potassium salts, using thermogravimetric analyzer in CO₂ medium. The study reported that switchgrass ash was impressive catalyst, with an almost eightfold increase in coal char gasification rate at 896 °C. These results indicate that biomass ash could provide an in situ and inexpensive catalyst to boost coal gasification. The switchgrass ash displayed remarkable catalytic activity when blended with the coal char in a 50:50 wt% mixture. A catalytic/synergistic effect was observed for biomass/fossil fuel mixtures with potassium-to-aluminum molar ratios beyond 1 [39]. A co-pyrolysis study of Park et al. [32] observed that the char yield during pyrolysis was relatively lower than the additive (or total) char yield that can be obtained if both fuels were decomposed individually. They also noted that the difference was more pronounced around 600 °C and disappeared as the temperature approached 800 °C and higher. Zhang et al. [30] also reported that synergy was pronounced at lower temperatures (600 °C) but reduced as temperature increased and was less pronounced around 720 °C. Gao et al. [45] made a similar observation. Another comprehensive study of co-pyrolysis and co-combustion is that of Kubacki [48]. The study involves the co-pyrolysis of different ranks of coal with biomass in different reactors. The study reported slight synergistic effects were observed in TGA study. The co-pyrolyzed coals in blends frequently had lower peak temperatures compared to coal alone, and higher volatile yields were produced. Higher gas yield was observed during co-pyrolysis. This effect was present for certain biomasses, viz. oat, straw, even after mineral materials were removed,

and hence this is not purely the result of catalytic ash components present in the biomass.

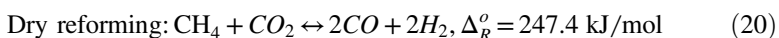
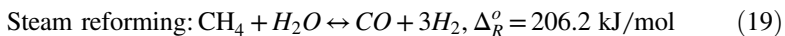
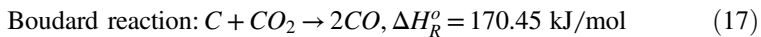
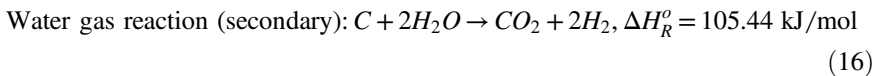
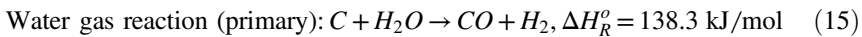
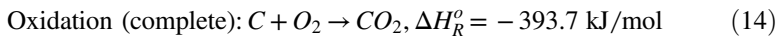
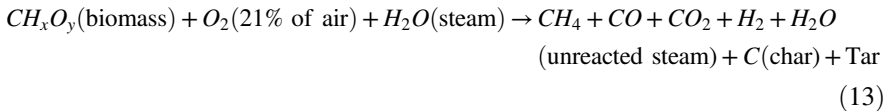
From this observation, we can conclude that synergy seems to be uttered by the pyrolysis/devolatilization step. Hence, the synergy effect occurring during the gasification is only the consequence of what has already taken place during the pyrolysis/devolatilization step. Summary of some passive/active synergistic effect during pyrolysis of coal/biomass blends drawn from TGA studies is given in Table 3.

Table 3 Summary of the literatures on synergistic effect during co-gasification of coal/biomass mixtures

Authors	Synergistic effect
Vamvuka et al. [28]	No synergetic effect is observed, each fuel decomposed independently in the mixture during co-gasification
Habibi et al. [9]	Potassium content in biomass deactivated by formation of aluminosilicates during co-gasification with coal char that hinders the synergy
Krerkkaiwan et al. [31]	Synergistic effect in coal/biomass blend occurs due to catalytic role of K and transfer of active OH and H radicals from biomass to coal
Park et al. [32]	Synergistic effect is observed in terms of higher yield of CO and CH ₄ concentration in producer gas for coal/biomass ratio of 40:60 wt% at 600 °C
Yuan et al. [33]	Synergistic effect is observed in terms of lower char yield and increase in volatile matters during co-pyrolysis
Masandi et al. [35]	Minerals in coal react with alkali and alkaline earth metals in biomass to form aluminosilicates which hinder gasification reactions
Collot et al. [36]	Positive synergy is observed due to presence of mineral materials present in biomass that play catalytic role during co-gasification
Kajitani et al. [37]	Synergistic effect diminishes at high temperature. However, at lower gasification temperatures, char reactivity slightly increased due to catalytic effect of mineral matters in biomass
Idris et al. [38]	No synergistic effect is observed, the coal/biomass blends show independent thermal decomposition as individual fuel
Masandi et al. [39]	Pyrolysis of coal/biomass blend occurs independently without any synergistic effect
Ding et al. [40]	A passive synergistic effect is observed by formation of KAlSiO ₄ during co-gasification of coal and biomass
Garcia-Perez et al. [41]	No synergetic effect in the co-pyrolysis of the coal/biomass blends, the total rate of weight loss is equal to the sum of weight loss of each fuel
Jones et al. [42]	Synergy observed in terms of decrease in aromatics content and increase in phenol content of pyrolysis products
Oney et al. [44]	Synergy is obtained for coal/biomass blends <33% due to presence of mineral matters in biomass that catalyzes co-pyrolysis reactions
Brown et al. [47]	Biomass ash is an impressive catalyst that enhances coal char gasification eightfold for coal/biomass ratio of 10:90 wt%

5 Gasification of Coal/Biomass Blends

Co-gasification of coal and various types of biomass blends is done to improve biomass gasification by decreasing the tar content in the producer gas. In addition, minerals present in the ash of biomass catalyze the gasification of coal. An added advantage of this process is improvement in the H_2/CO ratio in the produced gas, which is relevant from viewpoint of use of this gas for liquid fuel synthesis. Although the co-gasification is useful from a chemical point of view, various practical problems have also been associated with coal and biomass gasification on upstream, gasification, and downstream processes. In addition, during upstream processing, pretreatment of biomass and moisture content are very important. The choice of gasifier operation parameters (temperature, gasifying agent, and catalysts) decides product gas composition and quality. The overall reaction in an air and/or steam gasifier can be represented by Eq. 13, which proceeds with multiple reactions and pathways [49]. The process of biomass and coal gasification occurs through three steps. The initial devolatilization or pyrolysis occurs at lower temperature and produces volatile matters and char residue. Then, secondary reactions start involving the volatile products [50]. Finally, the gasification reaction of the remaining carbonaceous residue occurs with steam and carbon dioxide. Equations 14–20 represent volatile and char reactions. All volatiles and some tar are thermally cracked and broken down into simple gaseous products during gasification. The main reactions which occur during gasification of coal, biomass, or their blends are summarized below [51, 52].

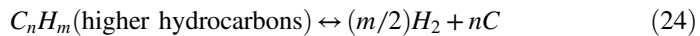
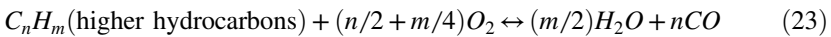
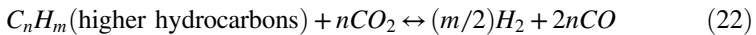
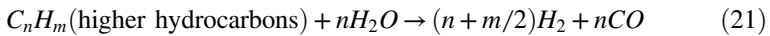


Co-gasification process and the composition of product gas depend upon several factors such as gasifying agent, gasification temperature, coal/biomass blends,

airflow rate etc. With increase in biomass content of the fuel, the gasification efficiency and CO, H₂, CH₄ production increase due to high ash content in biomass and low volatile content of coal [53]. However, Velez et al. [50] found that H₂ content in the producer gas increases for maximum 15% mixing of biomass with coal.

5.1 Effect of Bed Materials

The proper utilization of bed material in fluidized bed co-gasification not only accelerates the chemical reaction rate but also acts as a heat transfer medium. The presence of catalyst in the bed material during co-gasification influences the composition and heating value of the product gas. The hydrogen and carbon dioxide contents in the product gas increased with the use of bed materials during gasification, while the carbon monoxide content decreased. The exothermic water–gas shift reaction is enhanced by use of bed material, resulting in lower energy demand for gasification. The presence of bed material reduces the temperature of gasification and prevents solid agglomeration tendency of the bed. Pinto et al. [54] found that use of dolomite catalyst helped to reduce H₂S and to retain more than 90% sulfur in solid phase during co-gasification of Puertollano coal mixed with pine, petcoke, and polyethylene. The dolomite catalyst also reduced the formation of gaseous chlorine. The metal-based catalysts (such as Ni) are very outstanding in removal of tar. But, the deposition of carbon on the catalyst surface results in their fast deactivation. The catalytic reforming reactions by which tar is converted into useful gaseous compounds are given as follows [8]:



5.2 Effect of Gasifying Agent

Choice of the gasification medium is an important facet of design of gasification process, which contributes to the quality of the product gas. Generally, air is used as gasification agent in simplest gasification process. The product is a low-energy gas containing primarily H₂ and CO diluted with the N₂ from the air during air gasification. Very low airflow rate to the system results in low bed temperature, which produces higher tar and lower gas yields. Unlike air gasification, steam gasification

requires an external heat source to produce steam. Steam gasification produces a higher energy content producer gas with heating value 10–16 MJ/Nm³ and H₂ content 30–60 vol.% [55]. But, bed temperature decreased due to endothermic reactions and additional equipments and energy are required to increase the temperature to above 700 °C [56]. Oxygen-enriched air gasification provides a gas with medium heating value, but it necessitates membrane-based air filtration equipment, which essentially increases the cost of gasification process. With increase in O₂ concentration in the fluidizing gas from 20 to 100%, the concentrations of CH₄, H₂, and CO increased from 4 to 6%, 13 to 19%, and 25 to 55%, respectively [57]. Oxygen–steam gasification resulted in the increase in heating value of the fuel per unit mass of feedstock from 5 to 16 MJ/kg [58].

5.3 *Effect of Bed Temperature*

The reaction temperature is one of the important operating variables, which greatly affects the product gas composition and, hence, the calorific value of syngas. With the constant value of equivalence ratio, the gas heating value increases with the increase in temperature due to improved carbon conversion at higher temperature [59]. The rise of temperature favored the formation of hydrogen and hydrocarbons for further reactions, which lead to reduction of hydrocarbon content in the product gas. Pinto et al. [60] observed that CH₄ and hydrocarbons were reduced by 30 and 63%, respectively, while H₂ concentration increased by 70%, with increase in temperature from 750 to 890 °C during co-gasification coal/pine blends. Velez et al. [50] claimed that in temperature range between 810 and 850 °C, the water–gas shift reaction had a strong role in increasing the H₂ content in the fuel gas. At 850 °C, the Boudouard reaction dominated and consumed CO₂ produced through the water–gas shift reaction and, thus, increased the CO concentration in the product gas. A decrease in the CO/H₂ weight ratio was obtained at high temperature, which indicated high reaction temperature for producing H₂-rich gas [53].

5.4 *Effect of Equivalence Ratio*

Equivalence ratio expresses the amount of oxygen supplied for gasification relative to combustion. A typical range of ER values employed for gasification is 0.19–0.43 [61]. The gasifier temperature was found to increase with increase in the equivalence ratio, and this was attributed to increase in the exothermic reactions. Low equivalence ratio results in relatively low bed temperature, thus producing a lower gas and higher tar yields. Theoretically, optimum equivalence ratio from viewpoint of gasification is ~0.25. For ER <0.25, not all of the char is gasified, which essentially is energy loss due to underutilization of energy potential of biomass. At higher ER, complete oxidation of carbon results in rise of temperature inside the

gasifier. At ER ~ 0.25 , all the char is converted into product gas giving the highest energy of the producer gas. Kehzong et al. [62] observed that when ER was increased from 0.30 to 0.42, the total gas yield enhanced from 1.75 to 1.94 m³/kg fuel, though the syngas gas yield decreased from 0.98 to 0.93 m³/kg fuels, as more O₂ was provided for combustion. Ponzio et al. [63] also reported that ER ≥ 0.25 produced significantly higher yield of all gases, as compared to low ER of 0.19 during co-gasification. Similar observation was made by Pinto et al. [60] for co-gasification of coal and pine mixture.

5.5 Composition of Syngas

Syngas gas is the mixture of gas produced by gasification of organic materials at relatively low temperature. It consists of H₂, CO, CO₂, CH₄, and tar. The variations of each gas component with different parameters are briefly discussed below. Figure 3a–c shows the variation of syngas composition with ER (0.19–0.35) for different coal/biomass blends in our own study conducted in circulating fluidized bed gasifier [64]. The effect of the ER on the gas composition is mainly attributed to the oxidation reactions which release heat and create high temperature for the whole gasification process. It is considered that an increase in the ER led to further combustion of the product gas and dilution of the gas by nitrogen in air, resulting in a decrease in the concentrations of H₂ and CO. Conversely, CO₂ showed a slightly increasing trend with the increase in the ER. A higher value of the ER results in more CH₄ burning with O₂ and inhibiting the formation of CH₄ at higher temperature. Therefore, the volume fraction of CH₄ decreased with increasing ER. Sawdust has been used as the representative biomass in our study. Different biomass/coal ratios of 25:75, 50:50, and 75:25 wt% have been represented as follows: (A) 25% S + 75% C, (B) 50% S + 50% C, and (C) 75% S + 25% C.

5.6 H₂ Concentration

Co-gasification of coal with biomass having higher volatiles (viz. coffee husk) produced lesser quantity of H₂ as compared to gasification of individual coal [50]. The high volatile matter contents improved the release of combustible gases (such as H₂, CH₄, CO C_nH_n), which required a lower reaction temperature and hence caused a reduction in H₂ concentration. But, for the biomass having less volatile contents, higher operating temperature was required to obtain good products of combustion [50, 51, 65]. However, it was observed that simultaneous increase in biomass content and temperature in co-gasification led to higher contents of hydrogen [66]. Low volatile content biomasses and low-ranked coal are more suitable for significant H₂ production because low-ranked coals (with relatively high ash content) have higher reactivity than higher-ranked ones [67].

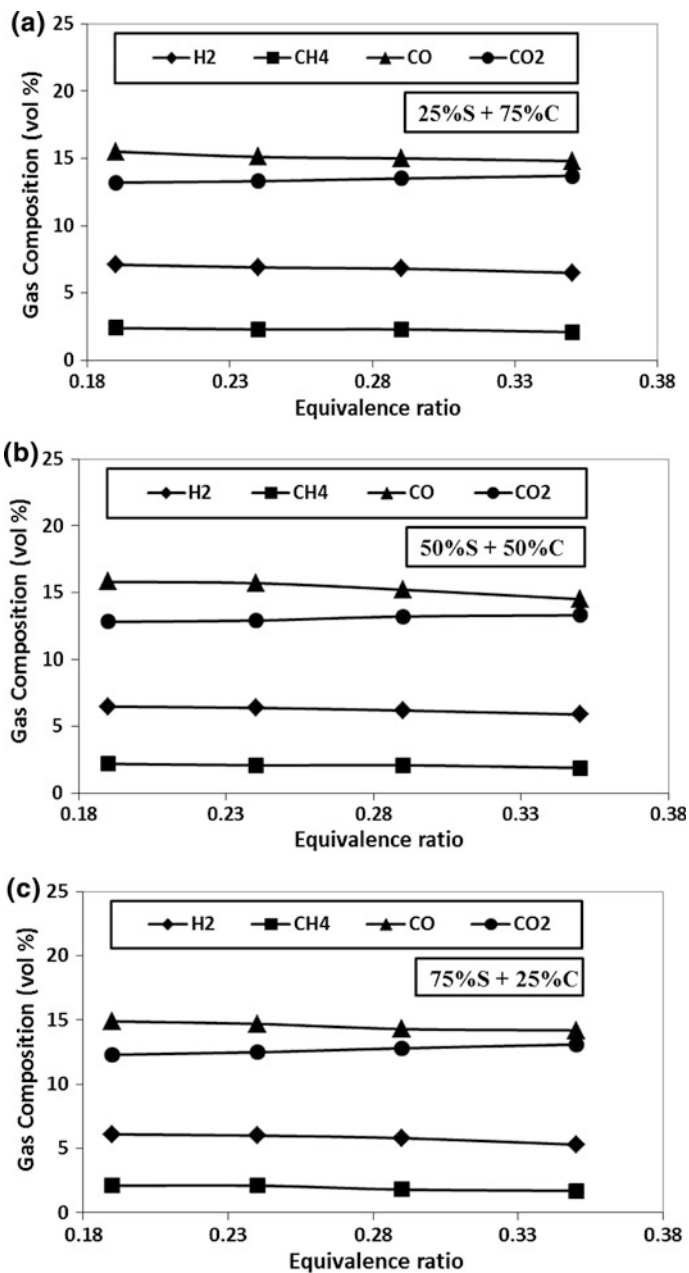


Fig. 3 Variation of gas composition with ER for different coal/biomass blends **a** 25% S + 75% C, **b** 50% S + 50% C, **c** 75% S + 25% C

5.7 *CO₂ Concentration*

In both biomass and coal gasification, high amount of CO₂ is produced due to the oxidation as well as water–gas shift reactions, which are very exothermic in nature. However, upon increasing the gasification temperature, the CO₂ concentration in the product gas starts decreasing due to increase in rates of endothermic reactions, which consume CO₂ [53, 65, 68, 69]. During co-gasification, CO₂ production is more than that of coal gasification because of higher O₂ contents in biomass than coal [63]. It is also reported that CO₂ production in co-gasification is reduced with the rise in temperature due to increase in consumption of CO₂ during dry reforming of CH₄, tars, and also occurrence of Boudouard reactions [51, 60, 65, 70, 71]. CO₂ content of producer gas is higher at relatively low temperature range of 810–850 °C due to impact of main water–gas shift reaction. However, Boudouard reaction becomes more dominant at high temperature, resulting in reduction in CO₂ concentration [50].

5.8 *CO Concentration*

In biomass and coal gasification, concentration of CO increases with increase in temperature due to an increase in the rate of both water–gas and Boudouard reactions [53, 68, 69]. CO contents in co-gasification are observed to be higher than that in coal gasification due to the greater reactivity of biomass compared to coal as well as due to the presence of excess O₂ in biomass. The rise in bed temperature leads to an increase in the production of CO in co-gasification because of the dominance of the Boudouard reaction [50, 66]. Pinto et al. [70] observed that carbon monoxide is mostly produced during oxidation reactions that are exothermic in nature, thus lowering CO production with the increase in temperature [72]. Hernandez et al. [73] stated that at longer residence times in air gasification, for all temperature ranges studied, more CO is produced, though the effect of residence time on the production of CO is lower compared to H₂ production. Hernandez et al. [66] observed that co-gasification using coal/biomass mass ratio of 20:80% can cause an increase in CO contents from 7.18–14% when temperature increases from 750–1050 °C. Pinto et al. [70] claimed that at higher temperature of ~830 °C, the CO production is slightly increased due to the consumption of CO₂ in dry reforming and Boudouard reaction [51].

5.9 *CH₄ and Other Hydrocarbons Concentration*

In gasification, methane is produced by methanation and methane steam reforming reaction, but CH₄ concentration starts consuming during combustion reaction. As a

result, CH_4 concentration does not change considerably with the variation of temperature [56]. In co-gasification, with the rise of temperature, both CH_4 and hydrocarbon concentrations decrease due to an increase in the reforming reactions [51, 69, 70]. It was observed that the concentrations of hydrocarbons are higher in co-gasification than in coal gasification because of the biomass content in co-gasification. The presence of biomass lowers the temperature in co-gasification, and so the concentrations of hydrocarbons are comparatively higher than those from coal gasification [50]. However, Pinto et al. [70] observed that during co-gasification of coal with edible waste at temperatures >850 °C, the concentration of C_nH_m decreases more due to the cracking and reforming reactions. Aznar et al. [71] have also studied co-gasification of coal, biomass and plastics, and reported a slight increase in CH_4 contents at temperatures >820 °C in the presence of dolomite catalyst due to an increase in the rate of methanation reaction. However, the concentration of light hydrocarbons decreased due to the cracking reactions at higher temperatures.

6 Conclusions

This chapter deals with the issue of gasification of coal/biomass blends. The basic idea underlying in gasification of coal/biomass blend is to attain synergy between the individual gasification of coal and biomass, where the kinetics of gasification of coal char is improved by biomass ash due to presence of alkali and alkaline earth metals in it. Synergistic effect in co-gasification has been in terms of reduction of activation energy of the fuel, which boosts the kinetics of gasification. Presence of alumina and silica in coal is unfavorable to synergistic effect, as silica and alumina block the catalytic action of alkali metals by formation of aluminosilicates during gasification. Furthermore, excessively high temperatures also hinder the synergy due to evaporative loss of alkali metals from biomass. The optimum coal/biomass ratio should be maintained to achieve maximum synergy.

The effects of various operational parameters, viz. temperature, bed materials, gasifying agents, equivalence ratio, on producer gas composition, and yield in the gasification process, are briefly discussed. Gasification temperature is a significant parameter in the process of gasification. The rise of gasification temperature leads to increase the H_2 content of the producer gas; however, the concentration will decrease if the biomass contains more volatile matters. The CO concentration also increases with the increase in gasification temperature due to increase in the rate of both water–gas and Boudouard reactions. However, heating value and producer gas composition, especially H_2 , CO, and CH_4 , can be varied with gasification medium. Unlike air gasification, steam gasification produces a higher energy content producer gas with heating value 10–16 MJ/Nm³ and H_2 content 30–60 vol.%.

In summary, the concept of co-gasification of coal/biomass blends has shown distinct merits and high promise in laboratory-scale studies, as compared to individual gasification of coal and biomass. Moreover, the co-gasification process also

helps in reduction of greenhouse gas emissions by partial replacement of fossil fuel with renewable feedstock of biomass. With further research and development endeavors on bench/pilot-scale co-gasification process, commercial implementation of biomass/coal gasification may be realized in near future.

References

1. International Energy Outlook (2013) EIA, DOE/EIA-0484
2. Rawat AS (1993) Indian forestry: a perspective. Indus publishing company, New Delhi, p 316
3. Arena U, Zaccariello L, Mastellone ML (2010) Fluidized bed gasification of waste-derived fuels. *Waste Manag* 30:1212–1219
4. Electricity sector in India (2017). https://en.wikipedia.org/wiki/Electricity_sector_in_India. Accessed on June 2017
5. Ananth P, Chikkatur (2008) A resource and technology assessment of coal utilization in India. Coal Initiative Reports White Paper Series, Pew Center on Global Climate Change, Cambridge October 2008
6. Balat M (2007) Influence of coal as an energy source on environmental pollution. *Energy Source Part A* 29:581–589
7. International Energy Agency (IEA) (2013). World energy outlook 2013. IEA, Paris, France
8. Mallick D, Mahanta P, Moholkar VS (2017) Co-gasification of coal and biomass blends: chemistry and engineering. *Fuel* 204:106–112
9. Habibi R, Kopyscinski J, Masnadi MS, Lam J, Grace JR, Mims CA, Hill JM (2013) Co-gasification of biomass and non-biomass feedstocks: synergistic and inhibition effects of switchgrass mixed with sub-bituminous coal and fluid coke during CO₂ gasification. *Energy Fuels* 27:494–500
10. Masnadi MS, Grace JR, Bi XT, Lim CJ, Ellis N, Li YH (2015) From coal towards renewables: catalytic/synergistic effects during steam co-gasification of switchgrass and coal in a pilot-scale bubbling fluidized bed. *Renew Energy* 83:918–930
11. Mukhopadhyay PK, Hatcher PG (1993) SG 38: hydrocarbons from coal, composition of coal, pp 79–118
12. Masnadi MS (2014) Biomass/fossil fuel co-gasification with and without integrated CO₂ capture. Dissertation, University of British Columbia, Canada
13. McKee DW (1983) Mechanisms of the alkali metal catalyzed gasification of carbon. *Fuel* 62:170–175
14. Yong Z, Mata V, Rodrigues AE (2002) Adsorption of carbon dioxide at high temperature: a review. *Sep Purif Technol* 26:195–205
15. McKee DW, Chatterji D (1975) The catalytic behavior of alkali metal carbonates and oxides in graphite oxidation reactions. *Carbon* 13:381–390
16. McKee DW (1982) Gasification of graphite in carbon dioxide and water vapor—the catalytic effects of alkali metal salts. *Carbon* 20:59–66
17. Walker PL, Mahajan OP, Komatsu M (1979) Catalysis of lignite char gasification by various exchanged cations-dependence of activity on reactive atmosphere. *Prepr Div Fuel Chem Am Chem Soc* 24:10–16
18. Tomita A, Takarada T, Tamai Y (1983) Gasification of coal impregnated with catalyst during pulverization: effect of catalyst type and reactant gas on the gasification of Shin-Yubari coal. *Fuel* 62:62–68
19. Veraa MJ, Bell AT (1978) Effect of alkali metal catalysts on gasification of coal char. *Fuel* 57:194–200
20. McCoy LR, Ampaya JP, Saunders RC (1983) Investigation of coal-gasification catalysis reaction mechanisms. Final technical progress report, October 1980–August 1982, Rockwell

- International Corp., Canoga Park, CA (USA). Energy Systems Group, Rockwell International Corp, Thousand Oaks, USA
21. Pullen JR (1984) Catalytic coal gasification. IEA Coal Research, London
 22. Lang RJ, Neavel RC (1982) Behaviour of calcium as a steam gasification catalyst. *Fuel* 61 (7):620–626
 23. Kopyscinski J, Rahman M, Gupta R, Mims CA, Hill JM (2014) K_2CO_3 catalyzed CO_2 gasification of ash-free coal. Interactions of the catalyst with carbon in N_2 and CO_2 atmosphere. *Fuel* 117:1181–1189
 24. Minchener AJ (1995) Combined gasification of coal with biomass and sewage sludge. In: *Proceedings of the 8th European biomass conference: biomass for energy, environment, agriculture, and industry*, Elsevier, Oxford, pp 1513–1519
 25. Biagini E, Lippi F, Petarca L, Tognotti L (2002) Devolatilization rate of biomasses and coal-biomass blends: an experimental investigation. *Fuel* 81(8):1041–1050
 26. Meesri C, Moghtaderi B (2002) Lack of synergetic effects in the pyrolytic characteristics of woody biomass/coal blends under low and high heating rate regimes. *Biomass Bioenerg* 23 (1):55–66
 27. Moghtaderi B, Meesri C, Wall T (2004) Pyrolytic characteristics of blended coal and woody biomass. *Fuel* 83(6):745–750
 28. Vamvuka D, Pasadakis N, Kastanaki E, Grammelis P, Kakaras E (2003) Kinetic modeling of coal/agricultural by-product blends. *Energy Fuels* 17(3):549–558
 29. Pan YG, Velo E, Puigjaner L (1996) Pyrolysis of blends of biomass with poor coals. *Fuel* 75 (4):412–418
 30. Zhang L, Xu S, Zhao W, Liu S (2007) Co-pyrolysis of biomass and coal in a free fall reactor. *Fuel* 86(3):353–359
 31. Krerkkaiwan S, Fushimi C, Tsutsumi A, Kuchonthara P (2013) Synergetic effect during co-pyrolysis/gasification of biomass and sub-bituminous coal. *Fuel Process Technol* 115:11–18
 32. Park DK, Kim SD, Lee SH, Lee JG (2010) Co-pyrolysis characteristics of sawdust and coal blend in TGA and a fixed bed reactor. *Bioresour Technol* 101(15):6151–6156
 33. Yuan S, Dai ZH, Zhou ZJ, Chen XL, Yu GS, Wang FC (2012) Rapid co-pyrolysis of rice straw and a bituminous coal in a high-frequency furnace and gasification of the residual char. *Bioresour Technol* 109:188–197
 34. Xu C, Hu S, Xiang J, Zhang L, Sun L, Shuai C, Chen Q, He L, Edreis EMA (2014) Interaction and kinetic analysis for coal and biomass co-gasification by TG–FTIR. *Bioresour Technol* 154:313–321
 35. Masnadi MS, Habibi R, Kopyscinski J, Hill JM, Bi XC, Ellis JLN, Grace JR (2014) Fuel characterization and co-pyrolysis kinetics of biomass and fossil fuels. *Fuel* 117:1204–1214
 36. Collot AG, Zhuo Y, Dugwell DR, Kandiyoti R (1999) Co-pyrolysis and co-gasification of coal and biomass in bench-scale fixed-bed and fluidized bed reactors. *Fuel* 78:667–679
 37. Kajitani S, Zhang Y, Umemoto S, Ashizawa M, Hara S (2009) Co-gasification reactivity of coal and woody biomass in high-temperature gasification. *Energy Fuels* 24:145–151
 38. Idris SS, Rahman NA, Ismail K, Alias AB, Rashid ZA, Aris MJ (2010) Investigation on thermochemical behaviour of low rank Malaysian coal, oil palm biomass and their blends during pyrolysis via thermogravimetric analysis (TGA). *Bioresour Technol* 101:4584–4592
 39. Masnadi MS, Grace JR, Bi XT, Lim CJ, Ellis N (2015) From fossil fuels towards renewables: inhibitory and catalytic effects on carbon thermochemical conversion during co-gasification of biomass with fossil fuels. *Appl Energy* 140:196–209
 40. Ding L, Zhang Y, Wang Z, Huang J, Fang Y (2014) Interaction and its induced inhibiting or synergistic effects during co-gasification of coal char and biomass char. *Biores Technol* 173:11–20
 41. Garcia-Perez M, Chaala A, Yang J, Roy C (2001) Co-pyrolysis of sugarcane bagasse with petroleum residue. Part I: Thermogravimetric analysis. *Fuel* 80(9):1245–1258
 42. Jones JM, Kubacki M, Kubica K, Ross AB, Williams A (2005) Devolatilisation characteristics of coal and biomass blends. *J Anal Appl Pyrol* 74(1–2):502–511

43. Ulloa CA, Gordon AL, García XA (2009) Thermogravimetric study of interactions in the pyrolysis of blends of coal with radiata pine sawdust. *Fuel Process Technol* 90:583–590
44. Onay O, Bayram E, Kockar OM (2007) Co-pyrolysis of Seyitömer lignite and safflower seed: influence of the blending ratio and pyrolysis temperature on product yields and oil characterization. *Energy Fuels* 21:3049–3056
45. Gao C, Vejehati F, Katalambula H, Gupta R (2009) Co-gasification of biomass with coal and oil sand coke in a drop tube furnace. *Energy Fuels* 24:232–240
46. Jeong HJ, Hwang IS, Hwang J (2015) Co-gasification of bituminous coal–pine sawdust blended char with H₂O at temperatures of 750–850 °C. *Fuel* 156:26–29
47. Brown RC, Liu Q, Norton G (2000) Catalytic effects observed during the co-gasification of coal and switchgrass. *Biomass Bioenergy* 18(6):499–506
48. Kubacki ML (2007) Co-Pyrolysis and co-combustion of coal and biomass. Dissertation, University of Leeds, Leeds, UK
49. Kumar A, Jones DD, Hanna MA (2009) Thermochemical biomass gasification: a review of the current status of the technology. *Energy* 2(3):556–581
50. Velez J, Chejne F, Valdes C, Emery E, Londoo C (2009) Co-gasification of Colombian coal and biomass in fluidized bed: an experimental study. *Fuel* 88:424–430
51. Andre RN, Pinto F, Franco C, Dias M, Gulyurtlu MAA (2005) Fluidized bed co-gasification of coal and olive oil industry wastes. *Fuel* 84:1635–1644
52. Fermoso JP (2009) Co-gasification of coal and biomass for the production of hydrogen. Dissertation, University of Oviedo, Spain
53. Lapuerta M, Hernandez JJ, Pazo A, Lpez J (2008) Gasification and co-gasification of biomass wastes: effect of the biomass origin and the gasifier operating conditions. *Fuel Process Technol* 89:828–837
54. Pinto F, Lopes H, Andre RN, Gulyurtlu I, Cabrita I (2008) Effect of catalysts in the quality of syngas and by-products obtained by co-gasification of coal and wastes. 2: heavy metals, sulphur and halogen compounds abatement. *Fuel* 87(7):1050–1062
55. Shen L, Gao Y, Xiao J (2008) Simulation of hydrogen production from biomass gasification in interconnected fluidized beds. *Biomass Bioenergy* 32:120–127
56. Umeki K, Yamamoto K, Namioka T, Yoshikawa K (2009) High temperature steam only gasification of woody biomass. *Appl Energy* 87:791–798
57. Bailie RC (1979) Hessleman gas generator testing for solar energy research institute. Contract No. AH-8-1077-1
58. Watkinson A, Cheng C, Lim C (1987) Oxygen-steam gasification of coals in a spouted bed. *Can J Chem Eng* 65:791–798
59. Li K, Zhang R, Bi J (2010) Experimental study on syngas production by co-gasification of coal and biomass in a fluidized bed. *Int J Hydrogen Energy* 35:2722–2726
60. Pinto F, Carlos F, Andre RN (2003) Effect of experimental conditions on co-gasification of coal, biomass and plastics wastes with air/steam mixtures in a fluidized bed system. *Fuel* 82 (15–17):1967–1976
61. Zainal ZA, Rifau A, Quadir GA, Seetharamu KN (2002) Experimental investigation of a downdraft biomass gasifier. *Biomass Bioenergy* 23:283–289
62. Kezhong L, Zhang R, Bi J (2010) Experimental study on syngas production by co-gasification of coal and biomass in a fluidized bed. *Int J Hydrogen Energy* 35(7):2722–2726
63. Ponzio A, Kalisz S, Blasiak W (2006) Effect of operating conditions on tar and gas composition in high temperature air/ steam gasification (HTAG) of plastic containing waste. *Fuel Process Technol* 87(3):223–233
64. Mallick D, Mahanta P, Moholkar VS (2017) Unpublished work
65. Pohorely M, Vosecky M, Hejdova P, Puncochar M, Skoblja S, Staf M (2006) Gasification of coal and PET in fluidized bed reactor. *Fuel* 85:2458–2468
66. Hernandez JJ, Aranda AG, Serrano C (2010) CO-gasification of biomass wastes and coal–coke blends in an entrained flow gasifier: an experimental study. *Energy Fuel* 24:2479–2488
67. Irfan MF, Usman MR, Kusakabe K (2011) Coal gasification in CO₂ atmosphere and its kinetics since 1948: a brief review. *Energy* 36:12–40

68. Asadullah M, Miyazawa T, Ito S, Kunimori K, Koyama S, Tomishige K (2004) A comparison of Rh/CeO₂/SiO₂ catalysts with steam reforming catalysts, dolomite and inert materials as bed materials in low throughput fluidized bed gasification systems. *Biomass Bioenergy* 26:269–279
69. Qin K, Lin W, Jensen PA, Jensen AD (2012) High-temperature entrained flow gasification of biomass. *Fuel* 93:589–600
70. Pinto F, Franco C, Andre RN, Miranda M, Gulyurtlu I, Cabrita I (2002) CO-gasification study of biomass mixed with plastic wastes. *Fuel* 81:291–297
71. Aznar MP, Caballero MA, Sancho JA, Frances E (2006) Plastic waste elimination by CO-gasification with coal and biomass in fluidized bed with air in pilot plant. *Fuel Process Technol* 87:409–420
72. Hernandez JJ, Aranda G, Barba J, Mendoza JM (2012) Effect of steam content in the air–steam flow on biomass entrained flow gasification. *Fuel Process Technol* 99:43–55
73. Hernandez JJ, Aranda AG, Bula A (2010) Gasification of biomass wastes in an entrained flow gasifier: Effect of the particle size and the residence time. *Fuel Process Technol* 9:681–692

Chemical Looping and Plasma Technologies for Gasification of Coal and Biomass

Barnali Bhui and Prabu Vairakannu

Abstract Gasification of solid fuels exhibits a vital role in power plants for electricity generation using gas turbines, fuel cells and for various chemical productions such as hydrogen, methanol, liquid hydrocarbons, etc. Chemical looping combustion (CLC) and plasma gasification are the recent emerging advanced technologies for the production of clean energy from solid fuels. CLC operation eliminates the energy penalty of air separation unit (ASU) in an oxy-fuel combustion unit and paves a way for carbon capture and storage. Another promising technology for the conversion of solid fuel into syngas is plasma gasification. Tar-free syngas with high-calorific value can be obtained in this technology. Further, co-gasification of coal and biomass is another option to utilize renewable energy, which reduces a considerable amount of greenhouse gas emission. In this chapter, the conversion efficiencies of solid fuels such as coal and biomass in the CLC technology are compared with liquid and gaseous fuels. The complexity of solid fuel-based CLC operation and future research scope of the CLC technology are discussed. Also, the percentage conversion of solid fuels and CO₂ yield in pilot plant-scale CLC experiments is reviewed. The syngas composition and carbon conversion efficiency of plasma gasification are compared for biomass and coal. The feasibility of co-utilization of coal and biomass in these gasification technologies is also explained.

1 Introduction

Coal and biomass play a crucial role in fulfilling energy demand of the present scenario. Direct combustion of these fuels produces thermal energy, which can be utilized for steam production in a boiler for power generation. Co-gasification of coal and biomass is beneficial as it reduces the dependency on fossil fuels along

B. Bhui · P. Vairakannu (✉)

Department of Chemical Engineering, Indian Institute of Technology Guwahati,
Guwahati 781039, Assam, India
e-mail: v.prabu@iitg.ernet.in

© Springer Nature Singapore Pte Ltd. 2018

S. De et al. (eds.), *Coal and Biomass Gasification*, Energy, Environment,
and Sustainability, https://doi.org/10.1007/978-981-10-7335-9_20

499

with reduction of greenhouse gas emission. Also, the co-combustion of high ash coal and biomass is advantageous due to the presence of high volatile matter in biomass. Alkali and alkaline earth metals in biomass ash can act as catalysts in gasification reactions.

Gasification is one of the thermochemical processes, which converts solid feedstock into syngas through partial oxidation using either air, steam, CO_2 , or their mixtures as gasifying agent. It is generally carried out at 800–1500 °C. In a gasifier, the solid fuel undergoes several thermochemical processes such as drying, pyrolysis, combustion, and gasification. Table 1 provides a list of chemical reactions, which occur in a gasifier. Drying is the removal of moisture from feedstock. It occurs relatively at low temperatures and thus, feedstock does not get decomposed at this temperature range (100–200 °C). The dried feedstock gets decomposed into tar, char, and volatiles at elevated temperature known as pyrolysis. Further, the heat liberated from the partial combustion of feedstock progresses the char gasification, which is an endothermic solid–gas reaction [67]. Thus, gasification occurs at low concentration oxygen atmosphere. Steam and CO_2 are potential gasifying agents for coal and biomass. Steam gasification produces a hydrogen-enriched syngas due to water gas shift reaction (reaction 5), whereas a CO-enriched syngas is formed during CO_2 gasification.

Coal would dominate the world energy market till 2030 [62]. Out of 223 gigawatt (GW) of total thermal energy (produced by coal, gas, and oil), coal produced 196 GW of energy till June 2017 (Government of India Ministry of Power). Biomass, a carbon-neutral energy source, becomes an attractive option to harness energy in small-scale industries. As biomass is abundantly available in nature, it could be considered as a viable energy source under economic conditions. Biomass gasification was originated in the 1800s for domestic purpose [10]. Biomass is highly oxygenated source as compared to coal or other feedstock because of its carbohydrate structure. Biomass is basically a lignocellulose component, which comprises of cellulose, hemicellulose, and lignin. Lignin mainly constitutes char content while cellulose and hemicellulose possess huge volatile matter [11].

The presence of alkali and alkaline metal (Na_2O , K_2O , and CaO) of biomass would result in positive synergy during co-gasification of coal and biomass [28, 46, 72]. Table 2 provides a comparative study of syngas composition of coal, biomass, and their blend-based gasification in fluidized and entrained bed gasifiers. Coal as a fuel produces high-calorific value syngas as compared to biomass. At high operating temperatures of a gasifier, the cracking and reforming reactions enhanced the production of hydrogen and CO.

Lignite coal under airstream gasification produced 226.8 kJ/mol calorific value of syngas. When biomass is blended with this coal, the calorific value of syngas is increased to 237 kJ/mol. With further increase in the percentage of biomass, its calorific value decreased. This is due to the reduction of total carbon content of fuel with increase in the percentage of biomass. Bituminous coal yields highest calorific value in oxy-steam gasification. Pine biomass produced a high yield of syngas as compared to other biomass. It produced 290 kJ/mol calorific value of syngas at 800 °C, whereas the blended pine and bituminous coal produced a

Table 1 Chemical reactions during gasification of solid fuels in a gasifier

Type of reaction	Reaction	ΔH_r (kJ/mol)
Pyrolysis	$\text{CHONS} + \text{heat} \rightarrow \text{CO} + \text{H}_2 + \text{CO}_2 + \text{H}_2\text{O} + \text{N}_2 + \text{CH}_4 + \text{Higher Hydrocarbons} + \text{Tar} + \text{Char}$	>0
	$\text{Char (C)} + \text{O}_2 \rightarrow \text{CO}_2$	-395.2
Oxidation	$2\text{C} + \text{O}_2 \rightarrow 2\text{CO}$	-227.4
	$\text{CO} + 0.5\text{O}_2 \rightarrow \text{CO}_2$	-284
	$\text{CH}_4 + 2\text{O}_2 \rightarrow 2\text{H}_2\text{O} + \text{CO}_2$	-803
	Tar reforming reaction	>0
	$\text{C}_n\text{H}_{2m} + n\text{H}_2\text{O}/\text{CO}_2 \rightarrow (n + m/2)\text{H}_2 + n\text{CO}$	>0
Hydrocarbon reforming	Hydrocarbon + $\text{H}_2\text{O}/\text{CO}_2 \rightarrow \text{H}_2 + \text{CO} + \text{CO}_2$	131.46
Water gas reaction	$\text{C} + \text{H}_2\text{O} \rightarrow \text{CO} + \text{H}_2$	-41.14
Water gas shift reaction (WGS)	$\text{CO} + \text{H}_2\text{O} \rightarrow \text{H}_2 + \text{CO}_2$	172.67
Boudouard reaction	$\text{C} + \text{CO}_2 \rightarrow 2\text{CO}$	206
Steam reforming reaction	$\text{CH}_4 + \text{H}_2\text{O} \rightarrow \text{CO} + 3\text{H}_2$	247.29
Dry reforming reaction	$\text{CH}_4 + \text{CO}_2 \rightarrow 2\text{H}_2 + 2\text{CO}$	-247.29
Methanation reaction	$2\text{CO} + 2\text{H}_2 \rightarrow \text{CH}_4 + \text{CO}_2$	-165
	$\text{CO}_2 + 4\text{H}_2 \rightarrow \text{CH}_4 + 2\text{H}_2\text{O}$	-74.87
Methane forming reaction	$\text{C} + 2\text{H}_2 \rightarrow 2\text{CH}_4$	-74.87

Table 2 Comparative study of syngas composition of coal, biomass, and their blend during gasification in steam atmosphere

Feedstock	Gasifier	Operating conditions	Operating parameters	Outlet gas composition	Calorific value of syn gas (kJ/mol)	References
Pine sawdust	Fluidized bed gasifier	Airstream	700 °C	CO-44%, H ₂ -21%,	247.52	[44]
			800 °C	CH ₄ -9% CO-37.5%, H ₂ -32%, CH ₄ -8% (vol. %)	247.73	
Pine bagasse and lignite coal	Fluidized bed gasifier	Airstream	Coal: Biomass			[4]
			100:0	CO ~ 19%, H ₂ ~ 45%, CH ₄ ~ 8%	226.83	
			60:40	CO ~ 26%, H ₂ ~ 38%, CH ₄ ~ 9%	237.72	
			40:60	CO ~ 21%, H ₂ ~ 37%, CH ₄ ~ 10%	229.17	
			850 °C	(vol. %)		
Low rank coal	Fluidized bed gasifier	Airstream	1040 °C	CO-19.2%, H ₂ -6.9%, CH ₄ -0%, CO ₂ -17% (vol. %)	71.03	[36]
Bituminous coal	Entrained flow gasifier	Oxygen-steam	1500 °C	CO-58.52%, H ₂ -27.68%, CH ₄ -2.95% (mol%)	256.26	[30]
Pine and bituminous coal (2:1)	Fluidized bed gasifier	Steam	1045 °C	CO-36%, H ₂ -17.66%, CH ₄ -1.76% (vol. %)	158.73	[38]
Bamboo	Downdraft gasifier	Steam	Moisture (%) -20%	CO-19.5%, H ₂ -18.8%, CH ₄ -1.25%, CO ₂ -11.2%	110.71	[12]
			Moisture (%) -5%	CO-20.5%, H ₂ -17.8%, CH ₄ -1.15%, CO ₂ -10.5%	110.31	
			850 °C	(vol. %)		

(continued)

Table 2 (continued)

Feedstock	Gasifier	Operating conditions	Operating parameters	Outlet gas composition	Calorific value of syn gas (kJ/mol)	References
Neem	Downdraft gasifier	steam	Moisture (%) -20%	CO-18.5%, H ₂ -18.2%, CH ₄ -1.35%, CO ₂ -11%	107.226	[12]
			Moisture (%) -5%	CO-19.2%, H ₂ -17.5%, CH ₄ -1.2%, CO ₂ -10.3%	106.31	
			850 °C	(vol. %)		
Eucalyptus	Fluidized bed gasifier	Steam	750 °C	CO-42%, H ₂ -2%, CH ₄ -15%	292.4	[15]
			880 °C	CO-42%, H ₂ -3%, CH ₄ -9% (mol%)	268.48	
Pine	Fluidized bed gasifier	Steam	750 °C	CO-42%, H ₂ -8%, CH ₄ -14%	298.9	[15]
			880 °C	CO-40%, H ₂ -6%, CH ₄ -12% (mol%)	296.56	

low-calorific-value syngas of 159 kJ/mol at 1045 °C. As high operating temperature enhances combustion reaction, the carbon content of solid fuel is burnt at such a high temperature.

Chemical looping combustion and plasma gasification are the recent emerging technologies for clean energy production using coal and biomass. Chemical looping concept uses oxygen carriers to oxidize solid fuels in a fuel reactor. Oxygen carriers act as a donor of oxygen molecules for fuel combustion as well as catalysts for char gasification and tar reforming reactions. Plasma gasification converts solid feedstock into rich syngas using plasma torch at high temperatures (1500–5000 °C). Tar content of coal and biomass is completely destructed in plasma gasification due to the cracking reactions of high hydrocarbons. Thus, a high syngas gas yield can be obtained in this technology.

In this chapter, the conversion efficiency of solid fuel and CO₂ yield under CLC process conditions is discussed and compared with liquid and gaseous fuels. The difficulty of solid fuel-based CLC operation is explained. Also, this chapter reviewed the pilot plants of CLC systems for solid fuels in order to show the technical feasibility for commercialization of this technology. The syngas composition and its calorific value of solid fuels during plasma gasification are reported. The effect of carrier gas on syngas composition of plasma gasification is discussed.

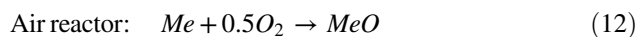
2 Advanced Gasification Technologies

Syngas can be produced by gasifying solid feedstock using air, steam, CO₂, or their mixtures. Air as a gasifying medium decreases the calorific value of syngas due to the dilution of N₂. Pure oxygen as the oxidizing medium may increase the calorific value of product gas but it would also increase the operational cost of gasifiers. Syngas from gasifiers can be utilized for hydrogen production or for electricity generation. In case of hydrogen production, a high-temperature reformer and a water gas shift reactor are required for the conversion of CO into H₂. Further, a CO₂ capture unit is required for the removal of CO₂ from H₂. However, the resultant hydrogen gas may be contaminated with a trace amount of CO, NO_x, and SO_x. The incorporation of these several downstream units would result in high energy penalty and reduces the overall efficiency of the process. These drawbacks can be overcome in chemical looping reforming technology (CLR), which produces high pure hydrogen.

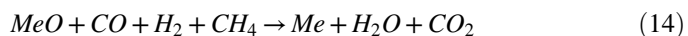
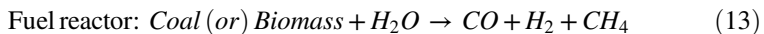
In case of gas turbine for electricity production, the combustor of a gas turbine requires pure oxygen to produce nitrogen-free flue gas for storage. However, the addition of an ASU unit for the production of pure oxygen would reduce the net thermal efficiency of power plants. This problem can be rectified in chemical looping combustion (CLC) technology.

2.1 Chemical Looping Combustion (CLC)

Chemical looping concept can also be referred as dual fluidized bed gasification. CLC technology separates oxygen from air through the oxidation of metal particles (Eq. 12) in an air reactor (AR).



Metal oxides from the AR are circulated to a fuel reactor (FR) for the oxidation of fuels. Firstly, solid fuel is converted into syngas using steam and CO₂. Secondly, metal oxides oxidize the resultant syngas into CO₂ and H₂O and produce a pure CO₂ stream, which can be stored without any further treatment. This process is referred as in situ gasification CLC technology.



Reduced metal particles from FR are recycled to AR for oxidation. Reduction and oxidation of oxygen carriers occur in a cyclic manner and hence, the concept is named as “chemical looping.” The heat of reaction in both reactors depends on the

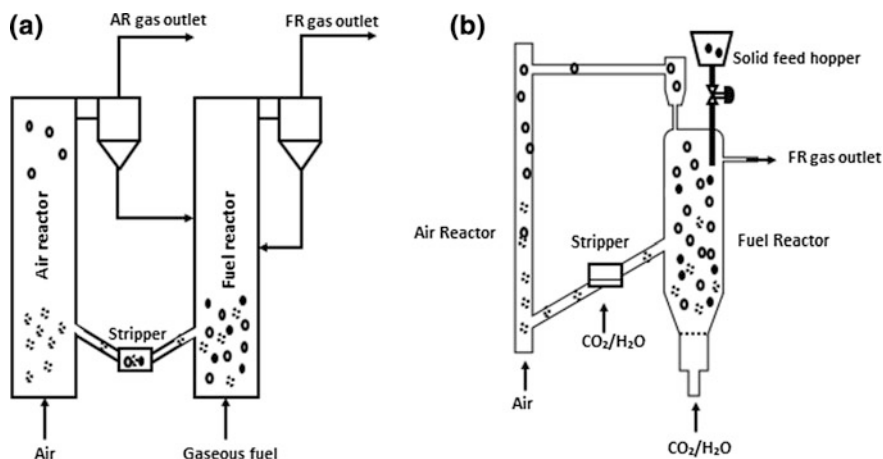


Fig. 1 Chemical looping setup in solid and gaseous fuels. (●—Fuel particles; ○—Oxidized oxygen carrier; ◐—Reduced oxygen carrier) [9, 14, 17, 39, 47, 58]

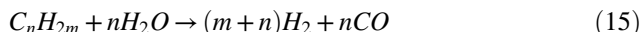
choice of fuel and metal oxides. This technology eliminates the use of ASU for the separation of oxygen from air.

Figure 1a, b shows the experimental setup of gas- and solid-based CLC reactors. Solid fuels such as coal and biomass can be gasified in a separate gasifier and the resultant syngas can be processed in CLC reactors. Figure 1a shows the reactor setup of gas fuel-based CLC process. Syngas is usually injected at the lower section of fuel reactors to provide counter-current mode of interaction with oxygen carriers [14, 18, 35, 39]. Also, one can use solid fuel directly in a CLC operation, which is termed as iG-CLC. Figure 3.1b shows the solid fuel-based reactor arrangement. Solid fuel is introduced at the upper section of fuel reactor via hopper and the fuel particles interact with CO₂/steam in a counter-current mode [9, 23]. A stripper is placed between air and fuel reactor to prevent the leakage of char into the AR [17, 47, 48, 58, 64]. The stripper is operated under bubbling fluidized mode for the transfer of carbon particles to the FR [50, 66].

2.2 Chemical Looping Gasification (CLG)

Chemical looping gasification (CLG) is a novel gasification technology, which is similar to the CLC technology. Metal oxides provide oxygen molecules for the partial combustion of syngas and this reaction liberates thermal energy for the progress of gasification reactions. This concept uses either two or three interconnected reactors in series known as air reactor, fuel reactor, and steam reactor. Interconnected fluidized bed enables high solid circulation rate. The gasification of solid fuel into CO and H₂

(Reaction 5–10) and further, the oxidation of syngas into CO_2 and H_2O with metal oxides (Reaction 15) would occur simultaneously in the FR.



At high temperatures, reverse water gas shift reaction would occur and might result in CO formation.

Figure 2 shows the schematic diagram of chemical looping gasification unit. It comprises of fuel reactor (1) and air reactor (6). Solid feedstock is usually fed by a hopper (2). FR is usually a bubbling fluidized bed reactor while AR is designed as a circulating fluidized bed reactor [14]. A cyclone separator (4) separates the mixture of reduced OC materials and syngas from the FR. The reduced OC is recycled to the AR and air (7) is introduced at the lower section of the AR (6). The heat required for gasification can also be supplied in the form of sensible heat of oxygen carriers from the AR to the FR. Metal oxide to fuel ratio is kept low in order to prevent the complete combustion of feedstock into CO_2 and H_2O [27].

Biomass is a suitable raw material for CLG as it contains 80% of volatile matter. Table 3 shows the syngas composition of biomass-based CLG. It can be noticed that with increase in the operating temperature of FR, a high-calorific-value syngas is obtained. In the CLG operation, CO-enriched syngas is reported under inert atmosphere whereas an equimolar percent of CO- and H_2 -based syngas is noticed

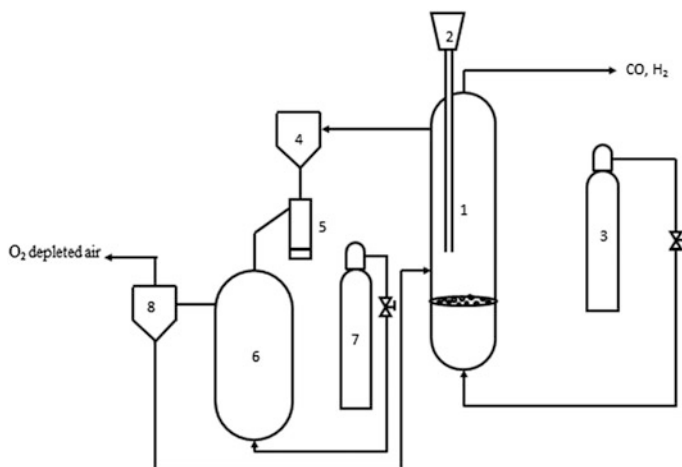


Fig. 2 Schematic layout of interconnected fluidized chemical looping gasification unit [14, 27]

Table 3 Comparison of syngas composition of biomass during chemical looping gasification (CLG) under inert and steam atmosphere

Feed	Oxygen carrier (OC)	Expt. setup	Fluidizing medium	Operating temperature (°C)	Gas composition (mol%)	Calorific value (kJ/mol)	References
Rice husk	Fe ₂ O ₃	Fluidized bed	Steam	800	CO-34%, H ₂ -38%, CO ₂ -15%	188.18	[17]
				900	CO-28%, H ₂ -30%, CO ₂ -36%	151.84	
Comcob	Mn ₂ O ₃	Simulation study	Steam	800	CO-40%, H ₂ -38%, CO ₂ -8%	205.16	[68, 69]
				1200	CO-55%, H ₂ -42%, CO ₂ -0%	257.29	
Pine	Hematite	Fluidized bed	Argon	650	CO-47%, H ₂ -16%, CO ₂ -22%	171.73	[20]
				800	CO-49%, H ₂ -21%, CO ₂ -17%	189.49	

under steam atmosphere. High operating temperature favored the release of volatiles from biomass, and thus, the calorific value is increased [20].

CaO is a cheaper metal oxide for CLG operation and also it acts as a catalyst for the production of hydrogen-enriched syngas [70]. Han et al. [19] claimed that CaO can also act as a catalyst for cracking of tar components in solid fuels. Further, CaO adsorbs CO_2 and thus, it enhances the percentage of hydrogen in syngas [2, 67].

2.3 Chemical Looping Reforming (CLR)

Chemical looping reforming (CLR) is an alternative method for the production of high pure hydrogen. It is similar to chemical looping combustion (CLC) technology. In this technology, solid fuel is converted into two separate gas streams. A pure CO_2 stream is obtained in the FR, whereas a high pure hydrogen can be produced in the steam reactor (SR). In this technology, an additional reactor (steam reactor) is required to connect with other reactors such as air reactor and fuel reactor. The reduced oxygen carriers from the FR are transferred into steam reactor (SR) for the oxidation of metal particles using steam. During the metal oxidation process, steam molecules are converted into hydrogen gas. The unoxidized metal particles in the steam reactor are recirculated to the AR to achieve complete oxidation. Thus, the metal/metal oxide particles are circulated between three interconnected reactors.

Figure 3 shows the schematic representation of the CLR technology. Iron-based OC exists in three thermodynamically stable form of oxides such as Fe_2O_3 , Fe_3O_4 ,

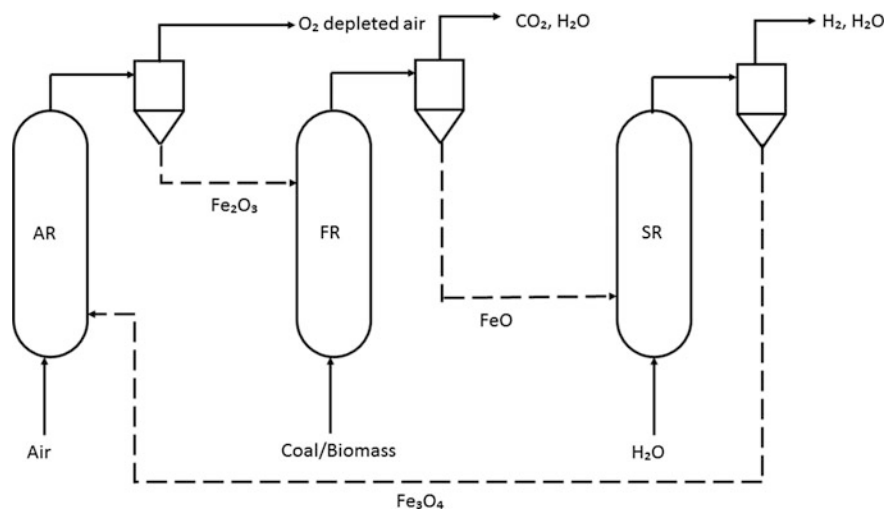
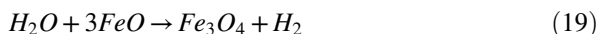


Fig. 3 Schematic illustration of chemical looping concept in hydrogen production [33, 53, 71]

and FeO. In the FR, the supplied fuel is converted into CO₂ and H₂O with the reduction of metal oxides. The reduced FeO from the FR is transferred into the SR. FeO is oxidized in the form of Fe₃O₄ in the SR. Further, Fe₃O₄ is transferred into the AR and gets converted into Fe₂O₃, which can be recycled into the FR for fuel oxidation [33, 53, 71]. The chemical reaction between steam and metal oxide in the SR is shown below:

In steam reactor,



2.4 Metal Oxides

Metal oxides such as Ni, Cu, Co Fe, Mn, etc., can be used as oxygen carriers. Cu, Co, and Mn possess a tendency to release its lattice oxygen at high temperature and the liberated-free oxygen molecule directly reacts with solid fuels and it is termed as chemical looping oxygen uncoupling (CLOU). Support materials such as Al₂O₃, TiO₂, ZrO₂, SiO₂, etc., are used to provide mechanical strength to oxygen carriers. Alumina-based support materials have been extensively used as it exhibit low agglomeration tendency, high thermal stability, and low attrition. Wastes such as manganese ore, red mud, perovskite from steel and alumina production industries and natural iron ores such as hematite, ilmenite can be used as a cheaper source of oxygen carriers in solid fuel-based CLC operation.

Table 4 provides a comparison study of reactivity of solid, liquid, and gaseous fuels under CLC operating conditions in terms of CO₂ yield and fuel conversion. CO₂ yield is defined as the molar percentage of CO₂ obtained in the flue gas of FR [68]. Copper-based oxides show highest reactivity with 99% of CO₂ yield as compared to Ni and Mn [56]. Cu and Mn have shown high reactivity with metal oxides due to its oxygen uncoupling property. However, Mn shows a lower reactivity than Cu due to high attrition tendency of Mn particles. Ni-, Mn-, Cu-based oxides are expensive and the use of these metal oxides for handling solid fuels leads to uneconomic conditions. Cheaper metal oxides such as ilmenite, hematite, magnetite, red mud, etc., can be used for solid fuel-based CLC operations. These metal oxides can be obtained as a cheaper source of waste material from several industries. The reactivity of hematite with bituminous coal shows a high CO₂ yield of 90% under steam and CO₂ atmosphere. Volatile matter in solid fuel plays a crucial role for enhancing the reactivity of metal oxides. Lignite coal possessing high volatile matter has shown a high reactivity with iron ore and achieved 90% of fuel conversion with 81% of CO₂ yield. However, in case of pet coke containing high fixed carbon, an average of 74% fuel conversion is achieved. In case of gas fuels, metal oxides have shown a high reactivity with a fuel conversion and CO₂ yield of 95%. Indirect method of solid CLC operation involves gasification of solid fuels in

Table 4 Comparative study of solid, gas, and liquid fuels using various metal oxides in CLC operation

Type	Fuel	Oxygen carrier (OC)	Type of bed	Operating temperature (°C)	Fuel Conversion (%)	CO ₂ yield (%)	References
Solid fuel	Petcoke	Mn ore	Bubbling fluidized bed reactor, Steam	940	68–76		[41]
	Coal	NiO	Spout fluid bed reactor, CO ₂ and Steam	970		96.3	[58]
	Pine	Fe ₂ O ₃	Bubbling fluidized bed, N ₂	900	90		[61]
	Lignite coal	Iron ore	Fluidized bed reactor CO ₂	900	91	81	[55]
	Bituminous coal	Ilmenite	Fast fluidized bed reactor, Steam	950	87		[1]
	Bituminous coal	Hematite	Spout fluid bed, Steam	970		93	[60]
	Bituminous coal	Hematite	Bubbling fluidized bed, CO ₂	900		92.8	[45]
	Syngas	Fe ₂ O ₃	Moving bed reactor	800	99.75	99.75	[39]
	Syngas	Fe ₂ O ₃	Moving bed reactor	900	~100	100	[66]
	Syngas	NiO	Fluidized bed reactor	800–900	>99		[29]
Gaseous fuel	Methane	CuO	Circulating fluidized bed reactor	~850	98	98	[37]
	Diesel	NiO	Circulating fluidized bed reactor	800	100		[16]
	Dodecane	NiO	Fluidized bed reactor	950	100	100	[24]
	Heavy oils from oil refinery	CuO NiO Mn ₃ O ₄	Bubbling fluidized bed reactor	800	99	~99 ~97 ~85	[56]
	Isopropanol solution	Fe ₂ O ₃	Moving bed reactor	900	100		[8]

a separate gasifier and the resultant syngas can be utilized in the CLC operation. However, it requires pure oxygen for the gasification of solid fuels in the gasifier. In the present study, liquid fuel CLC operation is also reviewed in order to compare the reactivity of solid fuels. Liquid fuels are superior to solid fuels as there is no char gasification in liquid fuels. However, heavy liquid fuels achieve slightly lower yield as compared to low molecular liquids due to high viscosity and sulfur content, which restricts the reactivity of oxygen carrier. Liquid fuels have shown high reactivity as compared to solid fuels.

The handling of solid fuel in a CLC operation is difficult due to the poor interaction between solid fuel and metal oxides. Especially, handling of Indian coal in the CLC process is more complex due to its high ash content. Co-combustion and co-gasification conditions of high ash coal and biomass can be highly suitable for the CLC operation. Table 5 provides a summary of pilot-scale studies in CLC process using solid, gas, and liquid fuels. Gaseous fuels such as syngas and natural gas have shown almost 100% fuel conversion efficiency irrespective of reactor choice (bubbling, circulating, or moving bed). However, solid fuel conversion was found to be lower due to the rate limiting step of char gasification reaction. The pilot-scale studies have shown that the fuel conversion is found in a wide range of 66–97%, which depends on its inherent properties and the choice of metal oxides. Thus, blended conditions of biomass and coal can enhance the reactivity of metal oxides.

The integration of co-gasification and chemical looping technology has several advantages.

- (i) Metal oxides can act as a catalyst for char gasification, water gas shift reaction, and Boudouard reaction.
- (ii) Biomass ash contains catalytic inorganic species, which is suitable for efficient char gasification.
- (iii) High volatile matter of biomass leads to high reactivity of metal oxides.
- (iv) The utilization of biomass reduces carbon emission into the atmosphere.

Research should be focused toward the direct utilization of solid fuels under blended conditions with suitable combination of metal oxides.

2.5 Plasma Gasification

Plasma is the fourth state of matter consisting of free electrons, neutral particles, and ions. The interaction of carrier gas with high energy source produces plasma plumes. Plasma creates high-temperature environment in electric arc discharge method ($>13,000$ °C) [13]. Plasma can be categorized into cold plasma (<4000 K) and hot plasma (4000–20,000 K) [57]. The rate of energy transfer from electron to molecules is low in cold plasma. In a conventional gasification unit, a sub-stoichiometric quantity of oxygen is utilized for the partial combustion of solid

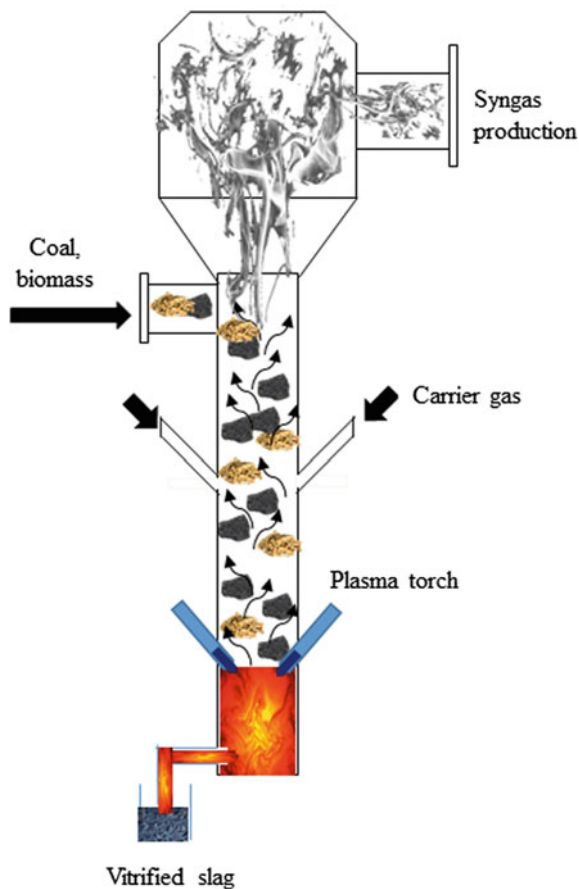
Table 5 Pilot-scale studies on coal and biomass-based CLC operation

Fuel	Oxygen carrier	Operating bed	Operating condition	Pilot plant size (kW _{th})	Fuel conversion (%)	Outlet gas composition	References
Bituminous coal	CuO	Circulating fluidized bed	Steam 950 °C	50	94.7	–	[3]
Sub-bituminous coal	Fe ₂ O ₃	Fixed bed reactor	950 °C	25	97	CO ₂ yield ~ 99%	[34]
Sub-bituminous coal	Fe ₂ O ₃	Moving bed reactor	835 °C	25	84.8	–	[6]
Bituminous coal	Ilmenite	Bubbling fluidized bed	Steam 1000 °C	10	64	–	[42]
Petcoke	Ilmenite	Fluidized bed	Steam	10	75	–	[7]
Bituminous coal	Ilmenite and manganese ore	Circulating fluidized bed	Steam 970 °C	100	~66	~74% sulfur is converted to SO ₂ in FR outlet	[40]
Natural gas	NiO	Circulating fluidized bed	Steam 747 °C	140	–	CO ₂ ~ 20%, H ₂ O ~ 50% CO-10%, CH ₄ ~ <1% (vol. %)	[54]
Natural gas	NiO	Circulating fluidized bed	Steam	140	>99	CO ₂ yield > 94%	[35]
Natural gas	NiO	Circulating fluidized bed	900 °C	120	~99	CO ₂ yield > 90%	[5]
Syngas	Fe ₂ O ₃	Moving bed reactor		2.5	>99	–	[34]
Residue from oil refinery	Ilmenite	Circulating fluidized bed reactor	950 °C	10	63–70	CO ₂ ~ 93%, CO ~ 3%, CH ₄ ~ 1.3%, HCs ~ 2.6% (vol. %)	[51]

fuels and the liberated heat is utilized for the gasification of char and the release of volatiles. Figure 4 shows the schematic representation of plasma gasification technology [13]. In the plasma gasification technology, the reaction between hydrocarbons of solid fuels and plasma at temperatures in the range of 2700–4500 °C cracks heavier components into lighter fractions (CO and H₂) with ash content as the residue. As the plasma torch is used as the energy source for gasification, the supply of pure oxygen for partial combustion of feed is not required. Also, the contamination of CO₂ with syngas can be avoided as compared to conventional gasification technology. A high-calorific syngas can be generated with a negligible tar content [26].

In plasma gasification, the carrier gas is allowed to pass between two electrodes under high voltage. Due to high potential difference, an electric arc is generated. This electric arc ionizes the carrier gas and a plasma plume is generated. This plasma plume at a temperature greater than 5000 °C decomposes solid feedstock [43] and progresses the pyrolysis and gasification reactions. The plasma electrons

Fig. 4 Schematic diagram of plasma gasification



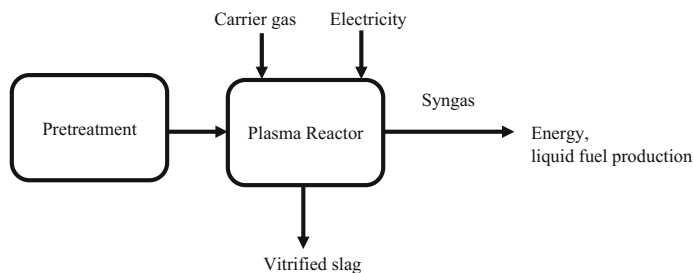


Fig. 5 Block diagram of plasma gasification

intensify the chemical oxidation process by reducing the activation energy of carbon conversion reactions. Plasma gasification technology requires carrier gas such as air, O_2 , or noble gas for plasma production. Plasma can be discharged using direct current (DC), radio frequency (RF), or microwave (MC) sources. In DC method, a high voltage is applied to electrodes to produce ions and electrons, which produces core temperatures greater than 10,000 K. However, the temperature in marginal region reaches only about 6000 K. The electrons get excited at this temperature range and produces ions with further collision. In case of RF, alternating current is applied between electrodes and produces a core temperature of about 8000 K [65]. Microwave method is economical as compared to other sources as it does not require any electrodes. Also, a low voltage supply is sufficient for the production of high-temperature plasma [22]. It is preferred over DC and RF as it has robust reactor design [31, 57]. Figure 5 shows the block diagram of plasma gasification. Solid feedstock should be pretreated for sizing of particles for plasma reactor.

Plasma gasification is an allothermal process and operated at atmospheric pressure. Allothermal process requires external heat to sustain its operating temperature (1500–5000 °C). It breaks down high molecular weight organic fractions into syngas and slag. This vitrified slag can be used for making building materials (tiles, bricks, etc.).

2.5.1 Choice of Plasma Carrier Gas

The choice of carrier gas affects the syngas composition during plasma gasification. Du et al. [11] conducted a comparative study to evaluate the effect of carrier gas on syngas composition. A low heating value of syngas is estimated for air as the carrier gas, and it is due to the dilution of syngas with N_2 .

Steam as the carrier gas gets dissociated into free radicals such as hydrogen, oxygen, and hydroxide at high plasma temperature. These reactive free radicals enhance the reaction rate [59]. The generated CO gas may get oxidized into CO_2 in presence of OH radical.



This technology is examined in pilot-scale level with a capacity of 12 ton/h feed rate at Swindon, UK. The sensible heat of hot syngas of plasma reactor can be used to produce steam for electricity generation. However, high operating cost of plasma reactor is the major drawback of this technology as the generation of plasma and the cost of electrodes are expensive.

2.5.2 Plasma Gasification-Based Syngas

Table 6 shows the composition of syngas obtained during plasma gasification. The reported syngas composition shows 25–30% of CO₂ and the rest of the gas constituted of H₂, CO, and CH₄. NO_x pollutants are generated with the use of air as the carrier gas due to high temperature of plasma. A high fuel conversion about 90–100% is reported for the steam and CO₂ atmosphere, whereas 65–85% of fuel conversion is noticed for air and N₂ atmosphere. This is due to the reactive atmosphere of the gasifying medium such CO₂ and H₂O. Low yield of syngas is obtained using argon as the carrier gas. This is due to the high ionization potential of argon gas, which consumes high energy [11]. Hrabovsky et al. [25] observed almost a tar-free syngas (>10 mg/Nm³) due to the progress of cracking and reforming reactions at elevated temperatures.

Tar is an undesired product in syngas and consists of a mixture of organic components of polyaromatic hydrocarbons (PAH) such as naphthalene, phenanthrene, anthracene, etc. These components are highly stable in the temperature range of 600–900 °C. High operating temperature of gasifiers reduces the quantity of tar due to the progress of cracking and reforming reactions. Phenolic components can decompose at high temperatures. The generation of polyaromatic hydrocarbon (PAH) was considerably low in plasma gasification as compared to conventional gasification [26].

Table 6 Calorific value and syngas composition of coal and biomass during plasma gasification

Feedstock	Type of plasma	Gas used	Product gas composition (vol.%)	Calorific value of syn gas (kJ/mol)	References
Bituminous Coal	Microwave plasma, 3500 K	Air	CO ~ 28.5%, CH ₄ ~ 1.5%, H ₂ ~ 8%, CO ₂ ~ 2%, O ₂ ~ 0%, N ₂ ~ 60%	112.05 NOx: 1431.5 ppm	[32]
Bituminous Coal	Direct current 3550 K	Air-steam	CO:26%, CH ₄ : 0%, H ₂ : 32.6%, CO ₂ : 0%, N ₂ : 37.4%, O ₂ : 4%	152.47 Carbon conversion (%) 90.2%	[50]
Sludge	Direct current 1373 K	Air	CO:22.4%, CH ₄ : 0%, H ₂ : 3.2%, CO ₂ : 5.2%, N ₂ : 57.6%	71.14 Toxicity > 0.002	[52]
Sawdust	Direct current 1633 K	CO ₂ , O ₂ and Ar	CO:60.8%, CH ₄ : 0.5%, H ₂ : 27.7%, CO ₂ : 5.4%, O ₂ : 0.7%, Ar: 4.9%	243.108	[25]
Sawdust	Direct current 1473–1673 K	CO ₂	CO:50.9%, CH ₄ : 2.3%, H ₂ : 41.6%, CO ₂ : 4.3%	263.16 Carbon conversion (%) 100%	[21]

3 Conclusions and Scope for Future Research

The conversion of coal and biomass into syngas through advanced gasification technologies such as CLC, CLR, and plasma technologies is feasible for the production of clean fuels. Plasma gasification leads to high yield of syngas without any residual matter. CLG generates syngas without using pure oxygen and CLR technology produces high purity hydrogen gas. Thus, the development of these advanced technologies would pave a path toward the production of clean and sustainable energy. Further, the future research scopes of these technologies are,

- (i) Research should be focused for the direct utilization of solid fuels using cheaper oxygen carriers in CLC technology. As Indian coal contains 40% ash content, the separation of ash and metal oxides in fuel reactors is difficult. Thus, cheaper metal oxides with high reactivity should be identified.
- (ii) As the conversion efficiency of solid fuels is less in CLC operation, co-combustion and co-gasification coal and biomass is an appropriate option for the CLC operation with a suitable gasifying medium.
- (iii) Pilot plant studies are required for plasma gasification to evaluate the feasibility of commercialization of the technology.

References

1. Abad A, Pérez-Vega R, Luis F, García-Labiano F, Gayán P, Adánez J (2015) Design and operation of a 50 kW_{th} Chemical Looping Combustion (CLC) unit for solid fuels. *Appl Energy* 157:295–303
2. Acharya B, Dutta A, Basu P (2009) Chemical-looping gasification of biomass for hydrogen-enriched gas production with in-process carbon dioxide capture. *Energy Fuels* 23(10):5077–5083
3. Adánez J, Abad A, Perez-Vega R, Luis F, García-Labiano F, Gayán P (2014) Design and operation of a coal-fired 50 kW_{th} chemical looping combustor. *Energy Procedia* 63:63–72
4. André RN, Pinto F, Franco C, Dias M, Gulyurtlu I, Matos MAA, Cabrita I (2005) Fluidized bed co-gasification of coal and olive oil industry wastes. *Fuel* 84(12):1635–1644
5. Bolhär-Nordenkamp J, Pröll T, Kolbitsch P, Hofbauer H (2009) Performance of a NiO-based oxygen carrier for chemical looping combustion and reforming in a 120 kW unit. *Energy Procedia* 1(1):19–25
6. Bayham S, McGiveron O, Tong A, Chung E, Kathe M, Wang D, Zeng L, Fan LS (2015) Parametric and dynamic studies of an iron-based 25-kW_{th} coal direct chemical looping unit using sub-bituminous coal. *Appl Energy* 145:354–363
7. Berguerand N, Lyngfelt A (2009) Chemical-looping combustion of petroleum coke using ilmenite in a 10 kW_{th} unit—high-temperature operation. *Energy Fuels* 23(10):5257–5268
8. Chiu PC, Ku Y, Wu HC, Kuo YL, Tseng YH (2013) Spent isopropanol solution as possible liquid fuel for moving bed reactor in chemical looping combustion. *Energy Fuels* 28(1):657–665
9. Cuadrat A, Abad A, García-Labiano F, Gayán P, Luis F, Adánez J (2011) Ilmenite as oxygen carrier in a chemical looping combustion system with coal. *Energy Procedia* 4:362–369

10. Demirbaş A (2001) Biomass resource facilities and biomass conversion processing for fuels and chemicals. *Energy Convers Manag* 42(11):1357–1378
11. Du C, Wu J, Ma D, Liu Y, Qiu P, Qiu R, Liao S, Gao D (2015) Gasification of corn cob using non-thermal arc plasma. *Int J Hydrogen Energy* 40(37):12634–12649
12. Dutta PP, Pandey V, Das AR, Sen S, Baruah DC (2014) Down draft gasification modelling and experimentation of some indigenous biomass for thermal applications. *Energy Procedia* 54:21–34
13. Favas J, Monteiro E, Rouboa A (2017) Hydrogen production using plasma gasification with steam injection. *Int J Hydrogen Energy* 42(16):10997–11005
14. Forero CR, Gayán P, García-Labiano F, De Diego LF, Abad A, Adánez J (2010) Effect of gas composition in chemical-looping combustion with copper-based oxygen carriers: fate of Sulphur. *Int J Greenhouse Gas Control* 4(5):762–770
15. Franco C, Pinto F, Gulyurtlu I, Cabrita I (2003) The study of reactions influencing the biomass steam gasification process. *Fuel* 82(7):835–842
16. García-Labiano F, de Diego LF, García-Díez E, Serrano A, Abad A, Gayán P, Adánez J (2017) Combustion and reforming of liquid fossil fuels through chemical looping processes: integration of chemical looping processes in a refinery. *Energy Procedia* 114:325–333
17. Ge H, Guo W, Shen L, Song T, Xiao J (2016) Biomass gasification using chemical looping in a 25 kW_{th} reactor with natural hematite as oxygen carrier. *Chem Eng J* 286:174–183
18. Gupta P, Velazquez-Vargas LG, Fan LS (2007) Syngas redox (SGR) process to produce hydrogen from coal derived syngas. *Energy Fuels* 21(5):2900–2908
19. Han L, Wan Q, Yang Y, Yu C, Fang M, Luo Z (2011) Hydrogen production via CaO sorption enhanced anaerobic gasification of sawdust in a bubbling fluidized bed. *Int J Hydrogen Energy* 36(8):4820–4829
20. He F, Huang Z, Li H, Zhao Z (2011) March biomass direct chemical looping conversion in a fluidized bed reactor with natural hematite as an oxygen carrier. In: 2011 Asia-Pacific power and energy engineering conference (APPEEC), pp 1–7
21. Hlina M, Hrabovsky M, Kavka T, Konrad M (2014) Production of high quality syngas from argon/water plasma gasification of biomass and waste. *Waste Manag* 34(1):63–66
22. Hong YC, Lee SJ, Shin DH, Kim YJ, Lee BJ, Cho SY, Chang HS (2012) Syngas production from gasification of brown coal in a microwave torch plasma. *Energy* 47(1):36–40
23. Hossain MM, Lasa HI (2008) Chemical-looping combustion (CLC) for inherent CO₂ separations—a review. *Chem Eng Sci* 63(18):4433–4451
24. Hoteit A, Forret A, Pelletant W, Roesle J, Gauthier T (2011) Chemical looping combustion with different types of liquid fuels. *Oil Gas Sci Technol* 66(2):193–199
25. Hrabovsky M, Konrád M, Kopecky V, Hlina M, Kavka T, Chumak O, Masláni A, Van-Oost G (2010) Plasma aided gasification of biomass and plastics using CO₂ as oxidizer. In: International Symposium on non-thermal/thermal plasma pollution control technology and sustainable energy, Canada
26. Hrabovsky M, Konrad M, Kopecky V, Hlina M, Kavka T, Van Oost G, Beekman E, Defoort B (2006) Gasification of biomass in water/gas-stabilized plasma for syngas production. *Czech J Phys* 56(2):B1199–B1206
27. Huang Z, He F, Zheng A, Zhao K, Chang S, Li X, Li H, Zhao Z (2013) Thermodynamic analysis and synthesis gas generation by chemical-looping gasification of biomass with nature hematite as oxygen carriers. *J Sustain Bioenergy Syst* 3:33–39
28. Jeong HJ, Park SS, Hwang J (2014) Co-gasification of coal–biomass blended char with CO₂ at temperatures of 900–1100 °C. *Fuel* 116:465–470
29. Johansson E, Mattisson T, Lyngfelt A, Thunman H (2006) Combustion of syngas and natural gas in a 300 W chemical-looping combustor. *Chem Eng Res Des* 84(9):819–827
30. Ju Y, Lee CH (2017) Evaluation of the energy efficiency of the shell coal gasification process by coal type. *Energy Convers Manag* 143:123–136
31. Kanilo PM, Kazantsev VI, Rasyuk NI, Schünemann K, Vavriv ED (2003) Microwave plasma combustion of coal. *Fuel* 82(2):187–193

32. Karpenko EI, Messerle VE, Ustimenko AB (2007) Plasma-aided solid fuel combustion. *Proc Combust Inst* 31(2):3353–3360
33. Khan MN, Shamim T (2016) Investigation of hydrogen generation in a three reactor chemical looping reforming process. *Appl Energy* 162:1186–1194
34. Kim HR, Wang D, Zen L, Bayham S, Tong A, Chung E, Kathe MV, Luo S, McGiveron O, Wang A, Sun Z (2013) Coal direct chemical looping combustion process: design and operation of a 25-kW_{th} sub-pilot unit. *Fuel* 108:370–384
35. Kolbitsch P, Bolhar-Nordenkampf J, Pröll T, Hofbauer H (2009) Comparison of two Ni-based oxygen carriers for chemical looping combustion of natural gas in 140 kW continuous looping operation. *Ind Eng Chem Res* 48(11):5542–5547
36. Kumar KV, Bharath M, Raghavan V, Prasad B, Chakravarthy SR, Sundararajan T (2017) Gasification of high-ash Indian coal in bubbling fluidized bed using air and steam—an experimental study. *Appl Therm Eng* 116:372–381
37. Langørgen Ø, Saanum I, Haugen NEL (2017) Chemical looping combustion of methane using a copper-based oxygen carrier in a 150 kW reactor system. *Energy Procedia* 114:352–360
38. Li K, Zhang R, Bi J (2010) Experimental study on syngas production by co-gasification of coal and biomass in a fluidized bed. *Int J Hydrogen Energy* 35(7):2722–2726
39. Li F, Kim HR, Sridhar D, Wang F, Zeng L, Chen J, Fan LS (2009) Syngas chemical looping gasification process: oxygen carrier particle selection and performance. *Energy Fuels* 23(8):4182–4189
40. Linderholm C, Schmitz M, Knutsson P, Lyngfelt A (2016) Chemical-looping combustion in a 100-kW unit using a mixture of ilmenite and manganese ore as oxygen carrier. *Fuel* 166:533–542
41. Linderholm C, Lyngfelt A, Dueso C (2013) Chemical-looping combustion of solid fuels in a 10 kW reactor system using natural minerals as oxygen carrier. *Energy Procedia* 37:598–607
42. Linderholm C, Cuadrat A, Lyngfelt A (2011) Chemical-looping combustion of solid fuels in a 10 kW_{th} pilot–batch tests with five fuels. *Energy Procedia* 4:385–392
43. Lupa CJ, Wylie SR, Shaw A, Al-Shamma'a A, Sweetman AJ, Herbert BM (2013) Gas evolution and syngas heating value from advanced thermal treatment of waste using microwave-induced plasma. *Renew Energy* 50:1065–1072
44. Lv PM, Xiong ZH, Chang J, Wu CZ, Chen Y, Zhu JX (2004) An experimental study on biomass air–steam gasification in a fluidized bed. *Bioresour Technol* 95(1):95–101
45. Ma J, Zhao H, Tian X, Wei Y, Rajendran S, Zhang Y, Bhattacharya S, Zheng C (2015) Chemical looping combustion of coal in a 5 kW_{th} interconnected fluidized bed reactor using hematite as oxygen carrier. *Appl Energy* 157:304–313
46. Mallick D, Mahanta P, Moholkar VS (2017) Co-gasification of coal and biomass blends: chemistry and engineering. *Fuel* 204:106–128
47. Markström P, Linderholm C, Lyngfelt A (2013) Chemical-looping combustion of solid fuels—design and operation of a 100 kW unit with bituminous coal. *Int J Greenhouse Gas Control* 15:150–162
48. Mattisson T, Lyngfelt A, Leion H (2009) Chemical-looping with oxygen uncoupling for combustion of solid fuels. *Int J Greenhouse Gas Control* 3(1):11–19
49. Mendiara T, Diego LF, García-Labiano F, Gayán P, Abad A, Adánez J (2014) On the use of a highly reactive iron ore in chemical looping combustion of different coals. *Fuel* 126:239–249
50. Messerle VE, Ustimenko AB, Lavrichshev OA (2016) Comparative study of coal plasma gasification: simulation and experiment. *Fuel* 164:172–179
51. Moldenhauer P, Rydén M, Mattisson T, Jamal A, Lyngfelt A (2017) Chemical-looping combustion with heavy liquid fuels in a 10 kW pilot plant. *Fuel Process Technol* 156:124–137
52. Moustakas K, Xydis G, Malamis S, Haralambous KJ, Loizidou M (2008) Analysis of results from the operation of a pilot plasma gasification/vitrification unit for optimizing its performance. *J Hazard Mater* 151(2–3):473–480
53. Phuluanglue A, Khaodee W, Assabumrungrat S (2017) Simulation of intensified process of sorption enhanced chemical-looping reforming of methane: comparison with conventional processes. *Comput Chem Eng* 105:237–245

54. Pröll T, Bolhàr-Nordenkamp J, Kolbitsch P, Hofbauer H (2010) Syngas and a separate nitrogen/argon stream via chemical looping reforming—a 140 kW pilot plant study. *Fuel* 89 (6):1249–1256
55. Rajendran S, Wong M, Stokie D, Bhattacharya S (2016) Performance of a Victorian brown coal and iron ore during chemical looping combustion in a 10 kW_{th} alternating fluidized bed. *Fuel* 183:245–252
56. Rydén M, Moldenhauer P, Mattisson T, Lyngfelt A, Younes M, Niass T, Fadhel B, Ballaguet JP (2013) Chemical-looping combustion with liquid fuels. *Energy Procedia* 37:654–661
57. Sanlisoy A, Carpinlioglu MO (2017) A review on plasma gasification for solid waste disposal. *Int J Hydrogen Energy* 42(2):1361–1365
58. Shen L, Wu J, Xiao J (2009) Experiments on chemical looping combustion of coal with a NiO based oxygen carrier. *Combust Flame* 156(3):721–728
59. Shin DH, Hong YC, Lee SJ, Kim YJ, Cho CH, Ma SH, Chun SM, Lee BJ, Uhm HS (2013) A pure steam microwave plasma torch: gasification of powdered coal in the plasma. *Surf Coat Technol* 228:S520–S523
60. Song T, Shen T, Shen L, Xiao J, Gu H, Zhang S (2013) Evaluation of hematite oxygen carrier in chemical-looping combustion of coal. *Fuel* 104:244–252
61. Sozen H, Guo-qiang W, Hai-bin L, Fang HE, Zhen H (2014) Chemical-looping gasification of biomass in a 10 kW_{th} interconnected fluidized bed reactor using Fe₂O₃/Al₂O₃ oxygen carrier. *J Fuel Chem Technol* 42(08):922–931
62. Sripada PP, Xu T, Kibria MA, Bhattacharya S (2017) Comparison of entrained flow gasification behavior of Victorian brown coal and biomass. *Fuel* 203:942–953
63. Ströhle J, Orth M, Epple B (2014) Design and operation of a 1 MW_{th} chemical looping plant. *Appl Energy* 113:1490–1495
64. Sun H, Cheng M, Chen D, Xu L, Li Z, Cai N (2015) Experimental study of a carbon stripper in solid fuel chemical looping combustion. *Ind Eng Chem Res* 54(35):8743–8753
65. Tang L, Huang H, Hao H, Zhao K (2013) Development of plasma pyrolysis/gasification systems for energy efficient and environmentally sound waste disposal. *J Electrostat* 71 (5):839–847
66. Tong A, Sridhar D, Sun Z, Kim HR, Zeng L, Wang F, Wang D, Kathe MV, Luo S, Sun Y, Fan LS (2013) Continuous high purity hydrogen generation from a syngas chemical looping 25 kW_{th} sub-pilot unit with 100% carbon capture. *Fuel* 103:495–505
67. Udomsirichakorn J, Salam PA (2014) Review of hydrogen-enriched gas production from steam gasification of biomass: the prospect of CaO-based chemical looping gasification. *Renew Sustain Energy Rev* 30:565–579
68. Wang X, Jin B, Zhu X, Liu H (2016) Experimental evaluation of a novel 20 kW_{th} in situ gasification chemical looping combustion unit with an iron ore as the oxygen carrier. *Ind Eng Chem Res* 55(45):11775–11784
69. Wang K, Yu Q, Qin Q, Hou L, Duan W (2016) Thermodynamic analysis of syngas generation from biomass using chemical looping gasification method. *Int J Hydrogen Energy* 41 (24):10346–10353
70. Weerachanchai P, Horio M, Tangsathikulchai C (2009) Effects of gasifying conditions and bed materials on fluidized bed steam gasification of wood biomass. *Bioresour Technol* 100 (3):1419–1427
71. Xiang W, Chen S, Xue Z, Sun X (2010) Investigation of coal gasification hydrogen and electricity co-production plant with three-reactor chemical looping process. *Int J Hydrogen Energy* 35(16):8580–8591
72. Xu C, Hu S, Xiang J, Zhang L, Sun L, Shuai C, Chen Q, He L, Edreis EM (2014) Interaction and kinetic analysis for coal and biomass co-gasification by TG–FTIR. *Bioresour Technol* 154:313–321

Author Index

A

Agarwal, Ramesh K., 331
Aghalayam, Preeti, 207
Arora, Pratham, 351
Attanoor, Suresh, 455

B

Banerjee, Subhodeep, 331
Baruah, Debarshi, 115
Bhaskaran, Sminu, 243, 425
Bhui, Barnali, 499
Buragohain, Buljit, 223

C

Chatterjee, Pradip K., 63, 93

D

De, Santanu, 63, 93, 243
Dhami, Harnek, 307
Dhar, Atul, 403

G

Ghosh, Sudip, 151
Gupta, Saurabh, 243, 425

H

Hoadley, Andrew, 351

I

Indrawan, Natarianto, 369
Izaharuddin, Ainul Nadirah, 307

K

Kalita, Pankaj, 115
Kamalanathan, Premkumar, 175
Karmakar, Malay K., 63, 93
Kaundal, Ankur, 403
Kumar, Ajay, 369

Kumar, Mayank, 281

Kumar, Sunil, 369
Kumar, Umesh, 307

L

Loha, Chanchal, 63, 93

M

Mahajani, Sanjay, 351
Mahanta, Pinakeswar, 223, 473
Mallick, Debarshi, 223, 473
Moholkar, Vijayanand S., 223, 473
Mukunda, H.S., 455

P

Paul, Manosh C., 307
Powar, Satvasheel, 403

R

Rajasekhar Reddy, B., 3
Ravi, M.R., 37

S

Salem, Ahmed M., 307
Sangeeta Kohli, 37
Sutardi, Tata, 307

U

Upadhyay, Rajesh Kumar, 175

V

Vairakannu, Prabu, 499
Vinu, R., 3

Y

Yang, Mengqiao, 331